OBSERVING AND MODELLING EXCEPTIONAL FLOODS AND RAINFALLS

edited by
ENNIO FERRARI
PASQUALE VERSACE

**1ST International Workshop
on Hydrological Extremes
AMHY-FRIEND group**

*University of Calabria,
Cosenza (Italy), 3-4 May, 2006*

OBSERVING AND MODELLING EXCEPTIONAL FLOODS AND RAINFALLS

edited by
ENNIO FERRARI
PASQUALE VERSACE

*1ST International Workshop on Hydrological Extremes
AMHY-FRIEND group*

University of Calabria,
Cosenza (Italy), 3-4 May, 2006

University of Calabria
Cosenza (Italy)
3-4 May, 2006

Observing and modelling exceptional floods and rainfalls

1ˢᵗ International Workshop on Hydrological Extremes

The workshop is a contribution of the AMHY-FRIEND group, topic "Extreme events", to UNESCO IHP-VI (2002-2007)

Proceedings of the Workshop

Edited by E. Ferrari and P. Versace

Soil Protection Department
Faculty of Engineering
University of Calabria (Italy)

Scientific Committee
Vito Copertino *(Potenza, Italy)*
Fabrizio Ferrucci *(Cosenza, Italy)*
Maria Carmen Llasat *(Barcelona, Spain)*
Eric Servat *(Montpellier, France)*
Pasquale Versace *(Cosenza, Italy)*

Organizing Committee
E. Ferrari (*Chairman*), D. L. De Luca, F. Cruscomagno, D. Biondi, G. Capparelli, V. De Matteis, M.A. Longo, D. Maletta, A. Senatore, T. Zaffino, G. Calcagno, F. Casacchia (*all at Camilab, http://www.camilab.unical.it*)

With the patronage of UNESCO IRD Institut de recherche pour le développement

Sponsorship UNIVERSITÀ DELLA CALABRIA Dipartimento di DIFESA DEL SUOLO CARTHEMA PROTEZIONE CIVILE CALABRIA

This book is dedicated to the memory of
VIOREL ALEXANDRU STANESCU
(1933–2006)

Viorel Alexandru Stanescu was the founder of the vanguard team in Romanian Hydrology. During his career he produced many highly valuable studies concerning the mathematical modelling of hydrologic phenomena.

After the engineer degree at the Bucharest Polytechnic Institute in 1956, he joined to the "Danube delta" team and then he was lead researcher at the Hydrology Department of the Institute of Hydrotechnics Studies and Research.

Finally he worked as a researcher at the Institute of Meteorology and Hydrology of Romania, which he directed for many years, and as professor at the Technical University of Civil Engineering Bucharest. While accomplishing these tasks, he proved his remarkable human qualities, his emotional and intellectual nobility, his creativity and social skills, leaving behind valuable followers to whom he has passed down something of his knowledge and more importantly from his passion and dedication.

Due to his studies and researches in the domain of Hydrology, Viorel Alexandru Stanescu became part of the hydrologists' world elite and was elected as expert in several international organizations. He published thirteen books, manuals and university courses and over 140 scientific works in Romania and abroad. He was rewarded for his activity with Romanian Academy awards, was a member of honour of the Hungarian Society of Hydrology and the president of the Romanian Association of Hydrology Sciences.

Among the many international projects that he coordinated with enthusiasm, since the early years he took part in the scientific activities of AMHY-FRIEND group for UNESCO, soon becoming a guide for all the colleagues who met him and greatly appreciated his unforgettable qualities as a man and scientist.

PRESENTATION

The reciprocal exchange of information and knowledge among researchers of extreme natural events and civil protection managers, daily involved in forecasting, coping or managing emergencies caused by hydrological and geological disasters, is an important task necessary for allowing the Institutions to face rapidly and efficiently with very dangerous situations.

From many years the Civil Protection Division of Calabria Region has started collaboration with the Research Institutions working throughout the territory, with the aim of make available tools for forecasting and prevention of occurrences of damaging events or to cope with emergency situations through the best available technologies.

Standard activity of Civil Protection Division concerns technological developments, through the standard use of high technology systems (regional warning systems, emergency telecommunications systems, geographical informative systems for emergency management), operative application of models and studies produced by experts in hydrological and geological risks, diffusion of knowledge of phenomena through promotion of specific studies and spreading activities of risk knowledge among people.

Within these activities, Civil Protection Division of Calabria Region has intended to support the International Workshop on Hydrological Extremes "Observing and modelling exceptional floods and rainfalls" which took place at the University of Calabria on 3rd and 4th May 2006, considering it as an opportunity greatly useful to promote comparison among researchers and managing personnel of Institutions and Administrations coping with hydrological extremes, working all over the countries within Mediterranean area.

It is an important occasion to promote exchange of experience and circulation of ideas that can contribute to better develop the scientific substratum in which Civil Protection Division of Calabria Region operates. The chance becomes even more meaningful for Calabria Region since different scientific contributions have been presented by engineers daily engaged in the regional Civil Protection structures, thus proving in such an eminent international assembly the high scientific levels reached in activities realized by the Civil Protection Division of Calabria Region.

Raffaele Niccoli

Manager of Civil Protection Division,
Calabria Region

Contents

Part 3
ADVANCES IN PEAK RIVER FLOW MODELLING THROUGH RAINFALL RUNOFF MODELS

INVITED LECTURE

FOREWORD

This book contains the proceedings of the 1st International Workshop on Hydrological Extremes that was held in Cosenza (Italy) on 3rd and 4th May, 2006, at the University of Calabria, with the title "Observing and modelling exceptional floods and rainfalls". It coped both with case studies of damaging floods and rainfalls and with advances in statistical analysis of hydrological extremes, mainly focusing at the researches developed for the topic "Extreme events" of AMHY (Alpine and Mediterranean Hydrology) group within FRIEND (Flow Regimes from International Experimental and Network Data) project, which is one of the crossing themes of the IHP-VI phase of UNESCO.

For over a decade all the people involved in AMHY–FRIEND group shared investigations on rare floods and heavy rainfalls and exchanged experiences in appointments like the present workshop, that was attended by national coordinators and researchers coming from 11 Mediterranean countries (Albania, Algeria, Bulgaria, France, Greece, Italy, Romania, Spain, Slovenia, Turkey, Yugoslavia). The relevance of the workshop is closely related to the increased vulnerability from hydrological events observed in the represented countries.

The workshop was divided in three sessions: Recent case studies of heavy rainfalls and floods (chairman M. Lang), Statistical and stochastic analysis of extreme events (chairman B. Bacchi), Advances in peak river flow modelling through rainfall-runoff models (chairpersons M.C. Llasat and V.A. Stanescu). A total of 24 works were presented and interesting discussions were raised. A brief outlook of the topic in charge of the international coordinator and the open discussion of proposals for defining future outlook of the topic concluded the workshop.

As collateral events followed: an invited lecture on "Remote sensing for prevention analysis of tsunami in Sri Lanka" by prof. F. Ferrucci (Project manager of Master Carthema, University of Calabria), a poster session of works on risk mapping by students of Master Carthema and the delivery of two thesis awards in memory of prof. Carlo Colosimo.

I wish to thank Camilab, Soil Protection Department and Master Carthema of University of Calabria for financing the workshop and the Civil Protection Division of Calabria Region for supporting this book. Thanks also to the Scientific Committee for judgments and suggestions on works and to all the people who helped in the organisation.

The workshop has confirmed once again the competence and the friendship among all the participants involved in the project, thus renewing our common believe that FRIEND could be not only the acronym of a scientific project but also a meaningful attempt to share knowledge and social interaction among people.

Ennio Ferrari

International coordinator of topic "Extreme events",
AMHY-FRIEND group

Observing and modelling exceptional floods and rainfalls
Proceedings of the AMHY-FRIEND International Workshop on Hydrological Extremes,
held at University of Calabria, Cosenza (Italy), May 3-4, 2006

ANALYSIS OF HYDROLOGICAL EXTREME EVENTS
IN AMHY-FRIEND GROUP

E. Ferrari

Department of Soil Protection "V. Marone", University of Calabria, Cosenza, Italy

ABSTRACT

In this work are briefly reviewed the main research lines and results related to the analysis of some hydrological extremes performed in recent years by the working groups involved in AMHY-FRIEND project, firstly as "Heavy rains" and "Rare floods" separate topics and then as "Extreme events" topic. Finally a synthetic presentation of both ongoing researches and outlooks for this latter new topic is shown.

1. INTRODUCTION

The AMHY (Alpine and Mediterranean Hydrology) group of FRIEND (Flow Regimes from International Experimental and Network Data) project covers a large range of topics, including frequency analysis of floods and low flow, investigation on Mediterranean storms, rainfall-runoff transformation, erosion and sediment transport and climate change (*Afouda et al.*, 1997; *Gustard and Cole*, 2002). Particularly for over a decade the international working groups involved in the analysis of intense rainfalls and floods have experienced common approaches to hydrological extreme frequency analysis, by applying various standard procedures to data base collected in different hydrological regions.

Until 2003 these working groups mainly coped with "Heavy rains" "Rare floods" topics separately, though often in a synergic way since the common objective of the characterization of the meteorological and hydrological sequences of events triggering flooding disasters. To this aim some specialized seminars about heavy rains and flash floods have been jointly organised within the activities of the IV (Rare Floods) and VI (Heavy Rains) topics, like it was during the annual meeting of AMHY-FRIEND group held on October 1998 at the Istanbul Technical University (Turkey) and on October 1999 at the University of Calabria (Cosenza, Italy). In these joint seminars, besides theoretical developments mainly related to the statistical analysis of rainfall and flood phenomena, several cases of flash floods produced by heavy rainfalls on different areas of Mediterranean countries (from small basins to very large drainage networks) have been analysed in detail, taking into account morphology, geology, land use and basin response to flood depending on antecedent moisture conditions (*Llasat et al.*, 1999).

1.1 Researches on "Heavy rains" topic

The main scientific activity of topic "Heavy rains", coordinated by M.C. Llasat (Spain), coped with the analysis of extreme rainfall events from meteorological, climatic and hydrological points of view. All countries involved in AMHY-FRIEND project participated actively to the researches, with Spain, France, Italy, Romania, Greece,

former Yugoslavia, Slovenia, Turkey and Moldavia among the most operative in rainfall researches. Particularly the Spanish GAMA group from University of Barcelona devoted great attention to the analysis of the meteorological and hydrological conditions triggering extreme rainfall events, in order to define features for classify different typologies of exceptional rainfalls. The exhaustive investigations allowed for assessments on the reliability of the most commonly used methodologies for the spatial characterization of convective storms. Results obtained through different approaches based on physical features of short time rainfall data taken from the meteorological radar, supported by rain gauges observations, provided a proposal of classification of precipitation structures in Mediterranean area (*Gustard and Cole*, 2002).

Good results came also from investigations focused on other specific questions about rainfall features, such as the analysis of anomalies in monthly rainfalls at large spatial scale, the possibility to obtain reliable regionalization of the different rainfall behaviours in Mediterranean countries, the optimal boundaries for obtaining practical results from these regional analyses, the relationships between physiographic and morphological features of basins and extreme rainfall data at different temporal aggregation for preliminary applications to ungauged basins.

Other scientific activities included simulations of rainfall hyetographs, intensity-duration-frequency analysis, performance analysis of the most common regional rainfall frequency distributions, rainfall forecasting, influence of relief on rainfall probabilistic distributions, climate evolution, stochastic analysis of non-periodic component of the annual and monthly rainfall process, implementation and enlargement of data bases of hydrological extreme events for European regions (*Afouda et al.*, 1997; *Gustard and Cole*, 2002).

1.2 Researches on "Rare floods" topic

Topic "Rare floods", coordinated by P. Versace (Italy), has been mainly directed at improving theoretical knowledge of flood phenomena and testing statistical procedures for flood frequency estimation. Most of the countries involved in AMHY-FRIEND contributed to the researches with very good analyses (France, Greece, Italy, former Yugoslavia, Spain, Turkey, Greece, Bulgaria, Albania, Romania and Slovenia).

Aiming at the practical mitigation of the inundation risk through a better estimation of flood with specified return period, attention has been focused on both at-site and regional estimation techniques of parameters of the most used probabilistic distributions.

As regards regional flood estimations, investigations based on the robustness and prediction capacity of some regional flood evaluation models commonly used in Europe (among the others the VAPI procedure in Italy, the AGREGEE model in France, the Modified Rational Method in Spain) were performed. These researches were validated in a crossed way on different national hydrological archives, thus encouraging improvement and synthesis of the various procedures. To this aim, some specific characteristics of the models have been successfully transferred from one method to another, thus pointing out the different features of flexibility and robustness of the regional models.

Meaningful improvements were obtained also in at-site flood evaluation procedures with important results obtained for flood quantile estimation, mainly for the interesting developments in data acquisition and analysis, concerning mainly the peaks over threshold sampling techniques, the use of historical information, new synthetic hydrograph computing methods (*Gustard and Cole*, 2002).

Another important research developed in "Rare flood" topic has been the exploitation of the links between flash floods and heavy rains, due to the increased frequency of floods caused by high intensities and short duration rainfalls. The interest in this issue is claimed by civil protection administrations for the shortage of time to activate any safeguard measures in the territories suffering from high risk of flash floods. These ongoing researches have tried to detect common meteorological and hydrological features responsible for the production of flash floods from the comprehensive rainfall-runoff analysis of some damaging event recently occurred in Mediterranean countries.

2. LATE SCIENTIFIC ACTIVITIES ON "EXTREME EVENTS" TOPIC

The "Extreme events" topic of AMHY-FRIEND group comes from the merging of the previous "Heavy rains" and "Rare floods" topics, discussed by the Steering Committee of AMHY-FRIEND project during the International Conference on Hydrology of the Mediterranean and semi-arid regions, held in Montpellier (France) on April 2003.

The scientific activities of the "Extreme events" topic, taking advantage of the skills of the various researchers previously interested in one of the topics described in section 1.1 and 1.2, mainly copes with comprehensive analyses of rainfall and flood events, also considering the physical links between phenomena as in the case of rainfall-runoff modelling.

In continuity with the past, attention is also given to comparative synoptic analyses of hydrological and meteorological data from simultaneous heavy rainfall events, which can produce floods in geographically distant regions with specific climatic features. The goal of the research is a better identification of the features triggering hydrological extremes and the comprehension of the rainfall-runoff dynamics of the different European climatic environments. Moreover several AMHY working groups involved in "Extreme events" topic have produced (or collaborated to) scientific reports concerning hydrological and meteorological analysis of the most damaging extreme events, in some cases also accounting for societal impacts and people perception of the events.

2.1 Development of rainfall analysis

Characterization of heavy rainfalls in Mediterranean area.
Exceptional storms recently occurred in the Mediterranean area have induced revision of the statistical distributions for rainfall estimation, particularly as regards the asymptotic tails over extreme values. To this aim, some regionalized approaches of heavy tailed probability distributions for estimation of rare daily rainfalls have been explored, for example through the statistical analysis of the coefficient of variation of the annual maximum daily rainfalls. The improved regional distributions have led to a significant increase in the estimation of rarer rainfall depths.

Other statistical analyses on heavy rainfalls events have been performed for FRIEND project in some regions of Europe (among the others: France, Portugal, Serbia and Italy), with results such as the frequency evaluation of rainfall events measured at large spatial scale, the intensity-duration-frequency curves for different return periods and basin area, the local estimations of probable maximum precipitation and empirical relationships for hourly and sub-hourly rainfalls.

Detection of trends, shifts and seasonality in precipitations.

Assessments on the possible existence of trends, shifts and seasonality in precipitations has been accomplished by means of the analyses of occurrence and magnitude of short duration rainfalls and, at a larger temporal scale, through trend analysis of cumulated monthly and annual precipitations. Principal aims of these ongoing researches, jointly performed by some working groups, are the comparison of the rainfall variability features in different regions and the detection of local relationships between short duration rainfalls and cumulated rainfalls at larger time scale.

The results have shown to depend on the time aggregation of the data and on the physical and climatic features of the examined area. In particular, evidence of significant decreasing trends in winter monthly rainfall values recorded in the most recent decades in southern Italy have been pointed out. On the contrary, anomalies and trend analyses of monthly rainfall series in Spain have shown no significant statistical results. As regards short duration rainfalls, in some AMHY countries exploratory analysis for trend detection based on statistical tests have exhibit no significant variation of rainfall frequency.

2.2 Development of flood analysis

Case studies of extreme floods.

In recent years, several serious floods due to heavy rainfalls hit Europe, thus suggesting the increase of frequency and magnitude of such extreme events. For the heaviest events, statistical analysis of ground-observed data and remote sensing data have been performed, thus characterizing causes and simulating effects of the phenomena (Spain, Romania, Bulgaria, France, Turkey, Italy).

Flood frequency analysis.

The return period of flood events recently occurred has been estimated by means of comprehensive regional approaches, taking into account the areal extension covered by precipitation heights greater than prefixed values. Regionalization approach to flood and rainfall frequency estimation confirms the hyper-exponential behaviour of extreme events, which can be interpreted by highly skewed probabilistic distributions. The ongoing research on the statistical features of the most important flood evaluation models has provided some practical improvements in flood quantile estimation procedures, due to the use of peaks over threshold sampling techniques and the enlarged data base due to historical information (Italy, France, Serbia, Spain, Turkey).

Spatial distribution of floods across Europe and climatic features.

Analysis of the spatial distribution of the most damaging floods occurred in some European countries has shown significant differences between countries due to the various climate features. Nevertheless, some common features for Spain, southern France and Italy have been identified: the inputs of southern warm air masses, increasing atmosphere humidity and producing intense rainstorms, which induce a high flash flood potential. On the contrary, in countries with more pronounced orography, like in central Europe, the relief has shown to constitute an important factor that overwhelms the differences in the climate features. In these regions, the most dangerous scenarios for flood risk is due to the presence of mountainous small basins with steep slopes, which if interested with heavy rainfalls can result in a flash flood potential comparable with that of the Mediterranean countries. The countries more directly influenced by the cold fronts

originating from the Atlantic Ocean also suffer from abundant and frequent though less intense rainfalls.

2.3 Analysis of the links between heavy rains and flash floods

The ongoing analysis of meteorological and/or hydrological links between flash floods and heavy rains copes with distributed modelling of rainfall-runoff transformation and atmospheric circulation pattern analysis.

Researches for FRIEND project on distributed event-based rainfall-runoff models in small experimental basins, based on both conceptual and physically-based schemes, generally have suggested that catchment runoff is mainly produced by saturation excess mechanism, while hortonian overland flow is associated only with high intensity rainfall. The validation of the models has been performed through general tests evaluating model ability in reproducing different runoff generation mechanisms, estimated spatial distribution of runoff production and model response plausibility for different hydrological situations.

Improvements of atmospheric and meteorological analysis aiming at predicting local intensity values and dynamics evolution of precipitations in Mediterranean countries has been performed through the application of special procedures, such as the classification of the most frequent circulation patterns which have shown to originate extreme events and the storm track analysis (Greece, Italy, Spain, France).

2.4 Arrangement of website with information on extreme events

The AMHY-FRIEND data base on extreme events has rapidly grown, since the high frequency of occurrence of floods caused by heavy rainfall intensities in the years 2002-06, which affected several countries of Europe causing enormous damages. Thus, aiming at contributing to a better knowledge of the risks arising from hydrological events, a new specific AMHY-FRIEND website for "Extreme events" topic is currently under construction (*www.camilab.unical.it/sito_amhy/home_page.htm*). The website contains information on working group activities, selected references to statistical procedures of extreme events analysis, appointments to meeting on hydrological extremes, links to focal points in hydrological extreme events topic and a database providing description and quantitative information on the most damaging rainfalls and floods recently happened in Mediterranean countries.

The database has been developed and successively implemented from various existing sources and personal contributions of AMHY working groups. For each events the database, though yet uncompleted, shows information at local spatial scale on features of extreme events, such as occurrence date, detailed localization, note and comments, affected region extensions, damages, casualties, main rainfall intensities and flood peaks, links to possible specific event reports or database with images and tables made available on the web.

2.5 Augmentation of data base and development of experimental basin network

Both the augmentation of the data base and the development of a network of experimental basins are special activities to encourage, since they can be very useful for statistical analysis of extreme events. As regards the augmentation of the available data, besides the more recent extreme events happened in Mediterranean countries, it has to be

noticed the acquisition of palaeoflood data from historical clues through reliable rating curves (by different European researches on peculiar French and Spanish rivers) and the increased availability of short aggregation time rainfall series and rating curves for water stage data provided by various national hydrographic services.

On the other side, the development of a network of experimental local basins with data taken from water levels and rainfall gauges can support investigation on rainfall-runoff transformation processes through better calibration of hydrological models. To this aim it is worthwhile to recall the possibility to synergize the efforts with some researchers of HELP project by sharing information and collaboration, both projects being interested to validate experimental basins for arranging unquestionable hydrological data base.

3. POSSIBLE DEVELOPMENTS OF THE TOPIC

The statistical analysis of the spatial distribution of hydrological extremes by means of application of procedures accounting for both observed data and physical characteristics of the basins is one of the possible developments of the topic "Extreme events", with the aim of improving estimation of hydrological extremes for ungauged sites. Moreover, further investigations on trend detection in time series of hydrological extremes, both for short duration rainfalls and monthly/annual cumulated rainfalls, could lead to more complete results on such a controversial issue. Both developments can take advantage of new data acquisition (palaeofloods and historical floods, shorter hourly rainfalls and rating curves for water stage levels from national hydrographical services) and more discerning statistical approach, such as the partial duration series analysis.

Combined analysis of meteorological and hydrological conditions triggering extreme events, which is one of the most peculiar issues of the topic, can be further developed with the growing availability of digital data on ground measurements, remote sensing, elevation model, land use maps and geophysical features of the area. This could lead to valuable results, such as a better identification of flood prone areas, due to the possibility to verify the inundated areas obtained from GIS processed images (supervised classification of cloud-free satellite images) through ground observations.

This can lead to a more reliable estimation of high quantiles from a combination of multiple data sources and regional approaches. Extreme event analyses based on these two kind of data (remote sensing and ground observations), though often focused on different spatial scales of investigation, have to be harmonized to delineate standard procedures and tentative arrangement of guidelines allowing for actual upgrading of used techniques and comparison of the results carried out in different environments.

Further directions in hydrological extreme investigations can cope with the temporal downscaling of hydrological extremes, the extension of analysis to the multivariate distributions, the spatial heterogeneity of regions, the updating of parameters estimation procedures in case of assessed trend, the identification of physical and/or meteorological characteristics of the catchments that cause similarity in flood response, the link between non-stationary models of hydrological extremes and meteorological variables, the incorporation of Bayesian methods into statistics of extremes to quantify uncertainty.

REFERENCES

Afouda, A., Gustard, A., Mkhandi, S., and G. Oberlin *(Scientific Eds.)* (1997), *FRIEND – Third report: 1994-1997*, Cemagref editions, Lyon (France).

AMHY-FRIEND (1998), Seminaire international annual du Groupe AMHY de FRIEND (1997-1998), Istanbul, Turkey, October 1998, UNESCO Technical Documents in Hydrology n°29.

Ferrari, E., *Frequency analysis of extreme floods*, International Workshop on Hydrological Extremes. Modelling and managing low flows, drougths and floods, Koblenz (Germany), July 5-8, 2004 (published on CD).

Gustard, A., and G.A. Cole *(Scientific Eds.)* (2002), *FRIEND – a global perspective 1998-2002*, CEH Wallingford (UK).

Llasat, M.C., Versace, P., and E. Ferrari *(Scientific Eds.)* (1999), *Heavy rains and flash floods*, Proceedings of the Joint Session of Topic IV (Rare Floods) and Topic VI (Heavy Rains) of FRIEND, UNESCO IHP-V 1.1 Project AMHY Group, Istanbul, October 1998, National Research Council, Group for Prevention from Hydro-Geological Disasters, Pub. 2049, Cosenza, Italy.

Servat, E. and J. Albergel *(Scientific Eds.)* (2002), *Hydrology of the Mediterranean Regions*, Proceedings of the International Seminar, Montpellier, France, 11-13 October 2000, UNESCO Technical Documents in Hydrology n°51.

Part 1
RECENT CASE STUDIES OF EXTREME HYDROLOGICAL EVENTS

Observing and modelling exceptional floods and rainfalls
Proceedings of the AMHY-FRIEND International Workshop on Hydrological Extremes,
held at University of Calabria, Cosenza (Italy), May 3-4, 2006

COMPARISON BETWEEN PROBABILISTIC AND DETERMINISTIC MODELS TO ANALYSE FLASH FLOOD EVENTS RECORDED IN CATALONIA, 2000-2005

V. Altava-Ortiz, A. Barrera, M.C. Llasat, and M.A. Prat

Group of Analysis of Adverse Meteorological Situations (GAMA), Department of Astronomy and Meteorology, University of Barcelona, Spain.

ABSTRACT

This contribution shows the results of applying two forecasting methods and their comparison in the study of five catastrophical events affecting Catalonia (NE Spain). These methods are the probabilistic Analogous method and the MM5 mesoscale deterministic model. They are applied to the following events: 9th-10th June 2000, 21st-23rd October 2000, 9th-11th April 2002, 8th-10th October 2002 and 6th-7th September 2004. In all of them, maximum accumulated precipitation recorded was up to 150 mm, flash floods occurred, and, as a result, 10 people died and damages exceeded 200 million euro. MM5 has been applied to carry out 48÷72h simulations, designed for three domains connected with two-way nesting, with 54, 18, 6 km horizontal grid resolution and 23 levels of vertical resolution. Full physics has been used and a Betts-Miller scheme is applied to parameterise convection in the first domain, Kain-Fritsch scheme in the second domain, whereas no convective parameterisation has been performed over the third domain. The Analogous method chosen to its application is based on the geopotential fields at 1000 hPa, 850 hPa and 500 hPa pressure levels. In order to consider the local features, two nested windows have been used in the Analogous method. The first one considers 30º-60º N latitude and 30ºW-30ºE longitude and the second one 37.5º-45º latitude and 5ºW-10ºE longitude, being centred over Catalonia. Results show a general underestimation of the maximum values for both methods. Nevertheless, results obtained as a whole show interesting results in the mark of the ensemble prediction procedure.

1. INTRODUCTION

Catalonia, located in the North-East region of the Iberian Peninsula, is affected periodically by extreme meteorological events. Its geography, with mountain ranges near the sea, and the Pyrenees in the north, provides this zone a very particular configuration (Figure 1). Its geographical location in the Mediterranean allows the interaction of sub-tropical and extra-tropical masses of air. In addition the mountains barrier position enhances the development of medium latitudes meteorological features.

The surface and even deep levels warm water in the Mediterranean favours the interchange of latent and sensible heat. As a consequence, its vertical thermodynamic profile often shows potential convective instability. That provides to the atmosphere state a great potentiality to become unstable when the synoptic situation is favourable, with great convective phenomena occurring enhanced by orographic effects (*Jansà*, 1997; *Llasat*, 2001; *Ceperuelo and Llasat*, 2004). This kind of events can usually be associated

with severe weather, which often causes a great amount of material damages and even lost of human lives (*Llasat et al.,* 2004).

Figure1. Catalonia location. Geophysical and hydrological subdivisions can be observed in the upper and bottom maps respectively.

A large number of meteorological studies have been carried out, aimed to analyse such kind of heavy rain events, going from the diagnosis to the forecasting, and using meteorological deterministic models or probabilistic ones (i.e. *Ramis et al.,* 1998*; Llasat et al.,* 2003*; Homar et al.,* 2002*; Mariani et al.,* 2005*; Barrera et al.,* 2005*; Rigo and Llasat,* 2005*; Romero et al.,* 2006*; Altava-Ortiz et al.,* 2006). Other studies paid special attention to the economical and social impact (*Llasat,* 2004*; Llasat et al.,* 2004*; Delitala,* 2005*; Brilly and Pollic,* 2005).

But how to consider an event as a catastrophic one when it happens is not as easy as it could seem. The magnitude and repercussion of a certain event can differ depending on the social impact, perception and so on. There are different classifications in order to subdivide heavy rainfall events depending on their intensity and duration, area affection, produced damages, etc. as well as other parameters like flow or social perception. *Llasat and Puigcerver* (1994) developed a list of objective requirements in order to consider an event as a catastrophic one:

- Accumulated rainfall exceeding 200 mm at least in one place.
- Accumulated rainfall over 100 mm in an area greater than 2000 km^2.
- Maximum rainfall in 24h exceeding 100 mm.
- One or more overflowed rivers.
- Important damages and casualties.

Taking into account this criterion, 5 cases have been finally selected: 9th-10th June 2000, 21st-23rd October 2000, 9th-11th April 2002, 16th-18th October 2002 and 11th-15th October 2005. The mesoscale MM5 model as well as the Analogous method has been applied in order to compare their capability to forecast or to reproduce the observed cumulated rainfall in cases of heavy rainfall events.

After the introduction of selected cases, the paper shows the data base and methodology for each method. A comparative analysis is made and conclusions are presented at the end.

2. MAIN SYNOPTIC FEATURES OF THE SELECTED EVENTS

Considering the five cases selected, it is possible to do an initial subdivision between events mainly with littoral affection and others with inland repercussions. Therefore, in the littoral group would be present the 21st-23rd October 2000, 16th-18th October 2002 and 11th-15th October 2005, and into the inland affection group would be the 9th-10th June 2000 and 9th -11th April 2002. Main affected areas are shown in Figure 2.
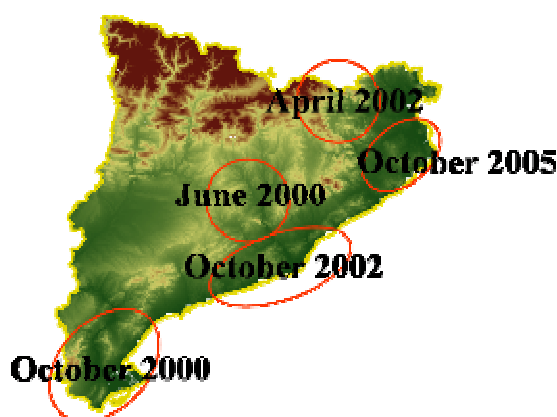
Figure 2. Main zones affected for each event.

In order to have a better understanding of each event, Figure 3 shows the main synoptic features of each one.

- *June 2000*
  The synoptic situation on 9th June was characterised by the entrance from the western part of the Iberian Peninsula of a cold front associated with a low situated to the north of the British Islands, while Catalonia itself was under the influence of an anticyclone that affected Central and Eastern Europe also. On 10 June a surface depression was forming over the Balearic Islands while a cold trough could be detected at upper atmospheric levels.
- *October 2000*
  The synoptic situation was characterised by the pass of an important trough moving from West to East of the Iberian Peninsula. Its intensification and strangulation produced the formation of a COL (Cut-Off-Low) above the Gulf of Cádiz. A low was formed over North Africa, as a consequence of the COL formation, producing an important wet, warm and potentially unstable air mass advection from the Mediterranean Sea towards the South of Catalonia. This situation remained during near three days, producing continuous and intense rainfalls over the prior mentioned regions.
- *April 2002*
  The presence of an extended anticyclone from the Scandinavian Peninsula to South Terranova produced the movement toward the Gulf of Cadis of a depression located around Madeira Islands. This configuration implied a southern wet and warm air mass over Catalonia. In the following days, this low was fed by an Eastern/North-eastern cold advection at upper levels, implying the pressure deepening.
- *October 2002*

On 8th October 12:00 UTC an intense trough associated to an Icelandic low crossed the Iberian Peninsula. Twelve hours after, the Icelandic cold low was divided in two lows and one of them moved to the NE of Spain, forming a COL remaining over it until 12:00 UTC of 10th October. That COL joined with a wet and warm Mediterranean flow produced high instability in Catalonia.

HGT 10th June 2000 00 UTC at 500 hPa

SLP 10th June 2000 00 UTC

HGT 23rd October 2000 00 UTC at 500 hPa

SLP 23rd October 2000 00 UTC

HGT 10th April 2002 00 UTC at 500 hPa

SLP 10th April 2002 00 UTC

HGT 10th October 2002 00 UTC at 500 hPa

SLP 10th October 2002 00 UTC

HGT 13th October 2005 00 UTC at 500 hPa

SLP 13th October 2005 00 UTC

Figure 3. Synoptic maps at 500 hPa and sea level pressure. One day for each event is presented.

- *October 2005*

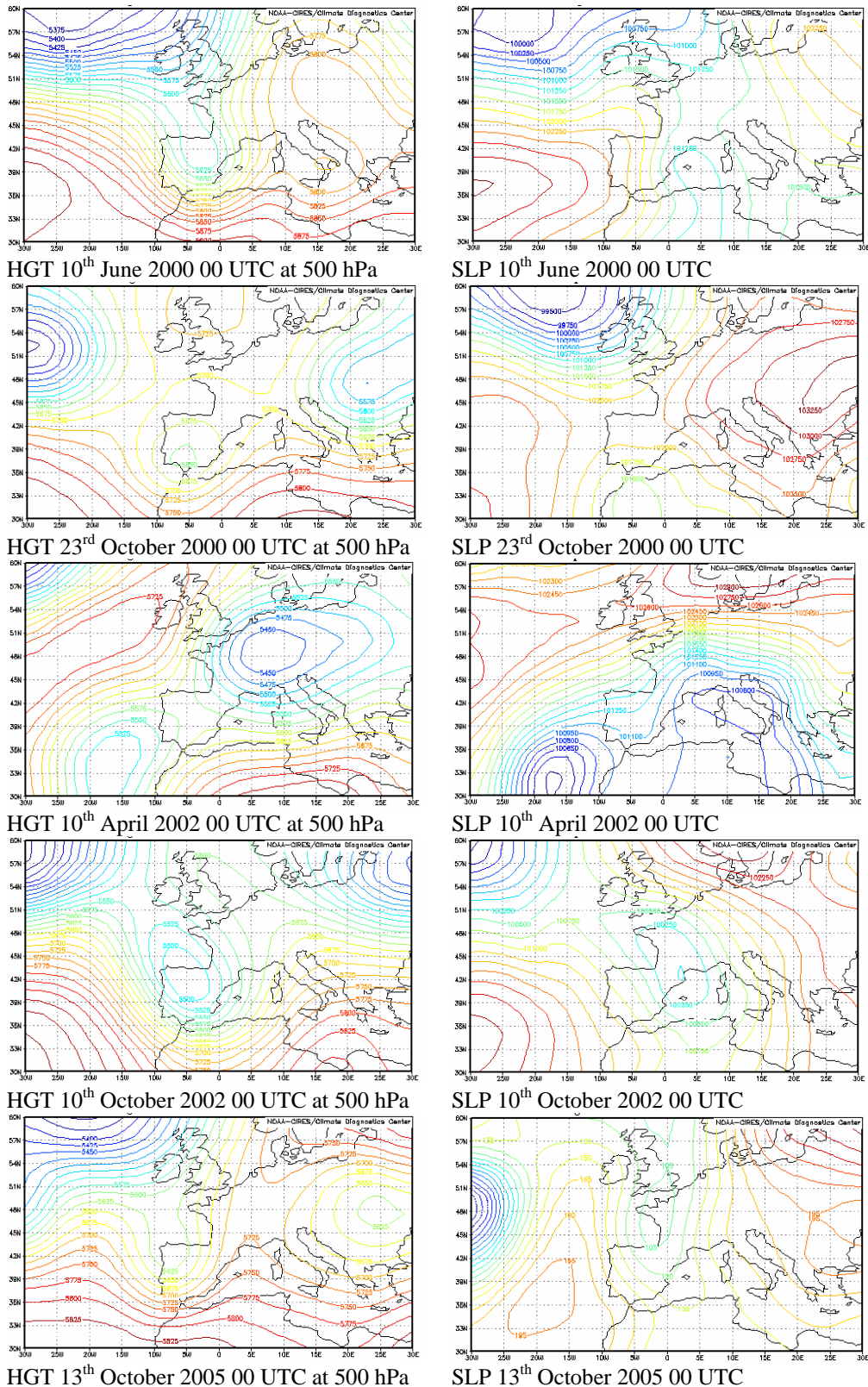 On 12th October a powerful anticyclone was located over Eastern Russia producing a high pressure blocking. At the same time, a trough was formed in front of the Portugal coast vertical. Due to the blocking made by the high pressure centre, this trough moved towards the South-East, until reached the centre of Iberian Peninsula, in the form of a very well-defined COL on 14th October.

3. DATABASE AND METHODOLOGY

First of all, a short introduction of the methods used at the present work is presented. That will provide a general overview of the different methodologies applied as well as the database used.

3.1 The MM5 model

The MM5 model is the fifth-generation NCAR / Penn State mesoscale model (*Grell et al., 1994; Dudhia et al., 2005*). It is the latest version in a series model that was developed from a mesoscale model used by Anthes at Penn State in the early 1970's, later documented by *Anthes and Warner* (1978). Since that time it has undergone many changes designed to broaden its applications. These include: a multiple-nest capability, non-hydrostatic dynamics, and a four-dimensional data assimilation capability (Newtonian nudging), increased number of physics options, and portability to a wider range of computer platforms, including OpenMP and MPI systems.

It is a limited-area, non-hydrostatic, terrain-following, sigma-coordinate model designed to simulate or predict mesoscale atmospheric circulation. The model is supported by several pre- and post-processing programs, which are referred to collectively as the MM5 modelling system. The MM5 modelling system software is mostly written in Fortran, and has been developed at Penn State and NCAR as a community mesoscale model with contributions from users worldwide. The MM5 modelling system software is freely provided and supported by the Mesoscale Prediction Group in the Mesoscale and Microscale Meteorology Division, NCAR (USA).

This numerical model has been run for a 48-72 h simulation period starting on the first day of each event at 00:00 UTC. Three domains connected with two way nesting and having 54, 18, 6 km horizontal grid resolution and 23 vertical levels have been used. The outer domain (domain 1) is centred in the NE Spain at geographical coordinate (39.0ºN, 0.0ºE). Initial and boundary conditions are obtained from the 2.5º resolution NCEP analyses available at 00:00 and 12:00 UTC, which are improved using surface and upper-air observations (ADP, Automated Data Processing observations from the NCEP). Full physics is used and a Betts-Miller scheme (*Betts and Miller,* 1993) is applied to parameterise convection for the first domain, Kain-Fritsch scheme (*Kain and Fritsch,* 1993) for the second domain, whereas no convective parameterisation is present over the third domain (Table 1). The convective parameterisation of the third domain is not critical in the study case. Instead of being characterised by a convective pattern, most of the rainfall quantities were recorded in the context of a warm-wet wind advection, triggered by orography. These parameterisations and resolutions have been used with reasonable results in other similar extreme meteorological events in the West Mediterranean area, as for example the cases of November 2001 (*Arreola et al.,* 2003),

June 2000 (*Mariani et al.,* 2005*; Romero et al.,* 2005), September 2002 and November 2002 (*Romero et al.,* 2005), October 2003 (*Altava-Ortiz et al.,* 2006)

Parameterisation	D1 (54 km)	D2 (18 km)	D3 (6 km)
Moisture scheme	Reisner 2	Reisner 2	Reisner 2
Cumulus scheme	Betts-Miller	Kain-Fritsch	None
Boundary layer	MRF	MRF	MRF
Atmospheric radiation	Cloud	Cloud	Cloud
Soil model	5-layer	5-layer	5-layer

Table 1. Scheme of the parameterisation and domains used in the MM5 simulations.

3.2 The Analogous method

As explained before, the Analogous method takes into account the weather observed in the past associated to certain meteorological variables in surface. When a meteorological situation is forecasted, several past situations are selected by means of the application of some similarity criteria. Since "Two atmospheric states are deemed 'analogous' when there is certain resemblance between them" (*Lorentz,* 1969), it is reasonable expecting similar behaviours on surface for two situations when the weather conditions are analogues.

Different criteria and variables can be selected in order to consider two states as analogous. At the present work, two criteria have been selected. The first one is a "criterion of proximity" in a space of *n* dimensions (*n* is related with the number of freedom degrees). The second one is a "criterion of correlation" between variables that characterise an atmospheric state. Only the states that have parameters higher than a prefixed threshold are selected as analogous. After doing the selection, the model outputs are calculated using the meteorological observations associated with the corresponding selected situations.

The "criterion of proximity" takes into account geopotential values at 1000 and 850 hPa levels, which provide a good description of the meteorological state of the atmosphere.

Two domains are involved: Domain 1, which is named the First Selection Window (FSW) and is delimited from 60ºN to 30ºN and from 30ºW to 30ºE. It has a 2.5º grid resolution. This first domain is useful to look for an analogous situation from a synoptic point of view. Due to the fact that heavy rainfall in Catalonia is usually produced by mesoscale processes it would be need to select those days that would have a similar meteorological situation around Catalonia. To get this purpose, a Domain 2 has been made. This domain is the Second Selection Window (SSW) and is centred in Catalonia. It is delimited from 37.5ºN to 45ºN and from 5ºW to 10ºE (Figure 4).

The FSW is an extend area and represents a considerate number of points where data are available. This fact is an advantage in the atmosphere description, but on the other hand, it holds a trouble due to the great number of freedom degrees, falling down the process. To decrease the number of freedom degrees, but trying to maintain a good system description, an EOF process has been performed. The first six Principal Components (PC) keep near 84% of system variance, which is accepted as a reasonable level. Taking each PC as independent from the others, the space which represents the considered meteorological state has six dimensions.
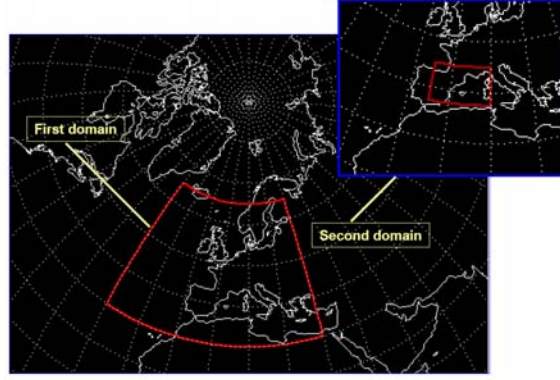
Figure. 4. Different domains used in the Analogous technique.

Therefore the considered analogous situations are those that lie in the interior of a six-ball of radius d in a 6-dimensional space. The radius is taken as a function of the distance, d, to the origin of the test day, t, as a follows:

$$\sum_{j=1}^{6}\left(Z_{ij}^{1000} - Z_{tj}^{1000}\right)^2 < d^2 \tag{1}$$

where Z_{ij} is the value of the variable Z_j on the day i, and Z_{tj} is the variable value on the forecasted day (test day). To calculate the distance " d " the procedure is as follows. Let D be the distance to the origin of the test day, so that:

$$D^2 = \sum_{i=1}^{6}(Z_i^{1000})^2 \tag{2}$$

The variable D^2 follows a χ^2 distribution law with N degrees of freedom, since Z_1, Z_2, Z_N are considered independent and identically distributed. For a law of χ^2 with *n* degrees of freedom, the function of density is given by the expression:

$$f(x) = \frac{x^{(n/2)-1} e^{-x/2}}{2^{n/2} \Gamma(\frac{n}{2})}, \quad \text{with} \quad \Gamma(n) = (n-1)! \tag{3}$$

As the first six PC have been retained, the density function takes the next form:

$$f(x) = \frac{x^2 e^{-x/2}}{16} \tag{4}$$

that corresponds to a Gamma function with parameters ($\lambda=3$ and $\rho=2$). Any quartile of this function of density has a typical deviation σ_D proportional to the size of the sample, m, that is, to the number of analogous situations for each test day. If 30 analogous days are considered then:

$$\sigma_D = \frac{1}{f(x)}\sqrt{\frac{p(1-p)}{m}} = \frac{1}{f(x)}\sqrt{\frac{p(1-p)}{30}} \tag{5}$$

in which, p is the probability calculated by interpolation based on a table of the Gamma distribution with six degrees of freedom.

For a number of variables between six and eight, *Duband* (1981) proposes the following expression:

$$d^2 = \omega^2 \sigma_D^2 \implies d = \omega\sqrt{\frac{1}{f(x)}\sqrt{\frac{p(1-p)}{30}}} \tag{6}$$

in which ω is a parameter that should be increased/decreased if the number of analogous situations are lower than 10 or more than 50.

17

The "criterion of correlation" is applied to select those days that have high correlation coefficient with the test day. The correlation coefficient used is the linear Pearson's one and the values to calculate the correlation coefficient are 13 PC: 6 from 1000 hPa, 6 from 850 hPa, and another one at 500 hPa pressure levels. These fields have been selected after testing different levels and taking into account the main factors responsible of flood generation in Catalonia (*Gibergans-Báguena et al.,* 1997*; Gibergans-Báguena,* 2001).

The vectors containing the values are:

$$\left(Z_{i1}^{1000}, Z_{i2}^{1000}, \ldots, Z_{i6}^{1000}, Z_{i1}^{850}, Z_{i2}^{850}, \ldots, Z_{i6}^{850}\ Z_{i1}^{500}, Z_{i2}^{500}, \ldots, Z_{i6}^{500} \right) \text{ for each day i}$$

$$\left(Z_{t1}^{1000}, Z_{t2}^{1000}, \ldots, Z_{t6}^{1000}, Z_{t1}^{850}, Z_{t2}^{850}, \ldots, Z_{t6}^{850}\ Z_{t1}^{500}, Z_{t2}^{500}, \ldots, Z_{t6}^{500} \right) \text{ for the test day.}$$

Candidate days that satisfied the next conditions (*Duband*, 1981) are selected as analogous ones:

$$u^2 = \frac{d^2}{r^2} < 6 \quad \text{and} \quad r^2 > 0.25 \tag{7}$$

It is needed paying attention to those days that have r < 0 (antithesis analogous day). They must be refused previously. The first step in the analogous selection is the application of the explained criteria above the FSW and a certain number of analogous days are selected. Afterwards, a second "criterion of correlation" is applied over the first step outputs, using the SSW. Days best correlated are considered the most similar to the test day. To avoid the possibility of ignoring a similar day in the FSW but with low correlation and high d, the thresholds used in Equation (7) can be relaxed in order to pick up more days.

4. RESULTS

The deterministic MM5 model, as well as the probabilistic one, the Analogous method, provides rainfall outputs in 24 hours and in its own grid resolution. Therefore a different kind of maps for each episode is obtained. Besides this, the MM5 provides an unique output with the total rainfall recorded in a certain time period (in this case, we have selected 24 hours) while the analogous method provides different probabilistic output. Table 2 shows the different probabilistic outputs supplied by the probabilistic method.

ERP(0.5)	Expected Rainfall Probability >0.5 mm/day
ERP(2)	Expected Rainfall Probability >2mm/day
ERP(10)	Expected Rainfall Probability >10 mm/day
ERP(20)	Expected Rainfall Probability >20 mm/day
ERP(50)	Expected Rainfall Probability >50 mm/day
MER	Maximum Expected Rainfall/day
AER	Average Expected Rainfall

Table 2. Probability thresholds and outputs obtained by the Analogous technique.

Among all possible combinations between parameterizations and domains, which can be applied in the MM5 model, we have used the physics contained in Table 1. This scheme is not so far from the scheme applied to do daily forecasting, but on the other hand it has been modified following the suggestions from different previous studies regarding extreme events. It would be possible improving results by testing specific

parameterizations and spatial resolution for each case, but the main idea has been to apply the same parameterization to all the cases and selecting the one that usually works better in all of them.

All maps showed have been obtained using the model reanalysis at 00UTC, with a temporal step of 24 hours. This means the rainfall probability and maximum expected rainfall which are shown in the respective maps, are valid from 00UTC of the considered day to 24 hours later. We have to note this fact, since different temporal steps could yield several probability/rainfall patterns.

Four maps have been selected to illustrate and comparing each case: two corresponding to the Analogous method output (a) and (b), another from the MM5 model (c), and the last one describing the real pattern and amount of rainfall recorded in Catalonia (d).

(a)   (b)

(c)   (d)

Figure 5. Model outputs for 10th June 2000; (a) Probability of exceeding 50 mm, (b) Maximum expected rainfall, (c) MM5 cumulated precipitation forecast, (d) Observed rainfall field.

On 10th June 2000 the maximum quantity of rainfall was recorded in the central part of the region (Figure 5d), with values above 200 mm. MM5 output place the maximum rainfall (more than 100 mm) in some central regions as well as in the north coast (Figure 5c). Although the maximum expected rainfall by the Analogous method gives the maximum in the south coast (Figure 5b), the probability of exceeding 50 mm identifies well the second maximum (Figure 5a). However in all cases there is an underestimation of the maximum rainfall.

On 22nd October 2000, rainfall quantities up to 150 mm were registered. Looking the deterministic MM5 output, values around 60 mm are expected in the same zone as the observed maximum, although this value is clearly under the actual one. Using the output maps of the Analogous method, probabilities of recording more than 50mm in 24 hours are mainly present in pre-littoral zones. The maximum expected rainfall on the contrary, despite of being like the real one, is located in the north.
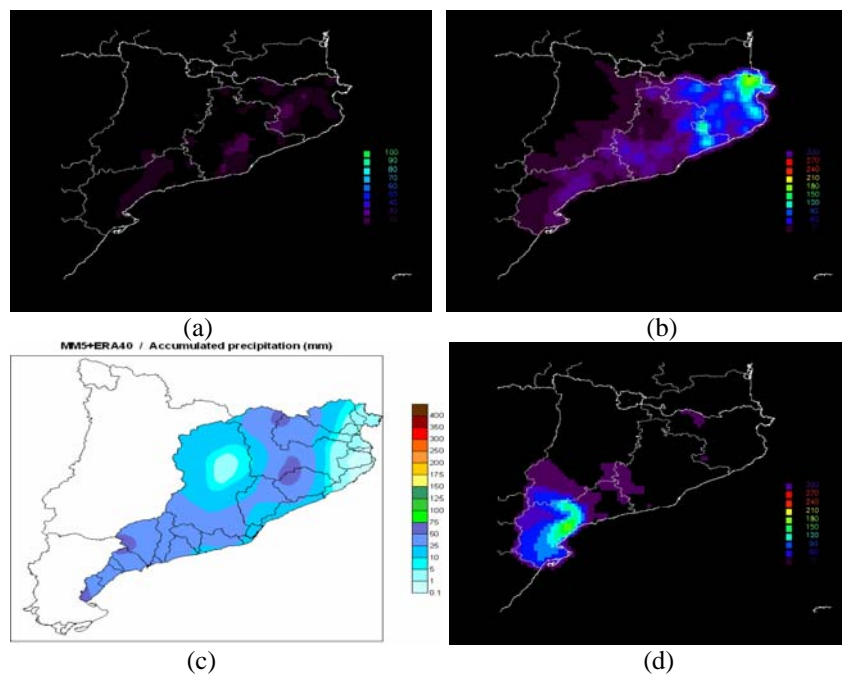
Figure 6. Model outputs for 22nd October 2000; (a) Probability of exceeding 50 mm, (b) Maximum expected rainfall, (c) MM5 cumulated rainfall forecast, (d) Observed rainfall field.
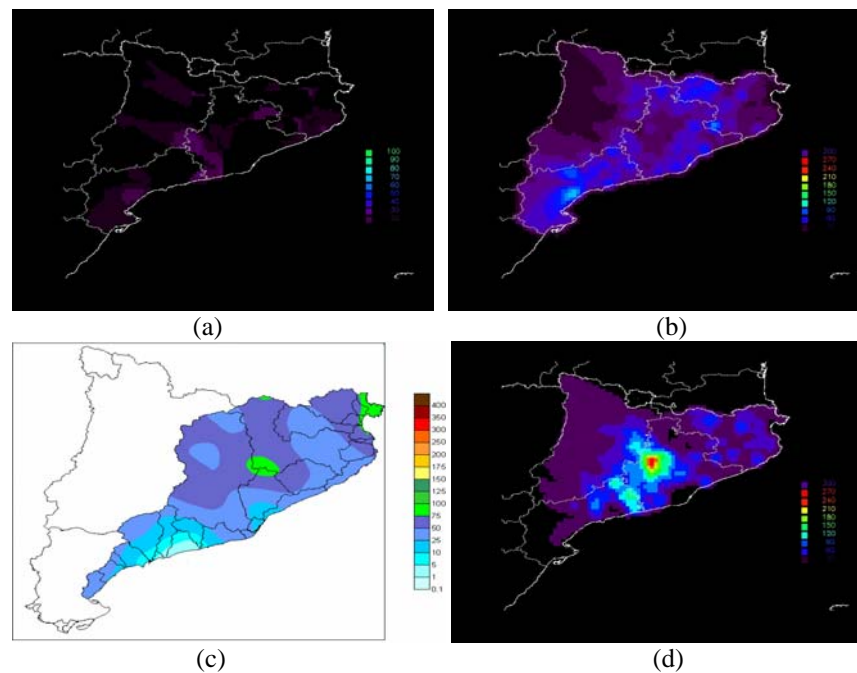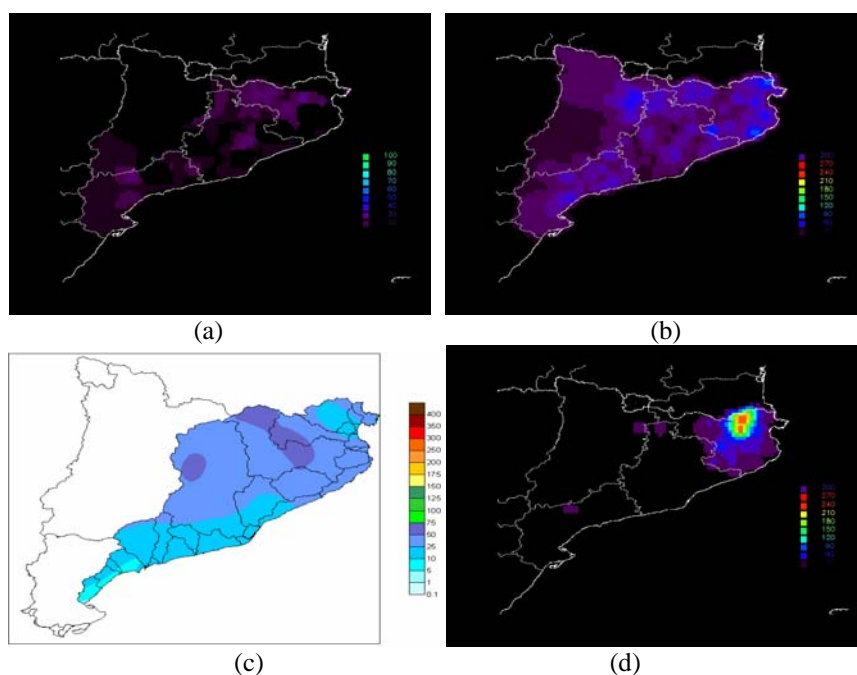

Figure 7. Model outputs for 11th April 2002; (a) Probability of exceeding 50 mm, (b) Maximum expected rainfall, (c) MM5 accumulated precipitation forecast, (d) Observed rainfall field.

On 11th April, values of 250 mm were recorded in the North region of Catalonia. The probability map of more than 50 mm/day, as well as the MER, gives values of 20% and 100 mm near the affected area respectively, although not in the same location. The MM5 model also suggests that maximum values will be in the north, but the in the range of 50÷75 mm.
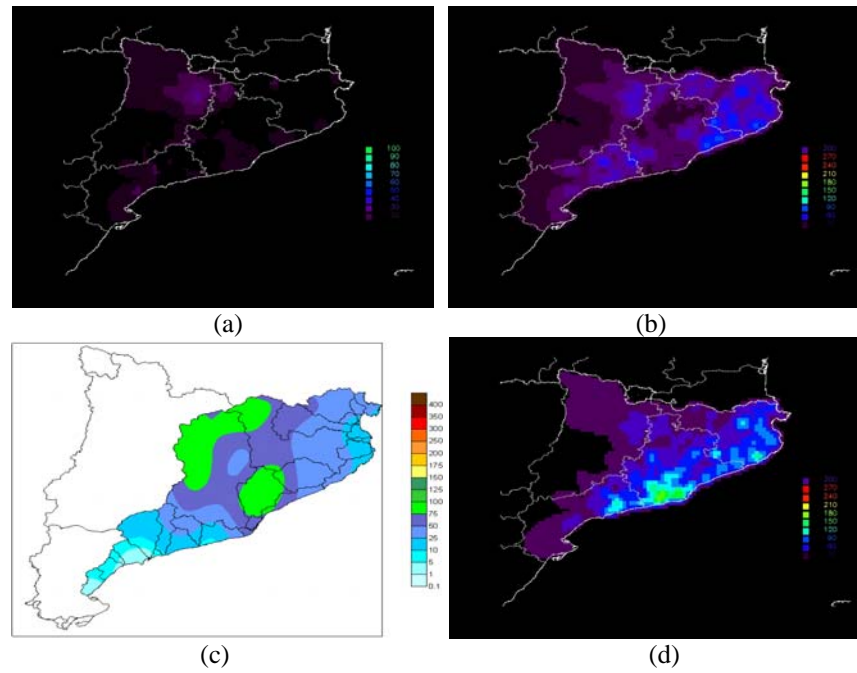
Figure 8. Model outputs for 9th October 2002; (a) Probability of exceeding 50 mm, (b) Maximum expected rainfall, (c) MM5 accumulated precipitation forecast, (d) Observed rainfall field.
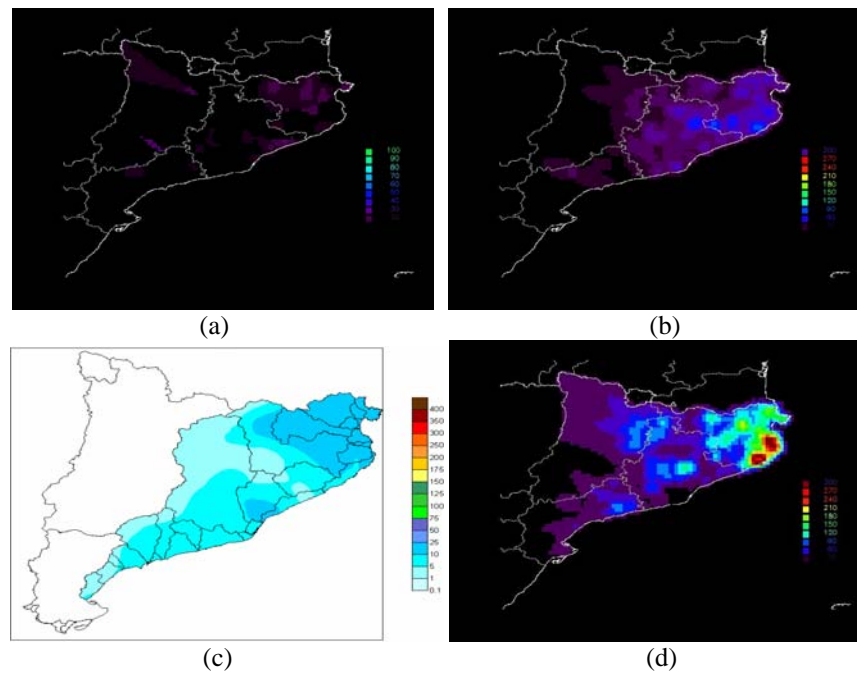
Figure 9. Model outputs for 13th October 2005; (a) Probability of exceeding 50 mm, (b) Maximum expected rainfall, (c) MM5 accumulated precipitation forecast, (d) Observed rainfall field.

On 9th October 2002, maximum values were recorded in the central Catalan coast where near 200 mm were accumulated. According to the MM5, values around 100 mm are expected close to the affected area. On the other side, the Analogous method suggests values of MER near 80 mm all around the central coast.

In this case, the analogous method provides quite good results in the event location, although maxima are below the observed rainfall. The MM5 rainfall pattern is similar to the observed one, but underestimated. Table 3 summarizes previous results.

Event	Analogous method		Deterministic method (MM5)	
	Location of maxima	Quantity of maxima	Location of maxima	Quantity of maxima
9-10 /VI/2000	NO	NO	YES	NO
21-23 /X/2000	NO	YES	YES	NO
9-11 /IV/2002	NO	NO	YES	NO
6-18 /X /2002	YES	NO	YES	NO
11-15 /X/2005	YES	NO	YES	NO

Table 3. Summary of the qualitative degree of skill in the rainfall forecasting.

5. CONCLUSIONS

In the present work a probabilistic and a deterministic model rainfall outputs have been compared for five heavy rainfall events that have affected Catalonia.

In general, all cases are underestimated by both techniques but the maximum rainfall location is quite well simulated, especially by the deterministic model.

However, the littoral events are better performed. That is more clearly seen in the case of the Analogous method. These kinds of events are the most common affecting Catalonia, and this fact enhances the capability of the probabilistic model to represent such cases.

When a more detailed study about these cases is carried out, mesoscalar processes are revealed to have an important role in main meteorological features development and generation. This fact is not correctly catch by the Analogous method.

On the other side, since the Analogous method has probabilistic outputs of exceeding a certain threshold, and the events analysed here were extremes, it is not easy to obtain a probability greater than 10-20% for the 50 mm/day rainfall threshold. This is an expectable result given that this quantity is not often reached.

In order to improve the Analogous method, future work contemplates to extend the period of the rainfall database. It theoretically will allow us to have more and more information about extreme events that took place in the past. This is an ambitious goal due to the difficulty of having extended daily precipitation records for a complete region. In addition, using different local criteria to select the cases considered as analogous could get better results.

Concerning the MM5 we hope to get more knowledge about processes generating extreme events in the Mediterranean, so that it would provide better parameterise for the physical relation between variables. The assimilation of real data, which nowadays is already in use, is also expected to improve the model outputs.

Therefore, studying extreme meteorological cases in different ways allows us to get better information about what happened. This kind of studies is included in what has been named as Ensemble Prediction Methods. This technique has been revealed as one of the most powerful to forecast rainfall events.

REFERENCES

Altava-Ortiz, A., A. Barrera, M.C. Llasat, M.A. Prat, J. Gibergans-Bàguena, and M. Barnolas (2006), Application of the MM5 and the analogous method to heavy rainfall event, the case of 16-18 October 2003 in Catalonia (NE Spain), *Adv. Geosciences*, *7,* 313–319.

Anthes, R.A., and T.T. Warner (1978), Development of hydrodynamic models suitable for air pollution and other mesometeorological studies, *Monthly Weather Review*, *106*, 1045-1078.

Arreola, J. L., V. Homar, R. Romero, C. Ramis, and S. Alonso (2003), Multiscale numerical study of the 10–12 November 2001 strong cyclogenesis event in the western Mediterranean, *Proc. of the 4th EGS Plinius Conference on Mediterranean Storms*, Alcudia (Spain), CD-Rom, sec. 1, num. 30.

Barrera, A., M.A. Prat, and M.C. Llasat (2005), Utilización del modelo MM5 para el estudio del episodio de fuertes lluvias y viento de octubre de 2003 en la zona del Empordà (NE Catalunya), *Revista del Aficionado a la Meteorología*, 36.

Betts, A. K., and J. Miller (1986), A new convective adjustment scheme. Part II: Single column tests using GATE wave, BOMEX, ATEX and Arctic air-mass data sets, *Q. J. R. Meteor. Soc.*, *112,* 693–709.

Brilly, M., and M. Polic (2005), Public perception of flood risks, flood forecasting and mitigation. *Nat. Hazard Earth Sys.*, *5,* 345-355.

Ceperuelo, M. and M.C. Llasat (2004), La Precipitación Convectiva en las Cuencas Internas de Catalunya, *Revista del Aficionado a la Meteorología*, 23 (available in http://www.meteored.com/ram/numero23/indice.asp).

Delitala, A.M.S (2005), Perception of intense precipitation events by public opinion, *Nat. Hazard Earth Sys.*, *5,* 499–503.

Duband, D. (1981), Prévision spatiale des hauteurs de précipitations journalières, *La Houille Blanche*, 7/8.

Dudhia, J., D. Gill, K. Manning, W. Wang, C. Bruyere, S. Kelly, and K. Lackey (2005), PSU/NCAR Mesoscale modeling system, *Tutorial Class Notes and User's Guide: MM5 Modeling System Version 3* (available in http://www.mmm.ucar.edu/mm5/documents/tutorial-v3-notes.html).

Gibergans-Báguena, J., M. C. Llasat, and J. Y. Rodríguez (1997), Daily rainfall identification by using an analogous method over local thermodynamic data, *Ann. Geophys.*, European Geophysical Society, C237.

Gibergans-Báguena, J. (2001), *Métodos hidrometeorológicos aplicados a la predicción de precipitación diaria en Catalunya*, University of Barcelona, Doctoral Thesis, Internal Publication.

Grell, G. A., J. Dudhia, and D. R. Stauffer (1994), A description of the fifth-generation Penn State/NCAR mesoscale model (MM5), *NCAR Technical Note*, NCAR/TN-398+STR.

Homar, V., R. Romero, C. Ramis, and S. Alonso (2002), Numerical study of the October 2000 torrential precipitation event over eastern Spain: Analysis of the synoptic-scale stationarity. *Ann. Geophys., 20*, 2047-2066.

Jansà, A. (1997), A General View about Mediterranean Meteorology: Cyclones and Hazardous Weather, *Proc. of the INM/WMO International Symposium on Cyclones and Hazardous*

Weather in the Mediterranean, Instituto Nacional de Meteorología and Universitat de les Illes Balears, Palma de Mallorca (Spain), 33-42.

Kain, J. S., and J. M. Fritsch (1993), Convective parameterization for mesoscale models: The Kain-Fritsch scheme, in: The representation of cumulus convection in numerical models, edited by: Emanuel, K. A. and Raymond, D. J., *Meteorological Monograph of the American Meteororological Society*, *46,* 165–170, 1993.

Llasat, M.C., and M. Puigcerver (1994), Meteorological factors associated with floods in the north-eastern part of the Iberian peninsula, *Nat. Hazards*, *9*, 81-93.

Llasat, M.C. (2001), An objective classification of rainfall events on the basis of their convective features: Application to rainfall intensity in the Northeast of Spain, *Int. J. Climatol.*, *21*, 1385-1400.

Llasat, M.C., T. Rigo and M. Barriendos (2003), The 'Montserrat-2000' flash-flood event: a comparison with the floods in the North-eastern Iberian Peninsula since the 14th century, *Int. J. Climatol.*, *23,* 453-469.

Llasat, M.C., M. Barnolas, M. Ceperuelo, M. Llasat, and M.A. Prat (2004), Algunos Aspectos Del Impacto Social De Las Inundaciones En Cataluña, *Revista del Aficionado a la Meteorología*, 20.

Llasat, M.C. (2004), La Vulnérabilité En Catalogne Et La Perception Sociale, *La Houille Blanche*, *6,* 71-75, (Ed. SHF), París (France).

Lorentz, E. N.(1969), Atmospheric predictability revealed by naturally occurring analogues, *J. Atmos. Sciences*, *26,* 636–646.

Mariani, S., M. Casaioli, C. Accadia, M. C. Llasat, F. Pasi, S. Davolio, M. Elementi, G. Ficca, and R. Romero (2005), A limited area model intercomparison on the "Montserrat-2000" flash-flood event using statistical and deterministic methods, *Nat. Hazard Earth Sys.*, *5*, 561-581.

Ramis, C., R. Romero, V. Homar, S. Alonso, and M. Alarcón (1998), Diagnosis and numerical simulation of a torrential precipitation event in Catalonia (Spain), *Meteorol. Atmos. Phys., 69,* 1-21.

Rigo, T., and M.C. Llasat (2005), Radar analysis of the life cycle of Mesoscale Convective Systems during the 10 June event, *Nat. Hazard Earth Sys., 5,* 1-12.

Romero, R., A. Martín, V. Homar, S. Alonso, and C. Ramis (2005), Predictability of prototype flash flood events in the western Mediterranean under uncertainties of the precursor upper-level disturbance, *Adv. Geosciences*, *7*, 55-63.

EXCEPTIONAL FLOOD OF SEPTEMBER 2002 IN ERZENI RIVER, ALBANIA

A. Selenica[1], M. Bogdani[2]

(1) Polytechnic University of Tirana, Albania.
(2) Institute of Hydrometeorology, Tirana, Albania.

ABSTRACT

The watershed of the Erzeni River is located in the central part of Albania. It has a surface of 663 km². The station Erzeni at Ndroq is equipped with an automatic hydrological station of type PM 346, installed in the framework of MED-HYCOS Programme. The climate of the watershed is a typical Mediterranean characterized by heavy rainfalls during the winter period. The annual average precipitation is 1400 mm and the maximum observed 24-hour rainfall is 153.5 mm. The last maximum peak discharge in this station was observed on 16/11/1962 and has a value of 794 m³/s. During the period 23ʳᵈ–25ᵗʰ September 2002, very high floods were observed in the majority of the Albanian rivers. An exceptional flood was observed in Erzeni River on 23ʳᵈ September 2002. During this flood the peak river stage was 21 cm above the highest historical river stage and the computed peak discharge has a value of 960 m³/s, having a discharge of 1.45 m³/s per km². Based on the hydrological data collected in this station and other information, the main characteristics of this flood, as the synoptic situation, the rainfall intensities, the river stages and flood hydrograph etc. are presented. An attempt is made to detect the flood trend in this river.

1. MAIN CHARACTERISTICS OF WATERSHED

The hydrographic basins of the rivers of Albania have a total area of 43,305 km², but only 28,748 km² are situated within the state territory of Albania. The remaining area, which mainly belongs to the catchments of the Rivers Drini and Vjosa, is situated in Greece, FYR of Macedonia Serbia, Montenegro and ONMI of Kosova. Albania is crossed by several rivers, in a general East-West direction: Drini, Mati, Ishmi, Erzeni, Shkumbini, Semani, Vjosa are the most important ones. The watershed of the Erzeni River is located in the central part of Albania. It has a surface of 663 km² and a mean altitude of 435 m; more than 50% of the watershed surface is situated above the altitude 700 m (Figure 1).

The watershed has characterized by a typical Mediterranean climate, with heavy rainfalls during the winter period. The annual average precipitation is 1400 mm and the maximum observed 24-hour rainfall is 153.5 mm. The last maximum peak discharge in this station was observed on 16/11/1962 and has a value of 794 m³/s.

The station Erzeni at Ndroq is equipped with an automatic hydrological station of type PM 346, installed in the framework of MED-HYCOS Programme.

2. SYNOPTIC SITUATION

The September 2002 was characterized by unstable weather with precipitations that covered all the territory. During this period, an unstable system of humid air mass, related to a cyclone structure placed on Genoa's gulf, and another one placed in the north of the Adriatic Sea, passed into Albanian territory. The Figure 2 shows the low–pressure centre developed in the northern part of the Adriatic Sea.
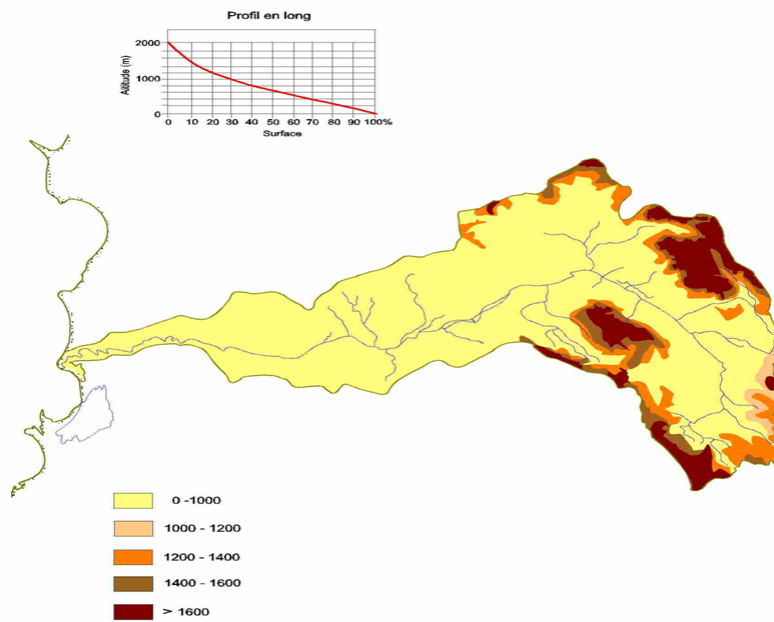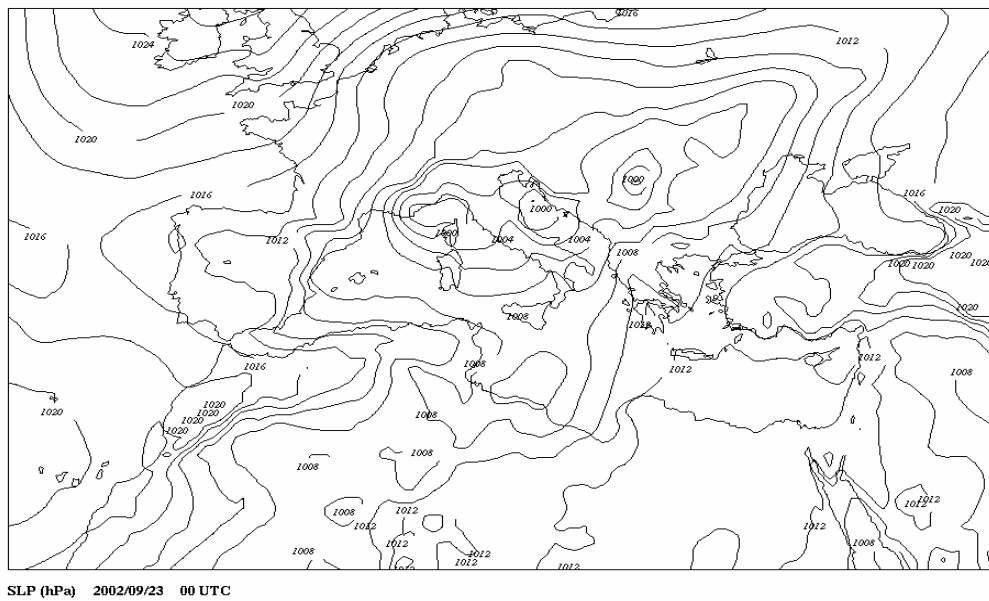

Figure 1. Watershed of Erzeni River.

Figure 2. Surface pressure of 23rd September 2002 at 00 UTC, from ECMWF–model analyses.
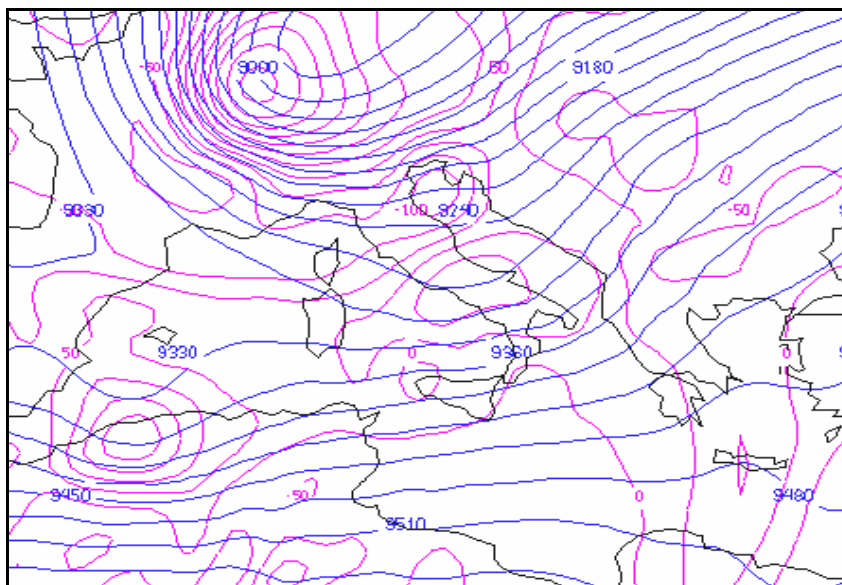
26

Figure 3. Geopotential and advection of vorticity at 300 hPa.

From Figure 3 it can be seen that there was not a real low–pressure centre over the Albanian territory, but the presence of a depression centre over the Genoa's gulf and another one located over the northern Adriatic Sea have had an important role in the creation of favourable conditions for high rainfall intensities.

We tried to analyze this situation in relation to Alpine cyclogenesis but, as we'll see later on, there is not a clear relation between them. The L–centre developed at low and medium levels while at high levels something was present just during the first hours of 23rd September (at 00 UTC, see the following picture) over the interested area. The convergence of the flow at low levels (before the 18:00 UTC and until the next day at 00 UTC) coincided to the divergence in high levels. There is no clear relation between the high and low level developments (in this time interval).

The convergence at low levels was forced by the low–pressure centre placed on Genoa's gulf, as well as by the other L-centre placed at north of Adriatic Sea and by a shallow cyclone centre placed in Southern Italy (it is seen only by MM5 Model). In the same time a warm moist air coming from the south had an important role in latent heat flux from the warm sea in this area. Thus, during the early hours of 22nd September, the low centre placed in the north of Adriatic Sea (at 00 UTC) reached a value of 1008 hPa, and the western wind speed achieved over 15 m/s, accompanied by a small jet stream placed in the Adriatic Sea, between Southern Italy and the western coast of Albania.

This low–centre developed continuously, extended all over the northern Adriatic Sea and decreased until 998 hPa at 18 UTC. At the same time, a small shallow cyclone with a pressure value of 998 hPa appeared in Southern Italy (it is seen by the MM5 model) and the wind became southern, with a speed of more than 15 m/s. This shallow centre developed quickly towards the east coast of Adriatic (over the north-western coast of Albania) and within 2 hours decreased from 998 hPa until 993 hPa.

A cold front accompanied this depression. Furthermore the speed of the southern wind achieved over 15 m/s, bringing a warm moist air. The earth temperatures were relatively normal, while in this period of the year the sea temperatures are high enough (the sea is still on its warm period, with a temperature approximately of 24.0 °C). All these

conditions were in favour of high rainfall intensities observed from 18:00 UTC until 06:00 UTC of 23rd September.
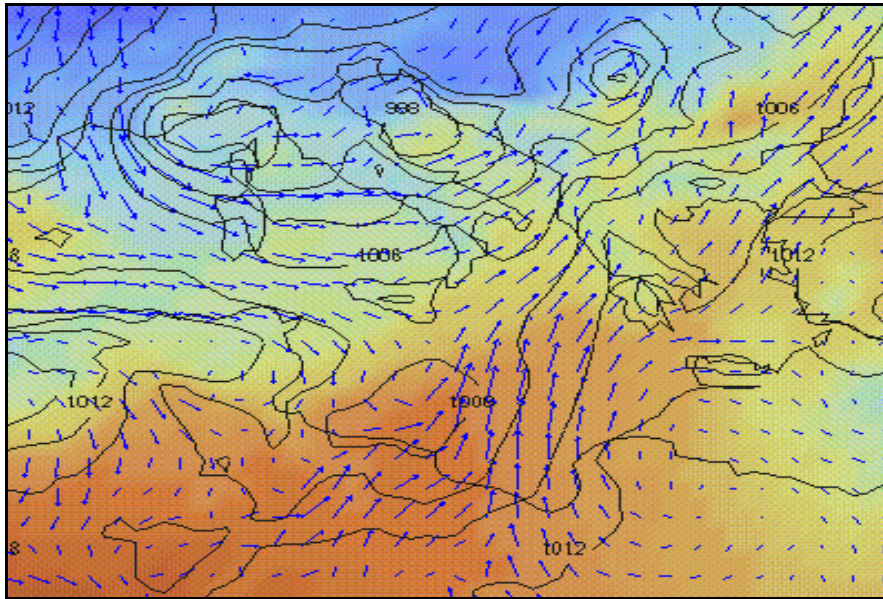
Figure 4. Surface pressure and the wind direction of 23rd September at 00 UTC (from the ECMWF–Model analysis by VIS5D Program).

3. RAINFALL INTENSITIES

The climate of Albania, in general, is Mediterranean with some degree of continentality in the mountainous regions of the country. The country combines a coastal plain in the West, with fairly high mountains: the highest point reaches 2751 m, while some ridges exceed 2000 m. The rain comes mainly with south-west winds and falls according to the obstacles encountered. This gives a variety of climates and rainfall patterns in the different regions of the country.

Thus, the average annual rainfall is around 1485 mm. The seasonal pattern is generally consistent with July, sometimes August, as the driest month and November, sometimes December, as the wettest one.

The precipitation regime in the southern part of Albania is generally of Mediterranean type, characterised by intensive showers during the winter. In the mountainous part of the Albanian catchments the precipitation are mostly in the form of snow.

The values of the highest 24 hour precipitation oscillate from 100 to 420 mm. The maximum values are observed in the Albanian Alps (420 mm in Boge) and in the southern mountainous region of Albania. The smallest values are observed in the eastern part of Albania (100 mm in Korca region).

Normally the highest values of 24 hour rainfall are observed during the wet season, but in recent years they have been observed in the late summer and early autumn too.

Coming back to the synoptic situation, the rain started on 21st September and reached its highest intensity between 22nd and 23rd September (about 18:00 UTC). In Table 1 are given the 24 hour precipitation registered during these days as well as maximum 24 values during last 50 years and mean monthly precipitation of September.

As it is seen from the Table 1, the 24 hour precipitations of 22nd September 2002 are quite high. Thus, for Tirana station, located in the middle of the watershed, the 24 hour

rainfall is almost 2 times higher than the monthly value for the September and close to the value of historical maximum value for the whole year (November 1962). At the same time, if we analyse the recorded mass curves of rainfalls (Figure 5) it can be seen that the values of rainfall for smaller durations (less than 6 hours) of 22nd September 2002 are higher than those of 15th November (historical maximum).

Location	Max of 24-hour rainfalls of September 1950–2002 (mm)		Annual maximum of 24-hour precipitation (mm)		Monthly rainfalls of September (mm)	24-hour rainfalls of 22nd Sept. 2002 (mm)
TIRANA	105.5	1985	153.5	15 Nov 1962	77.7	134.6
LEZHA	129.5	1972	160.1	10 Jun 1968	94.0	219.0

Table 1. Some 24-hour maximum rainfalls registered during the period 1951-2001.

This is the main reason why the peak discharge of the flood of the September 2002 is bigger than that of November 1962, which is the historical maximum flood observed in the rivers of Albania (except in the Erzeni River).
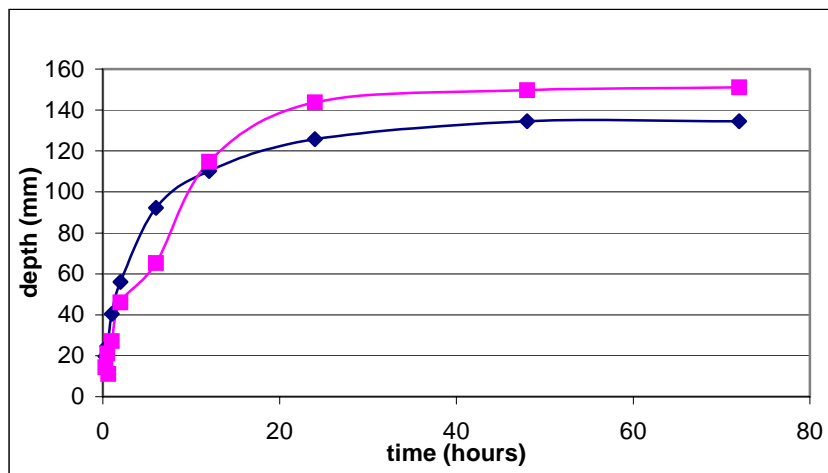
Figure 5. Mass curve of the rainfalls.

4. FLOOD HYDROGRAPH OF 22nd SEPTEMBER 2002

Among all flooding observed until now in the rivers of Albania the biggest are considered those of 1962-63 in relation to the occupation of the territory, duration and damages caused by them. These events occurred not only in Albania but also in almost all the Mediterranean basin and partly in the Western Europe. More intense events occurred in the south-western and eastern part of the Balkan Peninsula and Italy.

On 16th November 1962 high river stages were observed in the main network and tributaries of the main rivers of Albania. These river stages have overpassed those of the past floods (Figure 6).

Figure 6. Hydrometric station Erzeni Ndroq.

The low-lying fields of Thumana, Myzeqeja and Kavaja have been inundated. The waters of Shkumbini River joined those of the Semani in the field of Terbufi.

During the flood of November 1962 the waters of Erzeni inundated the lower part of watershed but the damages were less serious than in other rivers. The dykes in Erzeni River exist in the lower part of the river and are still in good conditions.

The flash flood of September 2002 was characterized by the occurrence of the peak of the flood within 6÷7 hours of the onset of the heavy rainfall. The flood conditions developed rapidly because the rainfall was so heavy, the ground was incapable of absorbing the water quickly enough, resulting in a very high runoff rate. The time to peak of this flood (from the beginning of the rainfall until the crest) was around 12 hours and the falling limb duration about 20 hours, providing a total base time about 40 hours long (Figure 7).

4.1 Data and methods

The fact that during last decades more frequent floods have been observed in the early autumn in some rivers of piedmont zone of Albania (as well as in other countries of Europe) and also some recent studies (*Kundzewicz et al.,* 2004*; Svensson et al.,* 2004), which analyse the trend in flood magnitude and frequency, incited us to think about this problem and try to detect such a trend in the flood series of Erzeni River (1949–2005).

Detection of trends in long time series is an important scientific issue. It is necessary if we are to establish the true effect of climate change in our hydrological systems, and it is fundamental for planning of future water resources and flood protection. Studies of trend detection are also of importance because of our need to understand the changes of the "natural" world. In view of the many dramatic recent floods, detection of trends in long time series of flood data is of paramount scientific and practical importance.
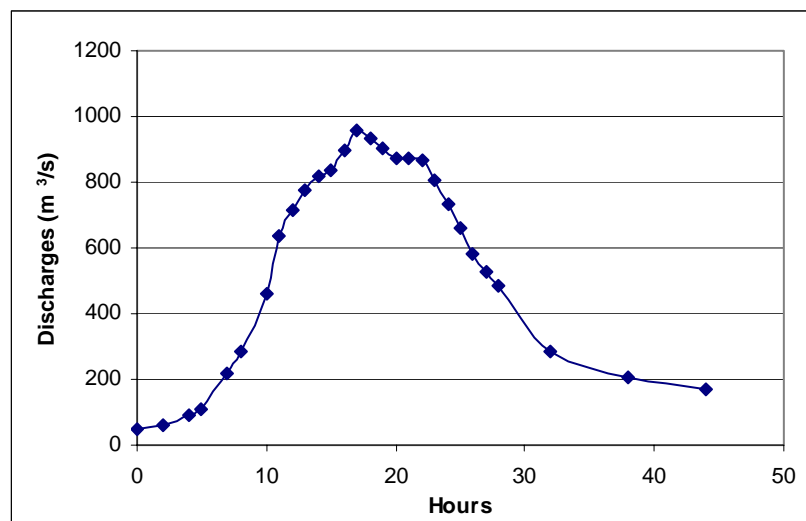
Figure 7. Flood hydrograph of 22nd-23rd September 2002 in station Erzeni at Ndroq.

The hypothesis that climate change will cause increases in frequency and severity of extreme hydrological events has resulted in growing recent interest in change detection in flow data.

Yet, to date, there is little concrete evidence of climate–induced change for river flood records. There are problems with strong natural variability and with data availability and quality. The search for weak changes in time series of hydrological data, which are subject to strong natural variability, is a difficult task, and the use of adequate data and good quality methodologies is essential.

Flood risk may have grown due to a range of land-use changes (deforestation, urbanization, reduction of wetlands and so on) which induce land-cover changes, hence hydrological systems modification. Flood risk may have grown due to considerable changes in socio-economics systems, such as economic development of flood-prone areas, with a general increase in population and wealth, which lead to increasing exposure and exacerbated flood losses. In many places flood risk is likely to grow, due to a combination of anthropogenic and climatic factors. According to last studies on climatic changes they are likely to play an important role in changing flood risk and vulnerability.

A statistically significant increase in global land precipitation over the 20th century has been noted. Instrumental records of land surface precipitation continue to show an increase of 0.5 to 1% per decade over much of mid and high latitudes of the northern hemisphere, particularly pronounced in autumn and winter. It is very likely (estimate of confidence: 90÷99 % chance) that in regions where the total precipitation has increased, there have been more pronounced increases in heavy and extreme precipitation events. Moreover, increases in heavy and extreme precipitation have also been documented even in the regions where the total precipitation has remained constant or slightly decreased.

The method used to estimate whether a significant positive or negative trend holds in flood magnitude and frequency is the linear regression. By this method a regression line fits to the series and the slope describes whether the trend is strong or not. The null hypothesis is that the slope of the line is zero.

However, the linear regression method requires the assumption of normal distribution and is very sensitive to outliers in the data; by ranking the observation and applying the non-parametric Mann–Kendall test, a more robust measure of trend is obtained

31

(*Kundzewicz and Robson,* 2004). This is a robust non-parametric test based on the tau statistic introduced by Kendall and adopted by Mann for time series analyses. In the software HYDROSPECT developed for the detection of trends in time series (*Radziejewski and Kundzewicz,* 2004) this test can only be applied to a series of ranks, so the raw data need to be pre-processed and ranks calculated. The test displayed is Kendall's sum (commonly denoted as S) divided by the square root of its variance under the hypothesis of independent and identically distributed observations. If x_1, x_2, …x_n is the time series values, where n is the time series length, then the test statistic is equal to:

$$\frac{1}{\sqrt{V}} S \tag{1}$$

where:

$$S = \sum_{i=1}^{n} \operatorname{sgn}(x_j - x_i) \tag{2}$$

and:

$$V = \frac{n(n-1)(2n+5)}{18} \tag{3}$$

HYDROSPECT employs a dedicated algorithm for computing this test efficiently, in order of n·log(n) operations, where n is the series length.

4.2 Results and discussion

In order to detect the trend of flood magnitude and frequency, in Figures 8 and 9 two different indices have been employed: the magnitude of peak-over threshold (POT_{mag}), and the frequency of peak over threshold (POT_{freq}). For this purpose the smallest annual flood for the whole period was selected as the peak over threshold. In this way we have two series: one series composed by the peak discharges of all the floods over the peak over threshold (114 m^3/s) and another series composed by the number of floods having a peak discharge greater than the value of peak over threshold. Finding a significant change in time series of river flow data by statistical testing is not difficult if a change results from a major human intervention in the river regime, such as dam construction. It is far more difficult to find a gradual change (e.g. related to climatic impacts) in the behaviour of flow extremes amidst strong natural variability. In Figures 8 and 9 the trend lines of POT_{mag} and POT_{freq} for Erzeni at Ndroq are respectively presented.
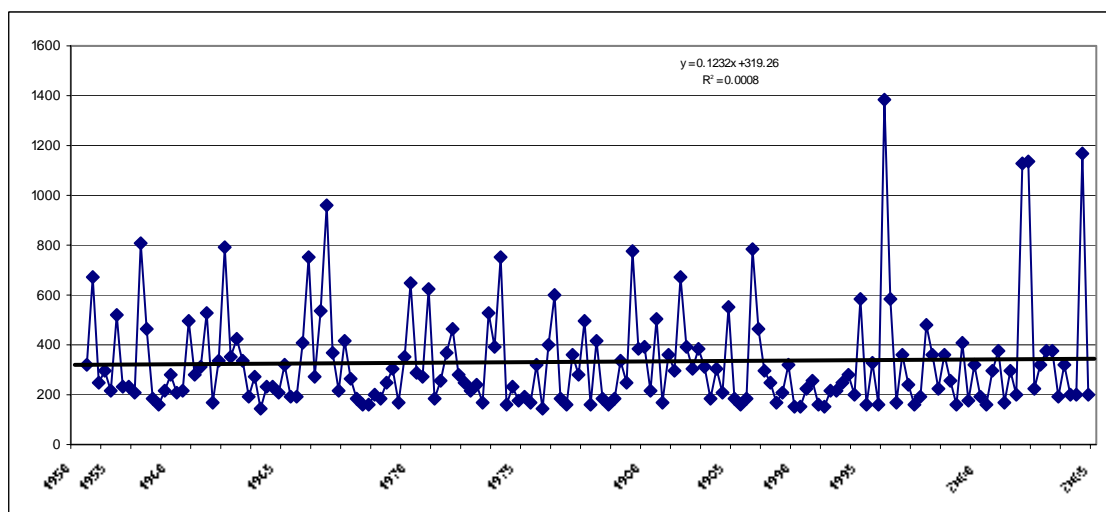

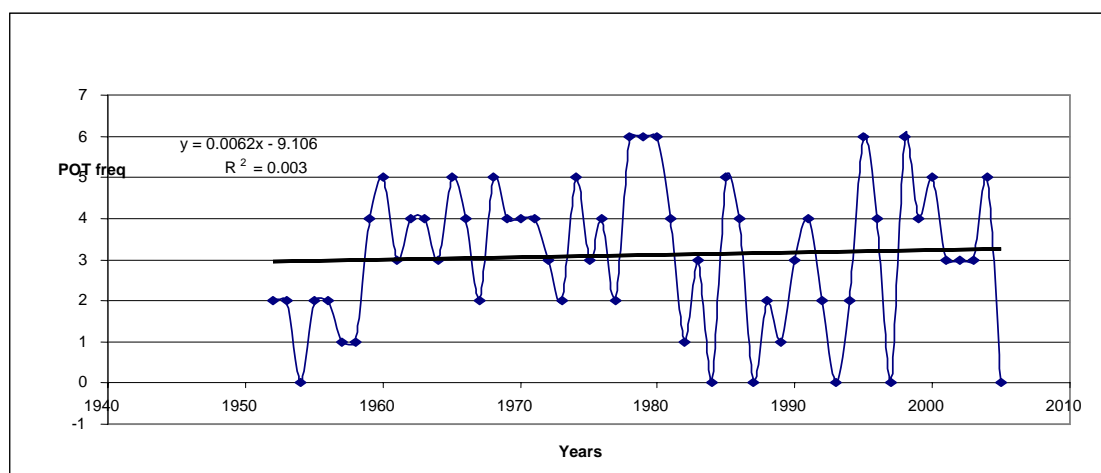**Figure 8.** Trend line of POT_{mag} for Erzeni at Ndroq.

Figure 9. Trend line of POT_{freq} for Erzeni at Ndroq.

From both figures it can bee seen that there is not any significant flood trend for this river. As a matter of fact the very issue of detecting a climate change signature in river flow data is complex. There is considerable evidence that increasing concentrations of greenhouse gases in the atmosphere cause global temperature rise. This, in turn, enhances evapotranspiration and precipitation in most areas, thus likely accelerating the hydrological cycle. Also the water vapour (major greenhouse gas) content of the atmosphere increases, which in turn may change cloud patterns and reflection of radiation.

The feedback mechanisms seem not yet well understood in quantitative terms. Runoff is basically a difference between precipitation and evapotranspiration (whose annual means are increasing in most cases) so the net effect on their difference is not intuitively clear, also because this difference is redistributed in time and space by river basin transfer functions. In order to detect a weak, if any, climate change component, it is necessary to eliminate other influences.

Apart from the inherent complexity of the issue of detecting a greenhouse component in flow records, there are serious problems with the data with which to work, and also with the methodology to detect changes.

In order to detect rigorously a weak greenhouse signal in a noisy, and highly variable, hydrological record, one needs an appropriate advanced methodology. Are trustworthy methodological tools available? The existing methods are based on three types of assumption commonly made when carrying out statistical tests: the form of the distribution, the constancy of it and the independence.

Radziejewski et al. (1998) composed performance of different tests for generated data contaminated by artificially introduced, and fully controlled, trends. All methods considered could detect stronger changes, in form of a gradual trend or abrupt jump, yet they could not detect weaker changes. The result of detection for short-lasting change (analogous to climate variability effects) was different for different tests. Beyond the "strength" of the trend or step-change, duration of occurrence of a trend is important. It is unlikely to detect a trend that has to not continue for a long time. In other terms, the run-up phase must be appropriate long.

5. CONCLUSIONS

The flood of September 2002 is the biggest flood observed from 1949. Field studies, based on flood marks investigation, show that this flood is at least as big as the flood of 1937. The combination of a depression centre on the Genoa's gulf, with another one located over the northern Adriatic Sea, and with a small shallow cyclone with a pressure value of 998 hPa in the Southern Italy, which brought a warm moist air with a speed of more than 15 m/s, have had an important role in the creation of favourable conditions for high rainfall intensities.

Using the regression linear method an attempt was made to detect the flood trend but no significant flood trend in Erzeni River was found. We will try to use in the future the same method, in the other rivers of Albania, in order to have a more convincible conclusion about flood trend in our region.

REFERENCES

Selenica, A. (2004), Risk assessment form flooding in the rivers of Albania, Proceedings of BALWOIS Conference, 25-29 May, Ohrid (Macedonia).

Selenica, A., *Risk assessment in Albania* (2003), Final Report, Publication of UNDP, Tirana, Albania.

Kundzewicz Z.W., D. Graczyk, T. Maurer, I. Przymusinska, M. Radziejewski, C. Svensson, and M. Szwed (2004), Detection of change in world-wide hydrological time series of maximum annual flow, *WMO/TD No. 1239*.

Svensson, C., Z.W. Kundzewicz, and T. Maurer (2004), Trends in flood and low flow series (POT), *WMO/TD- No.1241*.

Radziejewski, M., and Z.W. Kundzewicz (2004), Use and application of the HYDROSPECT data analysis system for the detection of changes in hydrological time series for use in WCP-Water and National Hydrological Services, *WMO/TD-No. 1240*.

Kundzewicz Z.W., and A.J. Robson (2004), Change detection in hydrological records. A review of the methodology, *Hydrol. Sci. J.*, *49*, 7-19.

Observing and modelling exceptional floods and rainfalls
Proceedings of the AMHY-FRIEND International Workshop on Hydrological Extremes,
held at University of Calabria, Cosenza (Italy), May 3-4, 2006.

RECENT EXTRAORDINARY FLOODS IN BULGARIA

S. Dakova

National Institute of Hydrology and Meteorology, BASc, Sofia, Bulgaria.

ABSTRACT
River flooding is a weather-related hazard causing catastrophic damages. After a long drought period of about twenty years, a few very heavy floods occurred between February and August 2005, which caused massive losses of livestock and immense damages to the infrastructure and economic activities. The 24-hour precipitations fallen with exceptional depth reaching 296 mm (on Montana and Vratza – towns in the west part of Bulgaria) have a probability of occurrence once in 1000 years. Some of the reservoirs reached their designed maximum volume and overflowed. The waters were spilling downstream, rupturing the dikes and inundating catastrophically everything on their way.
The causal factors of these very heavy rains are described. The significance of the meteorological input elements, the hydrographic basin parameters for runoff generation during extreme floods, the designed precipitation values used in the engineering practice and human activities concerning river channels were examined for Bulgarian rivers affected by the extraordinary floods. The analyses provide useful information about the frequency of flood occurrence, flood management and disaster prevention. The flood events in 2005 reminded us that wise management of water resources and strict observation of regulations for the operation of hydraulic constructions are the essence of their endurance.

1. INTRODUCTION

Drought and floods are the two sides of the "Hydrological Extreme" medal. Drought creeps very slowly with a cumulative impact. Slow initiation and an undefined end of the drought make the disaster elements hidden. It becomes evident much later, when the drought has already started. Because of that, it is difficult to choose the right time for taking defensive or remedial action. And vice versa, when the flood occurs every symptom is obvious and opportune measures may be taken, usually with the support of public opinion since the disaster is easily recognized by all. River flooding is a weather-related hazard, developing quickly, causing catastrophic damages. After a long drought period of about twenty years, a few very heavy floods occurred in Bulgaria between February and August 2005, which caused massive losses of livestock and immense damages to the infrastructure and economic activities. The houses of hundreds of people were flooded.

2. SYNOPTIC CONDITIONS

There are 3 types of synoptic situations causing floods in Bulgaria (*Latinov,* 2006):

- When Mediterranean cyclones pass over the southern part of the Balkan Peninsula, usually in the end of winter (February and March). Initially they provoke warm weather making snow melt. Later on, rainfall combines with snow melting producing the water for floods.
- Due to the intensive rains during the May-August period produced by cumulus-nimbus cloudiness, usually related to cyclones blocked over the Balkan Peninsula in great unsteadiness of air masses.
- During the autumn – due to slow moving cyclones and well shown convergent processes over the Balkan Peninsula

The occurrence of a synoptic situation of the first type in Central and East Bulgaria was a reason for the inundation in February 2005. Rains were unevenly distributed. They were most intensive in the southern areas with a Mediterranean climate influence, over the basins of the low stream of the Rivers Maritza and Struma, close to the border with Greece and Turkey. The proportion of the fallen precipitation to the mean one is 271%.

The second type is more frequently observed. It also occurred in 2005 and caused very heavy rains. The manifestation of the heavy rains in 2005 compared with the maximum and mean monthly precipitations observed for a period of 104 years (1901 to 2005) is graphically presented on Figure 1.
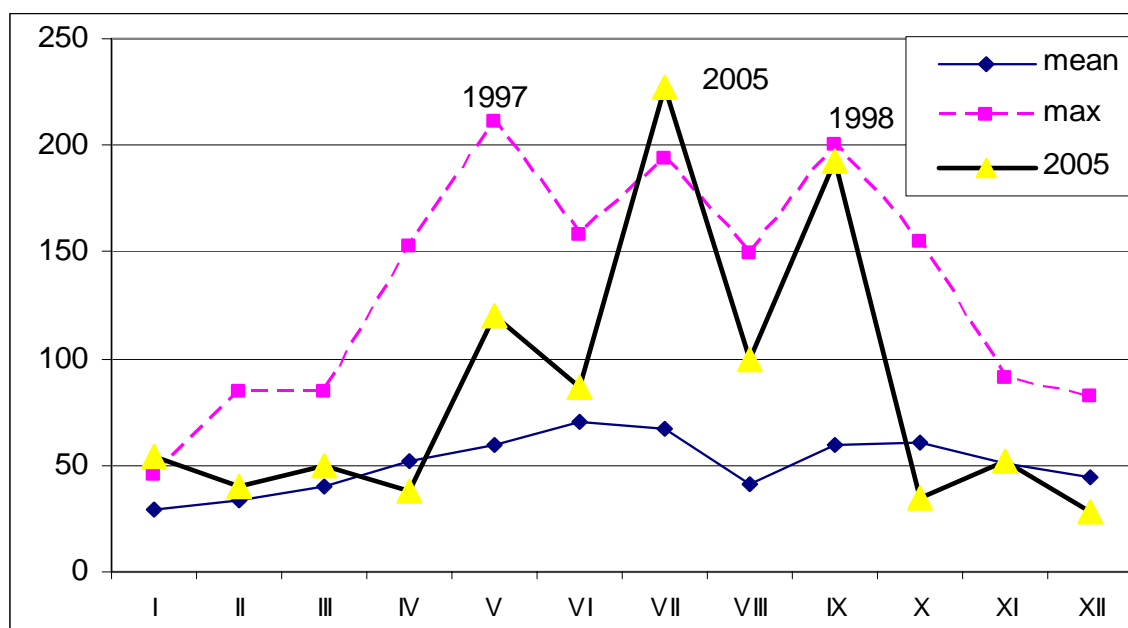

Figure 1. Comparative graphs of maximum and mean monthly precipitation for a 104-year period and maximum precipitations in 2005 fallen at the Obrastzov Chiflik station.

The multi-yearly variation of the precipitation during the period 1904-2005, smoothed by moving 5 year mean values, is presented graphically on Figure 2.
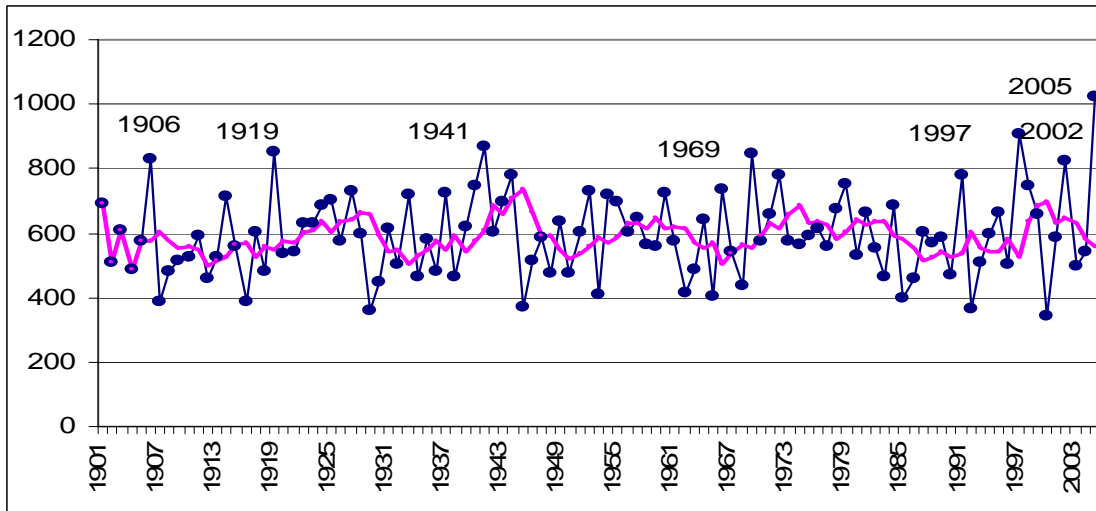
Figure 2. Multi-yearly variability of the annual sum of the precipitations.

The values of the extreme monthly amounts of precipitation fallen during the May–October period in the years with an annual sum over 800 mm are presented in Table 1.

Year	MAY	JUN	JUL	AUG	SEP	OCT	AnnSum
Mean	59.4	70.6	66.7	41.0	59.6	60.3	608.4
1906	137.3	120.6	153.4	37.0	11.4	72.7	828.8
1919	63.4	70.8	148.7	143.4	3.3	152.4	853.6
1941	86.3	262.5	130.1	51.4	40.9	85.8	867.6
1969	24.7	193.1	127.0	32.2	24.8	0.1	847.9
1991	211.5	37.8	193.5	55.0	14.1	59.4	779.0
1997	76.2	102.1	108.4	113.2	12.6	122.4	909.5
1998	102.1	59.5	51.6	17.8	199.9	78.8	747.4
2002	35.0	34.0	106.1	149.5	79.7	155.2	822.0
2005	119.7	86.9	227.3	99.3	192.2	34.6	1021.7

Table 1. Extreme monthly amount of precipitations (mm) fallen during the period May–October.

The proportion between the maximum sums of the precipitation and the respective mean monthly precipitations has reached 537÷625% in the west and central regions of Bulgaria. It must be pointed out that of all the 9 extreme annual sums, which occurred during the 104 years period, five occurred during the last fifteen years, i.e. their frequency for the last period has increased drastically to 34 %.

The long duration of the precipitation in 2005 is a very important cause for creating a flood. The value of the amount of rain Q≥30 mm/24h is usually used in Bulgaria as a criterion for heavy rains. The number of days with heavy rains estimated for the period 1961-2005 is presented in Figure 3.

It is evident that during the last fifteen years the number of days with heavy rains has increased. Heavy rains in 2005 lasted 28 days, that is why the soil was oversaturated and almost all fallen rain produced a flow.
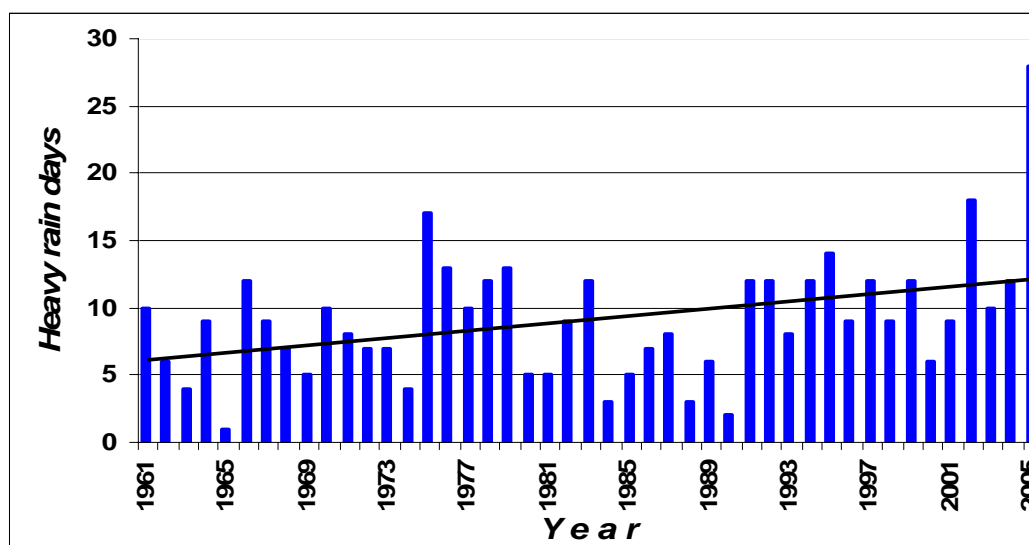
Figure 3. Heavy rain days (Q≥30 mm/24h) in more than 4 districts *(Simeonov et al., 2006).*

Moreover, the results from the analyses of precipitation support the statement that climate change will alter the frequency and magnitude of hydrological extremes. However, there is a broad agreement in the international scientific community about that.

3. WATER MANAGEMENT AND SOCIAL CONDITIONS

The physical and geographic conditions in Bulgaria usually generate spring and autumn floods and a very low flow to dryness in the summer. The mitigation of these extreme events was effectuated by constructing 2209 reservoirs with a total volume of $7172 \cdot 10^6$ m^3, the useful volume being $5997 \cdot 10^6$ m^3. This is almost 30% of the water resources of the country calculated for a wet year and 50 % for a dry year, respectively. Eighty-one reservoirs of a total volume of $6323 \cdot 10^6$ m^3 have been accepted as big. They have preliminary multi-purpose utilization. The remaining 2129 reservoirs have been preliminarily designed for irrigation and partially for water supply. They are small, with seasonal regulation and are managed by the "Irrigation systems" government company.

The Council on Water is directly subordinate to the Prime Minister and consists of representative experts from the Ministry of Agriculture, the Ministry of Public Works, and the Agency for Hydropower Production, hydrologists, and experts from other institutions related with the water. Managing the water resources of the country, the Council coordinated water demand and the functioning of hydraulic constructions until 1992. At that time floods weren't a menace because of the big total volume of the reservoirs and the wise management of water. Each autumn all reservoirs, including the smallest ones, received a directive related to the quantity of available water which had to be run off for prevention. Revision and correction of the river beds and dykes was done regularly.

The last fifteen years have been a transition period, when Bulgarian laws have been harmonized with European legislation, when property has changed its owner, etc. The management of these two thousand reservoirs and the adjoining constructions was neglected, except for these eighty one big reservoirs. Some of the small reservoirs were put in charge of the mayors of the nearby villages. Some of them were given for private

exploitation, transforming them into breeding pools, and bottom water outlets were walled off for keeping the fish. Others, the bigger ones (177 reservoirs) stayed under the control of the "Irrigation systems" company. Having in mind the severe crisis during the dry period, these reservoirs kept permanent over 80 % of their volume. It turns out that the rest 15÷20% were not enough for the retention of the occurred very big floods.

On the other hand, according to new legislation, river beds have to be maintained by the mayors of the territory of the villages and by no body between settlements. The dry period running the last almost 20 years created conditions for covering the river beds with trees and shrubs. They became a serious factor for backing the rivers and blocking the streamflow. This caused an overflow the bridges and even destruction of some of them.

4. FLOODS

The above-mentioned synoptic conditions have created a flow which is a few times bigger than the normal one. Almost eight months of 2005, six of them sequential, the discharge was so high as to be considered a disaster. Almost all the country was affected by the floods. The percentage of the registered flows related to the mean flow is presented in Table 2. Eighteen main rivers situated on Bulgarian territory are included. The location of the river in the country is marked with the first letter of the geographical cardinal points like: NWB is North-West Bulgaria, NCB is North-Central Bulgaria, SCB is South-Central Bulgaria, SEB is South-East Bulgaria and SWB is South-West Bulgaria.

N	River and place	situated	II	III	VI	VII	VIII	IX	X	XI
1	Topolovetz-v.Akatzievo	NWB	22.3	17.6	19.8	28.1	33.7	12.4	33.3	78.7
2	Ogosta-townMizija	NWB	133.6	100.6	73.4	188.7	**707.3**	193.7	357.8	263.1
3	Iskar-t.Novi Iskar	WB	80.7	124.1	399.6	241.3	**729.9**	324.2	228.8	168.8
4	Iskar –Orjahovo	NWB	114.2	127.4	346.5	268.4	**1083**	415.8	297.3	177.3
5	Vit v.Tarnene	NCB	127.9	79	243.3	450.4	**666**	612.7	223	288.5
6	Osam-Izgrev	NCB	144	99.3	238.7	610.8	538.7	1108	514	230.6
7	Jantra Karantzi	NCB	221.4	159.1	255.4	**1084**	441.5	956.9	516.7	418.9
8	Tcherni Lom-Shiokovo	NEB	89.8	78.4	231.9	601.3	191.5	446.8	341.3	258.9
9	Provadijska -Sindel	EB	94	122.4	111.8	**716.9**	180.7	219	138.9	96.6
10	Kamtchija-Grozdevo	EB	420.7	459.1	202.5	**905.4**	271.2	223.1	167.8	93.9
11	Sredetzka-Prohod	SEB	268	124.9	137.8	311.6	125.1	**1788**	110.5	152.1
12	Maritza –Pazardjik	SCB	81.6	129.8	431.9	395.1	**1988**	508.3	419.7	202.6
13	Maritza –Parvomaj	SCB	58.7	93.5	142.8	232.7	**661.3**	138.5	140.2	73.6
14	Maritza –Svilengrad	SEB	173.5	203	252.8	505.6	**780.9**	322.8	235.1	163.8
15	Arda-Vehtino	SEB	189.8	186.8	70.7	94.1	**681.3**	162.8	386.4	115.8
16	Tundja-Elhovo	CB	182	373.5	178.2	634.8	494.1	377.1	215.6	228.2
17	Mesta-Momina Kula	SWB	164.1	186.6	117.2	143.7	375.6	156.1	163.7	71.9
18	Struma-Marino Pole	SWB	189.5	246.7	167	153.2	229.8	132.2	122.3	64

Table 2. Percentage of the registered flows from the respective mean monthly flow in 2005.

It could be seen in the table that there are percentages near to and over the thousand. It is necessary to point out that this river flow is generated from the precipitation fallen over the basin, but also from the reservoir flow, running off after the earth dam has been

broken. Many very small irrigating reservoirs usually used for fish production have a burst dam. Besides, some reservoirs were full during the rainy period. The possibility for retention of the high wave is negligible. For instance, in the catchment area of the Iskar River (8642.2 km^2) there were a few small reservoirs which overflow, water was fallen volley to save the dam, and in some others the dams were torn, which accounted for the following form of the hydrograph:
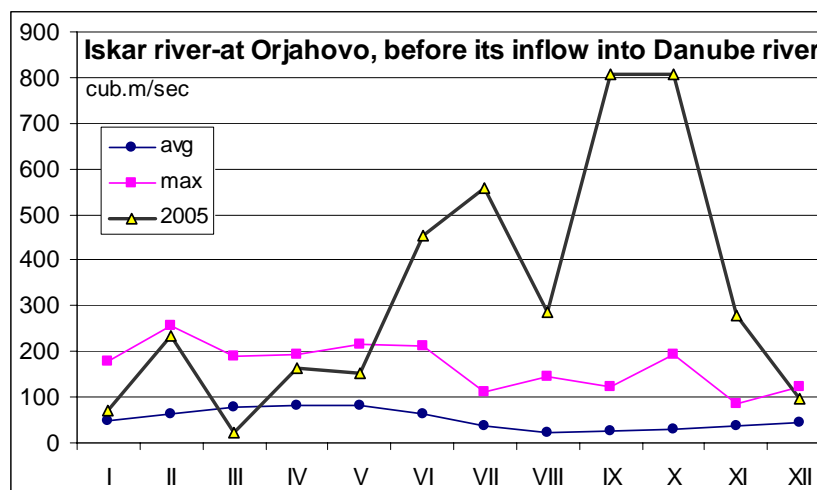
Figure 5. Discharge (m^3/s) of the Iskar River in 2005 compared with maximum and mean monthly flows.

Since water in the middle and low parts of the Iskar River has been used for irrigation, conductivity of the river bed was designed as IV class construction with a 5% probability of overflow. In the created conditions, the high wave has a probability of occurring once in a thousand years. It is natural that inundation would be a logical consequence.
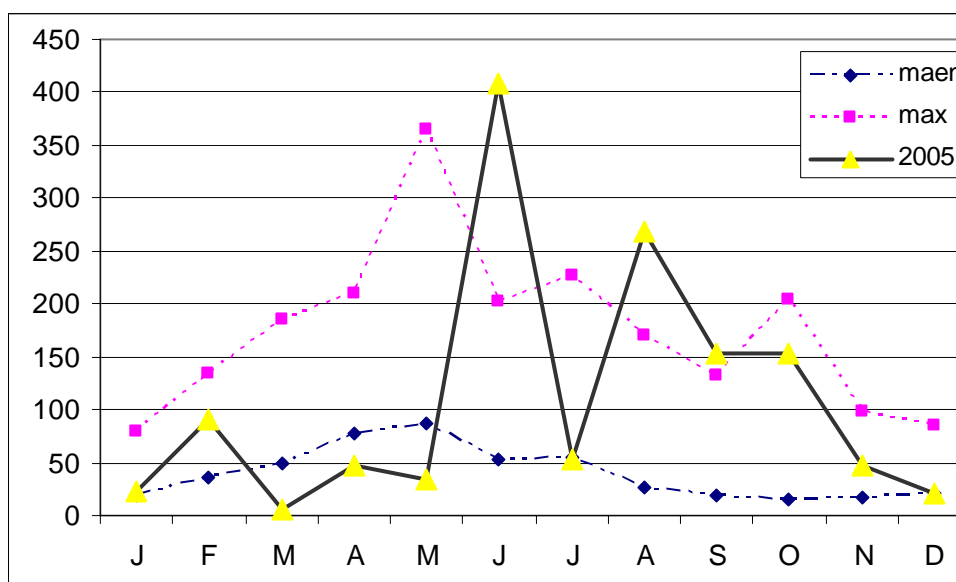
Figure 6. The Osam River flow (m^3/s) in 2005.

The maximum flow generated in the Osam River, in conditions of continental climate, has a frequency of occurrence once in 750 years. Generally, the hydraulic constructions

were designed for such values. The level of groundwater rose up to the surface. The damages in this basin came from the breaking of dykes and the shallow sewerage systems in the town.

In the basin of the Struma River which generates streamflow in Mediterranean conditions, the synoptic conditions were of the first type. The reservoirs were controlled; water was drawn out through hydropower plants. So, the situation was different from the previous one presented in Figure 6.
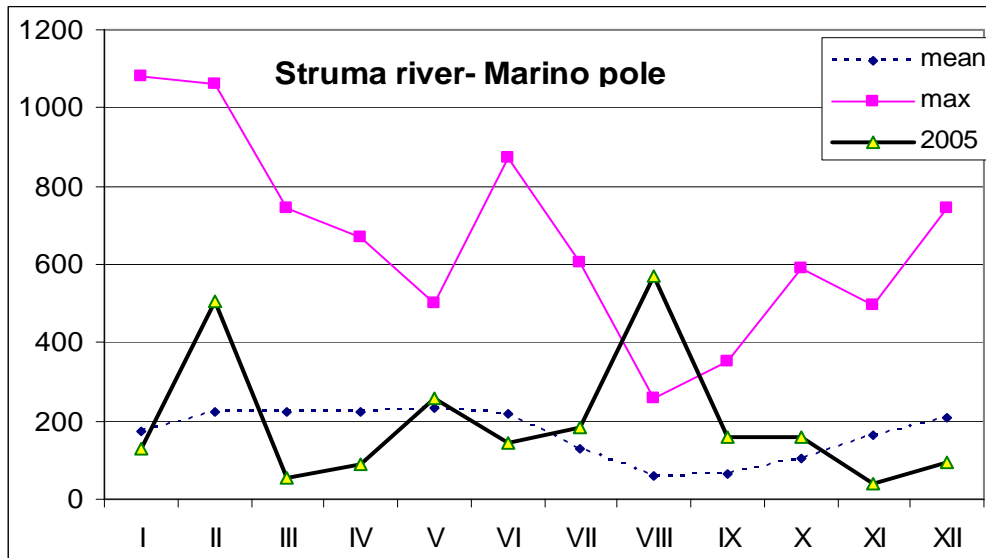
Figure 6. Discharge (m^3/s) of the Struma River at the Marino pole station in 2005 compared with the maximum flow which occurred in the respective month and the mean monthly flow.

It is obvious that 2005 was a very wet year. The water resources of the country amounted to $27391 \cdot 10^6$ m^3, having a 13% P, which corresponds to a very wet year, calculated back for a 50-year period.

|	
WR -25% P wet year	$23898 \cdot 10^6$ m^3
WR -50% P normal year	$19962 \cdot 10^6$ m^3
WR -75% P moderate dry year	$15656 \cdot 10^6$ m^3
WR 2001	$12466 \cdot 10^6$ m^3
WR 2002	$11134 \cdot 10^6$ m^3
WR 2003	$15174 \cdot 10^6$ m^3
WR 2004	$12466 \cdot 10^6$ m^3
WR 2005 -13% P	$27391 \cdot 10^6$ m^3

Table 3. Water resources (WR) of Bulgaria at different time levels and in 2005.

5. CONCLUSIONS AND CHALLENGES

The main conclusions and results from the above brief presentation of the 2005 floods could be summarized as follows:
- The recent inundations result both from very heavy rainfall (with a probability between 0, 0.1 and 0.001 P) and from the inadequate management of the small size reservoirs and the adjoining constructions.
- The frequency of occurrence of heavy rains during the last fifteen years is 0.34%.

- The conduct of precipitations supports the statement that climate change will alter the frequency and magnitude of hydrological extremes. Changes in the frequency of hydro-climatic extremes may be one of the most significant consequences of climate change.
- The frequency and magnitude of extreme precipitation also affect the hydrological extremes. The events (drought and floods) which occurred during the last three decades support the statement of an impact of climate change on runoff.
- The water resources obtained for 2005 have a 13% P, calculated from a distribution curve for a 60-year period (*Mandadjiev and Dakova,* 1996).
- The growing body of evidence suggests that certain aspects of our water resources are very sensitive to both climate and how we choose to manage our complex systems.

The flood events during 2005 reminded us that wise management of water resources and strict observation of regulations for the operation of hydraulic constructions are the essence of their endurance. They present us with a challenge to introduce further measures, some of which have already been initiated:

- As it was already mentioned above, the precipitation fallen in 2005 was extraordinary for the whole observation period and provoked heavy floods. So, the necessity for a reassessment of the conductivity of the corrected river beds, of the section of a river close to the reservoir dam, of the hydrological assurance of the reservoirs, etc. is imperative.
- Hydraulic constructions were designed using the information about precipitations and runoff available at that time. An updated reassessment of the designed high wave of the reservoirs will be another important activity.
- The Ministry of State Policy on the Disasters and Accidents has been set up and is already functioning.
- A new law about water management is in a process of preparation. It will clearly define the responsibility for maintaining river beds, dykes, and small reservoirs.

REFERENCES

Documents and Bulletins of Ministry of Environment and Water, Bulgaria (Data information obtained by NIMH –BASc).

Latinov, L. (2006), *Dangerous meteorological events in Bulgaria*, Book of Lectures edited by the Ministry of the State Policy on Disasters and Accidents.

Mandadjiev, D. and S. Dakova (1996), Influence of the drought continuing during last decades on the Bulgarian river discharge, *Bulgarian J. Meteorol. and Hydrol.*, 7.

Modev, S., and S. Kirilova (2006), *Reservoir influence on the flooded regions of the Republic of Bulgaria during the period 4-8.08.2005*, Report for the National Conference on Disasters and for the Meeting of the World Water Day, Sofia.

Simeonov, P., T. Marinova, and L. Bocheva (2006), *On frequency distribution and intensity of severe convective storms over Bulgaria*, BALWOIS Conference, Ohrid, Macedonia.

THE EXCEPTIONAL EVENT OF 12th AND 13th NOVEMBER 2004: PERFORMANCE OF THE CIVIL PROTECTION MONITORING SYSTEM OF CALABRIA REGION

S. Arcuri, L. De Felice, G. Iiritano, R. Niccoli

Calabria Region, Functional Centre, Civil Protection Division, Catanzaro, Italy.

ABSTRACT
The Functional Centre of the Calabria Region is an office of the regional Civil Protection Division. According to a specific task of the Civil Protection decree n. 3081/2000 (called "Soverato" decree), it has developed an early warning system for the geological and hydraulic risk based on rainfall thresholds. The system, currently operating, is based on a series of procedures finalized to the transmission of warning messages and, recently, has been adapted to the prescription contained in the Prime Minister Directive issued on the 27th February 2004. This latter encodes in uniform way all over the country the national warning system according to a combined management between a national level (managed by the National Department for the Civil Protection) and a regional level (managed by the regional Functional Centres).
The paper describes the behaviour of the regional warning system during the event that on 12th and 13th November 2004 involved large part of the regional territory.

1. THE REGIONAL WARNING SYSTEM

The regional warning system developed by the Functional Centre of the Calabria Region is based on the control and real-time monitoring of rainfall. When rainfall values overcome assigned threshold values, an alert message is transmitted to municipalities for the adoption of safeguard measures for the population safety.

The methodology of definition of the rainfall thresholds is applied to municipality territory and refers to two different scenarios of risk for hydrological and geological events (*Iiritano and Versace*, 1996; *Sirangelo*, 2001; *Iiritano et al.*, 2002; *Niccoli et al.*, 2004):

A) risk of erosion of the soil and small landslides;
B) risk of river bed erosion and localized river floods.

The first scenario (indicated in the following as A risk scenario) is related to the action of the rain in terms of superficial erosion or for soil infiltration (landslides). It's a widespread risk on the territory and, therefore, it involves all the calabrian municipality territories. The second scenario (indicated in the following as B risk scenario) is related to the precipitations that involve the whole catchment related to the river section the analysis is referred to. This risk is present along almost all the calabrian water courses.

The thresholds definition is based on the choice of appropriate precipitation values: the so-called "indicative rains" which can be associated to the phenomena described by the two mentioned risk scenarios.

The associated area and duration are intrinsic properties of the indicative rain. For each indicative rain value, a critical value has been characterized, called "critical rain": for

values bigger than this, the probability that the phenomenon can be primed is very high.

The system thresholds are a percentage of the critical rain. Different thresholds correspond to various percentages of the critical rain, and they are usually distinguished with increasing numbers (1, 2 and 3).

Considering the spatial scale of the warning system (municipality territory extent), in order to identify the critical values and thus the thresholds, it was necessary to characterize the "reference rain gauges" for every municipality in Calabria. Such real time rain gauges belong to the regional meteorological remote sensing network.

2. REFERENCE RAIN GAUGES

For the A risk scenario (risk of soil erosion and landslides) the choice of the reference rain gauges has been carried out according to the influence area of each gauge on the municipality territory. Each rain gauge belonging to the entire remote sensing network has been associated to an influence area using the method of Thiessen polygons. The weight of each gauge has been determined considering the ratio between the surface of the intersection Thiessen polygon - municipal territory and the surface of the municipality territory of interest.

The reference rain gauges have been chosen according to the following criteria: only one has been chosen in the case its weight is bigger than 80% (or 75% if none of the other gauges has a weight bigger than 20%). More gauges have been chosen on the contrary case.

For the B risk scenario (river bed erosions, localized floods), the reference critical sections have been preliminarily selected. For almost each municipality of Calabria at least one critical section has been selected (with the exception of mountainous municipalities with no rivers), generally in the lower valley zone or corresponding to bridges or crossings inside the inhabited areas.

For each critical section, the corresponding basin has been delimited, and it has been classified as small, medium or large according to the length, L, of the main channel. In particular, basins are classified as small when the length is less than 12 km, medium when L is between 12 and 36 km, large when L is longer than 36 km. The distinction is suggested by the fact that the critical rains, for river basins of various dimensions, are characterized by various durations, i.e. rains of short duration can generate critical conditions for small river basins but they do not have effects on the larger ones, and vice versa.

The procedure to select the reference rain gauges is analogous to the one relative to the A risk scenario, just referring to the area of the river basin and not to the municipality territory. Only one reference gauge has been assumed in the case its weight is over 80% (or 75% in the case none else of the other gauges has weight bigger than 5%). More rain gauges on the contrary case. It's totally similar to the A risk scenario, but considering 5% and not 20% as limit weight.

2.1 Indicative rains

The indicative rains are assumed equal to the weighted average of the precipitations measured by the reference rain gauges. The duration of indicative rainfalls is defined according to the risk scenario and the extent of the river basin, as presented in the

following table:

A Risk Scenario	B Risk Scenario		
	Small basins	Medium basins	Large basins
1, 3, 6, 12 hours	1, 3, 6 hours	3, 6, 12 hours	6, 12, 24 hours

2.2 Critical rains

The critical rains have been defined as indicative rains corresponding to a return period of 5 years, for the A risk typology, and of 10 years for B risk typology.

Since not all the rain gauges have time series long enough to carry out a reliable statistical analysis, the CDF curves have been determined only for the rain gauges with the longest series. The parameters of these curves have been considered as known constrained values for the application of an interpolation technique of geostatistics, in order to estimate the same parameters for the remaining network rain gauges with not long enough time series. Thus, finally, every gauge had its parameters.

The adopted CDFs are defined through the formula $h_{t,T} = at^n$, where t is the duration of the precipitation in hours, T is the period of return in years, $h_{t,T}$ is the rainfall with t as duration and T return period, a and n are the coefficients estimated through the interpolation technique of geostatistics for the gauges with short time series. All these parameters assume unique values for each return period.

2.3 Rainfall thresholds

Rainfall thresholds are defined on three levels, each one a percentage of the critical rain. In particular:
- threshold 1 (level 1): 60% of the critical rain
- threshold 2 (level 2): 80% of the critical rain
- threshold 3 (level 3): 100% of the critical rain

These percentages have been fixed according to the results of a back analysis that was carried out on some hourly rainfall time series of the past.

Finally, for each scenario the steps that led to the determination of the thresholds values are the following ones:
- choosing the reference rain gauges;
- estimating the values of a and n for every gauge;
- estimating the rain with return period equal to 5 and 10 years for each appropriate duration;
- calculating the average weighted on the single gauges;
- calculating the threshold values based on the described percentages.

Then a correspondence between rainfall thresholds and hazard level has been established:
- ordinary hazard: it corresponds to the threshold of level 1;
- moderate hazard: it corresponds to the threshold of level 2;
- high hazard: it corresponds to the threshold of level 3.

3. THE METEOROLOGICAL EVENT OF 12th AND 13th NOVEMBER 2004

The meteorological event of 12th and 13th November 2004 has been concentrated in the

24 hours between 6:00 a.m. of 12th November and 6:00 a.m. of 13th November.

The map of the rainfall of the event (Figure 2) shows how it interested the great part of the regional territory, with some peaks concentrated in some zones in which they are the first critical case in time series. In particular, in the rain gauge of Parenti (province of Cosenza) a total of 223,6 mm has been recorded, in Santa Cristina di Aspromonte (province of Reggio Calabria) 206.4 mm, in Tiriolo (province of Catanzaro) 181.6 mm, in Cerenzia (province of Crotone) 158.2 mm, Cirò Marina Volvito (province of Crotone) 127.6 mm and in Savelli (province of Crotone) 125.2 mm.

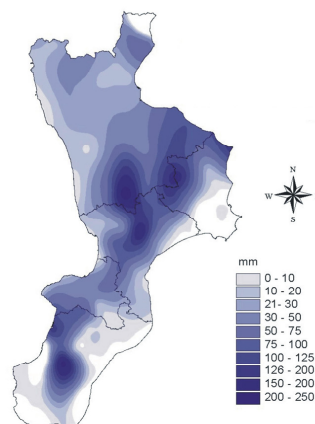**Figure 1.** Location of provinces of Calabria.

Figure 2. Rainfall distribution of meteorological event of 12th and 13th November 2004.

The perturbation has moved during the course of the event from the south-west side of the region towards the north-east, involving, progressively, the province of Reggio Calabria and marginally the one of Vibo Valentia and, subsequently, those of Catanzaro, Cosenza and Crotone. In the morning of 13th November the event completely ended. The temporal evolution of the perturbation is evidenced by the maps of the totals of accumulated precipitation in the consecutive periods of 6 hours, as reported in Figures 2, 3, 4 and 5.

In particular, Figure 3 shows the localization of precipitation in the Aspromonte area and in the flat territory around Gioia Tauro (province of Reggio Calabria). The maximum values have been recorded by the rain gauge of Santa Cristina d'Aspromonte with 105.2 mm and in the rain gauge of Gioia Tauro with 42.6 mm.

Figure 4 shows how the centre of the event has extended to the provinces of Catanzaro and Cosenza. In particular, from the city of Catanzaro to Savuto valley for the former, and from the Crati river basin northern Ionian coast for the latter. The maximum values have been recorded in the rain gauges of Parenti (province of Cosenza) with 102.2 mm, Rogliano (province of Cosenza) with 74.4 mm, Tiriolo (province of Catanzaro) with 59.2 mm, Gioia Tauro (province of Reggio Calabria) with 54.4 mm and Cropalati (province of Cosenza) with 47.2 mm.

From Figure 5 it is quite evident how the event by now has extended to the entire provinces of Catanzaro, Cosenza and Vibo Valentia with an increase of intensity also in the Aspromonte and in the flat area near Gioia Tauro. The maximum values have been

recorded in the rain gauges of Parenti (120.2 mm), Tiriolo (115.8 mm), Camigliatello (81 mm), Savelli and Cerenzia (68.4 mm), Feroleto della Chiesa (67.8 mm, province of Reggio Calabria) and San Pietro di Caridà (67.4 mm, province of Reggio Calabria). Finally, in Figure 6 an evident decrease of the precipitations, now only localized in the province of Crotone and, for a little portion, in provinces of Cosenza and Catanzaro, is shown.

The maximum values have been recorded in the rain gauge of Cirò Marina Volvito (114.4 mm), Pagliarelle (97.2 mm), Cotronei (90.6 mm), Cerenzia (72.6 mm), Catanzaro (55.4 mm) and Albi (51.0 mm, province of Catanzaro). For the rain gauges in which intense values of precipitation have been recorded during the evolution of the meteoric event, a statistical analysis on the maximum values of the 1hour, 3hour, 6hour, 12hour and 24hour duration precipitations has been carried out. As probabilistic model of the extreme values has been used the Two Components Extreme Value distribution (*Rossi and Versace*, 1982; *Rossi et al.* 1984).
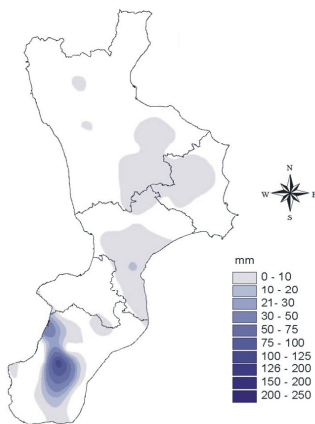

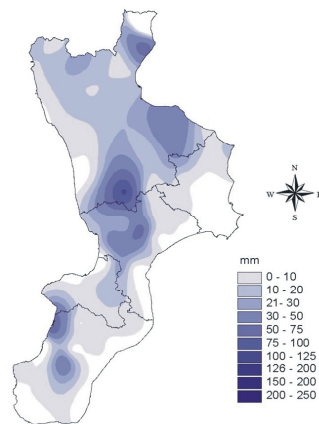**Figure 3.** Rainfall distribution from 6:00 to 12:00 of 12thNov.

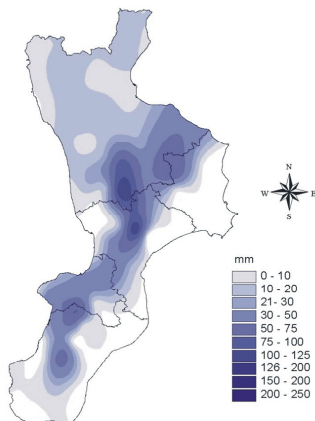**Figure 4.** Rainfall distribution from 12:00 to 18:00 of 12thNov.

Figure 5. Rainfall distribution from 18:00 to 24:00 of 12thNov.
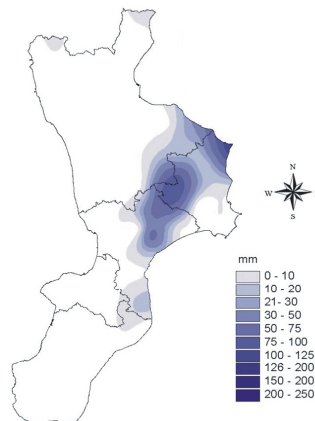

Figure 6. Rainfall distribution from 00:00 to 6:00 of 13thNov.

Finally, the map of the return periods of the precipitations fallen in the 24 hours, from 6:00 of 12th November to 6:00 of 13th November, at the third level of regionalization, has been elaborated (Figure 7).
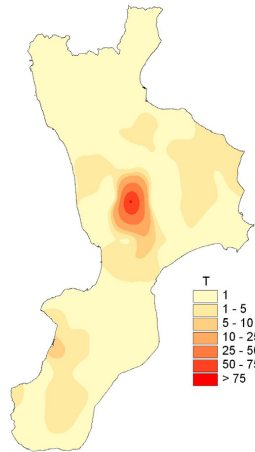
Figure 7. Return periods of rainfalls (from 6:00 of 12th November to 6:00 of 13th November).

4. THE SOFTWARE MOSIP

The Functional Centre has developed and currently employs the software MoSiP (Monitoring Pluviometric Situation) that visualizes the state of the hydro-geological risk on the territory. It's the user interface reporting on real time the situation of the warning system. It consists of a GIS interface, on which municipality territory borders and the connected risk levels are visualized.

A synthetic table, besides, shows for each municipality the risk level, evidencing the risk scenario, the values of the rainfall thresholds and of the corresponding indicative rain, the durations associated to the indicative rain and the trend of the values connected to each single risk.

In order to point out the immediate localization of the level of municipality hazard, different colours have been used: white for null hazard, yellow for ordinary hazard, orange for moderate hazard and red for high hazard.

The software executes the automatic data processing every 20 minutes, allowing to have a clear picture of the hazard level with the same temporal step. The interface easily provides for each municipality the relative information regarding the risks known in its territory.

4.1 Early warning system performance during the event of 12th and 13th November 2004

During the event, the system has marked the first overcoming of rainfall thresholds at 12:00 of 12th November, in the province of Reggio Calabria on the Aspromonte, with level 1 on 5 municipalities. But the situation at 13:20 evidenced, in the same zone, already 16 municipalities with surmounting of the third threshold level, therefore in high

hazard situation (Figure 8).

At the next time step (13:40) there was overcoming of threshold also for ten municipalities in the province of Catanzaro (Figure 9).

Figure 8. Rainfall overcoming situation at 13:20 of 12th November.
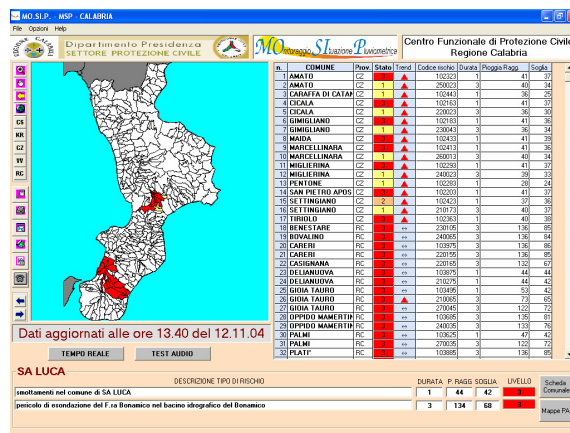
Figure 9. Rainfall overcoming situation at 13:40 of 12th November.

In the successive step, until 18:40, a progressive increase of the number of municipalities with no null hazard situation has been recorded. Practically all provinces have been interested, for a total number of 71 municipality territories with overcoming of threshold, a number of which consisting with elevate hazard from the Sila Plateau to the Tyrrhenian sea (Figure 10).

The number of municipalities involved in the event increases in a drastic way with the update of 23:00. It evidences an escalation of the number of high hazard, with 145 municipalities interested and persistence of the situations of high hazard in the zone of Sila (Figure 11).

During the night the situations of no null hazard have been recorded in the municipality territories of Crotone province, with the contemporary absence of hazard in the province of Reggio Calabria (Figure 12).
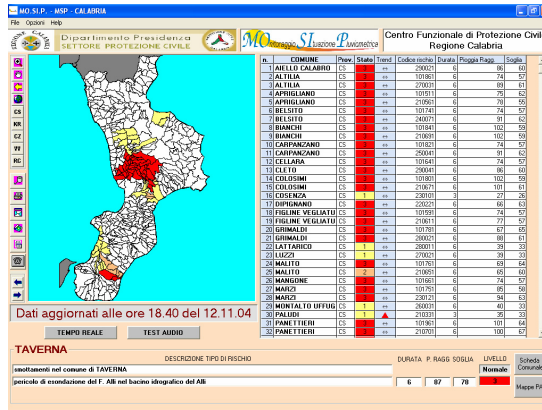
Figure 10. Rainfall overcoming situation at 18:40 of 12th November.
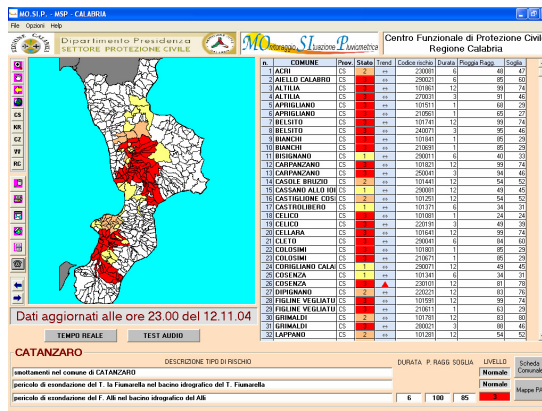
Figure 11. Rainfall overcoming situation at 23:00 of 12th November.
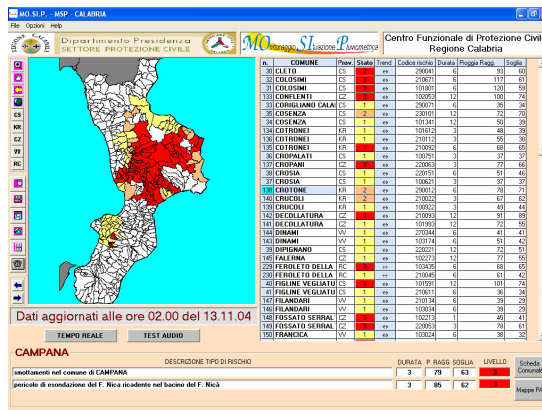
Figure 12. Rainfall overcoming situation at 02:00 of 13th November.

In particular the update at 2:00 counts 156 municipalities involved in no null hazard situation, the greater part with exceeding of third level thresholds. The number of the municipalities in no null hazard state becomes 162 with the update at 3:40 (Figure 13).

With the losing of strength of the meteorological event, the situation gets better, however, in the first morning (Figure 14), still a general situation of high hazard remains.
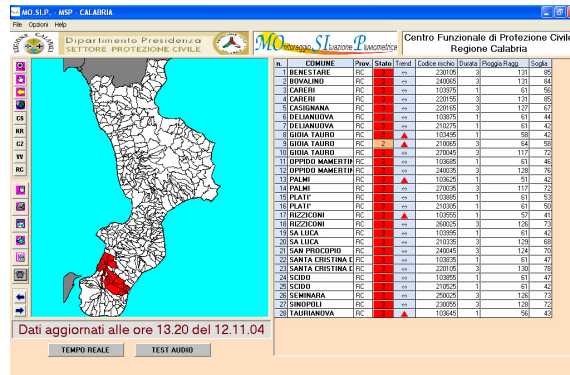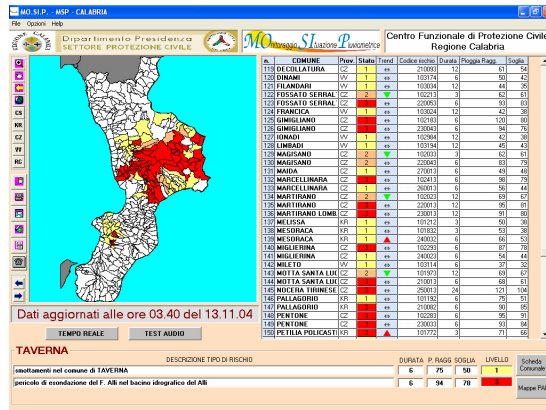

Figure 13. Rainfall overcoming situation at 03:40 of 13th November.
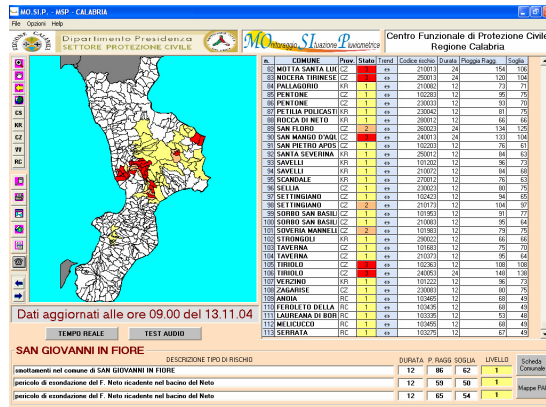
Figure 14. Rainfall overcoming situation at 09:00 of 13th November.

5. GROUND EFFECTS

The analysis of the ground effects caused by the event is based on the collection of the news reported by some local and national daily newspapers (*Pasqua and Petrucci,* 2007). Considering these information, some inspections have been made in the areas hit by the worst damages. Finally, a list of 38 municipalities was realized, in which all the risk scenario typologies were included, both for 12th and 13th November, as shown in Figure 15.
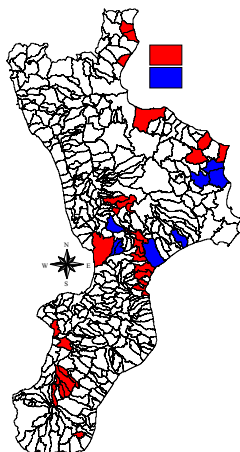
Figure 15. Municipalities affected by ground effects.

6. CONCLUSIONS

The behaviour of warning system of Calabria Region during the meteorological event between 12:00 of 12th November and 13:40 of 13th November has been analysed. The warning system marked meaningful hazard situations in 192 municipalities, of which 139 have been interested at least once by a high hazard situation and only 24 had ordinary hazard state.

The number of the municipalities for which exceeding of thresholds regarded exclusively the A risk scenario is 39. The same number regards the ones for which only B risk scenario thresholds were exceeded. Therefore, 114 municipalities have been interested by both the risk scenarios. For 38 municipalities a direct evolution from level 1 to level 3 has been recorded.

Actually has not been possible to carry out a systematic correlation between the hazard levels marked by the warning system and the real effects caused to the ground by the event. In any case, considering the collection of information regarding the damages induced by the meteorological event, it is possible to state that the system has found elevated hazard level in 30 out of the 38 municipalities for which damages were recorded (referring to both risk scenarios).

REFERENCES

Niccoli, R., G. Iiritano, S. Arcuri, A.Corina, and L. De Felice (2002), Regional warning system and operative tools for hydrologic monitoring in Calabria, Proceedings of the 1st Italian-Russian Workshop "New Trends in Hydrology", IRPI (CS), Rende (Italy).

Arcuri S., L. De Felice and G. Iiritano (2003), Software operativo per il monitoraggio del rischio idrogeologico in Calabria, Atti della VI Conferenza Italiana utenti ESRI, Sessione Ricerca & Applicazioni per l'Ambiente, Roma (Italy) *(in Italian)*.

Iiritano, G., and P. Versace (1996), Informazione pluviometrica in tempo reale e gestione dell'emergenza, Proceedings of the Workshop "La difesa dalle alluvioni", Florence (Italy) *(in Italian)*.

Iiritano, G., M.A., Longo and R. Niccoli (2002), Sul sistema di allertamento per il rischio idrogeologico della Regione Calabria: procedure operative, Proceedings of the Workshop "Conservazione dell'ambiente e rischio idrogeologico", Assisi (Italy), 513-521 *(in Italian)*.

Niccoli, R., G. Iiritano, S. Arcuri, A.C. Corina, L. De Felice and L. Marsico (2004), Il sistema di allertamento e gli strumenti operativi per il monitoraggio idrometeorologico in Calabria, Proceedings of the 1st Workshop MODECI, Cosenza (Italy), 25-36 *(in Italian)*.

Pasqua, A.A., and O. Petrucci (2007), Fenomeni di dissesto idrogeologico e danni indotti dalle piogge del novembre 2004**,** in: Rapporto dell'evento atmosferico abbattutosi sul territorio regionale nel Novembre 2004, Calabria Region, Catanzaro (Italy) *(in Italian)*.

Rossi, F., M. Fiorentino and P. Versace (1984), Two component extreme value distribution for flood frequency analysis, *Water Resour. Res., 20*(7), 847-856.

Rossi, F., and P. Versace (1982), Criteri e metodi per l'analisi statistica delle piene, Valutazione delle piene, CNR - P.F. Conservazione del suolo, n. 165, 63-130 *(in Italian)*.

Sirangelo, B. (2001), Linee guida per la determinazione delle soglie pluviometriche nei riguardi di vari tipi di rischio presenti sul territorio calabrese, *Internal Report*, Functional Centre, Calabria Region, Catanzaro (Italy) *(in Italian)*.

Observing and modelling exceptional floods and rainfalls
Proceedings of the AMHY-FRIEND International Workshop on Hydrological Extremes,
held at University of Calabria, Cosenza (Italy), May 3-4, 2006.

GREAT FLOODS IN ROMANIA IN 2005. LESSONS ON PREPAREDNESS AND PREVENTION ROLE IN FLOOD CONTROL

V. A. Stanescu, R. Drobot

National Institute of Hydrology and Water Management, Bucharest, Romania.

ABSTRACT

During 2005 very large floods occurred in Romania. The magnitude of the 2005 floods as compared with the historical ones occurred in Romania is presented. The initial meteorological conditions as well as the triggering intensive rainfalls are considered. The flood damages during 1993-2004 (about 0.8 billion of euro) as compared with 2005 (about 1.4 billion of euro) shows the greatness and aggressiveness of the floods in 2005. Their long duration along seven months with very small interruption periods outlines the stress induced in the population and the local and regional authorities. For each month, the maps of basins subject to flooding and time period when the peak discharges occurred are given in the paper. The largest floods of the year 2005 are the Banat region (especially Timis-Bega) and the Siret River basin. They are described in more detail starting with the generating rainfall, namely the isohyets maps and time distribution of them. The flood wave hydrographs are presented in the main points of confluences. To make a comparison with the recorded floods in the past the 2005 floods and the historical ones are centred at their peaks. Then the probability that is assigned to the recorded peak discharges is highlighted.

Considering the damages and the losses of lives as well as the manner in which the action for flood control have been conducted, the conclusions on the non-structural and structural measures aiming to improve the degree of preparedness, the prevention and operational intervention are highlighted in the last part of the work.

1. METEOROLOGICAL CONDITIONS

The most important meteorological peculiarity of the year 2005 was the huge amount of the precipitation fallen especially during the period April-October but also in January-March. As compared with the average annual amount of precipitation during the period 1961-1990, that is 647 mm, the total amount of precipitation in 2005 was 866.5 mm. In August the highest percentage of 124.2% over the average has been recorded. Important deviation from the average precipitation have been noticed in April (45.1%), July (46.3%) and September (90.4%). Important mention is made that the great quantities of rainfalls have been occurred during relatively short period of time, often preceded by prior rainy periods that brought the soil moisture near to saturation, thus favouring the production of heavy floods. In some areas, the effects of intense cumulonimbus vertically developed in the frame of a generalized rainfall event over large area led to the production of rainstorms, which resulted in outstanding flash floods over small catchments.
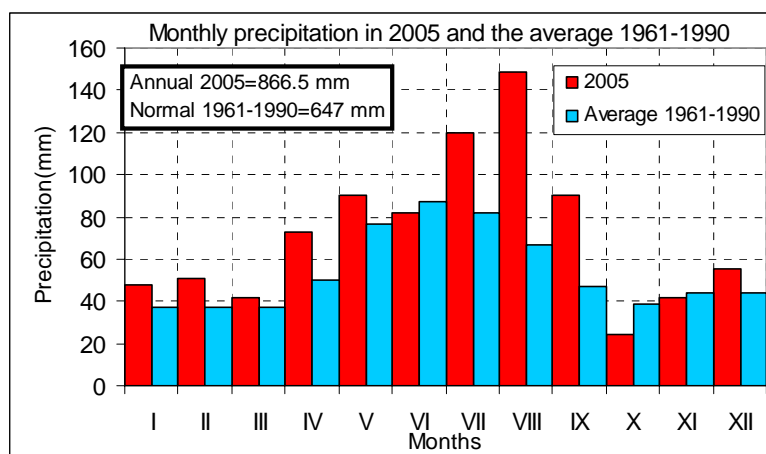
Figure 1. Monthly precipitation in 2005 and the normal amounts (after ANM-Romania).

In April, at 12 meteorological stations in Banat physiographic zone the normal value has been exceeded, at some of them the recorded amounts exceeded 200 mm. The great part of the rainfall amounts were recorded in a three short intervals in the second decade of the month. The rainfalls in May have been concentrated particularly in the southern part of the territory and heavy and intense rainfalls exceeded 100 mm at many stations from the Upper Olt, Arges and Ialomita-Prahova-Teleajen River basins.

The rainiest month was July when the outstanding quantities have been concentrated in a couple of days. Thus, in the Jiu, Lower Olt and Vedea River basins the amounts of the rainstorms exceeded 100 mm in less than 48 hours. In Table 1 the maximum rainfalls recorded at some pluviometric stations in 72 hours in the Jiu and Lower Olt River basins are presented. Also in Table 2 the maximum 48 hour rainfall in Vedea River basin are shown. In Siret River basin the rainfalls had impressive amounts, the highest ones exceeding 200 mm in 48 hours produced around large areas (a couple of thousands square kilometres).

JIU RIVER BASIN				LOWER OLT RIVER BASIN*			
River	**Station**	**Rainfall (mm)**	**Remarks**	**River**	**Station**	**Rainfall (mm)**	**Remarks**
Jiu	Rovinari	162	159 mm/48 hours	Cungrea	Căzănești	95	66.5 mm/48 hours
Jiu	Filiași	114	104 mm/48 hours	Teslui	Corbu	157	130 mm/48 hours
Jiu	Podari	108	104 mm/48 hours	Beica	Pleşoiu	131	
Bistriţa	Teleşti	139	136 mm/48 hours	Olteţ	Oteteliş	94	
Amaradia	Negoeşti	111		Mamu	Strejeşti	62	
Amaradia	Albeşti	146		Olt	Slatina	158	
Raznic	Breasta	156		*(*) 2nd July rainstorm in Inorog River basin at Maruntei station = 55mm/2 hours*			

Table 1. 72-hour rainfall from 6:00 of 1st to 6:00 of 4th July 2005 in southern zone of Romania.

In the hydrographical space Dobrogea at Casimcea station 73 mm of rainstorm from 6:00 to 9:00 of 3rd July 2005 have been recorded.

Consistent rainfalls have been also recorded from 3rd to 5th August (48 hours) in the catchments of Crisuri and Barcau Rivers, where the maximum amounts exceeded 70 mm. In the Jiu River basin located in the southern area of Romania (area about 10000 km^2),

between 4th and 6th August (48 hours) up to 100 mm has been recorded. Successively other 20÷30 mm has been added in the next two days.

River	Station	48-hour rainfall (mm)	Remarks
Vedea	Buzeşti	195	164 mm in 24 hours
Vedea	Văleni	218	168 mm in 24 hours (*)
Vedea	Videle	145	---
Vedea	Alexandria	121	100 mm in 24 hours
Cotmeana	Ciobani	183	160 mm in 24 hours (**)
Teleorman	Tătărăşti	156	130 mm in 24 hours
V. Câinelui	Vârtoapele	120	86 mm in 24 hours
Neajlov	Călugăreni	143	---

(*) Other remarkable rainfall intensity: 80 mm / 5 hours on 2nd July.
(**) Other remarkable rainfall intensity: 74 mm / 4 hours on 2nd July.

Table 2. 48-hour rainfalls from 6:00 of 2nd to 6:00 of 4th August in southern zone of Romania.

In Upper Olt River basin, from 5th to 9th August (96 hours) the maximum amounts ranged between 75÷115 while in Arges and Ialomita River basins in 72 hours (from 5th to 8th August) the maximum amounts ranged regularly between 80÷120 mm and locally exceeded 140 mm. In September heavy rains fell again over the southern area of the country in the Jiu, Arges, Ialomita, Vedea River basins. The quantities recorded between 19th and 25th of September at most representative stations are presented in the Table 3.

2. GENERAL CHARACTERIZATION OF THE FLOODS OCCURRED IN ROMANIA IN 2005

The year 2005 was one of the years with heavy floods in Romania. First, almost all of the territory of the country has been affected by flooding and second, these floods covered a long period of time from April to October. As compared with other rainy years in the past, the year 2005 shows often historical magnitudes of the peak discharges. Thus, as seen in Figure 2, the peak discharge of Siret River (basin area 42890 km^2) in 2005 has the maximum magnitude ever recorded, but also in the river basins from the southern part of the country the flood wave peaks, even if not the highest, are among the greatest historical ones. Quantitatively:

- at the meteorological stations Bucharest-Filaret: 264 mm, Mangalia: 254 mm, Bucharest Afumati: 264 mm, Sinaia: 247 mm, Bucharest-Baneasa: 229 mm, Ploiesti: 197 mm, Campina: 174 mm, Campulung: 156 mm;
- at Mangalia meteo station have been recorded 131 mm in about 3 hours;
- at Biruinta station have been recorded 155 mm in 3 hours.

Also, that is to be highlighted the fact that the 2005 flooding events occurred all around the territory of Romania, even if the flood peaks in the northern and central parts of the country have not reached historical magnitudes but they brought about important damages and lost of human lives. Moreover, apart from the regional flooding occurred on large and medium sized rivers, the flash floods produced in small basins accompanied by numerous terrain landslides completed the suite of disasters that stroke Romania in 2005.

The levels characterizing different stages of flooding event were exceeded during long periods of the months, when the floods occurred. These stages of flooding events are:

- Alarm level (AL), which shows the level above which a flooding is possible and therefore at this level the first preparative measures for flood defence must to be taken;
- Flooding level (FL), which shows the first steps of flooding over the river banks;
- Peril level (PL), which means a generalization of the inundation in the flooding prone areas, along the river course.

No.	River	Station	6:00 of 19th - 6:00 of 25th rainfall (mm)	No.	River	Station	6:00 of 19th - 6:00 of 25th rainfall (mm)
1	Arges	Cateasca	143	32	Badeni	Badeni	178
2	Arges	M. Spart	203	33	Colentina	Colacu	174
3	Arges	Gradinari	181	34	Ialomita	Moroieni	194
4	Arges	Budesti	183	35	Ialomita	Targoviste	175
5	Valsan	Bradet	96	36	Ialomita	Baleni	183
6	Valsan	Malureni	182	37	Ialomita	Silistea Sn.	221
7	R. Doamnei	B. Rusului	102	38	Ialomita	Cosereni	173
8	R. Doamnei	Darmanesti	189	39	Ialomicioara	Fieni	175
9	R. Doamnei	Ciumesti	177	40	Cricov D	Baltita	180
10	Bratia	Rausor	144	41	Prahova	Busteni	190
11	Bratia	Balilesti	161	42	Prahova	Campina	162
12	Rausor	Rausor	143	43	Prahova	Prahova	160
13	R. Targului	Voina	114	44	Prahova	Adancata	201
14	R. Targului	Voinesti	170	45	Doftana	Tesila	189
15	R. Targului	Piscani	203	46	Teleajen	G. Vitioarei	193
16	Argesel	Namaesti	144	47	Teleajen	M. Domn.	165
17	Argesel	Vulturesti	169	48	Jiu	Rovinari	128
18	Argesel	Mioveni	203	49	Jiu	Racari	154
19	Carcinov	Priboieni	152	50	Jales	Stolojani	123
20	Neajlov	V. Lat	201	51	Bistrita	Telesti	164
21	Neajlov	Calugareni	209	52	Gilort	Carbunesti	110
22	Dambovnic	Slobozia	127	53	Motru	Brosteni	125
23	Glavacioc	Crovu	131	54	Cosustea	Sisesti	113
24	Sabar	Poienari	190	55	Amaradia	Negoiesti	187
25	Sabar	Vidra	239	56	Bistrita	Genuneni	118
26	Potop	G. Foii	139	57	Topolog	Milcoiu	118
27	Dambovita	M. cu Flori	199	58	Luncavat	Otesani	107
28	Dambovita	Lunguletu	203	59	Pesceana	Zlatarei	115
29	Dambovita	Dragomiresti	211	60	Cungrea	Cazanesti	113
30	Dambovita	Budesti	145	61	Oltet	Otetelis	97
31	Rausor	Rucar	117	62	Iminog	Maruntei	137

Table 3. Rainfall recorded from 19th to 25th September 2005 in southern area of Romania (Arges, Ialomita-Prahova, Jiu and Lower Olt River basins).

It is worth to note that during a flooding event in a catchment all three characteristic levels can be found at different stations according to the manner of flood formation and routing of the floods along the tributaries and the main course.

Thus, a large coverage of the Romanian territory doubled of a long period of time of exceeding the flood characteristic levels constitute the main characteristics of 2005 flood

events. To highlight the ampleness and long-stressing duration of the floods in 2005, in the Figure 3 the coverage of the territory of Romania as well as the period of time when the flood characteristic levels have been reached are presented. Mention is made that the periods do not represent the duration of the flooding, which is much longer, but only the span of time when the exceedance of the AL, FL, or PL have been recorded. In the Figure 3 the interval of exceeding the flood characteristic levels in each month is also presented. Also, for each river basin affected by inundation, the variation range of the characteristic levels (alarm level, flooding level and peril level) is presented. Another peculiarity of the flooding events in Romania in 2005 is the repetition of flooding in some river basins during different months.
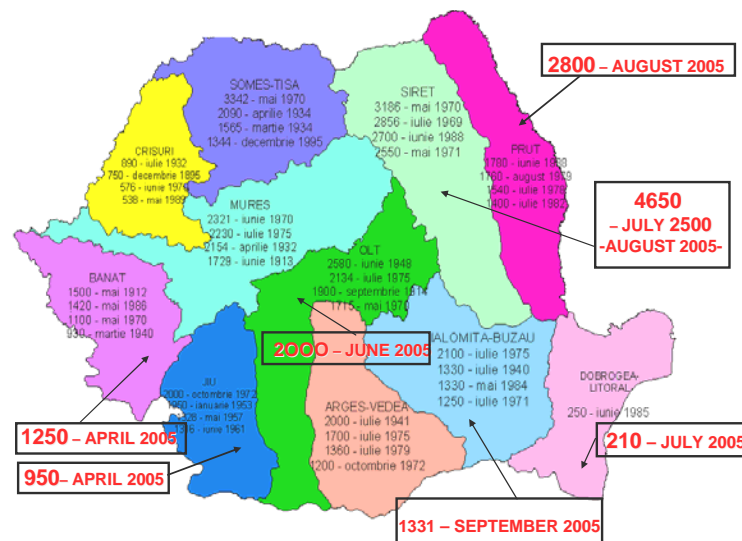
Figure 2. Historical flood peaks as compared with the floods in 2005
(*processed after National Administration "Romanian Waters*).

Thus, as one can see in Figure 3 more than once, the following major river catchments with significant basin areas and developed flood plains have been affected by flooding, namely: Vedea (5430 km^2, in June and July), Upper and middle Olt (14000 km^2, in April, May, July, August and September), Lower Olt (August and June), Arges-Ialomita-Prahova-Teleajen (22900 km^2, in May, June, July, August and September), Buzau (5264 km^2, in Mai, July, and September), CrisAlb-Cris Negru, Beretau (14860 km^2, in April, May, July and August), and Bahlui-Barlad (7220 km^2, in April, and August). The flood occurred in Ialomita River Basin in September was the second one as magnitude after that produced in July 1975, the April- flood in Timis-Bega River was also the third one, while the July- flood in Siret River basin was the first one in the historical series of peak discharges.

To make a comparison of the 2005 flood on different rivers in terms of the frequency (estimated by the statistical analysis of the series) the peak discharges corresponding to the recorded water stages above the peril levels have been considered.

The peak discharges recorded during the months with significant floods in 2005, at the gauging stations where the maximum water stages were above the peril levels (PL), have been plotted against the maximum discharges of different probabilities of exceedance, namely, 1% (once in 100 years), 2% (50 years), 5% (20 years), and 10% (10 years). The points placed at the right side of the 45° line (Figures 4) indicate the stations where the probability of exceedance is less than that is considered for all the stations which have

been deemed. It is noteworthy to observe in Figure 4a that in 10 stations (found at the right side of 45° line) the probability of the peak discharge was 1% or near this figure, while in Figure 4d all points (meaning the stations where the peak water stages were above the PL) are at the right side for the probability of 10%. Thus, in summer 2005 the floods had at least the 1/10 years frequency and many of them the frequency was even rarer (10 stations around 1/100 years, 20 stations around 1/50 years and less, 28 stations around 1/20 years and less) and 47 stations around 1/20 years and less. Some flash floods produced in small catchments had peak flows of very rare frequency.

Thus, the catastrophic flash floods occurred in September on Fernic River (189 km²) or on Cartal and Ramnic River basins had a frequency situated around 1/200 year and 1/300 year. Mention is made that the stations covered a large area (about 120000 km²) of Romania (237500 km²), namely all the southern, eastern and south-western parts of the country. Romania has long embankments of the river courses. The first dykes have been built ever since old times in the end of XVIII century. Nowadays, there are 18240 km of dykes and river course trainings, 1490 diversion works, over 400 significant water storages (permanent and non-permanent reservoirs) with 3700 billion m³, 1298 protected localities, 6100 roads and railways, 3100 socio-economic objectives and a protected area of 2.13 million ha.

In Figure 5 the situation of flood protection of the localities of Romania is presented.

Notwithstanding this capacity of protection, the 2005 floods brought about very great damages, particularly due to numerous ruptures of the dykes.

Due to the long period of stationing the high waters above the river banks, in the embanked sectors, failure of the dykes has been occurred, especially in Banat hydrographical area and in Siret River basin. These dyke ruptures brought about high damages, which probably would have been lesser in the absence of the dykes.

The total damages estimated in the period 1993-2004 were 29581 billion old ROL (about 0.8 billion of euro). If compared to the 50000 billion old ROL (about 1.4 billion of euro) produced only in 2005, the greatness and aggressiveness of the floods in the summer-autumn 2005 becomes clear. Yet, 76 losses of human lives have been reported.

In Figure 6 the total flood damages during the period 1992-2004 as compared with 2005 flood damages are presented. In 2005, 416995 ha have been flooded, 60828 homesteads affected, 4666.6 km of roads and 3244 bridges were damaged.

These immense damages, the high magnitude of floods with peak discharges exceeding frequencies rarer than 1/10 year and even 1/100 years, the territorial extension of them around almost all the country and the very long flood duration along seven months with very small interruption periods, outline the stress induced by these hazards in the affected population and the local and regional authorities.

Among the heaviest floods which have stricken Romania in 2005, those recorded in Timis-Bega River basin and in Siret River basin are noteworthy to be analyzed in more detail. First, these floods provoked the highest damages both due to high flooding water depths over very large areas and the long duration of the water that stagnated in the inundated zones. The long stagnation of waters in the flooded zones has been also the effect of a series of sequences of rainfalls which generates successive flood waves with very large volumes. For example, Timis River at the downstream station Sag (border of Romania with Serbia and Montenegro, see Figure 8) has a volume of 720 million m³ while the volumes of floods having similar peaks, which occurred in 1966 and 2000, had a volume representing about a third part of it.
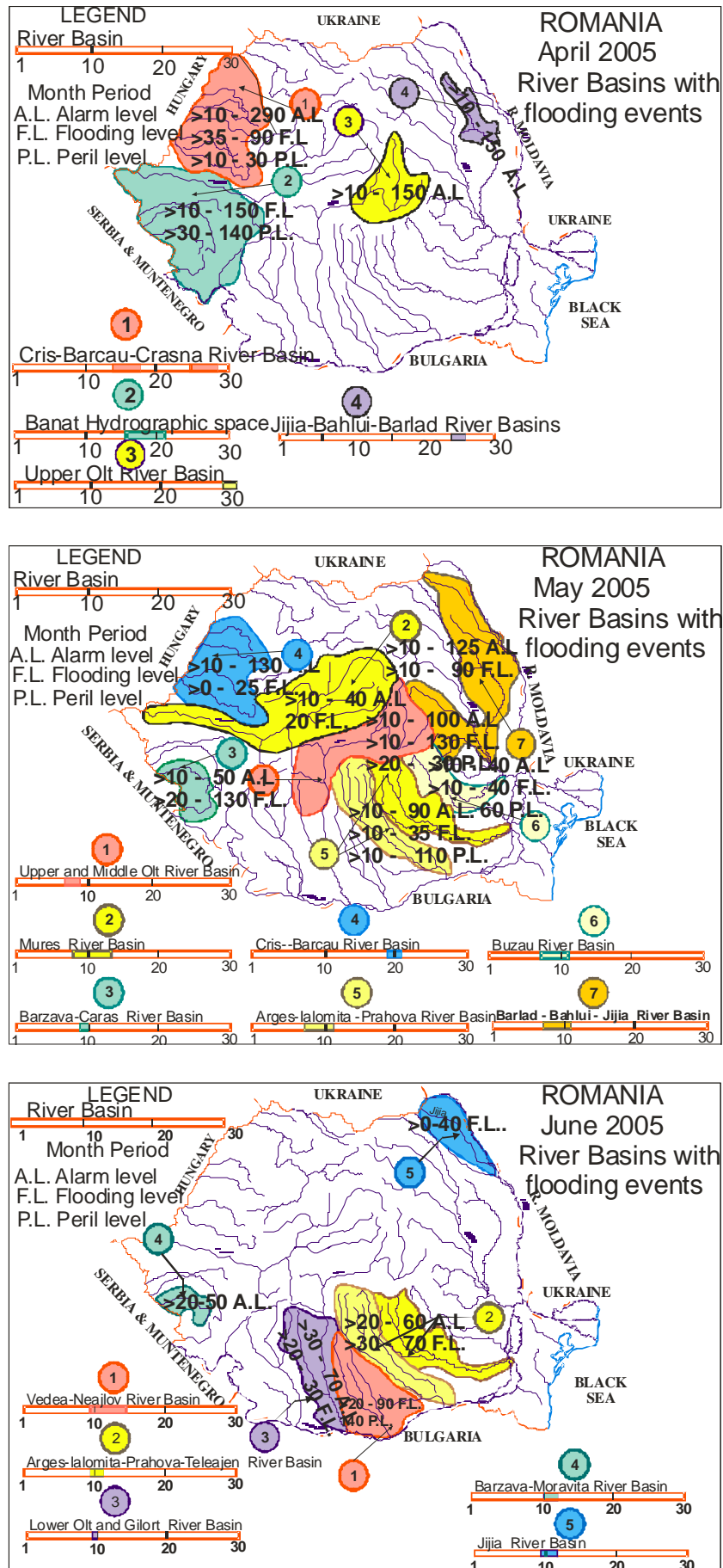
Figure 3a. Spatial distribution of the flood characteristic levels from April to June 2005.
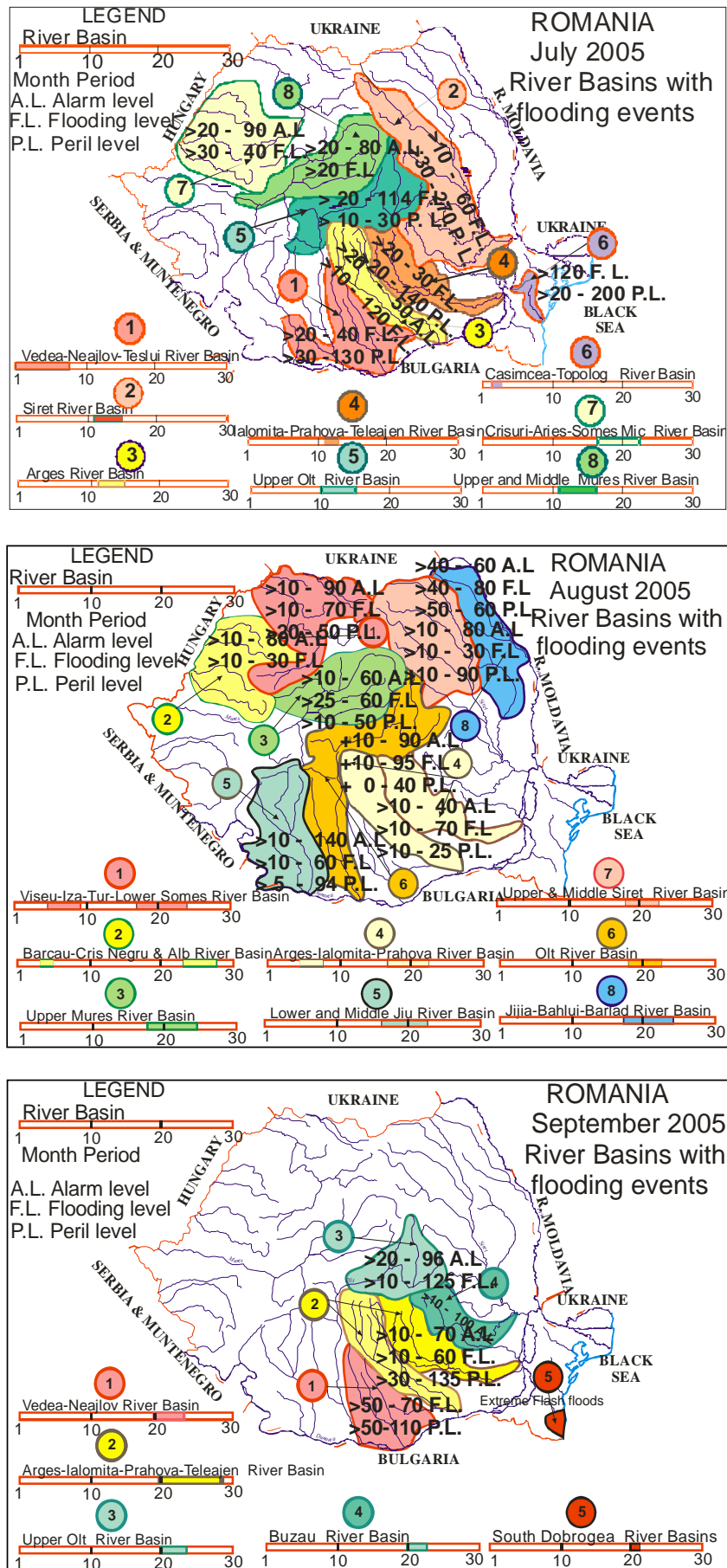
Figure 3b. Spatial distribution of the flood characteristic levels from July to September 2005.
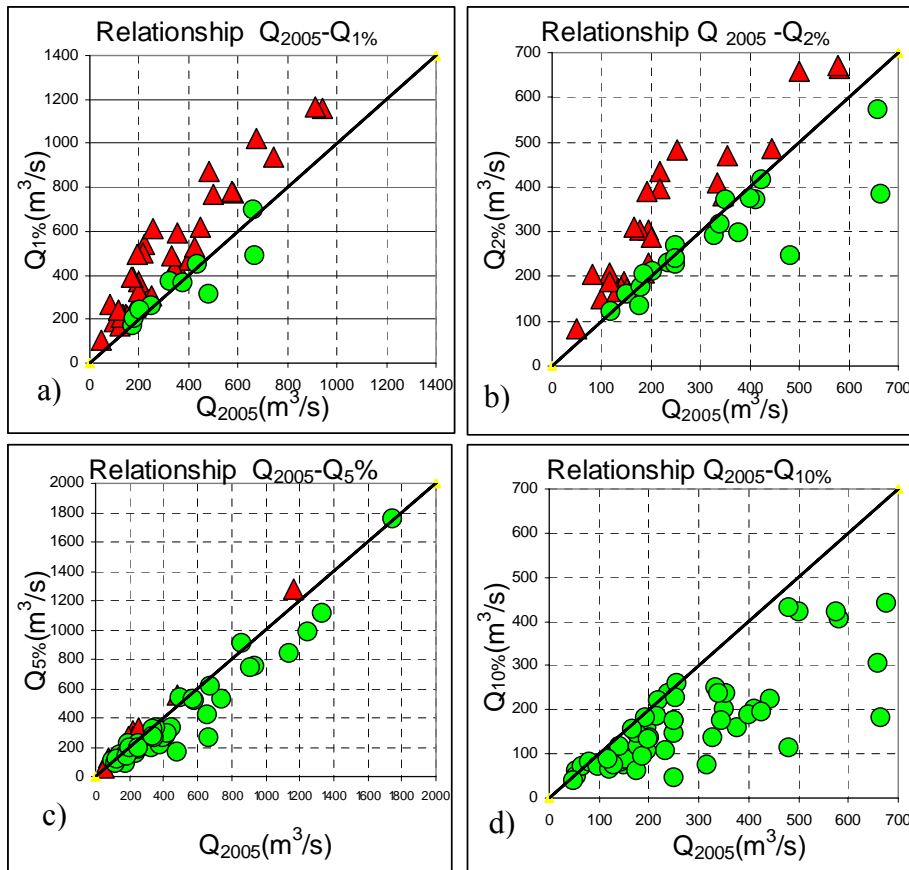
Figure 4. Peak flows in 2005 flooding events compared with those of different probabilities.
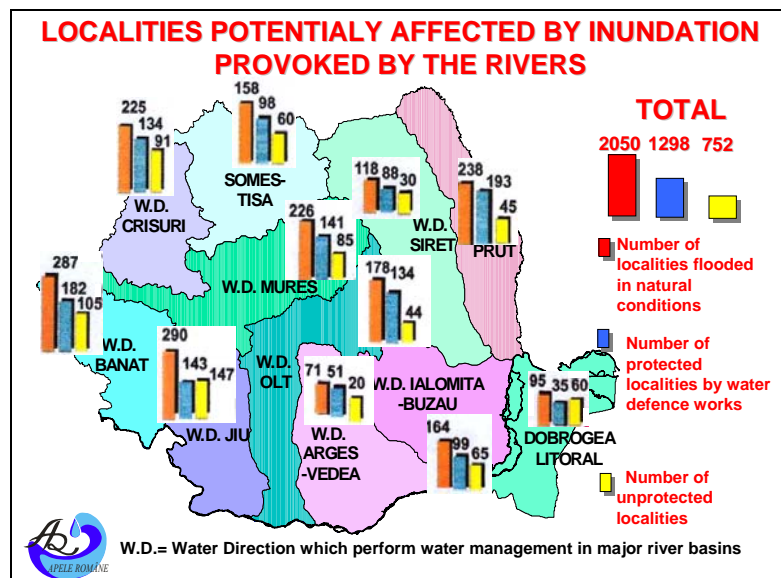
Figure 5. Protected and flood prone localities in Romania.
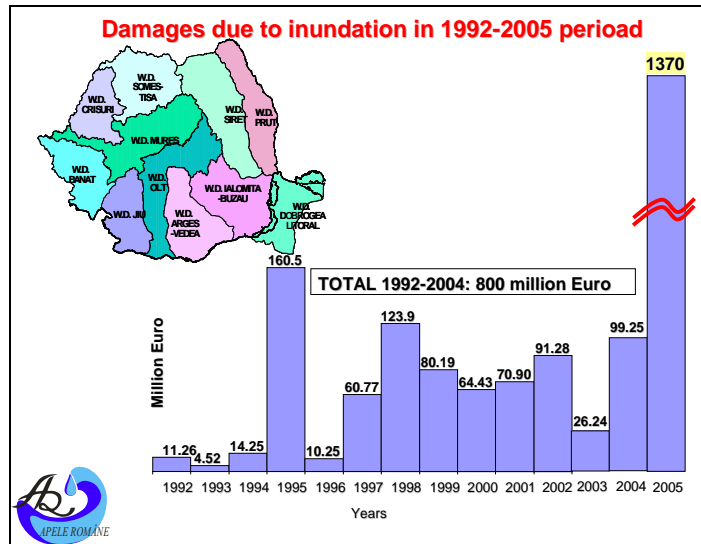
Figure 6. Flood damages during the period 1992-2005 (*processed after ANAR-Romania*).

3. THE FLOOD OF TIMIS-BEGA RIVER BASIN

As it can be seen from Figure 7, the flood of Timis-Bega River basin (7363 km[2]) has been provoked by a succession of three intense rainy periods from 14th to 22nd April. These intense rainfall periods were separated by intervals without precipitation ranging between 30-45 hours in the period 16th-17th April and 9-15 hours in 21st April 2005.

The nucleus of the rainfalls in the zones of flood formation ranged between 15-24 hours. The greatest amount of precipitation has fallen in the period 18th-22nd April. It is to note that in the period preceding the start of triggering rainfalls, a sudden warming has occurred, contributing to the snowmelt and therefore increasing the soil moisture with an equivalent that ranged between 25÷40 mm.
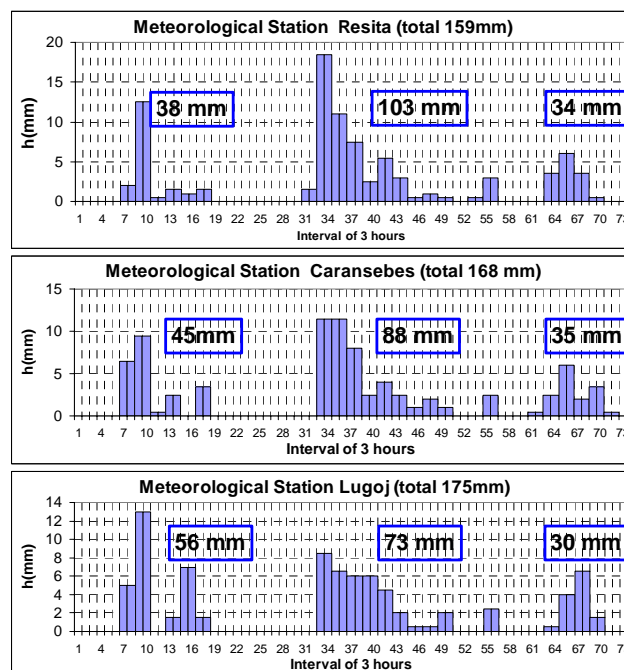
Figure 7. Time distribution of rainfall in Timis-Bega catchment.

In the mountainous part of the basin, the rainfall amounts, although significant, did not exceed 100-120 mm, while in the hilly areas located in the central zone of the catchment the total rainfall quantities exceeded 220 mm. Figure 8 shows the map of isohyets of total rainfall.

In the history of the great floods in this basin, those occurred in 1859, 1912, 1966, 2000 and 2005, which brought about inundation over large areas, were recorded (Figure 9). Some representative flood wave hydrographs along the main course of Timis River and Bega River (the main tributary of Timis River) are presented in Figure 10.

Similarly as that produced in 2000, the flood that occurred in April 2005 has been formed over entire catchment and all the contributions from tributaries led to a peak of 2% probability in the downstream sectors. For comparison, in Table 4 the peak discharges in 2005 and 2000 as compared maximum discharge of 1% probability are presented.

River	Station	Area (km^2)	Mean altitude H(m)	Q_{2000} (m^3/s)	Q_{2005} (m^3/s)	$Q_{1\%}$ (m^3/s)
Timis	Sadova	560	936	328	276	446
Timis	Caransebes	1072	765	441	425	650
Timis	Lugoj	2706	766	1246	1135	1225
Timis	Brod	5292	569	1200	1290	1451
Timis	Sag	6118	424	1100	1083	1425
Bega	Balint	1064	335	283	252	346
Bega	Chizatau	1660	278	352	346	482

Table 4. Comparative peak discharges in 2000, 2005 and Q_{max} of 1% probability.
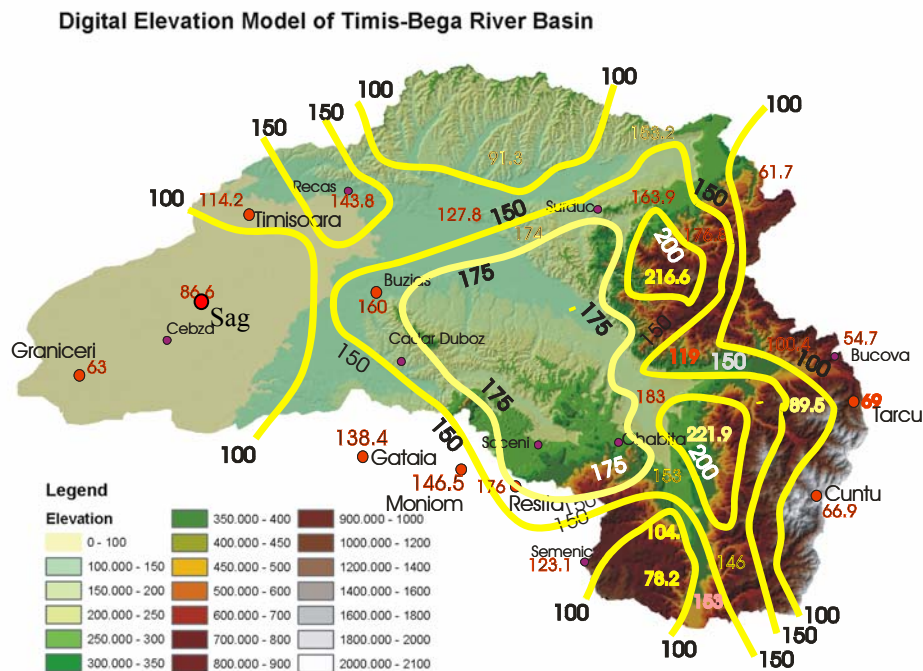
Figure 8. Total precipitation isohyets in the period 14th-22nd April 2005.
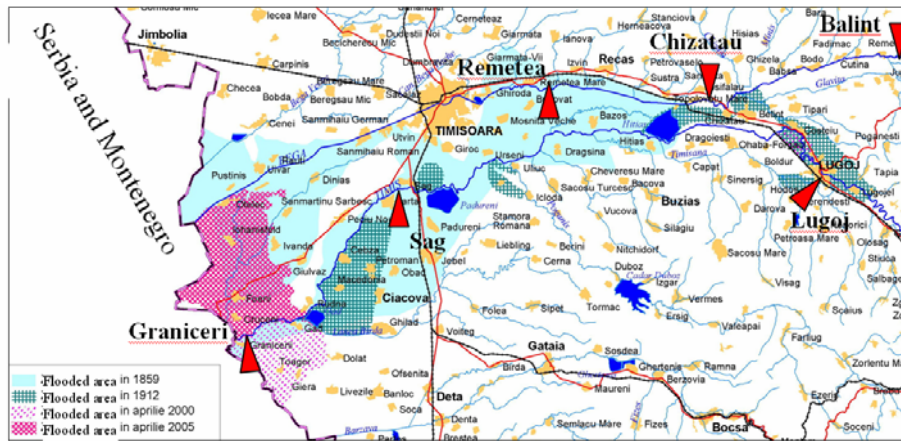
Figure 9. Areas flooded by the historical floods.
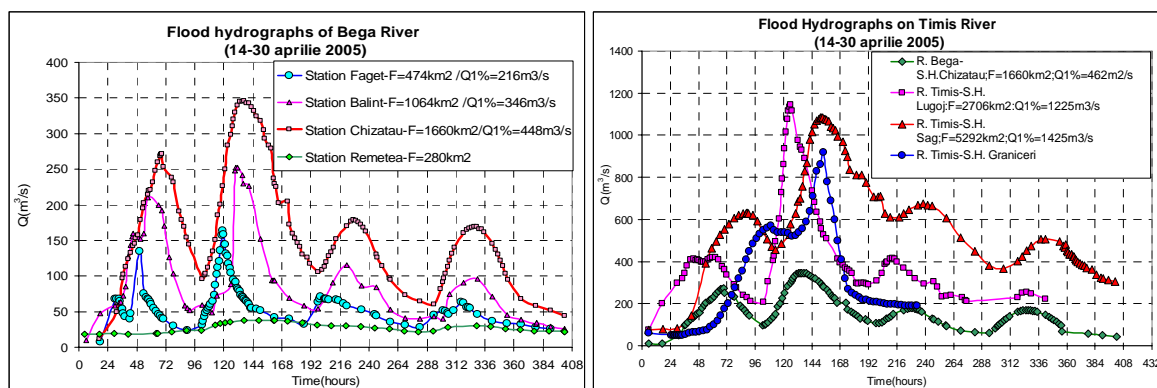
Figure 10. The hydrographs of Timis and Bega Rivers in April 2005.

For comparing the historical floods, these ones were overlapped by centring the peaks (Figure 11). Under the circumstances of the high levels of water in the embankment zone, from km 2 of the dyke, the dyke has ceased and a series of major ruptures have been produced, the water invaded the flood plain and formed an inundated area of about 30000 ha, where the depths reached over 2 m.
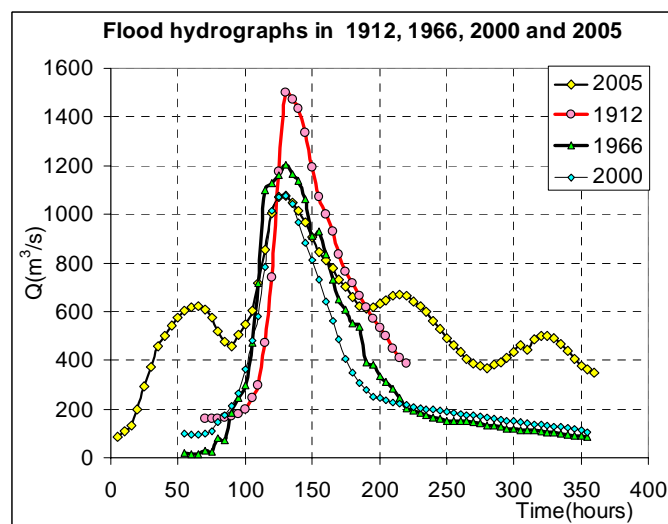
Figure 11. Overlapped historical floods.

Four villages completely flooded, 3644 homesteads and 2344 distressed people were the main damages. The reconstruction of the hydrograph in the section of the dyke rupture has been accomplished making use of a routing model. The volume of water spilled over the dyke rupture into the flooded area was of about 300 million m³ which has been drained both by pumps and gravitational (during more than one month).

4. THE FLOOD OF SIRET RIVER BASIN

The flood of Siret River basin has been provoked by a very intense rainfall distributed mainly over the middle and lower area of the catchment. The time distribution of the 2-day rainfall during 12nd-13rd July (Figure 12) shows a concentration in the first part of the interval. The total amount during the rainy period 10th-14th July reached over a large area more than 200 mm as seen in Figure 13.
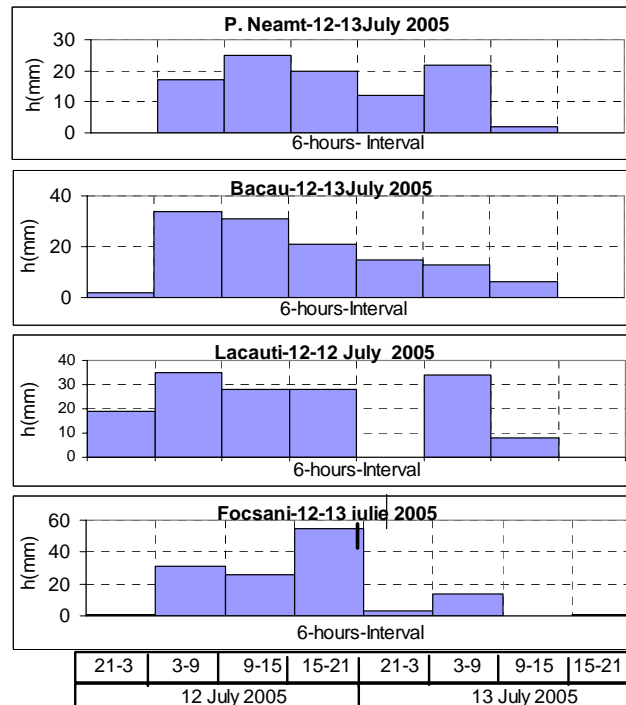
Figure 12. Time distribution of rainfall

Consequently to the isohyets map, that shows the distribution of the huge amounts of rainfall in the middle and downstream part of the basin, an outstanding flood peak was recorded in the downstream sector of Siret River at Lungoci station. The areas which provided greater contribution were Bistrita, Trotus and Putna Rivers. In these catchments (especially Trotus River basin) the flood peaks reached 1% probability and even less (Vranceni and Onesti stations). The upper sector of Siret River was not affected by significant flood. For example, at Dragesti station having a basin area of 11811 km² (as compared with that corresponding to Lungoci station that is 36036 km²), the peak discharge was 330 m³/s while the maximum discharge of 10% probability is 1375 m³/s.

Notwithstanding the weak inflow of the upper zone of the Siret basin, as a result of the composition of the floods occurred in the middle and downstream areas the maximum discharge at Lungoci station had a probability of 0.5% (frequency of 1/200 years).

The greatest historical floods of Siret River basin have been recorded in the years 1965, 1970, 1991 and 2005. For comparing the historical floods, these ones were overlapped by centring the peaks (Figure 14).

The Siret River flood brought about huge damages. Three villages have been completely destroyed while many others were partially flooded and road and railway infrastructures were heavily affected.

As a result of the major floods in 2005, a National Strategy of risk management on long term for enforcing the system of the hydraulic buildings for flood defence (prevention measures) as well as for improving the non-structural measures (preparedness and operational intervention) will be carried out. This will comprise the elaboration of the methodologies for hazard and risk maps, the methodology for assessing the flood damages and of the zones which should be inundated under control, guides for improving the awareness of the population coping with floods and feasibility studies and projects for developing the constructions aimed to make more efficient the flood control.

5. SHORT COMMENTS ON LESSONS OF THE 2005 FLOODS IN ROMANIA

Considering the damages and the losses of lives as well as the manner in which the action for flood control have been conducted, the conclusions on the non-structural and structural measures aiming to improve the degree of preparedness, the prevention and operational intervention are highlighted.
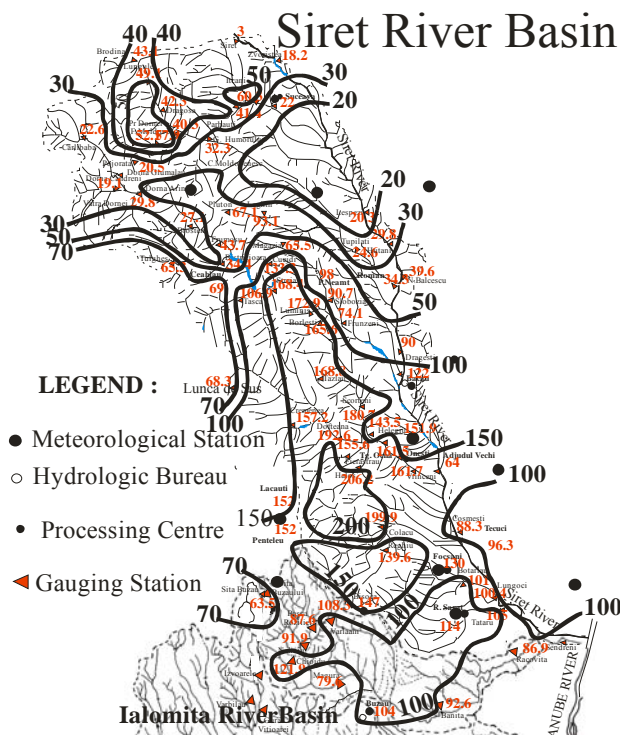
Figure 13. Isohyets of 12th-13th July 2005.
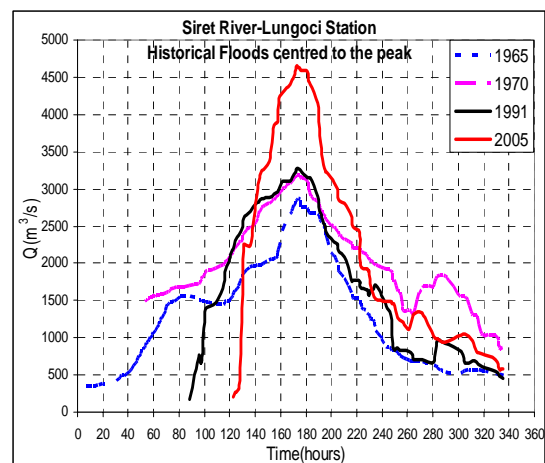
Figure 14. Overlapped historical floods.

Starting from the principle "more space for rivers" the many proposals for enhancing the actions of building non-permanent storages or "fusible dykes" on the tributaries and for enlarging the distance between dykes and the river bank were considered.

Compartmentalizing the embankments and building ring-shaped embankments around the localities are also foreseen.

The non-structural measures which are complementary to the structural ones have been also proposed. Among them, the role of flood forecast, expressed in terms of probability (Bayesian approach) and referred not only to the maximum peaks but equally to the volume and the shape of flood wave and the enhancement of the systems of dissemination, alarm and decision making for trigger actions have been highlighted.

The use of hydrologic/hydraulic models and GIS systems for assessing the multiple hydrological and meteorological scenarios of flood formation and routing, considering also embankment and dam failures, is to be considered in a national plan for flood control.

N	River	Station	Basin area (km^2)	Mean altitude (m)	Q_{2005} (m^3/s)	$Q_{0.5\%}$ (m^3/s)	$Q_{1\%}$ (m^3/s)	$Q_{2\%}$ (m^3/s)	$Q_{5\%}$ (m^3/s)	$Q_{10\%}$ (m^3/s)
1	Siret	Drăgeşti	11811	525	330	3060	2650	2485	1755	1375
2	Siret	Adjudul Vechi	20355	662	1637	4110	3205	2864	2157	1715
3	Siret	Lungoci	36036	539	4650	4510	3950	3425	2755	2220
4	Bistriţa	Bacau	3014	662	1150	1600	1300	1047	741	572
5	Trotuş	Vrânceni	4077	734	2800	2920	2500	2120	1670	1340
6	Trotuş	Tg. Ocna	2084	924	1260	1385	1200	1025	795	625
7	Trotuş	Onesti	2826	830	1680	1612	1397	1193	926	728
8	Putna	Boţârlău	2518	554	1323	2090	1790	1500	1130	855
9	Oituz	Fierastrau	263	810	378	435	370	300	220	160
10	Tazlau	Lucacesti	123	801	425	655	545	430	300	210
11	Putna	Colacu	1100	921	1510	1926	1650	1415	1190	898
12	Putna	Botarlau	2518	554	1323	2090	1790	1500	1130	855
13	Milcov	Golesti	395	410	600	920	780	670	525	420
14	Buzău	Racoviţa	5238	530	610	2805	2375	1945	1425	1035

Table 5. Comparative peak discharges in 2005 and Q_{max} of different probabilities.

These scenarios are to be specifically considered in the plans of operational measures which should be conceived as depending on the magnitude of floods and their peculiarities of time and space evolution.

REFERENCES

INHGA (2004), *Life-Timis: Protection of the River Life by Mitigation of Flood Damages*, European Commission, Directorate Environment, Direction LIFE-LIFE00ENV/RO/000986, 2000-2004.

Ministry of Environment and Water Management (2005), Analysis of the activities developed in 2005 for the management of the emergency situation generated by floods and the strategy for 2006 (*published on the internet site*).

Stanescu, V. Al., and R. Drobot (2005), The flood that took place between 14th and 30th of April 2005 in the hydrographical basin of Timis-Bega (in Romanian). *Hidrotehnica*, 7-8.

Stănescu, V.Al., and R. Drobot (2002), *Măsuri nestructurale de gestiune a inundaţiilor* (Non-structural measures for flood management), Editura H*G*A, Bucureşti (in Romanian).

THE DESTRUCTION OF THE BRIDGE OVER THE ZILIANA STREAM (GREECE) ON THE 28TH NOVEMBER 1998

M. Vafiadis, N. Efthymiou

Division of Hydraulics and Environmental Engineering, Department of Civil Engineering
Aristotle University of Thessaloniki, Greece.

ABSTRACT

In this paper are presented the facts and the research for causes and explications concerning the destruction of the bridge over the Ziliana Stream (Greece), at the 410.5 km of the National Road Athens-Thessaloniki on the 28th November 1998. This destruction is due to scouring of the abutments under a combination of adverse and mostly unforeseen circumstances.

1. INTRODUCTION

On the 28th November 1998, while for many days ugly meteorological conditions in the region of Platamonas Pieria prevailed, the bridge over the Ziliana Stream, at the 410.5 km position of the "New Athens/Thessaloniki Motorway", collapsed near the tolls station of Platamonas. The failure was expressed with the creation of big hole in the paving, just in front of a heavy lorry vehicle, that had just the time to stop by applying the brakes. In a few hours the destruction of the bridge was complete, causing the provisional break of the main communication way between Athens and Thessaloniki. Upstream and downstream of the bridge that collapsed, two new bridges were under construction for the Motorway (Figure 1).

More specifically, the end section of the Ziliana bridge, to Skotina side, on the New Athens-Thessaloniki Motorway was destroyed. This section of the bridge included a cantilever bridge with joists of variable cross-section, on two piers, of a total length of 25.00 m, a plate bridge of a length of 8.80 m and between these a transient embankment, of a length of 9.80 m, that was retained across with two retaining walls.

The collapse began little before the noon of 28th November 1998, during particularly high intense rainfalls, that had begun in the region many days before and which caused problems in many streams and damages in many technical works. The structures of the Ziliana bridge under examination had an age of the order of the 35÷40 years.

This work presents the results of the expertise and the relative research done in order to shed light on the true causes of this disaster. The destruction of the bridge happened because of the scouring at the foundations of the abutments and the retaining walls of the bridge, under a combination of unfavourable and mainly unanticipated conditions.

Figure 1. The Ziliana bridge afterwards the destruction. The circulation has been diverted on the new bridge of the right lane of the motorway Athens–Thessaloniki.

2. THE STATIC SYSTEM OF THE BRIDGE

The extreme right section of the bridge that collapsed, as for the watercourse, was composed by the following static components: a cantilever set of joists of variable cross-section with curved lower surface, connected with the plate of the deck. The central free opening was about 15 m large and the levers at both sides had openings of 5 m with a total length of the structure of 25 m.

Next to that, a landfill confined by retaining walls 9.80 m long is followed by a plate covered bridge-culvert with abutments formed by walls and a deck in form of a plate of reinforced concrete. It should be marked that this structure was open on the lower side, rendering the structure particularly vulnerable against potential scouring (Figure 2).
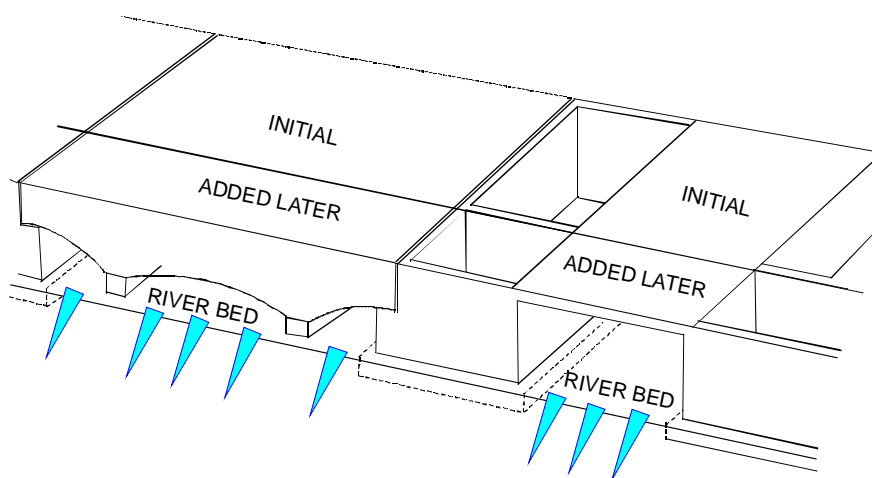

Figure 2. Sketch of the Ziliana bridge as it was before the destruction.

The destruction revealed that the bridge had been enlarged in width after its initial construction. The new part has been built in contact with the existing initial part. No document of this project is anymore available.

According to the contemporary knowledge and engineering practice these bridging structures of the Ziliana Stream would be characterized technically unacceptable. The solution that was applied, obviously for reasons of economy, the two bridges in outmost the watercourse with the completion of the middle interval with embankment interrupted, by small culverts, is judged without fail extraordinary and precarious.

3. HYDRAULIC AND HYDROLOGIC ANALYSIS

The Ziliana Stream constitutes a characteristic case of Greek winter ephemeral stream. It has a watershed about 150 km² large, with longest hydraulic path of a length of roughly 25 km, high altitudes and bents in his mountainous part, which determines a time of concentration of the order of the 2÷3 hours. Because of this relatively small time of concentration, on one side the danger for creation of flooding events is exceptionally increased, because the high rainfall has short durations, and on the other side it is impossible to appreciate the peak of the flood from only daily data.

The request for previous studies resulted only in a brief study of the contractor company for the new works, where however it is not reported expressly what is obtained from measurements and what constitutes simple estimates. The problem concerning the extent and reliability of the hydrologic studies for common technical works is the rule in Greece, due to the combination of insufficient regulation on the development of such studies, the restricted number of good available data, and the practice of simplified methodologies of calculation because of the lack of data.

The search for rainfall data in the services, which were likely to have them, resulted in very few exploitable data. Moreover, in order one to be able to argue and compare the faculty of the old structures to channel the flooding flows under the conditions that prevailed before and during their destruction on the 28th November 1998, the following elements would be known, that however it is not possible to be estimated afterwards the flood by inspection of the stream:
- the real profile and plane geometry of the Ziliana Stream, that constitutes the base for the choice, study and dimensioning of the old structures;
- the eventual gradual change of characteristics of the Ziliana Stream during the last 30 years, due to natural erosion or to illegal excavations upstream and downstream of the bridges;
- the probable previous scouring or excavation at the place of the old bridge;
- the condition of the levees and the watercourse of Ziliana Stream before the 28th November 1998 and the actual stream flow on that date.
  According to the available information:
- all involved institutions had have knowledge and had expressed it in various documents the facts that: a) the stream could present unexpected high flood flows; b) the insufficiencies of the old structures; c) the inevitable deterioration of these structures discharge capacity due to the construction of the new bridges; d) the need of a new regulation of watercourse of Ziliana Stream.
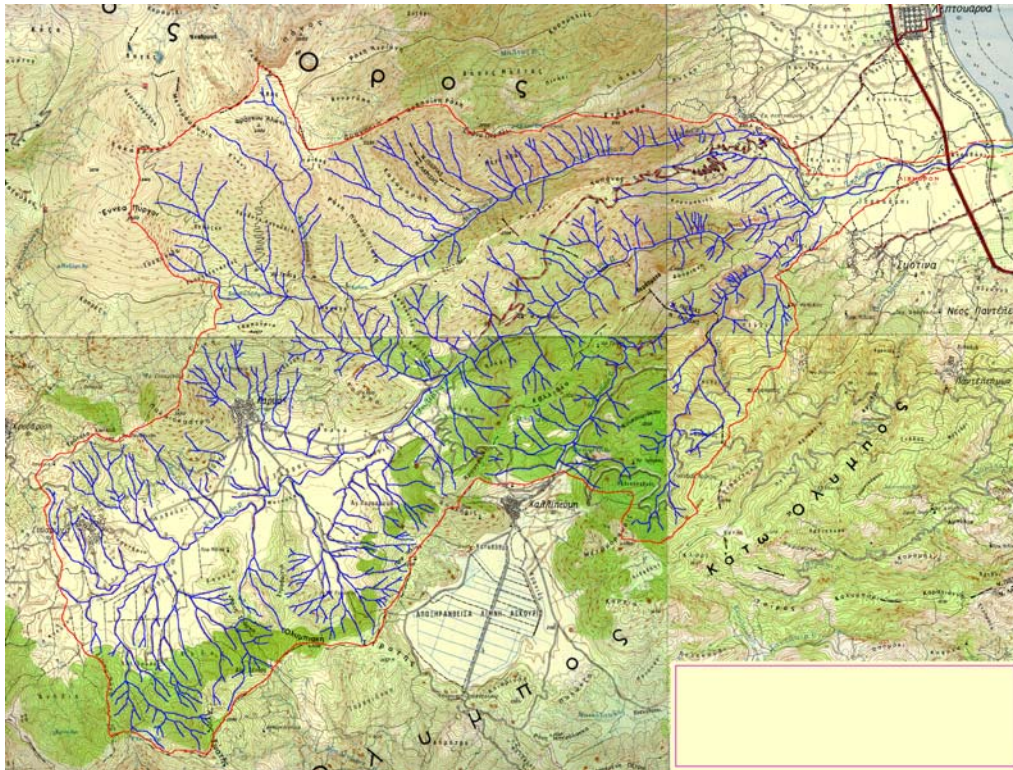
Figure 2. The watershed of Ziliana Stream.

- One can not accept, and neither reject, that the rainfall was exceptional on the base of the available daily data. The day of collapse was preceded by a period of many days with quite important rainfalls (166 mm of rain depth on the 23rd November 1998). The soil was saturated, the runoff coefficient increased, and probably local erosions and scouring occurred in the watercourse and the bridge, though not perceived by the persons in charge of various institutions before the destruction of the bridge, because of the practically continuous flows in the stream.
- The extent of erosion and scouring as they appear afterwards the bridge destruction did not allow a certain estimation of the prevailing situation in the watercourse before the 28th November 1998. No one can estimate the extent of probable excavations in the stream bed, because the natural erosion was much more intense and in larger extent, so that has changed completely the previous situation.
- a doubt concerning the time and the cause of destruction of downstream steps in stream bed (natural or anthropogenic destruction, before or during the flood) still exists. These steps carry an important part of the destruction responsibility for the growth of dangerous flow conditions that led to the erosion of the stream bed and the destruction of the old structures.
- The building of the new bridges considerably diminished the discharge capacity and the resistance of the old structures, not because of the reduction of the effective cross-section in the watercourse, but mainly because of the obstruction of certain openings and of the change of flow conditions due to the relative discrepancy of openings among the new and the old bridges. However the new bridges are much better drawn and built, so assuring to cope successfully with the future floods of Ziliana Stream.
- The type of shallow foundation of the old bridge and the various individual geometric characteristics played decisive role in destruction.
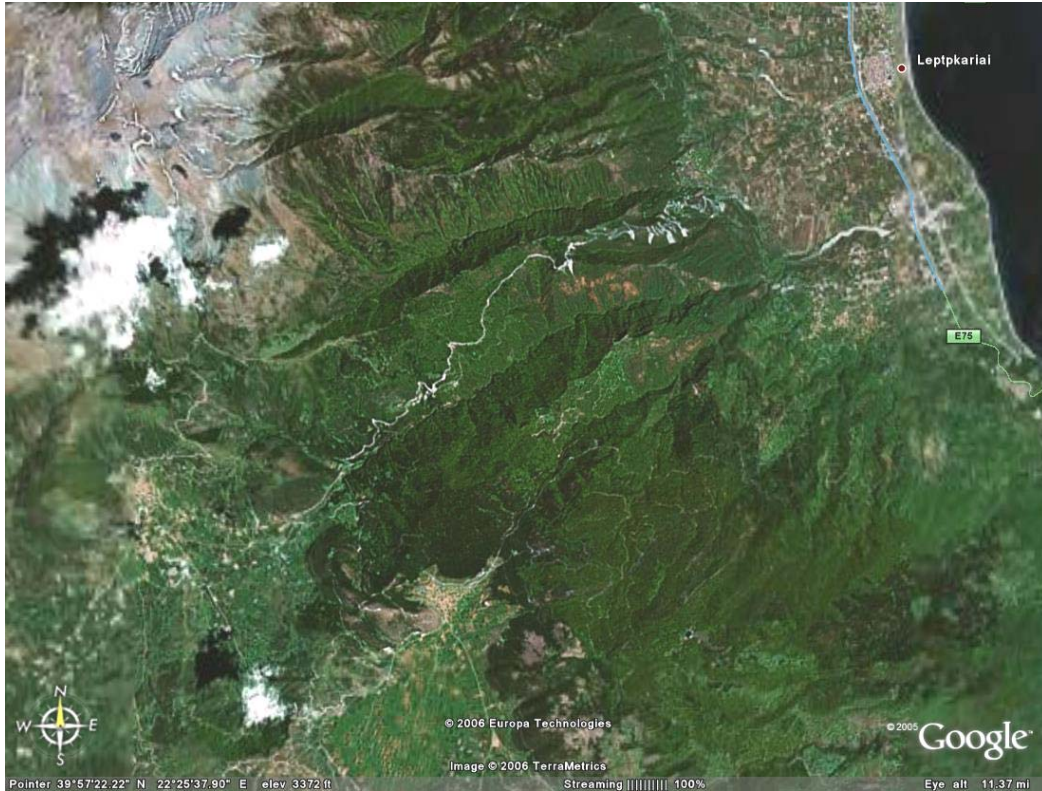
Figure 3. Aerial photography of the watershed of Ziliana Stream.
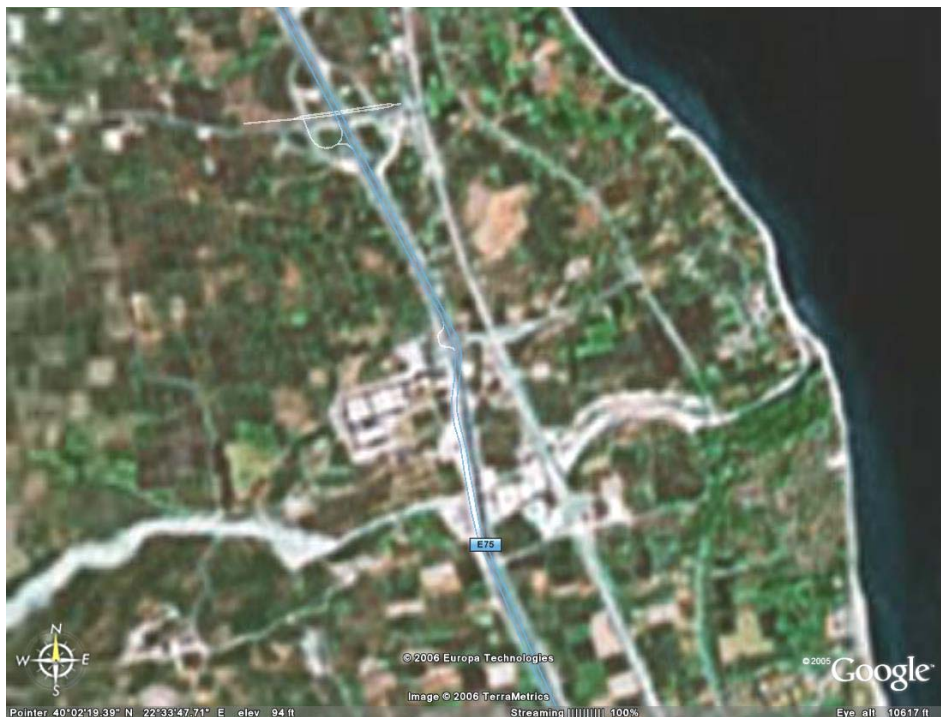
Figure 4. Aerial photography of the area of the bridges on Ziliana Stream.

4. QUESTIONS AND ANSWERS

Finally, which was the main reason that caused the bridge collapse ? It was the initial scouring of the ground to a level of 1.00 to 2.00 m, the wash out and the transport of the surrounding ground on which the foundations were based. The piers suffered important subsidence, resulting in a turn and displacement of carrying elements of the bridge.

What mechanisms led to the scouring of the bridge foundations ? The collapse was preceded by a quite long period of particularly intense rainfall which had as a consequence an important increase of the stream discharge.

The exceptionally high discharge, in combination with the slope of the stream flow, that was increased afterwards the destruction of the downstream steps, and with the width reduction of the watercourse in the place of bridges, caused the development of very high flow velocities, thus leading to the scouring of the stream bed, when the shearing force exceeded the ground resistance.

Did the effective water section of the stream under the bridge, that remained afterwards the works for the building of the new bridges, suffice for the flood flow ? It sufficed, as demonstrated by the fact that even during the peak flow in the effective section, the flow did not reach the upper structure of the bridge.
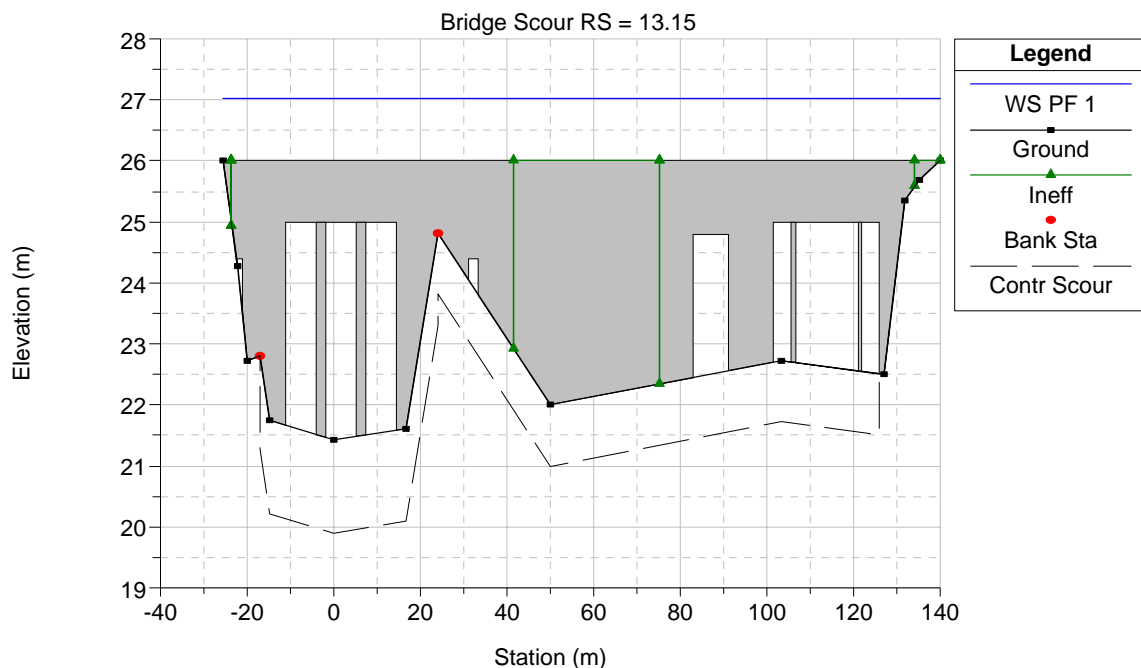
Figure 5. HEC-RAS simulation of the bridge scour.

5. RESEARCH

In order to determine the various missing data concerning the bridge destruction, many calculations and simulations have been carried on. Some calculations were made by applying analytical or empirical relations but the most complete simulations were realized using the HEC-RAS software (Figure 5). First, the river bed and the bridge geometry have been introduced to the program. Next, calculations were carried on for the discharge capacity of the stream, with and without bridges or steps. Finally, a scour

analysis for the 100-year estimated discharge (~900 m^3/s) and a sensitivity analysis have been carried out, taking into consideration the influence of discharge, bed material gradation and average diameter D_{50} of the bed material sediments for the calculated scour depth. The results have been analyzed and discussed.
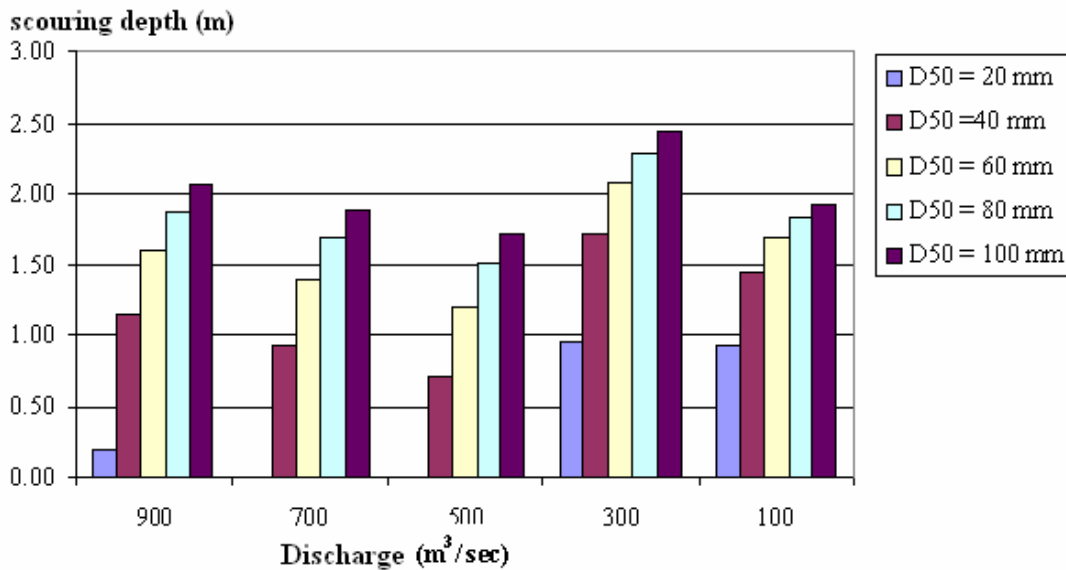
Figure 6. Comparison of the scouring depth for various combinations of discharge and D_{50}.

The most interesting outcome of this analysis is that for the case of the collapsed bridge, the most adverse discharge was lesser than half the 100-year estimated discharge (Figure 6). This is due to the combination of various hydraulic conditions that produced the most important velocities at the bridge section.

6. CONCLUSIONS

Apart from the various initial remarks presented previously, the conclusions drawn from the simulation of scouring have demonstrated again that sometimes an adverse combination of small effects can lead in a real disaster, although any important condition examined individually is quite securing !

Part 2
STATISTICAL AND STOCHASTIC ANALYSIS OF EXTREME EVENTS

Observing and modelling exceptional floods and rainfalls
Proceedings of the AMHY-FRIEND International Workshop on Hydrological Extremes,
held at University of Calabria, Cosenza (Italy), May 3-4, 2006

THE FLOODED AREAS RISK. ARGES BASIN APPLICATION

M.J. Adler, R. Amafteesei, R. Mic, V. A. Stanescu

National Institute of Hydrology and Water Management, Bucharest, Romania.

ABSTRACT

This paper shows an application of the procedure of the hydraulic model UNDA for flood risk map identification to the Arges river basin in Romania. The flood hydrographs have been determined by the use of QdF model, proposed by Cemagref, and of the Romanian NIMH model. In the case of QdF model, the hydrological study of rare observed floods aims to provide the mono-frequency synthetic hydrographs of the basin. On the other side, the NIMH model describes the flood wave through the maximum discharge of prefixed exceedance probability, the total duration of the flood hydrograph, the time to peak and the shape coefficient.

A regionalization procedure was applied to generate synthetic hydrographs, considered as input data for UNDA model. In order to achieve the maps of the flooding risk, have been used topographic data, GIS maps, flood hazard map, water management conditions in the river basin, data on the flood prone areas and technical regulations and standards concerning the accepted vulnerability.

The land uses located in the studied area in general satisfy the attribute of protected zone at inundation except two very critical zones concerning the communication ways.

1. INTRODUCTION

The philosophy of the project starts from the concept of a sustainable management of the Timis-Bega basin, including proper flood risk management. To attend the scope of the project a real time informational system was put in place in this demonstrative area, using replication of data at the level of the database. To this real-time data dissemination integrated monitoring and modelling system was performed and forecasted data are disseminated at all water users at the national level.

The increased use of floodplains in Arges basin has also seen an increase in the number of people and properties jeopardised in flood events and therefore it has resulted in parallel an increasing of the flood warning and forecasting needs and the importance to establish a ranked of flood risk areas to be implemented a national insurance program. At the same time, there has a shift in economic thinking towards a more attentive cost-benefit analysis of the water resources monitoring networks and towards the use of the high techniques in the acquisition, transmission, quality control, processing and dissemination of data. As a result, remote sensing data were added to the hydrological informational system to help in better defining the vulnerable areas. The final boot was integrating hazard and vulnerability data, to get a better defined flood risk regionalization.

2. DATA USED

The selected area at risk to be flooded was the river plain of the Arges river basin at the major confluence of the rivers Doamnei, Targului and Argesel. The hydrological study of rare, observed floods aims to provide the mono-frequency synthetic hydrographs (MFSH). These hydrographs are needed for hydraulic modelling of the flood flow and it concerns the pilot sub-basins of the Arges river basin (Table 1). The location of the considered stations is given in Figure 1.

River Basin	Station	Area (km^2)	Time period	Raingauge station
Raul Doamnei	Darmanesti	566	1959-1997	Vladesti
Raul Doamnei	Ciumesti	1736	1980-1997	Vladesti
Raul Targului	Piscani	830	1975-1997	Campulung
Argesel	Mioveni	230	1970-1997	Boteni

Table 1. Characteristic features of the basins.

Figure 1. Investigated area.
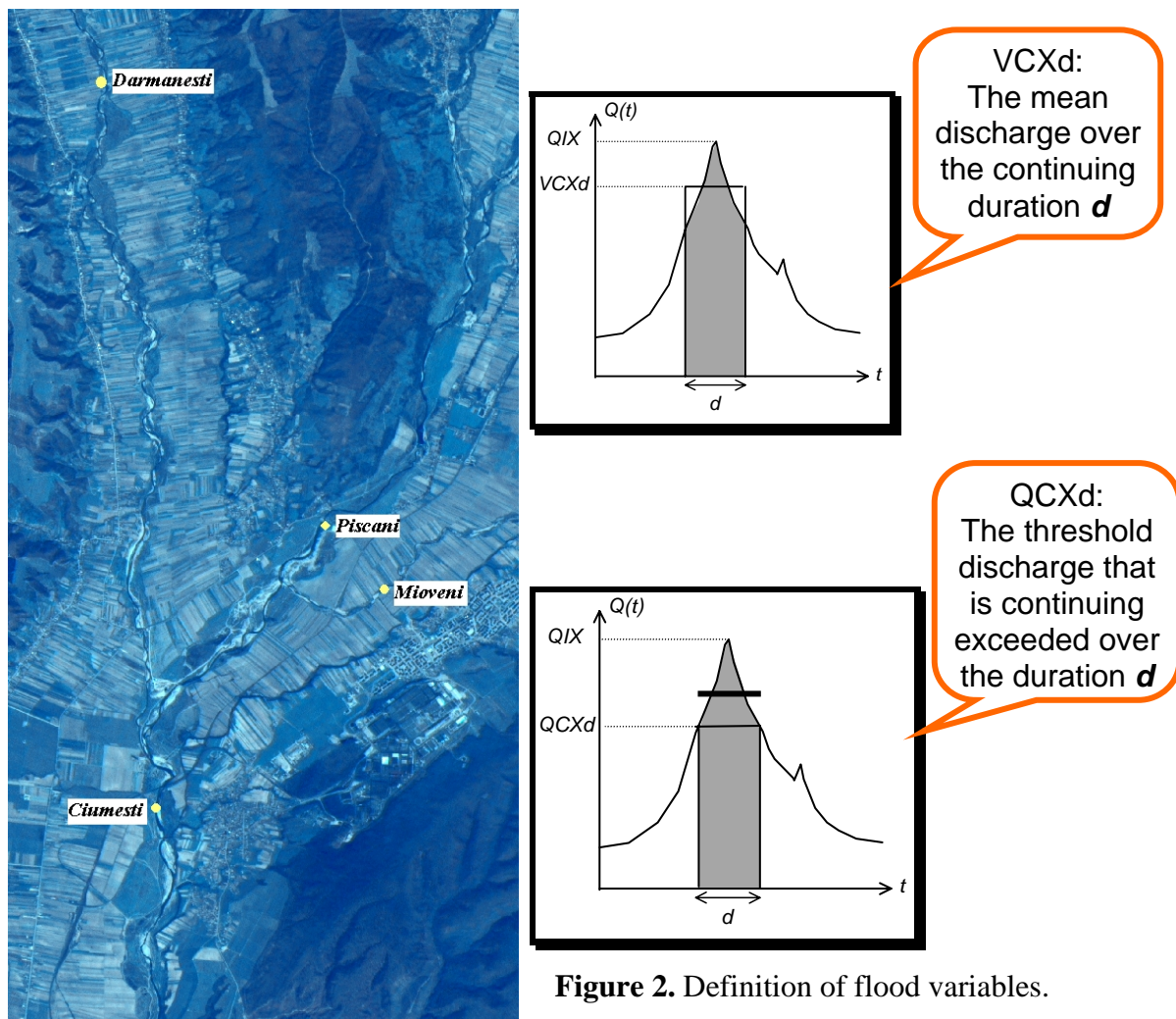
Figure 2. Definition of flood variables.

3. QdF AND NIMH MODELS FOR FLOOD HYDROGRAPHS OF DIFFERENT PROBABILITY OF EXCEEDANCE

In order to carry out the map of risk, the map of hazard has been previously determined. This is achieved by applying the hydraulic model UNDA for routing the flood hydrographs of different probability of exceedance. The flood hydrographs have been determined by the use of QdF model provided by Cemagref (Lyon, France) and by the NIMH model.

In the case of Cemagref model the hydrological study of rare, observed floods aims to provide the mono-frequency synthetic hydrographs (MFSH) starting from the from two hydrological variables: VCXd and QCXd (Figure 2). Then the distribution of the empirical frequency has been visualised and the exponential distribution has been checked and the probability law adopted (Figure 3).
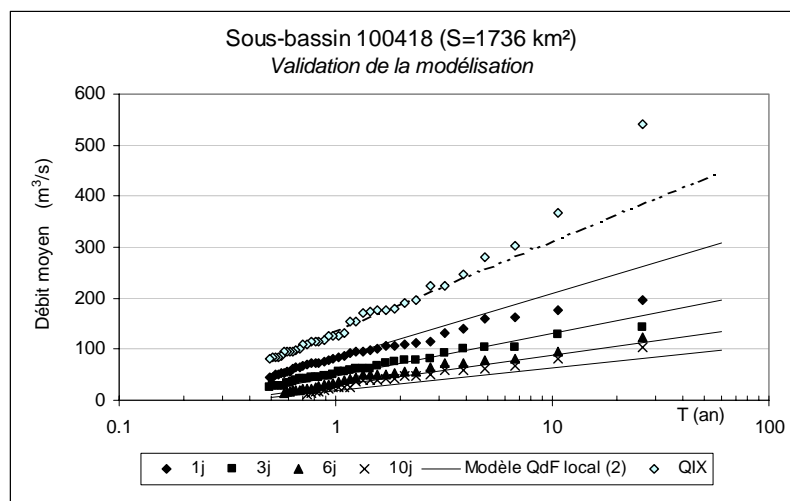
Figure 3. Application of QdF model.

Further on, the quantiles of the flood of the mean discharge VCX_d were determined in the recording domain. The characteristic duration D of the flood wave hydrograph represents the total duration of the flood hydrographs function of the peak discharge corresponding to return period of 10 years (Figure 4).
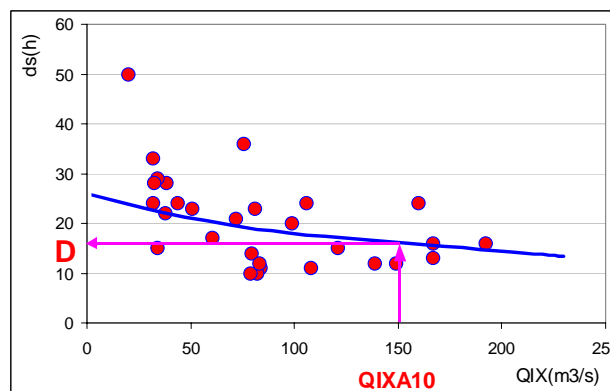
Figure 4. Identification of the characteristic duration D.

A regional QdF model has been then derived as can be seen below (Figure 5).

$$QCX_R(d,T) = \left[\left(\frac{x_2}{(x_1 \cdot \dfrac{d}{D} + x_2)^2} + x_3\right)\right] \cdot \ln(T) + \left[\left(\frac{x_5}{(x_4 \cdot \dfrac{d}{D} + x_5)^2} + x_6\right)\right] \cdot QIXA10$$
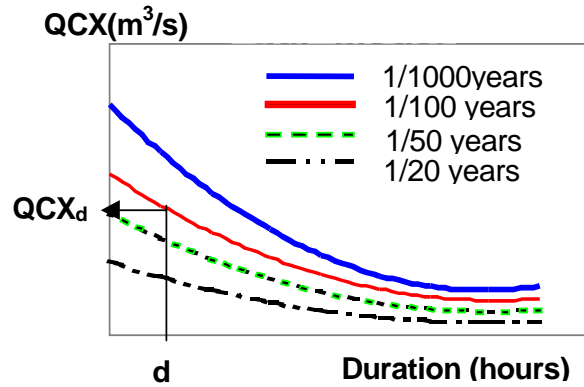
Figure 5. Qdf model.

On the basis of the QdF model, the mono-frequency synthetic hydrograph (MFSH) has been inferred as presented in Figure 6.
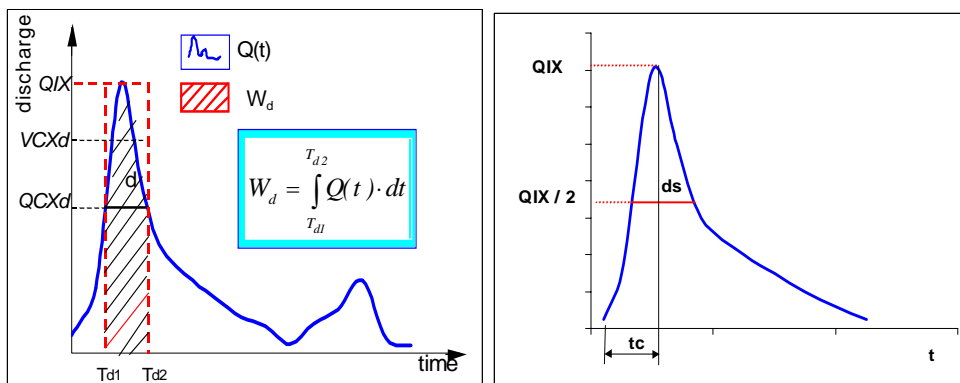
Figure 6. Assessment of the mono-frequency synthetic hydrograph (MFSH)

The NIMH model considers the following descriptors of the flood wave (Figure 7):

- The maximum discharge of certain probability p of exceedance, $Q_p^{(max)}$;
- The total duration of the flood wave hydrograph, T_{tot};
- The up-to peak duration (increase duration), T_{incr};
- The shape coefficient (compactness coefficient), $\gamma = \dfrac{W}{T_{tot} \cdot Q_p^{max}}$

The peak discharge is expressed in terms of the probability of exceedance $Q_p^{(max)}$ computed on the basis of the maximum annual discharges recorded over a long period of time at the gauging stations. Insofar as not all the stations within the Arges River Basin have long enough series a regionalization procedure was applied.
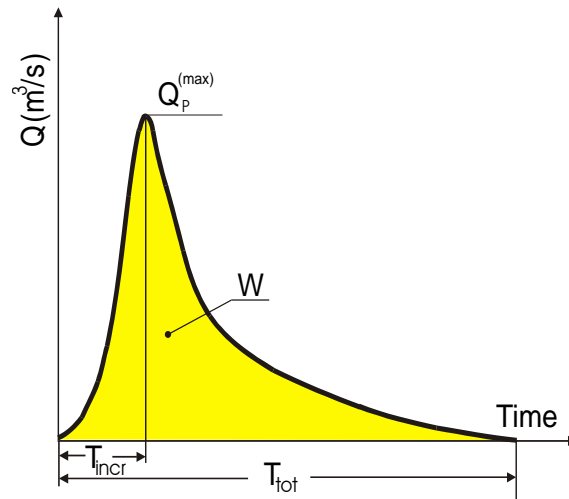
Figure 7. The NIMH model descriptors of the flood wave.

The regionalization function is of the type: $q_{max}^{p(\%)} = f\left(\dfrac{H_m}{\sqrt{F}}\right)$ where $q_{max}^{p(\%)} = \dfrac{Q_{max}^{p(\%)}}{F}$ is the maximum specific discharge, A the basin area and H_m the mean elevation. The shape of the regional relationships, obtained for the Arges zone and the other sixteen zones where the relationships are valid, were drawn in Figure 8.
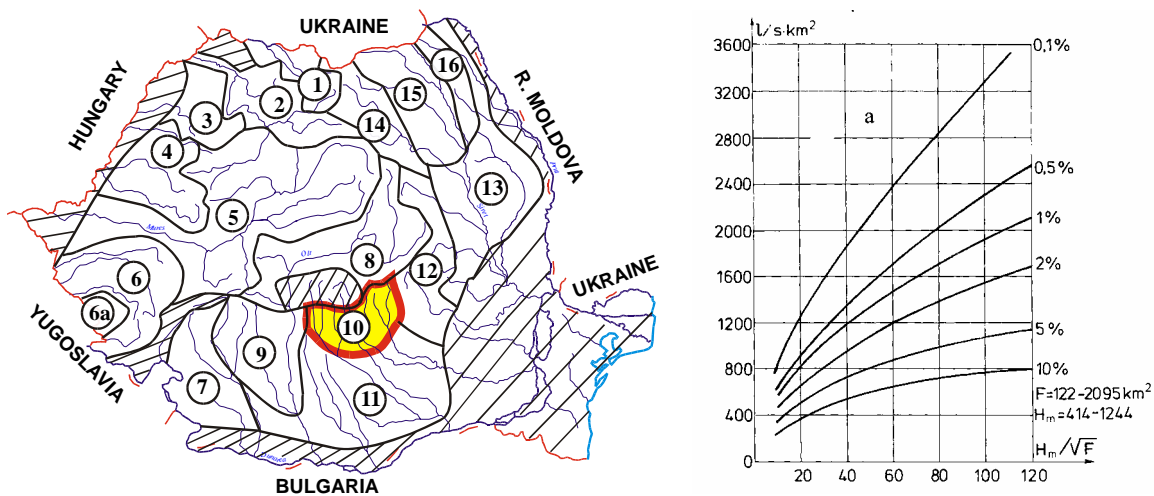
Figure 8. Regional relationships for maximum discharge derivation.

The flood shape characteristics are determined either on the basis of the recorded hydrographs at the stations or making use of regionalization procedures.

4. HYDRAULIC SIMULATION OF THE DIFFERENT FREQUENCY HYDROGRAPHS

The UNDA model simulates the one-dimensional, unsteady flows with free surface. It is based on the system of equations Saint Venant, numerically integrated in finite differentials on a rectangular network in the plane (x,t) in an implicit scheme with the linearization of the equations of Figure 9.

85
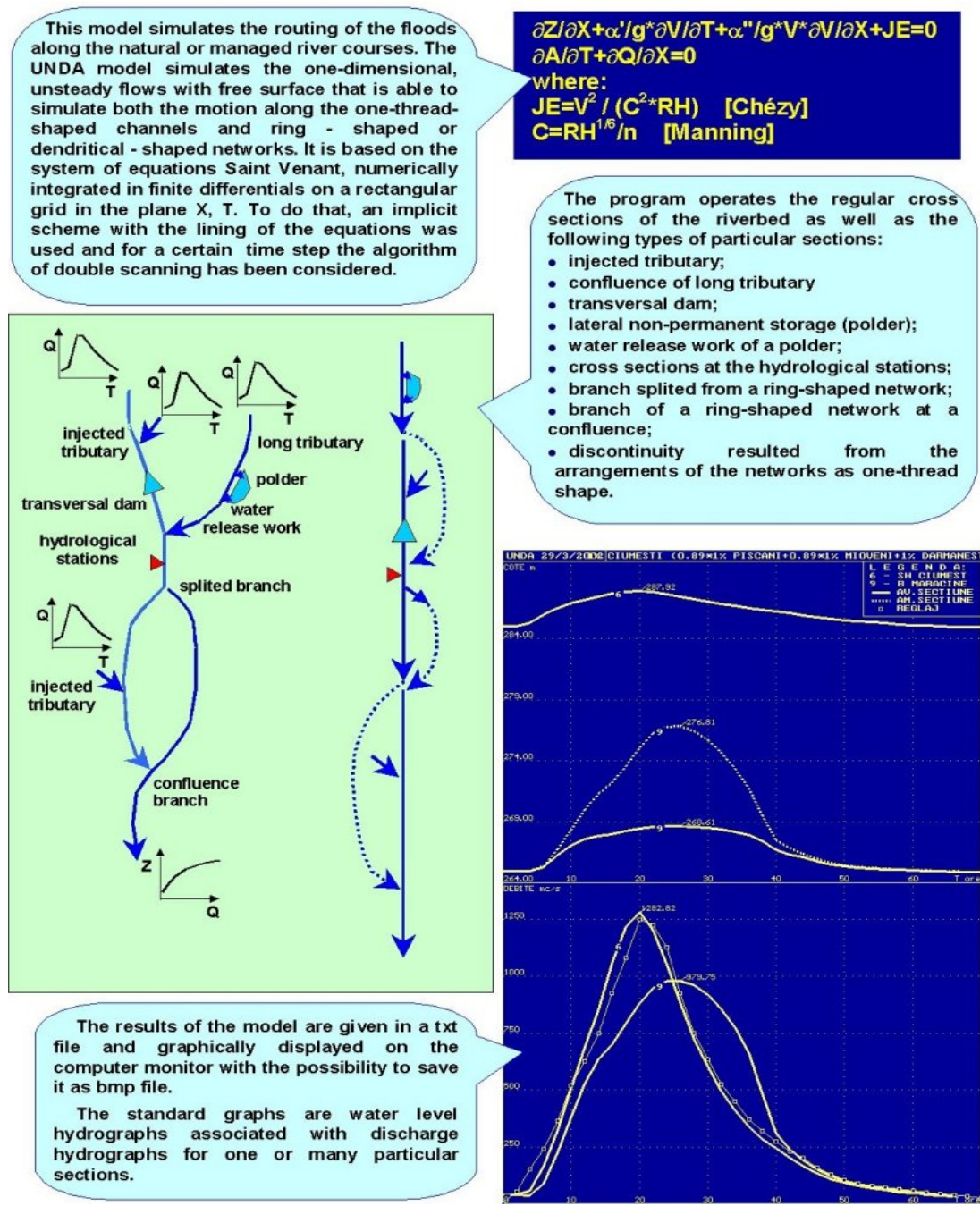
Figure 9. Outline of the UNDA model.

The calibration involves the use of 22 cross sections, out of which 7 are located at the road or railway bridges, distributed at a distance of 1 km, as follows: four sections on Argesel River, five on Targului and 13 on Doamnei River. Nine cross profiles (M1-M9 in Figure 10a) encompassing the non-permanent reservoir Maracineni (located at confluence of Arges and Doamnei Rivers) used for flood control, as well as the inner polder having an agricultural use, were considered (Figure 10 b).
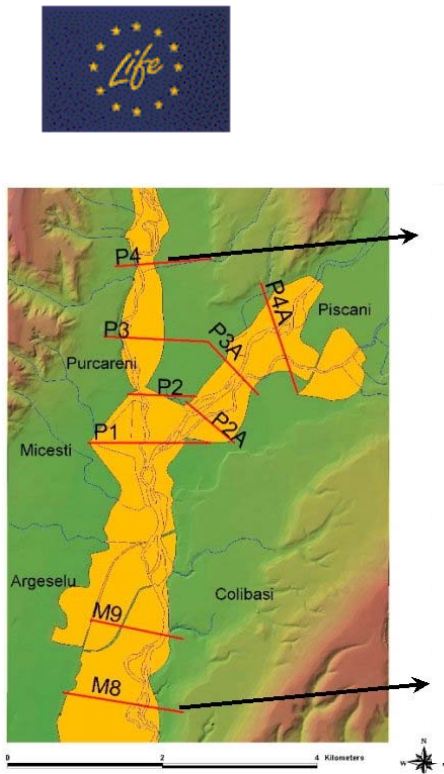
Figure 10 a. River sections.   **Figure 10b.** Scheme of the hydrographical network.
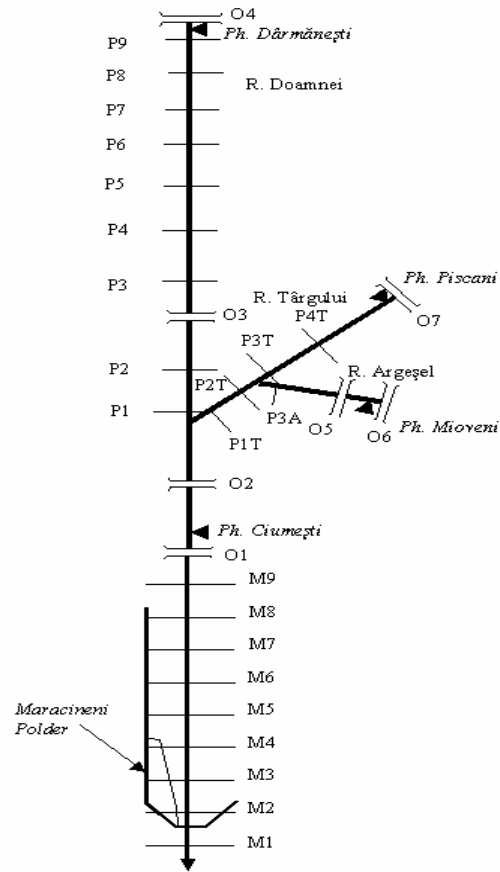
After running, the UNDA model provided the following results:

- kilometric position of the section;
- table with the geometrical and resistance characteristics;
- hydraulic works along the river;
- initial situation in the steady flow;
- table with results concerning the unsteady flow at every computing time in the particular sections;
- table with the maximum values (water levels and discharges) in all computing sections;
- table with the flood volumes for each section;
- list of the input discharge hydrographs;
- maximum error in estimating the differences of the water level in a specific point at a given moment;
- modulus value of the error in assessing the differences of the water level.

Taking into account the results provided by the model, the areas that are flooded for the peak discharges of 0.1%, 1%, and 10% probability of exceedance have been drawn as it is shown underneath.

In order to achieve the maps of the flooding risk the following data have been used: topographic data, GIS maps, flood hazard map, water management of he river basin, data on the flood prone areas (socio-economic and environment objectives) and the technical regulations and standards concerning the accepted vulnerability (Figures 11 and 12).
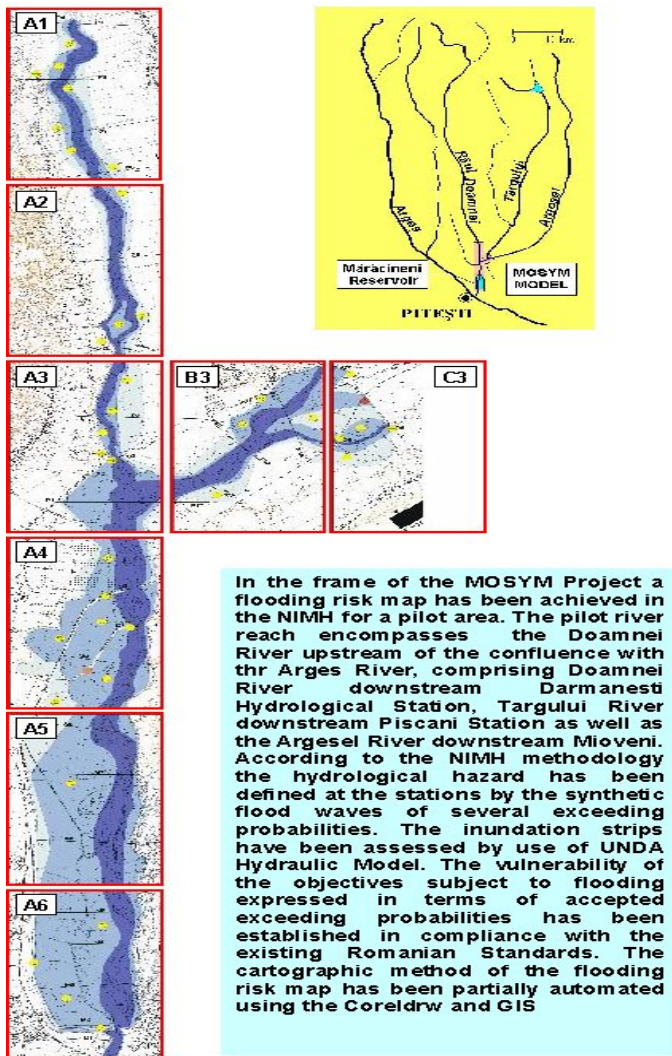
Figure 11. Flooding risk map.
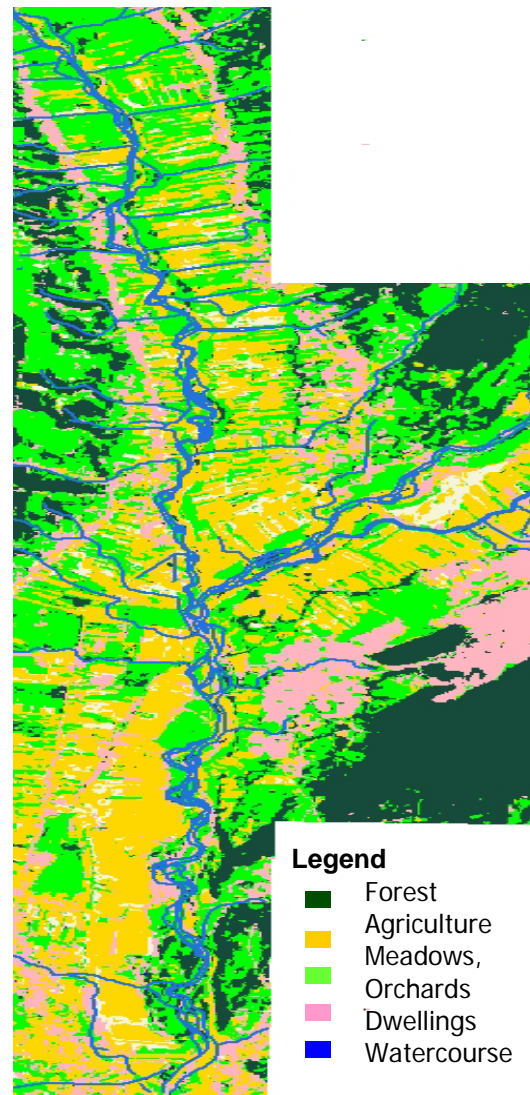
Figure12. Cover land use of Arges River.

In the frame of the MOSYM Project a flooding risk map has been achieved in the NIMH for a pilot area. The pilot river reach encompasses the Doamnei River upstream of the confluence with thr Arges River, comprising Doamnei River downstream Darmanesti Hydrological Station, Targului River downstream Piscani Station as well as the Argesel River downstream Mioveni. According to the NIMH methodology the hydrological hazard has been defined at the stations by the synthetic flood waves of several exceeding probabilities. The inundation strips have been assessed by use of UNDA Hydraulic Model. The vulnerability of the objectives subject to flooding expressed in terms of accepted exceeding probabilities has been established in compliance with the existing Romanian Standards. The cartographic method of the flooding risk map has been partially automated using the Coreldrw and GIS

Legend
- Forest
- Agriculture
- Meadows,
- Orchards
- Dwellings
- Watercourse

5. VULNERABILITY ESTIMATION

In order to determine the vulnerability map the land cover/land use map determined by GIS application was used. The flooding risk map is performed on the one hand, by identifying the parcels located in the contingency of the river bed that are able to be flooded with a given frequency and considering the "assumed" frequency of flooding, on the other. If the accepted frequency (probability of exceedance) is smaller than the assumed frequency, the parcel is considered endangered and vice-versa.

In Figure 12, the satellite map of the land-cover encompassing the five categories of uses is shown. The following five categories of the land cover are deemed: the forest, agriculture terrain, meadow and orchard zones, urban areas as well as the riverbeds. For the assumed probabilities the following values have been considered: forest area - 20%, agriculture terrain - 10%, meadows and orchards - 20%, dwelling in rural areas - 5%, communication ways - 1% dams and levees - 0.1%. The land uses located in the studied area in general satisfy the attribute of "protected" zone at inundation except two very critical zones concerning the communication ways which are located by circles marked in red colour on the map bellow, namely:

- The intersection of the modernized way Mioveni-Piscani with the railway Pitesti-Campulung, the flooding originating from the flood pain of Argesel River, downstream the bridge 06.
- On the road linking Ciumesti and Mioveni, after the high passage over the railway towards the bridge O1 (Figure 13).
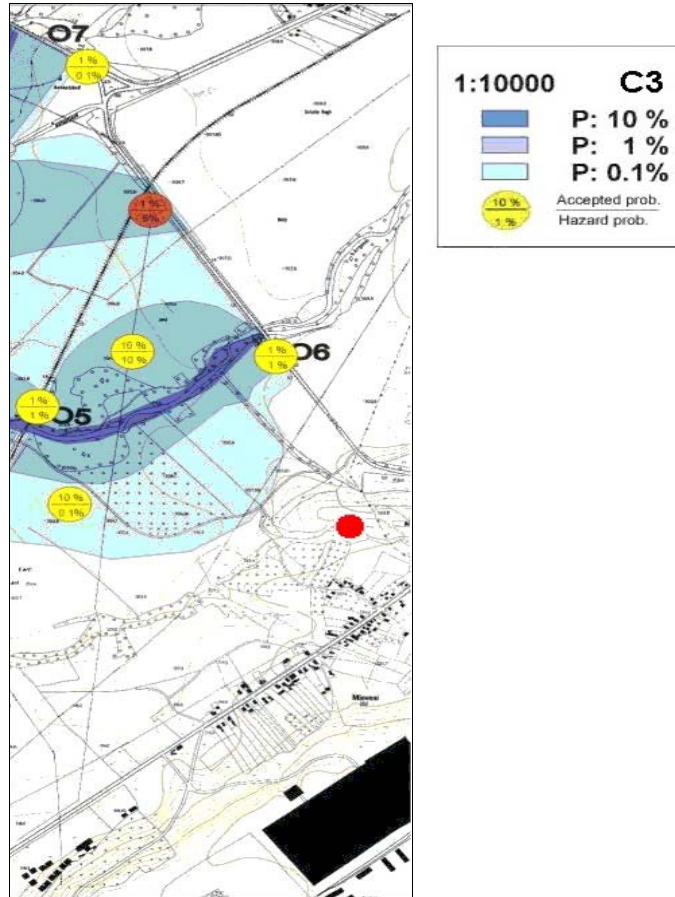
Figure 13. Area with high risk to be flooded (underprotected).

These two points are of an outstanding economic importance having a significant impact both on the railway circulation to and from Pitesti City (capital of the Arges County) and the Dacia-Renault industry of cars. In the range of the transited floods the Maracineni non-permanent water storage achieves to satisfy its designed role. At the 1% flood it performs a peak discharge mitigation of 25%, without jeopardising the agriculture terrain from upstream of the water storage.

The inner levee of the storage is not overflowed unless the probability of exceedance is less than 5%.

6. CONCLUSION

Using GIS facilities the risk maps were carried out for Arges pilot basin. Detailed definitions for common risk maps have displayed clearly the following basic information under a unique edition called "synthetic crossed form" and normally sufficient for any further use. If needed, further updated editions can be carried out. This synthetic form involves detailed information also displayable under annexed specialized forms:

- hazard aspects: either under a synthetic variable, or detailed with flood extensions, depths, velocities, duration, and their probabilities of occurrence;
- vulnerabilities aspects, mainly through their synthetic variable for helping the spatial comparisons (between the different land use along the river floodplain) and preparing the comparisons with the hazard synthetic one;
- water management aspects (volumes in excess, or available potential capacities for transitory storage);
- options of management solutions, either through hydraulic works, and/or through land use changes (or changed/adapted vulnerabilities for a remaining given land use).

The collaborations with SCOT for satellite data processing and with Cemagref for transferring the "Inundability" methodologies to the NIMH specialists were of the greatest interest for the developed application in Romania.

STRUCTURAL CHARACTERISTICS OF MAXIMUM FLOWS IN EASTERN BLACK SEA REGION, TURKEY

H. Aksoy[1], L. Kaynar[2] and N. Erdem Unal[1]

(1) Istanbul Technical University, Civil Engineering Dept., Maslak, Istanbul, Turkey.
(2) Su Yapi Engineering & Consulting Inc., Cankaya, Ankara, Turkey.

ABSTRACT
In this study, maximum values of daily average flows observed in eleven hydrometric stations in the Eastern Black Sea region (Turkey) are analyzed. The study investigates the structural characteristics such as randomness, jump, trend, and probability distribution function, of the time series. Outlier detection is also made. Tests available in literature are used for this purpose. The tests are Ellipse test for outlier detection, McGee test for randomness, nonparametric Spearman rank order correlation test for trend, the automatic segmentation procedure for jump, and Probability Plot Correlation Coefficient test for probability distribution function. The station-based analysis shows the presence of outliers in a number of stations. Data are found random that can be explained by the relatively less interrupted basins compared to the other regions in the country. No trend is found except for two stations only. Maxima are best fit by Weibull and Frechet distributions.

1. INTRODUCTION

It is usual that flow in a river exceeds the average conditions in wet periods, in particular, during the year. Depending on the region where the river goes through, this may result from a heavy rainfall or is observed after a snowmelt period. Similar cases can be observed if a huge amount of water is discharged through spillways of a reservoir located in the upstream of the region interested. All these may result in flood which is the case that not only the river channels but also surrounding areas have to transport water to downstream from upstream. However, when the river channel capacity cannot handle water coming from upstream to transport downstream, water flow becomes problematic and even dangerous for human life and properties. Because of that reason, flood analysis is a very important issue in hydrology.

With increase in population and industry, losses due to floods have become much more important than before. This has forced hydrologists and civil engineering practitioners to develop more precise methods for flood analysis. Therefore, flood frequency analysis, flood estimation, and updating flood for changing upstream and downstream conditions as well as climatological conditions are among the studies performed to make high level water in a river useful, not dangerous.

In this study, maximum flows observed during a hydrological year were taken from hydrometric stations in the Eastern Black Sea region in Turkey. The study investigates the structural characteristics such as randomness, jump, trend, and probability distribution function, of the time series. Detecting outliers that might present in the series was also considered. Tests available in literature were used for this purpose. The tests used are as

follows: Ellipse test for outlier detection, McGee test for randomness, non-parametric Spearman rank order correlation test for trend, the automatic segmentation procedure for jump, and Probability Plot Correlation Coefficient test for probability distribution function.

2. DATA USED

Eleven hydrometric stations operated by EIEI (Electrical Power Resources Survey and Development Administration) of Turkey, were incorporated into the study. Table 1 presents overall characteristics of the stations. Figure 1 shows their spatial distribution over the study area. Daily average flows were considered. The maximum of daily average streamflow recorded during a hydrological year was taken for consideration. Therefore, in this study, a time series of annual maxima of daily average streamflow data is made available from the observation.
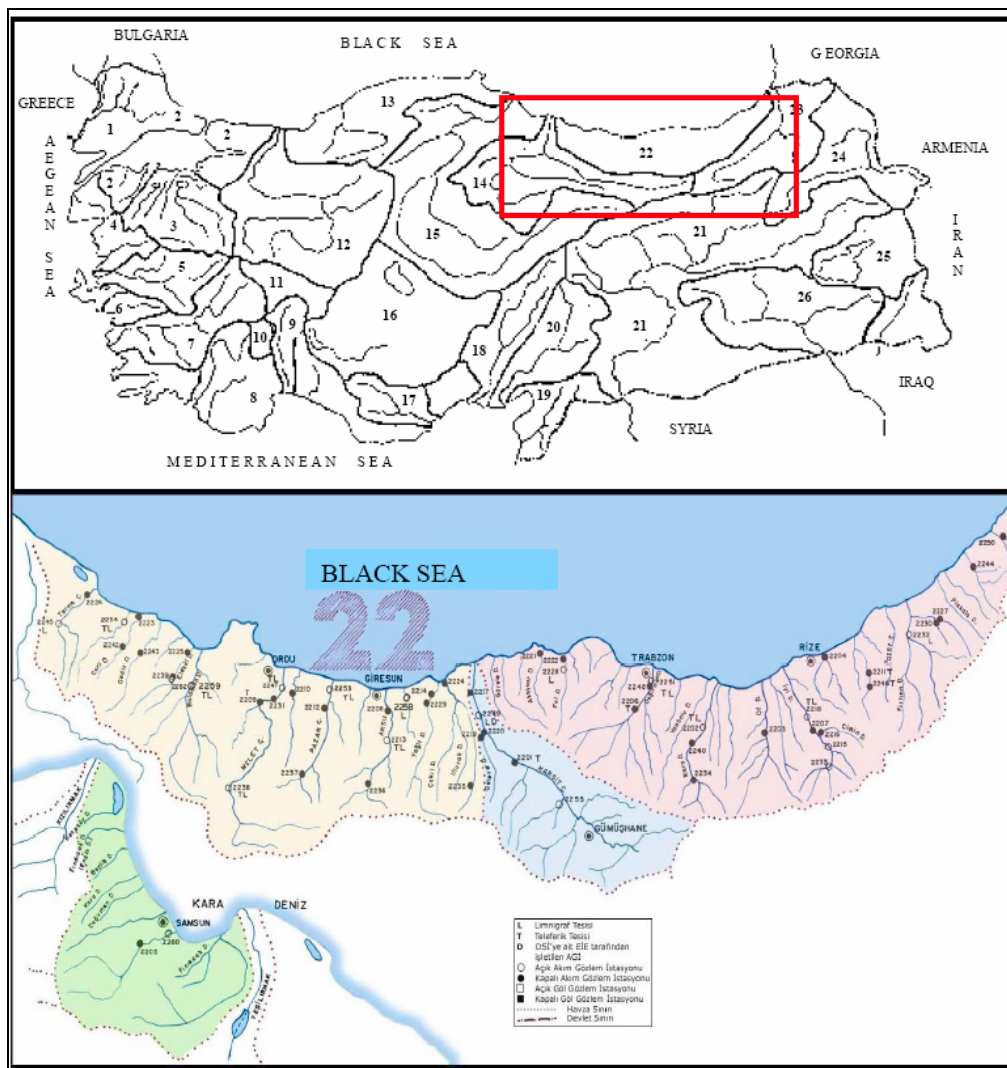
Figure 1. Layout of stations used in the study area.

Station	Length (year)	Drainage area (km²)	Elevation (m)	Average flow (m³/s)	Standard deviation (m³/s)	Median value (m³/s)	Coeff. of variation	Coeff. of skewness	Serial correlation coefficient	Max (m³/s)	Min (m³/s)
2202	25	608.8	350	94.06	31.00	90.0	0.32	1.21	0.130	182	59.8
2213	29	728.0	248	136.6	79.77	117.0	0.58	1.56	-0.123	400	44.2
2215	26	445.0	990	89.75	25.92	89.8	0.29	1.84	-0.200	184	51.0
2218	28	855.3	310	185.5	99.29	147.5	0.54	1.74	0.014	504	94.7
2228	25	219.6	17	66.86	38.76	61.2	0.58	0.75	-0.208	155	20.2
2232	27	940.0	160	185.6	98.19	155.0	0.53	2.85	-0.169	560	105.0
2233	27	249.2	1220	42.93	10.03	41.6	0.23	1.11	0.122	69.8	30.1
2238	26	1024.4	975	161.6	78.62	147.5	0.49	0.72	-0.005	345	57.6
2239	25	271.6	1070	134.6	114.6	95.6	0.86	1.49	0.050	442	22.6
2245	21	232.8	66	288.4	155.3	249.0	0.53	0.69	-0.060	598	69.3
2247	21	1859.2	40	629.2	369.8	540.0	0.59	0.46	-0.280	1274	133.0

Table 1. Characteristics of the stations.

3. TESTS

3.1 Outlier detection

Before a deeper analysis is made, a preliminary analysis of data should be performed. Such an analysis mainly starts with checking the homogeneity of the data sets. Outlier detection is a considerable effort to find out any outlier that might present in, and make the series non-homogeneous. Outlier detection was performed in this study, by using Ellipse test under the statistical package, *Statistica 6.0*. It is such a test that uses graphics and determines if any outlier is present. Any value lying out of area bordered by the ellipse is considered an outlier (*Santos and Henriques*, 1999; *Itibar*, 2005; *Kaynar*, 2005).

3.2 Randomness test

Randomness in a hydrological time series means that the data result from natural causes. If there is no randomness, then there is persistency which is typically quantified by serial correlation coefficient. An adopted version of a simple nonparametric run test was used in this study. The test is based on the median value of the observed time series. The null hypothesis is that the time series is random. Details of the test can be found in *Adeloye and Montaseri* (2002). The test consists of following steps:

a. The median of the observations is determined.

b. Each data items are examined whether or not it exceeds the median. If a data item exceeds the median, this is defined as a case of success, S, otherwise a case of failure, F.

c. The number of successes and failures are counted and denoted by n_1 and n_2, respectively.

d. The total number of runs (R) in the data set is determined. A run is a continuous sequence of successes until it is interrupted by a failure or vice versa.

e. The test statistics is computed by:

$$z = \frac{R - \left(\dfrac{2n_1 n_2}{n_1 + n_2} - 1\right)}{\sqrt{\dfrac{2n_1 n_2 \left(2n_1 n_2 - n_1 - n_2\right)}{\left(n_1 + n_2\right)^2 \left(n_1 + n_2 - 1\right)}}} \tag{1}$$

where z has a standard normal distribution under the null hypothesis, H_0, that the sequence of successes and failures is random.

f. Critical values of the standard normal distribution are obtained for the chosen significance level, α, and denoted by $\pm z_{\alpha/2}$.

g. The computed statistics z is compared to the critical values $\pm z_{\alpha/2}$. H_0 is rejected if $z < -z_{\alpha/2}$ or $z > z_{\alpha/2}$.

3.3 Jump test

Jump can be observed in hydrological time series due to natural or manmade causes. For instance, a wildfire in a forest-drainage basin affects the flow regime in the stream, and a jump might take place in the streamflow time series. A volcanic eruption or a landslide in the basin might cause considerable changes in the sediment transport capacity of, and, hence, flow in the stream. Climate change or variability due to global warming nowadays made the humankind to behave more carefully in responding such sudden changes.

For the jump analysis, the time series was first divided into sub-series (segments) by using the automatic segmentation procedure of *Hubert* (2000). The automatic segmentation procedure breaks the time series into as many segments with significantly different means as possible. The procedure is based on the minimization of the segmentation cost defined as the sum of squares of deviations from the average of each segment. If two or more segments are identified, the starting year of the last segment was chosen as the first year for splitting the time series. Then comparison was made between the segments before and after the chosen year. Once segmentation is completed the jump analysis was performed, for which details are taken from *Fanta et al.* (2001) and given below.

a. The time series is divided into several segments by the automatic segmentation procedure.

b. The mean of two consecutive segments ($\bar{y}_1$ and $\bar{y}_2$) are calculated and the length of the segments (N_1 and N_2) are determined.

c. The t-statistics is calculated by:

$$t = \frac{\left|\bar{y}_1 - \bar{y}_2\right|}{s\sqrt{\dfrac{N_1 + N_2}{N_1 N_2}}} \tag{2}$$

with $N_1 + N_2 - 2$ degrees of freedom. Parameter in equation (2) is the pooled variance given by:

$$s = \sqrt{\frac{\displaystyle\sum_{i=1}^{N_1}\left(y_i - \bar{y}_1\right)^2 + \sum_{j=1}^{N_2}\left(y_j - \bar{y}_2\right)^2}{N_1 + N_2 - 2}} \tag{3}$$

d. The null hypothesis, that shift in the mean is insignificant, is rejected if the sample t statistics in equation (2) is greater than the critical value of Student's t-distribution ($t_{1-\alpha/2}$, N_1+N_2-2) with N_1+N_2-2 degrees of freedom.

3.4 Trend test

Presence of a trend in a hydrological time series can be considered an indication of possible long-term changes such as climate change. The environment from which the data are taken out may be affected by mankind impacts as well as natural phenomena. Climate change (global temperature increase) can be considered the most important among others. It might be expected that the extremes of droughts and floods will become more common and even severe as a result of climate change.

Trend analysis in this study was performed by using the non-parametric Spearman rank order correlation coefficient test. The step by step explanation of the test is as follows for a time series y_i, $i = 1, .., n$, observed in time i:

a. Ranks, R_{yi}, are assigned to y_i, such that the rank 1 is assigned to the largest y_i and the rank n to the least y_i. Ties in the y_i are handled by assigning each of the tied observations the mean rank of those rank positions that they occupy.

b. The difference:

$$d_i = R_{yi} - i \tag{4}$$

is computed.

c. The coefficient of trend, r_s, is computed by:

$$r_s = \frac{1 - 6\sum_{i=1}^{n} d_i^2}{n(n^2 - 1)} \tag{5}$$

Under the null hypothesis that the time series has no trend, the variable:

$$t = r_s \sqrt{\frac{n-2}{1-r_s^2}} \tag{6}$$

has a Student's *t*-distribution with *n* − 2 degrees of freedom.

d. The critical values of the t-distribution for the chosen significance level, α, and n–2 degrees of freedom are obtained. For a two-tailed test, the critical values are denoted by $\pm t_{\alpha/2,n-2}$.

e. The values of t are compared to the critical values. H_0 is rejected if $t > t_{\alpha/2,n-2}$ or $t < -t_{\alpha/2,n-2}$.

3.5 Probability plot correlation coefficient (PPCC) test

The PPCC test was employed in this study to explore the best-fit probability distribution function. Following probability distributions were considered for the test: Normal, 2- and 3-parameter log-normal, 2-parameter gamma, Weibull, and Frechet. Several commonly used methods such as the Chi-squared and Kolmogorov-Smirnov tests are available for testing the goodness-of-fit of theoretical probability distribution functions to the hydrological time series data. The Kolmogorov-Smirnov (K-S) and χ^2 tests tend to result in high type II error. Therefore, the PPCC test was preferred in this study.

The test is based on the correlation coefficient between the ordered sample y_i ($y_1 \leq y_2 \leq \ldots \leq y_n$) and their corresponding fitted quantiles, $w_i = G^{-1}(1-p_i)$, where p_i, i=1, 2, …,

n, is the exceedance probability of y_i and $G^{-1}(\cdot)$ is the inverse of the cumulative distribution function of the theoretical probability distribution considered for the sample. However, it should be stressed that the test is not in the usual form given in *Vogel* (1986) and *Vogel and McMartin* (1991) for instance, but is an easier form detailed in *Adeloye and Montaseri* (2002). The difference between the two forms is that it is not required to find critical PPCC tables for every probability distribution functions tested. Instead, the probability distribution with the highest correlation coefficient with the observed time series is selected as the best-fit distribution.

The test has the following steps:

a. The sample is ordered from the smallest to the largest.

b. The exceedance probability, p_i, i = 1, 2,…, n, of each data item in the ordered sample is calculated by:

$$p_i = \frac{R_{yi} - 0.4}{n + 0.2} \tag{7}$$

c. The standard normal variate at p_i, z_{pi} is calculated by:

$$z_{pi} = \frac{(1 - p_i)^{0.135} - p_i^{0.135}}{0.1975} \tag{8}$$

d. For normal distribution, for instance, quantiles corresponding to the data items in the sample are calculated by:

$$w_i = \bar{y} + S_y z_{pi} \tag{9}$$

Equation (9) changes depending on what probability distribution is selected.

e. The correlation between y_i and w_i is calculated by:

$$r = \frac{1}{n-1} \sum_{i=1}^{n} \frac{y_i - \bar{y}}{S_y} \frac{w_i - \bar{w}}{S_w} \tag{10}$$

where $\bar{y}$ and $\bar{w}$ are the means, and S_y and S_w the standard deviations of y and w, respectively.

4. RESULTS

4.1 Outlier detection

As for examples, Figure 2 was given for stations 2218 and 2238. It can be seen that the maximum value of the streamflow in 1974 observed in station 2218 was replaced out the region which is then considered an outlier. For the station 2238 no outlier was assigned as all observed values were found in the area bordered with the ellipse of the significance level of 5%. No outlier was found for five stations (2233, 2238, 2239, 2245 and 2247) whereas outliers were detected for the remaining six stations (2202, 2213, 2215, 2218, 2228 and 2232).
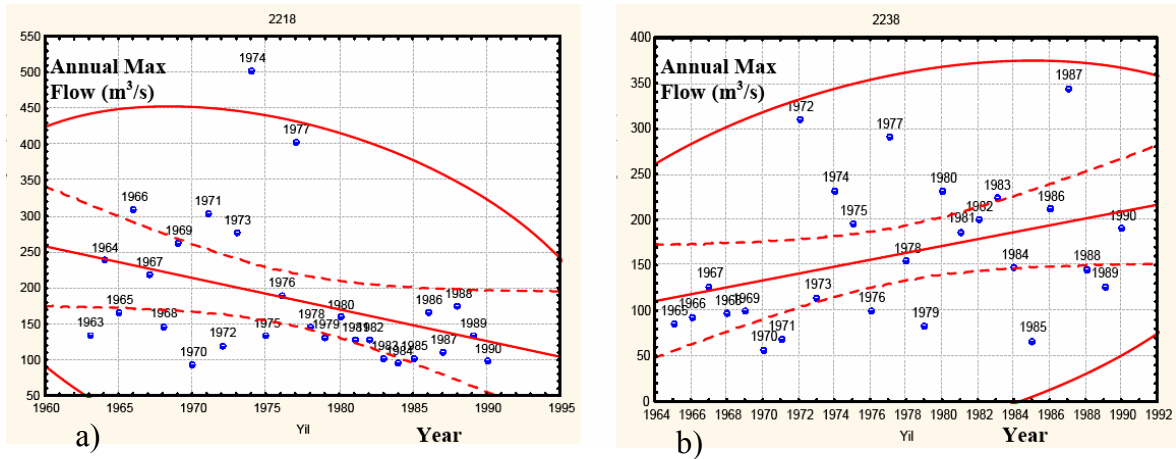
Figure 2. Outlier detection for stations 2218 (a) and 2238 (b) by using the Ellipse test.

4.2 Randomness

Table 2 summarizes results of the randomness test. Comparing the Z values in Table 2 to the critical value of 1.96 for the significance level of 5% indicates that all stations have random maximum streamflow data during the observation period. Physical interpretation of these results may be given in terms of the relatively less disturbed nature in the study area.

Station	N_1	N_2	R	Z	Result
2202	11	13	11	-0.806	Random
2213	13	12	14	0.213	Random
2215	11	13	13	0.035	Random
2218	13	15	17	0.802	Random
2228	10	12	11	-0.400	Random
2232	12	13	14	0.213	Random
2233	12	14	10	-1.580	Random
2238	12	14	12	-0.775	Random
2239	11	13	13	0.035	Random
2245	9	11	11	0.046	Random
2247	9	11	12	0.510	Random

Table 2. Randomness test.

4.3 Jump

Jump analysis made by the automatic segmentation procedure of *Hubert* (2000) resulted in no jump for every stations used. Therefore, the conclusion for the jump analysis is that there is no jump observed in the time series.

4.4 Trend

When the above detailed test was executed for the annual maximum data of each station, results in Table 3 were obtained. Following these results it can be said that there is no trend in the majority of the stations while only two stations (Figure 3) show the existence of trend in their annual maximum value of the daily average flow time series.

97

Station	r_s	t	$t_{critical}$	Result
2202	-0.368	-1.896	±2.08	No trend
2213	-0.170	-0.901	±2.07	No trend
2215	0.253	1.282	±2.08	No trend
2218	0.474	2.748	±2.07	Negative trend
2228	-0.164	-0.762	±2.09	No trend
2232	0.201	1.026	±2.07	No trend
2233	-0.067	-0.338	±2.07	No trend
2238	-0.398	-2.126	±2.087	Positive trend
2239	-0.248	-1.230	±2.08	No trend
2245	-0.140	-0.618	±2.11	No trend
2247	-0.392	-1.858	±2.11	No trend

Table 3. Results of the Spearman rank order correlation coefficient test to detect trend.
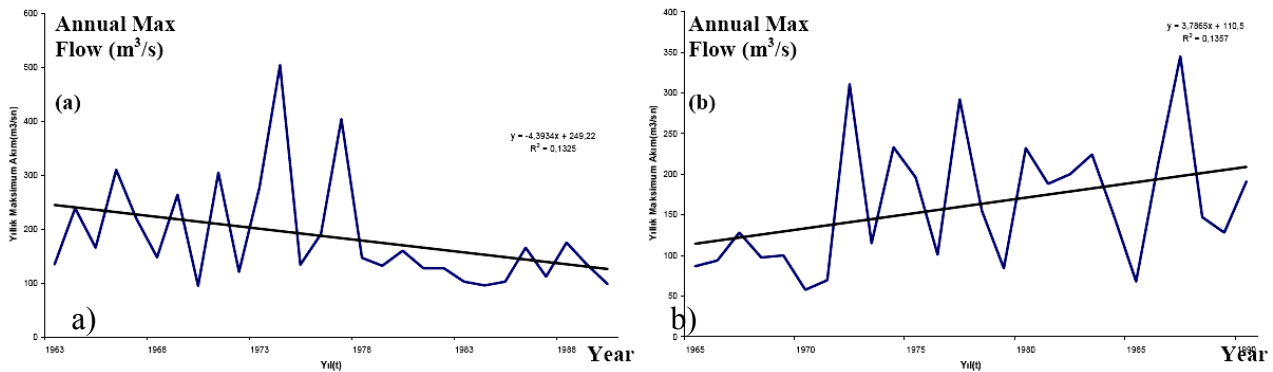
Figure 3. Linear trends fitted to stations 2218 (a) and 2238 (b).

4.5 Best-fit probability distribution

Comparison of correlation coefficients between the probability distribution chosen and the observed histogram shows how the selected distribution is applicable to the observed data. As said before, six probability distribution functions were selected and tested. Results were given in Table 4 from which it is concluded that the maxima series of the stations were best represented either by the Frechet or Weibull distribution in an equal chance while only one stations tended to obey the 2-parameter Gamma distribution.

Station → Distribution ↓	2202	2213	2215	2218	2228	2232	2233	2238	2239	2245	2247
Normal	0.994	0.929	0.914	0.895	0.964	0.792	0.953	0.970	0.907	0.975	0.968
LN2	0.984	0.993	0.945	0.976	0.976	0.891	0.978	0.985	0.980	0.969	0.941
LN3	0.984	0.993	0.945	0.976	0.976	0.891	0.978	0.985	0.980	0.969	0.941
G2	0.976	0.979	0.931	0.961	0.988	0.872	0.970	0.991	0.986	0.985	0.971
Weibull	0.943	0.964	0.898	0.992	0.988	0.832	0.936	0.987	0.976	0.991	0.986
Frechet	0.993	0.994	0.954	0.936	0.972	0.943	0.988	0.973	0.985	0.964	0.941

Table 4. PPCC test results.

5. CONCLUSIONS

After interpreting above given results the following conclusions are drawn from the study:

1. Outlier detection test was ended with outliers in six stations whereas no outlier in the remaining five was found.
2. Maxima in the daily average streamflow time series of the region is considered natural after the random structure of the time series was determined by the test employed in the study.
3. Only two stations were found with trend while no trend is detected in the majority of the stations.
4. No jumps were linked to stations at all.
5. Maxima in the region can either be best-fit by the Frechet distribution or Weibull both non-symmetrical.

Based on all these, it can be concluded that maximum flow may reach, in some stations, very high values that can result in floods. No or relatively less intervention by human to the river basins in the region may have effect on the random structure of the maxima series. Absence of jump and trend (except for two stations) can be considered another result of this. The skewed time series show the fit by the extreme value type distributions. Finally, it should be kept in mind that the study is not a regional analysis but is station-based. Therefore, a regional analysis can be employed.

REFERENCES

Adeloye, A.J., and M. Montaseri (2002), Preliminary streamflow data analysis prior to water resources planning study, *Hydrol. Sci. J.*, 47(5), 679-692.

Fanta, B., B.T. Zaake, and R.K. Kachroo (2001), A study of variability of annual river flow of the Southern African region, *Hydrol. Sci. J.*, 46 (4), pp. 513-524.

Hubert, P. (2000), The segmentation procedure as a tool for discrete modelling of hydrometeorological regimes, *Stoch. Env. Res. Risk A.*, 14, 297-304.

Itibar, M.D. (2005), *Probabilistic methods for structural characteristics of Aegean region stream flows*, MSc thesis, Istanbul Technical University, Institute of Science and Technology, Istanbul (Turkey) *(in Turkish)*.

Kaynar, L. (2005), *Analysis of maximum flows in the Eastern Black Sea region, by statistical methods*, MSc thesis, Istanbul Technical University, Institute of Science and Technology, Istanbul (Turkey) *(in Turkish)*.

Santos, M.J., and R. Henriques (1999), Analysis of the European annual precipitation series, *Technical Report to the ARIDE Project no.3*, Water Institute, Lisbon (Portugal).

Vogel, R.M. (1986), The probability plot correlation coefficient test for the normal, lognormal and Gumbel distributional hypotheses, *Water Resour. Res.*, 22 (4), 587-590.

Vogel, R.M., and D.E. McMartin (1991), Probability plot goodness-of-fit and skewness estimation for the Pearson type III, *Water Resour. Res.*, 27, 3149-3158.

Observing and modelling exceptional floods and rainfalls
Proceedings of the AMHY-FRIEND International Workshop on Hydrological Extremes,
held at University of Calabria, Cosenza (Italy), May 3-4, 2006.

APPROCHE METHODOLOGIQUE DE CALCUL DU DEBIT PLUVIAL EN CAS D'INSUFFISANCE DE DONNEES. CAS DE LA REGION DE TIPAZA, ALGERIE

I. Bouaïchi[1], B. Touaïbia[1] & F. Dernouni[2]

(1) Laboratoire d'Hydrologie, Ecole Nationale Supérieure de l'Hydraulique, Blida, Algérie.
(2) Laboratoire d'Hydraulique urbaine, Ecole Nationale Supérieure de l'Hydraulique, Blida, Algérie**.**

ABSTRACT
The objective of this work consists of an approach of regionalization of the climatic exponent using the calculation of the flow for the dimensioning of hydraulic networks in the case of insufficiency of data. The specific downpours are studied making it possible to build the curves of duration–intensity–frequency.
The linear interpolation by the method of Thiessen and the multivariate analysis were used for the determination of this exhibitor at the pluviometric stations deprived out of recording rain-gauges. The regionalization approach by the method of the kriging allowed the creation of a chart of isovalues of climatic exponent in the area of Tipaza prone to the flash floods.

1. INTRODUCTION

En Algérie, le problème des inondations en milieu urbain surgit souvent en raison d'un sous dimensionnement du réseau d'assainissement lié soit à un manque d'information ou à un manque d'étude appropriée conséquente quant aux pluies de courte durée.

La connaissance des observations pluviométriques constitue le seul outil pour la compréhension du comportement hydrologique d'un événement. Ainsi, il devient impératif de connaître les techniques appropriées pour obtenir le maximum d'information sur les échantillons, évaluer la qualité des conclusions déduites et quantifier le risque provenant d'une généralisation à partir de données partielles.

Les cumuls journaliers collectés sur les réseaux pluviométriques constituent l'essentiel de l'information acquise sur des périodes plus ou moins longues et des zones plus ou moins étendues. Son acquisition dépend essentiellement de la densité du réseau pluviométrique (*Remenieras,* 1979).

La cartographie directe des champs pluviométriques n'a de sens qu'au-delà d'une durée d'intégration, fonction à la fois, de la structure et du nombre des averses d'une part et de la densité de réseau d'autre part. Elle reste un outil d'investigation indispensable pour toute aide à la décision. La cartographie passe par la régionalisation dont l'objectif serait d'extraire de cet ensemble d'information, les paramètres pluviométriques nécessaires pour l'élaboration de cartes d'isovaleurs.

La région de Tipaza a constitué notre champ expérimental ayant pour objectif la régionalisation de l'exposant climatique b**,** entrant dans le calcul du débit pluvial.

2. PRESENTATION DE LA REGIONALISATION

Dans les pays en voie de développement, l'information hydrologique possède, en plus des erreurs traditionnelles dites systématiques, des incertitudes supplémentaires dues au manque d'uniformité dans la distribution du réseau de mesure, à la quasi-inexistence d'observations sur les bassins de faible superficie, à la faible quantité des données enregistrées et enfin au manque chronique de moyens financiers qui fréquemment paralyse les jaugeages et augmente les défaillances des séries continues (*Touaibia,* 2004).

La régionalisation des variables hydrologiques est un ensemble de procédure méthodologiques cherchant à exploiter au maximum les données existantes dans une région pour mieux les estimer et les étendre en des lieux où les données sont inexistantes (*Le Barbe et al.,* 1992).

Néanmoins, le problème que pose la régionalisation des paramètres hydrologiques est donc l'élaboration de méthodes qui permettent, compte tenu de l'information disponible, d'aboutir à des descriptions régionales, directement utilisable par les différents acteurs de l'eau.

3. PRESENTATION DE LA REGION DE TIPAZA

La région de Tipaza est une région côtière située à l'Ouest de la capitale Alger. Elle s'étend sur 120 km environ à partir de la commune de Douaouda du coté Est, jusqu'à celle de Damous du coté Ouest sur une largeur de 20 km environ vers le Sud. Elle se situe dans le grand bassin versant du côtier Algérois comprenant lui même 22 sous-bassins (Figure 1).
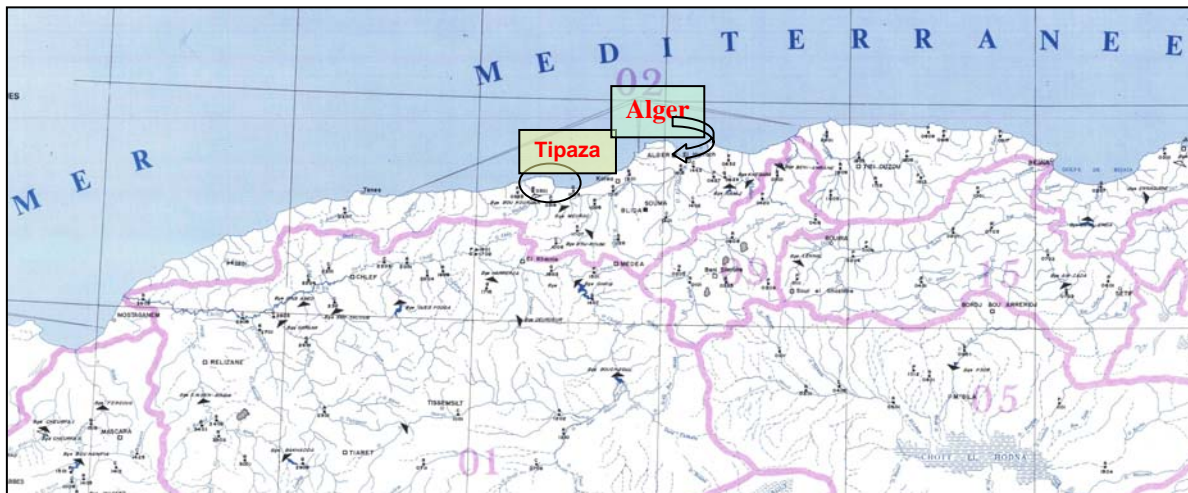
Figure 1. Situation géographique de la région de Tipaza.

La zone étudiée, d'une superficie de 3580 km² est équipée en 33 pluviomètres et 6 pluviographes. Tipaza, ville côtière et touristique connaît chaque année des inondations suite aux averses torrentielles. Le réseau d'assainissement de type unitaire ne supporte plus les débits pluviaux. Etant en pente, chaque averse crée un débit de ruissellement chargé, d'autant plus qu'à l'amont, la région de Tipaza jouit d'une agriculture d'autosubsistance.

4. CONSTITUTION DE LA BANQUE DES DONNEES

La région de Tipaza   possède un réseau de mesure météorologique très lâche datant de l'ère coloniale dont la majorité de ses stations a connu des ruptures dans leurs mesures. 39 stations pluviométriques sont réparties dans l'espace étudié (*ANRH,* 2005), d'une superficie de 3580 km², dont 6 d'entres elles sont équipés en pluviographes. Les données essentielles ont consisté en des séries de pluies annuelles, maximales journalières et de courte durée.

4.1 Identification des stations pluviométriques

Les stations équipées en pluviographes ont fait l'objet d'une étude poussée quand aux averses enregistrées. Les 33 autres stations étudiées sont munies simplement de pluviomètres car elles enregistrent seulement les pluies journalières. La position géographique des 39 stations est en Figure 2.
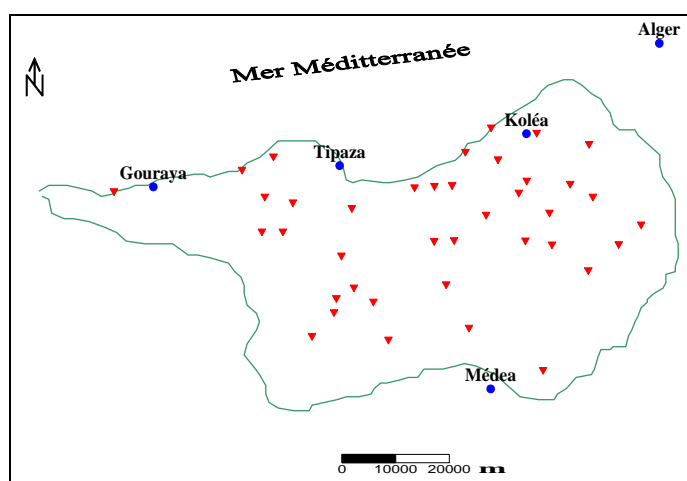
Figure 2. Position des stations pluviométriques.

5. APPROCHE METHODOLOGIQUE DE REGIONALISATION

Notre objectif est la régionalisation de l'exposant climatique. Toute la difficulté y réside car nous ne disposons que de 6 stations pluviométriques équipées en pluviographes. En réalité, la construction des courbes (IDF) à partir de la série des pluies maximales journalières d'une station, n'est qu'une approximation en absence des données exactes car, les intensités les plus importantes sont enregistrées pendant des intervalles de temps courts (*Llamas,* 1993). 2634 pluviogrammmes ont été dépouillées dont la durée de l'averse varie de 15 à 180 min. Des pas de temps de 15, 30, 45, 60, 90, 120, 150 et 180 min sont considérés permettant de tracer pour chacune des stations étudiées les courbes Intensité-Durée-Fréquence. La loi de distribution théorique loi Lognormale a donné le meilleur ajustement des pluies de courtes durées, au vu du test de Pearson χ^2 comparativement à la loi de Gumbel, pour la détermination des quantiles pour chaque pas de temps (*Dubreuil,* 1974).

La modélisation mathématique a permis d'établir une relation fonctionnelle de type puissance (*Dagnellie,* 1992) entre l'intensité moyenne maximale probable $\bar{i}_{t,p\%}$ et l'exposant climatique b de la forme : $\bar{i}_{t,p\%} = a\,t^{-b}$.

Pour chacune des stations étudiées, 6 exposants climatiques sont déterminés ce qui reste très insuffisant pour la régionalisation. Se basant sur la méthode de Thiessen (*Llamas,* 1993) des zones d'influence des 39 stations pluviométriques sont délimitées permettant par la méthode de l'interpolation linéaire de déterminer l'exposant climatique pour 6 stations supplémentaires, relevant le nombre à 12 stations. La zone d'étude étant étendue, le nombre de stations disposant d'un exposant climatique reste faible.

La représentativité des stations reste encore insuffisante pour l'élaboration d'une carte de l'exposant climatique. Pour étendre ce dernier aux autres stations, l'analyse multidimensionnelle est entreprise entre la variable à expliquer b et les variables explicatives, (coordonnées Lambert X et Y, Altitude Z, pluie moyenne interannuelle P_{an}, pluie maximale journalière $P_{max,j}$ et la moyenne des pluies maximales journalières $\bar{P}_{max,j}$ sur la période d'observations). Trois modèles sont établis b=f(X,Y,Z,P_{an}); b=f(X,Y,Z,$P_{max,j}$) et b=f(X,Y,Z,$\bar{P}_{max,j}$). La régression pas à pas est utilisée. La valeur du coefficient de corrélation multiple R_{mult} justifie le choix du modèle après vérification de sa valeur critique sur la table de Fisher (*Dagnellie,* 1992).

1ère modèle
$$b = -0{,}0004\,X + 0{,}0008Y - 0{,}0001Z + 0{,}0001\,P_{interan} + 0{,}25 \qquad R_{mult} = 0{,}46$$
$$(1)$$

2ème modèle
$$b = 0{,}000033\,X + 0{,}0038Y - 0{,}0002Z + 0{,}0013P_{max,j} - 1{,}1 \qquad R_{mult} = 0{,}89$$
$$(2)$$

3ème modèle
$$b = -0{,}00003\,X + 0{,}00094\,Y - 0{,}00009\,Z + 0{,}0024\bar{P}_{max\,j} - 0{,}03 \qquad R_{mult} = 0{,}73$$
$$(3)$$

Mathématiquement, au vu de R_{mult}, le modèle 2 devrait être retenu. Malheureusement les résultats sont surestimés comparativement à ceux du modèle 3 (Tableau 1) qui répondent mieux à la réalité. Aussi, le critère de Nash–Sutcliffe (1970) calculé à cet effet a donnée une valeur supérieure à 98%. Le modèle 3 a été retenu pour étendre l'exposant aux 27 autres stations existantes dans la région et pour lesquelles il n'y a aucune information sur les averses. Les résultats pour les trois modèles sont résumés dans le Tableau 1.

Au vu du Tableau 1, l'exposant climatique b est expliqué par le variable X, Y, Z et la moyenne des pluies maximales journalières soit le modèle 3. Pour mieux cerner cette extrapolation, le krigeage est entrepris (*Deutsch et al.,* 1998). La fonction de structure de l'exposant climatique ou variogramme expérimental est identifiée pour connaître le poids en chaque point de géoréférencement (*Chauvet,* 1999). Quatre modèles sont testés, le linéaire, sphérique, exponentiel et gaussien dont les résultats sont présentés dans le Tableau 2. La minimisation de l'erreur type a permis d'identifier le modèle gaussien comme étant le meilleur (Figure 3).

La fonction de la répartition spatiale de l'exposant climatique b suivant la distance h séparant les points de calcul est donnée par le modèle gaussien, soit:

$$\gamma(h) = 0.0025 \left[1 - e^{-\left(\frac{1.732\,h}{17.88}\right)^2} \right] \tag{4}$$

N°	Station	Code	Modèle 1	Modèle 2	Modèle 3
1	Bordj Ghobrini	20301	0.41	0.43	0.43
2	Menaceur	20303	0.39	0.41	0.44
3	Lazabane	20304	0.38	0.34	0.39
4	Meurad Barrage	20306	0.38	0.46	0.44
5	Djebadra	20307	0.36	0.32	0.38
6	Chechel phare	20312	0.42	0.49	0.45
7	Bellah RN11	20319	0.40	0.39	0.41
8	Hadjout (pont CW7)	20325	0.40	0.38	0.43
9	Boukourdane barrage	20329	0.39	0.40	0.44
10	Tombeau de la chrétienne	20402	0.38	0.40	0.41
11	Berrard (Ain Tagourait)	20403	0.39	0.43	0.42
12	Fouka marine	20405	0.40	0.49	0.44
13	Fouka ville	20406	0.38	0.55	0.42
14	Ain Beniam	21015	0.33	0.26	0.37
15	Hammam Righa	21016	0.35	0.40	0.41
16	Ameur El Ain	21020	0.38	0.35	0.39
17	Attatba Cave	21022	0.40	0.41	0.43
18	El Affroun (DNC 44)	21026	0.38	0.37	0.41
19	Chiffa (RN4)	21105	0.38	0.38	0.40
20	Fer a Cheval	21201	0.40	0.43	0.42
21	Beni Mered	21208	0.38	0.47	0.42
22	Boufarik Perinière	21209	0.39	0.47	0.43
23	Oued El Alleug	21210	0.39	0.43	0.42
24	Koléa secteur	21233	0.28	0.35	0.38
25	Passerelle	21307	0.37	0.35	0.41
26	Douera	21407	0.39	0.44	0.42
27	Douar Makli	21427	0.38	0.41	0.42

Tableau 1. Calcul de l'exposant climatique par les trois modèles.
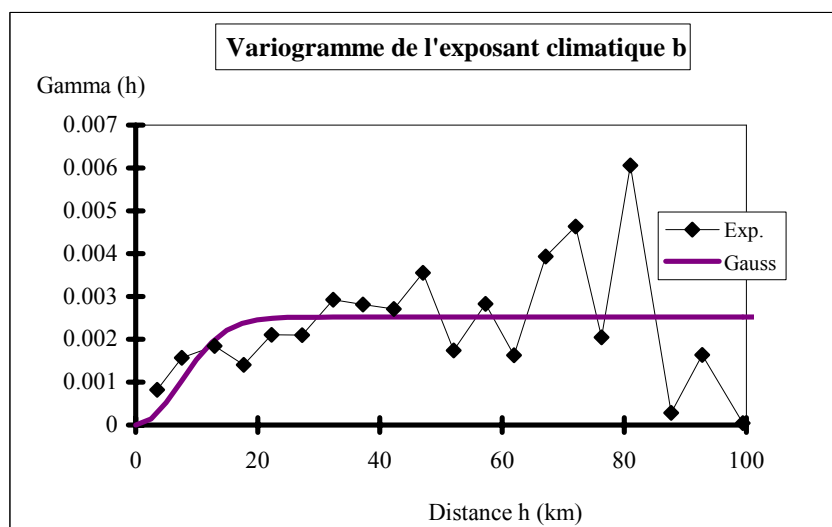
Figure 3. Variogramme expérimental.

Type de modèle	Portée	Palier	Pépite	Erreur type
Linéaire	99,45	0,0061	0	0,0022
Sphérique	99,45	0,0061	0	0,0025
Exponentiel	99,45	0,0061	0	0,0025
Gaussien	17,88	0,0025	0	0,0013

Tableau 2. Calcul des accroissements pour le variogramme.

6. CARTOGRAPHIE DU DEBIT PLUVIAL POUR UNE DUREE DE L'AVERSE DE 15MIN ET DE PERIODE DE RETOUR 10 ANS

Dans le domaine de l'assainissement urbain, le calcul de l'intensité moyenne maximale de durée 15 min et de période de retour 10 ans s'avère nécessaire pour la détermination du débit pluvial entrant dans le dimensionnement du réseau (*Bourrier,* 1997).

L'intensité moyenne maximale de durée 15 min et de probabilité 10% «$\bar{i}_{15mn,10\%}$» est déterminée à partir des courbes IDF pour les stations équipées en pluviographes et par l'expression (5) pour les autres stations. Elle correspond à la pluie maximale probable de durée 15 min «$P_{max,15min,10\%}$» rapportée à l'intervalle de référence 15 min.

$$\bar{i}_{15min,10\%} = P_{max,15min,10\%}/0.25 \quad (mm/h) \quad (5)$$

avec:

$$P_{15min,10\%} = P_{max,j,10\%} \left(\frac{0,25}{24}\right)^{b} \quad (mm) \quad (6)$$

où $P_{max,j,10\%}$ est déterminée après ajustement des pluies maximales journalières à la loi théorique de distribution de Gumbel.

L'approche méthodologique adoptée de calcul de l'exposant climatique a permis de calculer pour chacune des 39 stations, non seulement l'intensité moyenne maximale de durée 15 min et de période de retour 10 ans $\bar{i}_{15min,10\%}$, mais aussi le débit spécifique pluvial $M_{15min,10\%}$ correspondant, dont la connaissance du géoréférencement des stations pluviométriques nous a guidé vers l'élaboration d'une carte d'isovaleurs (Figure 4) d'égal débit pluvial pour une durée de l'averse de 15 min et de période de retour 10 ans.
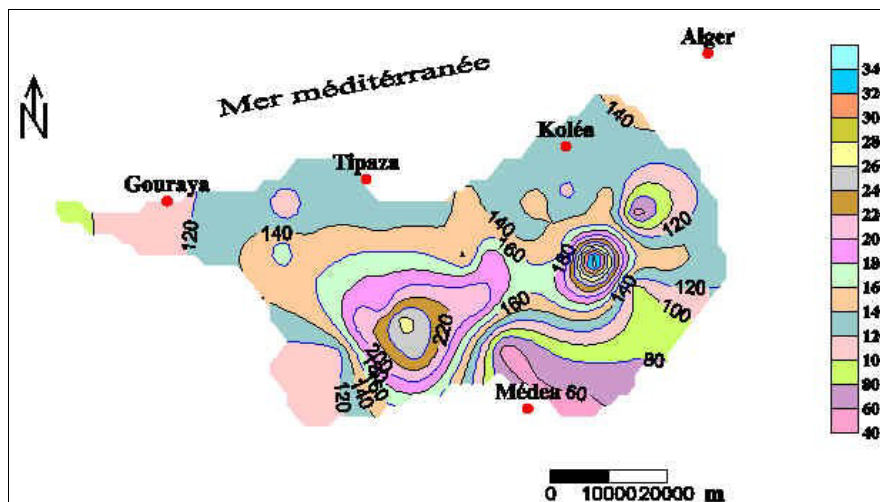
Figure 4. Carte en isolignes du débit spécifique pluvial [l s^{-1} . km^{-2}].

7. CONCLUSION

Compte tenu du manque d'information et de l'insuffisance des données dans cette région d'étude dans le contexte algérien, l'approche adoptée reste plausible. La carte établie pour une probabilité de 95 % reste un outil exploitable pour les bureaux d'études entreprenant le dimensionnement d'un réseau d'assainissement.

La ville de Tipaza enregistre un débit spécifique pluvial entre 120 et 140 l·s⁻¹ha⁻¹ pour une durée de l'averse de 15 min et une période de retour de 10 ans. En Algérie du Nord, les intensités créant des dégâts sont supérieurs à 24 mm/h, soit en terme de débit pluvial 67 l·s⁻¹ha⁻¹. Si, nous nous referons à cette dernière, Tipaza est sujette aux inondations à chaque fois que le débit pluvial dépasse 67 l·s⁻¹ha⁻¹. C'est ce que nous avons observé ces dernières années.

REFERENCES

ANRH (2002), *Données pluviométriques*, Document interne, Direction régionale, Blida, Algérie.

Bouaichi, I. (2005), Contribution à la régionalisation du débit pluvial dans la région de Tipaza, *Mémoire d'ingénieur d'Etat en Hydraulique*, Ecole Nationale Supérieure de l'Hydraulique, Blida, Algérie.

Bourrier, R. (1997), *Les réseaux d'assainissement. Calculs, Applications et perspective*, Lavoisier Tec et Doc, Paris.

Dagnellien, P. (1992), *Statistiques théorique et appliquée,* Tome 1, Presses agronomiques de Gembloux, Belgique.

Dubreuil, P. (1974), *Initiation à l'analyse Hydrologique*, Ed. Masson et CIE, ORSTOM, Paris.

Le Barbe, L., and E. Servat (1992), *Régionalisation en Hydrologie. Application au développement*. Huitièmes journées Hydrologiques de l'Orstrom. Edition Orstrom, France.

Llamas, J. (1992), *Hydrologie générale. Principes et applications,* 2ᵉᵐᵉ édition, Gaëtan morin, Québec.

Nash, J.E, and J.V. Sutcliffe (1970), River flow forecasting, through conceptual problems. Part I-A. Discussion of principles. *J. Hydrol., 10*(3), 282-290.

Réméniéras, G. (1979), *Hydrologie de l'ingénieur*, Collection des études et recherches d'électricité de France, Eyrolles.

Touaïbia, B. (2004), *Manuel Pratique d'Hydrologie,* Edition Madani, Blida, Algérie.

RAINFALL PREDETERMINATION IN MEDITERRANEAN CLIMATE USING REGIONAL APPROACH

L. Neppel, C. Bouvier, H. Niel

UMR HydroSciences Montpellier, Maison des Sciences de l'Eau, Université Montpellier II, France.

ABSTRACT

Usually the rainfall or peak discharges time series are too short to allow a precise estimation of the cumulative distribution of frequency (cdf) of the extremes values. In particular the shape of the tail of the cdf is subject to large uncertainties. The regional approach is a way to reduced them. It has been applied for local or punctual maximum annual daily rainfalls and for the maximum spatial mean rainfall observed during extreme daily rainfall events in South of France. It has been showed that their cdf are Frechet type rather then Gumbel type. That result does not seem to be related to the spatial dependency between the data. Also a framework for modelling spatial mean rainfall–area–frequency curves has been proposed, based on the scale properties of the spatial mean rainfall cdf.

1. INTRODUCTION

French Mediterranean regions are subject to heavy rainstorms that generate severe floods. Usually rainfall hazard studies and predetermination of discharge corresponding to a given return period are subject to large uncertainties due to sampling because of short time series. Enlarging the set of data can be done by two ways: regional or historical approach. In this paper we will focus on regional approach concerning extreme rainfall analysis in Mediterranean climate.

For risk assessment, hydrologists are interested by the maximum volume of rainfall over a given area, during a given duration. Usually it is described with i) the local or punctual cumulated frequency distribution of maximum rainfall over a year or a season, with eventually an areal reduction factors or ii) the cdf of the spatial mean rainfall over a given area. Whatever the case, a question which arise is the shape of the cdf. According to the theory of generalize extreme value three cases are possible (*Koutsoyannis* 2004a, *Beirlant et al.,* 2005):

i) the quantiles increase like the logarithm of the return period, noted log(T), which corresponds to the well known Gumbel distribution;

ii) the quantiles increase more rapidly than log(T) which corresponds to the Frechet type distributions;

iii) the quantiles reach a constant for T tends toward infinity which corresponds to the Weibull distributions.

The shape of the distribution has some obvious consequences in engineering, when a design storm or a design discharge has to be chosen. Several studies are interested in the extreme behaviour of maximum annual or seasonal rainfall like *Koutsoyannis* (2004b) and *Bacro and Chaouche* (2006): on the analysis of some long rainfall records around the

world, they concluded that local maximum rainfall cdf are from the Frechet type rather than Gumbel or Weibull family. Some other studies using rainfall simulator seem to lead to the same conclusions in Mediterranean area (*Arnaud and Lavabre,* 1999). On the other hand some argue that the Frechet type cdf can be explain by non-homogenous sample, and they use a combination of exponential cdf to model the daily maximum annual rainfall, each cdf corresponds to a given weather type (*Garçon et al.,* 2006). After a short presentation of the studied region and the data (section 2), we propose to analyse the asymptotic behaviour of extreme rainfall in the punctual or local case using punctual rainfall records (section 3) and in the spatial case (section 4) using spatial mean rainfall. A regional approach is used in both cases, as it has been shown that the weight of extreme event is better taken into account (*St Hilaire et al.,* 2003). A discussion follows in section 5.

2. STUDIED REGION AND DATA.

The region considered is the Cévennes-Vivarais Mediterranean Hydro-meteorological Observatory (OHMCV) observation domain (*Delrieux,* 2003): a 250x250 km² zone centred on the Cévennes mountains in South of France (Figure 1). The data are daily rain depths measured at the French Weather Service network. During the 1950-2003 observation period, the number of available daily rain gauges varies between 400 gauges to a maximum of near 600 gauges, with a mean density of 10 gauges for 1000 km². A sub domain is also defined, around 10000 km², with 165 daily rain gauges of at least 15 consecutive years of records during 1958 and 2002.
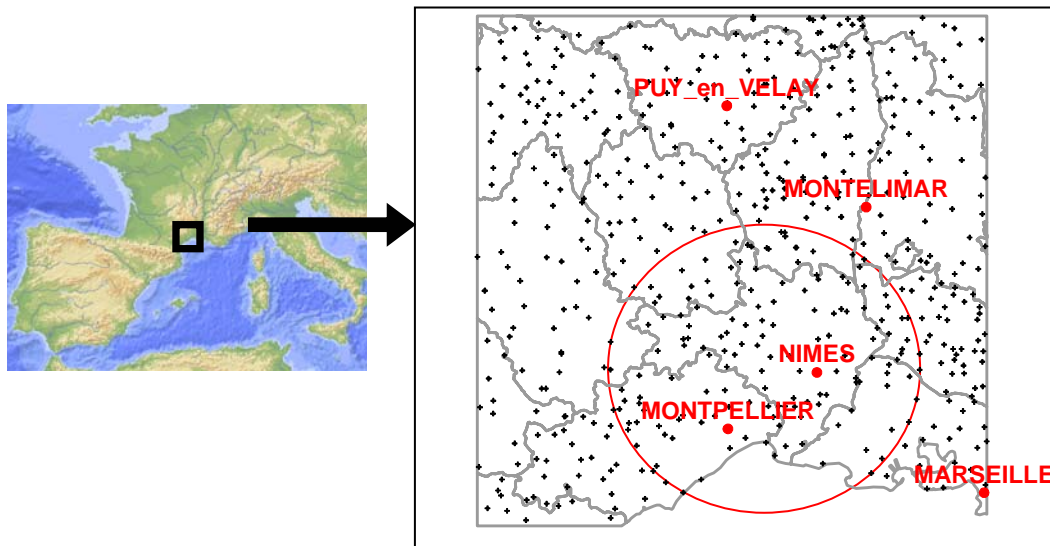
Figure 1. Location of the OHMCV observation domain and the sub region. The black points are the locations of the daily rain gauges of the French Weather Service in the year 2000.

3. REGIONAL CDF OF MAXIMUM ANNUAL DAILY RAINFALL

The general principles of regional method for rainfall or runoff analysis has been widely describe in several papers for example *Hosking* (1990), *Hosking and Wallis* (1993), *Rao and Hamed*, (2000), *Dominguez et al.* (2005). The method has been applied

on the maximum annual daily rainfall in the South of France. This part of the study concerns the sub domain presented in the previous section. The 165 rain gauges with records longer than 15 years during 1958-2002 have been selected. For each gauge the maximum annual daily rainfall has been sampled.

First the homogeneity of the region has been verified. The coefficient of variation (CV) of each gauge has been computed and it has been shown that the fluctuation of CV between all the gauges can be explained by sampling uncertainty (*Dominguez et al.,* 2005). We have defined at each gauge i the reduced variate Y_i:

$$Y_{i,j} = P_{i,j} / \overline{P}_i \qquad (1)$$

where $P_{i,j}$ is the daily maximum annual rainfall at the gauge i the year j and $\overline{P}_i$ is the mean maximum annual daily rainfall at the gauge i.

The two first moments of Y are constant and do not depend on the gauge i. Thus the hypothesis that all the Y_i variates are identically distributed can be done. A regional sample of 5120 the reduced variate Y is then constructed with all the gauges. According to theory of the extreme value, a GEV is fitted to the sample with the method of L-moment (*Rao and Hamed,* 2000). The probability p of non exceedance is given by:

$$p = \mathrm{Prob}(Y \leq y) = F(y) = \exp\left\{-\left[1 - k\left(\frac{y - u}{\alpha}\right)\right]^{1/k}\right\} \qquad (2)$$

where the estimation of the position, the scale and the shape parameters are respectively:

$$\widehat{u} = 0.79$$
$$\widehat{\alpha} = 0.29 \qquad (3)$$
$$\widehat{k} = -0.13$$

The maximum annual daily rainfall cdf at any gauge i is deduced from equation (2) by multiplying by $\overline{P}_i$. One can notice several points:

i) the shape parameter is negative and thus corresponds to the Frechet cdf (Figure 2). As it has been estimated with a sample of more than 5000 values, sampling uncertainties are quite reduced. Moreover, this value is near the result of *Koutsoyannis* (2004b) who has analysed 169 long series (at least 100 years) of different climates and found a shape parameter around –0.15;

ii) as consequences the Gumbel cdf used systematically to model the maximum annual rainfall frequency can lead to an under-estimation of the quantiles up to 50 % (*Dominguez et al.,* 2005).

Some argue that this "hyper exponential" behaviour could be explained by the spatial dependency between the maxima observed at different gauges and corresponding to the same event. This point has been analysed as follows: when a maximum annual daily rainfall correspond to the same event at different gauges, only the value distant from more than 80 km are selected in the regional sample. This distance corresponds to the distance of decorrelation between two rainfall measurements at a daily time step (*Neppel et al.,* 1998). The Figure 3 shows the regional cdf: despite of the spatial independence between the maxima at each gauge, the cdf is still a Frechet type.
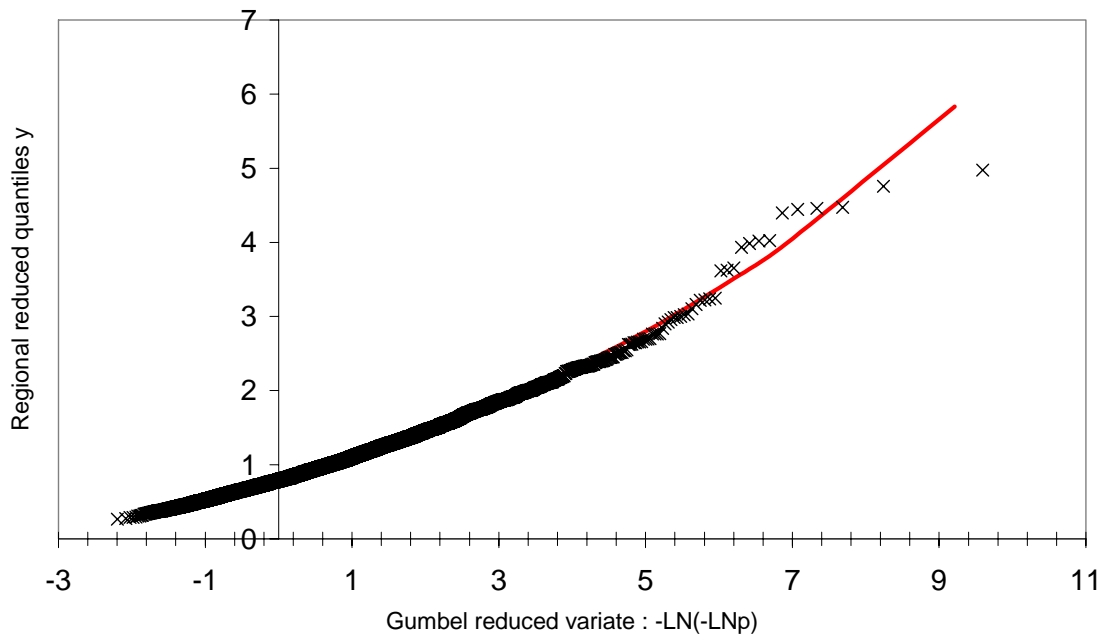
Figure 2. Regional cdf of the reduced variate Y in a Gumbel graph: comparison between the empirical frequencies obtained with the regional sample and the fitted GEV cdf.
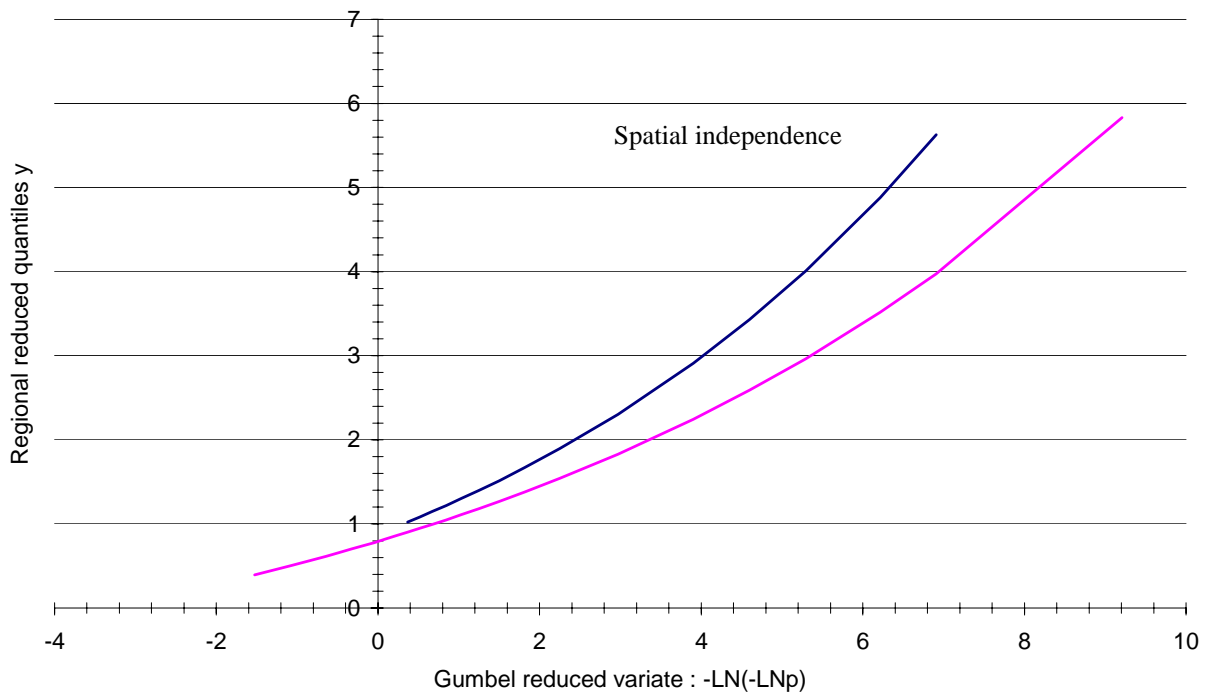
Figure 3. Comparison between the regional cdf with spatial dependence between maximum daily rainfalls and spatial independence between maximum daily rainfalls.

An interesting property of regional cdf is that it is less affected by sampling compared to local cdf. As an example the Table 1 shows the 10 and 100 years return period quantiles obtain at the Generargue gauge, using the local fitting of a GEV and the regional cdf. Two periods of observation are considered: 1939-2001 and 1939-

2002. In September 2002 occurred the highest rainfall event recorded in the region during the last 60 years, with an observation at Generargue of 540 mm/day. The Table 1 shows that the quantiles obtained with the local cdf varies up to 60% from a period to another, while the ones obtained with the regional cdf varies only of 7 %.

Quantiles	Maximum annual daily rainfall quantiles (mm/day)	
	Period 1939-2001	**Period 1939-2002**
T=10 years	a) 148 mm +/- 15 b) 157 mm	a) 178 mm +/- 30 b) 168 mm
T=100 years	a) 214 mm +/- 47 b) 265 mm	a) 336 mm +/- 145 b) 284 mm

Table 1. 10-years and 100-years return period quantiles at the gauge of Generargue for two different observation periods, with a) a local cdf estimation and b) the regional cdf rescaled at the Generargue gauge.

4. REGIONAL CDF OF THE DAILY MAXIMUM SPATIAL MEAN RAINFALL AT DIFFERENT SPATIAL SCALES

In this section we are interested by the maximum rainfall volume over different area S that falls during Mediterranean extreme events. We try to generalize the regional approach developed for the punctual maximum annual daily rainfall to the spatial mean rainfall. The aim is to analyse the asymptotic behaviour of the maximum spatial mean rainfall cdf of the extreme rainfall events.

4.1 Maximum spatial mean rainfall sampling.

During the 1950-2003 observation period a rainfall event is defined by a rainfall depths of at least 190 mm/day somewhere in the OHMCV observation domain. If this threshold is reached at a given date, all the daily rainfall depths measured at the rain gauge network are extracted from the French Weather Service Database. They are then used to map the event's daily rain field using a climatological kriging (*Bastin et al.,* 1984). 186 rainfall events have been selected.

For each event and for a given area S supposed to be rectangular, we search for the maximum rainfall volume over S (Figure 4). This procedure is repeated for 19 areas from 1 to 3500 km² and for the 186 rainfall events, leading to 19 samples of the 186 maximum rainfall volumes over an area S, noted L(S). What are the cdf of the L(S) samples and how do they vary according the spatial scale S ?

4.2 Distribution fitting.

The empirical frequency distributions of several L(S) variates are shown in Figure 5a. It appears that the structure of the curves "spatial mean rainfall – area – return period" (LST) are similar to IDF curves: if a cdf of L(S) for a given area is known, the cdf of the other L(S) variate for other area S can be deduced from the previous one, using a scale factor. To model the structure of the LST curves we have adapted the general method proposed by *Koutsoyannis* (1998) for modelling IDF curves: they are described by the ratio of two functions, the first one depends only on the return period and the second one represents the time scale relation. The same structure is used by replacing time by space.
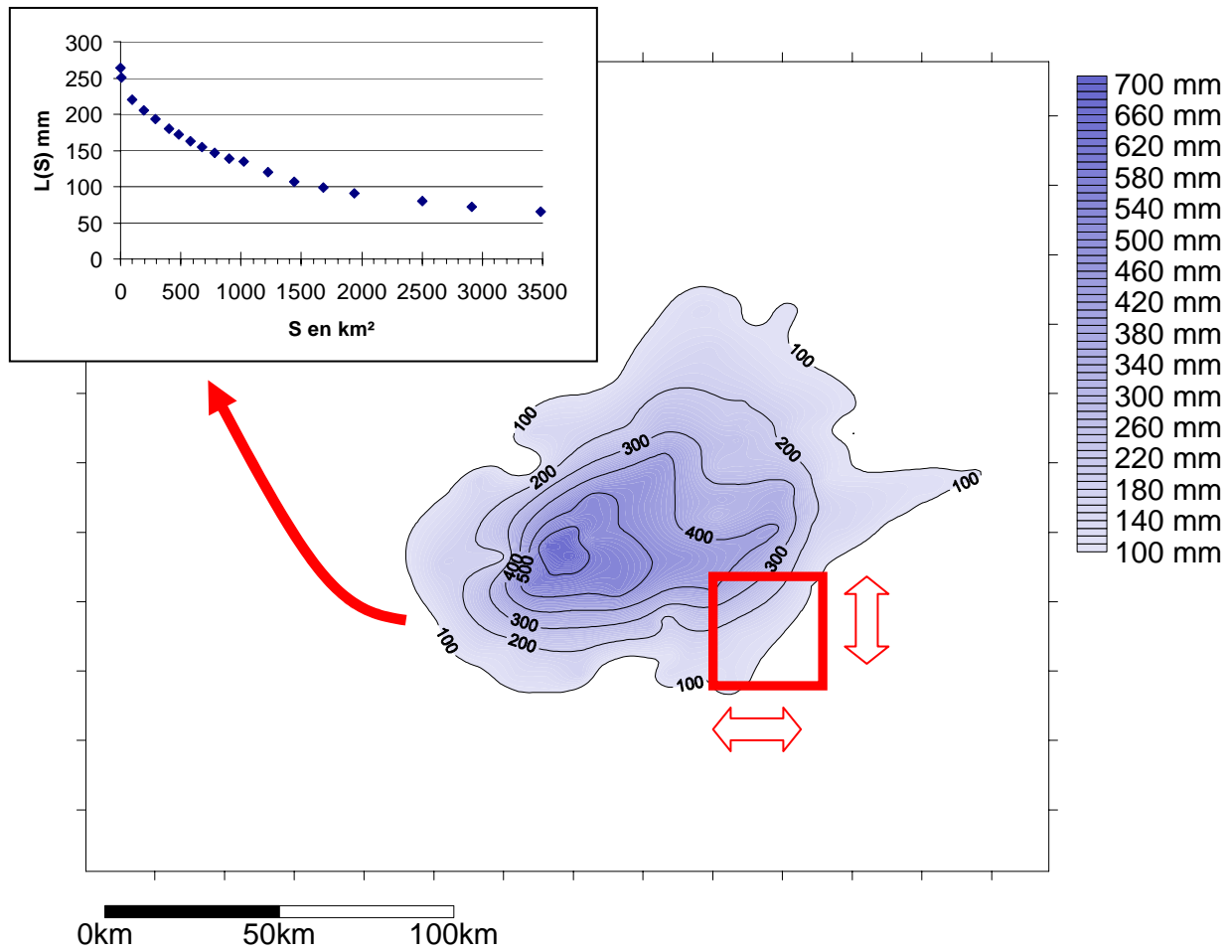
Figure 4. Illustration of the L(S) sampling procedure for the 8th September 2002 rainfall event. Daily rainfalls are in mm.

Thus the spatial mean rainfall over the area S corresponding to the T-return period can be obtain by a function a(T) which depend only on the return period T, divided by a function b(S) depending on the area S:

$$L(S,T) = a(T)/b(S) \qquad (4)$$

The a(T) expression depend on the cdf of the L(S) variate and the expression of b(S) describes the scale relation. The L(S) samples are peak over threshold samples. If the threshold is high enough the cdf of L(S) should be generalized Pareto distribution (GPD). We consider that this hypothesis is reached if the number of events over the threshold each year fits a Poisson distribution. This is obtained for rainfall events that reached at least 220 mm/day. The corresponding sample contains 103 events, i.e. an average of 1.91 events/year. Under the assumption of GPD distribution for the L(S) variate, equation (4) becomes:

$$L(S,T) = \frac{u + \dfrac{\alpha}{k}(1 - (\lambda T)^{-k})}{(S + \theta)^{\eta}} \qquad (5)$$

The three parameters u,α, k are respectively the position, the scale and the shape parameters of GPD distribution. θ and η depend on the scale relation between the L(S)

distributions. λ is the mean number of events exceeding the threshold per year. Let $\hat{L}(S_i)_j$ denote the spatial mean rainfall over the area S_i corresponding to the rank j in the sample and let $L(S_i)_j$ denote the theoretical quantile of rank j obtain with equation (5). We define the error function $e(u,\alpha,k,\theta,\eta)$ as follows :

$$ e = \frac{1}{n.ns} \sum_{i=1}^{ns} \sum_{s=1}^{n} \left[LN \frac{\hat{L}(S_i)_j}{L(S_i)_j} \right]^2 \tag{6} $$

The five parameters are obtained by numerical minimisation of e, where n is the L(S) sample size and ns the number of S value. The following set of parameters has been obtained: $\alpha= 153.2$, $u= 761$, $\theta= 151.09$, $\eta= 0.251$, $k=-0.14$. We note that (Figure 5b):

i) the shape parameter of the GPD distribution is negative, corresponding to the Frechet domain of attraction;

ii) the result seems to be coherent with the regional cdf of daily maxima annual rainfall: indeed if S reaches zero, the L(S,T) model gives the cdf of local or punctual distribution of daily rainfall over the 220 mm/day threshold. Remember a general statistical result: if the peak over threshold variates is GPD distributed then the maximum annual is GEV distributed with the same shape (*Beirlant et al.,* 2005). If we compare the shape parameter of the punctual regional cdf (eq. 2) with the one corresponding to the L(S,T) curves (eq. 5), we can see that this result seems to be verified, the both are comparable.

Also we must notice that the shape parameter of L(S) cdf is still influenced by the highest values unlike the regional cdf of punctual maxima annual daily rainfall. The k value is due to one event, the 8th September 2002 (around T=80 years return period), which gave the maximum value of L(S) whatever the area S. Thus, despite of a regional approach, sampling uncertainties remain very high.

5. DISCUSSION

Using regional approach, we have shown that the local maximum annual rainfall depth cdf correspond to Frechet cdf rather than Gumbel cdf. This result is consistent with other studies at other site and climate of the world. Moreover we suggest applying regional approach rather local cdf estimation which is more sensitive to sampling uncertainties.

Concerning the spatial mean rainfall over different areas, the results suggest also Frechet type cdf, which is coherent comparing to local approach. We should also notice that the LST curves we have presented do not correspond to the spatial mean rainfall cdf of a given catchment in the observation domain because the rainfall occurrence is not uniformly distributed in space. It must rather be interpreted with a meteorological point of view, as the maximum rainfall volume over different areas, during exceptional rainfall events. However we can notice that the spatial mean rainfall cdf of any catchment within the observation domain will be upper-bounded by the regional LST curves presented herein.

We also notice that another study base on historical approach yields to the same result concerning the cdf of maximum peak discharges of small basins (*Payrastre, 2005; Payrastre et al.,* 2005). Indeed on 4 small catchments (less than 200 km²) historical information about floods have been collected. Discharges of sever floods that occurred in

the 19th century have been estimated and this sparse information has been added to recent measurements to estimate the cdf of the highest discharge. If the cdf is estimated using only current measurements a Gumbel cdf is suggested by the data. Taking into account the historical information, even with large uncertainties, leads to a cdf of Frechet type.

All those results presented concern daily rainfall because of the obvious reason that daily rain measurements are much more dense in space and do have the longest records. Nevertheless if a time scale relation can be obtain via IDF curves for example, the regional approach could be extrapolated to shorter time steps. Studies are under going to extend the regional approach at shorter time steps using radar data.
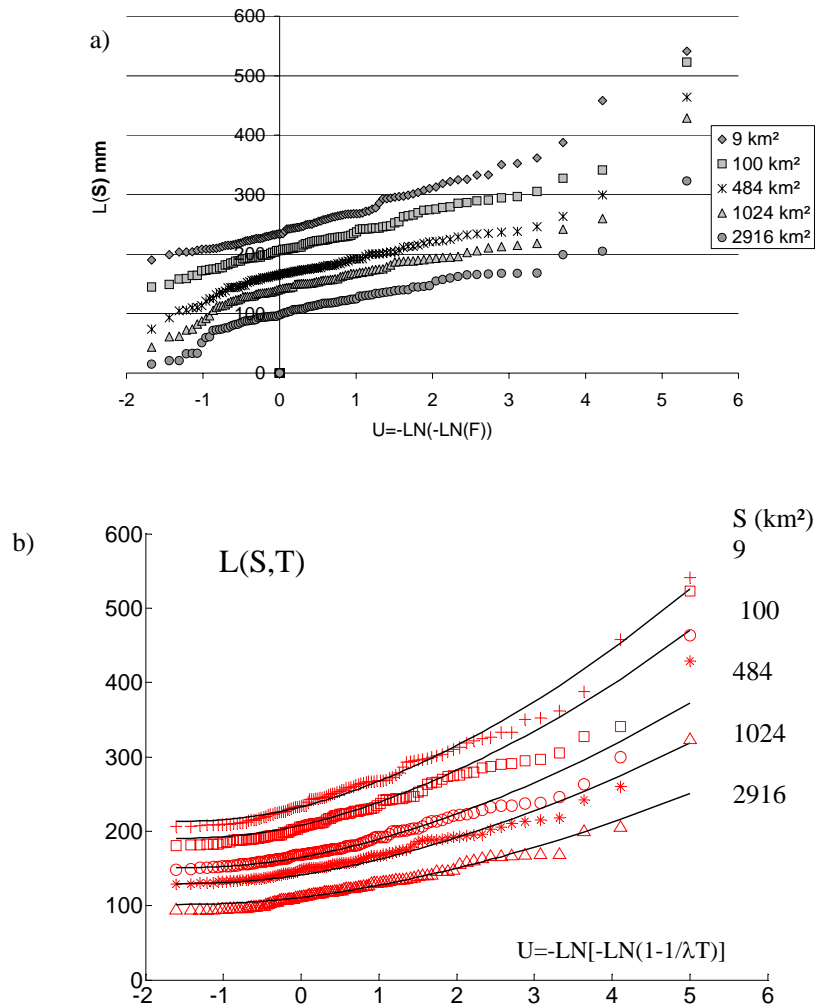
Figure 5. Empirical frequency of L(S) variate for different areas S in a Gumbel graph (a) and the thresholded L(S) cdf estimated with (5) (b).

REFERENCES

Arnaud, P., and J. Lavabre (1999), Using a stochastic model for generating hourly hyetographs to study extreme rainfalls, *Hydrol. Sci. J.*, *44*(3), 433-445.

Bacro, J.N., and A. Chaouche (2006), Incertitude d'estimation des pluies extrêmes du pourtour méditerranéen: illustration par les données de Marseille. *Hydrol. Sci. J.*, in press.

Bastin, G., C. Lorent, C. Duqué C., and M. Gevers (1984), Optimal estimation of the average areal rainfall and optimal selection of rain gauge locations, *Water Resour. Res.*, *20*, 463-470.

Beirlant, J., Y. Goegebeur, J. Segers, and J. Teugels (2005), *Statistics of Extremes, theory and applications*, Wiley Ltd.

Delrieu, G. (2003), L'observatoire Hydrométéorologique Méditerranéen Cévennes Vivarais, *La Houille Blanche*, *6*, 83-88.

Dominguez, R., C. Bouvier, L. Neppel and H. Niel (2005), Approche régionale pour l'estimation des distributions ponctuelles des pluies journalières dans le Languedoc-Roussillon (France), *Hydrol. Sci. J.*, *50*(1), 17-29.

Hosking, J.R.M., and J.R. Wallis (1993), Some statistics useful in regional frequency analysis, *Water Resour. Res.*, *29*(2), 271-281.

Hosking, J.R.M. (1990), L-moments: Analysis and estimation of distributions using linear combinations of order statistics, *J.R. Statist. Soc., B 52*(1), 105-124.

Koutsoyannis, D. (2004a), Statistics of extremes and estimation of extreme rainfall : I. Theoretical investigation, *Hydrol. Sci. J.*, *49*(4), 575-590.

Koutsoyannis, D. (2004b), Statistics of extremes and estimation of extreme rainfall : II. Empirical investigation of long rainfall records, *Hydrol. Sci. J.*, *49*(4), 591-610.

Koutsoyannis, D., D. Kozonis, and A. Manetas (1998), A mathematical framework for studying rainfall intensity-duration-frequency relationships, *J. Hydrol.*, *206*, 118-135

Neppel, L., M. Desbordes, and J.M. Masson (1998), Caractérisation spatiale de l'aléa climatique en région méditerranéenne : analyse statistique des surfaces pluvieuses, *Rev. Sci. Eau*, *2*,155-174.

Paquet, E., J. Gailhard, and R. Garçon (2006), Evolution de la méthode du Gradex : approche par type de temps et modélisation hydrologique, *Actes du Colloque Société Hydrotechnique de France*, Lyon, 37-50.

Payrastre, O., E. Gaume, and H. Andrieu (2005), Use of historical data to assess the occurrence of floods in small watersheds in the French Mediterranean area, *Adv. Geosci.*, *2*, 313-320.

Payrastre, O (2005), *Faisabilité et utilité du recueil de données historiques pour l'étude des crues extrêmes de petits cours d'eau. Etude du cas de quatre bassins versants affluents de l'Aude,* Thèse de doctorat, Ecole Nationale des Ponts et Chaussées.

Rao, A.R., and K.H. Hamed (2000), *Flood frequency analysis,* CRC Press LLC.

St-Hilaire, A., T.B.M.J. Ouarda, M. Lachance, B. Bobee, M. Barbet, and P. Bruneau (2003), La régionalisation des précipitations: une revue bibliographique des développements récents, *Rev. Sci. Eau*, *16*(1), 27-54.

DEVELOPMENT OF A REGIONAL FLOOD FREQUENCY ANALYSIS USING L-MOMENTS APPROACH FOR SICILY, ITALY

L. V. Noto, G. La Loggia and M. Cannarozzo

Dept. of Hydraulic Engineering and Environmental Applications, University of Palermo (Italy)

ABSTRACT

Extremely great floods are among environmental events with the most disastrous consequences for the entire world. Estimates of their return periods and design values are of great importance in hydrologic modeling, engineering practice for water resources and reservoirs design and management, planning for weather-related emergencies, etc. Regional flood frequency analysis resolves the problem of estimating the extreme flood events for catchments having short data records or ungauged catchments.

This paper analyzes annual maximum peak flood discharge data recorded from more than 50 stream flow gauging sites in Sicily, Italy to derive regional flood frequency curves. First these data are analyzed to point out some problems concerning the homogeneity of the single time series. On the basis of the L-moments and using cluster analysis techniques, the entire region is subdivided in five subregions whose homogeneity is tested using the L-moments based heterogeneity measure. Based on the L-moment ratio diagram and other statistic criteria, general extreme value (GEV) distribution is identified as the robust distribution for the study area. Regional flood frequency relationships are developed to estimate floods at various return periods for gauged and ungauged catchments in different subregions of the Sicily. These relationships have been implemented using the L-moment based GEV distribution and a regional relation between mean annual peak flood and some geomorphologic and climatic parameters of catchments.

This regional flood frequency analysis has been implemented within the GIS based tool SIRI (Sistema Informativo Regionale Idrologico), in order to complete the hydrological module necessary to compute the probable flow, for a selected risk level, at every point chosen by the user over the entire region of Sicily.

1. INTRODUCTION

Flood frequency evaluation has been a fundamental problem in engineering science and engineering hydrology. Design of different types of hydraulic structures and flood plain zoning, economic estimation of flood protection projects, etc. require information on flood magnitudes and their frequencies. Regional flood frequency analysis resolves the problem to estimate the extreme flood events for catchments having short data records or ungauged catchments by substituting space for time data from various sites.

Pilgrim and Cordery (1992) mention that estimation of peak flows on small to medium sized rural drainage basins is probably the most common application of flood estimation as well as being of greatest overall economic importance.

During 30 year the major effort was paid towards establishing effective procedures for

flood estimation in individual rivers for large geographic areas, including the possibility of merging regularities from different rivers of a region into a unified probability model (*NERC,* 1975). Substituting space for time data from various sites for estimating floods of different return periods, the hydrometric data within the homogeneous region as a whole can be used to obtain a number of empirical frequencies much greater than the case of an at-site estimate. According to *Wallis et al.* (1974), regionalization should always be used in statistical analysis of extreme hydrological events because of the large influence that higher moments exert on the shape of the tail of the distribution which are focused by practical applications.

In regional flood frequency analysis it is assumed that the data from all gauged sites in a region can be combined in such a way as to produce a single regional flood frequency curve called growth curve. This curve is applicable, after appropriate rescaling, anywhere in that region. The scaling operation is made usually using index flood approach first introduced by *Dalrymple* (1960), and since implemented on a regular basis (*Stedinger and Lu,* 1995). It was developed as a way of deriving a regional frequency curve. The underlying flood frequency distribution at each site is assumed to be identical, except for a site-specific scaling factor called index flood. In order to derive the index flood, traditional empirical methods based on , simple or multiple linear regression can be used (*Stedinger et al.*, 1992); these methods are often used to relate the index flood to physical characteristics of river basins such as climate, geomorphology, slope and land use. A comparison of some of those methods has been carried out by Grover et al. (2002).

Use of a generalized extreme value (GEV) distribution (*Jenkinson,* 1955) as a regional flood frequency model with an index flood approach has received considerable attention (*Chowdhury et al.,* 1991). Some of the flood frequency analysis studies include *Hosking and Wallis* (1988), *Potter and Lettenmaier* (1990) and *Iacobellis and Fiorentino* (2000). With regard to the regional flood frequency analysis in Sicily, two works have been carried out both using the TCEV distribution; the first (*Cannarozzo et al.,* 1995) developed a hierarchical regional flood frequency analysis suggesting a division of Sicily in three different homogeneous regions while the second (*Ferro and Porto,* 2006) showed that the division into three subregions proposed by *Cannarozzo et al.* (1995) is not necessary, and that a single theoretical growth curve is able to evaluate discharges associated with different return periods.

In this study a regional flood analysis has been performed for Sicily, Italy. Starting from hydrometric data recorded in more than 50 gauge sites over the island, the study has been first addressed to the identification of hydrometric homogeneous regions using the L-moments approach suggested by *Hosking and Wallis* (1993) together with cluster analysis techniques. Second, the analysis shows that, based on the GEV distribution, five growth curves with different empirical relationships for estimating the index flood could be used to evaluate discharges associated with different return periods anywhere over the entire island. Third, a Geographical Information System (GIS) based tool has been developed to allow the user to evaluate the flood discharge anywhere in Sicily using different methods.

2. L-MOMENTS METHOD

L-moments approach is a recent development in mathematical statistics which facilitates the estimation process in the frequency analysis (*Stedinger and Lu,* 1995). This

approach, introduced by *Hosking* (1990) is increasingly being used by hydrologists. The same author noted the benefits of L-moment ratios over product moment ratios in that the former are more robust in the presence of extreme values and do not have sample size related bounds. *Hosking and Wallis* (1997) pointed out that L-moments are an alternative system of describing the shapes of probability distributions. The L-moments are based on the probability weighted moments (PWMs) of *Greenwood et al.* (1979). Starting from PWMs, *Hosking* (1990) suggested the use of the L-moments defined as linear combination of PWMs. The $(r+1)^{th}$ L-moment, λ_{r+1}, is defined as:

$$\lambda_{r+1} = \sum_{k=0}^{r} p_{r,k}^* \beta_k \qquad (1)$$

where:

$$p_{r,k}^* = (-1)^{r-k} \binom{r}{k} \binom{r+k}{k} \qquad (2)$$

In particular, λ_1 is the mean of the distribution, λ_2 is a measure of the scale or dispersion and λ_3 and λ_4 are measures of skewness and kurtosis respectively.

In the regional frequency analysis dimensionless ratios between L-moment, called L-moment ratios (indicated as LMRs), are particularly useful. The LMRs are L_{cv}, L_{skew} and L_{kur} and they are analogous to the usual coefficient of variation, coefficient of skewness and coefficient of kurtosis. In particular the coefficient of variation is equal to $\tau = \lambda_2/\lambda_1$, while the others two LMRs (L_{skew} and L_{kur}) are given by

$$\tau_r = \frac{\lambda_r}{\lambda_2} \quad r = 3, 4 \qquad (L_{skew} \text{ for } r=3 \text{ and } L_{kur} \text{ for } r=4) \qquad (3)$$

The L-moments are similar to, but more convenient than, PWMs since they are more easily interpretable as measures of distributional shape. In particular, τ_3 and τ_4 (L_{skew} and L_{kur}) are dimensionless measures of skewness and kurtosis, respectively.

The sample estimation of L-moments can be expressed by:

$$l_{r+1} = \sum_{k=0}^{r} p_{r,k}^* b_k \qquad \text{with} \qquad b_r = n^{-1} \sum_{j=1}^{n} \frac{(j-1)(j-2)....(j-r)}{(n-1)(n-2)....(n-r)} x_j \qquad (4)$$

where x_j, for $j = 1,...,n$ is the ordered sample and n is the sample size.

The sample estimates of β_r and λ_r are unbiased while consistent but not unbiased estimators of the L-moment ratios τ and τ_r (L_{cv} and L_r) are (Hosking and Wallis, 1997):

$$t = L_{cv} = \frac{l_2}{l_1}, \qquad t_3 = L_{skew} = \frac{l_3}{l_2}, \qquad t_4 = L_{Kur} = \frac{l_4}{l_2} \qquad (5)$$

The values l_1, l_2, t_3, and t_4 are useful summary statistics of data sample and can be used to judge which distributions are consistent with a given data sample (*Hosking*, 1990). They can also be used to estimate parameters when fitting a distribution to a sample, by equating sample and distribution L-moments (*Hosking*, 1990). Recent researches (*Hosking et al., 1985; Wallis and Wood, 1985; Lettenmaier et al., 1987; Hosking and Wallis, 1988; Potter and Lettenmaier, 1990*) have shown that index flood procedures based on L-moments approach yield robust and accurate quantile estimates.

Zafirakou-Koulouris et al. (1998) mention that like ordinary product moments, L-moments summarize the characteristics or shapes of theoretical probability distributions and observed samples. Both moment types offer measures of distributional location

(mean), scale (variance), skewness (shape), and kurtosis (peakedness). The authors further mention that L-moments offer significant advantages over ordinary product moments, especially for environmental data sets, because of the following:

− LMR estimators of location, scale, and shape are nearly unbiased, regardless of the probability distribution from which the observations arise and can exhibit lower bias than conventional product moment ratios, especially for highly skewed samples;
− LMR estimators of L-CV and L-skewness do not have bounds, which depend on sample size as do the ordinary product moment ratio estimators of CV and skewness;
− L-moment estimators are linear combinations of the observations and thus are less sensitive to the largest observations in a sample than product moment estimators, which square or cube the observations;
− LMR diagrams are particularly good at identifying the distributional properties of highly skewed data, whereas ordinary product moment diagrams are almost useless for this task (*Vogel and Fennessey,* 1993).

3. THE CASE OF STUDY

The present study is carried out for the catchments of the largest island in the Mediterranean Sea: Sicily which extends over an area of 25700 km^2. The mean annual rainfall over the Sicily basins is about 715 mm (period 1921-2004). Annual maximum peak flood data of 72 stream flow gauging sites (Figure 1) and ranging over 7–65 years in record length have been provided for the study by UIR (*Ufficio Idrografico Regionale*).
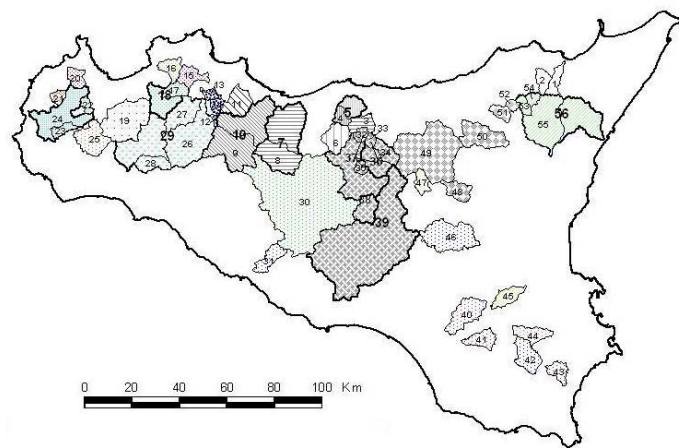
Figure 1. Catchments used in this regional flood frequency analysis

Following the suggestion reported in Bulletin 17B (Guidelines for Determining flood Flow Frequency by U.S. Department of the Interior Geological Survey) only data from sites with at least ten years in record length has been used, reducing the number of stations used in this study from 72 to 56. Catchment areas of these sites range from 10 (Eleuterio at Lupo) to 2000 km^2 (Imera Merid. at Drasi) and their mean annual peak floods vary from 0.78 to 2380 m^3/s; the maximum record length is 65 (Oreto at Parco) while the mean sample size is 22.

A summary check on hydrometric data finalized to point out lack of homogeneity in the original dataset has been carried out using the historical information provided by UIR. Through this control about 8% of original data have been removed because they

resulted not homogeneous with the remaining dataset. The main cause of this not homogeneity in data is the moving of the gauge sites.

3.1 Delimitation of homogeneous regions

The first step of the regional frequency analysis was the identification of the homogeneous regions. A homogeneous region, the fundamental unit of regional frequency analysis, is a set of gauge sites whose frequency distributions are approximately the same after an appropriate scaling operation. It can be assumed that the LMRs are the same for data from all sites within a statistically homogeneous region. The homogeneity of the proposed region is usually tested by calculating summary statistics of the at-site data and then comparing their variability with what would be expected for a homogeneous region.

3.1.1 Is the Sicily a homogeneous region?

Initially Sicily as a whole was assumed as a hydrometric homogeneous region and the truthfulness of this assumption was tested using two procedures suggested by *Hosking and Wallis* (1997): the discordancy measure D and the heterogeneity measure H.

The main goal of the discordancy measure D test is to identify those sites in which the sample LMRs are markedly different from the most of other sites. The discordancy measure can be used for two different purposes (*Hosking and Wallis,* 1997). First, at the beginning of the analysis it may applied to a large group of sites over a large geographical area. Sites with great errors in data will stand out from other sites and be flagged as discordant and therefore these ones have to be closely analyzed in order to detect errors in the recording or transcription of data or for sources of unreliability in the same data. Second, when homogeneous regions have been at least tentatively identified, the discordancy measure can be calculated for each site in the proposed region. If any site is then discordant with the whole region, the possibility of moving that site to another region should be considered.

Hosking and Wallis (1997) defined the discordancy measure (D_i) considering if there are N sites in the group. The discordancy measure for site i is defined as:

$$D_i = 1/3 \left[(u_i - \overline{u})^T (u_i - \overline{u}) S^{-1} \right] \qquad (6)$$

where $u_i = \left[L_{cv}^{(i)}, L_{skew}^{(i)}, L_{kur}^{(i)} \right]^T$ is a vector containing the three sample LMRs values for site i, $\overline{u}$ is the vector containing the unweighted average LMRs equal to $N^{-1} \sum_{i=1}^{N} u_i$ and S is the sample covariance matrix expressed by $S = (N-1)^{-1} \sum_{i=1}^{N} (u_i - \overline{u})(u_i - \overline{u})^T$.

Generally a site is discordant from the group as a whole if D_i is greater than a critical value that usually depends on the number of stations in the group (*Hosking and Wallis,* 1997). The same authors tentatively suggest $D_i \geq 3$ as a criterion for declaring a site to be discordant even if they advise to examine data for the sites with the largest D_i values, regardless of the magnitude of these values. Assuming the Sicily as unique homogeneous region, it is observed that D_i values of four gauging sites are greater than the critical value equal to 3. Data from these gauging sites are unsuitable for flood frequency analysis and then have been removed.

The inter-site variations in sample LMRs for the group of sites, for which a

homogeneous region would be expected, have been measured using the statistic H (heterogeneity measure). The inter-site variation of L-moment ratio is measured as the standard deviation (V) of the at-site L_{cv} weighted proportionally to the record length at each site. *Hosking and Wallis* (1997) suggest using L_{cv}, since between-site variation has a much larger effect on its value than variation in L_{skew} or L_{kur} on the variance of the estimates of the most of quantiles. The sample variance of L_{cv} is estimated as weighted standard deviation of the at-site sample L_{cv}:

$$V = \frac{\Sigma n_i \left(L_{cv}^{(i)} - \overline{L}_{cv} \right)^2}{\Sigma n_i} \tag{7}$$

where n_i is the sample size at site i and $L_{cv}^{(i)}$ and $\overline{L}_{cv}$ are respectively L_{cv} at site i and the average regional value of L_{cv}. To establish what would be expected of a homogeneous region, simulations are used. Using the regional weighted average statistics based on a four parameter Kappa distribution, 500 data regions have been generated. The inter-site variation of each generated region has been computed and the mean (μ_v) and the standard deviation (σ_v) of the computed inter-site variation is obtained. Then, heterogeneity measure H has been computed as:

$$H = \frac{(V - \mu_v)}{\sigma_v} \tag{8}$$

By comparing observed and simulated dispersion, H measures the heterogeneity of observed data, thus allowing to verify if they can be considered part of the same homogeneous region, i.e. if the LMR at site can be summarized by the regional average values. The criteria established by *Hosking and Wallis* (1993) for assessing heterogeneity of a region are:

> H<1   region is acceptably homogeneous,
> 1≤H<2   region is possibly heterogeneous,
> H≥2   region is definitely heterogeneous.

Other two heterogeneity indexes, called H_2 and H_3, have been calculated using respectively a measure based on L_{cv} and L_{skew} and a measure based on L_{skew} and L_{kur}. The values of heterogeneity measures computed by carrying out the 500 simulations mentioned above, based on the data of 51 sites are the following:

> H=7.72 H_2=3.83 H_3=0.87

H_2 and H_3 statistics lack power to discriminate between homogeneous and heterogeneous regions and rarely yield *H* values larger than 2 even for grossly heterogeneous regions while the H statistic has much better discriminatory power (*Hosking and Wallis*, 1993). For the reasons above mentioned and since the measure of H statistic for Sicily, using the data of 51 sites, was found to be much greater than 1.0, thus one can assert that the entire island of Sicily is not identifiable as a homogeneous region.

3.1.2 Hypothesis of the presence of three homogeneous subregions

As mentioned above, Sicily as a whole can not be considered a homogeneous region. For this reason a new hypothesis about a division of Sicily in different regions has to be considered. First, the division proposed by *Cannarozzo et al.* (1995) has been analyzed in order to verify the hydrometric homogeneity of the three different subzones proposed by the authors and obtained in an analogous work concerning the regional flood frequency analysis in Sicily (Figure 2).

Using the same equations above introduced, discordancy measure D and heterogeneity

measure H values have been calculated for each one of the three homogeneous subregions. The discordancy measure test permitted to mark six different sites as discordant.

In order to apply the heterogeneity measure H test, LMRs values have been calculated (Table 1). In the same table heterogeneity H values, obtained using the same procedures described in section 3.1.1, have been reported for each one of the three homogeneous subregions. The analysis of these values lead to assert that all the three subregions proposed by *Cannarozzo et al.* (1995) are definitely heterogeneous and thus they can not be used in a regional flood frequency analysis.
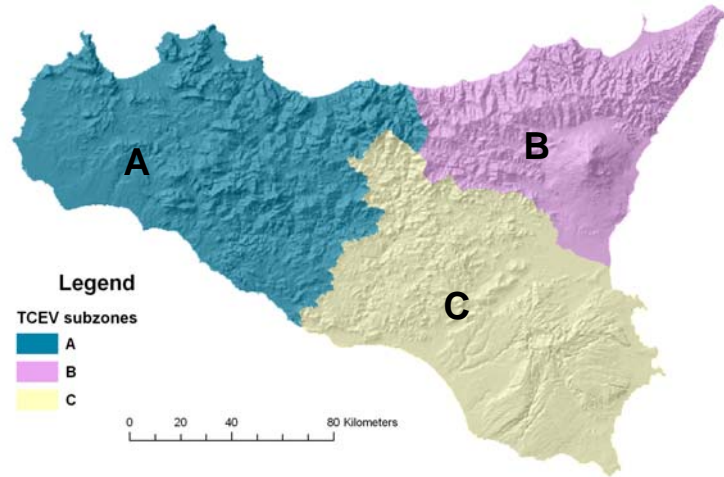

Figure 2. Homogeneous subzones delineated by *Cannarozzo et al.* (1995).

Zone	$\overline{L}_{cv}$	$\overline{L}_{skew}$	$\overline{L}_{kur}$	H	H_2	H_3
A	0.3848	0.2831	0.1712	**4.24**	1.84	0.15
B	0.2879	0.2244	0.1454	**2.31**	0.76	0.76
C	0.4303	0.2475	0.1649	**2.25**	2.94	2.13

Table 1. Regional average LMRs values and heterogeneity measures H under the hypothesis of 3 homogeneous regions proposed by *Cannarozzo et al.* (1995) *(heterogeneous regions are in italic)*.

3.1.3 Proposal for a new identification of homogeneous regions in Sicily

The previous hypotheses concerning the existence in Sicily of a unique homogeneous region (section 3.1.1) or three different homogeneous subregions (section 3.1.2) have been rejected by the use of heterogeneity measure H test and this causes the need to identify a new subdivision of Sicily in homogeneous regions.

The formation of regions was based on cluster analysis techniques which allow to create groups of objects, or clusters, in such a way that the profiles of objects belonging to the same cluster are very similar and the profiles of objects belonging to different clusters are quite distinct. In order to build the clusters, an agglomerative technique with standardized Euclidean metric was applied using six site characteristics: longitude and latitude of the watersheds centroids, mean annual precipitation of the watersheds, and the three LMRs.

The Ward's method (*Ward,* 1963) was applied as clustering algorithm. This method uses an analysis of variance approach to evaluate the distances between clusters and tends

to form clusters with equal number of sites. In short, this method attempts to minimize the sum of squares of any two clusters that can be formed at each step. By means of this analysis it has been created the hierarchical cluster tree which summarizes the information about the possible clusters. Five clusters were chosen to represent the homogeneous regions in Sicily even if the goodness of this choice has to be tested through the heterogeneity measure H. However, subjective adjustments have been necessary to improve the geographical coherence of regions and to avoid heterogeneity. The cluster analysis technique leads to identify the following five different hydrometric homogeneous regions, shown in Figure 5.
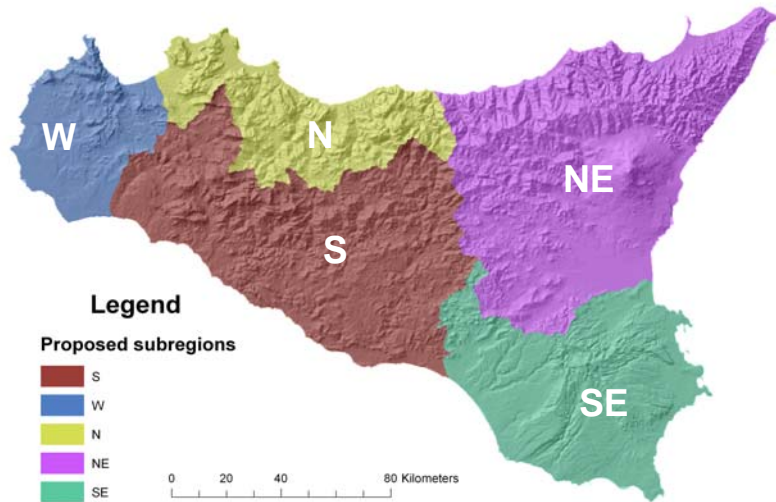

Figure 3. The five proposed homogeneous subregions.

The discordancy measure D test allowed to mark three different sites as discordant within each one of the five zones. Once discarded the discordant gauge sites, the heterogeneity measure H test has been applied to the remaining 52 sites, determining the regional average values of LMRs and the measure H values, using the same procedure shown in the previous sections (Table 2).

Zone	$\overline{L}_{cv}$	$\overline{L}_{skew}$	$\overline{L}_{kur}$	H	H_2	H_3
S	0.3840	0.2704	0.1824	0.29	1.00	1.23
W	0.4772	0.3589	0.2280	0.95	1.23	0.98
N	0.3763	0.2422	0.1471	0.86	1.41	0.22
NE	0.3513	0.2071	0.1486	1.04	0.87	-0.58
SE	0.4945	0.2542	0.1808	0.48	0.84	0.08

Table 2. Regional average LMRs values and heterogeneity measures H under the proposed hypothesis of five homogeneous regions.

The values of H based on the proposed regional subdivision leads to identify four of the five proposed regions as possibly homogeneous and one as probably heterogeneous (zone NE) even if the values of H is slightly greater than one (1.04).

3.2 Model selection

After the correct identification of the homogeneous regions, the subsequent step has been the choice of an appropriate frequency distribution for the regions; this has been achieved by comparing the moments of the distributions to the average moments

statistics obtained by regional data. The objective has been to identify from a number of candidate distributions, the one giving the best fit to the observed data. In this study, the L-moment ratio diagram and Z measure test proposed by *Hosking and Wallis* (1993) have been used to assess the goodness of fit of different distribution.

Assuming that sample L_{skew} and L_{kur} are exactly unbiased and the candidate distribution fitted by the method of L-moments has L_{skew} equal to the regional average $\overline{L}_{skew}$, it is possible to judge the quality of fit comparing the difference between the L_{kur} of the candidate distribution, indicated as L_{kur}^{DIST}, and the regional average $\overline{L}_{kur}$. In order to asses the significance of this difference, this one has to be compared with the sampling variability of $\overline{L}_{kur}$. This variability, described by σ_{kur}, the standard variation of $\overline{L}_{kur}$, can be obtained using repeated simulations of a homogeneous region with the candidate frequency distribution and gauge sites having record lengths equal to those of the observed data. Assuming these hypotheses, the Z index (goodness of fit measure) can be defined as:

$$Z^{DIST} = \frac{(\overline{L}_{kur} - L_{kur}^{DIST})}{\sigma_{kur}} \tag{9}$$

Obviously small values of $|Z^{DIST}|$ are consistent with the candidate distribution being the true underlying frequency distribution for the region. The fit is considered to be adequate if $|Z^{DIST}|$ statistic is sufficiently close to zero; a reasonable criterion being $|Z^{DIST}|$ - statistic less than 1.64 and this criterion then corresponds to acceptance of the hypothesized distribution at a confidence level of 90%. A difficulty associated with this procedure is that a separate set of simulations have to be made for each candidate distribution to obtain the appropriate σ_{kur} value. In practice, it should be sufficient to assume that σ_{kur} is the same for all the fitted distributions having the same L_{skew}. In this way σ_{kur} values can be obtained by the same simulations used in the calculation of the heterogeneity measure described in section 3.1.1.

For Sicily four different candidate probability distributions have been used: General Extreme Value (GEV), Generalized Logistic (GL), Pearson type-III (P3) and Generalized Pareto (GP). By simulating 500 regions having no cross or serial correlation with sites having the same record lengths as their real world counterparts, the *Z* measures have been calculated for the candidate distributions and for the five homogenous regions using the (15) (Table 3).

Distribution	S		W		N		NE		SE	
	$\overline{L}_{kur}$	Z	$\overline{L}_{kur}$	Z	$\overline{L}_{kur}$	Z	$\overline{L}_{kur}$	Z	$\overline{L}_{kur}$	Z
GL	0.228	1.34	0.274	0.50	0.216	2.75	0.202	1.51	0.220	0.77
GEV	0.198	0.29	0.253	0.12	0.169	1.18	0.166	0.48	0.189	0.16
P3	0.149	-1.41	0.176	-1.30	0.102	-0.66	0.137	-0.33	0.146	-0.68
GP	0.121	-2.41	0.187	-1.08	0.169	-2.57	0.081	-1.89	0.110	-1.39

Table 3. L-kurtosis and Z measure values for the four different candidate distributions and for each one of the proposed homogeneous regions.

By the analysis of Table 3, probability candidate distributions GL and GP have to be excluded because the values of Z index for zones N, NE and S are greater than the critical value 1.64. Among the two remaining candidate distributions, GEV and P3, the first has to be preferred since it shows the best performance, on average, over the five regions.
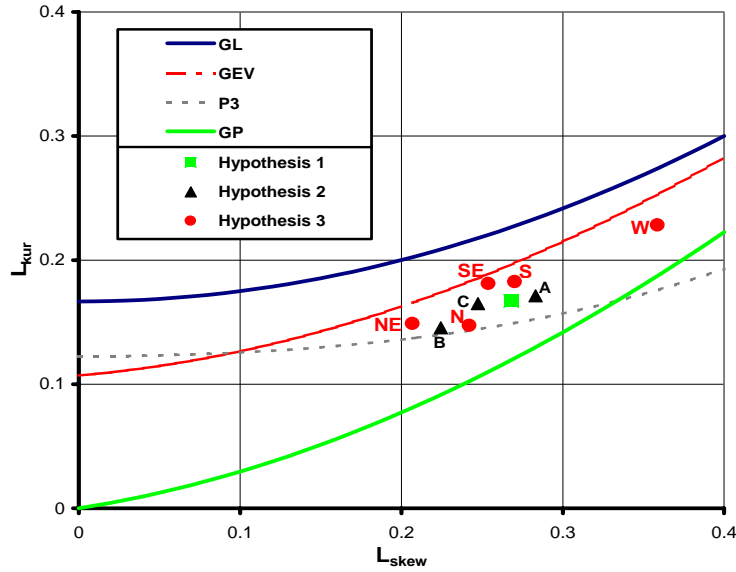
Figure 4. The LMRs diagram for the four candidate distributions (GL, GEV, P3 and GP) and for the three hypotheses discussed in sections 3.1.1, 3.1.2 and 3.1.3 *(Hypothesis 1 concerns Sicily as homogeneous region, Hypothesis 2 concerns Sicily divided in three homogeneous regions and Hypothesis 3 concerns the proposed subdivision in five different homogeneous regions)*.

Same information can be obtained from the analysis of Figure 4. In the L-moment ratio diagram shown in this figure, the points defined by the regional average values of L-skewness and L-kurtosis for the five homogeneous regions (Hypothesis 3 red circles), lie closest to the GEV distribution while the point correspondent to the Hypothesis 1 (Sicily as a unique homogeneous region) and the points correspondent to Hypothesis 2 (Sicily divided in three homogeneous regions proposed by *Cannarozzo et al,* 1995) lies closest sometimes to the P3 distribution, sometimes to the GEV distribution.

3.3 Results

The GEV distribution has been identified as the robust distribution for the study area; hence, regional flood frequency relationships have been developed using this distribution. The frequency relationship for GEV distribution can be written taking into account the relationship between probability and return period as:

$$x(T) = u + \frac{\alpha}{k}\left\{ 1 - \left[\ln\left(1 - \frac{1}{T} \right) \right]^{k} \right\} \tag{10}$$

where u, α and k are the location, scale and shape parameters. The parameters of the GEV distribution in terms of L-moments are (*Hosking and Wallis,* 1993):

$$u = l_1 + \frac{\alpha[\Gamma(1+k)-1]}{k}, \qquad \alpha = \frac{k l_2}{\Gamma(1+k)\left(1 - 2^{-k}\right)} \qquad \text{and} \qquad k = 7{,}859z + 2{,}955z^2 \tag{11}$$

with $z = \frac{2l_2}{l_3 + 3l_2} - \frac{\ln 2}{\ln 3}$ where l_1, l_2, l_3 are the sample L-moments above described.

In order to obtain the relationship Q-T, the index flood method has been applied, by calculating the flood discharge for fixed return period using the following expression:

$$Q_T = K_T^R Q_m \tag{12}$$

where Q_m is scale factor called index flood and K_T^R is the probability distribution of the

frequency factor, called growth curve which represents the T-years quantile of the normalized regional GEV distribution. The growth curve depends only on the return period and the GEV parameters and it has a unique expression valid over the entire homogeneous region given by:

$$K_T^R = u^R + \alpha^R \Big/ k^R \left\{ 1 - \left[-\ln\left(1 - \frac{1}{T}\right) \right]^{k^R} \right\}$$ (13)

where u^R, α^R and k^R are the regional parameters of GEV. These values can be estimated by means of (11) using the regional average of normalized L-moments instead of the at-site L-moments. These parameters are estimated as the weighted average of the at-site normalized L-moments (*Wallis,* 1985). Thus, the regional average of normalized L-moments can be obtained as following:

$$l_r^R = \sum_{k=1}^{N} w_K \left[\frac{l_r}{l_1} \right] \Big/ \sum_{k=1}^{N} w_K$$ (14)

in particular:

$$l_1^R = 1, \qquad l_2^R = \frac{\sum_{k=1}^{N} w_K \left[\frac{l_2}{l_1} \right]}{\sum_{k=1}^{N} w_K}, \qquad l_3^R = \frac{\sum_{k=1}^{N} w_K \left[\frac{l_3}{l_1} \right]}{\sum_{k=1}^{N} w_K}$$ (15)

where N is the number of gauges sites and w_k are the weights. A simple choice is $w_k = n_k$, where n_k is the sample size for the site k. However weighting by the sample size when some sites have much longer records may give them undue influence. A better choice which limits the weight assigned to sites with longer records can be the following one:

$$w_k = \frac{n_k n_r}{n_k + n_r}$$ (16)

where n_r is a weighting parameter whose value depends on the region heterogeneity. By substituting the average normalized L-moments in (11), the regional parameters of GEV, u^R, α^R and k^R, can be determined for each one of the five homogeneous regions (Table 4).

Figure 5. Growth curves (GEV distribution) for the five proposed homogeneous zones.
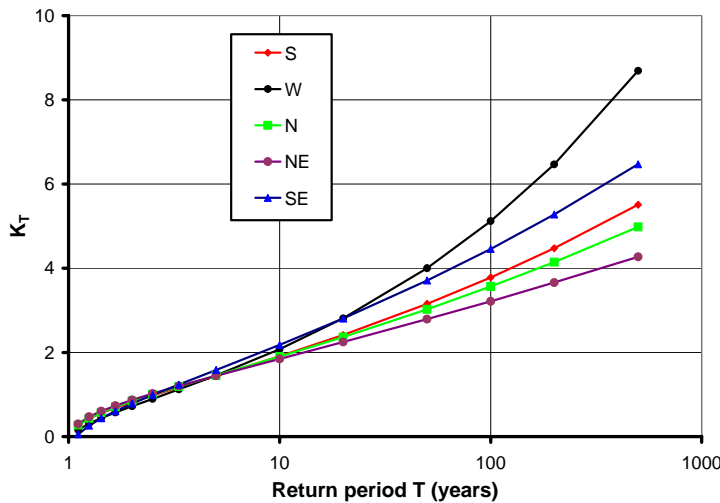
Zone	u^R	α^R	k^R
S	0.645	0.472	-0.151
W	0.531	0.496	-0.275
N	0.661	0.485	-0.110
NE	0.695	0.479	-0.057
SE	0.550	0.625	-0.127

Table 4. GEV regional parameters for the GEV distribution for the five proposed homogeneous zones.

3.4 Using the Q-T relationship in ungauged sites

In order to estimate the T-year return period flood at a site, the assessment of index flood is required. It has become a common practice among hydrologists to estimate the index flood by the at-site sample mean. *Dalrymple* (1960) warned about using the at-site sample mean, which gives the same weight to all observations and is therefore more sensitive to large sampling errors of extreme observations. For ungauged catchments at-site mean can not be computed in absence of the observed flow data. In such a situation index flood estimation can be achieved using different methods. The approach first depends on the available information. Also, one must consider the reliability (acceptable level of uncertainty) that one calls for the statistical predictions in a specific application, because the degree of complexity may differ from one method to another, so requiring a great effort in data collection and model development. Due to their simplicity, regressive methods are the most used methods to estimate the index flood. These methods link Q_m to some catchment characteristics such as climatic indexes, lithological and pedological parameters, land coverage and geomorphic parameters. In general, regressive methods have the following structure:

$$Q_m = const \prod_{i=1}^{N_{par}} C_i^{b_i} \qquad (17)$$

where the constant, const, and the exponents b_i, are determined through a multiple regression of the logarithmic transform of the observed mean, $\log(Q_m)$, against the logarithmic transform of the different parameters, $\log(C_i)$ (*NERC*, 1975). Owing to a limited number of the gauged sites in a homogeneous region for model calibration, one has to consider a truthful number of regression parameters, in order to guarantee reliability and robustness of the statistical model. Even though these formulae are able to explain a high fraction of the variability of Q_m logarithmic transform, the related explained variance is pretty moderate.

In this work, the index flood Q_m has been directly estimated as sample mean for the gauged sites while a regressive analysis has been carried out for the ungauged catchments. The first step of this analysis has been the identification of catchment parameters to be used and it has been followed by the determination of most significative parameters and by the estimation of the regression coefficients.

The most of the catchment characteristics used in this analysis comes directly from the SIRI (*Sistema Informativo Regionale Idrologico*) (*Noto et al.*, 2001) or is easily derivable within it; among these characteristics, the following ones have been computed: the basin area (A_r) [km^2], the mean areal annual precipitation (A), [mm], the average basin elevation (H_m), [m], the longest drainage path (L_{max}), [m], the average slope basin (S_m), [%], the mean areal value of Curve Number (CN), [-], the scaling coefficient of depth-duration-frequency curves (a), [mm], and the mean areal rainfall depth for return periods 2 and 5 years and durations equal to 3, 6, 12 and 24 hours (h_{2-3}, h_{2-6}, h_{2-12}, h_{2-24}, h_{5-6}, h_{5-12}, h_{5-24}).

Stepwise regression has been used to select the optimal set of variables reflecting the geomorphologic and climatic effects. This method adds additional independent variables one by one, in successive steps, each raising the dimensions of the analysis by one. The most promising independent variable, i.e. the one that provides the greatest reduction in the unexplained variation in the dependent variable (index flood), is selected at every stage.

The stepwise regression has been performed using the variables above mentioned. The use of stepwise regressive analysis has led to the determination of four different types of equations, as function of the number of included parameters. Table 5 shows these four equations together with the root mean square error (RMSE) and the amount of response variability explained by the model (i.e. the coefficient of determination) (R^2).

N° of parameters	Regressive model	R^2	RMSE
1	$Q_m=0.866494 \, Ar^{0.8774}$	0.7734	0.5526
2	$Q_m=0.007585 \, Ar^{0.87774} \, h_{2\text{-}24}^{1.0574}$	0.8018	0.5216
3	$Q_m=0.017982 \, Ar^{0.8661} \, h_{2\text{-}12}^{-1.7117} \, h_{2\text{-}24}^{1.9079}$	0.8131	0.5067
4	$Q_m=0.143159 \, Ar^{1.0105} \, L_{max}^{-0.2805} \, h_{2\text{-}12}^{-1.6643} \, h_{2\text{-}24}^{2.4833}$	0.8313	0.4915

Table 5. Regressive equations for the estimation of index flood Q_m.

The proposed regionalization procedure has been implemented in the SIRI. This system, based on the ArcView GIS environment allows the determination of maximum probable discharge all over the Sicilian basins. The prediction of flood discharge is performed using two different approaches: direct and indirect analysis. The former provides the flood discharge for desired return period by means of a regional analysis of data coming from the stream gauge sites using the proposed GEV distribution and the TCEV (*Cannarozzo et al.,* 1995). The latter uses hydrologic models which enable to transform the rainfall recorded on the gauges over the watershed into discharge at the outlet. A preliminary probabilistic analysis of the rainfall over the whole watershed using one of the many rainfall probability distribution function implemented in the system (GEV, TCEV; EV1, EV2) and the following simulation of the rainfall-runoff transformation are carried out. Concerning the transformation of rainfall into runoff, two models have been included in the proposed methodology: the runoff coefficient Ψ and the SCS-CN method (*U.S. Dept. Agric., S.C.S.,* 1972) while the transformation of rainfall excess to direct runoff is carried out using the unit hydrograph (UH) (Sherman, 1932) derived by means of the topographic information contained in the DEM. Besides, the SIRI offers to the user the possibility to compare the flood discharge estimation obtained by different approaches and by different models.

4. CONCLUSION

A common problem in many areas of environmental engineering is that to estimate the return period of rare geophysical events, such as extreme floods, for a site or group of sites. Nowadays there is an increasing interest in this estimation process especially for ungauged areas or for sites characterized by a short sample length.

The study presented herein reports a regional analysis carried out in Sicily, Italy, aimed to evaluate the relationship between flood discharge and return period anywhere over the entire island. A careful screening of data coming from about 70 stream gauging sites, with the use of discordancy measures test allowed to verify the suitability of these data for regional flood frequency analysis. The Sicily was analyzed firstly as a whole and then as three smaller subregions proposed in a previous work. The whole region and the subregions did not pass the regional homogeneity test and a new identification of homogeneous subregions has been carried out using cluster analysis technique. In this

way five homogeneous subregions were delineated and heterogeneity measure test confirmed their hydrometric homogeneity.

Using the L-moment ratio diagram and the Z statistic criteria, GEV distribution has been identified as the most robust distribution among four candidate distributions for all the proposed subregions of the Sicily. The estimated regional growth curves were significantly different for the five different subregions, confirming the non-homogeneity of the whole region. To estimate floods of various return periods for gauged catchments in the study area, the mean annual peak flood of the catchment may be multiplied by corresponding values of the growth factors, computed using the GEV distribution. For estimation of floods for ungauged catchments of the study area, the same values of growth factors have to be multiplied by the index flood computed using a multi-regressive approach that incorporates climatic and geomorphologic basin characteristics within a GIS environment.

REFERENCES

Cannarozzo, M., F. D'Asaro, and V. Ferro (1995), Regional rainfall and flood frequency analysis for Sicily using the two component extreme value distribution, *Hydrol. Sci. J.*, *40*(1), 19-42.

Chowdhury, J.U., J.R. Stedinger, and L.H. Lu (1991), Goodness-of-fit tests for regional Generalized Extreme Value flood distributions, *Water Resour. Res.*, *27*(7), 1765–1776.

Dalrymple, T. (1960). Flood frequency analysis, *Technical Report Water Supply Pap.*, 1543-A, U.S. Geol. Surv.

Ferro, V., and P. Porto (2006), Flood frequency analysis for Sicily, Italy, *J. Hydrol. Eng.*, *(11)*2, 110-122.

Greenwood, J.A., J.M Landwehr, N.C. Matalas, and J.R Wallis (1979), Probability weighted moments: definition and relation to parameters of several distributions expressible in inverse form, *Water Resour. Res.*, *15*, 1049–1054.

Grover, P.L., D.H. Burn, and J.M. Cunderlik (2002), A comparison of index flood estimation procedures for ungauged catchments, *Can. J. Civil Eng.*, 29(5), 734–741.

Hosking, J.R.M. (1990), "L-moments: analysis and estimation of distributions using linear combinations of order statistics". *J. R. Stat. Soc.*, *B 52*, 105-124.

Hosking, J.R.M. (1996), Fortran routines for use with the method of L-moments-, version 3, *Res. Rep. RC20525, IBM Res.*, Yorktown Heights, NY

Hosking, J.R.M, and J.R. Wallis (1988), The effect of intersite dependence on regional flood frequency analysis, *Water Resour. Res.*, *24*(4), 588-600.

Hosking, J.R.M, and J.R. Wallis (1993), Some statistics in regional frequency analysis, *Water Resour. Res.*, *29*(2), 271-181.

Hosking, J.R.M., and J.R. Wallis (1997), *Regional frequency analysis: an approach based on L-moments,* Cambridge University Press, Cambridge, U.K.

Hosking J.R.M, J.R Wallis, and E.F. Wood (1985), *An appraisal of regional flood frequency procedure in the UK studies*, Report 30, 85-109.

Iacobellis, V., and M. Fiorentino (2000), Derived distribution of floods based on the concept of partial area coverage with a climatic appeal, *Water Resour. Res.*, *36*(2), 469-482.

Jenkinson, A.F. (1955), The frequency distribution of the annual maximum (or minimum) of meteorological elements, *Q. J. R. Meteorol. Soc.*, London, 81, 158-171.

Lettenmaier, D.P., J.R Wallis, and E.F. Wood (1987), Effect of regional heterogeneity on flood frequency estimation, *Water Resour. Res.*, *23*(2), 313-323.

National Research Council (1988) Estimating Probabilities of Extreme Floods, Methods and Recommended Research, *Report by the Committee on "Techniques for Estimating Probabilities of Extreme Floods"*, Nat. Academy Press, Washington D.C.

NERC - Natural Environment Research Council (1975), *Flood studies report, Vol. I - Hydrologic studies, NERC*, London.

Noto, L., G. La Loggia, and M. Pirrello (2001), Un Sistema Informativo Territoriale per l'analisi del rischio idraulico delle infrastrutture viarie, *V Confer. Nazionale ASITA* (in Italian).

Pilgrim, D.H., and I. Cordery (1993), Flood Runoff, in *Handbook of Hydrology*, ed. D.R. Maidment, McGraw-Hill Inc., New York, 9.1-9.42.

Potter K.W., and D.P. Lettenmaier (1990), A comparison of regional flood frequency estimation methods using a resampling method, *Water Resour. Res., 16*(3), 415-424.

Sherman, L.K. (1932), Streamflow from rainfall by unit-graph method, *Eng. News Rec., 108*, 501-505.

Stedinger, J.R., and L.H. Lu (1995), Appraisal of regional and index flood quantile estimators, *Stoch. Hydrol. Hydraul., 9*(1), 49–75.

U.S. Dept. Agric., Soil Conservation Service (1972), *SCS National Engineering Handbook*, Sec.4, Hydrology.

U. S. Geological Survey (1982), Guidelines for determining flood flow frequency, *Bulletin #17B of the Hydrology Subcommittee,* Reston, Virginia. 14-20.

Vogel, R.M., and N.M. Fennessey (1993), L moment diagrams should replace product moment diagrams, *Water Resour. Res., 29*(6), 1745-1752.

Wallis, J.R., and E.F. Wood (1985), Relative Accuracy of Log Pearson III Procedures, *J. Hydraul. Eng., 111*(7), 1043-1056.

Wallis, J.R., N.C. Matalas, and J.R. Slack (1974), Just a moment!, *Water Resour. Res., 10*(2), 281–289.

Ward, J. H. (1963), Hierarchical grouping to optimize an objective function, *J. Am. Statistic. Assoc., 58*, 236-244.

Zafirakou-Koulouris, A., R. Vogel, S. Craig, and J. Habermeier (1998), L-moment diagrams for censored observations, *Water Resour. Res., 34*(5), 1241-1249.

Observing and modelling exceptional floods and rainfalls
Proceedings of the AMHY-FRIEND International Workshop on Hydrological Extremes,
held at University of Calabria, Cosenza (Italy), May 3-4, 2006

UNCERTAINTY IN FLOOD ESTIMATION BY PARTIAL DURATION SERIES

J. Plavšić

Faculty of Civil Engineering, University of Belgrade, Serbia.

ABSTRACT
Flood frequency analysis (FFA) in hydrologic practice is essentially based on fitting of a theoretical probability distribution to observed flood data, meaning that some amount of uncertainty is always associated with the results of FFA. For FFA that is based on series of annual maximum floods, uncertainties have been investigated in detail and can be readily found in literature on hydrologic statistics. On the other hand, that is not the case with uncertainties in FFA based on partial duration series (PDS). The majority of work in this area is devoted to sampling properties of quantile estimates from the Poisson-exponential model of PDS, while models based on distributions other than combination of Poisson and exponential have been dealt with to much lesser extent. The paper briefly presents methodology for assessment of uncertainties in theoretical PDS models and factors affecting this uncertainty are described on several examples in order to describe the value of information on uncertainty for flood frequency analysis.

1. INTRODUCTION

Flood risk management relies heavily on flood frequency analysis, which is the primary tool for establishing a relationship between magnitude of flood and its probability of occurrence. Traditional approach to frequency analysis of floods is based on annual maxima series, which consist of maximum flow rates from each year within the observation period. This approach is commonly used in hydrologic practice because its requirements for data are low and the statistical apparatus and calculations are rather simple. The drawback of annual maxima series is that they include just one flow rate from a year, meaning that some relatively small values from dry years are included in data series and some "second greatest" values from wet years are not included. Alternatively, flood frequencies can be obtained using partial duration series, which consist of flood peaks exceeding some threshold value. It is considered that partial duration series contain more information on floods than annual maxima series.

Statistical analysis of partial duration series involves comparatively more complex methods than annual maxima series, since it is actually based on stochastic processes. The whole procedure is nowadays usually referred to as the peaks over threshold (POT) method. The theoretical basis for development of the POT method was set by work of Todorović (*Todorović, 1970; Todorović and Zelenhasić,* 1970). He has formulated a stochastic model of floods in which the time of flood peak occurrence (and consequently the number of peaks in a time interval) and the peak magnitude are both random variables. In terms of stochastic processes, this model can be categorized as a marked point process. Todorović has originally developed his model for a sequence of independent and identically distributed peaks, but the mathematical description of the model is general enough so that it can also be used for other cases as well (see e.g.

Rosbjerg, (1985) for dependent peaks and *Todorović and Rousselle* (1971) for non-identically distributed peaks). *Todorović and Zelenhasić* (1970) have chosen Poisson process as the process of peak occurrence and exponential distribution as the distribution of peak magnitude.

The POT method was further developed in several directions. *Todorović and Rousselle* (1971) have introduced seasonal variations of flood occurrence into the model. *North* (1980) has also considered inhomogeneous time process. *Ashkar and Rousselle* (1983a,b; 1987) examined assumptions about Poissonian flood count and exponential flood magnitudes and conditions for their fulfilling. As an alternative to Poisson distribution for flood count, negative binomial distribution was proposed by *Calenda et al.* (1977), and later by *Cunnane* (1979). Binomial distribution for flood count has been used to lesser extent (e.g. *Van Montfort and Otten,* 1991). In addition to the exponential distribution, other distributions used for flood magnitudes include two-parameter gamma (*Zelenhasić,* 1970), general Pareto (e.g. *Wang,* 1991*; Rosbjerg et al.,* 1992), and Weibull (*Vukmirović and Petrović,* 1997) distributions. Todorović has applied similar methodology to other hydrologic processes, including rainfall, dispersion in rivers and in porous media, and sediment transport (e.g. *Todorović and Yevjevich,* 1969*; Todorović,* 1975).

Uncertainties in flood estimates obtained from the partial duration series were first discussed for the Poisson-exponential model by *Cunnane* (1973), who derived an expression for the variance of flood quantile estimate. Other authors have dealt with the same problem, adopting different approaches of lesser or greater complexity, discussed later in more detail.

2. BRIEF DESCRIPTION OF THE POT METHOD

The stochastic model of floods introduced by *Todorović and Zelenhasić* (1970) considers the flood peaks X_i within a time interval (0, t] that exceed certain threshold x_0 (Figure 1). Then:

$$Z_i = X_i - x_0, \quad i = 1, 2, \dots \tag{1}$$

are flood exceedances or peaks over threshold. Each Z_i is a random variable, which occurs at random time τ_i. The number of exceedances in (0, t] is also a random variable, denoted by $\eta(t)$, and actually represents a discrete stochastic process. The greatest of all exceedances Z_i in time interval (0, t] is the random process $\chi(t)$:

$$\chi(t) = \sup\{Z_i; 0 < i \leq \eta(t)\} = \sup\{Z_i; \tau_i \leq t\}, \quad t \geq 0 \tag{2}$$

In other words, $\chi(t)$ is the maximum discharge above the chosen threshold in an arbitrary, but fixed, time interval. Under assumption that the exceedances are independent and identically distributed, and under assumption that the peak magnitudes are independent of their time of occurrence, distribution of the greatest exceedance can be expressed as (*Todorović and Zelenhasić,* 1970):

$$F(z; t) = P\{\chi(t) \leq z\} = P\{\eta(t) = 0\} + \sum_{n=1}^{\infty} [H(z)]^n \cdot P\{\eta(t) = n\} \tag{3}$$

where $H(z) = P\{Z_i \leq z\}$ is probability distribution function of exceedances.

If the time interval (0, t] is one year, then $\chi(t)$ is the annual maximum exceedance above x_0. If an annual maximum discharge is denoted with $X(t) = \chi(t) + x_0$, then the distribution function of annual maxima is:
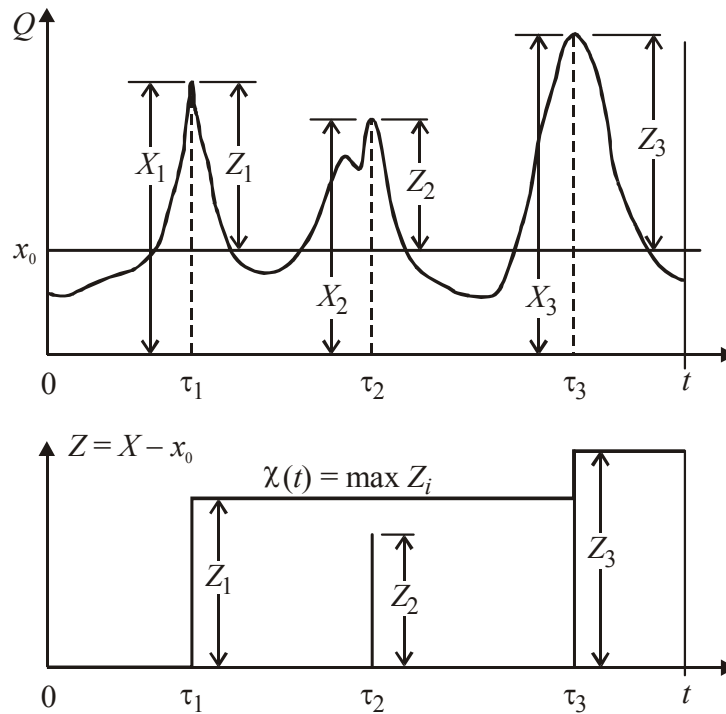
Figure 1. River hydrograph and exceedances above a threshold as a random process.

$$F(x) = P\{X(t) \le x\} = P\{\chi(t) \le x - x_0\} = \sum_{n=0}^{\infty}[H(x - x_0)]^n \cdot P\{\eta(t) = n\}, \quad x > x_0 \quad (4)$$

The above distribution function is valid only for $x > x_0$, i.e. for discharges greater then the threshold value, while it is not defined for smaller discharges, i.e. for $x < x_0$. The value of the distribution function of annual maximum discharge for $x = x_0$ is equal to the probability that there are no exceedances above x_0 during the year:

$$F(x_0) = P\{X(t) \le x_0\} = P\{\eta(t) = 0\} \quad (5)$$

Expressions for specific POT models (specific combinations of distributions for the number of peaks and for the peak magnitude) can be derived from the general equation (4). Distribution functions (both direct and inverse form) for several POT models are shown in Table 1.

In practice, partial duration series for a selected threshold is analyzed in three steps:
a) fitting the distribution of the number of peaks, $p_n = P\{\eta = n\}$ (choosing between Poisson, binomial and negative binomial distribution);
b) fitting the distribution of the exceedances, $H(z)$ (exponential, Weibull, etc.);
c) using parameters of distributions adopted in steps 1 and 2 to calculate distribution of annual maximum exceedance, $F(x)$.

If $F(x)$ is distribution function of annual maximum, then the classical definition of return period T can be used:

$$T(x) = \frac{1}{P\{X > x\}} = \frac{1}{1 - F(x)}, \quad x > x_0 \quad (6)$$

In this way, estimates based on partial duration series can be compared to those based on annual maximum series. *Todorović and Zelenhasić* (1970) showed that this expression also represents the average number of years when the first exceedance of the value x occurs.

Model	Distribution function	Inverse distribution function (quantile)
Poisson / Exponential **P**(Λ)+**E**(β)	$F(x) = \exp\left\{-\Lambda \exp\left(-\dfrac{x-x_0}{\beta}\right)\right\}$	$x(F) = x_0 + \beta[-\ln(-\ln F) + \ln \Lambda]$
Poisson / General Pareto **P**(Λ)+**GP**(k,b)	$F(x) = \exp\left\{-\Lambda\left(1 - k\dfrac{x-x_0}{b}\right)^{1/k}\right\}$	$x(F) = x_0 + \dfrac{b}{k}\left[1 - \left(\dfrac{-\ln F}{\Lambda}\right)^k\right]$
Poisson / Weibull **P**(Λ)+**W**(γ,β)	$F(x) = \exp\left\{-\Lambda \exp\left[-\left(\dfrac{x-x_0}{\beta}\right)^\gamma\right]\right\}$	$x(F) = x_0 + \beta[-\ln(-\ln F) + \ln \Lambda]^{1/\gamma}$
Binomial / Exponential **B**(Λ,b)+**E**(β)	$F(x) = \left\{1 - \dfrac{\Lambda}{b}\exp\left[-\dfrac{x-x_0}{\beta}\right]\right\}^b$	$x(F) = x_0 + \beta \ln\left[\dfrac{\Lambda}{b(1 - F^{1/b})}\right]$
Neg. binomial / Exponential **NB**(Λ,a)+**E**(β)	$F(x) = \left\{1 + \dfrac{\Lambda}{a}\exp\left(-\dfrac{x-x_0}{\beta}\right)\right\}^{-a}$	$x(F) = x_0 + \beta \ln\left[\dfrac{\Lambda}{a(F^{-1/a} - 1)}\right]$

Table 1. Overview of direct and inverse forms of distribution functions for different POT models.

On the other hand, some authors (e.g. *Rasmussen and Rosbjerg*, 1989) prefer to assume the Poisson process for the number of peaks and to perform only the second step of the above three. In that case, return period has to be defined on the basis of H(z), resulting in:

$$T_{PDS}(x) = \frac{1}{\lambda[1 - H(x - x_0)]}, \quad x > x_0 \tag{7}$$

where λ is the intensity of the Poisson process, i.e. the average number of peaks per year.

The relationship between the two definitions of return period is given with a well known expression:

$$T_{PDS}(x) = \frac{1}{\ln T(x) - \ln[T(x) - 1]} \tag{8}$$

Differences between the two definitions are significant only for short return periods (shorter than 10 years). Main difference is that classical return period $T(x)$ is greater than 1 year, while $T_{PDS}(x)$ may be shorter than 1 year. However, the latter definition of return period is not suitable if a POT model with a non-Poissonian distribution for the number of peaks is used.

3. ASSESSMENT OF UNCERTAINTIES IN THE POT SERIES

3.1 Measures of uncertainty in POT models

The usual task in flood frequency analysis is to estimate a design flood associated with some level of risk (expressed e.g. in terms of the return period). Another task may be to estimate the risk for a specific flood magnitude. Essentially, these two tasks involve the

same procedure of choosing a suitable POT model for floods and estimating distribution parameters. Of course, parent (or 'true') distribution of flood population is never known since its unknown parameters can only be estimated from a sample. For example, for a POT model with three parameters (e.g. a_1, a_2, a_3), it can be said that it has unknown parent distribution $F(x; a_1, a_2, a_3)$ and distribution $F(x; \hat{a}_1, \hat{a}_2, \hat{a}_3)$ estimated from the sample, as shown in Figure 2. Consequently, a quantile estimate $\hat{x}_T$ (or an exceedance probability estimate $\hat{p}_x$ for a given flood magnitude x) from the chosen POT model depends on parameter estimates, which in turn depend on sample properties. As any other estimate from sample, quantile estimate $\hat{x}_T$ is a random variable, having probability density function $f_{\hat{x}_T}(x)$ and properties such as mean $E[\hat{x}_T]$ and variance $\text{var}[\hat{x}_T]$. These properties actually describe uncertainty in estimating $\hat{x}_T$.
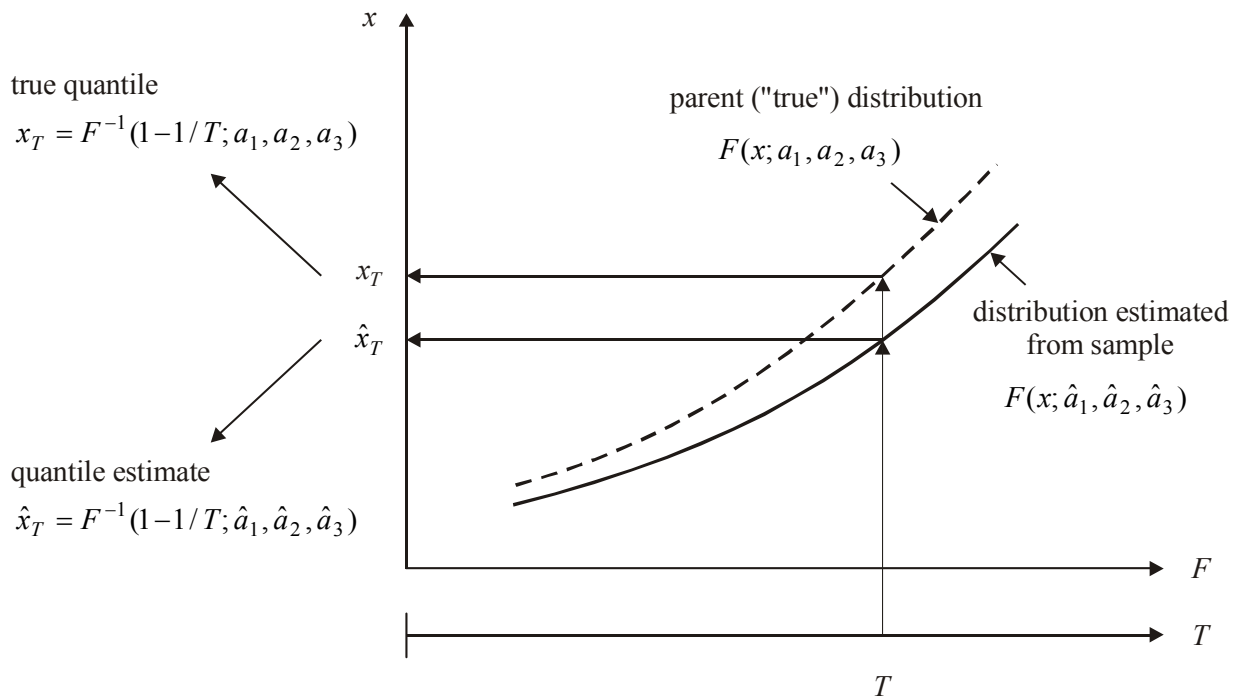
Figure 2. Discrepancy between unknown parent distribution and estimated distribution.

Commonly used measures of uncertainty are bias B, standard error SE and root mean square error RMSE, defined respectively here for quantile estimate:

$$B[\hat{x}_T] = E[\hat{x}_T] - x_T, \quad SE[\hat{x}_T] = \sqrt{\text{var}[\hat{x}_T]}, \quad RMSE[\hat{x}_T] = \sqrt{\text{var}[\hat{x}_T] + B^2[\hat{x}_T]} \quad (9)$$

When considering uncertainties in quantile estimate $\hat{x}_T$, it is easier to work with the exceedance quantile $\hat{z}_T = \hat{x}_T - x_0$ because the effect of the threshold x_0 is eliminated. There is no loss of generality in this because the following is valid for the bias and the variance of the quantile estimates:

$$B[\hat{x}_T] = B[\hat{z}_T], \quad \text{var}[\hat{x}_T] = \text{var}[\hat{z}_T] \quad (10)$$

3.2 Approaches to assessment of uncertainties

In general, there are several approaches for obtaining uncertainties. If the probability density function $f_{\hat{x}_T}(x)$ of quantile estimate $\hat{x}_T$ is known, then it is possible to estimate $E[\hat{x}_T]$ or $\text{var}[\hat{x}_T]$ directly. *Ashkar and Rousselle* (1981) derived probability density

function of the quantile estimate, $f_{\hat{x}_T}(x)$, for the P+E model of POT series, and later *Nachtnebel and Konecny* (1987) obtained virtually the same results. This approach was also used by *Rasmussen and Rosbjerg* (1989), who used $f_{\hat{x}_T}(x)$ to obtain $E[\hat{x}_T]$ and $\text{var}[\hat{x}_T]$. However, for other POT models it is practically impossible to define $f_{\hat{x}_T}(x)$.

The most common approach is based on expansion of quantile estimate $\hat{x}_T$ into Taylor series in which higher-order derivatives are neglected, where quantile estimate is treated as a function of parameter estimates, such as $\hat{x}_T = g(\hat{a}_1, \hat{a}_2, \hat{a}_3)$. This approach leads to the well-known formulae for variance and expectation of a function of random variables, which for quantile estimate read:

$$
\begin{aligned}
\text{var}[\hat{x}_T] &\approx \sum_i \text{var}[\hat{a}_i] \left(\frac{\partial g}{\partial \hat{a}_i}\bigg|_\mu \right)^2 + 2\sum_{i \neq j} \text{cov}[\hat{a}_i, \hat{a}_j] \left(\frac{\partial g}{\partial \hat{a}_i} \frac{\partial g}{\partial \hat{a}_j}\bigg|_\mu \right) \\
E[\hat{x}_T] &\approx g\big|_\mu + \frac{1}{2}\sum_i \text{var}[\hat{a}_i] \frac{\partial^2 g}{\partial \hat{a}_i^2}\bigg|_\mu + \sum_{i \neq j} \text{cov}[\hat{a}_i, \hat{a}_j] \frac{\partial^2 g}{\partial \hat{a}_i \partial \hat{a}_j}\bigg|_\mu
\end{aligned}
\tag{11}
$$

where $\big|_\mu$ means that the function g and its derivatives are evaluated at point $(\mu_{\hat{a}_1}, \mu_{\hat{a}_2}, \mu_{\hat{a}_3})$. This approach was used by *Cunnane* (1973) and *Rosbjerg* (1985) for the P+E model, and by *Rosbjerg et al.* (1992) for the P+GP model. The above formulae are also referred to as asymptotic formulae because they actually describe properties of estimates for large sample sizes.

It is also possible to employ Monte Carlo simulations to obtain mean and variance of quantile estimates. An advantage of this approach is that uncertainties for small sample sizes can be assessed. However, this approach cannot be expected to be applied in everyday practice. Monte Carlo simulations were used for the P+E model by *Tavares and da Silva* (1983) and for the P+GP model by *Rosbjerg et al.* (1992).

In the inverse task of estimating probability for a given flood *x*, it is a matter of preference whether this probability would be expressed as a non-exceedance probability (or cumulative distribution function) F_x, exceedance probability $p_x = 1 - F_x$ or return period $T_x = 1/p_x$; sometimes, risk $R_x = 1 - F^L$ defined as probability of exceedance in L years is also used. Approaches for assessment of uncertainties in probability estimates are the same as for quantile estimates. For the P+E model, *Ashkar and Rousselle* (1981) applied direct approach of deriving probability density function for the return period estimate $\hat{T}_x$, while *Rasmussen and Rosbjerg* (1989) used the same approach focusing on return period estimate from partial duration series $\hat{T}_{PDS,x}$ and risk estimate $\hat{R}_x$. However, mean and variance can be obtained only for $\hat{R}_x$ and not for $\hat{T}_x$ or $\hat{T}_{PDS,x}$. *Rasmussen and Rosbjerg* (1989) also used the Taylor series approach and referred to the corresponding results as to 'approximation formulae'. Defining probability density function for other POT models is practically impossible.

The results of uncertainty assessment for all POT models mentioned in Table 1 are described in detail in the study by *Plavšić* (2005). The study includes uncertainties in both quantile and probability estimates. For models with general Pareto and Weibull distributions, two common parameter estimation methods are considered: the method of moments and the method of probability weighted moments. The results of various authors for the P+E model are systematically compared for quantile and probability

estimates. Uncertainties in quantile estimate for the P+GP model are adjusted from the results of *Rosbjerg et al.* (1992). Uncertainties in probability estimate for the P+GP model, as well as uncertainties for both quantile and probability estimates for other models (P+W, NB+E and B+E) are developed using the Taylor series expansion approach. Assessment of all these uncertainties can be found in *Plavšić* (2005). The subsequent sections illustrate the main results and conclusions from this study on several examples.

3.3 Factors affecting uncertainty in POT models

Effect of record length. Uncertainties are, of course, the greatest if the frequency analysis is performed with the shortest records. Record length in POT series is represented not only by the number of years in record N, but also by the total number of peaks M or the average number of peaks per year $\Lambda = M/N$. In general, uncertainties in POT models decrease with an increase in total record length M, and with and increase of both N and Λ. To illustrate the effect of the record length on uncertainties, the gauging station at Bezdan on the Danube was chosen with 70 years of record (the longest hydrologic record in Serbia). Four POT series were extracted from the original record, with length of 10, 30, 50 and 70 years, as shown in Table 2. The series with smaller number of years were made with lower threshold so that the average annual number of peaks is higher, and vice versa. Figure 3 presents the relative standard error and the relative bias of quantile estimate for the P+W model. It can be seen that very short series such as 10 or 30 years create much larger uncertainties, even with a high average annual number of peaks Λ. This means that it is not correct to assume that a large number of peaks in partial duration series would 'compensate' the small number of years; therefore, the POT method should not be abused in this direction.

Series	*N*	Λ
1961-1970	10	5.9
1951-1980	30	4.2
1941-1990	50	2.5
1931-2001	70	1.04

Table 2. Partial duration series of flows on the Danube at Bezdan
for analysis of the effect of record length.

Effect of shape parameter of exceedance distribution. Uncertainties in POT models with two-parameter distributions for exceedances are most affected by values of shape parameters of these distributions (parameter k of the general Pareto distribution, and parameter γ of the Weibull distribution; see Table 1). This is expected since these distributions may be quite different for different values of their shape parameters. For example, the general Pareto distribution is upper-bounded for positive *k*, while it is not bounded for negative k; this not only reflected on the shape of the distribution, but also on the uncertainties.

Uncertainties become very large in some ranges of values of shape parameters. Knowing which these ranges are is useful in the process of selecting a distribution for peaks: if fitted shape parameter is within a range of values with large uncertainties, then perhaps another distribution should be fitted to the series in hand.

Figure 4 shows the effect of shape parameters of P+GP and P+W models on uncertainties of quantile estimates. The diagrams in Figure 4 present theoretical results for a series with N=30 years of record and Λ=2 peaks per year in average. Uncertainties are large where the general Pareto parameter k is negative and the Weibull parameter γ is smaller than 1.
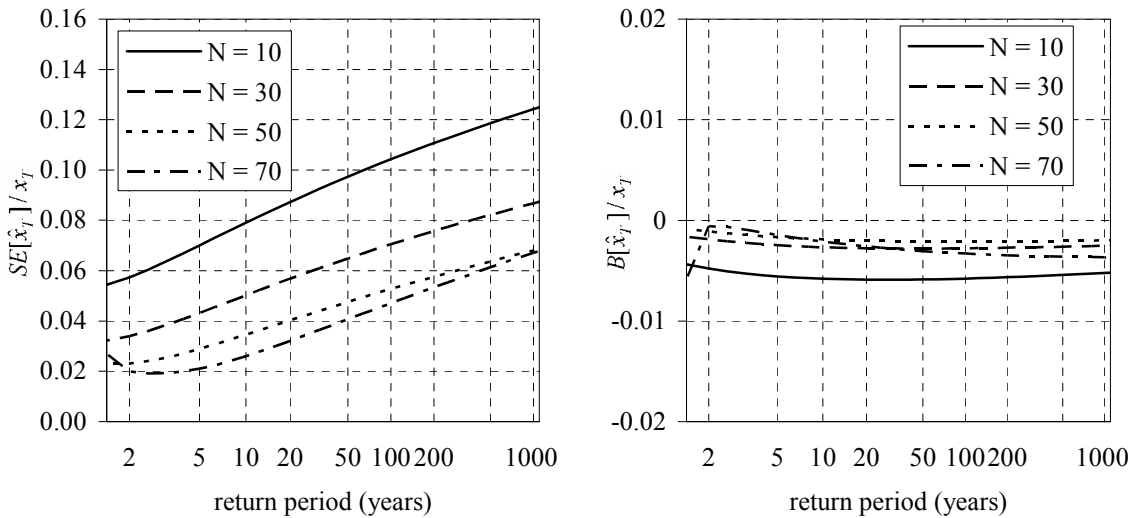

Figure 3. Relative standard error (left) and relative bias (right) of quantile estimate by the P+W model for different number of years in the record (station Bezdan on the Danube).

Effect of the parameter estimation method. The choice of the method for estimation of parameters also affects uncertainties. The most common method for estimation of the Weibull and general Pareto distributions are the classical method of moments (MOM) and the method of probability weighted moments (PWM). No particular conclusions can be made in favour of one or the other method. The two methods sometimes produce significantly different results in terms of uncertainties, and sometimes they give the same results (Figure 5).

The MOM method is not applicable with the general Pareto distribution for values of shape parameter $k \leq -0.5$. Uncertainties are very large for $-0.5 \leq k \leq -0.2$ and even cannot be calculated using the asymptotic formulae for $k \leq -0.25$. For reasonable record lengths and for $k > -0.2$, the MOM method gives smaller uncertainties then the PWM method, while the PWM method is better than the MOM method for $k \leq -0.2$.

The effect of the method is somewhat smaller for the POT models with Weibull distribution. Bias in quantile estimate obtained by the MOM method abruptly increases for the values of shape parameter γ in the range between 0.5 and 1. Relative standard error of quantile estimate is very similar for both parameter estimation methods.

3.4 Uncertainty as an additional criterion for selecting a POT model

Uncertainties may be a good additional criterion for selecting an appropriate model for a partial duration series. Several examples are shown to illustrate how uncertainties can support this process.
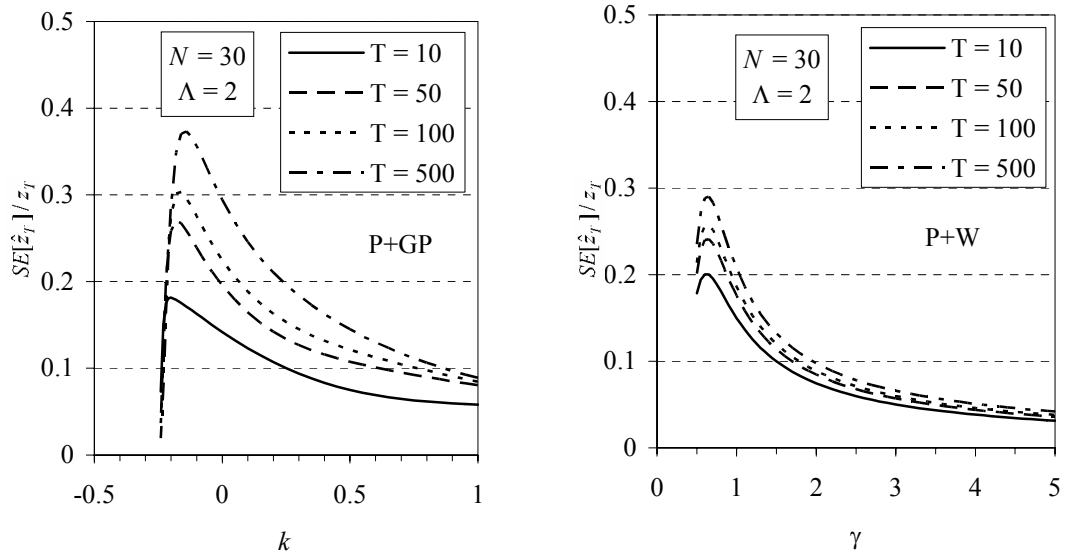
Figure 4. Relative standard error of exceedance quantile estimate by the P+GP model (left) and by the P+W model (right) vs. values of shape parameters k and γ of general Pareto and Weibull distributions, respectively, for several values of return period T.
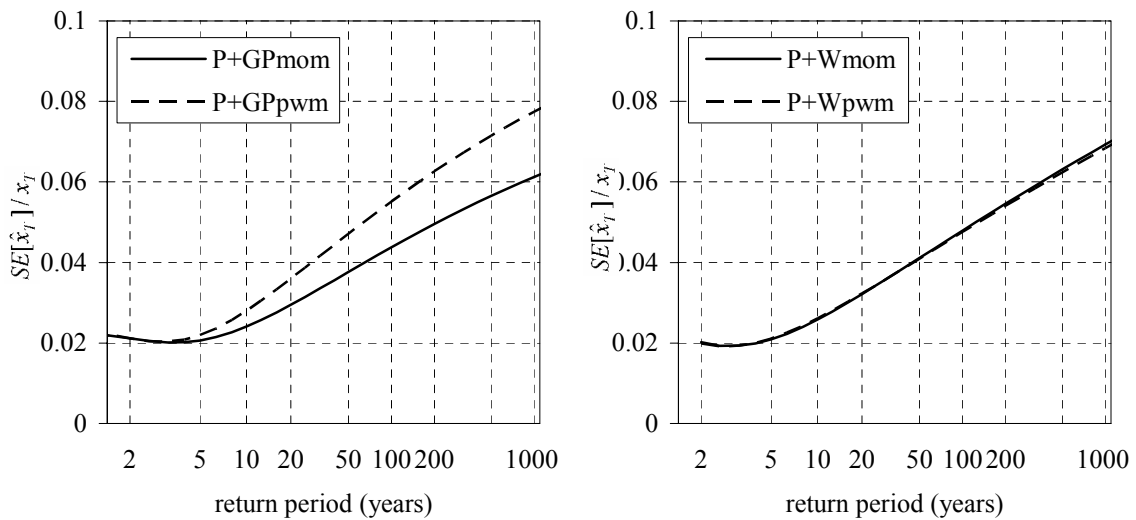

Figure 5. Relative standard error of quantile estimate by the P+GP model (left) and by the P+W model (right) for two methods of parameters estimation, MOM and PWM (station Bezdan on the Danube).

Sometimes fitting POT models to some series, usually those with no outliers and small skewness, yields inconclusive results in sense that all the fitted models give very similar distributions. In such cases, goodness-of-fit tests also give very similar results and it is not possible to objectively select 'the best' model. Figure 6 presents such a case for the station Bezdan on the Danube for the threshold of 5000 m^3/s.
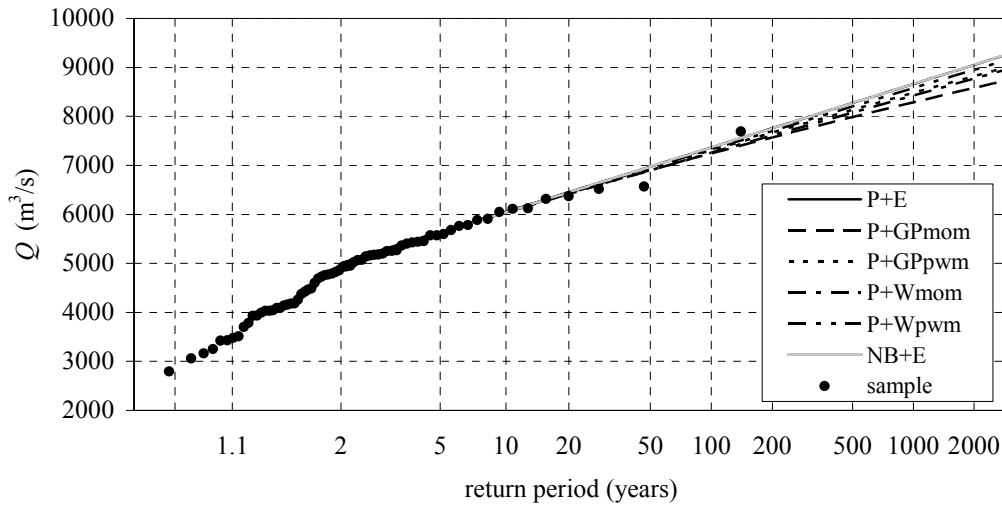
Figure 6. Distributions of floods for the station Bezdan on the Danube for threshold of 5000 m³/s according to different POT models.

However, if uncertainties of the same models are plotted (Figure 7), then it can be seen that some models produce higher uncertainties then others. Models P+E and P+NB, having the smallest relative standard error of quantile estimate, are overlaid on the graph in Figure 7. In such a case, when other criteria are not helpful to decide on the best model, the model with the smallest uncertainty can be selected (in this case model P+E).

Selecting the model with the smallest standard error gives the narrowest confidence interval (Figure 8).
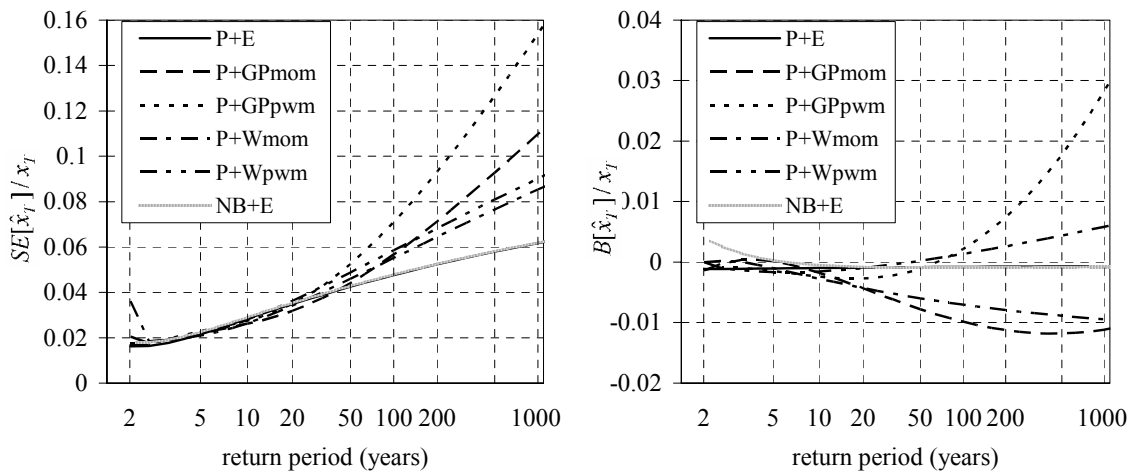
Figure 7. Relative standard error (left) and relative bias (right) of quantile estimate by different POT models for the station Bezdan on the Danube and threshold of 5000 m³/s.

3.5 Uncertainty in probability estimation

The general conclusion about uncertainties in estimating probability (either exceedance probability or return period) for a give flood magnitude is that the greater the flood, the greater the uncertainty. More precisely, uncertainties become very large for values corresponding to 'true' return period that exceeds the number of years of record.

Figure 9 presents an example of flood frequency distribution for station Lopatnica Lakat on the Ibar River in Serbia, where the maximum observed flood is $Q_{max} = 1520$ m³/s. An 80% confidence interval for the estimate of exceedance probability is also

plotted in Figure 9. According to the best fitted model (P+W), return period of Q_{max} is about 120 years, while the confidence interval indicates that the 'true' return period is somewhere between 70 and 700 years! From this example it can be concluded that estimating the return period of an observed flood is quite unrewarding task.
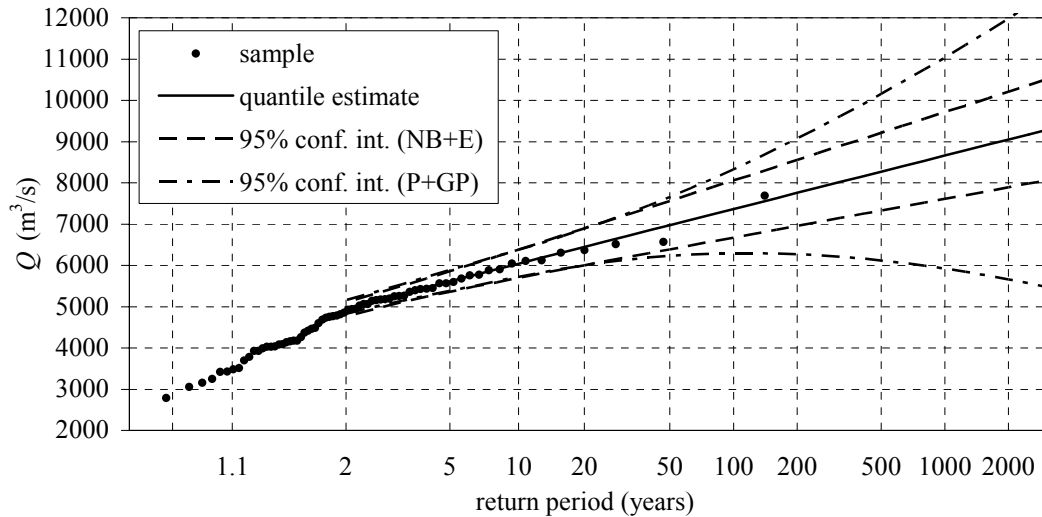

Figure 8. Confidence interval of 95% for flood quantile estimates at the station Bezdan on the Danube for threshold of 5000 m^3/s, for POT models with the smallest and the greatest uncertainty.

4. CONCLUSIONS

It is difficult to formulate a general conclusion about uncertainties in partial duration series, especially when it is clear that many factors affect these uncertainties. The most easily observable issue is that the uncertainties are the largest for the shortest records, and not only for a small total number of peaks, but also for the small number of years combined with a relatively large number of peaks. This proves that the POT method should not be misused with short records in terms of the number of years. Uncertainties are affected also by the values of shape parameters of distributions for peaks that are part of POT models (such as the general Pareto and Weibull distributions), as well as by the method for parameter estimation. Also, uncertainties can be a good additional criterion in selecting an appropriate model for a given partial duration series.

Flood frequency analysis is just one step in water resources engineering and management projects focused on estimation of risks and damages from floods, planning and design of structures and measures for protection from floods and associated phenomena such as erosion or landslides. Flood frequency analysis is supposed to provide design floods for a given probability of occurrence as criteria for design purposes, or an estimate of probability of occurrence of some critical events. Uncertainties are always present in flood risk analysis, and will always be present. They are inevitably transferred to further results, such are the dimensions of flood protection structures or estimated damages. Yet, there is a prevailing tendency in hydrologic practice to neglect uncertainties and to treat the results of flood frequency analysis as certain (even deterministic) values. It can also be found in practice that the uncertainties are compensated by choosing a higher return

period or simply by selecting a distribution producing the highest floods ('justified' by being on the safe side).
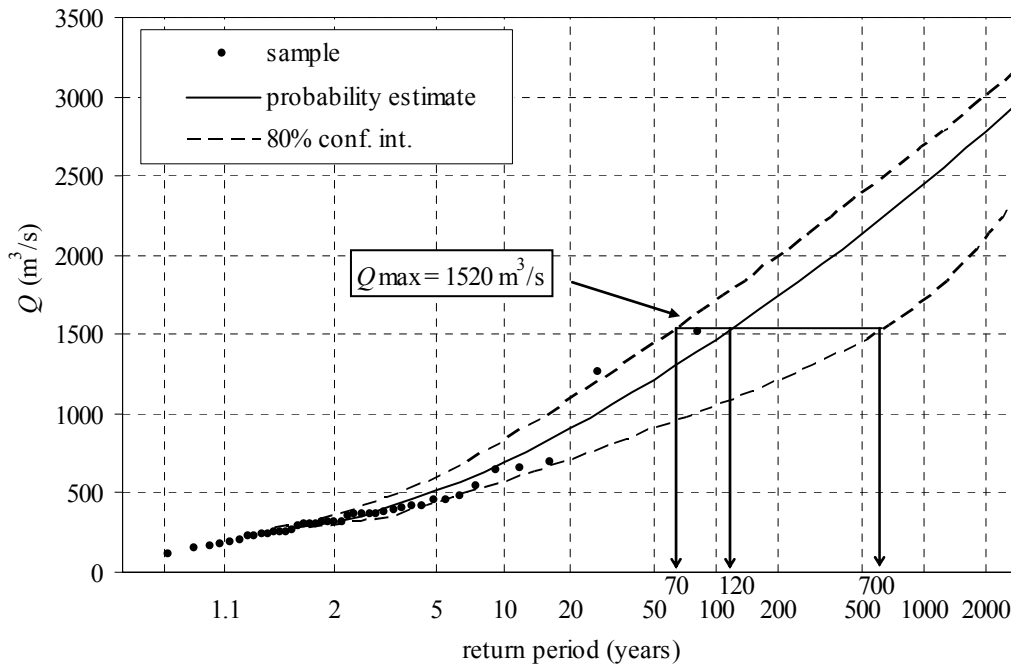

Figure 9. Confidence interval of 80% for exceedance probability of floods at the station Lopatnica Lakat on the Ibar River (P+W model with threshold of 280 m³/s); for the maximum observed flood of 1520 m³/s, confidence limits for return period are 70 and 700 years.

Although uncertainties cannot be avoided, knowing their magnitude (or at least their order of magnitude) and taking them into consideration is important in order to be aware of limitations of designed structures or flood protection measures. Taking uncertainties into consideration in flood risk analysis contributes to better technical and flood management solutions and to the decision-making process on acceptable flood risk.

REFERENCES

Ashkar, F., and J. Rousselle (1981), Design discharge as a random variable: a risk study, *Water Resour. Res.*, *17*(3), 577-591.

Ashkar, F., and J. Rousselle (1983a), Some remarks on the truncation used in partial flood series models, *Water Resour. Res.*, *19*(2), 477-480.

Ashkar, F., and J. Rousselle (1983b), The effect of certain restrictions imposed on the interarrival times of flood events on the Poisson distribution used for modeling flood counts, *Water Resour. Res.*, *19*(2), 481-485.

Ashkar, F., and J. Rousselle (1987), Partial duration series modeling under the assumption of a Poissonian flood count, *J. Hydrol.*, *90*, 135-144.

Cunnane, C. (1973), A particular comparison of annual maxima and partial duration series methods of flood frequency prediction, *J. Hydrol.*, *18*, 257-271.

Cunnane, C. (1979), A note on the Poisson assumption in partial duration series models, *Water Resour. Res.*, *15*(2), 489-494.

Nachtnebel, H.P., and F. Konecny (1987), Risk analysis and time-dependent flood models, *J. Hydrol.*, *91*, 295-318.

North, M. (1980), Time-dependant stochastic model of floods, *J. Hydr. Div.*, *106*(5), 649-665.

Plavšić, J. (2004) *Analysis of flood risk estimation by partial duration series*, Ph.D. thesis (in Serbian). Faculty of Civil Engineering, University of Belgrade, Serbia.

Rasmussen, P.F., and D. Rosbjerg (1989), Risk estimation in partial duration series, *Water Resour. Res.*, *25*, 2319-2330.

Rosbjerg, D (1985), Estimation in partial duration series with independent and dependent peak values, *J. Hydrol.*, *76*, 183-195.

Rosbjerg, D., H. Madsen, and P.F. Rasmussen (1992), Prediction in partial duration series with generalized Pareto-distributed exceedances, *Water Resour. Res.*, *28*, 3001-3010.

Tavares, L.V., and J.E. da Silva (1983), Partial duration series method revisited, *J. Hydrol.*, *64*, 1-14.

Todorović, P. (1970), On some problems involving random number of random variables, *Ann. Math. Stat.*, *41*(3), 1059-1063.

Todorović, P. (1975), A stochastic model of dispersion of sediment particles released from a continuous source, *Water Resour. Res.*, *11*(6), 919-925.

Todorović, P., and J. Rousselle (1971), Some problems of flood analysis, *Water Resour. Res.*, *7*(5), 1144-1150.

Todorović, P., and V. Yevjevich (1969), *Stochastic processes of precipitation*, Hydrology Paper No. 35, Colorado State University, Fort Collins.

Todorović, P., and E. Zelenhasić (1970), A stochastic model for flood analysis, *Water Resour. Res.*, *6*(6), 1641-1648.

Van Montfort, M.A.J. and A. Otten (1991), The first and the second e of the extreme value distribution EV1, *Stoch. Hydrol. Hydraul.*, 69-76.

Vukmirović, V., and J. Petrović (1997), Flood flow analysis using renewal processes, *UNESCO-IHP V Tech. Documents in Hydrology No. 11* (Annual FRIEND-AMHY meeting, Thessaloniki, 1995), 159-169.

Wang, Q.J. (1991) The POT model described by the generalized Pareto distribution with Poisson arrival rate, *J. Hydrol.*, *129*, 263-280.

Zelenhasić, E. (1970), *Theoretical probability distributions for flood peaks*, Hydrology Paper No. 42, Colorado State University, Fort Collins.

Observing and modelling exceptional floods and rainfalls
Proceedings of the AMHY-FRIEND International Workshop on Hydrological Extremes,
held at University of Calabria, Cosenza (Italy), May 3-4, 2006

INVESTIGATION INTO RAINFALL VARIABILITY AT MONTHLY TIME AGGREGATION SCALE

B. Sirangelo, E. Ferrari

Soil Protection Department "V. Marone", University of Calabria, Cosenza, Italy.

ABSTRACT
With the aim of exploring possible trends in hydrological variables, in this work the presence of significant variation in recent rainfall regime of Crati River basin in Southern Italy (about 2500 km²) has been investigated. The rain gauges network used for the analysis consists of 70 instruments, whose observations span from 1921 to 2000 with a few missing years. The climatic variable employed for trend evaluation is the monthly rainfall height, averaged over the whole basin through a spatial non-statistical interpolation of point rainfall heights.
Seasonality has been modelled by assuming the existence of a deterministic component in the discrete domain through Fourier analysis. The statistical exploration of the residuals has been focused with reference to decades 1981-1990 and 1991-2000 by means of a cross-validation procedure, which shows clear evidence of decreasing monthly rainfalls recorded in the most recent decades. The comparisons among residuals of different decades have been based on normal probability plots, non-parametric tests, among which the two-sample Kolmogorov-Smirnov test, and some other tests based on stochastic independence, such as the Anderson test.

1. INTRODUCTION

Only in recent years the impacts of human activities on environment have been investigated, especially as regards those activities delivering great amount of gases as a residual that are supposed producing an increase of the mean temperature on the earth. Less evident, and yet less simple to explain, seem to be the impacts on the rainfall regime. This can be due either to a lesser rainfall sensitivity to the ongoing changing trend or to the difficulty in evaluating changes of an intermittent random variable like meteoric precipitation.

Assessments on the possible existence of notable changes in rainfall characteristics of a drainage basin, though not verifiable for a certainty, are very important for most of the engineering applications of water resources supply and management. Moreover, if reliably assessed, non-stationary features of rainfall phenomenon should imply the adequacy of the procedures for statistical evaluation of hydrological variables, though criteria for possible appropriate modifications are not yet well defined (*IPCC*, 2001).

Within this debated question, it is important to perform rigorous and objective statistical analyses of rainfall observations (*Hirsch et al.*, 1992; *Chin*, 1995; *WMO*, 2000; *Burn and Hag Elnur*, 2002). Following this direction, this work tries to contribute to climatic change discussion through assessment of existence of significant variation in recent rainfalls of the Crati basin, the greatest basin of Calabria (Southern Italy). The data

used in the statistical analysis are the monthly rainfalls observed in a set of 70 rain gauges spanning from 1921 to 2000, with some lack of data during the 1941-1950 decade.

2. RAINFALL ANALYSIS

2.1 Evaluation of monthly-averaged mean areal precipitations

Statistical analysis of significant variations in pluviometric features has been focused on the daily rainfalls averaged on the basin extension at a monthly temporal scale. Evaluation of monthly-averaged mean areal rainfalls has been performed through surface spline, the most efficient non-statistical technique of spatial interpolation that is a dual formulation of the kriging method (*Cressie*, 1991).

The mathematical structure of the spatial function interpolating rainfall heigths of month j and year i, $h_{i,j}(x, y)$ can be posed in the form (*Yu*, 2001):

$$h_{i,j}(x, y) = a_0^{(i,j)} + a_1^{(i,j)}x + a_2^{(i,j)}y + \sum_{m=1}^{N^{(i,j)}} \left[K_m^{(i,i)}\delta(d_m) + d_m^2 \ln d_m^2 \right] c_m^{(i,j)} \tag{1}$$

where $\delta(.)$ indicates Kroneker's delta, $d_m^2 = (x - x_m)^2 + (y - y_m)^2$, with x_m and y_m spatial coordinates of $N^{(i,j)}$ functioning rain gauges, and rigidity factors $K_m^{(i,j)}$ are zero in the case of interpolating functions exactly reproducing values observed at rain gauges. For month j and year i, the effective estimation of $N^{(i,j)} + 3$ coefficients $a_0^{(i,j)}$, $a_1^{(i,j)}$, $a_2^{(i,j)}$ and $c_m^{(i,j)}, m = 1, 2, ..., N^{(i,j)}$ is obtained from the solution of the system of $N^{(i,j)} + 3$ linear algebric equations:

$$\begin{bmatrix} \underline{\underline{F}}^{(i,j)} & \underline{\underline{B}}^{(i,j)} \\ \underline{\underline{B}}^{(i,j)T} & \underline{\underline{0}} \end{bmatrix} \cdot \begin{bmatrix} \underline{c}^{(i,j)} \\ \underline{a}^{(i,j)} \end{bmatrix} = \begin{bmatrix} \underline{h}^{(i,j)} \\ \underline{0} \end{bmatrix} \tag{2}$$

where $\underline{\underline{F}}^{(i,j)}$ is a matrix $N^{(i,j)} \times N^{(i,j)}$ with elements $f_{mn} = d_{mn}^2 \ln d_{mn}^2$ for $m \neq n$ and $f_{mn} = 0$ for $m = n$, with $d_{mn}^2 = (x_n - x_m)^2 + (y_n - y_m)^2$, $\underline{\underline{B}}^{(i,j)}$ is a matrix $N^{(i,j)} \times 3$ with elements $b_{m1} = 1$, $b_{m2} = x_m$, $b_{m3} = y_m$, $\underline{c}^{(i,j)}$ is a vector $[c_1^{(i,j)}, c_2^{(i,j)}, ..., c_{N^{(i,j)}}^{(i,j)}]^T$, $\underline{a}^{(i,j)}$ is a vector $[a_0^{(i,j)}, a_1^{(i,j)}, a_2^{(i,j)}]^T$ and $\underline{h}^{(i,j)}$ is a vector $[h_1^{(i,j)}, h_2^{(i,j)}, ..., h_{N^{(i,j)}}^{(i,j)}]^T$ formed by rainfall heigths of month j and year i observed at rain gauges.

Once the interpolating functions have been determined, the mean areal rainfall heigths of month j and year i are evaluated by:

$$\overline{h}_{i,j} = \frac{1}{S} \iint_{\Sigma} h_{i,j}(x, y) dx dy \tag{3}$$

where Σ is the domain of the basin and S its extension. Surface integral of (3) can be numerically evaluated.

2.2 Modelling of average monthly rainfalls

In order to homogenize the different durations of the months by means of a common time unit equal to the average monthly duration, $\Delta t = 365.25 / 12$ days, rainfall amounts $\overline{h}_{i,j}$ have been multiplied by the ratio between Δt and the duration of month j (in days). The adjusted monthly rainfall amounts can be interpreted as a sample series, with constant

step Δt, of a continuous integrated stochastic process $\{\overline{H}_{i,j}\}$ in which i and j are the index of the year and the index of the month respectively.

The process $\{\overline{H}_{i,j}\}$ is previously normalized through the power function:

$$Y_{i,j} = \left(\overline{H}_{i,j}\right)^{\lambda} \tag{4}$$

with constant λ, aiming to create a transformed process $\{Y_{i,j}\}$ as near as possible to a normal process (*Box and Cox*, 1964). Then the transformed process $\{Y_{i,j}\}$ is deseasonalized and standardized by means of the reduced random variable Z:

$$Z = \frac{1}{\upsilon_{Y_j}}\left[\frac{Y_{i,j}}{\mu_{Y_j}} - 1\right] \tag{5}$$

where μ_{Y_j} and υ_{Y_j} are, respectively, mean and coefficient of variation of the process.

The mean μ_{Y_j} and the coefficient of variation μ_{Y_j} are considered periodic functions with period equal to $12\Delta t$ and are approximated through a finite expansion of Fourier series:

$$\mu_{Y_j} \cong \widetilde{\mu}_{Y_j} = \frac{1}{2}a_0^{(\mu)} + \sum_{k=1}^{n_a^{(\mu)}}\left[a_k^{(\mu)}\cos\left(\frac{\pi k}{6}j\right) + b_k^{(\mu)}\mathrm{sen}\left(\frac{\pi k}{6}j\right)\right] \tag{6}$$

$$\upsilon_{Y_j} \cong \widetilde{\upsilon}_{Y_j} = \frac{1}{2}a_0^{(\upsilon)} + \sum_{k=1}^{n_a^{(\upsilon)}}\left[a_k^{(\upsilon)}\cos\left(\frac{\pi k}{6}j\right) + b_k^{(\upsilon)}\mathrm{sen}\left(\frac{\pi k}{6}j\right)\right] \tag{7}$$

where $n_a^{(\mu)}$ is the number of harmonics, $a_0^{(\mu)}$, $a_k^{(\mu)}, b_k^{(\mu)}; k = 1,...,n_a^{(\mu)}$ are Fourier coefficients for the mean and $n_a^{(\upsilon)}, a_0^{(\upsilon)}, a_k^{(\upsilon)}, b_k^{(\upsilon)}; k = 1,...,n_a^{(\upsilon)}$ are the analogous quantities for coefficient of variation.

These parameters can be evaluated as:

$$a_0^{(\mu)} = \frac{1}{6}\sum_{j=1}^{12}m_{Y_j} \qquad a_k^{(\mu)} = \frac{1}{6}\sum_{j=1}^{12}m_{Y_j}\cos\left(\frac{\pi}{6}kj\right) \qquad b_k^{(\mu)} = \frac{1}{6}\sum_{j=1}^{12}m_{Y_j}\mathrm{sen}\left(\frac{\pi}{6}kj\right) \tag{8}$$

$$a_0^{(\upsilon)} = \frac{1}{6}\sum_{j=1}^{12}v_{Y_j} \qquad a_k^{(\upsilon)} = \frac{1}{6}\sum_{j=1}^{12}v_{Y_j}\cos\left(\frac{\pi}{6}kj\right) \qquad b_k^{(\upsilon)} = \frac{1}{6}\sum_{j=1}^{12}v_{Y_j}\mathrm{sen}\left(\frac{\pi}{6}kj\right) \tag{9}$$

where the sample statistics are:

$$m_{Y_j} = \frac{1}{N_{a,j}}\sum_{i=1}^{N_{a,j}}\overline{h}_{i,j}^{\lambda} \qquad v_{Y_j} = s_{Y_j}/m_{Y_j} \qquad s_{Y_j}^2 = \frac{1}{N_{a,j}}\sum_{i=1}^{N_{a,j}}\left(\overline{h}_{i,j}^{\lambda} - m_{Y_j}\right)^2 \tag{10}$$

in which $N_{a,j}$ is the number of observation years available for the month j.

Accepted a constant value of parameter λ, the number of harmonics to be used, both for mean and coefficient of variation, can be fixed equal to the minimum number so that monthly values of $\widetilde{\mu}_{Y_j}$ and $\widetilde{\upsilon}_{Y_j}$, estimated through (6) and (7), be within confidence intervals of sampling mean m_{Y_j} and coefficient of variation v_{Y_j} for each specified level of significance α.

As regards the sample mean m_{Y_j}, the bounds of confidence intervals can be easily evaluated remembering that Y_j and consequently sample mean are approximately normal,

for large $N_{a,j}$, with mean and variance evaluated as m_{Y_j} and $s_{Y_j}^2 / N_{a,j}$. So, for a specific significance level α, the confidence interval is given by:

$$\left[m_{Y_j} - x_{1-\alpha/2}\, s_{Y_j} / \sqrt{N_{a,j}}\, ; m_{Y_j} + x_{1-\alpha/2}\, s_{Y_j} / \sqrt{N_{a,j}} \right] \tag{11}$$

where $x_{1-\alpha/2}$ is the quantile $1-\alpha/2$ of standard normal distribution. More complex is the identification of the confidence intervals of sample coefficient of variation that is characterised by a probabilistic distribution not easily identifiable and usable, though the variance is easily obtained (*Kendall and Stuart*, 1973). Nevertheless, since Y_j is an approximately standard normal variable, confidence intervals can be evaluated through Monte Carlo techniques.

2.3 Analysis of reduced variable Z

The removal of the periodicity of the monthly-averaged mean areal rainfalls provide a stochastic process $\{Z\}$ which can yet contain a residual correlation. To verify if the process $\{Z\}$ can be defined as purely random, the classical Anderson test has been applied. The test is based on the property that, for a purely stationary and independent gaussian process, the sample correlation coefficients:

$$r_{Z,k} = \left[p_Z^{(1,N-k)} - m_Z^{(1,N-k)} m_Z^{(1+k,N)} \right] / \left[s_Z^{(1,N-k)} s_Z^{(1+k,N)} \right] \tag{12}$$

where:

$$p_Z^{(1,N-k)} = \frac{1}{N-k} \sum_{n=1}^{N-k} z_n z_{n+k} \qquad m_Z^{(1,N-k)} = \frac{1}{N-k} \sum_{n=1}^{N-k} z_n \qquad m_Z^{(1+k,N)} = \frac{1}{N-k} \sum_{n=1+k}^{N} z_n$$

$$s_Z^{(1,N-k)} = \sqrt{\frac{1}{N-k} \sum_{n=1}^{N-k} z_n^2 - \left(m_Z^{(1,N-k)} \right)^2} \qquad s_Z^{(1+k,N)} = \sqrt{\frac{1}{N-k} \sum_{n=1+k}^{N} z_n^2 - \left(m_Z^{(1+k,N)} \right)^2}$$

in which $z_1, z_2, \ldots, z_N$ is the sample of Z values evaluated through (5), are approximately distributed through a normal distribution with mean and variance provided by $-1/(N-k)$ and $(N-k-1)/(N-k)^2$ respectively. Confidence intervals, with significance level α, are expressed as:

$$\left[-\frac{1}{N-k} - x_{1-\alpha/2}\, \frac{\sqrt{N-k-1}}{(N-k)}\, ; -\frac{1}{N-k} + x_{1-\alpha/2}\, \frac{\sqrt{N-k-1}}{(N-k)} \right] \qquad k = 1,2,\ldots \tag{13}$$

Hypothesis of purely randomness for process $\{Z\}$ cannot be rejected if $r_{Z,k}$ values (k=1, 2,…) are in between bounds of confidence intervals.

A further verification of hypothesis refers to the capacity of relationship (4) to lead to an approximately normal variable Y_j and then, through (5), to an approximately standard normal variable Z. Besides graphical evidence of linear trend of $z_1, z_2, \ldots, z_N$ values on normalized plot, statistical tests can be effected about skewness and kurtosis coefficients. As previously stated, under hypothesis of normal process the sample skewness coefficient:

$$g_{1,Z} = \frac{1}{N} \sum_{n=1}^{N} \left(\frac{z_n - m_Z}{s_Z} \right)^3 \tag{14}$$

where:

$$m_Z = \frac{1}{N} \sum_{n=1}^{N} z_n \qquad\qquad s_z = \sqrt{\frac{1}{N} \sum_{n=1}^{N} z_n^2 - m_Z^2}$$

for large N values, can be considered normally distributed with zero mean and variance equal to $[6N(N-1)]/[(N-2)(N+1)(N+3)]$. Confidence interval, with significance level α, is:

$$\left[-x_{1-\alpha/2}\sqrt{\frac{6N(N-1)}{(N-2)(N+1)(N+3)}}; x_{1-\alpha/2}\sqrt{\frac{6N(N-1)}{(N-2)(N+1)(N+3)}} \right] \tag{15}$$

Hypothesis of normal process for $\{Z\}$ cannot be rejected if $g_{1,Z}$ value is in between bounds of confidence interval. More difficult is the identification of confidence interval for sample kurtosis coefficient:

$$g_{2,Z} = \frac{1}{N}\sum_{n=1}^{N}\left(\frac{z_n - m_Z}{s_Z} \right)^4 \tag{16}$$

that is characterised by a probabilistic distribution not simple to derive and use, though variance can be easily obtained (*Kendall and Stuart*, 1973). Nevertheless, since Z is an approximately standard normal variable, confidence intervals can be evaluated through Monte Carlo techniques.

2.4 Use of the model

The modelling of monthly-averaged rainfalls can allow to assess the existence of statistically significant variations in pluviometric features of the basin. With this aim, let $\overline{h}'_{i,j}$ be the observations of the process $\{\overline{H}_{i,j}\}$ for a period of N'_a years, for which the shift of rainfalls from the previously modelled stationary model has to be verified. Based on $\overline{h}'_{i,j}$ values, the series $z'_1, z'_2,...,z'_{N'}$, with $N' = 12N'_a$, and the corresponding ranked sample $z'_{(1)}, z'_{(2)},...,z'_{(N')}$ can be evaluated through relationships (4) and (5).

Each of these values can be interpreted as a realization of the order statistics of Z, so it can be evaluated if they belong or not to the confidence intervals with significance level α. Since Z variable follows a standard normal distribution, lower and upper bounds of confidence intervals of order statistics $z'_{(n'),\alpha/2}, n' = 1,2,...N'$ and $z'_{(n'),1-\alpha/2}, n' = 1,2,...N'$ can be evaluated by resolving equations:

$$\frac{\alpha}{2} = I\left[\Phi\left(z'_{(n'),\alpha/2} \right); n', N' - n' + 1 \right] \qquad 1 - \frac{\alpha}{2} = I\left[\Phi\left(z'_{(n'),1-\alpha/2} \right); n', N' - n' + 1 \right] \tag{17}$$

where $\Phi(x)$ is the standard normal density function and $I(x;a,b)$ is the standard incomplete beta function.

A different verification can be based on the comparison of sample $z'_1, z'_2,...,z'_{N'}$ with an analogous control sample $z''_1, z''_2,...,z''_{N''}$, related to a period of $N''_a = N''/12$ years, within the temporal period for which the process $\{\overline{H}_{i,j}\}$ is considered stationary. In this case, by means of a jackknife approach, data referred to the control period sample $z''_1, z''_2,...,z''_{N''}$ are excluded from data used for calibration of model of monthly-averaged rainfalls.

The two-sample Kolmogorov-Smirnov test can be used to verify if samples $z'_1, z'_2,...,z'_{N'}$ and $z''_1, z''_2,...,z''_{N''}$ belong to the same world. To this aim, let's define the maximum difference between the step functions $\varphi'_{N'}(z)$ and $\varphi''_{N''}(z)$ of the two samples:

$$D_{N',N''} = \sup_z \left| \varphi'_{N'}(z) - \varphi''_{N''}(z) \right| \tag{18}$$

where:

$$\varphi'_{N'} = \begin{cases} 0 & \text{for} \quad z < z'_{(1)} \\ n'/N' & \text{for} \quad z'_{(n')} \leq z < z'_{(n'+1)} \\ 1 & \text{for} \quad z \geq z'_{(N')} \end{cases} \qquad \varphi''_{N''} = \begin{cases} 0 & \text{for} \quad z < z''_{(1)} \\ n''/N'' & \text{for} \quad z''_{(n'')} \leq z < z''_{(n''+1)} \\ 1 & \text{for} \quad z \geq z''_{(N'')} \end{cases}$$

The hypothesis that the two samples belong to the same world, with significance level α, has to be rejected if $D_{N',N''}/\sqrt{1/N'+1/N''}$ is greater that critical value $\delta_{1-\alpha}$ obtained by resolving the equation:

$$1 - \alpha = \frac{2\pi}{\delta_{1-\alpha}} \sum_{k=1}^{\infty} \exp\left[-\frac{1}{2}\left(\frac{(2k-1)\pi}{2\delta_{1-\alpha}} \right)^2 \right] \tag{19}$$

valid for great enough values of N' and N''.

3. RESULTS FROM APPLICATION ON CRATI BASIN

3.1 Features of the Crati basin

The drainage basin of Crati River is the largest basin of Calabria region (Southern Italy), with an area of about 2448 km². Climatic features of the basin are due both to the atmospheric perturbations mainly coming from the Atlantic Ocean and to temperate air masses coming from the sub-Sahara region due to the expansion of the Azores High anticyclone. Pluviometric features are constrained by the particular orography of the basin, bounded at north by the Pollino Mountains, at west by the Coastal Chain and at south-east by the Sila Plateau. The Crati River tends towards the north, flowing down to the Ionian Sea in a north-eastern direction. A set of 33 rain gauges are placed within the basin, though further 37 rain gauges positioned in neighbouring rivers have been taken into account (Figure 1). Most of the available daily rainfall series have 50÷70 years of data. The mean number of active rain gauges, for each decades of the considered time series, is shown in Table 1.
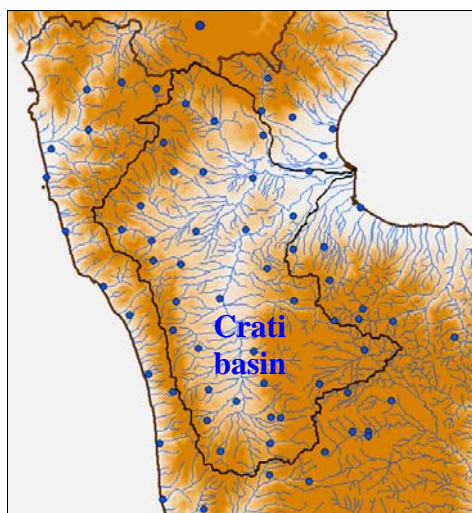
Decade	Mean number of active rain gauges
1921-1930	41,2
1931-1940	35,2
1941-1950	4,9
1951-1960	49,2
1961-1970	62,3
1971-1980	59,5
1981-1990	51,0
1991-2000	44,6

Figure 1. Rain gauges used in the analysis.   **Table 1.** Mean number of rain gauges per decade.

The values of monthly-averaged rainfalls for Crati basin have been obtained from at-site monthly rainfalls through the spline procedure described in section 2.1 (*Sirangelo and*

Ferrari, 2003). Actual observation period is formed only by 1921-1930, 1931-1940, 1951-1960, 1961-1970, 1971-1980, 1981-1990 and 1991-2000 decades, since 1941-1950 decade has not been used for the short number of contemporary active rain gauges. With reference to summer months and for small areas of the basin, $h_{i,j}(x,y)$ function shows negative values that have been substituted by null values. The values of monthly-averaged rainfalls over the whole basin $\overline{h}_{i,j}$, obtained by spline integration, have been compared to those obtained through Voronoy-Thiessen polygon method. Observed differences are generally limited to some unit percent, with maximum value slightly greater than 10%.

3.2 Calibration of the model

The parameter values estimated by modelling the monthly-averaged precipitations over the Crati basin are shown in Table 2. The estimations have been evaluated by using monthly rainfall heights observed in the 5 decades 1921-1930, 1931-1940, 1951-1960, 1961-1970 and 1971-1980, for a total of N=600 values and $N_{a,j}$=50 values. As previously stated, rainfall data recorded in 1981-1990 and 1991-2000 decades have not been used for model calibration, thus allowing for the verification of the non-stationarity of the rainfalls observed in these last decades compared to the rainfalls observed in the previous ones. Figures 2 and 3 show the estimated functions $\widetilde{\mu}_{Y_j}$ and $\widetilde{\upsilon}_{Y_j}$ and the corresponding confidence intervals for the significance level α=0.05. For both the mean and the coefficient of variation, two harmonics seem to be sufficient for a good interpolation.

Transformed exponent			$\lambda = 1/2$			
Mean	$n_a^{(\mu)}$	$a_0^{(\mu)}$	$a_1^{(\mu)}$	$b_1^{(\mu)}$	$a_2^{(\mu)}$	$b_2^{(\mu)}$
	2	18,00	4,08	1,74	0,02	-1,04
Coefficient of variation	$n_a^{(\upsilon)}$	$a_0^{(\upsilon)}$	$a_1^{(\upsilon)}$	$b_1^{(\upsilon)}$	$a_2^{(\upsilon)}$	$b_2^{(\upsilon)}$
	2	0,694	-0,116	-0,075	0,033	0,087

Table 2. Estimation of parameter values of finite expansions of Fourier series for monthly-averaged mean areal rainfalls of Crati basin.
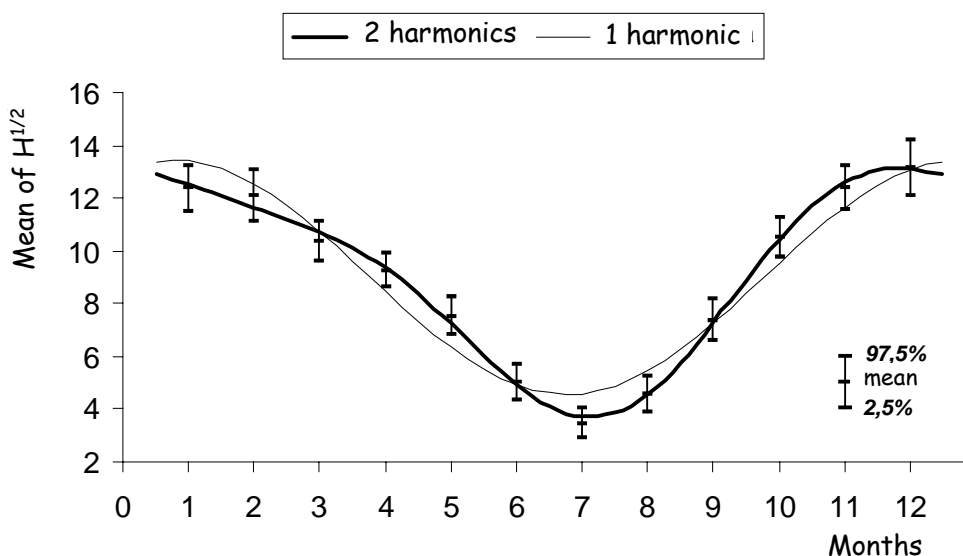
Figure 2. Monthly mean μ_{Y_j} interpolated by finite expansions of Fourier series.
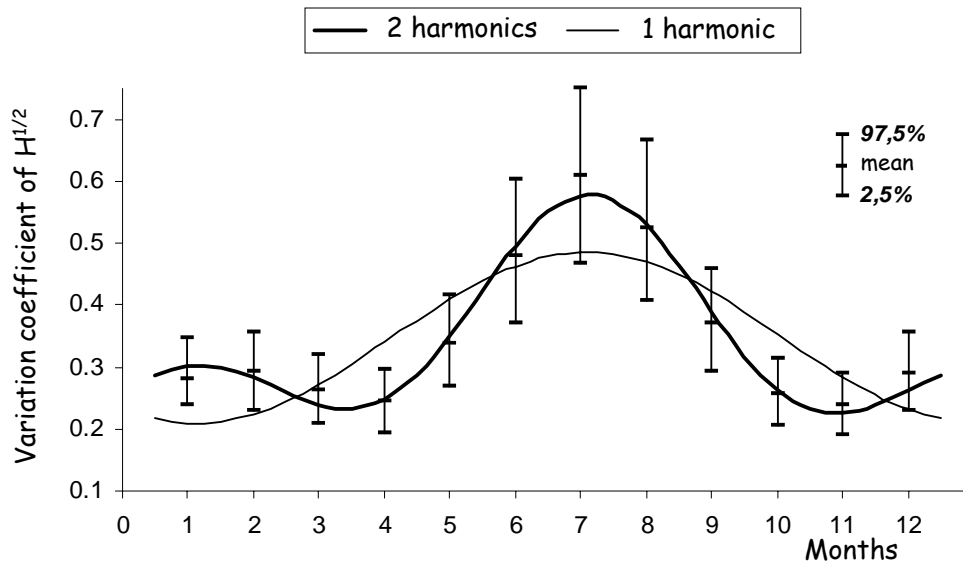
Figure 3. Monthly coefficient of variation υ_{Y_j} interpolated by finite expansions of Fourier series.

3.3 Verification of the model

The power transformation and the removal of the periodicity from monthly-averaged mean areal rainfalls provide a process {Z} for which cannot be rejected the hypothesis of absence of correlation, as shown from the Anderson test with significance level α=0.05 (Figure 4).

Moreover, standard variable Z seems to be normally distributed, since tests on both skewness and kurtosis coefficients show sample values $g_{1,Z}$=−0.051 and $g_{2,Z}$=2.74 that belong to confidence intervals, equal to $[-0,196; +0,196]$ and $[2,65; 3,42]$ respectively, for the significance level α=0.05. The normal probabilistic plot of N=600 sample values of Z is shown in Figure 5.
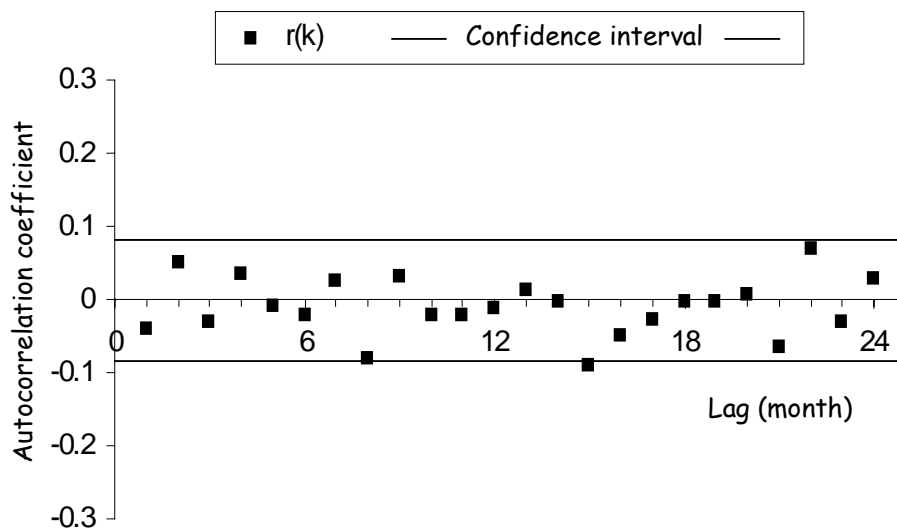
Figure 4. The Anderson test for serial correlation of monthly-averaged mean areal rainfalls with significance level α=0.05.

156
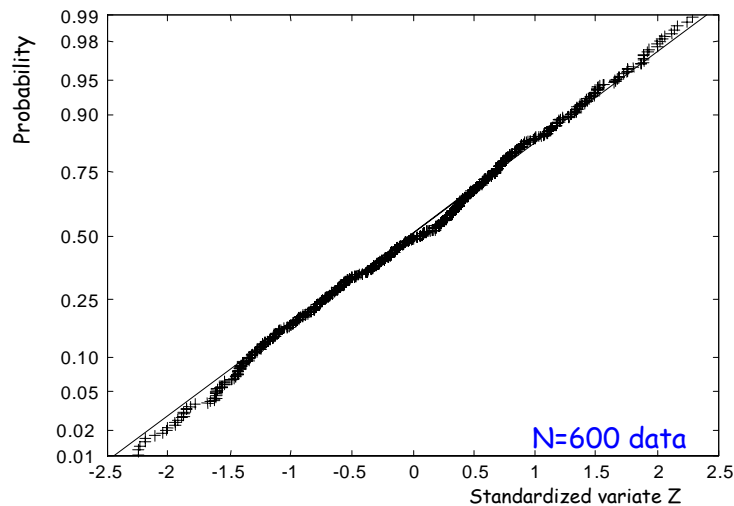
Figure 5. Sample values of standard variable Z in normal probabilistic plot.

3.4 Analysis of 1981-1990 and 1991-2000 decades

The verification of possible existence of statistically significant variations in pluviometric features of Crati basin has been effected with reference to 1981-1990 and 1991-2000 decades, whose values have been excluded from the calibration procedure of the partial Fourier series model.

For both 1981-1990 and 1991-2000 decades, the sample $z'_{(1)}, z'_{(2)}, ..., z'_{(N')}$ with $N'=120$ have been evaluated and compared with the confidence intervals of the corresponding order statistics of Z variable, computed for the significance level $\alpha=0.05$. As can be seen from Figure 6, for both decades the most part of the data show a high departure from confidence intervals, thus pointing out non-stationarity features of monthly-averaged mean areal rainfalls of the Crati basin.

The presence of observed values of Z variable notably lesser than the lower bounds of confidence intervals allows to assess the statistical significance of rainfall reduction during the last two temporal decades on Crati basin. Just as a comparison, values of Z variable $z'_{(1)}, z'_{(2)}, ..., z'_{(N')}$ for 1971-1980 decade, also used for model calibration, are all inside the confidence limits, as clearly visible in Figure 6.

Assessment on the existence of statistically significant variation in pluviometric features of Crati basin for 1981-1990 and 1991-2000 decades also arises from the repeated application of the two-sample Kolmogorov-Smirnov test, as described in section 2.4.

The sample values of the statistic $D_{N',N''}$ have been compared to critical value $D_{N',N''}=0.175$ for each paired samples $z'_1, z'_2, ..., z'_{N'}$ and $z''_1, z''_2, ..., z''_{N''}$ (with dimension $N'=N''=120$) corresponding to two different decades (Table 3). Data values of 1981-1990 and 1991-2000 decades have been always kept out from data set needed for calibration of the partial Fourier series model.

The results confirm that values observed in 1981-1990 and 1991-2000 decades cannot be considered as belonging to the same statistical world of the remaining decades. A very few exceptions appear from the comparisons between 1981-1990 and 1921-1930 and between 1981-1990 and 1971-1980, nevertheless in these cases the values of $D_{N',N''}$ are very near to the critical ones.
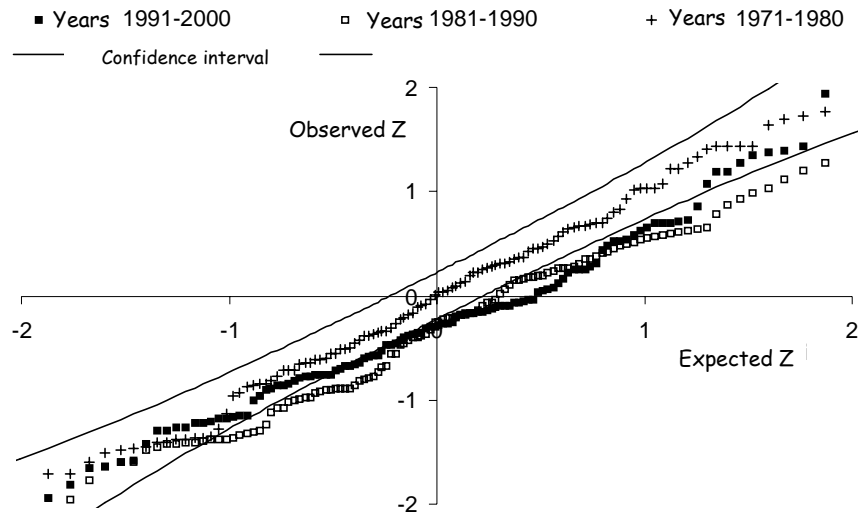
Figure 6. Comparison among the sample values $z'_{(1)}, z'_{(2)}, \ldots, z'_{(N')}$ of 1981-1990 and 1991-2000 decades and the confidence intervals of Z variable for the significance level $\alpha = 0.05$.

Decade	Statistic $D_{N',N''}$ (critical value = 0.175)						
	1991-2000	1981-1990	1971-1980	1961-1970	1951-1960	1931-1940	1921-1930
1991-2000	-----	0.133	0.192	0.250	0.242	0.225	0.183
1981-1990	no reject.	-----	0.167	0.192	0.242	0.200	0.142
1971-1980	rejection	no reject.	-----	0.092	0.125	0.067	0.092
1961-1970	rejection	rejection	no reject.	-----	0.142	0.092	0.133
1951-1960	rejection	rejection	no reject.	no reject.	-----	0.100	0.158
1931-1940	rejection	rejection	no reject.	no reject.	no reject.	-----	0.117
1921-1930	rejection	no reject.	no reject.	no reject.	no reject.	no reject.	-----

Table 3. Results from the two-sample Kolmogorov-Smirnov test (significance level $\alpha = 0.05$).

4. CONCLUSIONS

Statistical analysis of monthly-averaged mean areal rainfalls of Crati basin (Italy) has been performed through an interpolation technique using finite expansions of Fourier series. Results obtained from residual analysis, based on some classical parametric and non-parametric tests, such as the two-sample Kolmogorov-Smirnov test, have shown that the clear reduction in rainfall amounts observed in 1981-1990 and 1991-2000 decades cannot be due only to sampling variability.

More precisely, results obtained from the application of the tests have proved that the variation observed in monthly rainfalls can be considered a statistically significant non-stationary feature of the rainfall phenomena, confirming what seems to be a characteristic feature of the climatic behaviour of many Mediterranean countries in the last years. If confirmed in the future, these results will bring important implications to engineering problems of water resources supply and management.

A further development of the analysis accomplished in this work will cope with the verification of the presence of non-stationary features in shorter time aggregation rainfalls exceeding prefixed thresholds values.

REFERENCES

Box, G.E.P., and D.R. Cox (1964), Analysis of transformation, *J. Royal Stat. Society, B, 26*, 211-243.

Burn, D.H., and M.A. Hag Elnur (2002), Detection of hydrologic trends and variability, *J. Hydrol., 255*, 107-122.

Chin, D.A. (1995), A Scale Model of Multivariate Rainfall Time Series, *J. Hydrol., 168*, 1-15.

Cressie, N.A.C. (1991), *Statistics for Spatial Data*, Wiley, New York, N.Y., USA.

Hirsch, R.M., D.R. Helsel, T.A. Cohn, and E.J. Gilroy (1992), Statistical analysis of hydrologic data, in *Handbook of Hydrology*, D.R. Maidment (Editor in Chief), Chapter 17, McGraw-Hill, pp.55.

IPCC (2001), *Climate Change 2001. Impacts, Adaptation and Vulnerability*, Cambridge University Press.

Kendall, M.G., and A. Stuart (1973), *The Advanced Theory of Statistics*, Griffin, London, U.K.

Sirangelo, B., and E. Ferrari (2003), Una verifica statistica della presenza di variazioni nella pluviometria recente relativa ad un bacino dell'Italia meridionale, in Atti del Convegno: La difesa idraulica del territorio, Trieste (Italy), 583-594 *(in Italian)*.

WMO (2000), *Detecting trend and other changes in hydrological data*, Z.W. Kundzewicz and A. Robson (Editors), TD-No.1013.

Yu, Z.W. (2001), Surface interpolation from irregularly distributed points using surface splines, with Fortran program, *Computer & Geosciences, 27*, 877-882.

MODELISATION DU REGIME DE CRUES DES BASSINS VERSANTS: APPLICATION ET UTILITE DES HYDROGRAMMES SYNTHETIQUES MONO–FREQUENCE HSMF

A. Yahiaoui[1], B. Touaibia[2]

(1) Département d'Hydraulique, Centre Universitaire de Bechar, Algérie
(2) Laboratoire d'Hydrologie, Ecole Nationale Supérieure de l'Hydraulique, Blida, Algérie

ABSTRACT

La modélisation du régime de crues d'un bassin versant est très importante en matière d'étude et d'estimation des débits de crues rares et extrêmes. Elle permet d'étudier le phénomène des inondations d'une zone à risque à partir des hydrogrammes synthétiques préalablement établis. En effet, l'Hydrogramme Synthétique Mono–Fréquence (HSMF) est un des outils de synthèse des régimes de crues des bassins versants déterminés après modélisation de la relation Débit–durée–Fréquences (QdF) développée au Cemagref de Lyon selon une approche multi–durées et multi–fréquences des crues observées. QdF est un modèle continue de prédétermination des crues fréquentes à rares d'un bassin versant (observé ou non), qui permet de répondre à une conception de gestion intégrée des cours d'eau et de leurs bassins versants. L'utilité de la méthodologie QdF réside d'une part à la modélisation du régime de crue d'un bassin versant et d'autre part à la détermination des Hydrogrammes Synthétiques Mono–Fréquence et leurs utilités en matière de détermination de l'aléa. L'application de cette méthodologie de modélisation sur le bassin versant de l'Oued Mekkera zone à risque vis-à-vis des inondations, permet de mieux connaître la nature du régime de crue en vue de prendre des mesures de préventions nécessaires contre ces inondations.

1. INTRODUCTION

Les recherches menées ces dernières années au Cemagref de Lyon, autour de la modélisation régionale, ont permis d'aboutir à la mise au point de modèles synthétiques QdF (Débit–durée–Fréquence) et par la suite les hydrogrammes synthétiques mono – fréquence (HSMF) qui permettent une représentation du régime de crue d'un bassin versant. Les origines de cette modélisation ont été présentées par *Oberlin et al.* (1989).

Une constatation générale (*Prudhomme,* 1995) est que les recherches en hydrologie montrent peu de modèles synthétiques régionaux traitant des débits seuils ou débits moyens suivant une approche multi–durées et multi–fréquences des crues. La modélisation QdF a été établie à partir des observations des pluies et des débits d'un bassin versant particulièrement choisi et représentatif d'une typologie des régimes d'écoulements, ce qui lui confère une large représentativité spatiale. Les variables hydrologiques des modèles QdF sont nécessaires pour que leurs définitions et leurs choix puisent être mieux perçus, de les présenter parmi l'ensemble des variables hydrologiques du régime de crue d'un bassin versant.

Lors de l'étude des régimes de crues des bassins versants, il est nécessaire, pour la bonne compréhension des développements ultérieurs, de prêter une attention particulière

à la notion de la "durée" qui intervient dans un bon nombre de concepts hydrologiques concernant en particulier la définition et le choix des variables hydrologiques, la caractérisation de l'écoulement d'un bassin versant, la demande sociale en matière de besoins, de risques de dégâts, etc., toutes choses étroitement liées aux événements hydrologiques temporels (*Galéa et al.,* 1997).

2. VARIABLES HYDROLOGIQUES

L'enregistrement limnigraphique associé aux courbes de tarage, permet d'obtenir un hydrogramme continu Q(t) (Figure 1).
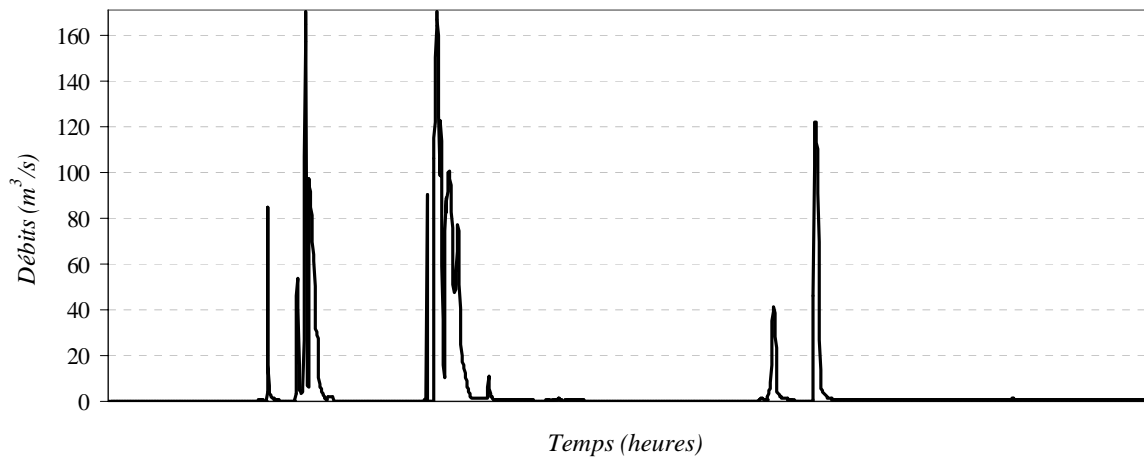
Figure 1. Chronique annuelle des débits de 1996/97 (station de Sidi Bel Abbès).

Pour chaque année, cette information doit être synthétisée par des variables hydrologiques représentatives de la variabilité temporelle du régime hydrologique du bassin versant. Deux variables hydrologiques caractérisent le régime hydrologique d'un bassin versant pouvant être obtenus directement à partir de la chronique Q(t) à savoir:
- Le débit moyen (volume) VCd: l'intégration de la chronique Q(t) sur une durée continue d permet d'obtenir le volume d'eau écoulé pendant cette durée (Figure 2). La quantité obtenue est un débit caractéristique (Volume) sur une durée fixe d. Ces débits sont très utilisés en hautes et moyennes eaux, un peu moins en basses eaux.
- Le débit seuil QCd: cette variable correspond à une notion de débit qui est toujours dépassé ou non dépassé pendant une durée d (Figure 2).

Les débits caractéristiques de périodes continues d'écoulement peuvent être échantillonnées à partir d'une chronique de débit Q(t) continue journalière (débit moyen journalier). La technique d'échantillonnage à partir de la chronique Q(t) des VCd et des QCd relatifs à une année donnée (Figure 2) procède au balayage de tout l'hydrogramme Q(t). Ce balayage, obtenu grâce au déplacement d'un intervalle mobile de durée d d'une fraction de temps ε choisie égale à un jour permet de déterminer (365-d) valeurs en VCd et QCd (Figure 3).

La portion de courbe Q(t) correspondant à chaque période fournit un débit seuil QCd minimum (dépassé) et un seuil maximum (non dépassé) ainsi que le débit moyenne VCd résultant pratiquement de son intégration ou de la moyenne des débits qui existent dans l'intervalle de durée d.

Le classement des débits QCd et VCd pour une période donnée permet d'obtenir deux autres caractéristiques QCXd et VCXd, qui sont respectivement, le débit (Q) seuil Caractéristique continûment dépassé ou non dépassé sur la durée d maXimal dans l'année et débit moyen (Volume) Caractéristiques sur la durée d, maXimal dans l'année.
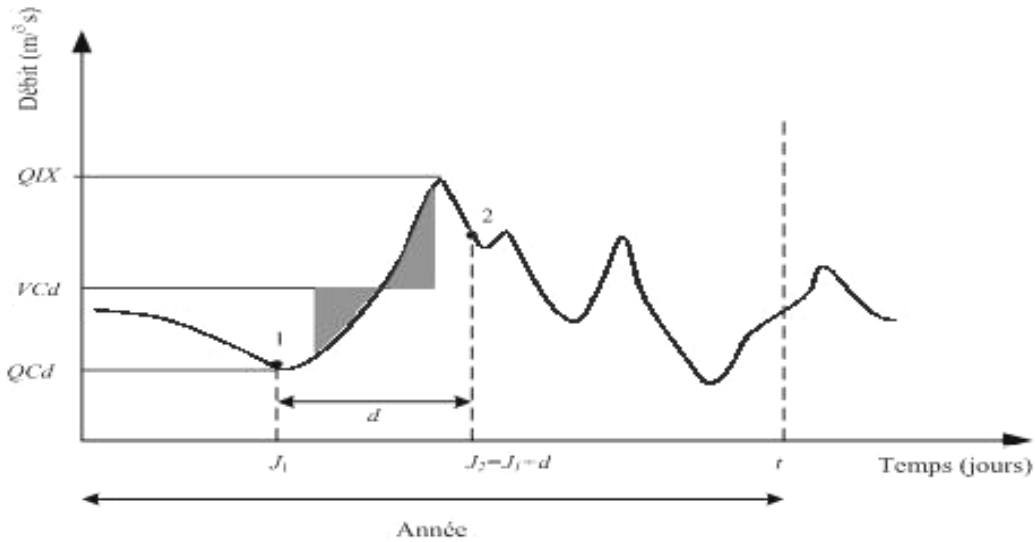

Figure 2. Détermination des caractéristiques du régime d'écoulement VCd et QCd.
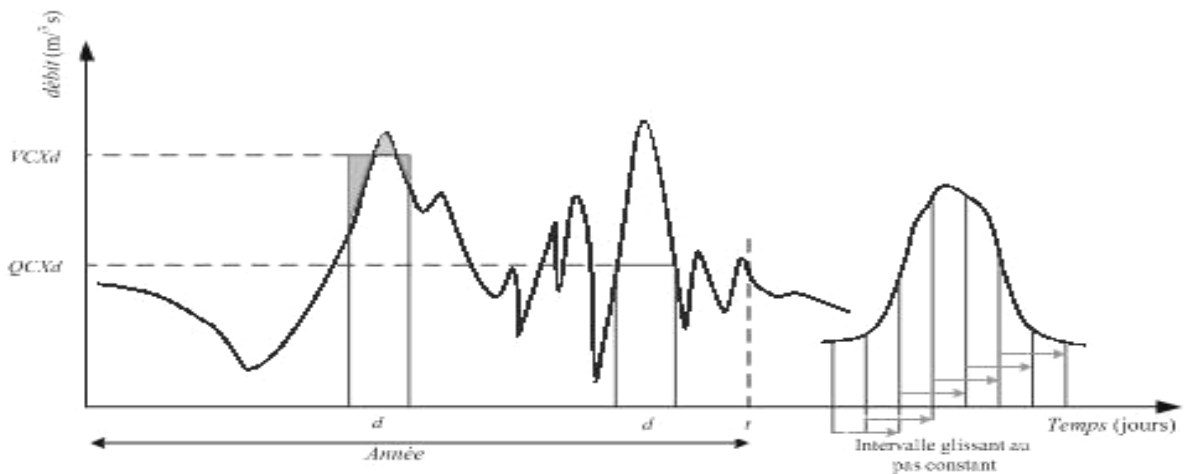

Figure 3. Définition des caractéristiques du régime de crue d'un bassin versant VCXd et QCXd.

3. MODELISATION HYDROLOGIQUE

L'analyse statistique montre qu'il est possible, à partir d'un échantillonnage multi–durées de chroniques hydrométriques supposées stationnaires, de décrire les caractéristiques de crue du bassin versant étudié en Débit–durée–Fréquence (*Gilard,* 1998*; Gilard et Gendreau,* 1998). La série des débits relative à la durée d suivent une fonction croissante de la période de retour T, et pour une période de retour donnée, les débits suivent une fonction décroissante de la durée.

Les travaux menés sur la base des concepts de la méthode de Gradex (*Guillont et Duband,* 1967*; CFGB,* 1994) et des méthodes dérivées tel que le modèle AGREGEE (*Margoum,* 1992*; Margoum et al.,* 1994*; Lang,* 1997) montrent que cette description en

Débit–durée–Fréquence peut être étendue en extrapolation aux périodes de retour rares et extrêmes tout en conservant la régularité des dépendances (*Galéa et al.,* 1997).

Les travaux de synthèse sont réalisés sur la description de l'hydrogramme synthétique mono-fréquence HSMF d'une station hydrométrique à partir de trois paramètres caractéristiques du bassin versant à savoir:

- Le débit (Q) Instantané maXimum Annuel décennal (10) QIXA10.
- La durée caractéristique de la crue de bassin versant D.
- Le temps de montée caractéristique de la crue du bassin versant t_m.

4. DETERMINATION DES CARACTERISTIQUES DU BASSIN VERSANT

La détermination des caractéristiques nécessite désormais, les crues et les chroniques de débits moyens journaliers enregistrées à une station hydrométrique ou à l'exutoire du bassin versant. En plus des données hydrométriques, les données pluviométriques sont présentées sous forme de précipitations maximales annuelles moyennes.

Le bassin versant ainsi considéré est celui de l'Oued Mekerra (Figure 4) situé dans le nord ouest algérien, de superficie de 3000 km^2. Son cours d'eau principal est de 125 km de long avec une pente de 5.5 %. Le bassin versant a une forme allongée d'orientation sud nord. La station hydrométrique de Sidi-Bel-Abbès (Code 110301) se situe à l'exutoire du bassin dont leurs données hydrométriques sont utilisées à l'analyse du régime de crues du bassin versant.
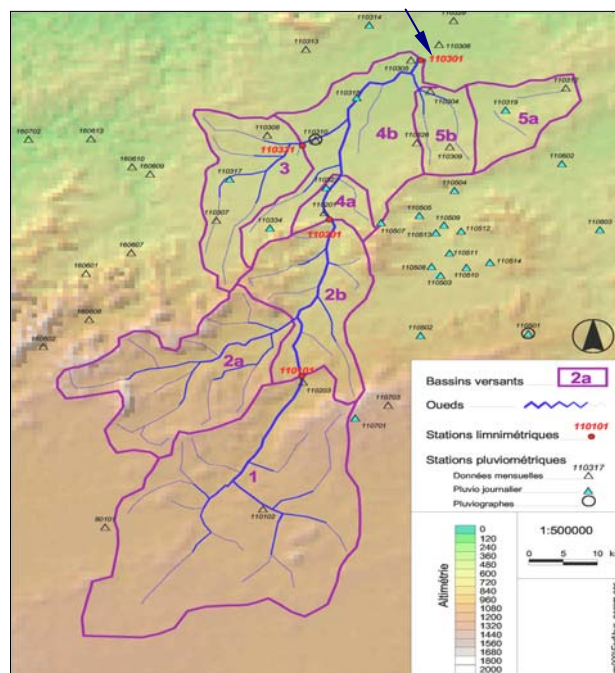
Figure 4. Bassin versant de l'Oued Mekerra et station hydrométrique de Sidi-Bel-Abbes.

4.1 Estimation de QIXA10

Le débit QIXA10 est estimé après l'ajustement de la série des débits moyens maxima journaliers annuels QIX à une loi de type exponentielle simple à deux paramètres (position et échelle) (Figure 5).

L'adéquation de loi à été faite par trois tests à savoir:

- le test de coefficient de corrélation PPC (Probability Plot Correlation),
- le test de RMSD (Root Mean Square Deviation),
- le test de KS (Kolmogorov – Smirnov).

QIXA10 est le débit décennal obtenu directement de la droite d'ajustement pour une période de retour T=10 ans (1-F_{exp}=0.1), qui vaut dans le cas du bassin versant de l'Oued Mekerra:

$$QIXA10 = 110 \, m^3 / s$$
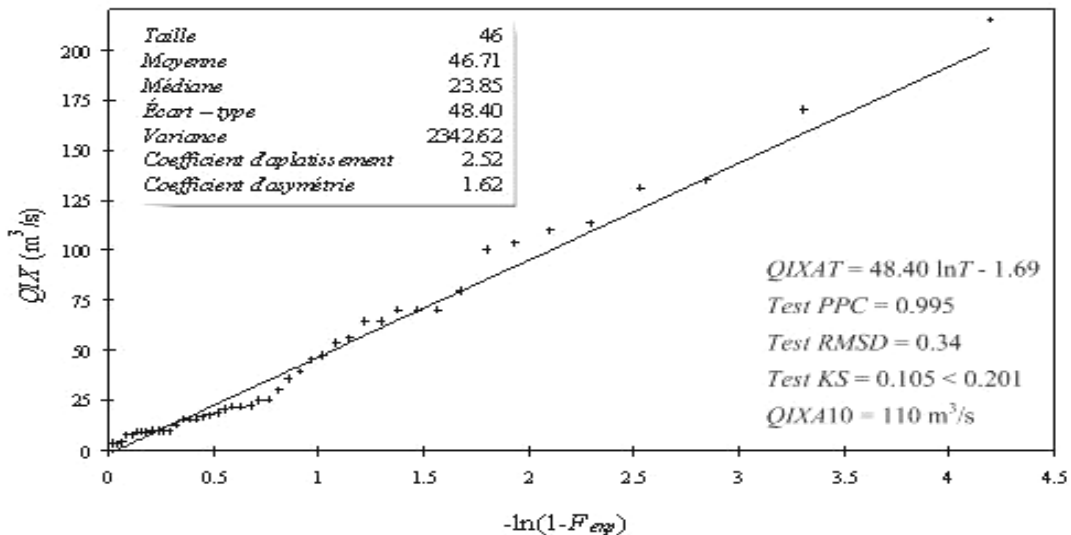
Figure 5. Caractéristiques et ajustement de la série des *QIX* à une loi exponentielle.

4.2 Durée caractéristique de la crue D

Par définition, la durée caractéristique de la crue d'un bassin versant, c'est-à-dire la durée pendant laquelle la moitie du débit de pointe est continûment dépassé (Figure 6).

Pour chaque crue i observée, les caractéristiques Qs_i, ds_i et t_{mi} doivent être déterminé suivant la procédure décrite dans la Figure 6. Traçons dans le plan (Qs; ds) l'ensemble des points observés ainsi que leurs courbe médiane conditionnelle (Figure 7).
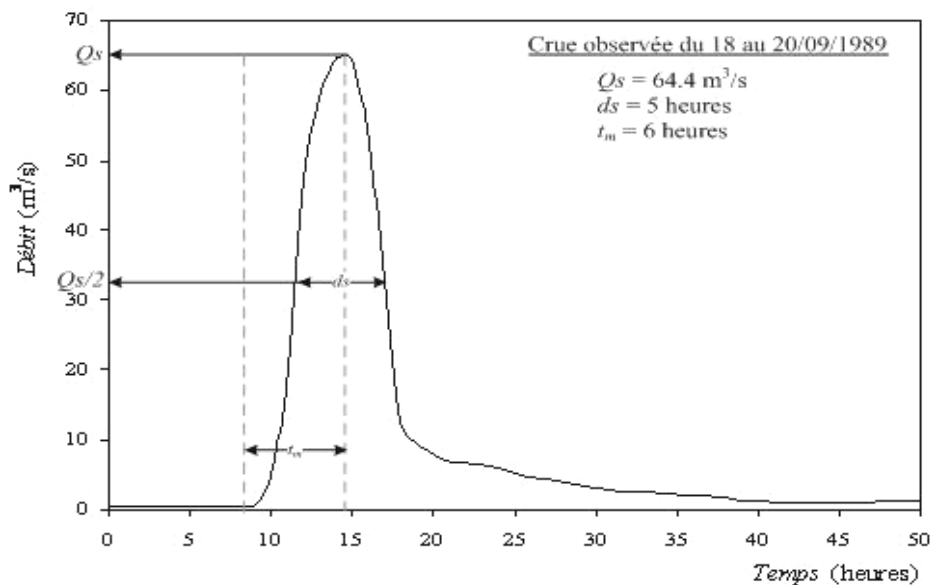
Figure 6. Caractéristiques et ajustement de la série des QIX à une loi exponentielle.

L'allure de la médiane conditionnelle traduit la variation moyenne du temps ds en fonction de la variation moyenne des débits de pointe Qs des crues du bassin versant, par conséquent la durée caractéristique D de la crue correspond au débit caractéristique QIXA10 (Figure 7), qui vaut dans ce cas D=10 heures.
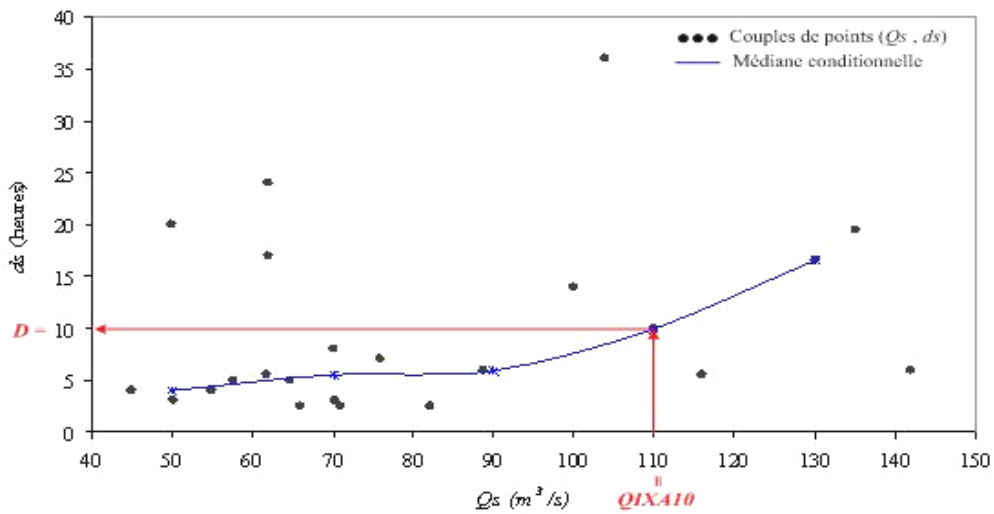
Figure 7. Détermination de la durée D caractéristique de la crue.

4.3 Temps de montée caractéristique de la crue t_m

Avec la même procédure, le temps de montée caractéristique de la crue correspond au débit caractéristique QIXA10 (Figure 8), vaut dans ce cas t_m=13 heures.
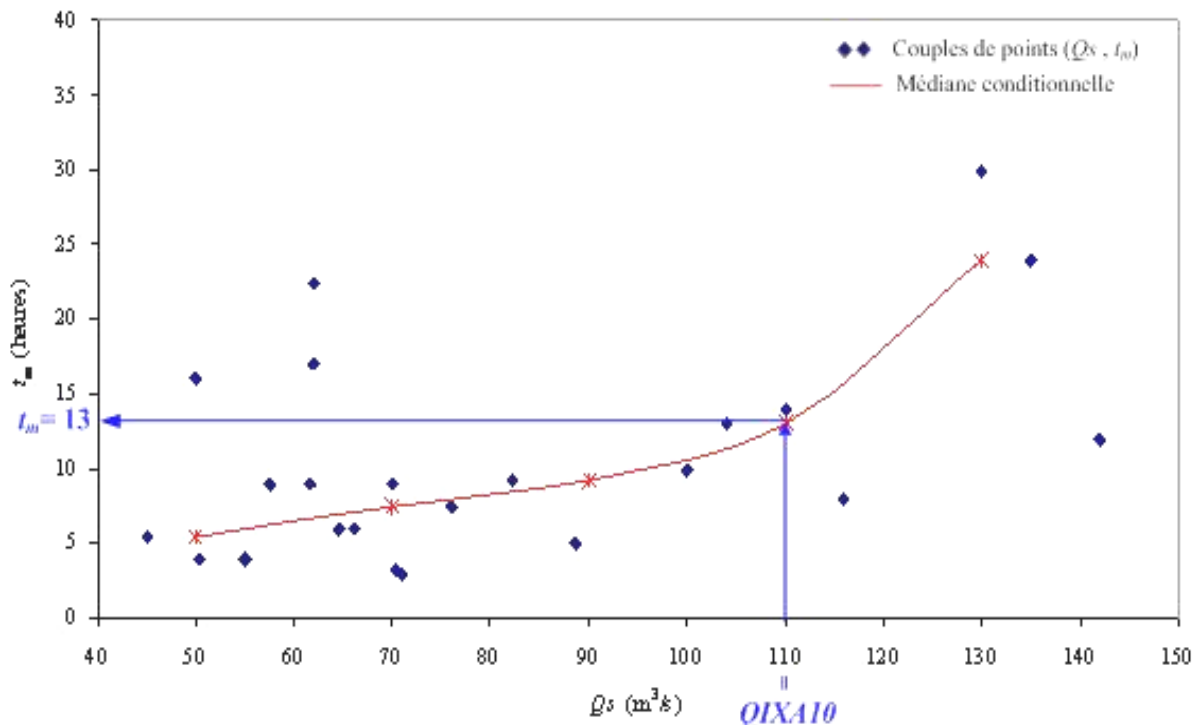
Figure 8. Détermination du temps de montée t_m caractéristique de la crue.

Les caractéristiques QIXA10 et D peuvent être déterminés par des formules empiriques (*CTGREF*, 1980):

$$QIXA10 = R\left(\frac{PJXA10}{80}\right)^2 S^{0.8} \tag{1}$$

$$D = \exp\left(-0.69 + 0.32\ln S + 2.2\sqrt{\frac{P_A}{PJXA10}\frac{1}{t_a}}\right) \tag{2}$$

où:

QIXA10 : en m^3/s P_A : pluie annuelle moyenne (mm)

D : en heures   S : surface du bassin versant (km^2)

R : coefficient régional t_a : température moyenne annuelle (°C)

PJXA10 : pluie journalière décennale (mm)

Une modélisation adimensionnelle rendant compte de la typologie des écoulements, est donnée par l'équation suivante (*Galéa et Prudhomme,* 1993, 1997):

$$\frac{QCXTd}{QIXA10} = \begin{cases} \dfrac{A_q\left(\frac{d}{D}\right)\ln T + B\left(\frac{d}{D}\right)}{QIXA10} & \text{si } 0.5 \leq T \leq 10 \\[2em] \dfrac{QCX(10,d)}{QIXA10} + \dfrac{A_p\left(\frac{d}{D}\right)}{QIXA10}\ln\left(1 + \dfrac{A_q\left(\frac{d}{D}\right)}{A_p\left(\frac{d}{D}\right)}\dfrac{T-10}{10}\right) & \text{si } 10 \leq T \leq 1000 \end{cases} \quad \frac{D}{2} \leq d \leq 5D$$

où :

$$\frac{A_q\left(\frac{d}{D}\right)}{QIXA10} = \left(\frac{1}{x_1\frac{d}{D} + x_2}\right) + x_3 \qquad \frac{B\left(\frac{d}{D}\right)}{QIXA10} = \left(\frac{1}{x_4\frac{d}{D} + x_5}\right) + x_6 \qquad \frac{A_p\left(\frac{d}{D}\right)}{QIXA10} = \left(\frac{1}{x_7\frac{d}{D} + x_8}\right) + x_9$$

A_q et A_p sont respectivement les Gradex des débits et des pluies:

$$A_q = \frac{dQ(T)}{d\ln T} \quad ; \quad A_p = \frac{dP(T)}{d\ln T}$$

La durée d est toujours comprise entre D/2 et 5D c'est-à-dire, elle peut être choisie dans l'intervalle $[5,50]$ heures pour le cas de l'Oued Mekerra.

Le modèle adimensionnel (Vandenesse, Florac ou Soyans) est caractérisé par un jeu de neuf paramètres x_i (Tableau 1), choisis en fonction de critères utilisant des informations pluviométriques (Gradex) et des informations locales en l'occurrence QIXA10 et D (*Galéa et Prudhomme,* 1993).

Type du modèle	x_1	x_2	x_3	x_4	x_5	x_6	x_7	x_8	x_9
Vandenesse	3.970	6.480	0.010	1.910	1.910	0.097	3.674	1.774	0.013
Florac	3.050	3.530	0.000	2.130	2.960	0.010	2.780	1.770	0.040
Soyans	2.570	4.860	0.000	2.100	2.100	0.050	1.490	0.680	0.017

Tableau 1. Paramètres pour les modèles en débit seuil (QCX).

Le modèle de Vandenesse caractérise un régime de crue soutenu sur les fréquences observables. Les événements exceptionnels sont peu différents des événements rares et les crues sont plus volumineuses que pointues.

Le modèle de Florac définit un régime d'écoulement rapide, avec un certain stockage de pluies. Cela conduit à des événements très courants, différents des événements moyens, eux-mêmes très différents des événements rares. Les crues sont pointues, peu volumineuses, mais s'inscrivent dans la durée de restitution du stockage pendant les crues.

Le modèle de Soyans définit un régime d'écoulement rapide, mais avec un très faible stockage sur le bassin versant. Les événements moyens, les crues étant très pointues et peu volumineuses, en général, la durée caractéristique de crues D est relativement faible (*Gilard et Gendreau,* 1998).

5. CHOIX DU MODELE QdF

Pour affiner le choix du modèle QdF, il importe de disposer de critères quantitatifs plus objectifs que les éléments qualitatifs, ces critères reposent sur la comparaison entre les caractéristiques de débit QIXA10 et la durée D du bassin versant étudié et le régime pluviométrique dans lequel il se situe, qui s'analyse simplement pour les Gradex des pluies observées (*Gilard,* 1998). Des études menées sur une tendance de bassins versants dans des contextes hydrologiques différents ont permis de définir des règles de choix des modèles QdF (*Prudhomme,* 1995) deux limites :

$$A_p(d) = \frac{QIXA10}{0.768\dfrac{d}{D} + 2.332} = L_1 \quad \text{(Limite Vandenesse – Florac)}$$

$$A_p(d) = \frac{QIXA10}{0.419\dfrac{d}{D} + 1.580} = L_2 \quad \text{(Limite Florac – Soyans)}$$

Ces limites ont été définies sur la base d'une centaine de couples expérimentaux qui se caractérisent par une certaine dispersion des échantillons analysés. Aussi il convient de travailler sur plusieurs durées différentes pour obtenir le meilleur résultat.

Le Gradex des précipitations en m^3/s pour une durée d est exprimé par:

$$A_p(d) = \frac{G_p S}{3.6d}$$

où: G_p est le Gradex des pluies exprimé en mm d'eau et S est la surface du bassin versant en km^2, le Gradex G_p n'est autre que la pente de la droite d'ajustement de Gumbel de la série des pluies maximales annuelles (Figure 9).

L'ajustement adéquat des pluie à la loi du Gumbel montre que le Gradex des pluie vaut G_p=6.47 mm d'eau, alors pour une durée d égale à 24 heures, le Gradex A_p en m^3/s correspondant et les deux limites L_1 et L_2 des modèles QdF valent respectivement 224.65, 26.35 et 42.54 m^3/s ce qui permet de dire que le bassin versant de l'Oued Mekerra est de type Soyans. Alors l'expression finale du débit QCXT(d) est donc:

$$QCXT(d) = \begin{cases} 110\left[\left(\dfrac{1}{2.570\dfrac{d}{10}+4.860}\right)\ln T + \dfrac{1}{2.100\dfrac{d}{10}+2.100}+0.050\right] & \text{si } \begin{cases} 0.5 \le T \le 10 \\ 5 \le d \le 50 \end{cases}, \\[2em] QCX10(d)+110\left(\dfrac{1}{1.490\dfrac{d}{10}+0.680}+0.017\right)\ln\left(1+\dfrac{\dfrac{1}{2.570\dfrac{d}{10}+4.860}}{\dfrac{1}{1.490\dfrac{d}{10}+0.680}+0.017}\dfrac{T-10}{10}\right) & \text{si } \begin{cases} 10 \le T \le 1000 \\ 5 \le d \le 50 \end{cases}. \end{cases}$$

Connaissant l'expression de débit QCXT(d), il est très facile de tracer les courbes QdF. Dans un plan de coordonnés (durée d; Débit) la courbe $QCXT(d)$ peut être tracée pour une période de retour T fixée (Figure 10).
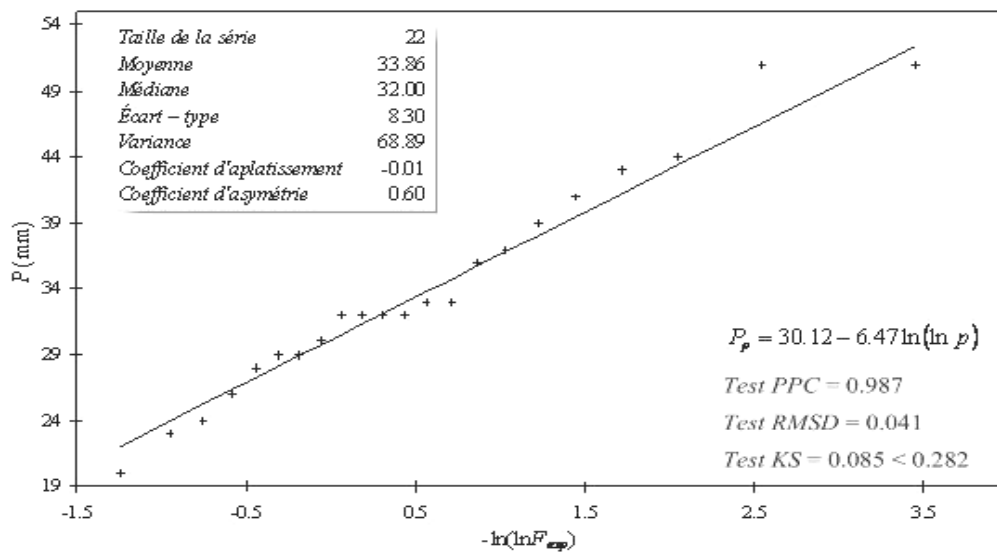
Figure 9. Ajustement des pluies à une loi du Gumbel.
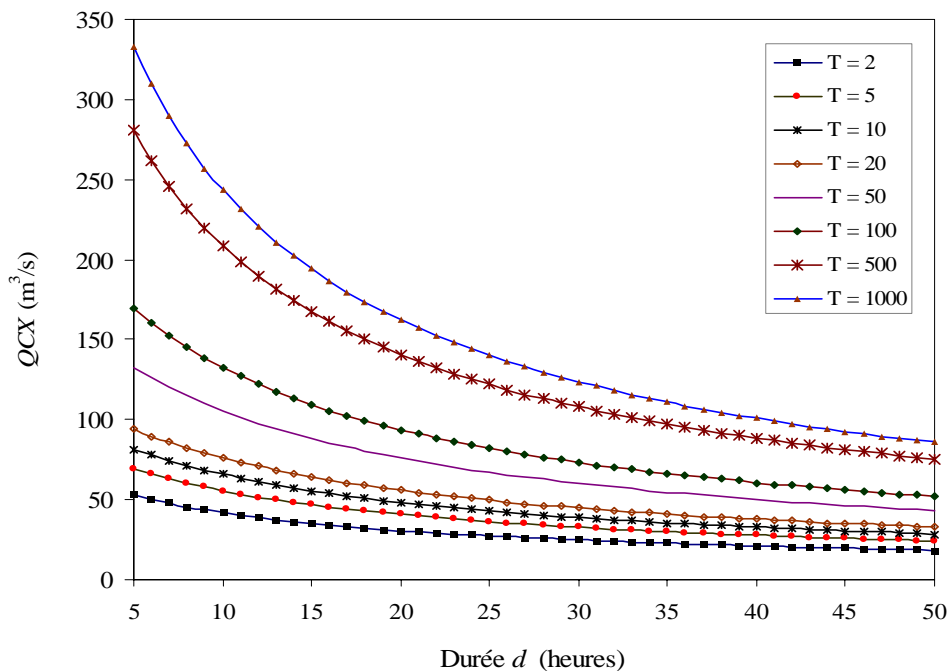
Figure 10. Courbes QdF des débits seuils QCX du bassin versant de l'Oued Mekerra.

6. CONSTRUCTION DES HSMF

Les Hydrogrammes Synthétiques Mono–Fréquence sont construits en faisant une première hypothèse sur le temps de montée des crues (Figure 8) et une hypothèse, qui consiste à assurer une montée linéaire de l'hydrogramme entre un débit de base initiale qui peut être le quantile de débit continûment dépassé pendant une durée de 30 jours pour une période de retour de un an (c'est-à-dire QCX1(720 h) = 6.22 m^3/s), et la pointe de crue ou le débit instantané maximum de la période de retour considérée QIXT (Figure 11).
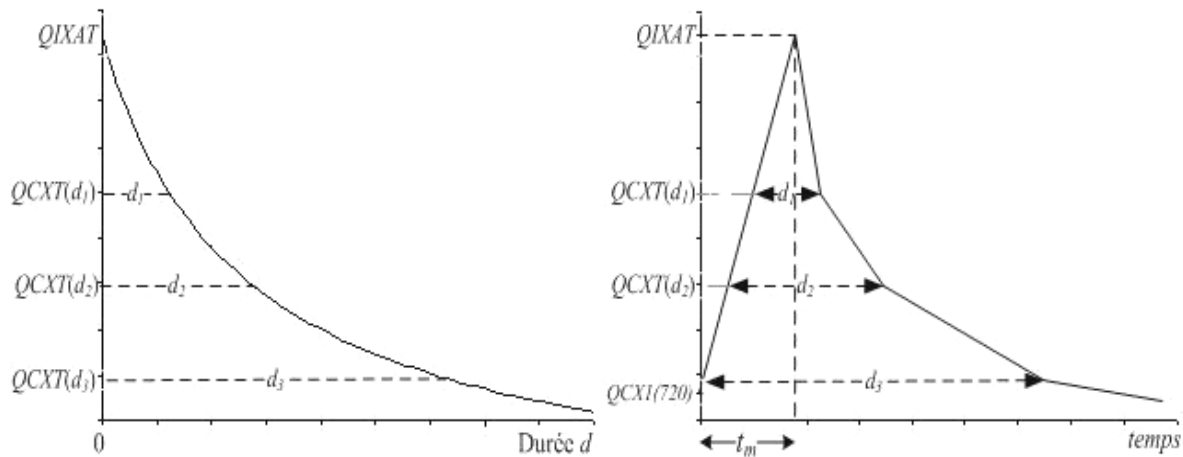
Figure 11. Procédure de construction des Hydrogrammes Synthétique Mono-Fréquence HSMF.

Cette procédure de construction (Figure 11) permet d'avoir les différents hydrogrammes synthétiques mono-fréquence de l'Oued Mekerra (Figure 12).
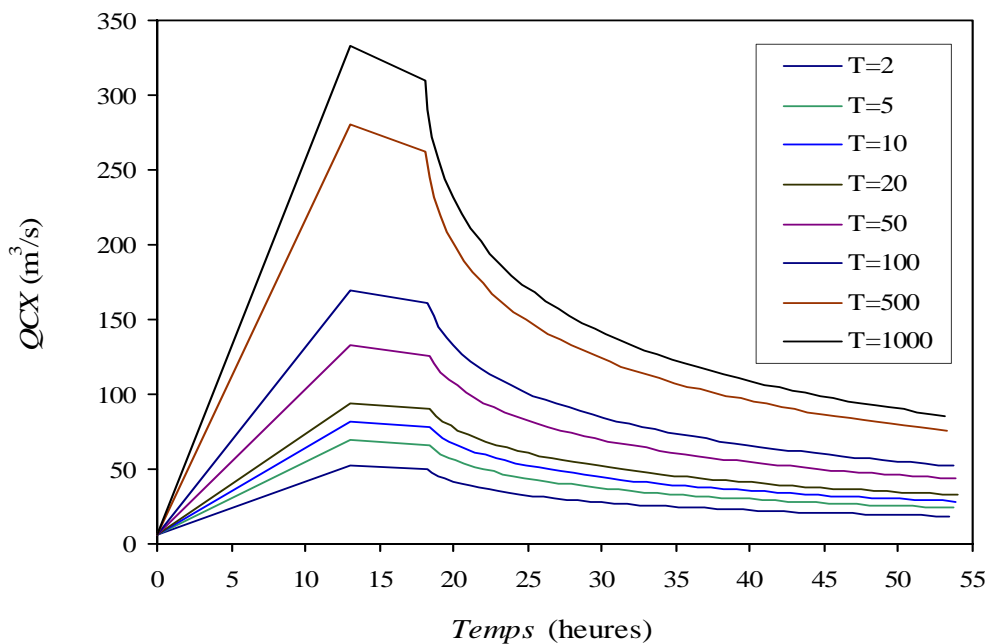
Figure 12. Hydrogrammes Synthétiques Mono-Fréquence du bassin versant de l'Oued Mekerra.

7. APPLICATION ET UTILITE DES HSMF

Les hydrogrammes synthétiques Mono–Fréquence HSMF ne sont pas des hydrogrammes observés qu'ils présentent la caractéristique d'être mono-fréquence, c'est-à-dire que, quelle que soit la durée considérée, le débit continûment dépassé par ces hydrogrammes est le quantile de débit seuil de même fréquence.

Cette propriété assure une cohérence entre ces hydrogrammes et les quantiles de débit moyen correspondant comme l'on mis en évidence les études théoriques réalisées sur ces opérateurs hydrologiques. En conséquence, leur utilisation dans les études d'inondabilité (*Gilard,* 1998) assure la cohérence entre les effets de laminage ou de gestion des volumes étudiés et la quantification des variables synthétiques permettant de définir le risque.

Les événements de crue observés réellement dans les cours d'eau ne peuvent pas être qualifiés en terme de fréquence ou période de retour pour la bonne raison que celle – ci varie suivant la durée sur laquelle on analyse le phénomène observé. Pour cette raison il ne nous semble pas pertinent d'analyser les risques d'inondation sur la base de crues réelles qui peuvent être pessimiste en pointe et optimiste en volume ou inversement.

Les apports au modèle hydraulique vont pouvoir être calculés simplement à partir des modèles QdF. Si l'on travaille en régime permanent, la lecture des débits instantanés maxima obtenus pour différentes périodes de retour donne les débits correspondant aux entrées des modèles hydrodynamiques (type Saint-Venant). Si l'on travaille en régime transitoire, il est nécessaire au préalable de construire des hydrogrammes synthétiques mono–fréquence.

Une autre utilité des hydrogrammes synthétiques mono–fréquence, est sont utilisation dans le laminage des crues dans un but de déterminer la hauteur déversée à travers un évacuateur de crue d'un barrage, car ces hydrogrammes sont aussi une caractéristique hydrométrique du bassin versant.

8. CONCLUSION

L'étude du régime de crues d'un bassin versant est souvent faite par des méthodes qui ne tiennent compte que du débit instantané seulement comme paramètre principal dans l'estimation des crues rares et extrêmes pour telle ou telle période de retour.

Les crues dévastatrices qui sont dues spécialement à des fortes précipitations, conduisent à des inondations catastrophiques (inondation de 10/12/2001 à Alger). Ainsi, il est nécessaire de prendre en compte d'autres facteurs qui permettant d'interpréter la crue comme phénomène exceptionnelle et aléatoire, à savoir: le débit instantané maximal annuel décennal QIXA10, la durée caractéristique D et le temps de montée t_m de la crue qui sont les paramètres de la crue caractéristique du bassin versant, qui traduit le régime de crue d'un bassin versant et à partir desquels, les courbes QdF et par conséquent les hydrogrammes synthétiques mono-fréquences HSMF peuvent être facilement déterminés pour différentes périodes de retour.

L'établissement des hydrogrammes synthétiques mono-fréquence HSMF du bassin versant de l'Oued Mekerra a permis de donner une information très intéressante en matière d'interprétation du régime des crues bassin, en plus, l'aléa d'une inondation peut être déterminé par un modélisation hydrodynamique des équations de Saint-Venant avec la considération du débit entrant est le débit maximum dans l'hydrogramme synthétique mono-fréquence.

REFERENCES

C.F.G.B. (1994), Les crues de projet des barrages: methods du GRADEX; Design flood determination by the Gradex method, 18e Congrès CIGB-ICOLD, *Bulletin du Comité Français des Grands Barrages*, n°2, Nov. 1994, Français–Anglais, 96 p.

C.T.G.R.E.F. (1980), Synthèse nationale sur les crues des petits bassins, Fascicule 2: la méthode SOCOSE, Fascicule 3: la méthode CRUPEDIX, 39 p.

Galéa, G., and C. Prudhomme (1997), Notion de bases et concepts utiles pour la compréhension de la modélisation synthétique des régimes de crues des bassins versants au sens des modèles QdF, *Revue des Sciences de l'Eau*, *1*, 83-101.

Galéa, G., and C. Prudhomme (1993), Characterization of ungauged basins floods behaviour by upstreaming QdF models, 2nd International Conference FRIEND on Flow Regimes from International Experimental and Network Data, Technische Univesität Braunschweig, RFA, *IASH Publication n° 221*, 229-240.

Gilard, O., (1998), *Les bases techniques de la méthode Inondabilité*, Cemagref Edition, 207 p.

Gilard, O., N. Gendreau (1998), Inondabilité: une méthode de prévention raisonnable du risque d'inondation pour une gestion mieux intégrée des bassins versants, *Revue des Sciences de l'Eau*, *3*, 429-444.

Guillont, P., and D. Duband (1967), La méthode du Gradex pour le calcul de la probabilité des crues à partir des pluies, *Journées de SHF*, question 1, rapport 7, Paris.

Lang, M. (1997), New developments with AGREGEE, a statistical modeling hydrometeorological information, in *FRIEND projects H-5-5 and H-1-1, Third report 1994-1997*, edited by Oberlin G. and Desbos E., Cemagref Editions, 181-191.

Margoum, M. (1992), Estimation des crues rares et extrêmes: Le modèle AGREGEE. Conception et premières validations, Thèse de doctorat, Ecole des mines de Paris, Cemagref Lyon, GIS Hydrologie FRIEND-AMHY, 252 p.

Margoum, M., G., Oberlin, M., Lang, and R. Weingartner (1994), Estimation des crues rares et extrêmes: principes du modèle AGREGEE, *Hydrologie Continentale*, Vol. *9*(1), 85-100.

Oberlin, G., H. Ben Mansour, and R. Ortiz (1989), Generalization and standardization for 3 types of flow-duration-frequency curves in flood regime description and transfer, FRIEND, Bolskesjö, AISH n°187.

Prudhomme, C. (1995), Analyse et régionalisation des régimes hydrologiques méditerranéens, Thèse de Doctorat en hydrologie, Cemagref–Lyon, Division Hydrologie–Hydraulique, LHM, Montpellier II.

Prudhomme, C. (1995), Modèles synthétiques des connaissances en hydrologie: application à lu régionalisation des crues en Europe alpine et méditerranéenne, Thèse de doctorat spécialité mécanique, hydrologie Sciences de l'eau et l'aménagement, Université de Montpellier II, Cemagref–Lyon, 397 p.

Observing and modelling exceptional floods and rainfalls
Proceedings of the AMHY-FRIEND International Workshop on Hydrological Extremes,
held at University of Calabria, Cosenza (Italy), May 3-4, 2006

REGIONAL FREQUENCY ANALYSIS OF RAINFALL EXTREMES IN TUSCANY

E. Caporali[1], E. Cavigli[1], A. Petrucci[2]

(1) Department of Civil Engineering, University of Florence, Italy
(2) Department of Statistics, University of Florence, Italy

ABSTRACT

The first and the second level of a hierarchical approach to regional frequency analysis of annual maximum of rainfall height for storm durations of 1 hour, 3, 6, 12, and 24 hours in Tuscany, are here described. Over a territory of about 22000 km², the data of 470 rain gauges, in the period from 1923 to 2002, have been collected and investigated. Particularly 295 time series larger than 10 years, characterized by a low spatial correlation and included in each of the five dataset (i.e. storm durations of 1, 3, 6, 12, 24 hours), have been selected. The statistical homogeneous zones and sub-zones have been defined using the L-moments method. The regional frequency analysis has been carried out on the basis of a two components extreme value distribution and the parameters have been evaluated with the joint ML estimation method. The growth factors, of the second level of the hierarchical regional frequency analysis, have been estimated for each sub-zones and return period up to 200 years. A third level of the regional frequency analysis is also here proposed, using a multivariate regressive model to assess the index rainfall value for storm duration from 1 to 24 hours and a given return period, in any location of the studied territory. A preliminary investigation has been carried out using the Mean Annual Precipitation (MAP). Particularly the relation between MAP and the rainfall extreme values at the rain gauge sites for a given storm duration and an assigned time period have been investigated. Daily registrations from 1970 to 2004 of a dataset of 601 rain gauges have been analysed to obtain the MAP value at each measurement site. Inverse distance weighted method has been used to elaborate the spatial distribution of MAP. The results show that the MAP values are nearly sufficient for the estimation of the index value for one of the three sub zones defined at the second level of the hierarchical approach. The analysis has been carried out fitting a regression model on MAP values and on other geographic and climatic characteristics such as elevation, aspects and mean value of the annual maximum rainfall with given time duration.

1. INTRODUCTION

In frequency analysis of hydrological extremes the two parameters probability distributions usually are not able to fit correctly the observations characterized by more intense and rare events, i.e. they are not able to model adequately the upper tail of extreme rainfall events (*Rossi et al.*, 1984). Distributions with more than two parameters better represent the data recorded at the gauge station but need of a larger amount of data. For their application, a regional analysis based on a high number of time series recorded at different measurement stations, belonging to the same homogenous hydrological region, is recommended. The criteria of homogeneity can be defined considering physical

or climatic conditions or equivalent statistical parameters (*Haan*, 1994). With this type of analysis the sample size is larger than that of each single time series. The probability of including in the frequency analysis a larger number of events characterized by high return periods increases and the estimation of rare events becomes more reliable.

To identify possible homogeneous zones (*Haan*, 1994) for the regional analysis, the spatial distribution of L−coefficient of variation and L−skewness for each dataset have been investigated (*Hosking,* 1990) and results obtained on the regional frequency analysis of annual maximum of daily rainfall (*Sorbi*, 1997; *Tartaglia*, 2001) have been considered.

In this study the TCEV - Two Components Extreme Value distribution (*Rossi et al.*, 1984) on five dataset of extreme rainfall (i.e. storm durations of 1, 3, 6, 12, 24 hours), is applied. The distribution follows the hypothesis that, the first component describes the more frequent events characterized by a low magnitude. The second component describes the outliers, characterized by more intense and rare events.

Each component is described by a set of parameters evaluated using the joint ML estimation method (*Gabriele et al.*, 1994), at the first and second level of regionalization, based on a hierarchical procedure proposed in the Italian research project VaPI - Valutazione delle Piene in Italia (*Versace*, 1994). The third level of the regional frequency analysis is also investigated, using a multivariate regressive model to assess the index rainfall value (*Dalrymple*, 1960), for storm duration from 1 to 24 hours and a given return period, in any location of the studied territory. A preliminary investigation has been carried out using the Mean Annual Precipitation (MAP) (*Alila*, 1999). Particularly the relation between MAP and the rainfall extreme value at the rain gauge sites for a given storm duration and an assigned time period has been investigated.

2. DATA SAMPLE

The analysis has been carried out over a territory of about 22000 km^2, on a set of 470 rain gauges, of time series (storm durations 1, 3, 6, 12, 24 hours) of annual maximum of rainfall, recorded from 1923 to 2002.

Even if there is a spatial dependence among the time series, the regional analysis is more accurate than the local one (*Hosking and Wallis*, 1988), for this reason only sites with high correlation coefficient (more than 0.8), and within a distance of 50 km have been excluded (*Tartaglia*, 2001).

The study has been carried out on 293 time series, longer than 10 years extracted by the above described data set (Table 1). All the following analysis have been reiterated for the dataset with time series longer than 20, 30, 40 years.

3. HOMOGENOUS ZONE INVESTIGATION

Preliminarily the sample L-coefficient of variation and sample L-skewness for each dataset has been calculated and their means have been evaluated (Figure 1) with the aim to understand if, for each duration-data set, there was the possibility to maintain the same zone identification. The analysis shows that the sample L-skewness depends by rainfall duration more than the L-coefficient of variation; however the hypothesis of same zone division for the different duration can be maintained.

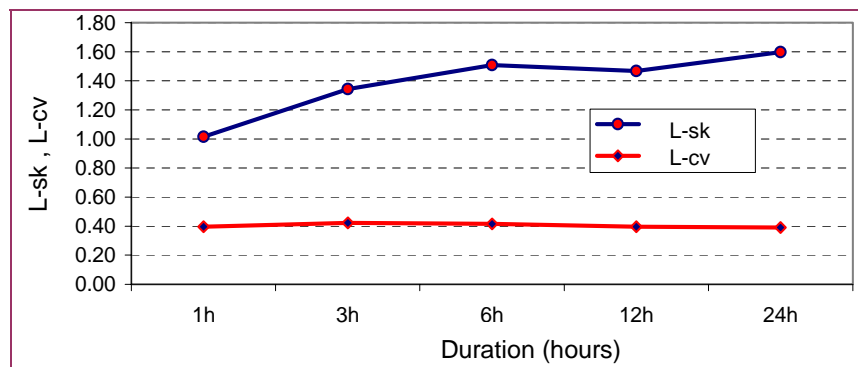| Time series longer than	N° of sites	N° of data	N° of data per site
10 years	293	8949	30.5
15 years	226	8155	36.1
20 years	173	7267	42.0
25 years	147	6689	45.5
30 years	124	6085	49.1
35 years	112	5704	50.9
40 years	95	5067	53.3
45 years	77	4316	56.1
50 years	61	3578	58.7

Table 1. Consistence of the time series database.

Figure 1. Succession with the duration of the mean of the sample L-coefficients, for time series longer than 30 years.

The spatial distribution of L-coefficient of variation and L-skewness, for each dataset, has been also investigated (*Hosking*, 1990). An inverse distance weighted interpolation method has been used to predict the value for any unmeasured site and a 2x2 km grid has been generated (Figure 2).
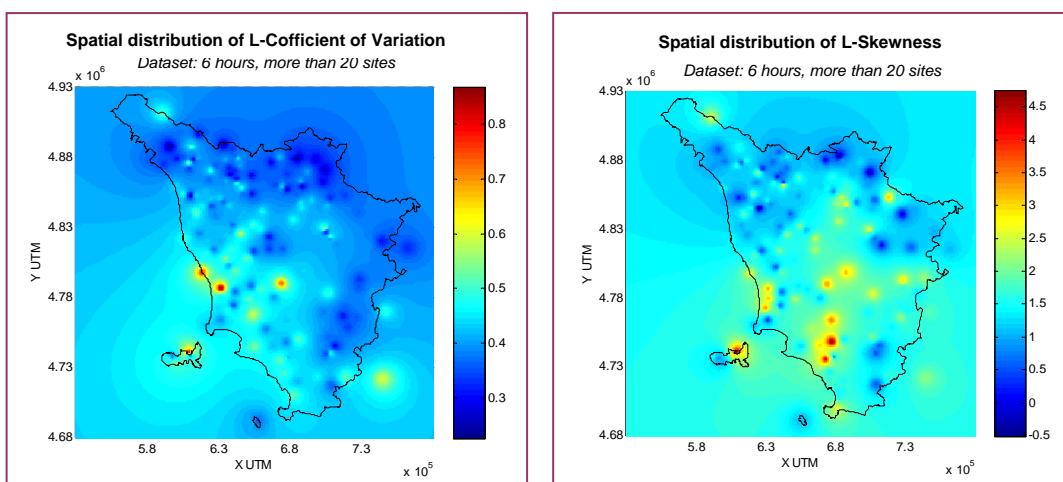
Figure 2. Spatial distribution of L-coefficient of variation and L-skewness.

On the basis of the achieved results and the results obtained on the regional frequency analysis of annual maximum of daily rainfall (*Sorbi*, 1997; *Tartaglia*, 2001) three hypotheses have been considered for Tuscany region:

1. unique homogeneous zone and unique sub-zone;
2. unique homogeneous zone and three sub-zones (North, Centre, South);
3. three homogeneous zones (North, Center, South), each one coincident with a correspondent sub-zone.

For each hypothesis the parameters Λ_*, θ_* e Λ_1 of the TCEV distribution, for the first and second level of hierarchical regional analysis, have been evaluated using the joint ML estimation method (*Gabriele and Iiritano*, 1994).

Fitting tests have been carried out on the obtained results. Particularly the χ^2 test, the Students t test on the mean and Wilcoxon test have been used. The tests don't give the same positive results on the different data samples. The hypotheses that at the same time satisfy the tests have been investigated, in particular, on the larger data samples of 30 and 40 years. The better fitting are those obtained for the hypothesis that consider the Tuscany region divided in three homogeneous zone: North, Centre and South, and three coincident sub-zones.

4. HOMOGENOUS ZONE DEFINITION AND TCEV GROWTH FACTOR ESTIMATION

The hypothesis that gives better results considers the Tuscany region divided in three homogeneous zones, North, Centre and South, coincident with their sub-zones.

Tuscany divided in 3 homogeneous zones: NORTH, CENTRE and SOUTH								
NORTH homogeneous zone and sub-zone								
	20 years			30 years			40 years		
	Λ_*	θ_*	Λ_1	Λ_*	θ_*	Λ_1	Λ_*	θ_*	Λ_1
1h	0.049	1.794	16.735	0.062	1.78	16.435	0.073	1.798	16.869
3h	0.255	2.254	20.986	0.227	2.307	20.739	0.195	2.373	20.647
6h	0.176	2.61	25.602	0.162	2.701	25.277	0.142	2.81	25.042
12h	0.174	2.412	30.053	0.175	2.446	30.048	0.165	2.51	29.43
24h	0.087	2.452	28.975	0.11	2.451	30.648	0.106	2.473	30.164
CENTRE homogeneous zone and sub-zone								
	20 years			30 years			40 years		
	Λ_*	θ_*	Λ_1	Λ_*	θ_*	Λ_1	Λ_*	θ_*	Λ_1
1h	0.058	1.49	12.865	0.008	3.155	12.815	0.029	1.021	12.28
3h	0.194	2.271	15.597	0.14	2.282	14.774	0.22	1.895	14.521
6h	0.114	2.907	17.904	0.108	2.808	17.059	0.171	2.149	16.916
12h	0.082	3.131	18.552	0.083	3.119	17.879	0.074	2.908	17.553
24h	0.062	4.053	21.021	0.06	4.275	20.442	0.056	3.983	20.517
SOUTH homogeneous zone and sub-zone								
	20 years			30 years			40 years		
	Λ_*	θ_*	Λ_1	Λ_*	θ_*	Λ_1	Λ_*	θ_*	Λ_1
1h	0.03	1.01	13.791	0.029	1.015	14.258	0.028	1.012	14.903
3h	0.605	1.605	15.172	0.516	1.601	15.004	0.083	1.57	15.567
6h	0.169	1.974	19.625	0.145	2.035	18.838	0.113	1.863	18.093
12h	0.082	2.698	24.076	0.089	2.722	23.644	0.072	2.703	23.262
24h	0.065	3.169	28.06	0.066	3.298	26.742	0.054	3.245	25.949

Table 2. TCEV distribution parameters for the 1st and 2nd level of hierarchical regional analysis.

Some examples of distribution function for the TCEV evaluated standardized variable *y* are reported in the following (Figure 3).
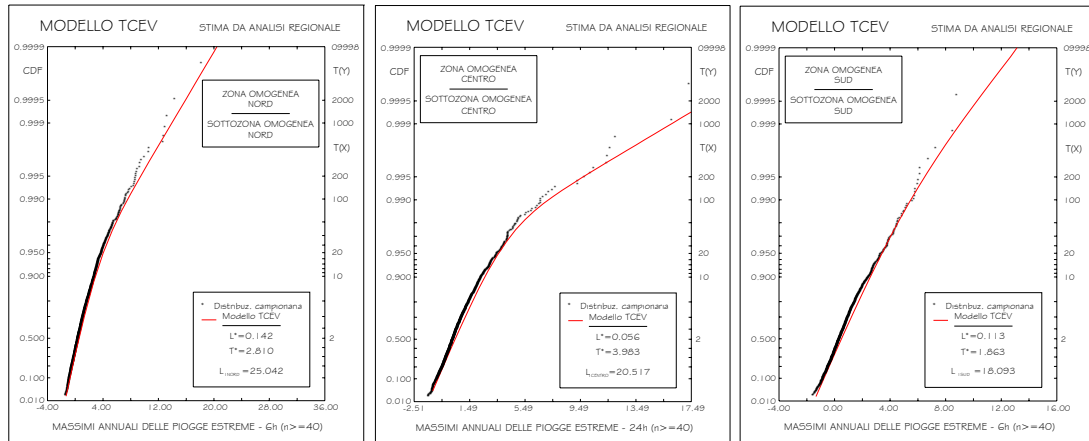

Figure 3. Distribution functions of the standardized variable y for the time series longer than 40 years, with Tuscany region divided in three homogeneous zones and three sub-zones.

For each storm duration, the growth factor k, at the first and second level of hierarchical regional analysis, has been calculated (Figure 4) using the expression:

$$k = \frac{X_{Tr}}{\mu(X_{Tr})}$$

where X_{Tr} is the rainfall depth at return time T_r and $\mu(X_{Tr})$ is the index rainfall at return time T_r (*Dalrymple*, 1960).
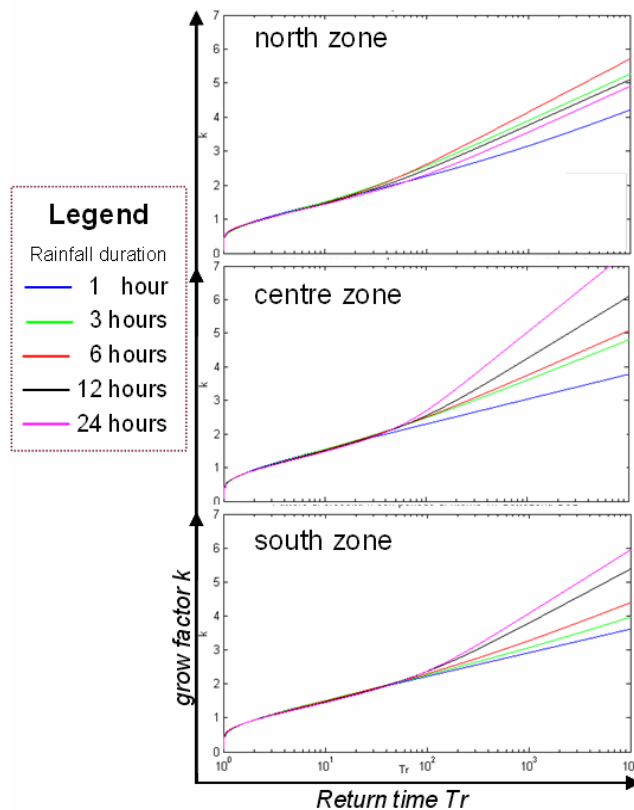
Figure 4. Growth factor k of TCEV distribution vs return time T_r for different storm duration.

5. THE INDEX RAINFALL OF THE THIRD LEVEL OF HIERARCHICAL REGIONAL ANALYSIS

Investigations carried out on different territories (*Alila*, 1999; *Brath et al.*, 2003) show that rainfall extremes could be considered as a function of the Mean Annual Precipitation (MAP) value. The at-site MAP value has been calculated using daily registrations in the period 1970-2004, of a dataset of 601 rain gauges. Inverse distance weighted method has been used to elaborate the spatial distribution of MAP in the analysed territory (Figure 5).

At the same time, on each rain gauge site, a local extreme value analysis with GEV - Generalized Extreme Value distribution (*Alila*, 1999; *Brath et al.*, 2003; *Gellens*, 2002) has been carried out. The following hypothesis has been assumed: the rainfall local extreme estimation at the gauge site corresponds to the estimated regional extreme, i.e. the product between growth factor and the index rainfall value.

At each site the index rainfall has been calculated and its relationship with the Mean Annual Precipitation – MAP value (*Alila*, 2000) has been investigated.

It is shown from the investigation that only the north zone gives interesting results that could encourage the use of MAP as unique value for the estimation of the index rainfall ($R^2 \geq 0.8$) for each duration and given return period.
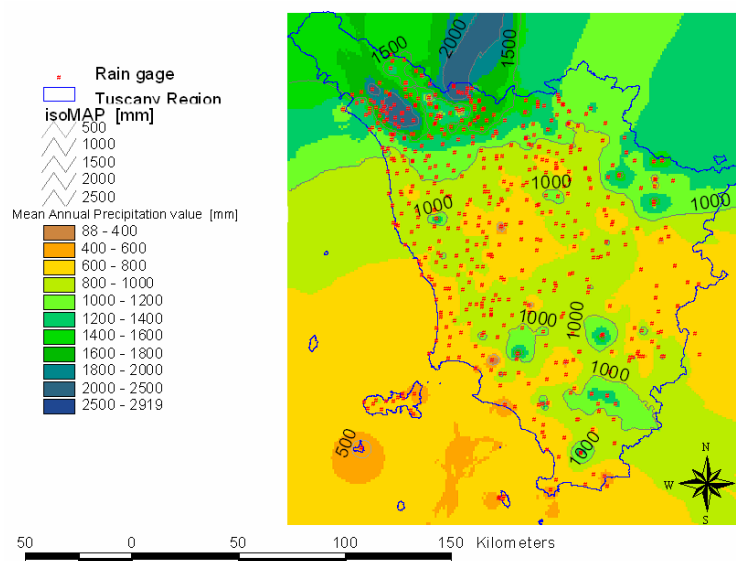
Figure 5. Mean Annual Precipitation map for Tuscany region (1970-2004).

6. CONCLUSION AND FUTURE DEVELOPMENTS

The MAP value alone is not able to completely describe the index rainfall, although the acceptable results on the North zone. For this reason the possibility of using a multi-regressive analysis, that includes other characteristics related to the territory, is going to be investigated. In fact in the more diffused geophysical models the equations can be easily approximated using multiregressive models (*Castrignanò et al.*, 2005). The equation that models the index rainfall will involve territory characteristics such as elevation (DTM) and aspects. After some preliminary elaborations, rather important seems to include in the model the mean value of the time series of measured extreme rainfall, used in the growth factors estimation. Being the time series valid at the

measurement site they have been interpolated with the kriging method applied to the recorded time series for each storm duration. The exponential semivariogram is the one that gives: standardized mean nearest to zero; smallest RMS prediction-error; average prediction standard error nearest to the RMSPE and standardized RMSPE nearest to one.

The elaborations for the estimation of the parameters model are still in progress. At the moment a model for each rainfall duration has been implemented. In the future the analysis will involve the development of a unique model dependent also by the storm duration.

REFERENCES

Alila, Y. (1999), A hierarchical approach for the regionalization of precipitation annual maxima in Canada, *J. Geoph. Res.*, *104*(D24), 31645-31655.

Alila, Y. (2000), Regional rainfall depth-duration-frequency equations for Canada, *Water Resour. Res.*, *36*(7), 1767-1778.

Brath, A., A. Castellarin, and A. Montanari (2003), Assessing the reliability of regional depth-duration-frequency equations for gaged and ungaged sites, *Water Resour. Res.*, *39*(12), 1367-1378.

Castrignanò, A., N. Lopez, and M.S. Caradonna (2005), L'impiego di parametri topografici per migliorare la precisione della stima della precipitazione, *Proceedings of the meeting AIAM 2005 (Agrometeorologia, risorse naturali e sistemi di gestione del territorio)*, 77-78 (in Italian).

Dalrymple, T. (1996), Flood Frequency Analysis, U.S. *Geological Survey Water-Supply Paper* 1543-A, GPO, Washington, D.C..

Gabriele, S. and G. Iiritano (1994), *Alcuni aspetti teorici ed applicativi nella regionalizzazione delle piogge con il modello TCEV*, CNR-GNDCI, pubb. n. 1098 (in Italian).

Gellens, D. (2002), Combining regional approach and data extension procedure for assessing GEV distribution of extreme precipitation in Belgium, *J. Hydrol.*, *268*, 113-126.

Haan, C.T. (1994), *Statistical Methods in hydrology*, The Iowa State University Press, Ames.

Hosking, J.R.M. and J.R. Wallis (1988), The effect of intersite dependence on regional flood frequency analysis, *Water Resour. Res.*, *24*(4), 588-600.

Hosking, J.R.M. (1990), L-moments: Analysis and Estimation of Distributions using Linear Combinations of Order Statistics, *J. of Royal Stat. Soc.*, *Series B*, *52*, 105-124.

Rossi, F., M. Fiorentino, and P. Versace (1984), Two-Component Extreme Value Distribution for Flood Frequency Analysis", *Water Resour. Res.*, *20*(7), 847-856.

Sorbi, A. (1997), Le piogge estreme in Toscana, Graduation thesis (unpublished), Engineering Faculty, University of Florence, Italy (in Italian).

Tartaglia, V. (2001), Vulnerabilità idraulica degli attraversamenti ferroviari di corsi d'acqua in Toscana, Graduation thesis (unpublished), Engineering Faculty, University of Florence, Italy (in Italian).

Versace, P. (1994), Descrizione della procedura VAPI, VAPI project, National report, CNR-GNDCI, U.O. 1.15, Soil Protection Department, University of Calabria, Cosenza (in Italian).

Part 3
ADVANCES IN PEAK RIVER FLOW MODELLING THROUGH RAINFALL RUNOFF MODELS

Observing and modelling exceptional floods and rainfalls
Proceedings of the AMHY-FRIEND International Workshop on Hydrological Extremes,
held at University of Calabria, Cosenza (Italy), May 3-4, 2006

FLOOD SIMULATION AND ESTIMATION IN THE TEVERE RIVER: A DETERMINISTIC AND PROBABILISTIC APPROACH

B. Bacchi[1], G. Grossi[1], L. Pennesi[2], P. Potenza[2], R. Ranzi[1], A. Schiavoni[2]

(1) Dept. of Civil Engineering, Architecture, Soil and Environment, University of Brescia, Italy
(2) ITALECO S.p.a., Roma

ABSTRACT

Eight floods observed at the Ponte Nuovo stream gauge station, draining an area of 4147 km² in the Upper Tevere River basin in Central Italy, were simulated using a conceptual hydrological model with distributed parameters. Hourly hyetographs and hydrographs of the flood events were recorded at several rain gauge and stream gauge stations to enable a realistic description of the rainfall field and the model verification in several nodes of the river network. For the flood routing, both over the hillslopes and along the channel network, a dynamical Muskingum-Cunge method was applied, with different parameters describing the overland and channel flow. For the net rainfall computation a modified version of the standard SCS-CN procedure was applied. In the application of this method it was observed, indeed, that the storm runoff volume was sensitive to the precipitation measured in the 30 days prior to the flood event, instead of the 5 days, as recommended by the standard practice. As a consequence of this "experimental" result a WAPI30 index is to be computed to define the soil storage capacity parameter. As an alternative method a distributed runoff coefficient approach was also explored to compute the surface runoff production. This method results as being more 'robust' with respect to the inter-event variability of net-rainfall volumes and storm hyetographs than the non-linear SCS-CN. Some numerical experiments suggest applying this method for flood prediction in the Upper Tevere basin.

1. INTRODUCTION

The flood plains of the Tevere River in the vicinity of Ponte Nuovo gauge station, as well as upstream the Corbara dam, were affected in the past and also recently by several high floods, which flooded and caused severe damages to the adjacent alluvial plains. To this extent there are still rumours of the events that occurred in April 2004 and autumn 2005, for the latter even the city of Rome was alerted and some urban areas downstream the city were evacuated (*Mele et al.,* 2006).

As far as flood protection is concerned, structural and non-structural measures can be adopted, each characterised by a different degree of protection and a different efficiency in reducing potential damages. National and regional offices aimed at the prevention of the effects of hydro-geological hazards are recently paying increasing attention to warning systems; this is a consequence of the fact that society hardly accepts structural solutions (levee building, net reservoirs, river restoration,…), mainly because of economic and social costs. An early flood warning, when issued in time, could in fact give a chance to the inhabitants to become aware of the potential danger, and eventually to move from the threatened areas. Therefore the scientific community is nowadays

solicited towards this type of approach, aiming at improving the reliability of operative forecasting systems. From this comes the motivation for a definition of an optimised hydrological flood model for the Tevere River basin, upstream the section of Ponte Nuovo (4147 km²), including most of the mountainous area of the basin as well as the Chiascio subbasin on the left side.

The generation of surface and subsurface runoff and its routing through the river network is a typical space distributed process, since a high spatial variability is shown by the precipitation rate, the infiltration and overland flow velocity and the sub-surface water movements. Therefore the use of mathematical distributed models able to compute the river discharge as a function of space and time is suggested, instead of the use of lumped models computing the discharge only as a function of time in a prefixed number of river sections. Among the hydrological distributed models, event scale flood models can simulate the generation of quick surface and subsurface runoff and its routing along the hillslope and in the river network, but they do not take into account the evapotranspiration and the soil moisture updating processes between two subsequent events. The distributed approach allows the flood hydrograph simulation at any point of the river network, avoiding the sometimes dangerous spatial extrapolation of the lumped results. In addition, a number of experiments conducted by several authors (*Rosso*, 1994; *Ranzi and Rosso*, 1994) showed the applicability and efficiency of these models.

For these reasons a distributed hydrological model was selected to simulate the hydrological response of the Tevere River watershed: the model is called DIMOSOP and it was already applied in previous studies concerning different watersheds, with reduced size and higher slopes with respect to the Tevere River basin, such as the Entella River, the Mella River (*Ranzi et al.*, 2002) and the Toce River (*Bacchi and Ranzi*, 2003) watershed. As a result of the distributed simulation, flood hydrographs were provided for some selected river sections. Some refer to simulated events that occurred in the past, some were 'synthetically' generated through the application of the intensity-duration-frequency curves.

The same flood events were also simulated through a lumped model, in order to verify the level of improvement in the results provided by more detailed models. The aim of this analysis was in fact to verify if the distributed model, requiring detailed information on the geography, the topography, the geology and the soil properties of the site, can provide results closer to the observations than a lumped model, requiring only some information on the average basin condition.

2. THE DISTRIBUTED FLOOD MODEL

The distributed approach to the physical-mathematical modelling of the hydrological response is based on a discretization of the basin in unit cells, linked one another and small enough to allow a deterministic representation of the physical processes of interest. The model is based on mass, motion and energy conservation, where state parameters can be considered uniform within each cell. The elemental flows are then integrated, following an hydraulic routing model along each cell cascade, representing a slope surface, and along the river network. In this way the flow is simulated for each cell of the basin, using digital elevation models (DEM).

It is here worth to remember that a complete simulation of the flood generation mechanism should take into account the two main contributions to the rise of the river

water level: flows with high routing velocity, that are surface runoff and interflow, and slower flows, due essentially to groundwater flow. The information needed for the use of a distributed model of runoff are rarely available even for small basins. For this reason the distributed model was focused on the hillslope runoff, ruled by more easily estimated parameters like slope and hillslope and bed river roughness.

2.1 Surface runoff generation

The time evolution of runoff produced in a given river basin depends on the water movement over the hillslopes and along the river network. The hillslope response to the meteorological forcing depends on the topographic and geomorphologic characteristics of the hillslope itself. The hillslope is in fact a morphologic unit, bounded by a surface with variable slope and made of not homogeneous land cover, soils and rocks; inside the water moves in three dimensions both at the surface and below. In order to simulate the soil response to the meteorological forcing a parameterisation of the rock and the soil permeability is necessary. The evapotranspiration process is not accounted, because the water loss due to this phenomenon during a flood event is usually negligible when compared to the other processes influencing runoff generation.

At the hillslope scale, the first process to be considered is the separation between the slow groundwater flow and the rapid runoff generation in the river network, due to overland flow and inflow. In this work the model proposed by the United States Soil Conservation Service, the Curve Number model (*USDA-SCS,* 1985), is used. This procedure was originally suggested for the computation of surface runoff for small rural ungauged watersheds and it is still widely used in hydrological practice and applied research (*Mishra and Singh,* 2004*; Rinaldo et al.,* 2004); the model allows the computation of the precipitation lost because of the soil absorption and it assumes that in a flood event, the specific volume of surface runoff, Q, is proportional to the precipitated one, P, reduced by the initial loss, I_a, as the ratio between the specific infiltrated volume and a specific volume representing the potential retention S.

The total runoff volume, in other words, can be obtained through the well known expression:

$$Q = \frac{(P - I_a)^2}{P - I_a + S} \qquad (1)$$

where S [mm] is directly related to the CN index:

$$S = \left(\frac{100}{CN} - 1\right) \cdot 254 \qquad (1')$$

In order to apply the procedure to each cell of the basin, it is therefore necessary to know, not only for each cell but also for each time step, the precipitation and the absorption properties represented by the storage parameter. The information about the space variability of the hydraulic properties of the soil is also necessary.

The information needed for the definition of the soil absorption 2D-map concerns the lithology of the upper soil layer and the land use. The initial conditions, i.e. the soil water content in each cell at the beginning of the flood event, are derived from an antecedent precipitation index referred to 5 days before the event (API5), on the basis of which the Antecedent Moisture Condition (AMC) is selected. The lithology and the land use are necessary to estimate, by a cross-tabulation of their classes, the hydraulic properties of the soil and it is here worth to notice that the result is subjective, to some extent.

2.2 The routing scheme

DIMOSOP (DIstributed hydrological MOdel for the SOP[1]) is the hydrological rainfall-runoff model used for this study. It is based on a representation of the river network through junctions of channel segments draining the cells of the basin, as first developed by *La Barbera* (1990). Effective rainfall generation processes, described by the conceptual scheme of the CN index was coupled to the routing processes along the river network following the procedure first proposed by *Mancini* (1991). The original code assumed that in each elemental cell of the basin a channel was present and that each channel was joining the downstream channels, reproducing the routing mechanism as described by the Muskingum-Cunge scheme.

The original structure was modified to introduce both the non-linear routing scheme, and, afterwards, a separation between routing on the hillslope (overland flow) and along the river network. For this reason it is assumed that for the source cells draining an area lower than a fixed threshold value, the routing scheme of the overland flow is a linear reservoir (*Ranzi et al.,* 2002). In this way the sum of the precipitation and of the outflow of the adjacent upstream cells becomes the total inflow to the downstream cell. The modified model was previously applied to the Entella watershed, in Liguria (Italy), to the Mella watershed (in the Province of Brescia, Italy) and to the Toce watershed (Piedmont, Italy; *Ranzi et al.,* 2003*; Bacchi and Ranzi,* 2000*; Grossi and Kouwen,* 2004). Finally, after several improvements it is here applied to the Tevere watershed; DIMOSOP takes into account the rain and snow partitioning of precipitation and the snowmelt on the basis of a simple temperature index model. It also accounts for the presence of reservoirs along the river network.

Soil permeability characteristics were not calibrated: they were estimated on the basis of permeability and land use maps and kept constant for all the simulated events. The river bed is assumed to have a rectangular shape with a given base/height ratio. Hillslope roughness was fixed on the basis of literature data (*Emmett,* 1970) and channel roughness was estimated according to the stage-discharge curves available for some hydrometric stations (*Bencivenga et al.,* 2001).

The flow routing along the river network is represented through a dynamic Muskingum-Cunge scheme, where the parameters depend on the current computed discharge. The discharge $Q_{x+Dx,t+Dt}$ at the grid point with coordinate x+Dx and at time t+Dt is explicitly computed as a function of the discharge computed at the previous spatial grid point, having coordinate x, at time t and t+Dt, and of the discharge computed for the current spatial grid point at time t, plus the contribution of the lateral and direct inflow, p_t, distributed over the cell:

$$Q_{x+\Delta x,t+\Delta t} = C_1 Q_{x,t+\Delta t} + C_2 Q_{x,t} + C_3 Q_{x+\Delta x,t} + C_4 p_t \qquad (2)$$

The travel time constant involved in the analytical definition of the C_k coefficients is computed as a function of the current discharge, as suggested by *Ponce and Yevjevich* (1978) and adopted by *Orlandini and Rosso* (1998) and *Ranzi et al.* (2002).

3. THE TEVERE WATERSHED AT THE SECTION OF PONTE NUOVO

3.1 The digital terrain model of the Tevere watershed at the section of Ponte Nuovo

---

[1] The Special Observing Period of the 'Mesoscale Alpine Programme' (*Bougeault et al.*, 2001).

The study area includes the Tevere River watershed upstream its junction with the Chiascio River, south of Perugia, that is upstream the gauged section of Ponte Nuovo, including part of the territories of three different administrative regions (Emilia Romagna, Toscana and Umbria). The drained area of the watershed is 4147 km^2 wide, the maximum height is 1570 m, the average height is 523 m, the zero water level at the closure section is 163.02 m a.s.l. (from 1927 up to 1969).

The digital elevation model (DEM) has a grid size of 250 m, which is actually enough to reproduce the spatial variability of the elevation in the study area, as it is shown in Figure 1. On the basis of the DEM, all the information collected concerning the lithology and the land use, by the interpretation of a geologic map by CNR-IRPI (*Cardinali et al.,* 2001), was then used to produce the CN parameter map (with reference to average soil moisture conditions), necessary for the estimate of the surface runoff production for each cell (Figure 2).

3.2 The hydrometeorological dataset

Given the high frequency of occurrence in the last twenty years of high flood events in the upper Tevere watershed, the hydrological model was used to simulate some of the events recently occurred. The aim is twofold. On one hand, to test the ability of the model to reproduce the rainfall-runoff processes in a context completely different from the one for which it was developed. On the other hand, the model is used assuming synthetic scenarios with the aim of reproducing a "T-year flood" event using an areal intensity-frequency rainfall event, spatially distributed, of the same T-year return period. For this reason hydrometric and pluviometric observations referring to the period 1994-2001 were collected; within this observation period, the eight flood events described in tab. 1 were selected.

The available rainfall observations, sampled every 30 minutes, are those recorded at the 36 rain gauges located inside the Tevere basin or in the nearby area. On the other hand the rainfall series are not continuous and the point observations are not always all available, but they can change from one event to the other.

Available water level observations, again sampled every 30 minutes, are those recorded by the hydrometric stations located along the Tevere River and along its tributaries (Figure 1). A reliable stage-discharge relationship was available for the Ponte Nuovo section, but other gauged sections can be used as check-points to verify the likelihood of the simulated discharge hydrographs with respect to the recorded time-level hydrographs.

4. THE SIMULATION OF THE OBSERVED FLOOD EVENTS

As mentioned above, the distributed model was first applied to simulate the flood events for which rainfall observations recorded by several rain gauges within the basin, as well as hydrometric observations in some gauged sections, were available (Table 1).

For each of the selected events, the available rainfall series were recorded by a different set of rain gauges, on average well distributed over the basin, because of the lack of records in some of the 36 gauged stations. However it was possible to compute the Thiessen polygons (that is the contributing area for each station, necessary to assign the rainfall value to each cell) for the basin, that is the weights for each station to be

included in the computation of the areal average. An example is shown in Figure 1b.

Date of the event	Time period (h)	Q_0 $(m^3 \cdot s^{-1} \cdot km^{-2})$	API_5 (mm)	$WAPI_{30}$ (mm)	Vegetative period	Q_{obs} (mm)
04/01/94	120	0.024	16	43	no	7.16
30/12/95	120	0.010	35	35	no	15.27
17/11/96	90	0.004	20	21	no	20.31
14/12/96	120	0.011	18	42	no	15.83
01/06/97	120	0.004	2	14	yes	17.14
04/12/98	120	0.015	14	27	no	10.63
09/02/99	120	0.007	7	24	no	15.90
24/12/00	216	0.004	1	21	no	49.55

Table 1. Flood events observed in the Tevere basin and simulated by the hydrological model.
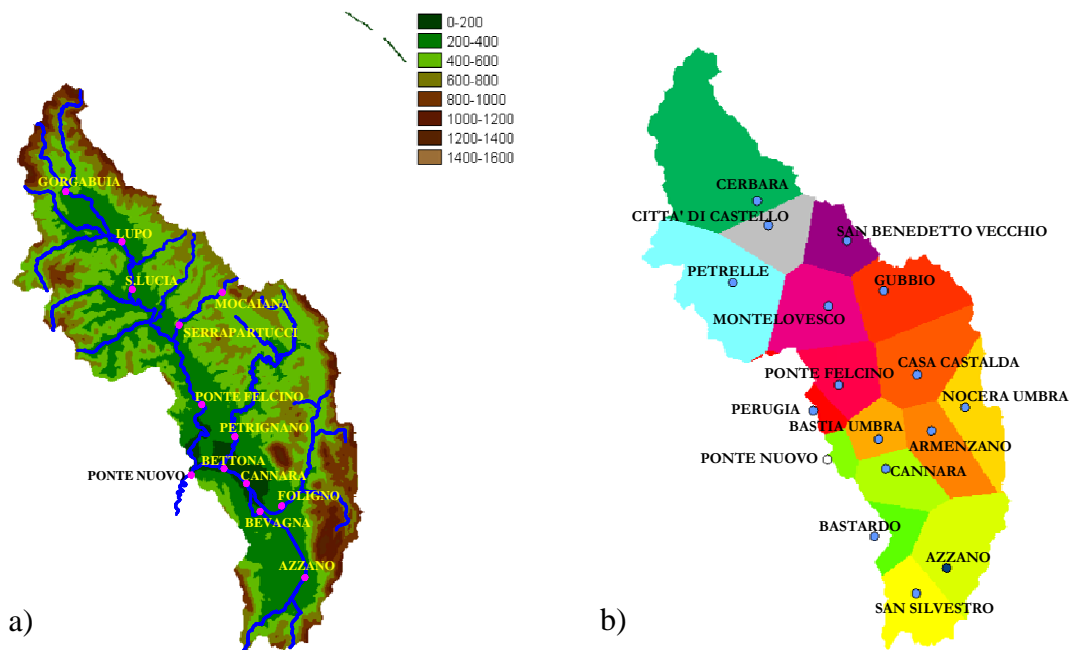
Figure 1. The Tevere basin at the section of Ponte Nuovo: a) the digital elevation model, b) Thiessen polygons for the available rain gauges for the events 1994-1995.

The outlet sections of the 13 subbasins for which the flood hydrograph was reproduced were selected where the hydrometric stations are located (Figure 1a). With the exception of the Ponte Nuovo section though, the stage-discharge relationships are not known; therefore, for the other closure sections, it is not possible to translate water level observations into discharge values. In any case water level observations are not enough for a volume check, but they do allow a check of the timing of the simulated hydrograph with respect to observed one; for this reason the flood hydrograph was reproduced and checked in each subbasin closure section.

As described in paragraph 2, the Antecedent soil Moisture Condition (AMC) was first selected with respect to standard criteria based on the API_5, that is the total precipitation recorded in the five days before the event. Results obtained with this procedure showed a very poor reproduction of the rainfall-runoff processes. As a matter of fact, the CN method is very sensitive to the initial soil moisture condition of the basin. Then a better definition of the AMC is needed.
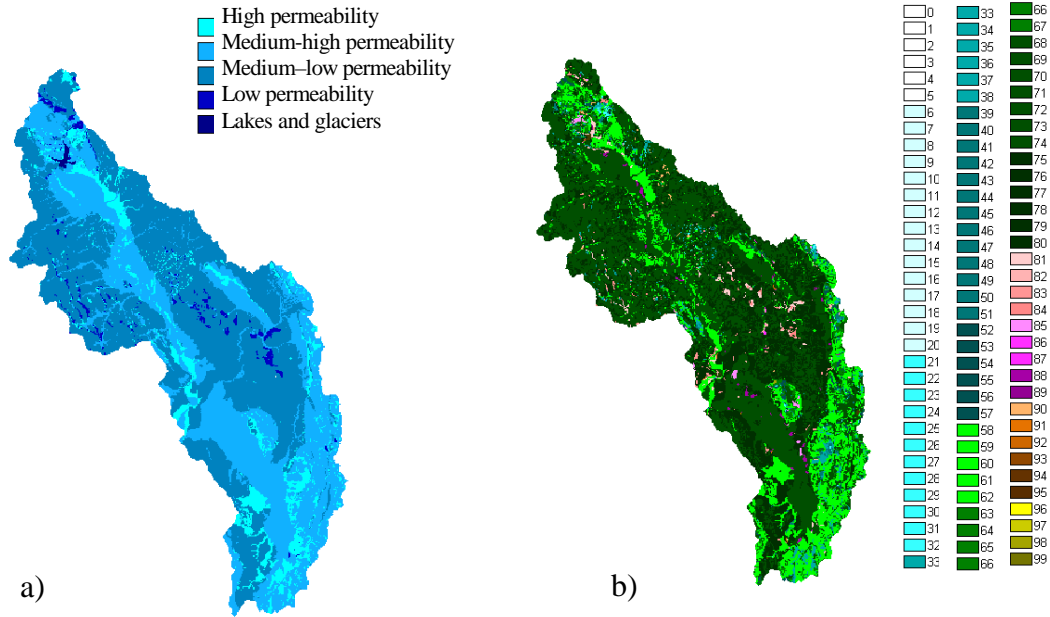
Figura 2. The Tevere basin at the section of Ponte Nuovo: a) permeability map, b) CN map for intermediate soil moisture conditions.

A way to improve this definition was suggested by the awareness that the CN-SCS methodology was developed for small basins where the 'memory' of the previous storm event is not longer than a few days. When the model is applied to medium-sized alpine catchments (e.g. the Toce River or the Mella River) the simulation results are in good fit with observations, given the fast hydrologic response due to the high slopes of the drained surface and the small depth of the soil layer. When the same model is applied to a larger catchment with relevant alluvial plains and mild surface slopes, the influence of the antecedent precipitation can be relevant.

In order to improve the performance of the model, the CN method was again applied but the AMC was selected with a different procedure: a precipitation index based on the 30 days before the event was used, as suggested by *Natale and Savi* (2004) for the Tevere River. As a measure of the soil moisture content, an index, named WAPI30, of the baseflow before the storm is here adopted:

$$\text{WAPI30} = \sum_{i=1}^{30} h_{-i} \left(1 - \phi\right) \cdot e^{-i/k} \tag{3}$$

where ϕ is the runoff coefficient and h_{-i} is the precipitation fallen in the ith day before the storm. WAPI30, that is the sum of the precipitation fallen in the antecedent 30 days differs from a standard 'antecedent precipitation index' because of the factor $(1-\phi)$, here introduced to take into account that only the infiltrated portion of the precipitation participates to the base flow, and of the factor $e^{-i/k}$, which is actually a way to assign a different weight to the antecedent precipitation as a function of the occurrence time. The adopted index is then a weighed API30 (WAPI30).

In the second step of the model initialisation, a tentative was carried out to apply this procedure, where the index WAPI30 is computed, assuming that the unsaturated soil surface layer is acting as a linear reservoir characterised by the time parameter k=24h (*Heggen*, 2001), accordingly to what was observed on the Tevere basin for the extreme flood events. Results of the API5 and WAPI30 indexes are reported for each event in Table 1.

After a first analysis of the baseflow index (WAPI30) it was clear that a new definition of the upper and lower limits of the AMC classes was necessary. In fact when the 30 days before the event are considered, instead of only 5, the total amount of rainfall affecting AMC might increase; consequently the limits of the three initial soil moisture classes have to be reset. It has also to be expected that for some events the AMC class changes: for example for the events that occurred in January 1994 and in December 1996 the highest soil moisture class is now expected.

In order to fix the new limits of the three classes, the events characterised by high antecedent precipitation were assumed to belong to AMC III, while those with low precipitation were forced to belong to AMC I; the range between the lower and upper limit of each class was also increased, accordingly to the expected increase in the total rainfall amounts before the storms. The new expected limits are reported in tab. 2. For values of WAPI30 belonging to the class AMCII, that is between 20 and 40 mm during the vegetation rest season, and between 43 and 63 mm during the growing season (obtained from the rest season limits by adding the same shift, 36-13, between the lower limits in the growing, 36, and in the rest season, 13, for the standard AMCI class), the following relationships can be used:

API5=13+0.75×(API30-20)   for the vegetation rest season
API5=36+0.85×(API30-43)   for the vegetation growing season

where a scaling factor is introduced to rescale the ranges of the standard API5 (respectively 13÷28 for the rest season and 36÷53 for the growing season) to the range of the WAPI30 classes.

AMC class	Rainfall in the 30 days before the event (weighted as suggested by eq.3)	Rainfall in the 5 days before the event
I	<20mm	<13 mm
II	20-40 mm	13-28 mm
III	>40 mm	>28 mm

Table 2. New limits for the initial soil moisture condition for the vegetation rest season.

Vegetation rest and growing season were actually not distinguishable from the observation because only one of the selected events should be strictly considered in the growing season.

No change in the initial soil moisture class and in the computed hydrograph resulted for the three events which were satisfactorily simulated with the standard procedure (November 1996, June 1997, December 1998): no change in the soil moisture class means no change in the hydrograph reproduction. On the other hand the initial soil moisture condition changes for the other 5 events and therefore also the simulated hydrograph changes. Figure 3 shows the plots of the simulated hydrographs obtained with the WAPI30 index and the new AMC definition.

The simulation of the flood events with the proposed procedure of AMC definition and the distributed model is more satisfactory than the standard one. Therefore the performance of this flood model is acceptable for some practical applications. The most meaningful required performances with respect to a potential use of the flood model for flood forecasting purposes is in the value of the peak discharge and of the timing of the simulated peak with respect to the observed one. From this point of view, looking at Table 4, the error in the peak discharge value results, in most cases, lower than 10% (5

events out of 8) and only for December 2000 the error is relevant (27 %).
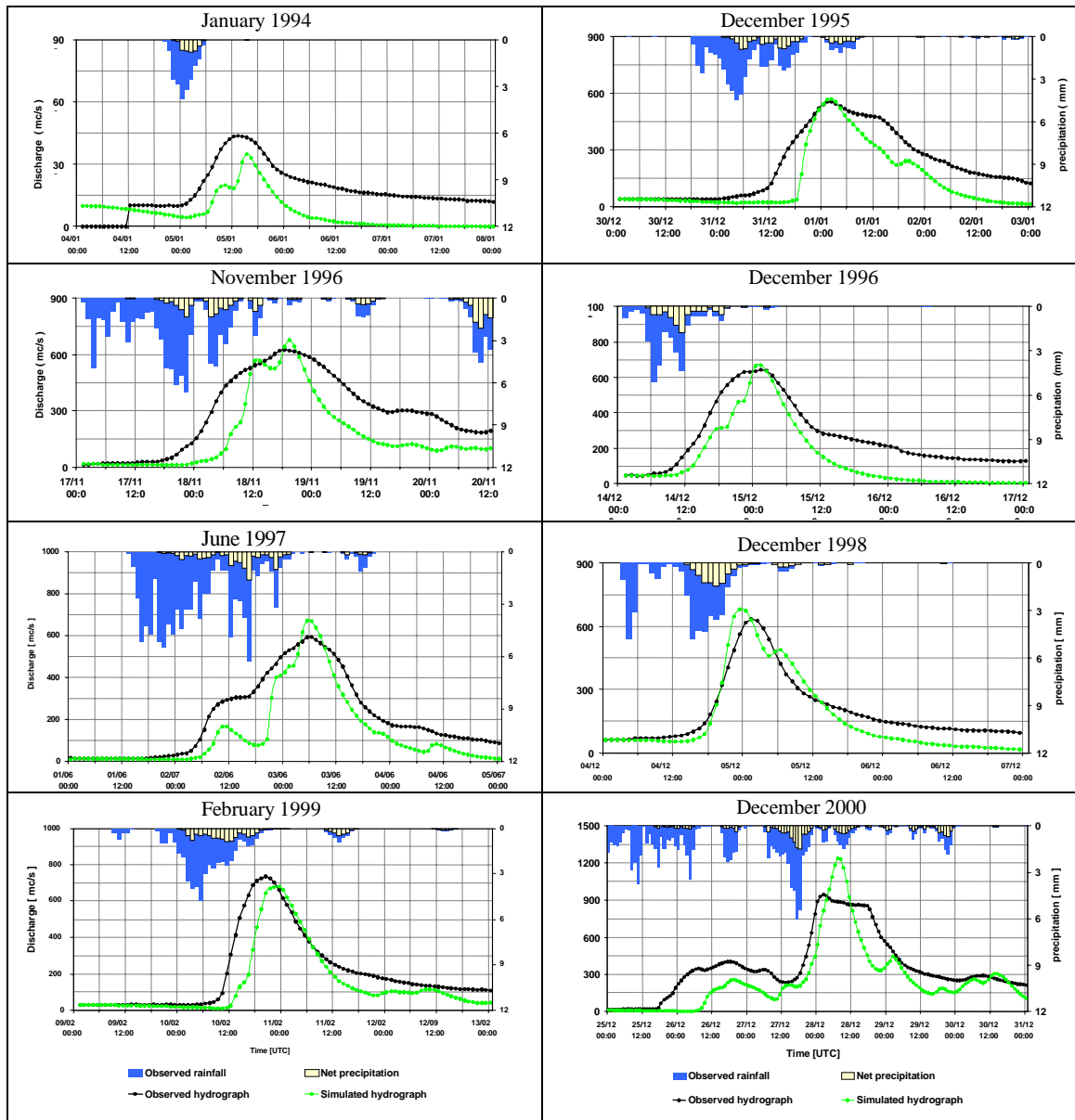
Figure 3. Observed and simulated hydrograph for the eight selected events.

	Event								mean
	4th Jan. 94	30th Dec. 95	17th Nov. 96	14th Dec. 96	1st Jun. 97	4th Dec. 98	9th Feb. 99	24th Dec. 00	
AMC	III	II	II	III	I	II	II	II	-
Q_{OBS} (m^3/s)	438	556	628	644	594	635	736	944	647
Q_{SIM} (m^3/s)	349	570	677	669	672	681	682	1203	688
% Error peak discharge	- 20	2	8	4	13	7	- 7	27	4
t_{sim}-t_{obs} (hours)	2	0	1	0	- 1	- 2	3	5	1
V_{OBS} (mm)	7.16	15.27	20.31	15.83	17.14	10.63	15.90	49.55	18.97
V_{SIM} (mm)	3.12	9.46	11.91	7.69	11.27	7.37	10.44	32.89	11.77
% Error runoff volume	- 60	- 38	- 41	- 51	- 34	- 31	- 34	- 34	- 40
Mean of the % absolute error on the peak discharge	11	Mean of the % absolute error on the runoff volume		40	Mean of the % absolute error on the timing (hours)				1.75

Table 3. Results of the distributed simulation for the observed floods (CN Method-API30).

The timing between the simulated and the observed peak is also very good: for 6 out of 8 events the time shift is shorter than 2 hours and only for the 2000 flood the time delay is significantly higher (5 hours).

Moreover a significant underestimation of the flood volume (40% on average) is observed, indicating that the subsurface component of the hydrograph, which is neglected in the model, is indeed relevant in the basin.

4.1 Verification with the runoff coefficient approach

In order to verify the suitability of the distributed model as an absorption soil model different from CN and to avoid the uncertainties due to the definition of the soil moisture condition before the event, a tentative simulation with a distributed runoff coefficient approach was carried out: at each time step, a fraction $(1-\phi)$ of precipitation is absorbed, while a fraction ϕ is rejected by the soil, where ϕ is the dimensionless runoff coefficient, with a value ranging from 0 to 1.

Of course the method was applied in a mode which was forced to be consistent with the spatial variability of the distributed model with respect to the average observed runoff coefficient. This implied first the estimate of the average runoff coefficient (ϕ=28%, as obtained through a least squares procedure). Then the CN value exceeded in the 28% of the cells of the basin was obtained by the CN cumulative frequency distribution. This CN value (76) was finally used to reclassify the CN map so that each cell with CN greater or equal to 76 were considered impervious and the CN value was forced to 100, while for the other cells a CN value equal to 1 was assigned because they are assumed to be completely pervious. In this way a scenario simulating a distributed runoff coefficient was created.

Results obtained with the distributed runoff coefficient approach can be globally accepted, since most of the simulated events show negligible differences with the method previously described, proving the reliability of the model application, even though in some cases the discrepancy between the simulated and the observed hydrograph is not negligible (November 1996, June 1997, December 2000).

Results are shown in Table 4: it is clear that the error in the peak discharge is lower than 15-20% for 5 out of 8 events, while the peak discharge is definitely overestimated only for June 1997 event.

	Event								mean
	4th Jan. 94	30th Dec. 95	17th Nov. 96	14th Dec. 96	1st Jun. 97	4th Dec. 98	9th Feb. 99	24th Dec. 00	
AMC	III	II	II	III	I	II	II	II	-
Q_{OBS} (m³/s)	438	556	628	644	594	635	736	944	647
Q_{SIM} (m³/s)	429	578	913	523	1000	733	797	547	690
% Error peak discharge	- 2	4	45	-19	68	15	8	-42	10
$t_{sim}-t_{obs}$ (hours)	0	-7	-7	-4	- 20	- 2	-2	6	-4.5
V_{OBS} (mm)	7.16	15.27	20.31	15.83	17.14	10.63	15.90	49.55	18.97
V_{SIM} (mm)	3.46	10.45	18.66	6.75	22.28	9.67	10.65	23.90	13.23
% Error runoff volume	- 52	- 32	- 8	- 57	30	-9	- 33	- 52	- 26.6
Mean of the % absolute error on the peak discharge	25	Mean of the % absolute error on the runoff volume		34	Mean of the % absolute error on the timing (hours)				6

Table 4. Results of the distributed simulation for the observed floods (runoff coeff. approach).

When the timing between the simulated and the observed peak is considered, the model is simulating the peak earlier, with good timing for half of the events and quite a long delay (20 hours earlier) for the event occurred in June 1997, which turns out to be a difficult simulation exercise as the high errors show. However, in summary, it can be assessed that this procedure is reliable enough. It can be preferred to the standard CN method approach based on the API5 estimate also because the event simulation can be carried out without the estimate of the initial soil moisture condition. When the AMC class is selected, instead, on the basis of the API30 value, better performances can be obtained.

5. THE SIMULATION OF THE SYNTHETIC HYDROGRAPHS

By analysing the performances of the distributed model used to simulate the eight flood events occurred in the Tevere basin since 1994 up to 2001 it was possible to find a reliable modelling framework. At this point it is also interesting to force the model with a precipitation with given return period with the aim of reproducing a flood of the same frequency. The procedure used, based on the joint use of precipitation depth-duration frequency curves for the basin and observed hyetographs, is shown in the next paragraphs. A second matter concerns the validation of simulated scenarios. For this purpose it seems reasonable to verify the ability of the model to reproduce peak discharges for the closure section, the only one with suitable hydrometric observations. At this section, in fact, a suitable probabilistic model of the yearly maximum peak discharge can be inferred, since the annual maximum of peak flow was measured from 1925 up to 1970 and can be integrated with recent observations. For the discharges observed in the Tevere River at the section of Ponte Nuovo a Gumbel distribution (Extreme Value distribution type I) was assumed, as suggested by *Bencivenga et al.* (2001). As a consequence, to the eight selected flood events a return period shorter than 10 years is assigned.

The maximum rainfall depth $h_{d,T}$ for a given duration d and return period T was evaluated on the basis of the depth duration curves of the stations for which high intensity precipitation observations are available. Each depth-duration curve provides a point value of $h_{d,T}$, but usually average values over the whole basin and/or over a part of it are needed. In order to estimate the mean areal value of rainfall depth for a given duration and return period two procedures can be adopted. The first involves for each return period the estimate of the point depth duration curve for the corresponding Thiessen polygon: the average rainfall depth over the basin area is then computed as a weighed mean of the rainfall depth for each polygon, the weights being the ratio between the area of each polygon and the total area of interest. The second procedure involves the estimate of a unique areal-average depth duration curve through a weighed mean of the parameters of the point depth-duration curves, as shown in the following expression:

$$h_{A,T,d} = \left(\sum_{i=1}^{N} \frac{A_i}{A} a_{i,T} \right) \cdot d^{\left(\sum_{i=1}^{N} \frac{A_i}{A} n_{i,T} \right)} \qquad (4)$$

where the brackets include spatial averages of the parameters a and n usually used in Italy for the representation of the $h_{d,T}$ curves at a given return period T, N is the number of rain gauges in the basin, A is the area of the basin, A_i is the area of the polygon pertaining to

the ith rain gauge.

For the point precipitation reduction factor a value of 0.91 was found through the relationship formulated by *Moisello and Papiri* (1986), on the basis of the analysis of a quite long series of rainfall data for a relatively dense network of rain gauges around the city of Pavia. Accordingly, for the area of 4147 km^2 and duration of 30 hours the previous value is found. The duration of the rainfall event was established on the basis of the estimated concentration time t_c. It is here worth to remark that if the relationship suggested by the U.S. Weather Bureau had been used, a value of 0.92 would have been found.

Once the rainfall depth of the design storm event has been fixed, a synthetic hyetograph of the event can be built, selecting the spatial and temporal distribution of rainfall. As far as the spatial distribution is concerned, the spatial variability of rainfall observed during some flood events has to be preserved, as suggested for instance by *Recaldini* (2004) and *Castelli et al.* (2006).

In this work, in order to reproduce a realistic spatial and temporal distribution of rainfall, each of the analysed events is assumed to be representative of the spatial and temporal distribution of rainfall after it has been rescaled in a proper way. For each of the eight selected events, the maximum rainfall depth ADO=$h_{max,d}$ with the same duration d of the critical event (assumed to be 30 hours) is computed. Then, the critical areal rainfall depth with a given return period ADDF=$h_{A,T,tc}$ previously computed, is divided by ADO and the ratio RF=ADDF/ADO is quickly obtained. By multiplying each observed hyetograph by the respective value of RF, the areal mean value ADDF is precisely reproduced. In this way the spatial and temporal distribution of the events observed in the Tevere River basin at Ponte Nuovo is preserved. When each of the available events is rescaled, actually only one particular event is considered, one out of an infinite number of possible hyetographs, corresponding to the areal rainfall depth computed for a given return period. For this reason the simulations are considered to be all "equally realistic" and therefore all representative of potential flood scenarios. The procedure is then validated by averaging the computed peaks and comparing them to those estimated "at-site" from the probability distribution of peak discharges. In Table 5 the average peak discharge of the simulated scenarios are compared to the peak discharges Q_T inferred from the probability distribution.

As shown in Table 5, for the events having a return period of 10, 100 and 200 years, the results obtained with the distributed runoff coefficient approach are quite satisfactory, with an error on the peak discharge lower than 10% for 12 cases out of 18. The percentage error decreases when the event with the poorest performances is not considered, that is the one occurred in December 1998, probably as a consequence of the rainfall short duration and low depths that actually occurred.

It was in fact observed that also the events occurred in January 1994 and December 1996, not listed in the table but again with rainfall durations shorter than the one of the critical event (30 hours) and rainfall depths very low (around 30 mm all together), are not to be considered representative, as explained earlier. One of the advantages of the procedure used to determine the synthetic hyetograph is actually to maintain the same spatial and temporal distribution of the observed storm. This means though that if the rainfall has a short duration (as in January 1994, in December 1996 and partially in December 1998), the obtained design event will have the same duration and the intensity will be higher, even too much high, causing an overestimate of the peak discharge in the

distributed model.

The results of the simulations show also that a linear relationship can be observed between rainfall and peak discharge, as expected form the distributed model coupled to the runoff coefficient approach.

		Retun period (years)	10	100	200
		Q_{cr} (m^3/s)	1107	1538	1665
30th December 1995	CN procedure	Q_{sim} (m^3/s)	1740	2930	3329
		% error peak discharge	57	90	100
	Runoff coeff. approach	Q_{sim} (m^3/s)	1140	1655	1777
		% error peak discharge	3	8	7
17th November 1996	CN procedure	Q_{sim} (m^3/s)	1072	2311	2951
		% error peak discharge	- 3	50	77
	Runoff coeff. approach	Q_{sim} (m^3/s)	1099	1570	1750
		% error peak discharge	- 1	2	5
1st June 1997	CN procedure	Q_{sim} (m^3/s)	1290	2906	3244
		% error peak discharge	16	89	95
	Runoff coeff. approach	Q_{sim} (m^3/s)	1000	1548	1668
		% error peak discharge	- 10	1	0
4th December 1998	CN procedure	Q_{sim} (m^3/s)	1621	3403	3741
		% error peak discharge	46	121	125
	Runoff coeff. approach	Q_{sim} (m^3/s)	1514	2246	2369
		% error peak discharge	37	46	42
9th February 1999	CN procedure	Q_{sim} (m^3/s)	804	2069	2780
		% error peak discharge	- 27	34	67
	Runoff coeff. approach	Q_{sim} (m^3/s)	1250	1920	2203
		% error peak discharge	13	24	32
24th December 2000	CN procedure	Q_{sim} (m^3/s)	1280	2992	3767
		% error peak discharge	15	94	126
	Runoff coeff. approach	Q_{sim} (m^3/s)	1103	1604	1798
		% error peak discharge	0	4	8

Table 5. Comparison between estimated and simulated discharges for a given return period.

Instead, when the CN method is used, different results are obtained. In this case the difference in the peak discharge is low only for a return period of 10 years, that is not so strange since all the eight events used for the calibration have a return period lower than 10 years. When higher return periods are considered (and therefore higher rainfall depths) the model provides much higher peak discharges, and the difference between the two estimates of the peak discharge can be higher than 100% (T=200 years).

With reference again to the CN method, the relationship between peak discharges and rainfall is not linear and the results obtained, quite different from event to event, show the marked influence of the rainfall spatial distribution on runoff discharges. The last observation is true of course also for the runoff coefficient approach.

In summary it can be stressed that for rainfall depths lower than the design depth for a 10 years return period, the model is reliable. On the other hand, for less frequent events the two approaches have to be distinguished, because quite high peak discharges are obtained with the CN method. Events characterised by rainfall duration lower than the concentration time are not to be considered for scenarios purposes.

6. COMPARISON WITH A LUMPED MODEL

Since lumped hydrological models are easy and quick to apply, results of a lumped model are compared to the distributed simulation obtained with the quite complex procedure explained in the previous paragraphs.

Lumped models describe the hydrological response of the basin through very simple conceptual schemes preserving the water balance of the basin and usually rely on elemental analogical schemes that can be combined in different ways to reproduce the involved hydrological processes. In order to develop this kind of models two 'lumping' actions are performed:

- input (total rainfall) and output (runoff) definition, observed or estimated with reference to a particular location within the basin, not to the actual spatially distributed variables;
- global evaluation of the pedological, morfological and hydrological structure of the basin through global parameters, not dependent again from its spatial variability.

For the mathematical simulation of a flood event, the definition of the hyetograph of the spatial rainfall intensity i(t) and the discharge only at the outlet section is therefore required.

Then, for the estimate of the effective rainfall, the value of the CN parameter and of the maximum capacity S can be assigned, together with the parameters' values of a routing model for the simulation of the flood hydrograph. For this study a Nash model was used.

Good results are obtained when the runoff coefficient approach is used for the simulation of the events of Table 1. The error in runoff volume is lower than 20% for 5 out 8 events, while the peak discharge is even better reproduced: for 5 out of 8 events the error is lower than 10% while for 7 out of 8 the error is lower than 20%. Moreover, the time shift between the simulated and the observed peak discharge is shorter than that obtained with the CN method coupled to the distributed model: 1-2 hours. Therefore the last procedure gives a chance to apply a reliable lumped model for the simulation of flood events for the Tevere River at Ponte Nuovo, leaving a useful warning time that Civil Protection Services have to manage in case of potential hydro-geological risk.

As already explained for the distributed model, also for the lumped model scenarios with a given return period were built.

Again, the analysis was carried out for return periods of 10, 100 and 200 years. Peak discharges and rainfall values characterising this low frequency events are the same reported in the previous analysis but here the approach is different: the hyetograph is assumed to be constant, with duration equal to the basin concentration time (30 hours).

Discharges corresponding to the selected return period were estimated on the basis of the synthetic hyetograph and using:
- the CN-SCS method, with average CN value equal to 71, AMC class II and initial abstraction equal to the 20% of the potential retention S,
- the runoff coefficient approach, with the average runoff coefficient.

In order to represent the response of the river network, a Nash model was used, calibrating the value of the parameters (the time constant k and the number n of reservoirs) on the basis of the eight available events, that is:

$$k = 8 \text{ h} \qquad n = 3$$

Also for the lumped model it can be assessed that the runoff coefficient approach

provides results in agreement with the peak discharges inferred from the statistical distribution, with errors on the peak discharges lower than 5%. The CN approach leads to different results: the error is low only for a 10 year return period (2%), while for longer return periods the discharge is definitely overestimated (the error increases up to 40%).

The results of the simulations in the distributed and lumped conceptualisation are quite interesting. The two models behave in a similar way even if they show some differences due to the type of spatial representation they rely on. In both cases results are satisfactory when the runoff coefficient approach is used but the simulated discharges are too high when the CN method is used.

It is here worth to notice though how for the less frequent events the observed peak discharges are affected by the routing effects produced by areas adjacent to the river bed. An overestimate of the simulated discharge obtained by applying rainfall-runoff models not taking into account these phenomena is then to be expected

On the other hand results of the application of a lumped model to the Tevere River at Ponte Nuovo show that results are globally satisfactory, when a runoff coefficient equal to 31% (the arithmetic mean of the observed selected events) is used. Results of the peak discharge simulation obtained with the distributed and with the lumped model are summarised in the following Figures 4a and 4b, referring respectively to the CN-WAPI30 procedure and to the runoff coefficient approach.

7. CONCLUSIONS

The increasing frequency of severe flood events in the Upper Tevere watershed has motivated the set up of a distributed hydrological model to simulate some flood events that have occurred in the past years. Then a series of synthetic hyetographs were generated for several sections of the river network and for several return periods, up to the outlet section at Ponte Nuovo. The synthetic storms preserved the shape and the spatial distribution of the observed hyetographs during some intense observed events, so that their mean areal rainfall depth was set equal to the one inferred for the given return period.
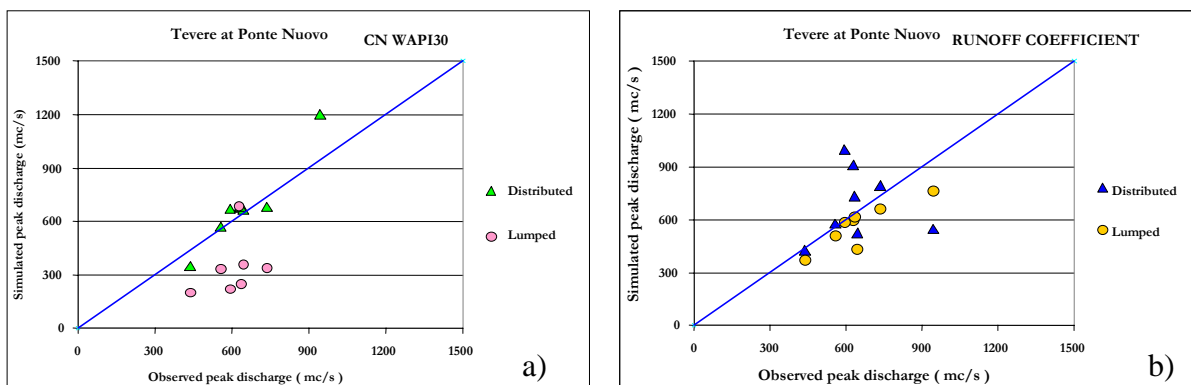
Figure 4. Comparison between observed and simulated discharges: CN-API30 coupled to a lumped and a distributed model (a) and runoff coefficient coupled to a lumped and a distributed model (b).

Obtained results showed how the runoff coefficient approach provides peak discharges at the section of Ponte Nuovo in agreement with the corresponding statistical flood

quantiles, while the distributed CN method, for return periods longer than 100 years, leads to a strong overestimate of peak flow retrieved from the statistical analysis of a quite long series of annual maxima. This is due to the fact that with the CN method the soil saturation is reached quickly and a larger volume of surface runoff is produced. It is not to be neglected though that the hydrological model of runoff production and propagation is expected to overestimate peak discharges even with return periods longer than 5 years, also because it does not take into account the possible overflow and routing effects of floodplain areas during less frequent floods. It is then correct that the model based on the CN-WAPI30 estimate provides higher peaks. When coupled to a hydraulic model able to account for the geometry of the perifluvial bands, the simulations could be more reliable.

In order to evaluate the advantages and the disadvantages of a distributed approach with respect to a lumped one, results obtained with the two approaches are compared.

In summary, it can be assessed, with some caution, that both approaches (distributed with CN-WAPI30 or a lumped runoff coefficient approach) give satisfactory results. It is worth to remark though that the distributed model can better take into account the real spatial distribution of precipitation and of the hydro-geological, morphological and hydrographic characteristics of the basin. With a distributed approach also the flood hydrographs at any selected point of the river network can be reproduced and this is a requirement for hydraulic models used to simulate overflows. It is an advantage of the distributed approach, mainly for large watersheds as Tevere River at Ponte Nuovo, because the flood event simulation can be validated at intermediate sections and the hydrological processes inducing runoff generation and its propagation to the outlet can be better analysed for each subbasin.

REFERENCES

Bacchi, B., and R. Ranzi (editors) (2000), Runoff and Atmospheric Processes for flood Hazard Forecasting and Control, Contract ENV4-CT97-0552, Final Report, Brescia.

Bacchi B, and R. Ranzi (2003), Hydrological and meteorological aspects of floods in the Alps: an overview, *Hydrology and Earth System Sciences*, *7*(6), 784-798.

Bencivenga, M., G. Calenda, and C.P. Mancini (2001), Ricostruzione storica delle scale di deflusso delle principali stazioni di misura nel bacino del fiume Tevere – Il secolo XX, Presidenza del Consiglio dei Ministri, Istituto Poligrafico e Zecca dello Stato (in Italian).

Bougeault, P., P. Binder, A. Buzzi, R. Dirks, R. Houze, J. Kuettner, R.B. Smith, R. Steinacker, and H. Volkert (2001), The MAP Special Observing Period, *Bull. Am. Met. Soc.*, *82*, 433-462.

Cardinali, M., G. Antonini, P. Reichenbach, and F. Guzzetti (2001), Photo-geological and landslide inventory map of the upper Tiber River basin, Italy, *GNDCI publ. n°2116*, Rome.

Castelli, F., F. Caparrini, and L. Castellani (2006), Flood frequency mapping through the distributed modeling and precipitation pattern modulation, *Atti del XXX Convegno di Idraulica e Costruzioni Idrauliche*, Casa Editrice Università La Sapienza, Roma.

Emmet, W.W. (1970), The hydraulics of overland flow on hillslopes, *Geol. Survey prof. paper 662-A*, United States Government Printing Office, Washington.

Grossi, G., and N. Kouwen (2004), Intercomparison among hydrologic simulations coupled to meteorological predictions provided by different mesoscale meteorological models, *Atti del XXIX Convegno di Idraulica e Costruzioni Idrauliche*, Trento, 7-10 settembre 2004, Editoriale Bios, Volume 2, 265-271.

Heggen, R.J. (2001), Normalized antecedent precipitation index, *J. Hydraul. Eng., ASCE*, *6*(5).

La Barbera, P. (1990), Problemi di preannuncio di eventi estremi: modelli geomorfoclimatici, meccanica del debris-flow, Linea 3, *CNR-GNDCI Report*.

Mancini, M. (1991), Modelli idrologici superficiali nella pianificazione di bacino, Ph.D. dissertation, Politecnics of Milan (in Italian).

Mele, F., A. Sabene, G. Pellegrino, G. Borzillo, and F. Napolitano (2006), La gestione in tempo reale della piena del novembre-dicembre 2005 nel bacino del fiume Tevere, Atti del XXX Convegno di Idraulica e Costruzioni Idrauliche, Casa Editrice Università La Sapienza, Roma (in Italian).

Mishra, S.K., and V.P. Singh (2004), Validity and extension of the SCS-CN method for computing infiltration and rainfall-excess rates, *Hydrol. Proc.*, *18*(17), 3323-3345.

Moisello, U., and S. Papiri (1986), Relazione tra l'altezza di pioggia puntuale e ragguagliata, Atti del XX Convegno di Idraulica e Costruzioni Idrauliche, Padova, 615-631 (in Italian).

Natale L., and F. Savi (2004), Analisi Monte Carlo degli scenari di inondazione di Roma, in *Grandi Bacini Idrografici*, Atti dei Convegni Lincei, n. 198, Accademia Nazionale dei Lincei, Roma (in Italian).

Orlandini, S., and R. Rosso (1998), Parameterization of stream channel geometry in distributed modelling of catchment dynamics, *Water Resour. Res.*, *34*(8), 1971-1985.

Ponce, V.M., and V. Yevjevich (1978), Muskingum-Cunge method with variable parameters, *J. Hydraul. Div., ASCE*, *104* (HY12).

Ranzi, R., B. Bacchi, and M. Bocchicchio (2002), Effect on floods of recent afforestation and urbanisation in the Mella River (Italian Alps), *HESS*, *6*(2), 239-265.

Ranzi R., B. Bacchi, and G. Grossi (2003), Runoff measurements and hydrological modelling for the estimation of rainfall volumes in an alpine basin, *Quart. J. Royal Met. Soc.*, *129*, 653-672.

Ranzi, R., and R. Rosso (1994), Scale effects in distributed modeling of energy exchange between snow fields and atmosphere, in *Advances in Distributed Hydrology*, edited by R. Rosso, A. Peano, I. Becchi, and G.A. Bemporad, Water Resour. Publ.

Recaldini, M. (2004), Modello distribuito di piena del Fiume Tevere a Ponte Nuovo, Graduation thesis (unpublished), University of Brescia, A.A. 2003-04.

Rinaldo A., M. Marani, G. Botter, S. Silvestri, A. Bellin, R. Rigon, M. Ferri, F. Baruffi, and A. Rusconi (2004), Sul tempo di Ritorno delle piene: Metodi Geomorfoclimatici-Montecarlo e Fiume Brenta chiuso a Bassano, in *Grandi Bacini Idrografici*, Atti dei Convegni Lincei, n. 198, Accademia Nazionale dei Lincei, Roma.

Rosso, R. (1994), An introduction to spatially distributed modeling of basin response, in *Advances in Distributed Hydrology*, edited by R. Rosso, A. Peano, I. Becchi, and G.A. Bemporad, Water Resour. Publ.

USDA-Soil Conservation Service (1985), *National Engineering Handbook*, Section 4-Hydrology, Washington D.C.

Observing and modelling exceptional floods and rainfalls
Proceedings of the AMHY-FRIEND International Workshop on Hydrological Extremes,
held at University of Calabria, Cosenza (Italy), May 3-4, 2006

SNOWMELT PROCESSES WITHIN THE EXPERIMENTAL BASIN OF "FIUMARELLA OF CORLETO"

D. Carriero, S. Manfreda, M. Fiorentino

Dept. of Engineering and Environment Physics, University of Basilicata, Potenza, Italy

ABSTRACT

The experimental basin of "Fiumarella of Corleto" has been monitored for four years since September 2002. It is provided of an instrumentation that includes one complete meteorological station, three rain gauges and one hydrometer at the outlet. The basin is characterized by conspicuous snowfall during winter periods. For this reason, one of the rain gauges is provided of a heat resistance that allows to quantify the snowy precipitation. Such data has been used to improve a conceptual model for rainfall-runoff simulation by means of a snowmelt module based on the use of degree-day factors or, for smaller time scales, degree-hour factors. The model is a semi-distributed one, where the basin is subdivided in elevation bands accounting for the spatial distribution of snowy coverage, precipitation and temperatures. It was found that the snowfall produces delayed response in the streamflow and also ignoring this process may cause significant errors in the flow discharge estimation during flood events.

1. INTRODUCTION

The application of rainfall-runoff models should be tested using data of experimental basins with detailed hydrological information in space and time. Generally, measurement errors and rough resolution of data may produce a misinterpretation of rainfall-runoff processes specially when we are dealing with different runoff generation processes. For instance, the snowmelt process plays an important role in the runoff generation mechanisms when the sample watershed is located at high altitude. In those cases, detailed measurements of temperature, snow precipitation and a detailed digital elevation model are necessary.

In the last few years, numerous hydrological models have been developed. The *WMO* (1986) operated an intercomparison of conceptual rainfall-runoff models paying attention to their attitude for operational use. Most models consist of two components: a snowmelt module, which simulates the snow accumulation and melting, and a transformation module simulating the streamflow at the outlet. The snowmelt models can be classified into "index" or "energy balance" models: the former are generally based on temperature data whose spatial distribution is evaluated by means of a lapse rate, while the second requires a greater number of meteorological data (solar radiation, air humidity, wind speed, etc.).

The "energy balance" approach allows to better evaluate the spatial distribution of the snow coverage over the basin, that can be validated by observed data as those derived from point measurements, remote sensing images or aerial photos. For instance, *Blöschl et al.* (1991a, b) proposed an energy based model for the estimation of the spatial distribution of the snow water equivalent, but they had serious difficulties in the use of

point measurements since the water equivalent may vary significantly over small distances. Therefore, given the influence of the topography, the wind and the gravity effects, the authors proposed a linear interpolation of the snow water equivalent as a function of the local elevation, the slope and curvature.

A detailed snowmelt simulation is described in the work of *Zanotti et al.* (2004) where an energy-based snow module is proposed for the GEOTOP model (*Bertoldi et al.,* 2004): the soil-snow energy and mass exchanges are involved together with a runoff production module. Great attention is paid to the soil characteristics whose parameterization is fundamental for a correct schematization of the physical processes involved. Snow accumulation and successive melting are calculated following the UEB scheme (*Tarboton and Luce,* 1996), an energy-based one-layer snow model that is physically consistent but computationally efficient enough to be used in a basin-scale distributed model. The daily snow water equivalent simulated shows a good fitting with the observed one obtained by means of data of daily snow depth and average snow density at different stratigraphic profiles. It is besides highlighted the effect of slope and aspect: snow cover is much more shallow or nearly absent in steep south-facing slopes.

The increasing availability of meteorological data drives many researchers to develop "energy balance" models with an increasing complexity and difficult to be tested. The *WMO* (1986) analyzing various kind of models highlighted that the temperature represents the main factor for the evaluation of the snow precipitation and, after the accumulation in the snow pack, of the melting portion. For these reasons, simple models based on the degree-day method, where the daily snowmelt depth is computed by means of a melting factor and of the temperature, have a great diffusion. In the years they were improved incorporating the radiation data in the snowmelt equation (*Brubaker et al.,* 1996).

The study cases presented in the literature are generally mountain basin in which it is easily distinguishable an accumulation and a melting period with the individuation of the runoff component caused by the snowmelt. In the present work the sample watershed, afterwards described, is on the Apennine with a mean altitude of about 1000 m. In this case, the snowmelt contribution to the streamflow, less consistent in comparison with the mountain basins, shows a delayed response and smoothing effects on the basin hydrograph. This behaviour is particularly evident at scale event during which other physical quantities (e.g., solar radiation) play a secondary role: that justifies, in this study, the use of a simple model based only on temperature data.

The paper is organized as follow: in the first part the basin is described in all its physical and hydrological characteristics, in the second part the results of a semi-distributed simulation model are showed with particular attention to the snowmelt processes that characterize a considerable number of flood events.

2. "FIUMARELLA OF CORLETO" EXPERIMENTAL BASIN

The "Fiumarella of Corleto" River is an affluent of the Sauro River (Agri basin) located in Basilicata region (Southern Italy), with an area of about 33 km^2, a mean altitude of 1050 m (ranging from 650 to 1500 m), characterized by a sub-humid climate (mean annual precipitation 720 mm). The mean annual number of flood events is 10, in particular in winter and spring period with about the 50% of them characterized by a snow contribution.

The great interest developed on this basin, by now monitored from September 2002, grows up from its particular land use, characterized by forest for the right hillslope and by prevalent agricultural crops for the left one, that allows to study the two respective hydrological response (*Fiorentino et al.,* 2006). This is described on the land system map (Figure 1a), elaborated by *Santini et al.* (1999), where each unit is identified by a specific vegetation and soil type: the first attribute allows the definition of a land use map (Figure 1b) the second is only a qualitative description of the soil. For this reason, the second aspect was deepened for the definition of the soil physical characteristics by means of the data obtained along two linear transects established at the opposite sides of the stream channel (*Romano and Palladino,* 2002). Every transect is constituted by 88 undisturbed soil cores spaced 50 m apart that have been analysed by means of laboratory measurements in order to define: texture, organic matter, etc. The geographical intersection of the transect points with the unit map allowed the characterization of almost all units with the definition of the mean value of the features previously described. For the zones without available information, the data was integrated with a land system map of the whole Agri basin whose soil classification was realized according to the HYPRES (HYdraulic PRoperties of European Soil) database that defines also the hydraulic characteristics (*Carriero et al.,* 2005). The soil characterization is articulated in the following physical quantities: texture, according USDA classification, organic carbon, thickness.
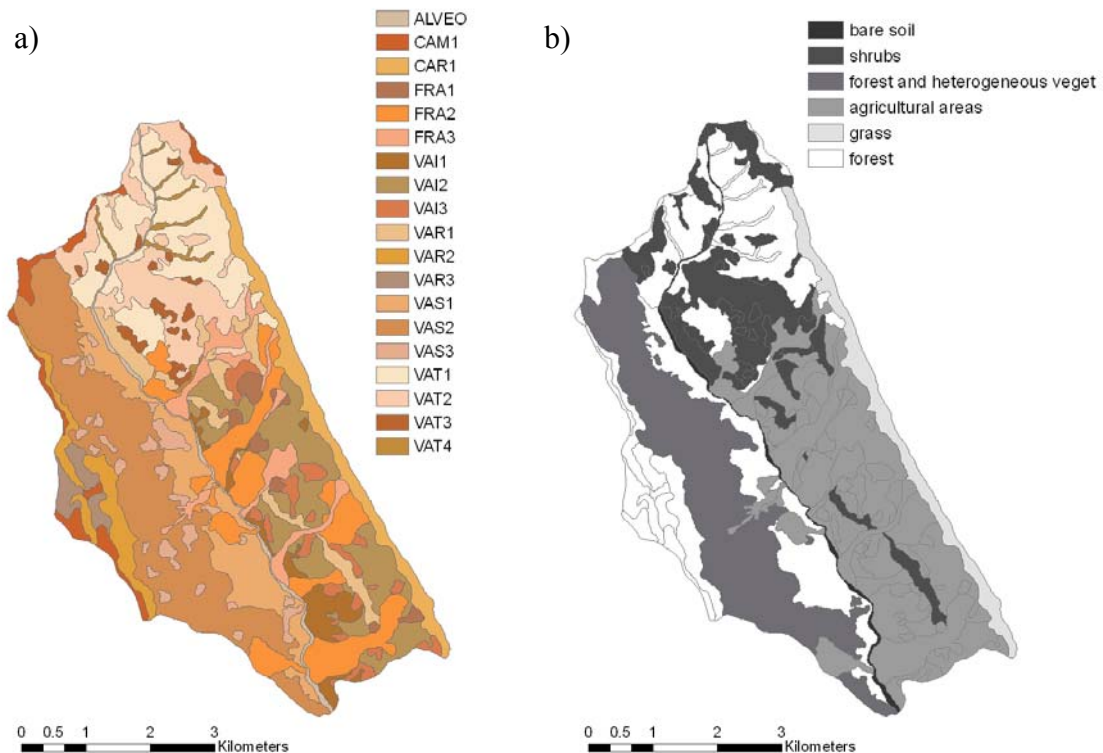
Figure 1. Land system map (a) and land use map (b) of the Fiumarella of Corleto.

The use of simplified techniques allows to define the hydrological quantities generally required by the simulation models such as: field capacity, water content at saturation, etc. These are the ptf (Pedo Transfer Functions), statistical functions that allow to derive the hydraulic soil characteristics from the physical ones. In particular, we used for the estimation of soil water content at saturation θ_s (*Saxton et al.,* 1986):

$$\theta_s = 0.332 - 7.251 \cdot 10 - 4(\% \text{ sand}) + 0.1276 \cdot \log_{10}(\% \text{ clay}),$$

for the estimation of the residual water content θ_r (*Vereecken et al.,* 1989):

$$\theta_r = 0.015 + 0.005(\% \text{ clay}) + 0.014(\% \text{ C}_{\text{organic}}),$$

for the evaluation of the field capacity θ_c (*Rawls et al.,* 1982), hypothesized as the value of the water content at the potential h=-33 kPa:

$$\theta_c = 0.2576 + 0.002 \text{ (\% sand)} + 0.0036 \text{ (\% clay)} + 0.0299 \text{ (\%C organic)}.$$

Finally another ptf (*Cosby et al.,* 1984) was used for the estimation of the hydraulic conductivity at saturation K_s:

$$K_s = 0.6096 \cdot 10 - 0.6 + 0.0126(\% \text{ sand}) - 0.0064(\% \text{ clay}).$$

The resulting physical and hydraulic characteristics of soil are given in Table 1.

Unit	% Clay	% Sand	% Silt	Depth (cm)	Porosity Index	Organic matter	θ_c	θ_r	θ_s	K_S (mm/h)	Land use
Alveo	0	0	0	70	4.5	0	0.35	0.15	0.45	12	bare soil
Cam1	29.17	34.97	35.85	72	8.4	2.66	0.372	0.198	0.494	11.45	forest
Car1	27.8	30.81	41.4	90	6	1.86	0.352	0.18	0.494	10.35	grass
Fra1	41.65	15.07	43.28	53	10	1.76	0.43	0.248	0.528	5.35	agricultural areas
Fra2	41.65	15.07	43.28	53	10	1.76	0.43	0.248	0.528	5.35	agricultural areas
Fra3	41.65	15.07	43.28	53	10	1.76	0.43	0.248	0.528	5.35	agricultural areas
Vai1	41.65	15.07	43.28	53	10	1.76	0.43	0.248	0.528	5.35	agricultural areas
Vai2	31.53	21.59	46.88	80	8.4	1.93	0.386	0.2	0.508	7.5	agricultural areas
Vai3	42.22	18.49	39.28	80	10	2.73	0.454	0.264	0.526	5.86	agricultural areas
Var1	38.37	17.12	44.51	60	7.6	2.65	0.441	0.244	0.522	5.96	shrubs
Var2	37.65	33.79	28.55	20	8.4	4.68	0.465	0.269	0.509	9.76	forest
Var3	38.01	25.46	36.53	60	8.4	2.73	0.425	0.243	0.515	7.63	forest
Vas1	35.46	23.19	41.35	70	8.4	2.9	0.426	0.233	0.513	7.41	forest
Vas2	42.67	17.16	40.16	60	10	2.71	0.458	0.266	0.528	5.6	forest & heter. veget.
Vas3	47.68	16.17	36.15	50	10.8	3.02	0.487	0.296	0.534	5.05	forest & heter. veget.
Vat1	MF	MF	MF	35	6.5	MF	0.406	0.2	0.5	7.5	forest
Vat2	MF	MF	MF	35	6.5	MF	0.406	0.2	0.5	7.5	shrubs
Vat3	MF	MF	MF	35	6.5	MF	0.406	0.2	0.5	7.5	shrubs
Vat4	MF	MF	MF	35	6.5	MF	0.406	0.2	0.5	7.5	forest

Table 1. Physical and hydraulic characteristics of the land system units (MF*: medium-fine*).

The hydrological data is recorded by three stations, two of which located on opposite hillslopes, in consideration of the different land use previously described, and the third at the basin outlet (Figure 2). The station n.1 (at 1115 m a.s.l.) is composed by a rain gauge, that becomes a snow gauge at low temperatures with the activation of a heat resistance, a temperature sensor (active from September 2002), and sensors for the measurement of the solar radiation, air relative humidity, wind velocity and direction, soil moisture (TDT) (active from November 2004). The station n.2 (at 680 m a.s.l.) is composed by a rain gauge and an ultrasound hydrometric sensor, while the station n.3 (at 1040 m a.s.l.) is equipped simply with a rain gauge.

METEO-HYDROLOGICAL STATION

RAIN GAUGE (sept. '02)

Station 3

Station 1

Station 2

HYDROMETER AND RAIN GAUGE
(sept. '02)
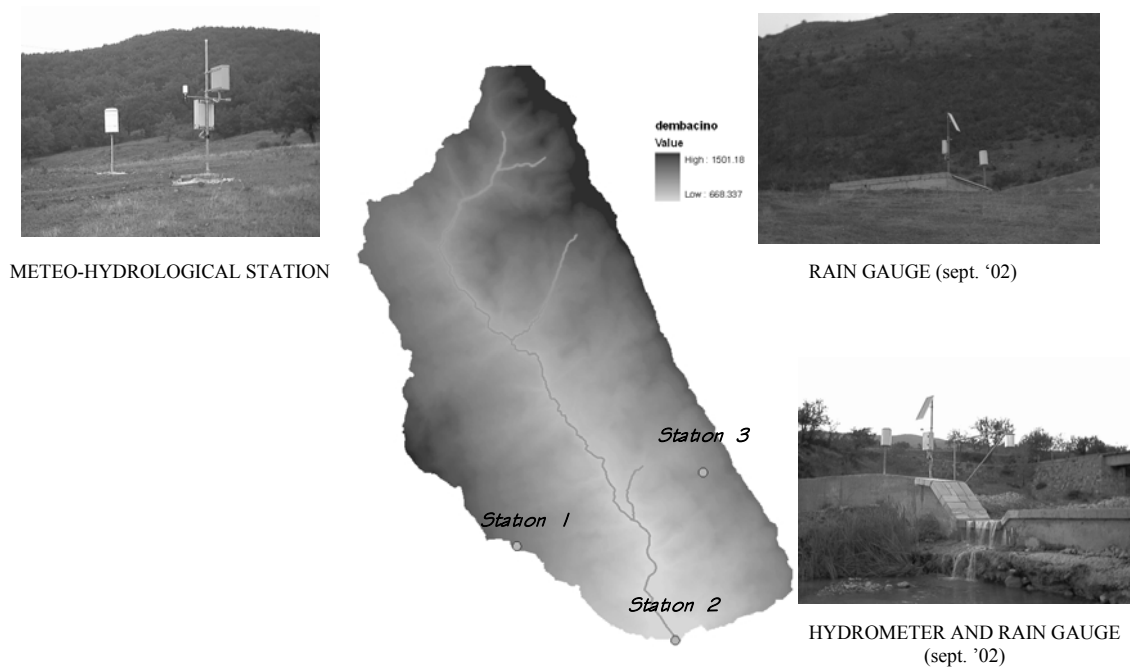
Figure 2. Description of the hydrological instrumentation and the structure of the experimental basin described through a high resolution DEM (1x1 m).

3. ANALYSIS OF THE HYDROLOGICAL DATA

The recorded database was used to investigate on the flood events and their main hydrological characteristics (lag-time, recession curve constants, etc.) in order to deepen the watershed hydrological response and, successively, to utilize the same parameters in the simulation model.
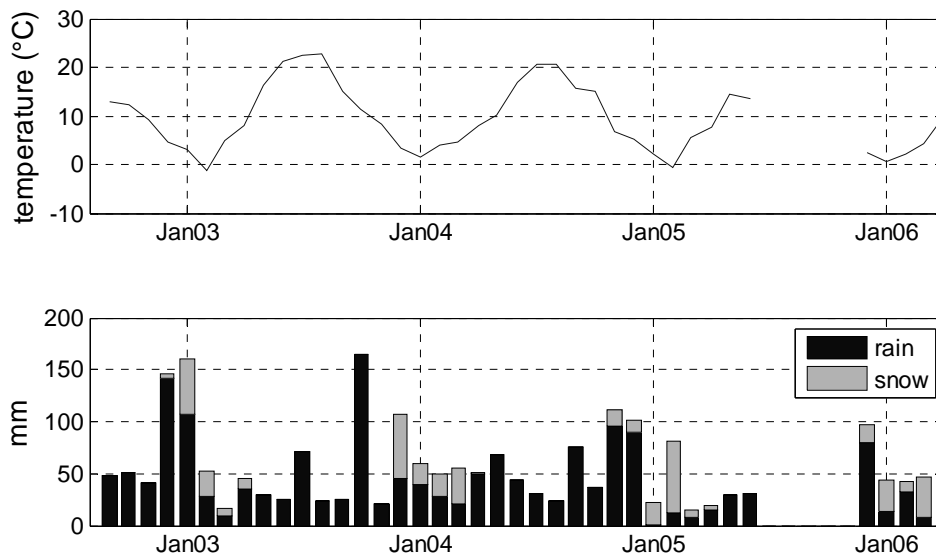
Figure 3. Measurements of monthly average temperature and monthly precipitation given as the sum of rain plus snow (distinction is based on temperature) at the station n.1.

During the winter period, the monthly mean temperature (Figure 3) is very close to the 0°C and consequently the snowy precipitation volumes, evaluated on the basis of the temperatures as afterwards better explained, are conspicuous for these periods and not

negligible for an hydrological study and a consequent simulation.

From the recorded hydrographs, it is possible to derive the recession curves constants k interpolating the flow data with an exponential equation $Q=Q_0 \cdot e^{-t/k}$. The successive step is the separation of the hydrograph in order to define the effective rainfall volume and the lag-time of each flood event. All this quantities are investigated in comparison with the flood peaks with interesting results, as it can be seen in Figure 4. The lag-time and the surface recession constants have a decreasing dispersion with the increase of flood magnitude: this is probably due to a change in the behaviour of the basin response under intense and severe precipitations that may produce the saturation over the whole basin even in presence of heterogeneous soils (in terms of physical characteristics and vegetation coverage). In this case, the role held by the snow, which will be better described in the simulations, can be considered negligible because it doesn't influence in a determinant way the tendency in the graphs.
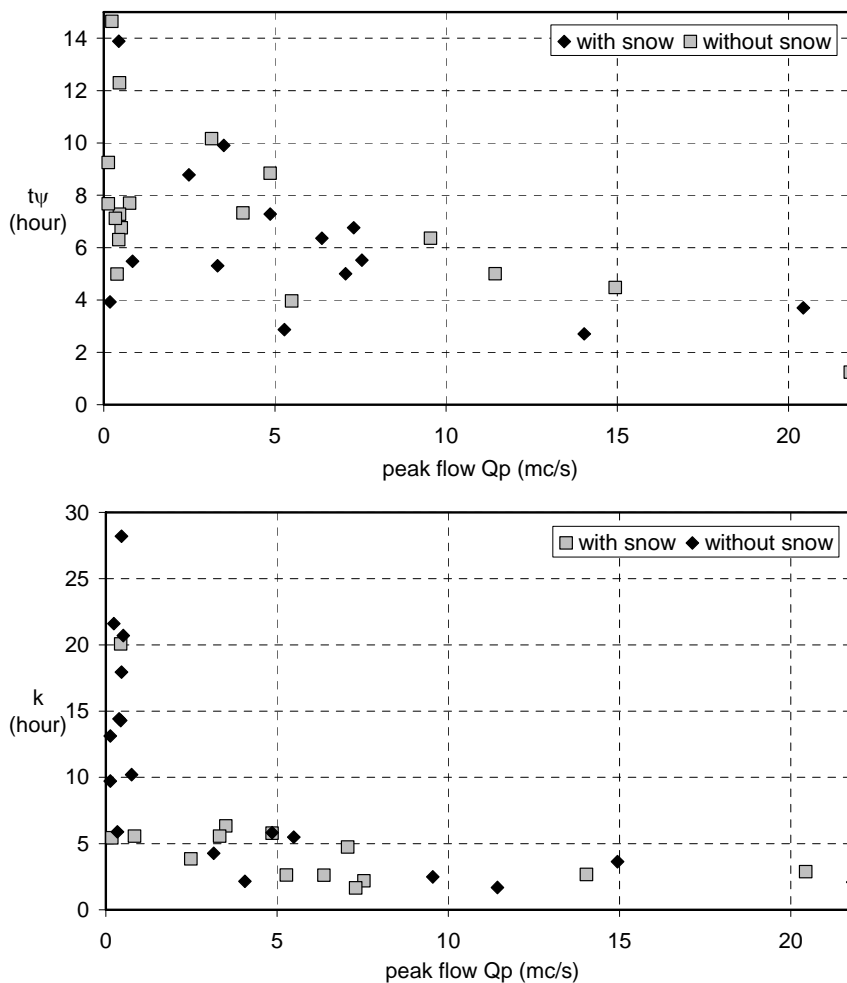
Figure 4. Lag-time and recession curve constants of the streamflow due to the surface runoff as a function of the basin floods peak.

4. RAINFALL-RUNOFF SIMULATION MODEL WITH SNOWMELT MODULE

The hydrological simulation is operated by means of a semi-distributed model, the AD3 that is an evolution of the concentrated one AD2 (*Fiorentino and Manfreda,* 2004*; Manfreda,* 2005). The AD3 is a physically based model that schematizes the basin as

sequence of buckets in series representative of altitude bands. The temperature of each band is calculated from those measured at the station n.1 assuming a lapse rate of 6.5°C.

The water balance equations are governed by threshold parameters that allow to estimate the main outflow components (surface runoff, subsurface runoff, base flow). Such parameters are derived from the main catchment physical characteristics: the maximum water storage volume of the single bucket is determined as $S_{max}=\theta_s \cdot D$ where θ_s is the soil water content at saturation and D is the soil thickness, while the water storage volume at field capacity is $S_c=\theta_c \cdot D$ where θ_c is the water content at field capacity. When the water volume S_t at the time t exceeds S_c we have the generation of the subsurface runoff RI_t while when it exceeds S_{max} we have the generation of the surface runoff (saturation excess) that, summed to the quantity $C \cdot S_t/S_{max} \cdot P_t$, supplies the P_n (net precipitation), with C runoff coefficient (hortonian process), depending to the slope and the vegetation coverage, and P_t the total precipitation. All the water volume involved in the balance equation are transformed in the respective flows by means of the linear reservoir law $Q_t=W_t/k$ where the own recession constants (surface, subsurface, deep) for the main outflow components are calculated interpolating the observed data as previously explained. The complete description of the soil water balance is schematized in the Figure 5.
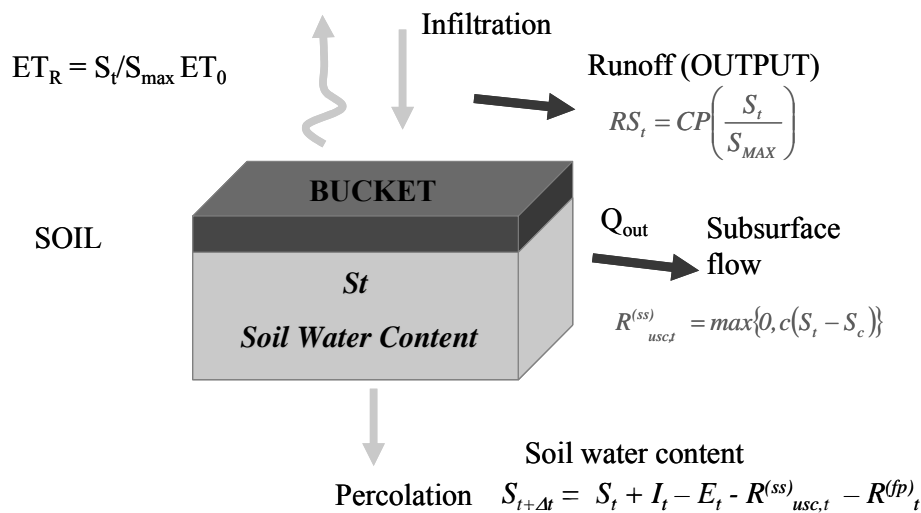
Figure 5. Schematization of the soil water balance within the model AD3.

The evolution from the AD2 into the AD3 model is made including a snowmelt module based on the degree-day method: this is an empirical method that simplifies the melting dynamic as a function of the variations in the air temperature neglecting the effects of solar radiation, air humidity, wind, etc. The choice of a simulation module based only on temperature data is due to the fact that the record of temperature was significantly longer than other variables and also because within the simulation model quantities like the solar radiation are negligible at the event scale. Besides, the use of a simplified method facilitates the analysis on the final basin outflow because of the limited number of model parameters.

The control volume is represented by the snow pack whose water content is quantified by the snow water equivalent (SWE) i.e. the equivalent depth of water of a snow cover: it is the result of the balance between snowmelt and refrozen water (Figure 6).
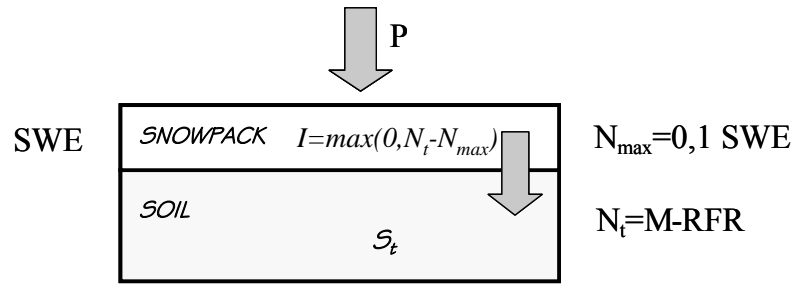
$$M = M_f(T_a\text{-}T_0) \qquad RFR = M_{fr}\,(T_a\text{-}T_n)$$

Figure 6. Snowmelt module.

The snowmelt process simulation is based on the simple equation:

$$M = M_f\,(T_a\text{-}T_0)$$

where M (mm) is the melting water depth, M_f (mm/°C) is the melt factor, T_a (°C) the mean air temperature and T_0 (°C) the base temperature. M_f depends on the snow density and it generally varies from 3.5 to 6 mm/°C (lower values are recommended for fresh snow and for snow cover under forest canopy), while T_0 is assumed equal to 0 °C (*Gray and Prowse,* 1993). Part of the melting water refreezes, RFR (mm), when the air temperature $T_a < T_n$:

$$RFR = M_{fr}\,(T_a\text{-}T_n)$$

with M_{fr} refreezing factor, generally equal to 0,05 mm/°C, and T_n reference temperature, about -1,5 °C. M and RFR contribute to the mass balance of the SWE. A threshold parameter is represented by the snow pack water capacity retention (N_{max}): all the water at the liquid state that overcomes this value infiltrates into the soil. In general, the water holding capacity of the snow pack decreases as melting occurs. During the melting process an acceptable value relating to real systems is between 2 and 15%; the value of freshly fallen snow can be as high as 55%; ten percent is a typical average value used in many models (*Bergström,* 1976).

In consideration of the various atmospheric requirements for snowfall formation, a single value of the air temperature cannot be taken as a discrimination parameter between snow and rain. In the simulation, it is assumed a temperature interval in which the precipitation is a mixture of rainfall and snow as defined by the *U.S. Army Corps of Engineers* (1998):

$$P_s = P\text{-}P_r \qquad \text{with} \qquad P_r = \begin{cases} P & T_a \geq T_r \\ P \cdot \dfrac{T_a - T_b}{T_r - T_b} & T_b < T_a < T_r \\ 0 & T_a \leq T_b \end{cases}$$

where:
T_a is the air temperature;
T_r is the air temperature value above which all the precipitation is considered liquid;
T_b is the air temperature value below which all the precipitation is considered snowy;
P is the total precipitation measured at the snow gauge;
P_r is the estimated liquid precipitation;
P_s is the estimated snowy precipitation.

The values of T_r and Tb chosen for this case of study are respectively 3 °C and 0 °C.

This kind of module was originally created for daily balance but considering the short lag time and duration of the floods of the studied watershed, it was adapted at hourly scale with encouraging results.

5. RESULTS AND DISCUSSION

The results showed several differences between a simulation with and without the snowmelt module. In the three cases reported herein, it was necessary the use of a snowmelt module in order to increase the predictive capabilities of the model. In the Figure 7 (4th February 2003 event), it may be noticed that the use of a snowmelt module causes a smoothing effect on the second peak flow occurring during a drop in the air temperature.

The Figure 7 (3rd January 2004 event) also demonstrates how the model capability have been improved changing the simulated hydrograph: in fact the hyetograph presents two precipitation events separated by an interval of one hour that should cause the generation of two distinct peak flows. The snowmelt process produces a delay effect on the basin response that unifies the two precipitation contributions in a unique peak flow. It can be also noticed a significant difference in the components of the simulated streamflow. Including the snowmelt module in the simulation, we obtain a reduction of the superficial runoff volume with consequent increasing of the subsurface one. This is a consequence of the surface runoff simulation mechanism based on the hortonian process in which only the precipitation at liquid state is involved; the snow, instead, accumulates in the snow pack that, melting, increases the soil water content and consequently the subsurface runoff characterized by a slower hydrologic response. The surface runoff volume production visible in the simulation is mostly due to the soil saturation.

Finally, the Figure 8 (21st February 2005) describes the combination of the model applications at daily and hourly scale: through the use of a continuous simulation at the daily scale has been possible to evaluate the initial moisture condition and also the snow cover caused by antecedent snowfall, removing, in this way, the underestimation observed in the initial part of the simulated hydrograph obtained with AD3 without snowmelt module. As in the previous case we observed a significant increase of the subsurface runoff and a reduction of the surface runoff for the same reasons explained before.
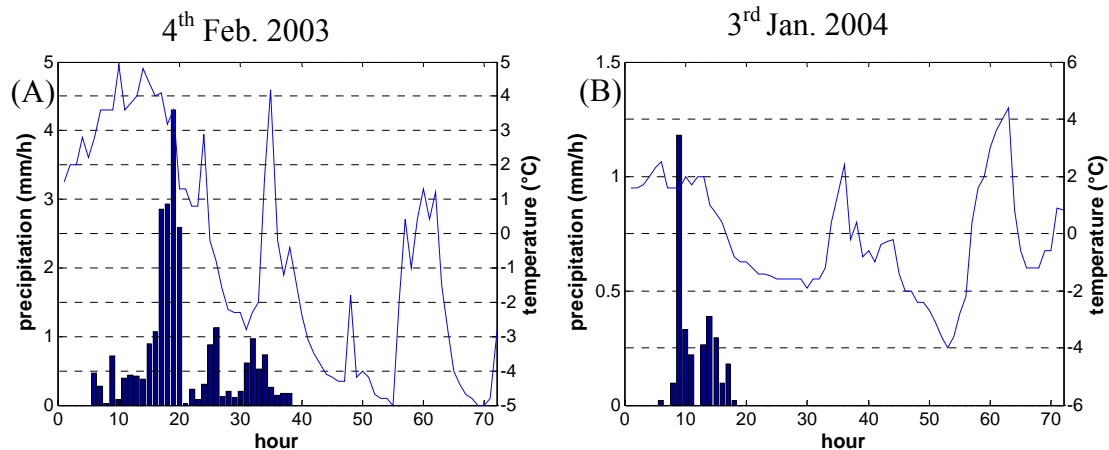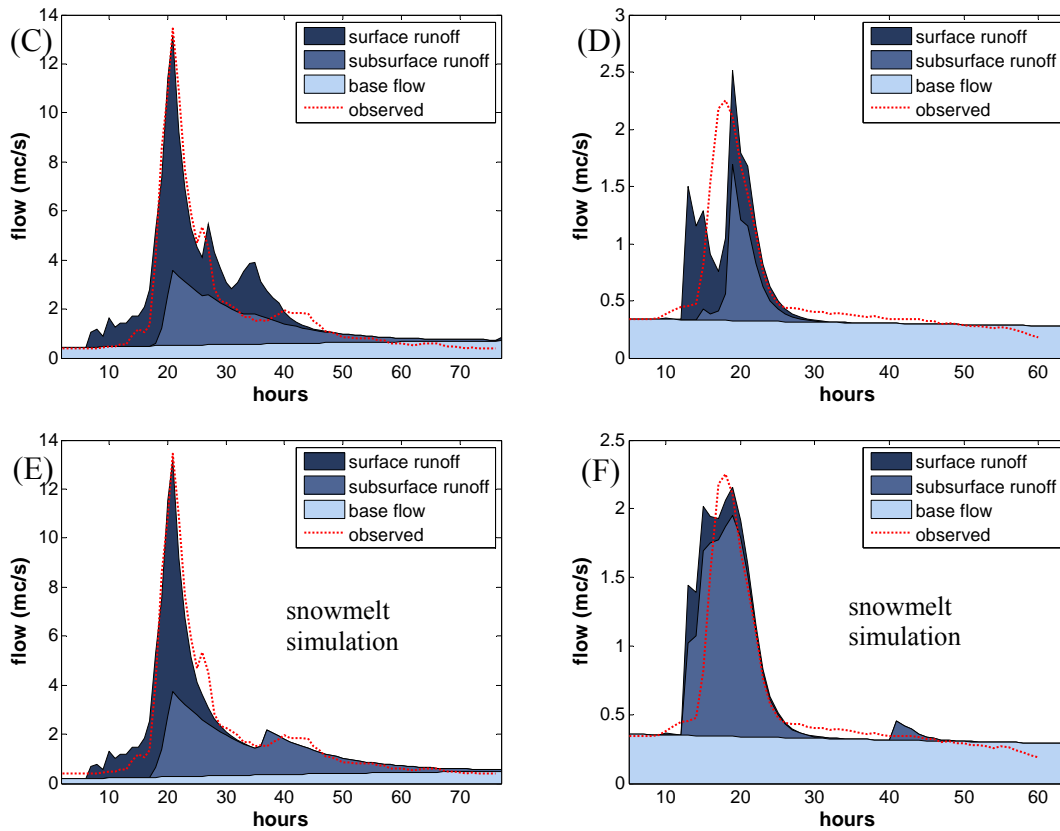
Figure 7. Results of the model AD3 obtained using the model under two different configurations one neglecting the presence of snowmelt process (C and D) and the second accounting for the snowmelt (see E and F). Graphs describe from the top: the recorded hyetograph and air temperature during the flood events of 4th Feb. 2003 (A) and 3rd Jan.2004 (B), the comparison of the recorded with simulated streamflow obtained using the AD3 without and with the snowmelt module.
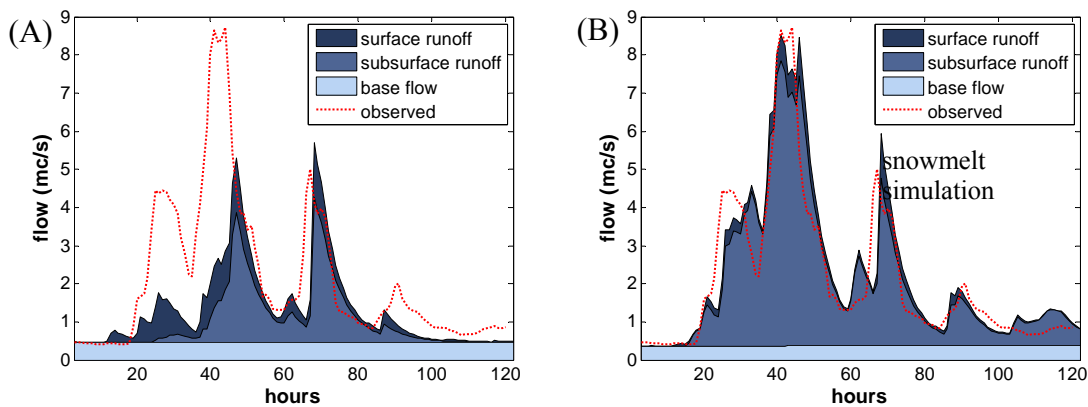
Figure 8. Results of the AD3 model during the flood event of the 21st Feb. 2005 using the model with the two variant described in Figure 7.

6. CONCLUSION

The snowmelt process involves a series of physical quantities that increase the complexity of simulations. For Apennine basins, it is not possible to separate clearly an accumulation period from a snowmelt period because the temperature, during the winter

period, is frequently very close to the threshold of 0°C. On the other hand, if the snowmelt is neglected, this may produce significant errors in the models outcomes in the simulation of flood events characterized by snowfall.

The presented study case deals with a small Apennine basin with a mean altitude of about 1050 m, in which almost the half of the flood events is characterized by presence of snowfall. In the first part, the analysis of the main hydrological parameters (lag-time and curve recession constants) of the recorded flood events show a dispersion of data decreasing with the floods magnitude. In fact, for high peak flows a great part of the watershed is involved in the runoff generation, so the dynamic of the entire basin prevails over the hydrological peculiarities of the single sub-zones.

In the second part, the hydrological simulations were used to validate the semi-distributed model AD3 developed from the precedent AD2 with the addition of a snowmelt module. In spite of a reduced number of parameters requested by the model, the goodness of the simulation results offer interesting arguments of discussion: in particular the snowmelt process produces two visible effects the smoothing of the peak flows and a delay in the basin response. This effect is due to the fact that the snowmelt produces an increase of the subsurface runoff, slower than the surface runoff.

REFERENCES

Bergström, S. (1976), Development and Application of a Conceptual Runoff Model for Scandinavian Catchments, *Bulletin Series* A, *No. 52*, Lund University, 134.

Bertoldi, G., D. Tamanini, F. Zanotti, and R. Rigon (2004), GEOTOP: a hydrological balance model. Technical description and programs guide, University of Trento (Italy) E-Prints. http://eprints.biblio.unitn.it/archive/00000551/ (4 April 2004).

Brubaker, K., A. Rango, and W. Kustas (1996), Incorporating radiation inputs into the snowmelt runoff model, *Hydrol. Process., 10*, 1329-1343.

Bloschl, G., R. Kirnbauer, and D. Gutknecht (1991a), Distributed Snowmelt Simulations in an Alpine Catchment: I. Model Evaluation on the Basis of Snow Cover Patterns, *Water Resour. Re*s., *27*(12), 3171-3179.

Bloschl, G., D. Gutknecht, and R. Kirnbauer (1991b), Distributed Snowmelt Simulations in an Alpine Catchment: II. Parameter Study and Model Predictions, *Water Resour. Res.*, *27*(12), 3181-3188.

Carriero, D., N. Romano, and M. Fiorentino (2005), A simplified approach for characterizing soil hydrologic behavior at basin scale, *Rivista di Ingegneria Agraria*, submitted.

Cosby, B.J., G.M. Homberger, R.B. Clapp, and T.R. Glinn (1984), A statistical exploration of the relationships of soil moisture characteristics to the physical properties of soils, *Water Resour. Res.*, *20*, 682-690.

Fiorentino, M., D. Carriero, V. Iacobellis, S. Manfreda, and I. Portoghese (2006), MEDCLUB - starting line and first activities, in *Predictions in Ungauged Basins: Promises and Progress* edited by M. Sivapalan, T. Wagener, S. Uhlenbrook, E. Zehe, V. Lakshmi, Xu Liang, Y. Tachikawa and P. Kumar, IAHS Publ. 303.

Fiorentino, M., and S. Manfreda (2004), La Stima dei Volumi di Piena dell'Adige a Trento con riferimento al Rischio di Inondazione, *Proceedings of 29° Convegno di Idraulica e*

Costruzioni Idrauliche, Trento, Editoriale Bios, Vol. 2, 115-122 (in Italian).

Gray, D.M., and T.D. Prowse (1993), Snow and floating ice, Chapter 7, in *Handbook of Hydrology*, edited by D.R. Maidment, McGraw-Hill, New York, 7.1-7.25.

Manfreda, S. (2005), La Simulazione Idrologica, Dispense di Idrologia, *Report del Dipartimento di Ingegneria e Fisica dell'Ambiente*, pp. 21 (in Italian).

Rawls, W.J., D.L. Brakensiek, and K.E. Saxton (1982), Estimation of soil water properties, *Trans. ASAE, 25*, 1316-1320.

Romano, N., and M. Palladino (2002), Prediction of soil water retention using soil physical data and terrain attributes, *J. Hydrol. 265*, 56–75.

Santini, A., A. Coppola, N. Romano, and F. Terribile (1999), Interpretation of the spatial variability of soil hydraulic properties using a land system analysis, in *Soils*, edited by J. Feyen and K. Wiyo, Modelling of Transport Processes, p. 491-500, Wageningen Pers, Wageningen, The Netherlands.

Saxton, K.E., W.J. Rawls, J.S. Romberger, and R.I. Papendick (1986), Estimating generalised soil-water characteristics from texture, *Soil Science Society of America Journal, 50*, 1031-1036.

Tarboton, D.G., and C.H. Luce (1996), Utah energy balance snow accumulation and melt model (UEB). Computer model technical description and users guide, Utah Water Research Laboratory, Utah State University and USDA Forest Service Intermountain Research Station.

U.S. Army Corps of Engineers (1998), Engineering and Design. Runoff from Snowmelt, *Engineer Manual 1110-2-1406*, Washington.

Vereecken, H., J. Maes, J. Feyen, and P. Darius (1989), Estimating the soil moisture retention characteristic from texture, bulk density and carbon content, *Soil Science, 148,* 389-403.

World Meteorological Organization (1986), Intercomparison of models of snowmelt runoff, *Oper. Hydrol. Rep. 23*, WMO Publ. 646, Geneva.

Zanotti, F., S. Endrizzi, G. Bertoldi, and R. Rigon (2004), The GEOTOP snow module, *Hydrol. Process. 18*, 3667–3679.

RAINFALL AND HYDROMETRIC THRESHOLDS FOR FLOOD WARNING. THE ESARO RIVER CASE STUDY

G. Mendicino

Soil Protection Department "V. Marone", Università della Calabria, Cosenza (Italy)

ABTRACT

Rainfall thresholds are an easy method aimed at increasing the efficiency of a flood warning system, providing some hours in advance information useful to decide whether or not set an alarm off and activate all the required protection measures. These thresholds represent the cumulative rainfall depths which generate critical discharges in given river sections, and they are capable of performing a warning without the necessity of running real time numerical models.

Rainfall thresholds have been evaluated for different sections of the Esaro River (Crotone, Southern Italy) using the flood event semi-distributed model WRROOM, for different antecedent moisture conditions and taking into account storage and control structures within the basin. Three synthetic hyetographs with different shape and duration as input model were used. The reliability of the proposed approach has been finally verified by generating 200 years of synthetic rainfall on the Esaro River basin, analyzing the right, false and missing warnings pointed out by the system

1. INTRODUCTION

Flooding cannot be completely avoided, but damages from severe flooding can be reduced if effective flood prevention schemes are realized. Flood warning systems assume an important role because they provide some hours in advance information useful to decide whether or not set an alarm off and activate all the required protection measures.

Traditional flood warning systems are mainly based on water levels or discharges in critical river sections, and through a more or less complex modeling, they search to extend the lead time and to reduce the uncertainty associated with the forecast. Basins in southern Italy are characterized by critical fluvial sections draining small areas (100-1000 km^2) which can include steep slopes mountains. Frequently, these basins show very short times of concentration which cause fast rainfall-runoff transformations, and then the forecasting based on hydrological processing of the observed rainfall is not sufficient to guarantee adequate times of intervention. In this case, quantitative rainfall forecasting carried out through the coupling of hydrological models with numerical weather models allows to extend the lead time of these basins.

The a priori knowledge of dangerous precipitation fields is then useful to perform a warning without the necessity of running real time models, which is based directly on the comparison between forecasted rainfall and critical values, called rainfall thresholds. These thresholds represent the cumulative precipitation values which define, for a given duration and soil moisture state, the total amount of rainfall which causes flooding damages. Flood warning systems including this kind of thresholds can supply the traditional ones in case the other systems fail or for a rough estimation of the predicted rainfall risk.

In this paper a framework for the estimate of warning rainfall thresholds on an urbanized basin in southern Italy (Esaro River, Crotone), endowed by storage and control structures, and frequently affected by extreme flood events, is described. Specifically, for three different river sections the anthropic effects on the total amount of rainfall which causes flooding damages are shown. Finally, the proposed rainfall thresholds have been verified through the generation of 200 years of synthetic rainfall with the aim of analyzing right, false and missing warnings pointed out by the flood forecasting system.

2. RAINFALL THRESHOLDS

The use of rainfall thresholds in flood hazard context is not widespread because of fact that there is not a formal definition for them. Using the analogy with the rainfall thresholds applied in geology (*Annunziati et al.*, 2000; *Costa and Frattini*, 2001), they could be defined as the cumulated volume of rainfall during a storm event which could be critical for a flood hazard in a specific location corresponding with a river section (Figure 1).

Different criteria have been suggested starting from those based on unconditional precipitation thresholds (direct approach) where early flood warning must be issued according to more general estimates like 50 mm of rainfall forecasted for the next 6 hours, or to local time series from which thresholds were evaluated making reference to assigned return period T (*Iiritano and Versace*, 1996; *Mendicino et al.*, 1998; *Sirangelo*, 1994). Obviously, the effects of 50 mm of rain in 6 hours or the risk levels associated to a given return period are quite different if rain fall over a dry or a saturated watershed.
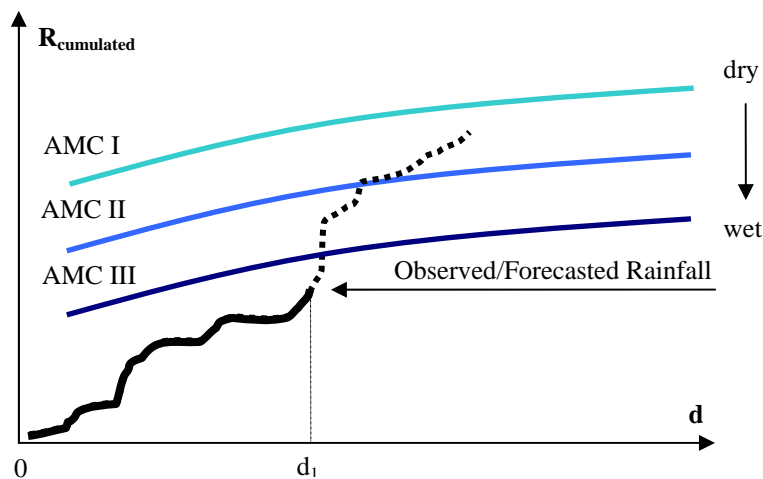
Figure 1. Representation of the rainfall thresholds, i.e. a cumulated volume versus the duration of the event, for different soil moisture states.

Within a basin soil moisture state strongly influences the surface runoff production corresponding to a storm event. Then, rainfall thresholds must depend explicitly on the Antecedent soil Moisture Conditions (AMC) of the basin, since a given rainfall volume which is not of any danger for the basin in a dry condition, it could be critical when the same basin is found in wetter conditions. *Mancini et al.* (2002) used an indirect estimate of the AMC according to the Soil Conservation Service definition (*SCS*, 1986), where AMC classes (I-dry, II-medium and III-wet) are depending on the amount of precipitation fallen in the previous five days (Figure 1). These AMC classes were utilized within a rainfall-

runoff distributed model to solve the inverse hydrological problem, which is to define that amount of rainfall which produces a given flooding discharge in a river section.

Specifically, the inverse hydrologic problem is solved starting from critical discharges (hypothesized as that discharge which guarantees 1 m average gap between floodplain and levees in a critical river section). Assuming the rainfall uniformly distributed over the basin, three different types of hyetograph are considered: constant intensity, linear increasing intensity and linear decreasing intensity. Each hyetograph is utilized as input in the rainfall-runoff transformation model by considering the three different antecedent moisture conditions of the basin. For a given critical discharge, for every combination of the conditions mentioned above and for every given duration, through an automated iterative procedure applied on the rainfall-runoff transformation model all the points which compound the thresholds are achieved. In Figure 2, an example of the resulting rainfall thresholds for the gauge Acqua della Quercia (Esaro River basin, Crotone) is shown: total critical rainfall is computed for the three AMC classes, for the three hyetograph types and for 1-3-6-12-24 hours duration. The values so estimated are linked together to give the critical pluviometric lines. Furthermore, if storage structures are present along the river network, then the amount of runoff stored during a flood involves, for the same critical discharge, a general increase in the rainfall threshold values (Figure 3). In some cases, the storage effect given by a reservoir decreases with the increase in rainfall duration. In fact, when long rainfall events occur active storage capacity is filled and the rainfall threshold tends to reach its original value.

3. HYDROMETRIC THRESHOLDS

Rainfall thresholds estimation, such as mentioned above, requires the solution of the inverse hydrological problem. This problem starts by determining the critical discharges (hypothesized as that discharge which guarantees 1 m average gap between floodplain and levees in a critical river section) observed along the river channels of a given basin. These critical values can be determined by analyzing the hydraulic characteristics of the whole river network. Different models are available to compute water surface elevation at given locations of interest within a basin, varying from kinematic and diffusion to dynamic wave routing. Channel slope and propagation upstream due to disturbances such as tides, tributary inflows, bridges or reservoir operations (Figure 4) can involve the necessity of using more simplified approaches such as that suggested by the model package "River Analysis System" (RAS) by the US Army Corps of Engineers – Hydrologic Engineering Center (HEC) HEC-RAS (http://www.hec.usace.army.mil/software/hec-ras/). This model includes: a steady flow model (the computing routine SNET); an unsteady flow model (the routine UNET); the consideration of a wide range of hydraulic works, bridges, storage areas; facilities for hydraulic design such as computation of localized scour at the piles of a bridge. Making reference to the SNET routine, the computational procedure is based on solution of the one-dimensional energy equation using the standard step method. Profile computations begin at a cross-section with know or assumed starting conditions and proceed upstream for subcritical flow or downstream for supercritical flow. Subcritical profiles are constrained to critical depth or above, and supercritical profiles are constrained to critical depth or below.

Once the critical discharges have been evaluated, the amounts of rainfall which produce the same flooding discharges in assigned river sections are achieved by means of a rainfall-

runoff model. For this work a semi-distributed object-oriented model has been utilized, the Watershed Rainfall Runoff Object Oriented Model (WRROOM) developed in the past years at the CAMILab (*Calabretta et al.*, 2000; *Biondi et al.*, 2002) of the Soil Conservation Department of the University of Calabria.
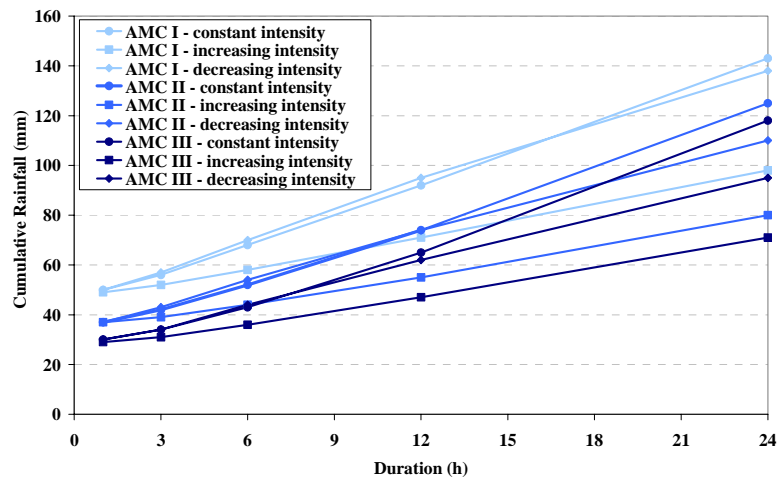
Figure 2. Thresholds for the rainfall gauge Acqua della Quercia (Esaro River basin, Crotone). Total critical rainfall is computed for the three AMC classes, for the three hyetograph types and for 1-3-6-12-24 hours duration.
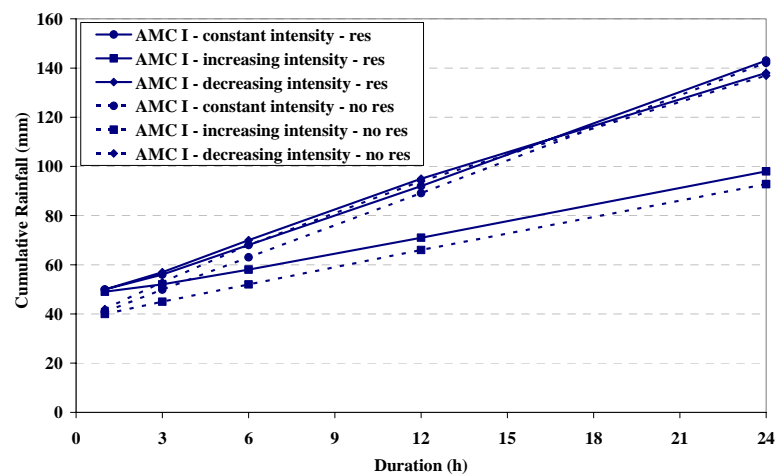
Figure 3. Thresholds for the rainfall gauge Acqua della Quercia (Esaro River basin, Crotone). Total critical rainfall is computed for the AMC I class, for the three hyetograph types, considering both the effects caused by the presence (res) and the absence (no res) of a reservoir.

Within this model, basic components of the basin are defined as "objects". They are containers of characteristic data (properties, parameters) and methods which simulate different hydrological processes: infiltration losses, runoff transformation, channel routing, etc. (Table 1).

Basins characterized by runoff generation not totally dominated by hortonian mechanism, can also be analyzed by means of a method based on a dunnian approach, simulating overland flow generation on hillslopes through a grid based water balance (*D'Odorico et al.*, 1998). A combined translation and storage model and a first-passage-time distribution unit pulse response function can be used for routing the excess precipitation over the watershed to produce runoff at its outlet (*Olivera and Maidment*,

1999). To obtain total runoff hydrograph, baseflow is added as a weighted average of the streamflow runoff and the baseflow at the previous time interval.
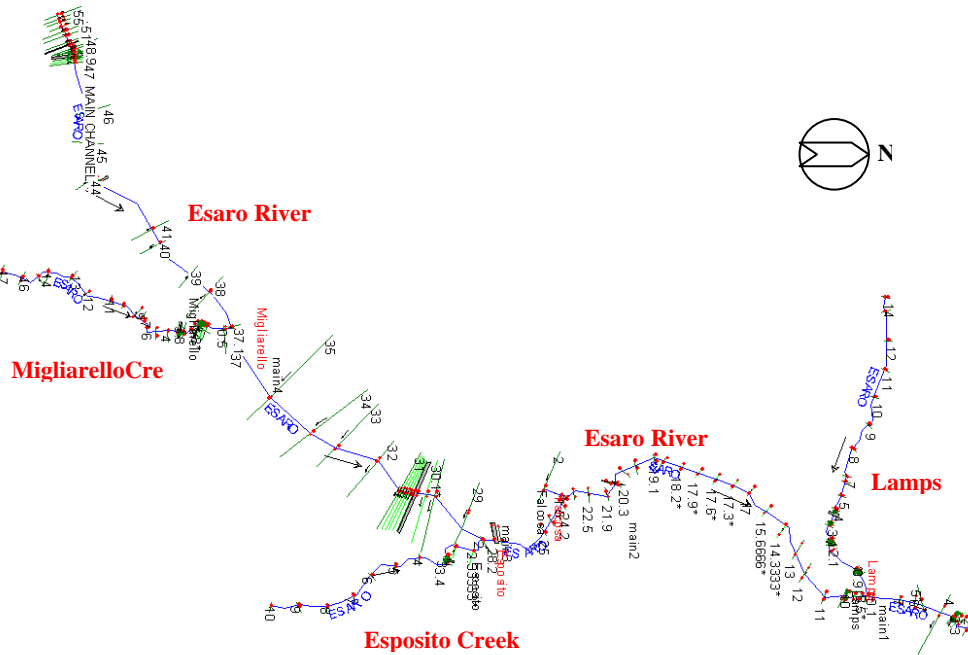
Figure 4. Esaro River network characterized by tributary inflows, bridges and reservoirs (HEC-RAS schematic river system).

BASIN, JUNCTION, GAUGE, RESERVOIR		REACH
Infiltration Losses	Initial/Constant method SCS Curve Number Green-Ampt Dunnian approach	Lag method
Runoff Routing	Clark Modified Diffusive	**Channel Routing** Muskingum
Baseflow	LowPass	
Storage-Outflow relationship (reservoir only)	Level-Pool Runge-Kutta (4th order)	Muskingum-Cunge

Table 1. List of objects and functions available into the WRROOM model.

Three methods are available regarding the routing of the flow through the channel network to the outlet: lag method, Muskingum and Muskingum-Cunge respectively. The latter method incorporates stream channel geometry in the distributed modeling of watershed dynamics combining "at-a-station" and "downstream" fluvial relationships to obtain laws of variability in space and time for water surface width (*Orlandini and Rosso*, 1996).

Computation according to the defined topological scheme proceeds from upstream elements in a downstream direction till a gauge is reached. Then parameters values are automatically adjusted to produce an optimal fit between simulated and observed hydrographs. The optimal fit is obtained minimizing the magnitude of an object function by means of univariate gradient method based on an iterative Newton scheme or using a global approach based on a shuffled complex evolution method.

4. THE ESARO RIVER BASIN

The basin analyzed in this study is that corresponding to the Esaro River (Crotone, Southern Italy). This basin is located at 39°55'*N* and 17°05'*E* (E.D.) and is characterized by large and smooth hills without any kind of relief with a maximum altitude of 242 m above sea level. It is approximately 107 km^2 in size, the corresponding length of the watershed is about 61 km while the main channel is 18 km long. The basin is about 105 m above sea level and the average incline of the slope is 1.74% (Figure 5).

The main geomorphologic characteristic is the high capacity to produce runoff, because the soil characteristics show little permeable clay, without significant erosion. To this aim, a rough estimate of runoff recorded for about 20 years in the southern Italian rivers shows a mean annual flood per unit area of about 1.0 m$^3 \cdot$s$^{-1} \cdot$km^{-2}, which appears lower than 3.5 m$^3 \cdot$s$^{-1} \cdot$km^{-2} observed in the Esaro River basin.

The climatic characteristics of the area can be summarized:
- a mean annual precipitation of about 800 mm, lower than the mean regional values (about 1170 mm);
- the number of rainy days equal to 60÷70, lower than the mean regional values (about 87 days);
- the monthly rainfall distribution like the typical regional behavior (6÷7% in summer, 70÷80 between October and March).

The maximum daily rainfall values recorded in the past by the rain gauges close and inside the basin are 264.0 mm (1934, Cutro), 200.2 mm (1957, Crotone), 200.0 mm (1972, Acqua della Quercia), with the highest value of 400.0 mm recorded at Petilia Policastro in 1943. In the case of highest short duration rainfalls, the maximum historical values observed in Crotone rain gauge are 90.0 mm (1 hour), 102.0 mm (3 hours), 114.0 mm (6 hours), 207.0 mm (12 hours) and 233.6 (24 hours).

Regarding the floods occurred on the Esaro River basin, only 6 events were recorded during the period 1962-67. These events were reproduced using WRROOM model with the aim of determining the optimal parameter values to be used in the inverse hydrological problem. According to the SCS-CN method used to simulate rainfall infiltration in the soil, it was observed a good agreement between the estimated CN values and those derived by optimization procedures. Specifically, for all the recorded flood event in Table 2 are shown the estimated and optimized CN values together with the return periods of peak flows and concurrent rainfalls.

Data in Table 2 points out that return periods of flood events occurred very soon after another storm (3rd and 5th floods of Table 2) are about 3÷4 times the value of the return periods of the concurrent rainfalls. This involves that hydrological responses of the Esaro River basin (mainly characterized by clayey soil) are strongly conditioned by the antecedent moisture conditions. Previous rainfalls not only increase soil moisture up to the saturation value, but also allow the swelling of the clay within the basin, determining very high runoff coefficient values. These particular rainfall-runoff transformation dynamics have been further verified during the last disastrous flood event of 14th October 1996, where just a few days before another similar high rainfall had filled the clayey soil of the basin up to saturation, without producing damages.

Figure 5. Esaro River basin and tributaries.

Order	Date	AMC	CN estimated	CN optimized	T rainfall (years)	T floods (years)
1	21.11.1960	I	66	67	1.6	1.2
2	09.11.1962	II	82	85	26.0	27.0
3	15.11.1962	III	92	90	4.5	20.0
4	30.10.1964	II	82	86	2.1	2.2
5	01.11.1964	III	92	99	2.2	7.3
6	07.12.1966	III	92	93	1.5	3.0

Table 2. Estimated and optimized CN values with return periods of peak flows and concurrent rainfalls.

Furthermore, to make more critical flood events along the urban reach of the Esaro River the presence of narrow spans of railway and road bridges, together with the growing urban development on the flood plains that greatly reduced available volumes for water temporary storage. Backwater effects caused by these changing in the channel configuration were observed during the flooding of Crotone in October 1996, producing destruction of infrastructures and great damages to public and private buildings.

To partially solve flooding damages, after the October 1996 different structural works and non-structural measures were carried out. Specifically, at the centre of the basin (Acqua della Quercia) a little reservoir was realized with the aim of increasing the water temporary storage during floods. Moreover, a real-time monitoring system (Figure 6a) was also realized based on the data recorded by 4 rainfall gauges (Acqua della Quercia – R1, Salica – R2, Papanice – R3 and Crotone – R4) and by 2 water levels gauges (Forcosa Bridge – WL1 and Esaro Bridge – WL2). According to the geographic position of rainfall gauges R1, R2 and R3, and starting from Acqua della Quercia reservoir downward to the Esaro outlet, three critical sections (CR1, CR2 and CR3) were detected to determine the rainfall thresholds on the whole basin. Schematically, figure 6b shows these sections and the corresponding subbasins (1, 2 and 3) closed by the same ones.

The former section CR1 (Figure 7) was assumed downhill the reservoir, corresponding to the narrow span of the Forcosa bridge (WL1 Station). This section has been hypothesized as representative of the high portion of the basin (Subbasin 1), and the corresponding critical discharge was utilized in the inverse hydrological problem to determine the rainfall thresholds for gauge R1.

219
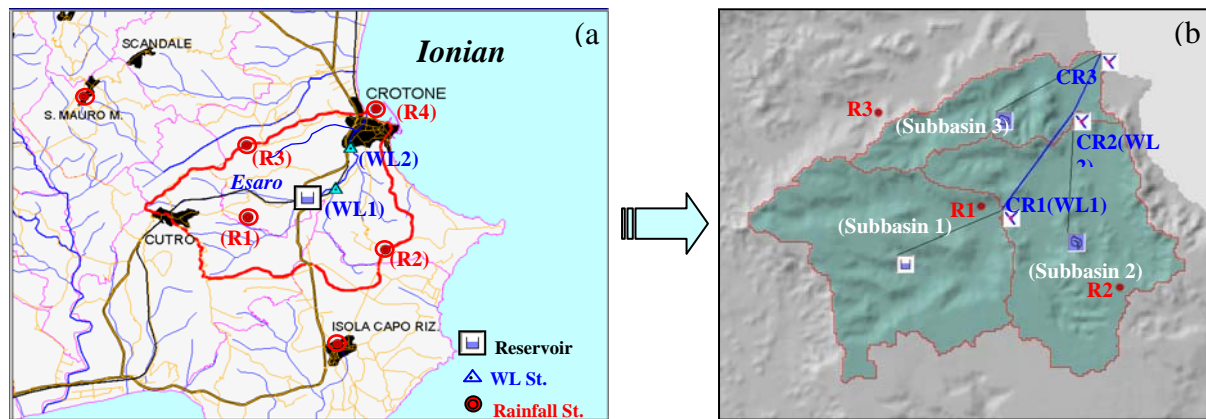
Figure 6. Real-time network of rain and water level gauges (a) and subdivision of the Esaro River basin according to the critical sections detected on the whole basin.

Figure 7. Critical section corresponding to a narrow span represented by the Forcosa bridge.

The other two sections were considered close the main critical urban area represented by the railway station in Crotone (Figure 8): one on the Esaro River (CR2 or WL2 Station), corresponding to the road bridge along Nicoletta Street; the other (CR3) on the Lamps Creek before the flowing into the Esaro River. The CR2 section has been hypothesized as representative of the urban portion of the Esaro River basin (Subbasin 2), and the corresponding critical discharge was utilized in the inverse hydrological problem to determine the rainfall thresholds for gauge R2. Finally, the critical discharge achieved on the Lamps Creek was used to estimate the rainfall thresholds for gauge R3 with the aim of performing a warning on the remaining part of the basin (Subbasin 3).

5. RESULTS

Esaro River network has been schematized within the HEC-RAS software (Figure 4) and for each of the three analyzed sections the corresponding critical discharge was achieved. Specifically, for the CR1 shown in Figure 7 (Forcosa Bridge - WL1), the hydraulic simulations carried out for the whole river reach pointed our a critical value of 120 m^3 s^{-1} (Figure 9), while for the critical sections shown in Figure 8 the simulations

pointed out 300 m^{3}s^{-1} for the Esaro River section CR2 (Figure 10) and 80 m^{3}s^{-1} for the Lamps Creek section CR3 (Figure 11) respectively.

Figure 8. Critical sections considered for the critical urban area in Crotone: one on the Esaro River (CR2), corresponding to the road bridge along Nicoletta Street, the other (CR3) on the Lamps Creek before the flowing into the Esaro River.

These critical discharges were used as input within the WRROOM model to solve, for each assigned AMC class, the inverse hydrological problem. Specifically, the topological scheme adopted for the simulation of the hydrological responses of the Esaro River basin is that shown in Figure 12.

Simulations have been carried out considering the SCS-CN method for infiltration losses, the effects of the reservoir were evaluated through the level pool approach, whilst a first-passage-time distribution unit pulse response function (*Olivera and Maidment*, 1999) was used for routing the excess precipitation over the watershed to produce runoff at its outlet. Finally, the inverse hydrological procedure applied for each critical section detected over the Esaro River basin produced the rainfall thresholds shown in Figures 12, 13 and 14.
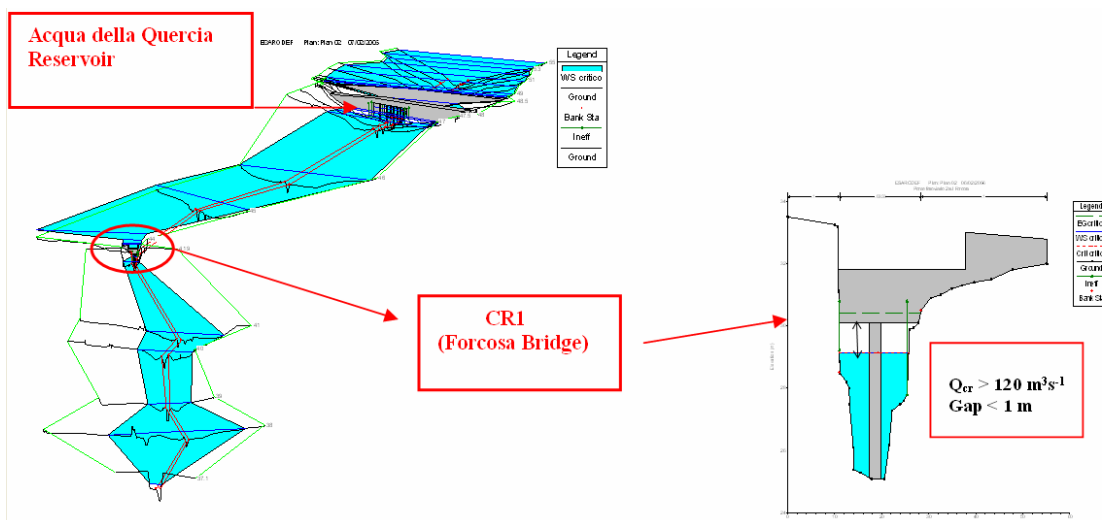
Figure 9. Critical section CR1 for the Forcosa Bridge (*hydraulic schematization in HEC-RAS*).

221
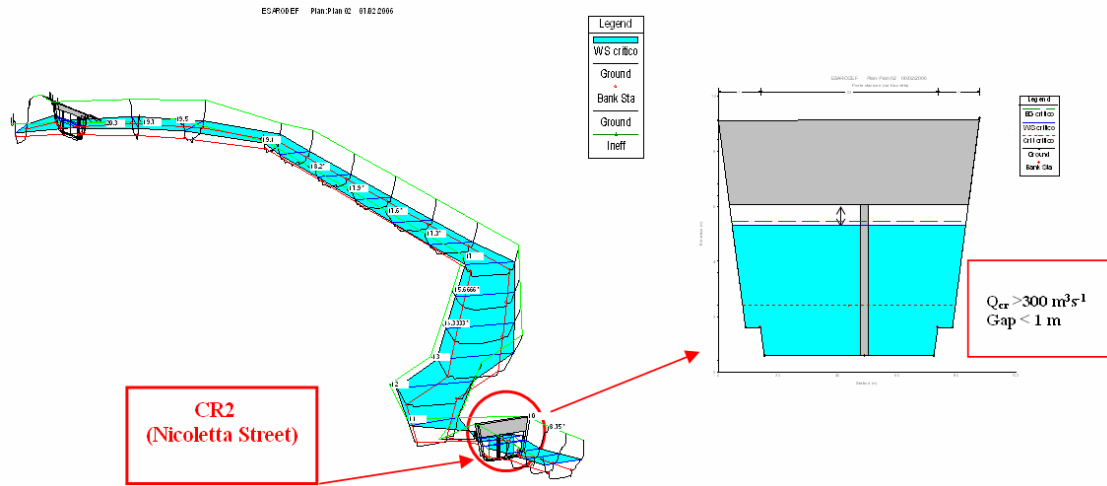
Figure 10. Critical section CR2 for the Road Bridge along Nicoletta Street.
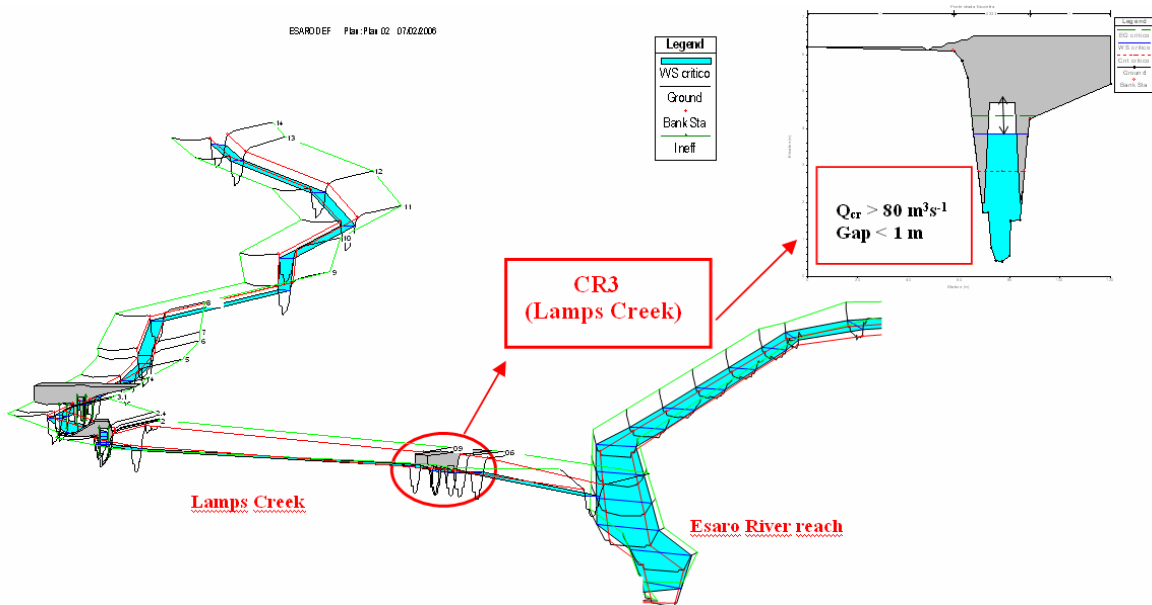
Figure 11. Critical section CR3 for the Lamps Creek before flowing into the Esaro River.
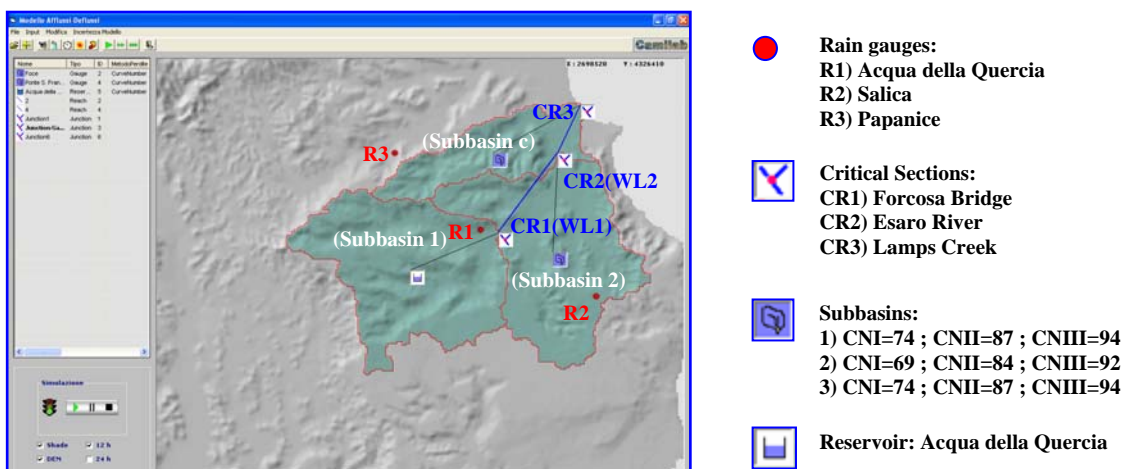
Figure 12. Topological scheme adopted for the simulation of the hydrological responses of the Esaro River basin.

222
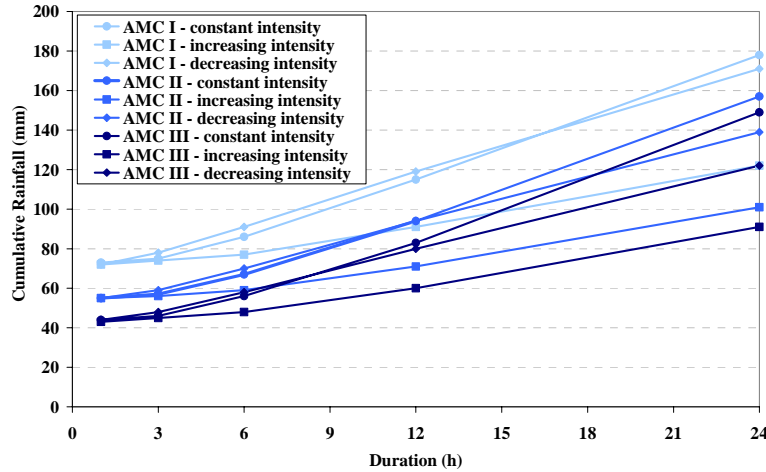
Figure 13. Thresholds for the rainfall gauge R2 (Salica). Total critical rainfall is computed for the three AMC classes, for the three hyetograph types and for 1-3-6-12-24 hours duration.
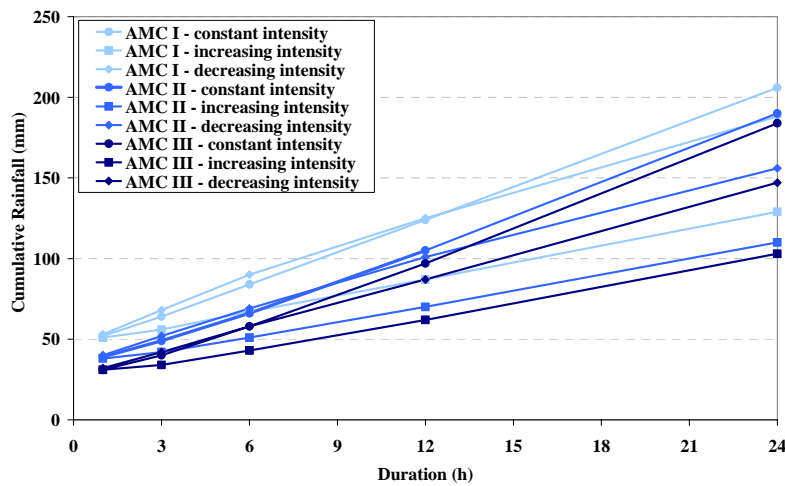
Figure 14. Thresholds for the rainfall gauge R3 (Papanice). Total critical rainfall is computed for the three AMC classes, for the three hyetograph types and for 1-3-6-12-24 hours duration.

From these figures it is possible to observe that higher critical conditions occur for AMC III class and for the increasing intensity hyetograph, since in this case all the precipitation is almost transformed in surface runoff.

Specifically, rainfall thresholds determined for gauge R1 (Acqua della Quercia) resulting lower than those achieved for the urban part of the basin, have to be referred only to eventual hydraulic failures occurred on the upstream areas of the basin. Concerning the rainfall thresholds determined for gauge R2 (Salica), these make reference to the critical values capable of producing flooding in the urban area of Crotone. Finally, the rainfall threshold values of gauge R3 (Papanice), which have been only determined for the Lamps Creek subbasin and in particular for the critical section before the urban confluence with the Esaro River, were reduced for 12 and 24 hours duration. These latter values were assumed equal to those of gauge R2 with the aim of guarantying a limit safety condition for both the critical section CR3 (Lamps Creek) and the CR2 (Esaro River) when rainfall data recorded by gauge R2 is unavailable.

For each of the three rain gauges R1, R2 and R3, thresholds achieved using the inverse hydrological problem were compared with those determined considering only the rainfall

time series for assigned return periods T (direct approach). Direct thresholds were detected from a previous analysis carried out by the Ufficio Idrografico e Mareografico - Centro Funzionale Meteo Idrologico della Regione Calabria - on the rainfall gauges spatially distributed on the whole Calabrian region. In this study, through a back-analysis approach has been pointed out that return periods changing from 20 to 50 years can be used as indicators for flood warnings. Figures 15, 16 and 17 show for each of the rainfall gauges considered within the Esaro River basin the comparison between the two criteria used to determine rainfall thresholds respectively.
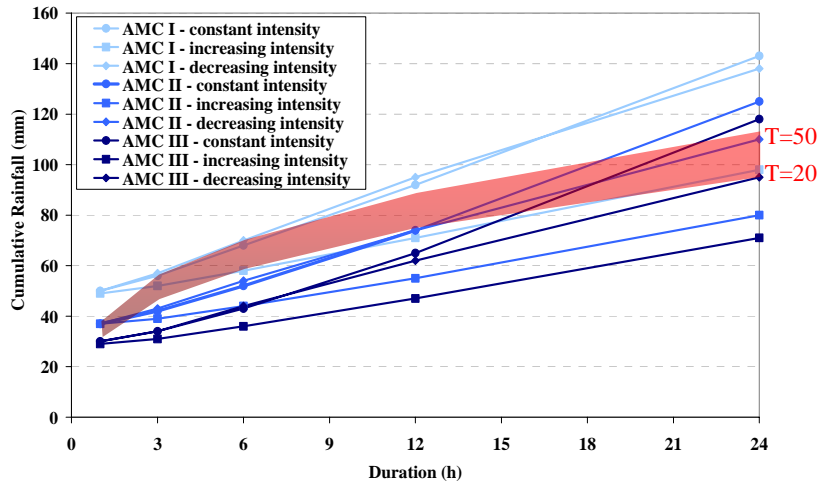
Figure 15. Rainfall gauge R1 (Acqua della Quercia): comparison between rainfall thresholds using inverse hydrological problem and through statistical analysis for return periods of 20 and 50 years.
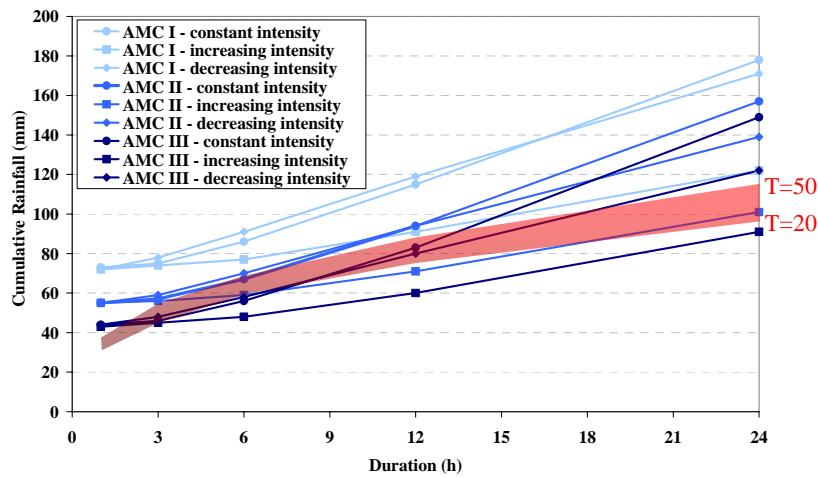
Figure 16. Rainfall gauge R2 (Salica): comparison between rainfall thresholds using inverse hydrological problem and through statistical analysis for return periods of 20 and 50 years.

The interesting aspect highlighted by these comparisons is to note for standard antecedent moisture condition (AMC II) that, if do not attend anthropic actions aimed at changing the morphological characteristics of the river sections, which are the results of a dynamic equilibrium between fluvial system and meteorological forcing, the analyzed approaches tend to be similar for rainfall durations varying from 3 to 12 hours, as well as the critical sections CR2 and CR3 located in the urban area of Crotone. When the presence of narrow spans or railway and road bridges greatly change the natural channel configuration, such as

the case observed in the critical section CR1, then the direct thresholds are not suitable to detect warning conditions, apart from the antecedent moisture soil class (Figure 15).
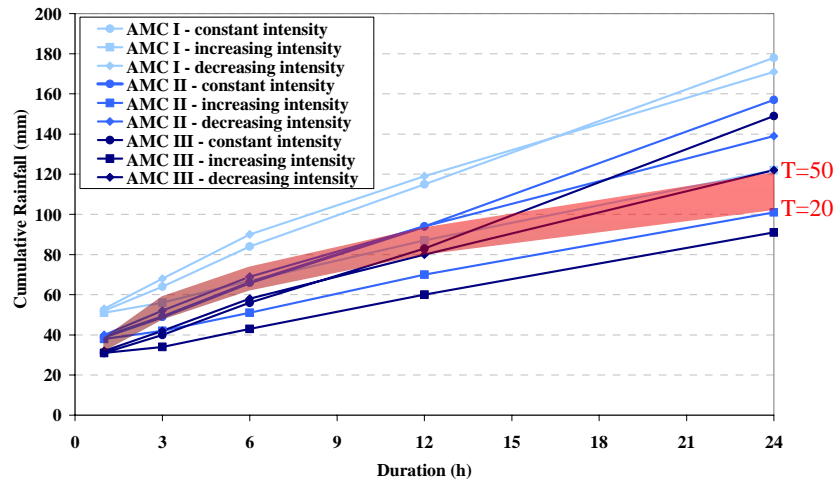
Figure 17. Rainfall gauge R3 (Papanice): comparison between rainfall thresholds using inverse hydrological problem and through statistical analysis for return periods of 20 and 50 years.

Finally, for the same standard antecedent moisture condition can be observed how the direct thresholds appeared precautionary for rainfall characterized by very short durations.

6. RELIABILITY ANALYSIS

The number of available historical events recorded on the Esaro River network is not large enough for robust statistical analysis. With the aim of increasing the number of events a 200 years rainfall data series has been synthetically generated according to Neymann Scott Rectangular Pulses (NSRP) algorithm (*Sirangelo*, 1994). Only rainfall gauge R4 (Crotone) was considered within the basin, because just for it was available a long sub-hourly time series. For this station the NSRP parameters were achieved both for winter and summer periods. The synthetic rainfall data was verified analyzing its capability in reproducing extreme events. This has been carried out comparing observed and synthetic Intensity-Frequency-Duration curves for different return periods T (T=20 and 100 years). Figure 18 shows the good agreement between the two set of curves.

Rainfall has been considered uniformly distributed over the basin and a transformation into runoff has been carried out with the WRROOM model. For each critical river section a number of significant events characterized by peak flow values greater than the 70% of the critical discharge was achieved. It can be seen how the number of significant events is great enough to guaranty the strength of the reliability analysis, varying from a minimum of 361 events for rainfall gauge R2 (Salica) to a maximum of 625 events for rainfall gauge R1 (Acqua della Quercia). Of these events, those greater than the critical discharges resulted: 384 events for rainfall gauge R1 (Acqua della Quercia); 205 events for rainfall gauge R2 (Salica) and 281 events for rainfall gauge R3 (Papanice). According to the significant events, all the Esaro River rainfall thresholds were verified in terms of right warning, false warning, no warning, missing warning and late warning (Figure 19).

The sum of right warning and no warning represents the thresholds efficiency. The difference between 1 and the false alarms percentage defines the safety factor of the system

and, finally, the sum of missing warning and late warning gives the bad working of the system. Tables 3, 4 and 5 summarize the percentage values of the different warnings encountered during the thresholds reliability analysis for each type of hyetograph considered. Specifically, the linear increasing intensity hyetograph resulted the more reliable to be used in the monitoring system, giving in all the cases the highest efficiency.
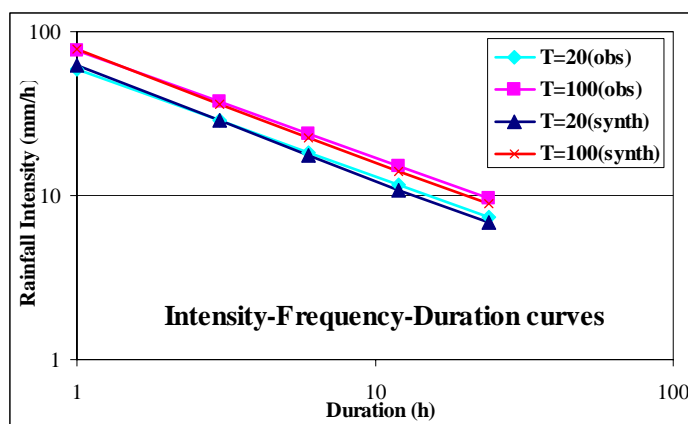
Figure 18. Observed and synthetic Intensity-Frequency-Duration curves for different return periods T (T = 20 and 100 years).

7. CONCLUSION

In the last decade the interest toward natural disasters is increased, specifically in the case of damages owing to floods. This trend is due to the increase of both flood events frequency and economic damages which appear higher because of the increased value of properties subject to risk. Southern Italy is a territory historically interested by very rapid and intense flood events, and only recently different flood warning systems for the vulnerability reduction of the region have been developed. Basins are characterized by critical fluvial sections draining small areas determining very short times of concentration which require a priori knowledge of dangerous precipitation fields with the aim of extending the lead time of the same basins.

Warning systems based on rainfall thresholds show the merit to synthesize in a critical rainfall height value all the complexity of the phenomena involved in the river floods generation. For this reason the a priori hydrological analysis has to guarantee the correct representation of the flood phenomena occurring in a river basin. The rainfall amount, which for a given duration causes the rising of the flood hydrograph up to the achievement of the critical discharge in an assigned river section, also defined as rainfall threshold, has been evaluated as inverse solution of the classic rainfall-runoff transformation phenomenon. With the aim of reducing the uncertainty related to the non-linearity of the rainfall-runoff transformation, three different antecedent soil moisture conditions were considered according to the definition suggested by the Soil Conservation Service, as well as three different types of hyetograph were considered (constant intensity, linear increasing intensity and linear decreasing intensity) to represent the typical behaviour of temperate climates.

The number of available historical events recorded on the Esaro River network was not large enough for robust statistical analysis, then a 200 years rainfall data series has been synthetically generated determining a set of flood events where the warning system has

shown efficiency values greater than the 60% for all the types of hyetograph considered. For the linear increasing intensity hyetograph these efficiency values were greater than the 70 %, with a maximum value of the 82%.
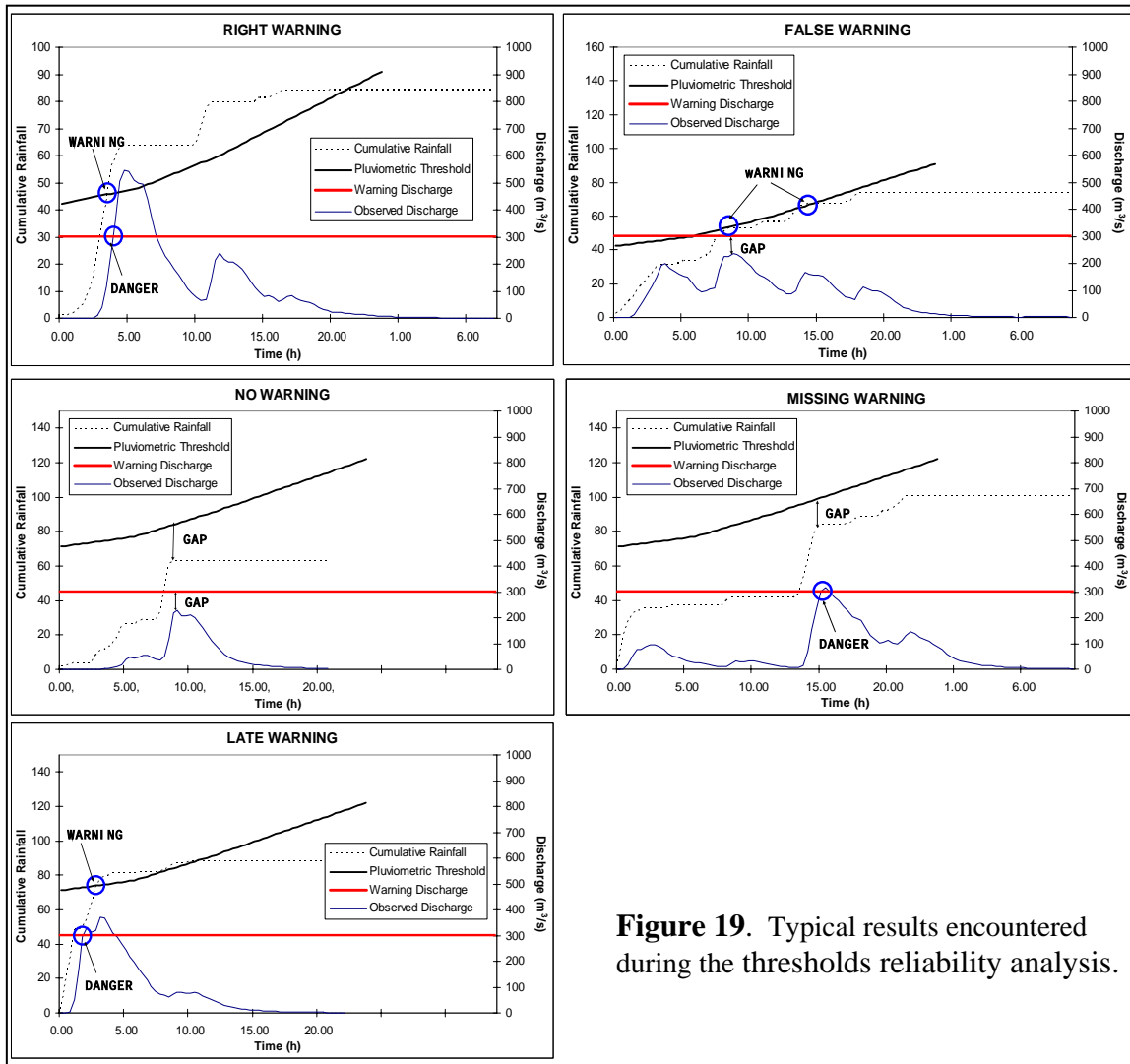
Figure 19. Typical results encountered during the thresholds reliability analysis.

ACQUA DELLA QUERCIA	(R1)		
Significant events	625		
Critical events	384		
	Constant	Increasing	Decreasing
Right warning	37.92%	**54.08%**	37.60%
False warning	2.40%	**13.12%**	1.92%
No warning	36.16%	25.44%	36.64%
Missing warning	22.88%	**7.04%**	23.04%
Late warning	0.64%	0.32%	0.80%
EFFICIENCY	74.08%	79.52%	74.24%

Table 3. Percentage values of the different warnings considered during the thresholds reliability analysis: rainfall gauge R1 (Acqua della Quercia).

SALICA	(R2)		
Significant events	361		
Critical events	205		
	Constant	Increasing	Decreasing
Right warning	29.92%	**48.75%**	27.98%
False warning	0.55%	**9.70%**	0.28%
No warning	42.66%	33.52%	42.94%
Missing warning	26.87%	**8.03%**	28.81%
Late warning	0.00%	0.00%	0.00%
EFFICIENCY	72.58%	82.27%	70.91%

Table 4. Percentage values of the different warnings considered during the thresholds reliability analysis: rainfall gauge R2 (Salica).

PAPANICE		(R3)	
Significant events	435		
Critical events	281		
	Constant	Increasing	Decreasing
Right warning	29.20%	**52.18%**	26.90%
False warning	2.99%	**14.25%**	1.38%
No warning	32.41%	21.15%	34.25%
Missing warning	34.71%	**12.18%**	29.43%
Late warning	0.69%	0.23%	1.15%
EFFICIENCY	61.61%	73.33%	61.15%

Table 5. Percentage values of the different warnings considered during the thresholds reliability analysis: rainfall gauge R3 (Papanice)

REFERENCES

Annunziati, A., A. Focardi, P. Focardi, S. Martello, and P. Vannocci (2000), Analysis of the rainfall thresholds that induced debris flows in the area of Apuan Alps - Tuscany, Italy (June 1996 Storm), *Proceedings of EGS I Plinius Conference on Mediterranean Storms*, Ed. Bios, 485-493.

Biondi, D., G. Mendicino, and P. Versace (2002), Modelli semi-distribuiti "object-oriented" per la previsione delle piene fluviali, *Atti del XXVIII Convegno di Idraulica e Costruzioni Idrauliche*, Potenza, Vol. I, 441-452 *(in Italian)*.

Calabretta, G., G. Mendicino, and P. Versace (2000), Un modello semidistribuito per la previsione delle piene fluviali in piccoli bacini idrografici, *Atti del XXVII Convegno di Idraulica e Costruzioni Idrauliche*, Genova, Vol. II, 33-41 *(in Italian)*.

Crosta, G.B., and P. Frattini (2001), Coupling empirical and physically based rainfall thresholds for shallow landslides forecasting, *Proceedings of EGS III Plinius Conference on Mediterranean Storms*, Ed. Bios.

D'Odorico, P., M. Marani, and R. Rigon (1998), Questioni geomorfologiche e previsione delle piene nei bacini fluviali, *Atti del XXVI Convegno di Idraulica e Costruzioni Idrauliche*, Catania, Vol. II, 73-84 *(in Italian)*.

Iiritano, G., and P. Versace (1996), Informazione pluviometrica in tempo reale e gestione dell'emergenza, *Atti del Convegno su: La Difesa dalle Alluvioni*, Firenze *(in Italian)*.

Mancini, M., P. Mazzetti, S. Nativi, D. Rabuffetti, G. Ravazzani, P. Amadio, and R. Rosso (2002), Definizione di soglie pluviometriche di piena per la realizzazione di un sistema di allertamento in tempo reale per il bacino dell'Arno a monte di Firenze, *Atti del XXVIII Convegno di Idraulica e Costruzioni Idrauliche*, Potenza, Vol. II, 497-505 *(in Italian)*.

Mendicino, G., G. Iiritano, and P. Versace (1998), Il preannuncio di piena nei piccoli bacini. Il caso dell'Esaro di Crotone, *Atti del XXVI Convegno di Idraulica e Costruzioni Idrauliche*, Catania, Vol. II, 273-285 *(in Italian)*.

Olivera, F., and D. Maidment (1999), Geographic Information System (GIS)-based spatially distributed model for runoff routine, *Water Resour. Res.*, *35*(4), 1155-1164.

Orlandini, F., and R. Rosso (1996), Sull'onda di piena diffusiva nei reticoli di drenaggio naturali, *Atti XXV Convegno di Idraulica e Costruzioni Idrauliche*, Torino, Vol. I, 265-276 *(in Italian)*.

SCS – Soil Conservation Service (1986), *National Engineering Handbook*, Section 4, Hydrology, Rev. Ed., U.S.D.A., Washington D.C., U.S.A.

Sirangelo, B. (2004), Un modello poissoniano non omogeneo per l'analisi delle precipitazioni cumulate su lunghi intervalli temporali, *Idrotecnica*, *3*, 125-158 *(in Italian)*.

RECENT ADVANCES IN RAINFALL-RUNOFF MODELLING: EXTRAPOLATION TO EXTREME FLOODS IN SOUTHERN FRANCE

C. Bouvier[1], P.A. Ayral[2], P. Brunet[1], A. Crespy[1], A. Marchandise[1], C. Martin[3]

(1) HydroSciences Montpellier, IRD, UMR 5569 CNRS-IRD-UM1-UM2, Montpellier, France
(2) Ecole des Mines Alès, Centre de Recherche LGEI, Alès, France
(3) UMR 6012 "ESPACE" CNRS, Université de Nice-Sophia-Antipolis, Nice, France

ABSTRACT

The extrapolations in time and space of hydrological models suppose that the models lie on strong physical basis, or that the behaviour of the models has been carefully checked for a given application. We study here the problem of simulating extreme floods from rainfall-runoff models. The case study is the Gardon of Anduze, where the floods are very irregular like in most of Mediterranean areas. The first part of this paper describes the basin, while insisting on the experimental aspects which show that soils saturation processes are predominant in this basin. The second part analyzes the performances of 2 rainfall-runoff models (TopModel and distributed-SCS) for simulating 50-years period return flood, those models being calibrated with "normal" floods. Both models perform well in calibration, but significant differences are found in extrapolation to the extreme flood. This difference seems mainly due to the way that the initialization of soil moisture is made.

1. INTRODUCTION

The Mediterranean basins of the south of France are frequently prone to fast risings, whose consequences can be catastrophic (Nîmes in 1988, Vaison the Roman in 1992, departments of the Aude in 1999 or Gard in 2002). The levels in the rivers can rise up of more than ten meters in a few hours, under the effect of precipitations locally exceeding several hundred mm in 24 h (*Neppel et al.*, 2007, this conference).

To protect the populations from floods, the strategies consist for example in predetermination, i.e. the assessment of flow levels or speeds associated with various periods of return, or in short-term forecasting. The first one aims at designing Plans of Prevention of the Risks of Floods (PPRi), implying specific urban development and hydraulic works in the critical areas; the second one allows the population to be prepared and safe before and during the floods.

In both cases, the rainfall-runoff models are used very much, because the hydrometric data are relatively more seldom than the rainfall records. The interest of these models is not only to simulate hydrographs which have not been observed on a given catchment (during large time periods, or extreme events), but also to take into account the impact of local modifications of the catchment or the climate, and at last, to be applied in ungauged basins. These extrapolations suppose however that the models lie on strong physical basis, or that the behaviour of the models has been carefully checked for a given application.

We will study here the problem of simulating extreme floods from rainfall-runoff models. The case study is the Gardon of Anduze, where floods are very irregular like in most of Mediterranean areas. In September 2002 occurred a 50-year return period flood of which the peak flow largely exceeded (about 3 times) those observed since 1992 (Figure1). This is due to the fact that Mediterranean floods are subject to high increase when rainfall exceeds a given threshold depending on the basin and the initial moisture conditions. In this context, the questions that will be addressed in this paper are: which models are able to simulate efficiently both normal and extreme floods, and b) why those models do simulate efficiently, or not.

Q m3/s
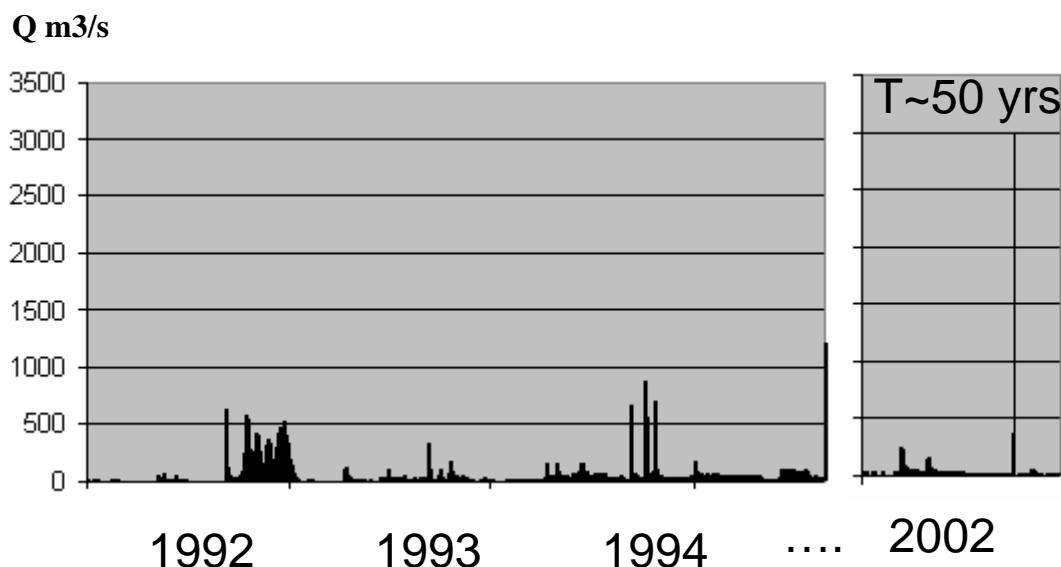
Figure 1. View of some peak flows, from 1992 to 2002.

The paper is organized in two parts. The first part describes the basin, while insisting on the experimental aspects which highlight the flow processes at hillslope scale. We will present the hydrodynamic properties of the soils, the measurement flows at plot scale, the application of electrical measurements in order to characterize the soil moisture and its evolution in time and space. The second part analyzes the performances of two models for simulating the 50-years return period 2002-flood, those models being calibrated with "normal" floods: the first model is an empirical distributed SCS runoff model, and the second one is the physically-based TopModel. The interpretation of the parameters of both models will be also discussed in this part.

2. OBSERVATIONS ON HILLSLOPE FLOW PROCESSES

The study area is the Gardon of Anduze, which lies nearly 70 km northeast of Montpellier, in the Cévennes mountainous area. The area of the catchment is 525 km^2. On this basin, the floods mainly occur in autumn, during very intense rainy events that may reach several hundred millimetres in 24 h. In September 2002, the daily rainfalls reached locally more than 600 mm. Every year, several events exceed a 100 mm rainfall in 24h. The flood rising times are short, ranging from 3 to 5 hours in this basin; runoff coefficients depend on the rainfall amounts, they can reach 0.5÷0.6 in the extreme cases.
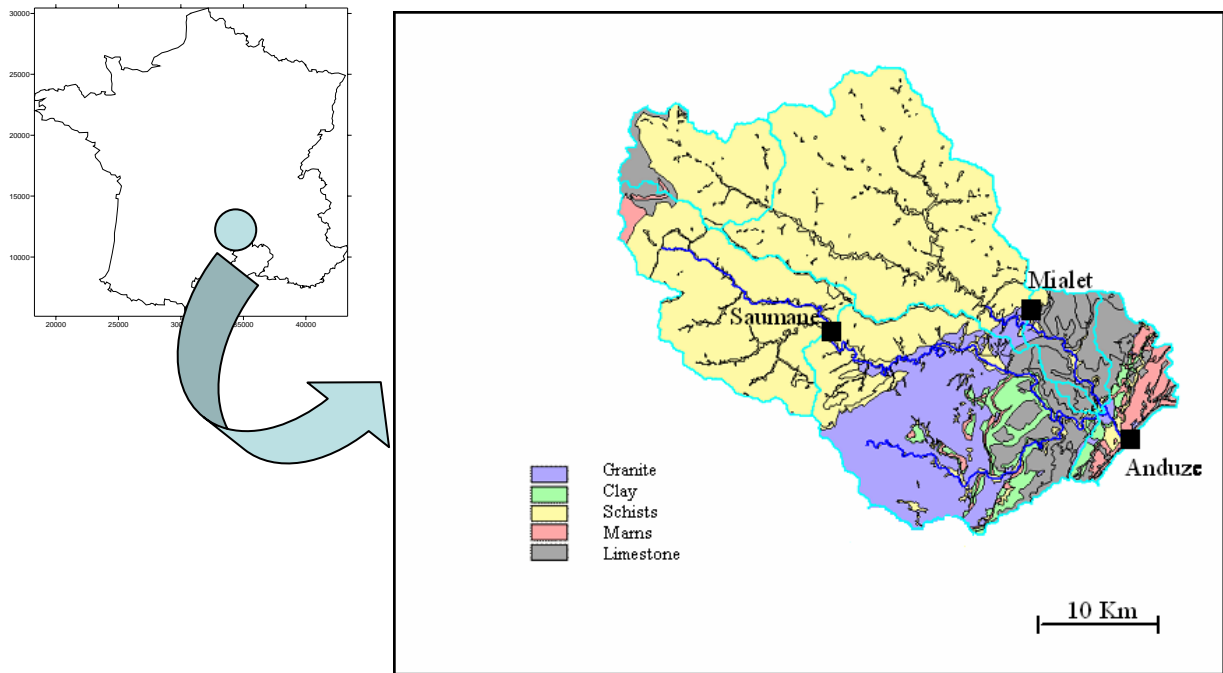
Figure 2. Main geological units of the Gardon of Anduze.

The elevations range from 100 to 900 meters, the slopes are very steep, 40% in average. The basin has three main units: schist (dominant, 60 %), granite and limestone. A typical scheme of the hillslope organization of soils is shown in Figure 3, corresponding to the dominant schist unit. The soils are relatively thin, from 10 to 100 cm or more.
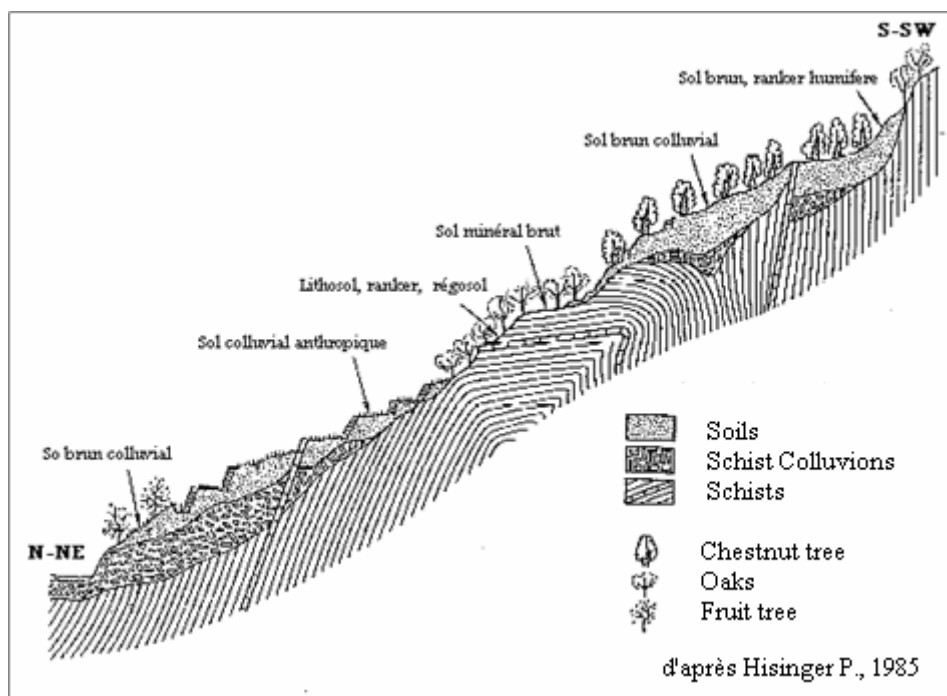
Figure 3. View of a typical hillslope in schist unit *(from BD INRA, http://sol.ensam.inra.fr/bdsollr/Asp/Default.asp)*.

231

The hydraulic conductivities have been measured at site, with a disk infiltrometer (Figure 4a): measures have been made in 4 plots, at various depths, and were found to be quite uniform in space (Figure 4b) and depth. Hydraulic conductivities at saturation are very high, ranging from 200 up to 600 mm·h^{-1} and exceeding rainfall rates. Thus, complete infiltration of rainfall is expected, when soils are not saturated.
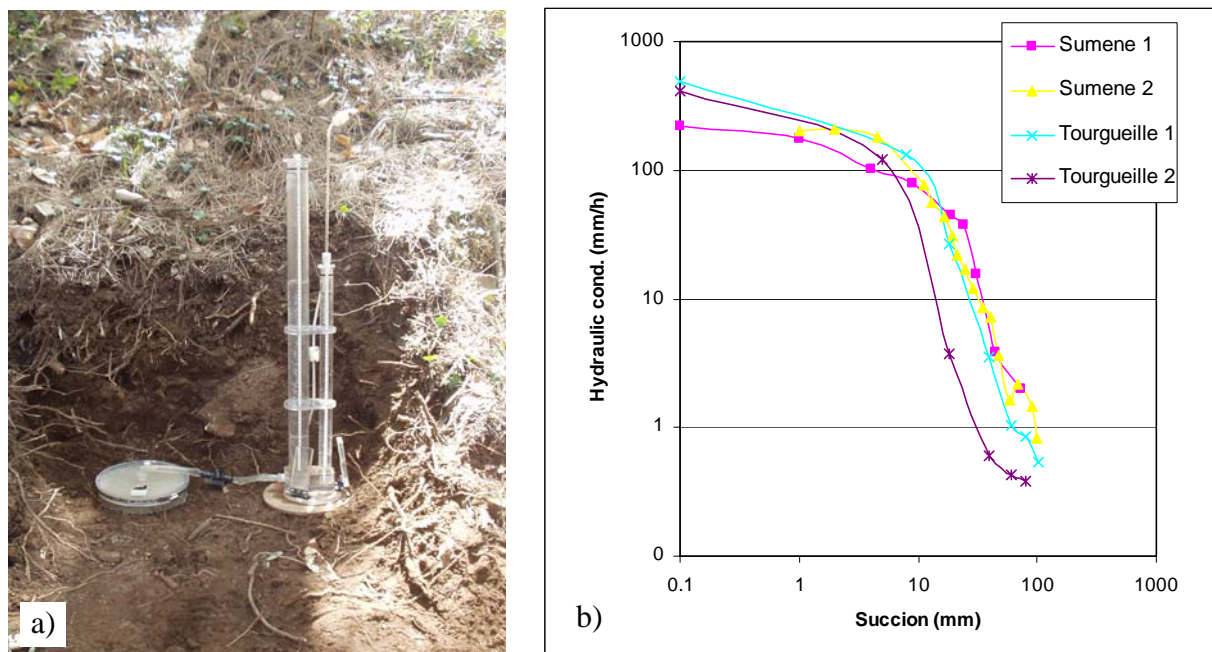
Figure 4. a) Disk infiltrometer device; b) Comparison of surface hydraulic conductivities K(Φ) in 4 plots.

Experiments at plot scale confirm complete infiltration. Artificial rainfalls were performed on six 1-m^2 plots, collecting only surface runoff, and on 2 10-m^2 plots, collecting both surface and sub-surface runoff (Figure 5). Results show that surface runoff is generally very low (less than 5 %), even when rainfall intensities reach 200 or 300 mm·h^{-1}. Sub-surface runoff can be very important, ranging from 30 to 60 %. However, it is expected than under natural rainfall, the surface runoff could be much more important, because in this case, the soil saturation can occur more quickly, due to a generalized sub-surface flow at hillslope scale. Furthermore, the lateral sub-surface runoff speeds have also been measured under artificial rainfalls, using various devices as salt tracers or downstream electrical measures: these speeds were found to be 3-5 cm/min in most cases.

At hillslope scale, evidence of saturation soil processes was provided from piezometers. Two of them were located at the hillslope foot, in soils where depths are about 50÷60 cm: the measures clearly show that water tables can develop in the soils during rainy events, but that evolution in time of this water tables is very short (Figure 6); they disappear in a few hours after rain stop. Thus, soils can saturate during the most intense rainy events, and in this case generate surface runoff and flash floods. The fact that saturation time is very short also means that the extension of saturated areas will not be correlated with base flow, of which variations are very slower than soil saturation dynamics.

10 m², slope 30%

Rainfall intensity
~ 200 mm/h

Lateral flow
3-5 m/h

Sub-surface **30-60 %**
runoff
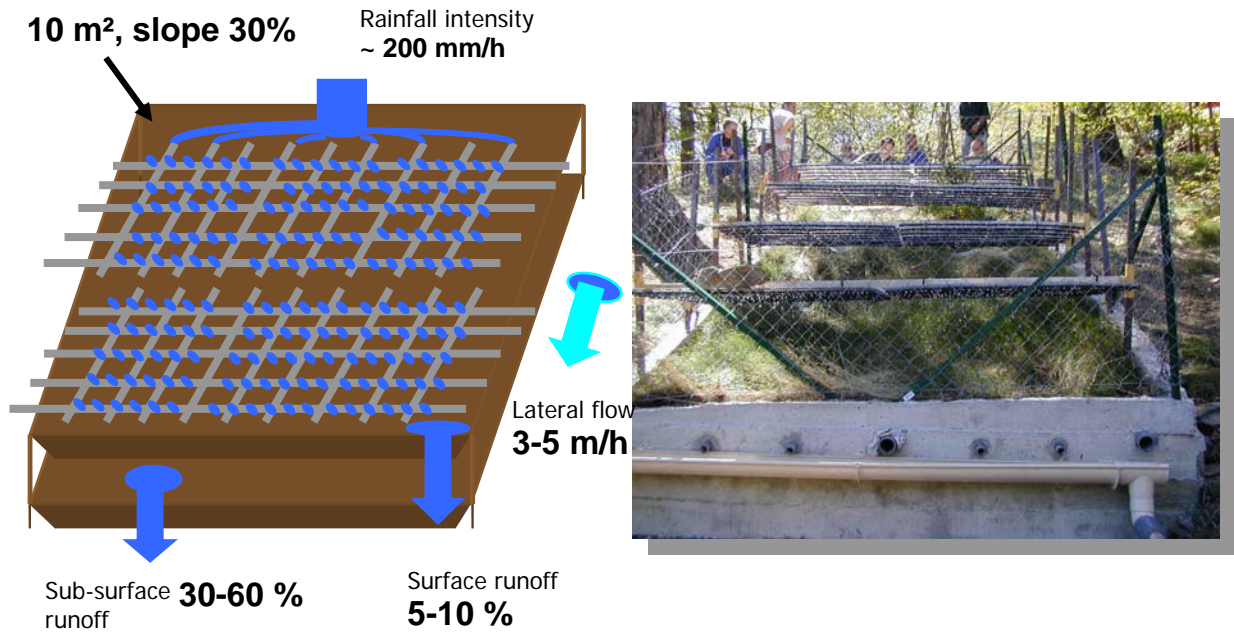
Surface runoff
5-10 %

Figure 5. Experimental device of both surface and subsurface runoff measurement.
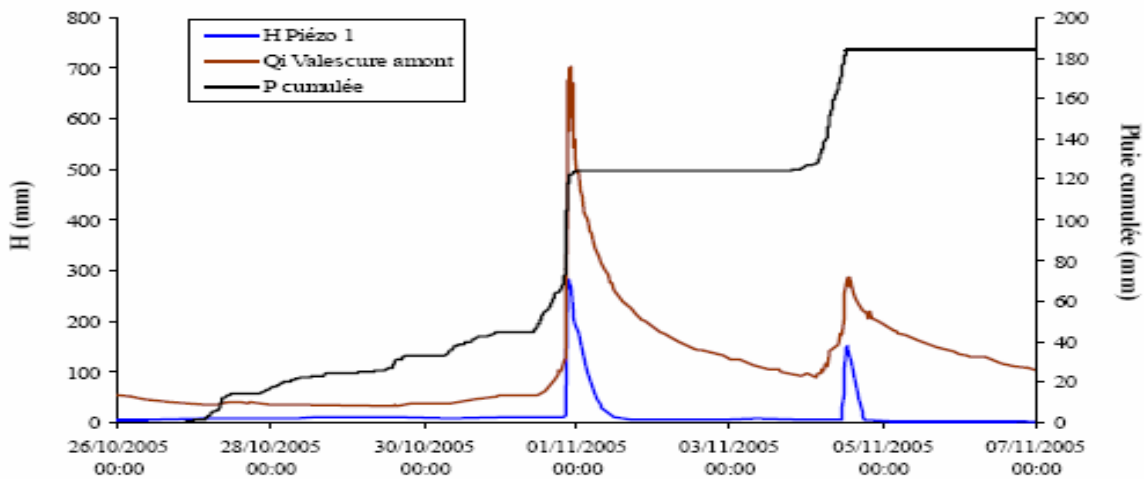
Figure 6. Variations in piezometric levels (blue) during flood (brown) and rain (black) events downstream a 1-km^2 basin.

Water contents in the unsaturated area were also measured at both event or year scale, by using TDR probes. At event scale, water contents are found to increase very quickly, which is consistent with the high hydraulic conductivities of this kind of soils. Like piezometers measurements, water contents are also able to quickly decrease, back to initial conditions in less than 24h when they exceed 15% (Figure 7a). For water contents lower than 15%, the matricial forces between soil and water remain predominant, and water content does not come back to initial conditions (Figure 7b). In this case, water remain adsorbed to soil much more time, as shown by yearly-measurement of water content (Figure 8): this example shows that the water contents depend on both seasonality and soil depth. However, they are found to be quite uniform between September and April, decreasing then during the hottest months (June to August), and finally quickly increasing when the first rains occur in autumn. This cycle is quite important to be known, in order to initialize correctly the hydrological models. It is also seen that the

233

beginning of autumn is a very critical period for short-term forecasting, because of high variability of water contents and occurrence of heavy storm water.
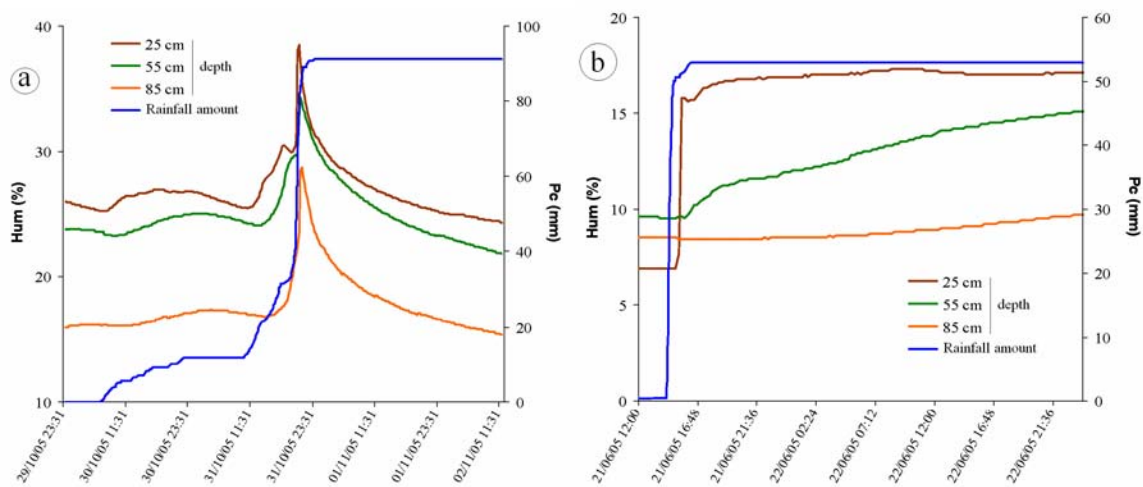
Figure 7. Event-scale variations of water contents at different depths : a) in moderately wet initial conditions, b) in dry initial conditions.
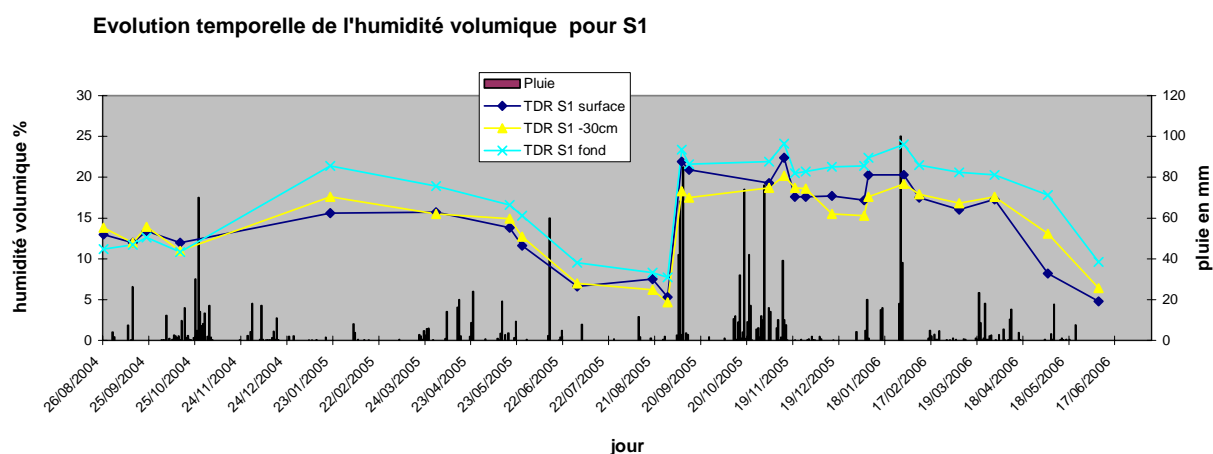
Figure 8. Seasonal variations of water contents at various depths.

In conclusion, the amount of the observations and experiments carried out on the basin of the Gardon of Anduze are very coherent, and show that the formation of the flash floods is mainly related to saturation processes of the soils. From a spatial point of view, the basin proves to be very homogeneous, regarding the hydrodynamic properties of the soils, whether schists or granites. This homogeneity makes more reliable the global signification of the observations carried out on local scales. We've thus got accurate description of the main soils characteristics, as well as the water contents and their evolution in time. These elements will make it possible to evaluate the performances of hydrological models, and to appreciate the corrections that should be brought furthermore. This is the object of the following part.

3. RAINFALL-RUNOFF MODELLING

Two models were selected: TopModel, which should be very convenient because of predominant variable source area processes, and SCS model, in a distributed version.

TopModel is a well-known physically-based model (see for example *Franchini et al.*, 1996, *Ambroise et al.*, 1996), which has received lot of improvements since its earlier version (*Beven and Kirkby*, 1979). Very briefly, it consists in assuming that runoff coefficient at a given time is due to the proportion of saturated cells in a basin. This proportion depends on the average saturation deficit in the basin, and on the distribution of the so-called topographic index. The average saturation deficit is processed by means of a balance between the recharge (depending on hydraulic conductivities) and the discharge of soils (Darcy's law). Initial average deficit depends on the base flow, which is supposed to indicate the extension of saturated areas. Only two runoff parameters were used here, to fit runoff conditions at the event scale: the hydraulic conductivities at saturation at the soil surface, K_o (m s^{-1}), and the coefficient f (m^{-1}) of the exponential decrease $K(z)=K_o.e^{-f.z}$ of the hydraulic conductivity at saturation with depth

SCS is an empirical model (see for example *Lyon et al.*, 2004), assuming that runoff coefficient is based on a relationship between rainfall amounts and a reservoir capacity S. Although SCS is commonly interpreted as direct surface runoff, it can also describe soils saturation processes. The version that we used here considers that the infiltration fills a soil reservoir, of which level is processed by means of a balance between the infiltration and the discharge of soils (linear reservoir). Initial reservoir levels are 0 at the beginning of each event, which means that soil moisture conditions are dry before rain. In our case, the initial soil moisture conditions do not take into account any previous event or any index of antecedent rainfalls. As well as in Topmodel, only two parameters were used here to fit the runoff conditions at the event scale:
- S (m), the reservoir capacity;
- ds (s^{-1}), coefficient of the exponential decrease of water level in soil reservoir with time.

Both models thus simulate the runoff contribution from a given cell at a given time. The elementary contributions are then routed to the outlet using the same routing model, which combines translation (V_o parameter, m s^{-1}) and storage (K_o parameter, ad.). The same parameters have been used for both models, so that differences only come from runoff parameters and concepts. Complete equations of both models that were used here could be found in ATHYS documentation (http://www.athys-soft.org).
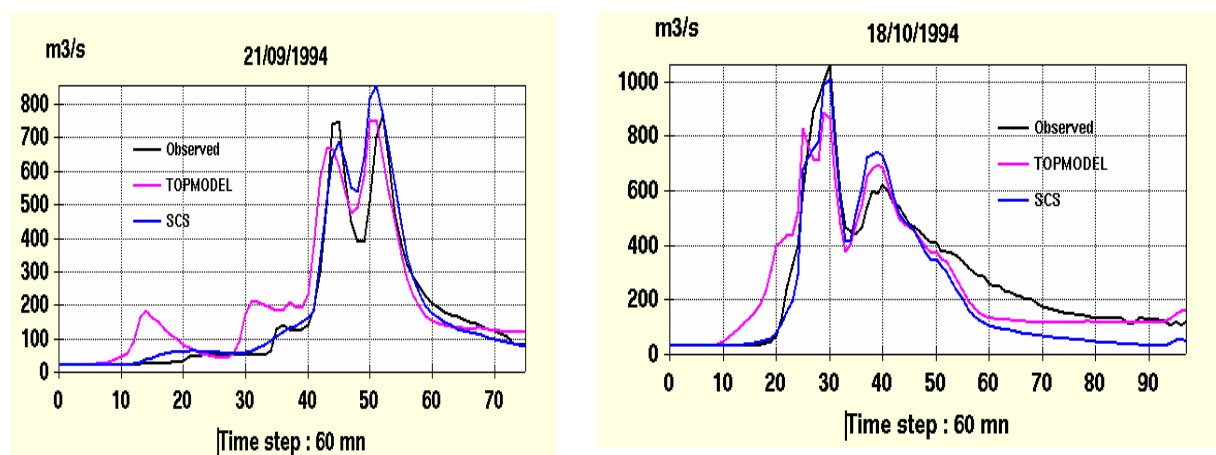
Figure 9. Calibration of both models with 1994 floods.

The models have then been calibrated from a sample of 3 floods in 1994, whose peak flows are respectively 770, 1060, 820 $m^3 s^{-1}$. It was found that both models can simulate efficiently those floods (Figure 9). Final parameters are K_o=6 m h^{-1} and f=10 m^{-1} for Topmodel, S=300 mm and d_s=1.15·10^{-5} s^{-1} for SCS. Both models were then applied to the main flood of 2002, whose peak flow is more than 3 times large than those of the 1994 floods. The previous calibration of both models has been kept, to illustrate the performances of the 2 models in extrapolation towards the extremes. It can be seen this time that the performances of the 2 models are clearly different, extrapolation with model SCS being largely better than the one provided by TopModel (Figure 10).
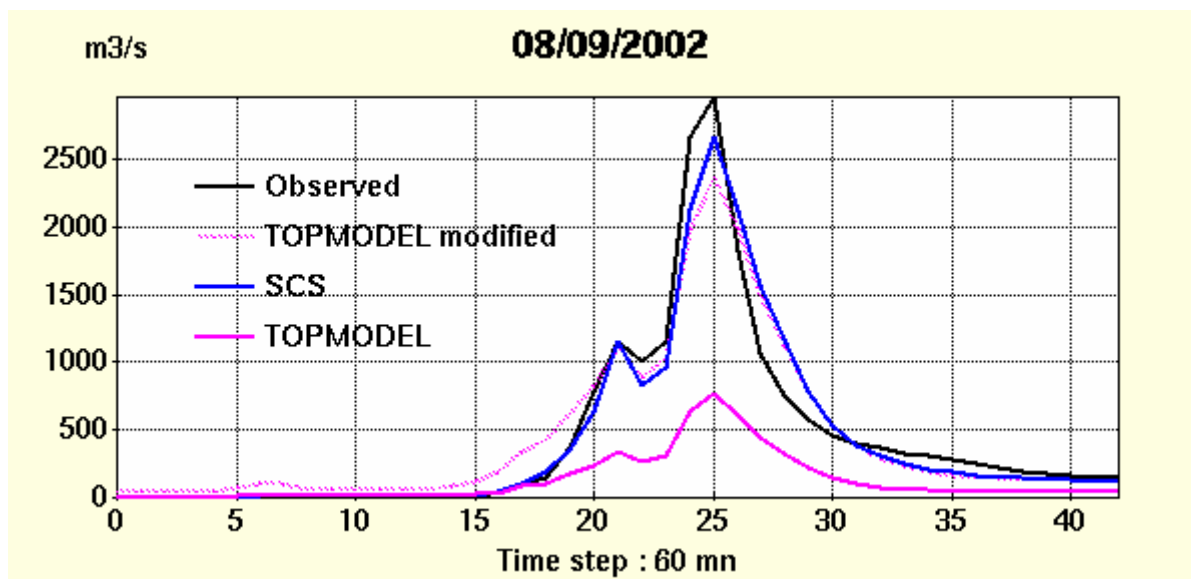
Figure 10. Simulation of 2002-flood with parameters calibrated for 1994 floods.

Numerical and physical biases could be mentioned to explain TopModel behaviour. From a numerical point of view, biases in parameter assessment can be due to the grid size of the MNT (*Franchini et al.*, 1996) or the computation algorithm of the topographic index (*Saulnier et al.*, 1997); *Saulnier and Datin* (2004) have noted that the water budget is incorrect when the proportion of saturated surfaces is high, and have brought the adapted corrections; equivalence of several set of parameters could also make that the selected set of values would not be convenient for extrapolation ("equifinality"). From a physical point of view, biases can also result from the assumptions made on the vertical profiles of hydraulic conductivities (*Ambroise et al.*, 1996), or from the anisotropy of vertical and lateral hydraulic conductivities. Other causes can be mentioned, scale effects, additional physical processes like translational flow, groundwater ridging.

Some tests, dealing with a modification of the vertical profile of hydraulic conductivities, with other algorithm to compute the topographic index, or simulations made with other set of parameters did not bring significant improvements. Nevertheless, it will be necessary to deepen.

We think however that the major problem is related to the initialization of the average deficit on the basin, and with the relation imposed by Topmodel between the base flow and this deficit. This relation is written:

$$\bar{\delta} = -\frac{1}{f} \times \mathrm{Ln}(\frac{Q_b}{A \times T_0 \times \exp(-\bar{\tau})}) \qquad (1)$$

236

where $\bar{\delta}$ is the mean deficit, in m, Q_b the base flow, in m^3s^{-1}, A the area of the basin, in m^2, T_0 the hydraulic transmissivity (K_o/f), in m^2s^{-1}, and $\bar{\tau}$ the mean topographic index (here ~6.6).

The 3 floods of 1994 occurred in moderately wet conditions, with base flows being respectively 20, 30 and 50 m^3s^{-1}. The corresponding initial average deficits derived from (1) are respectively: 182, 141, 90 mm. The flood of 2002 occurs at the beginning of the autumn rainfalls, in dry conditions. The base flow is about 3 m^3s^{-1}, and the average deficit calculated by the model is equal to 371 mm. The differences in average deficit are 200 mm and more, between dry and moderately wet conditions. Such variation does not seem realistic if one refers for example to at-site measurements of soil moisture, which were carried out on the basin, in top of slope as in bottom of slope. If considering that soil moisture is nearly 20 % in moderately wet conditions and 5 % in dry conditions, then that average porosity and average depth of soils are respectively 0.4 and 0.5 m, thus initial deficit would be 100 mm in moderately wet conditions and 175 mm in dry conditions. It can be seen that the difference is much smaller than the difference deriving from (1). Finally, another TopModel simulation was made, relaxing (1) for setting the initial deficit: starting for example with an initial deficit of 200 mm is shown to be much more efficient (Figure 10, curve Topmodel modified).

From a physical meaning, the bias which is supposed to appear when relating the spatial extension of saturated areas with base flow could arise because the base flow is mainly generated by deep and slow groundwater circulation (in schist fractures or granite alterits), while saturation of soils results from fast vertical filling occurring at the event scale, because of high hydraulic conductivities, weak thickness of soils and very strong rainfall intensities.

In addition, the SCS model shows that the initial deficit does not seem to be so discriminating for a correct simulation of the floods. Indeed, this model always considers the same conditions of initial soil moisture or deficit. The fact that the accuracy of the simulations do not depend whether initial moisture conditions are moderately wet or dry suggest that the initial conditions are relatively not very variable from one event to another.

4. CONCLUSIONS

The principal conclusions of this paper relate on the nature of the processes originating the flash floods, and to the modelling of these processes.

As first conclusion, the case of Gardon of Anduze shows that flash floods can be generated by processes of soils saturation, which result from high hydraulic conductivities, strong rainfall intensities and low thickness of the soils. However, these soils are likely to store several hundreds of millimetres of water. Beyond this rainfall threshold, the surface flows will be quickly activated, which mainly explain the typical behaviour and threshold effect of the Mediterranean basins.

As second conclusion, the hydrological models must be tested, when it is possible, on their capacity to be extrapolated towards the extremes. The example presented here shows that two models can have equivalent performances to reconstitute a set of current floods, and to diverge notably in extrapolation towards the extremes. It is also seen that if

physically-based modelling must be sought, it must be based on well identified processes. As an alternative, empirical modelling can also provide interesting results.

As third conclusion, the physical interpretation of the models supposes to get a real and objective knowledge of the characteristics of the basins, namely soils and water contents. It must be stressed to carry out more systematic explorations of these features, in order to describe not only their mean values, but also the variability in space of these values, by means of statistical distributions. In that sense, geophysical investigation applied to the surface formations could supply very efficient tools.

REFERENCES

Ambroise, B., K.J. Beven, and J. Freer (1996), Towards a generalisation of the TOPMODEL concepts: topographic indices of hydrological similarity, *Water Resour. Res.*, *32*(7), 2135-2145.

Beven, K.J., and M.J. Kirkby (1979), A physically based variable contributing area model of basin hydrology, *Hydrol. Sci. Bull.*, *24*(1), 43-69.

Franchini, M., J. Wendling, C. Obled, and E. Todini (1996), Physical interpretation and sensitivity analysis of the TOPMODEL, *J. Hydrol.*, *175*, 293-338

Gaume, E., M. Livet, M. Desbordes, and J.P. Villeneuve (2004), Hydrological analysis of the river Aude, France, flash flood on 12 and 13 November 1999, *J. Hydrol.*, *286*, 135–154.

Lyon, S.W., M. Todd Walter, P. Gerard-Marchant, and T.S. Steenhuis (2004), Using a topographic index to distribute variable source area runoff predicted with the SCS curve-number equation, *Hydrol. Process.*, *18*, 2757–2771.

Neppel, L., H. Niel, and C. Bouvier (2007), Rainfall and runoff predetermination in Mediterranean climate: regional and historical approaches, *this volume (Proceedings of International Workshop on Hydrological Extremes: "Observing and modelling exceptional floods and rainfalls", University of Calabria, Rende (CS), Italy, 3-4 May 2006)*.

Saulnier, G.M., K. Beven, and C. Obled (1997), Digital elevation analysis for distributed hydrological modelling: reducing scale dependence in effective hydraulic conductivity values, *Water Resour. Res.*, *33*(9), 2097-2101.

Saulnier, G.M., and R. Datin (2004), Analytical solution to a bias in the TOPMODEL framework balance, *Hydrol. Process.*, *18*(**7**)*,* 1195–1218.

FLASH FLOOD OCCURRENCE VERSUS IDF CURVES ESTIMATION

M. Vafiadis

Division of Hydraulics and Environmental Engineering, Department of Civil Engineering, Aristotle University of Thessaloniki, Greece

ABSTRACT
The Mediterranean cities suffer from frequent storm generated local flash floods. The extreme intensity rainfall over urban areas presents an important variability in time and space. This variability is usually unknown and underestimated. In absence of a very dense rain gauge network, the IDF curves computation is based on the "most representative" nearby station. The study of 50 years of data and Press information from Thessaloniki (Greece) shows that such a point statistic estimation does not represent adequately the actual flash flood danger for the surrounding urban area.

1. INTRODUCTION

In Mediterranean and semi arid regions, flash floods occur unexpectedly with most catastrophic results. The intensities and the total amount of rainfall recorded during such flash floods are beyond any normal extreme values statistical computation. During the last decade the most catastrophic storms all around Greece precipitated 150 mm to 350 mm (Corinth, 12 January 1997) during single events of a total duration not exceeding 6 hours, when the normal annual precipitation totals are 400 to 800 mm. Flash floods are unexpected localized phenomena of a very short ("flash") duration. In this case, any flood protection solution based on emergency planning or alarm systems is excluded. Therefore, a very good estimation of the maximum probable rainfall is necessary for any urban drainage project. This value is generally the outcome of an intensity-depth-frequency (IDF) curve analysis. The statistical analysis of complete or partial annual extreme series, and the necessary probability curve fitting, gives for such extreme values important return periods.

In urban areas the drainage basins are small scale. The areas are of the order of 10 km^2 or less, and the relative concentration times of the order of 5÷15 min. The usual density of recording rain gauges does not exceed 1 recording rain gauge over 100 km^2. This unique recording rain gauge provides data for extreme intensities and IDF curves computation. These curves then are accepted for the entire urban area. The question of representativeness of the data collected at a single point arises again. An overview of relevant literature and a historic research all over Greece for flash floods occurrences, catastrophic results and relative data, leaves a feeling that this catastrophic evidence is not as rare as the data analysis shows. The present study for the urban area of Thessaloniki shows that the well established statistical methodology for the depth-duration-frequency analysis does not produce frequencies or intensities that are proven by the experience. Hence a need to reconsider the procedure for the estimation of project values to be used in urban drainage planning: Instead of single station analysis, one has to consider the realization of extreme rainfall intensities over a more or less broader area

representing some hydrologic homogeneity. The question of hydrologic homogeneity, the representativeness of the obtained project precipitation values and the "probable" probabilities of such high values, are important research and discussion subjects.

2. THE STUDY AREA

Thessaloniki is the second largest urbanized area in Greece, with almost 1 million inhabitants. This 2300 years old city is a modern town, practically rebuilt after the two world wars. It has the form of an "8" with the city center in the narrower part and two large, still expanding areas, West – North-West and East – South-East of the city center, along the Thermaikos bay coast. A ring drainage channel protects the city against the flooding flow coming down from the surrounding hills.

Three good meteorological stations operate in this area:
1. The "Mikra" (NWS: National Weather Service) station in the "Macedonia" airport, 12 km south from the center;
2. The "Sindos" (CRI: Cotton Research Institute) station in the industrial zone, 12 km west from the center;
3. The "Thessaloniki" meteorological station of the University in the campus, in the center of the town.(AUTh: Aristotle University of Thessaloniki).

The data from the "Thessaloniki/AUTh" are regularly published and therefore available. The tables 1÷5 are based on the data from this station, which is considered as the "more representative" for the urban area.

The mean annual precipitation is ~450 mm, the number of wet days in a year ~100 and the number of days with snowfall usually does not exceed 2÷3 each year.
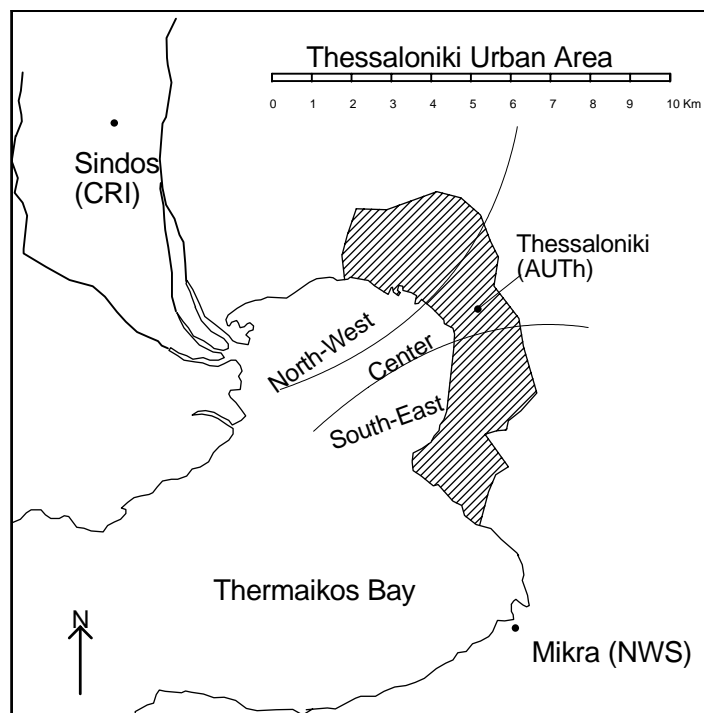
Figure 1. Study area.

3. THE FLOODING EVENTS

The research based on the local newspapers for a period of 50 years (1945-1994), revealed 10 important flooding events in the urban area of Thessaloniki. The importance of these events counts for considerable housing and property damage, cars destruction and water levels exceeding 0.5 m over the street pavement.

Return Period (years)	5 min (mm)	10 min (mm)
60	19.0	35.0
30	16.2	20.0
20	11.5	18.1
15	10.5	17.5
10	10.0	15.0
5	8.5	12.0
2	5.5	9.1
1.0	3.6	7.0

Table 1. Empirical Probabilities for 5 min and 10 min extreme rainfall intensities recorded at the Meteorological Station of the University of Thessaloniki, during the period 1930-1990.

The "subjective" information concerning duration and localization of each event ("Hellinikos Vorras", "Makedonia"), has been related to the "objective" meteorological information from MS/AUTh (Observations Météorologiques de Thessaloniki), and is presented on Table 2. Table 1 shows the empirical probabilities (plotting positions) for 5 min and 10 min extreme rainfall intensities recorded at the Meteorological Station of the University of Thessaloniki during the period 1930-1990. Tables 3, 4 and 5 present the daily, 10 min and 5 min rainfall depth maxima. The shaded data represent the data for which a major flood event is reported in daily local press.

Some expected but also some unexpected facts is the outcome of this work:
1. flooding events affecting restricted areas are frequent enough: 10 local floods in 50 years (T=5 years);
2. no flood event appears to happen systematically every time when maximal rainfall intensities are recorded by the recording rain gauge. The rainfall intensities during such flooding events are often quite normal. The global floods, large area floods, are practically non existent. The floods affected areas 5÷20 km^2. The total area we consider is ~150 km^2, but more than half of this area is the surrounding forest area drained by the ring flood protection channel of the town;
3. the total duration of rainfall producing local floods is between 20 min and 120 min;
4. the total flooding time does not exceed 2÷6 hours;
5. the maximum intensities for 10 min rainfall duration produced the most of the floods;
6. all the events have been produced during the "dry" season, and most of them in the afternoon. This means that they are local storm events;
7. the comparison among the various recorded intensities that produced no flood and the intensities that produced a local flood permits the suspicion that locally the rainfall intensity was more important than this one recorded by the nearby meteorological station;
8. deforestation, urbanization and drainage network efficiency do not provide explanations for these floods, because recorded rainfalls of the same importance did

not produce, under similar conditions equivalent flooding events.

| Date | Press Information | | | Meteorological station records (Thessaloniki Univ.) | | | |
	Time (hours:min)	District	Duration (min)	Total depth (mm)	Total duration (min)	Extreme intensity rain depth (mm)	Extreme intensity duration (min)
3-9-1947	7:15 pm	All districts	30	36.2	80	8.5	10
19-7-1952	4:30 pm	Center,East	60	43.6	150	11.7	5
13-5-1961	5:15 pm	East	30	54.1	440	8.5 16.0	5 10
19-9-1967	10:15 pm	Center,West	80	28.4	80	10.5 24.0	5 15
4-8-1968	Noon	East	35	16.9	35	4.0	5
8-7-1970	2:00 am	West		40.9	835	8.0	5
15-7-1972	Afternoon	West	70	48.7	80	19.0 24.3 38.0	5 10 20
18-7-1976	Morning	Center,East	30	28.2	70	17.5	10
1-10-1981	Night	Center	20	12.6	190	4.5	10
17-8-1988		All districts	20	21.3	50	13.8	10

Table 2. Important local flooding events in Thessaloniki.

Date	Total Rain Depth (mm)	Duration (hours:min)	Duration (min)	Mean Intensity (mm/hour)	Extreme Intensity Rain Depth (mm)	Extreme Intensity Duration (min)
13/12/1947	51.7	11:45	705	4.4	2.8	10
17/11/1949	44.4	07:10	430	6.2	4.5	10
30/10/1950	44.3	06:05	365	7.3	--	--
26/10/1951	45.3	15:15	915	3.0	2.6	10
19/7/1952	43.6	02:30	150	17.4	11.7	5
7/12/1952	64.3	24:00	1440	2.7	1.8	10
2/2/1954	53.3	23:00	1380	2.3	2.3	10
2/6/1956	56.3	03:15	195	17.3	10.0	5
27/6/1957	41.6	12:05	725	3.4	3.0	10
28/6/1957	51.1	20:00	1200	2.6	1.0	10
24/10/1957	41.0	03:15	195	12.6	--	--
11/9/1960	42.1	19:10	1150	2.2	3.0	10
13/5/1961	54.1	07:20	440	7.4	8.5	5
3/9/1964	49.6	23:00	1380	2.2	1.7	10
7/12/1966	41.7	11:10	670	3.7	3.5	10
30/9/1967	50.9	02:40	160	19.1	20.0	10
2/12/1969	45.8	11:35	695	4.0	1.5	10
8/7/1970	40.9	13:55	835	2.9	8.0	5
20/4/1972	54.2	19:55	1195	2.7	7.4	10
15/7/1972	48.7	01:20	80	36.5	19.0	5
31/12/1974	54.5	23:45	1425	2.3	6.1	10
28/10/1978	62.7	24:00	1440	2.6	2.0	10
24/7/1979	53.5	05:45	345	9.3	10.0	5
20/10/1980	45.7	22:10	1330	2.1	10.2	10
18/11/1982	74.0	16:00	960	4.6	7.8	10
29/11/1982	50.2	19:25	1165	2.6	3.0	10
24/11/1985	98.0	24:00	1440	4.1	5.6	10
16/2/1986	40.8	24:00	1440	1.7	1.4	10
18/11/1987	50.7	14:10	850	3.6	1.3	10

Table 3. Maximum daily rain depths (*Meteorological station of Thessaloniki University*).

Date	Total Rain Depth (mm)	Duration (hours:min)	Duration (min)	Mean Intensity (mm/hour)	Extreme Intensity Rain Depth (mm)	Extreme Intensity Duration (min)
3/9/1947	36.2	01:20	80	27.2	8.5	10
17/5/1949	27.1	02:35	155	10.5	13.5	10
14/5/1955	19.7	05:55	355	3.3	8.3	10
8/10/1956	22.0	06:30	390	3.4	8.2	10
21/9/1960	25.7	02:25	145	10.6	11.0	10
13/5/1961	54.1	7:20	440	7.4	16.0	10
25/5/1963	18.7	02:10	130	8.6	9.0	10
22/7/1963	18.0	01:25	85	12.7	9.0	10
19/9/1967	28.4	1:20	80	21.3	18.0	10
30/9/1967	50.9	02:40	160	19.1	20.0	10
5/8/1969	11.0	00:50	50	13.2	10.8	10
30/5/1971	35.2	07:25	445	4.7	8.5	10
3/7/1972	17.9	04:40	280	3.8	9.3	10
15/7/1972	48.7	01:20	80	36.5	24.3	10
15/6/1973	17.8	1:10	70	15.3	8.9	10
23/5/1975	12.2	00:40	40	18.3	9.0	10
21/6/1975	24.2	05:20	320	4.5	9.1	10
22/6/1975	11.5	01:15	75	9.2	9.6	10
18/7/1976	28.2	01:10	70	24.2	17.5	10
18/10/1976	21.2	03:50	230	5.5	10.0	10
28/5/1977	14.8	05:15	315	2.8	8.8	10
4/7/1980	25.2	06:15	375	4.0	12.1	10
20/10/1980	45.7	22:10	1330	2.1	10.2	10
28/7/1981	10.8	12:30	750	0.9	10.2	10
30/6/1983	35.9	07:50	470	4.6	10.0	10
21/6/1987	24.4	05:15	315	4.6	11.5	10
12/8/1987	16.8	01:15	75	13.4	11.9	10
31/7/1988	22.3	02:55	175	7.6	10.5	10
17/8/1988	21.3	00:50	50	25.6	13.8	10
22/5/1989	19.3	01:20	80	14.5	10.0	10
17/6/1989	39.6	10:30	630	3.8	13.0	10
20/5/1990	24.2	03:30	210	6.9	10.0	10

Table 4. Maximum 10 minutes rain depths (*Meteorological station of Thessaloniki University*).

4. CONCLUSIONS

When the extreme rainfall intensities analysis rely on a unique recording rain gauge, the resulting IDF curves give no good information for urban flooding protection. These point estimates can not assess the areal variability of short duration precipitations. The reason is that some extreme intensities occurring in small distances from the precipitation measuring station are not detected at all. For drainage areas of the order of 10 km^2 and concentration times of the order of 10 min, a dense recording rain gauge network, with a rain gauge density of 1 rain gauge for 10 km^2 of drained surface is needed, if IDF curves for local flash flood protection projects have to be computed. This is not usually possible, for technical and economic reasons. On the other hand, an increased return period for new projects, does not provide a good solution, because the real return period remains unknown. This simple approach could also lead to legal troubles concerning the responsibilities of the services and the engineers in charge for the non flooding safety.

Date	Total Rain Depth (mm)	Duration (hours:min)	Duration (min)	Mean Intensity (mm/hour)	Extreme Intensity Rain Depth (mm)	Extreme Intensity Duration (min)
17/9/1949	24.5	11:15	675	2.2	8.4	5
1/3/1951	19.0	09:50	590	1.9	16.2	5
5/4/1951	37.8	14:00	840	2.7	5.1	5
3/7/1951	27.6	08:00	480	3.5	7.5	5
19/7/1951	16.3	08:45	525	1.9	4.7	5
19/7/1952	43.6	02:30	150	17.4	11.7	5
22/5/1953	18.7	02:50	170	6.6	5.5	5
26/5/1953	11.6	01:00	60	11.6	8.0	5
9/10/1954	10.8	03:55	235	2.8	4.5	5
14/7/1955	31.7	02:00	120	15.9	4.5	5
9/10/1955	37.9	09:20	560	4.1	8.5	5
2/6/1956	56.3	03:15	195	17.3	10.0	5
20/11/1956	14.2	07:15	435	2.0	7.0	5
2/10/1957	21.0	01:55	115	11.0	9.4	5
27/6/1959	11.7	01:35	95	7.4	5.9	5
13/5/1961	54.1	07:20	440	7.4	8.5	5
30/5/1964	39.5	05:35	335	7.1	9.0	5
10/7/1967	29.3	08:45	525	3.3	6.0	5
19/9/1967	28.4	01:20	80	--	10.5	5
7/7/1970	24.1	10:00	600	2.4	6.7	5
8/7/1970	40.9	13:55	835	2.9	8.0	5
15/7/1972	48.7	01:20	80	36.5	19.0	5
17/7/1972	26.4	01:51	111	14.3	9.5	5
15/10/1972	38.1	18:50	1130	2.0	6.0	5
20/6/1975	34.4	05:50	350	5.9	9.8	5
7/8/1975	27.5	02:45	165	10.0	4.8	5
18/7/1976	28.2	01:10	70	--	9.0	5
25/5/1978	14.2	01:20	80	10.7	7.0	5
29/5/1978	21.7	04:15	255	5.1	6.5	5
24/7/1979	53.5	05:45	345	9.3	10.0	5
5/9/1979	31.1	02:40	160	11.7	8.4	5

Table 5. Maximum 5-min rain depths (*Meteorological station of Thessaloniki University*).

Therefore, instead of point statistical estimation method, we need an areal flash flood frequency estimation method. This method must combine in one data set the extremes from more than one station in the same area, thus providing spatial information that has to be adequate also for regions in the same area where no data exist. Such a procedure, with a sound theoretical support, is not available at the present time. Finally the hydrological planning and the statistical analysis of data have to be done in parallel with the drainage or flood protection project elaboration, in order to minimize costs and optimize necessary works and structures. This can be done by application of some kind of multi-criteria and multilevel protection scheme, based on a cost-risk-benefit analysis.

REFERENCES

Observations Météorologiques de Thessaloniki. Université de Thessaloniki, 1946-1995.

Hellinikos Vorras, Daily newspaper, Thessaloniki.

Makedonia, Daily newspaper, Thessaloniki.

Observing and modelling exceptional floods and rainfalls
Proceedings of the AMHY-FRIEND International Workshop on Hydrological Extremes,
held at University of Calabria, Cosenza (Italy), May 3-4, 2006

CALIBRATION AND VALIDATION OF A RAINFALL-RUNOFF MODEL SIMULATING INFILTRATION AND SATURATION EXCESS

P. Versace, B. Sirangelo, D. Biondi

Soil Protection Department "V. Marone", University of Calabria, Cosenza, Italy.

ABSTRACT

This paper deals with a rainfall-runoff model which represents the most relevant hydrological processes involved in storm runoff production. The modelling framework considers evapotranspiration, infiltration with continuous soil moisture accounting, lateral moisture transfer in the saturated zone and surface runoff routing. The model explicitly accounts for spatial variability in precipitation fields, land-surface descriptors and moisture dynamics. It also enables runoff generation via a variety of mechanisms. The main objective of the study was a general assessment of the capabilities and limitations of the model, testing as much as possible and making use of both conventional strategies and more subjective and qualitative assessments. Preliminary applications are presented that illustrate the model ability to reproduce, through a lumped approach in parameter values, physically significant dynamics for a small Mediterranean catchment. The calibrated model performs well in reproducing observed outflow hydrographs. Further model performance evaluations put emphasis on sensitivity of different runoff generation mechanisms and analyse the major controls exerted on different model outputs, such as discharge, groundwater head and soil moisture content. The tests also involve quantification of parameter uncertainty through the GLUE approach.

1. INTRODUCTION

There are two main application areas for rainfall-runoff models: a model may be used to improve understanding of real-world processes by investigating, typically within research programs, the effects of making certain modelling assumptions, i.e. as tool for hypothesis testing (*Grayson et al.*, 1992); the second use is the application of models as predictive tools in real time warning systems.

In both cases the need for proper validation techniques is generally recognised (*Ewen and Parkin*, 1996; *Christiaens and Feyen*, 2002): whatever the complexity of the modelling structure, which clearly relates to the modelling objectives, model results should be critically assessed in order to obtain appropriate confidence in their reliability.

Indeed, modelling practice always requires a pragmatic approach: model concepts are often developed using partial and imperfect knowledge about many of the dominant processes, as well as data and resource constraints often limit calibration and evaluation. These problems lead to non-unique solutions for the parameter calibration (parameter equifinality), and hence on one hand to the need for the quantification of the uncertainties associated with model parameters and model structure, on the other to the search for reductions with advancements in information and measuring technology and an improved understanding of the physics and effective representation of the associated hydrological processes.

Obviously the type of model application, i.e. investigative versus predictive, has profound implications on both model structure and model calibration/validation. For practical applications, where the purpose of the modelling is to make predictions rather than to gain insight into spatial catchment behaviour, a suitable reproduction of observed hydrographs outside the calibration period may be in many cases sufficient. Models of different complexity can achieve this task satisfactorily. However, today, uncertainty analysis is considered a mandatory step in the prediction context and has to be communicated in the appropriate manner to the decision maker or stakeholder in order to enable a critical assessment of output reliability.

When dealing with more complex, distributed or physically based, rainfall-runoff models it has been pointed out numerous times (*Rosso et al.*, 1994) that verification against discharge data alone is poorly consistent with such multiresponse data modelling. Even if the model can be shown to accurately simulate aggregated processes, that does not give any guarantee that the model provides accurate simulations of all the underlying processes. Ideally, in this case, the internal behaviour, in terms of simulated patterns of state variables and model outputs, should be tested, but, there are rarely sufficient field data for such tests, often limited to small experimental catchments.

Validation methodologies have been subject to considerable discussion and dispute during the past decades with both practical and philosophical undertones (*Anderson and Bates*, 2001). Most of the traditional validation tests in current use were discussed by *Klemeš* (1986); *Refsgaard and Knudsen* (1996) and *Grayson and Bloschl* (2000) emphasised the different requirements for calibration and validation of lumped and distributed models. Recent studies explored the possibility of a better use of the information available, like "soft data", i.e. qualitative knowledge from the experimentalist (*Seibert and Mc Donnell*, 2002), or results from virtual experiments (*Weiler and McDonnell*, 2004), to be used not only to calibrate models but also to help to strengthen the confidence in simulated responses and to check on the consistency of internal model structures and simulations.

This paper introduces an original rainfall-runoff model and illustrates its development, calibration and validation for a Southern Italy catchment. The main features of the model components are presented. The task was to design a model with a level of complexity suited to the amount and the quality of the available data, which basically simulates the key processes of the hydrological cycle involved in storm runoff production, at a small-medium size catchment scale. It also enables to produce a variety of outputs, like soil moisture content and water table depth, which are going to be the object of future field surveys.

In addition the extensive analyses followed in evaluating processes conceptualisation and calibrated parameters are described. A general assessment of the capabilities and limitations of the proposed model was performed: the idea behind was that as much as possible must be tested, making use of both conventional strategies and more subjective and qualitative assessments. A three step approach was taken in model validation. First a traditional split-sample test was carried out. In the second validation step, emphasis was focused on the question of a more general validity and physical soundness of the proposed approach. This task was performed testing the model against hydrological common sense, without the benefit of data. Finally, the GLUE approach was used in quantification of the uncertainty associated with model parameters

2. THE RISE MODEL

2.1 Model structure description

RISE (Runoff by Infiltration and Saturation Excess) is a process-oriented rainfall-runoff model, essentially conceived for applications to small and medium size catchments. It considers both conceptual and physically-based schemes to represent the primary processes of the hydrological cycle, and has been designed through a stepwise approach, with the aim of a realistic description of the mechanisms that are assumed to be dominant in controlling storm runoff production and saturated area space-temporal dynamics.

RISE accounts for spatial distributions of precipitation input and catchment surface characteristics according to the available DEM (Digital Elevation Model) resolution. The elements of this computational grid need to be marked as hillslope or channel cell.

Two modules compose the modelling framework (Figure 1): a soil module that aims at simulating processes involved in surface runoff generation, and a module that reproduces surface runoff routing.

The RISE runoff generation module provides several contributions to storm runoff, spatially distributed over the catchment. The most commonly distinguished processes are represented: runoff produced through limited infiltration capacity (hortonian overland flow); runoff due to saturation of the soil (saturation excess); exfiltration of soil water out of the soil (return flow); fast lateral sub-surface flow.
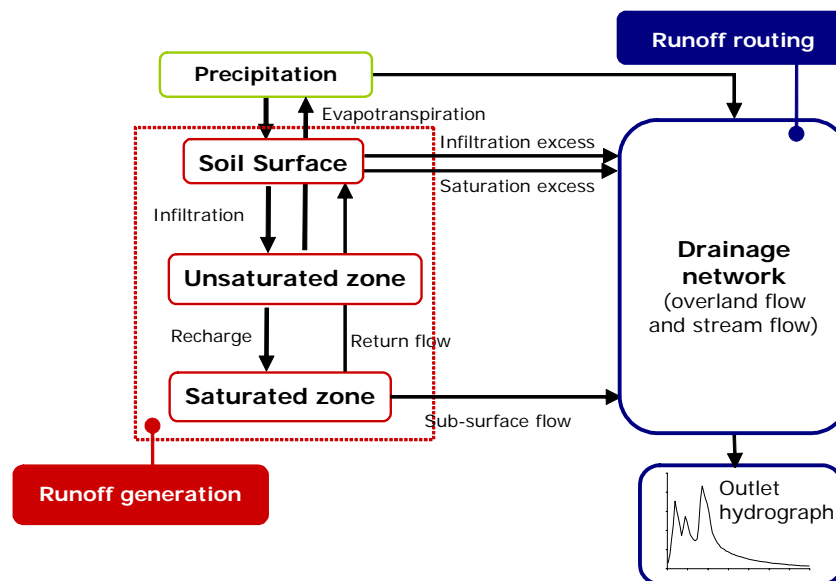
Figure 1. Flow chart of the RISE modelling framework.

To model the dynamics of fluxes and storage processes of water in the top layer of the soil, each grid cell is partitioned into an unsaturated and a saturated zone, with a boundary moving up and down depending on water table level position. Internal variables behaviour, like soil moisture content and water table level, is also represented coupling the one-dimensional representation of the upper soil zone to the more detailed quasi-three dimensional approach for the lower saturated soil zone, where lateral hydrologic fluxes are deemed to be essentials.

A conceptual description is applied in the surface runoff (stream flow and overland

flow) routing module, adopting the Geomorphic Instantaneous Unit Hydrograph (GIUH) approach in the formulation proposed by *Rinaldo et al.* (1995).

For reasons of briefness some model equations which are standard for physically based models are not reported here; more details about model features are in *Versace et al.* (2004) and *Biondi* (2004).

2.2 Unsaturated zone component

The local water balance of the upper unsaturated soil layer is performed during storm-interstorm sequences by calculating the vertical water fluxes between soil, vegetation, and atmosphere. The key variable is the average soil moisture content, which is updated by solving the following continuity equation:

$$z_1 \frac{d\theta}{dt} = \phi(\theta) - R(\theta) - ET \qquad (1)$$

where z_1 is the thickness of the unsaturated layer, θ is the average volumetric soil moisture content, ϕ represents the infiltrated precipitation input, R is the downward flux that recharges the grid cell water table, and ET the evapotranspiration.

The actual infiltration rate, ϕ, in a Horton-type formulation of the infiltration process, corresponds to the rainfall rate, p, limited by the infiltration capacity, f. The latter is assumed to vary between f_{min} and f_{max}, as a non-linear function of θ:

$$f(\theta) = f_{min} + (f_{max} - f_{min}) \left(\frac{\theta_s - \theta}{\theta_s - \theta_r} \right)^n \qquad (2)$$

where θ_r and θ_s represent respectively residual and saturated soil moisture content, and n is a shape factor. Equation (2) provides an empirical expression of the tendency for infiltration capacity to be reduced in response to the actual storage in the unsaturated zone. The minimum infiltration capacity, f_{min}, as assumed in many formulations of the infiltration process, corresponds to the vertical component of the saturated hydraulic conductivity, $K_v^{(s)}$.

The downward flux R is estimated, neglecting the soil matrix potential gradient, according to the Brooks and Corey relationship.

The evapotranspiration flux is taken into account as a water loss in the continuity equation. This loss may be a known quantity, if observations are available, and directly introduced as an input to the model. Otherwise potential evapotranspiration can be estimated internally by means of the physically-based Penman-Monteith equation if required data are available; when local soil moisture content falls below the 60% of its saturation value, actual evapotranspiration is calculated reducing linearly the potential one.

Equation (1) is solved numerically, by applying a simple explicit forward Euler scheme, to yield a first estimation of soil moisture content, which will be referred to as $\theta_{t+\Delta t}^*$. This value is updated after the simulation of saturated zone processes, in order to account for the effect of the water table dynamics on the geometry of unsaturated zone and to maintain the water mass balance.

Within this module, spatially distributed local contributions to storm runoff may occur either as a result of the infiltration capacity or of the total cell capacity being exceeded.

2.3 Saturated zone component

Sub-surface flow in the saturated soil layer is routed laterally downslope till channel elements with an explicit grid cell approach based on that proposed by *Wigmosta et al.* (1994).

The representation of water table development and lateral flow delivery follows the well known Dupuit-Forchheimer assumption. The computational scheme assumes that each grid cell can exchange water with its eight adjacent neighbours. The rate of saturated sub-surface flow $Q_{i,j,k}$ of cell i,j to (or from) its neighbour in the k flow direction (numbered from 0 to 7 in a clockwise direction beginning with the upper left-hand node) is calculated as:

$$Q_{i,j,k} = -T_{i,j,k} b_{i,j,k} J_{i,j,k} \qquad (3)$$

where $T_{i,j,k}$ is the transmissivity at cell i,j corresponding to the k direction, $J_{i,j,k}$ is the local hydraulic (water table) gradient in the k direction, $b_{i,j,k}$ is the width of flow, again in the k direction, estimated as proposed by Quinn et al. (1995). A linear transmissivity profile, and therefore a constant lateral saturated hydraulic conductivity $K_h^{(s)}$, is assumed in the saturated soil thickness $z_2 = Z - z_1$.

The partitioning of outflow from each grid cell is recalculated each time step based on the local hydraulic gradient, thus relaxing the usually adopted kinematic wave approximation, which defines the subsurface flow direction a priori by the surface topography, and the steady state assumption which are often assumed to simplify the model structure, parameterisation, and calculations.

The adopted approach enables a more accurate description in modelling the formation of shallow water tables and the propagation of a transient saturated wave: this condition is representative of many Mediterranean catchments where sub-surface flow is activated only during heavy rainfall events and rarely reaches steady-state conditions.

The change in local hydraulic head over the time step Δt is given by:

$$h_{i,j}^{t+\Delta t} = h_{i,j}^{t} + \frac{1}{\Delta\theta_{i,j}^{t}}\left[\frac{Q_{net_{i,j}}}{A} + R_{i,j}^{\Delta t/2}\right]\Delta t \qquad (4)$$

where $Q_{net_{i,j}}$ is the net saturated subsurface flow for cell i,j given by the sum of the inflows and outflows contributes in each direction; $R_{i,j}^{\Delta t/2}$ is the time averaged rate of recharge to water table from t to t+Δt; *A* is the grid cell area, $\Delta\theta_{i,j}^{t}$ equals $(\theta_s - \theta)$ if water table rises, whereas corresponds to $(\theta_s - \theta_{fc})$ in the case of falling water table, with θ_{fc} the field capacity moisture content.

For those cells flowing directly into a "channel" cell, water table gradient is estimated as the average value of the up-gradient surrounding cells, or is approximated by the local ground surface slope. Their contributions determine the sub-surface flow component of the outlet hydrograph. A return flow input available for the surface runoff routing module comes from the exfiltration of soil water when water table intersects ground surface.

2.4 Unsaturated - saturated zone interaction

A simple conceptual description of the interaction between the saturated and unsaturated zone is implemented in order to account for influence on the soil water content in the unsaturated layer under a changing water table, which represents a moving boundary between the two zones.

The basic assumptions can be briefly resumed as follows. If the water table rises, growth of the saturated zone reduces the unsaturated thickness, where soil moisture content remains constant (as it is assumed that water occupies the voids of the porous medium). The process is reversed when water table falls: a certain portion of saturated zone changes its status to 'unsaturated', characterized by a soil moisture content at field capacity. The average value of soil moisture content on the upper soil layer is updated according to the following mass (water) balance condition:

$$\theta_{t+\Delta t} = \frac{\theta_{fc}(z_1^{t+\Delta t} - z_1^t) + \theta_{t+\Delta t}^* z_1^t}{z_1^{t+\Delta t}}$$

(5)

where z_1^t and $z_1^{t+\Delta t}$ are the unsaturated soil thickness at time t and t+Δt, and $\theta_{t+\Delta t}^*$ is the soil moisture content previously estimated through equation 1.

2.5 Surface runoff routing

Given the soil module outlined above, local contributions to surface runoff are conceptually routed to the catchment outlet by means of the Geomorphologic IUH formulation proposed by *Rinaldo et al.* (1995). A rescaled geomorphologic width function accounts for a different dynamic characterization for hillslopes and stream network introducing a ratio r=u_c/u_h (u_c is the mean celerity in channels and uh the analogous for hillslopes) in the length computation of hillslope path. The probability density function, f(t,x), of travel times in the drainage network is the inverse Gaussian distribution, i.e. the impulse response of the convective diffusive equation representing the flow routing. Other two parameters, assumed uniform throughout the basin, characterize the hydraulic component of the GIUH: the celerity u_c and the longitudinal diffusivity, D_L.

3. STUDY SITE

The applications reported here refer to the test site of the Turbolo Creek catchment (29 km^2), a tributary of the Crati River, located in Southern Italy. The catchment, has a mean slope of 28%, and ranges in elevation from 75 m a.s.l. up to 1015 m a.s.l.. In the western part of the basin the underlying geology consists of metamorphic rock (15%), whereas sand (48%), silty-clay (21%) and alluvial deposits (16%) crop out moving towards terminal sections. Wooded areas (31%) together with olive groves (36%) and agricultural practice (16%) represent the dominant land use. Urbanisation is less than 2% of the total catchment area. More catchment's features are reported in *Taddei and Terranova* (1993).

The climatic conditions strongly affect the seasonal runoff cycle of the torrent which, not being recharged by a significant groundwater reservoir, runs practically dry for long periods and sometimes floods during the winter. Previous studies, based on the superimposition of several physical factors which have the major controls on runoff processes, showed an extensive area affected by the presence of lithotypes with high infiltration capacity and a limited bent for surface runoff production.

The hydro-meteorological database used within this study comprises rainfall, temperature, and discharge values sampled with a 20 minutes temporal resolution.

Eight flood events occurred in 1988 and during the period 2000-2001 have been selected. Table 1 provides a summary of their main characteristics.

Precipitation and temperature were collected in up to 3 stations located within or nearby the basin and are spatially distributed according to the Thiessen polygons method. Runoff measures refer to two locations: events I, II e III concern a stream gauge (drainable area of 29.2 km^2), located at the confluence with the Crati River. After 2000 hydrometric data relate to a gauging station which drains 26 km^2.

Storm event	Date (mm/dd/yy)	Peak discharge (m^3 s^{-1})	Rainfall depth (mm)	Runoff coefficient	API$_5$ (mm)	API$_{30}$ (mm)
I	01/30/88	9.57	54.2	0.32	14.4	64.0
II	02/05/88	7.28	10.2	0.26	3.8	115.0
III	02/09/88	8.64	19.6	0.36	33.8	132.0
IV	01/05/01	7.28	23.0	0.22	15.2	169.2
V	01/08/01	5.83	40.0	0.19	26.8	193.0
VI	01/14/01	4.08	20.4	0.20	27.6	242.8
VII	12/23/01	5.10	19.8	0.25	12.6	117.0
VIII	12/25/01	14.32	42.8	0.33	41.0	147.0

API$_k$ = antecedent precipitation index calculated as the sum of the precipitation backward in

Table 1. Main characteristics of the selected events.

4. MODEL SET-UP AND CALIBRATION

Catchment topography is described by a DEM based on a 30 m resolution mesh. A GIS-based analysis was performed to automatically extract the drainage network from DEM; a $13.5 \cdot 10^4$ m^2 (15 pixels) threshold flow accumulation area for channel initiation was determined through a comparison with the blue lines of topography.

Although most of the RISE parameters have a physical meaning and the model has been designed to incorporate a completely general set of parameter spatial distributions, owing to a lack of site-specific information and to facilitate model calibration, the applications reported here were restricted to a lumped definition of parameters. Spatial variability in the catchment was not considered and 'effective' parameter values were estimated.

Some of the soil parameters were derived empirically from the texture of the main soil type of the catchment, namely the sandy clay soil. The remaining parameters were estimated by calibration through a global optimisation technique, the SCE-UA (Shuffled Complex Evolution - University of Arizona) algorithm (*Duan et al.*, 1992), against the event occurred on 30th January 1988 characterized by a fairly complex shape.

Given the model outlined above, the storm simulation required a consistent definition of soil moisture and water table initial conditions. A realistic spatially distribution of water table depths was assessed by simulating a groundwater recession, without precipitation, from a full saturated state: the assumed distribution was that obtained when subsurface flow reaches the observed initial discharge of the investigated event.

Initial soil moisture, indeed, was uniformly set at a value, θ_0, which was treated as a tuning variable and calibrated. Besides, to have a reasonable distribution of soil moisture content according to the observed precipitation, a 'warm up' period of a month was included at the beginning of the event simulation. Best results were found with the

parameter values reported in Table 2.

The model performed well in simulating the calibration event (Figure 2) showing a good ability to reproduce the value and the timing of observed peaks as well as the overall shape of the hydrograph: the Nash and Sutcliffe model efficiency (R_{eff}) was found to be equal to 0.81 and the values of percentage errors on peak discharge (δQ) and runoff volume (δV) were 7.6 % and 7.4 % respectively.

Parameter	Description	Unit	Value
Z	Soil depth (*)	m	1
f_{max}	Maximum infiltration capacity	m s^{-1}	0.0005
$K_v^{(s)} = f_{min}$	Vertical saturated hydraulic conductivity	m s^{-1}	$9.6 \cdot 10^{-8}$
$K_h^{(s)}$	Horizontal saturated hydraulic conductivity	m s^{-1}	$7.1 \cdot 10^{-5}$
n	Shape factor of the infiltration capacity equation	-	3.75
c	Pore disconnectedness index in Brooks and Corey equation (*)	-	10.4
θ_s	Saturated soil moisture content (*)	-	0.45
θ_r	Residual soil moisture content (*)	-	0.05
θ_0	Initial soil moisture content	-	0.30
θ_{fc}	Field capacity (*)	-	0.22
u_c	Streamflow velocity	m s^{-1}	0.91
r	Ratio (stream velocity/ hillslope velocity)	-	72
D_L	Hydrodynamic dispersion	m^2 s^{-1}	10800

(*) *Non calibrated parameter estimated on the basis of soil geometry and characteristics*

Table 2. Model parameters: optimised values for the calibration event.

5. MODEL VALIDATION

A three step approach was taken in the validation of the model. Firstly a split-sample test was carried out using the other selected events. In the second validation step, emphasis was focused on the question of a more general validity and physical soundness of the proposed approach. As stated in the introduction a satisfactory calibration against catchment outflow does not ensure about accuracy of internal catchment processes model representation. A further evaluation of simulated processes was therefore pursued using internal catchment variables as much as possible. As streamflow data have only been measured for a single gauging station, and presently no soil moisture and water table depth data are available, this task was carried out testing the model conceptualisation via basic principle and standards that are usually referred to as hydrological common sense, without the benefit of data.

Even though the main goal of the modelling practice is to accurately reproduce observed data, this subjective assessment was adopted as a complementary procedure to allow the judgement of how reasonable the structure, the underlying assumptions and the behaviour of internal catchment processes are.

Finally, as crucial part of model evaluation, Generalised Likelihood Uncertainty Estimator (GLUE) was used as a tool for parameter uncertainty assessment.
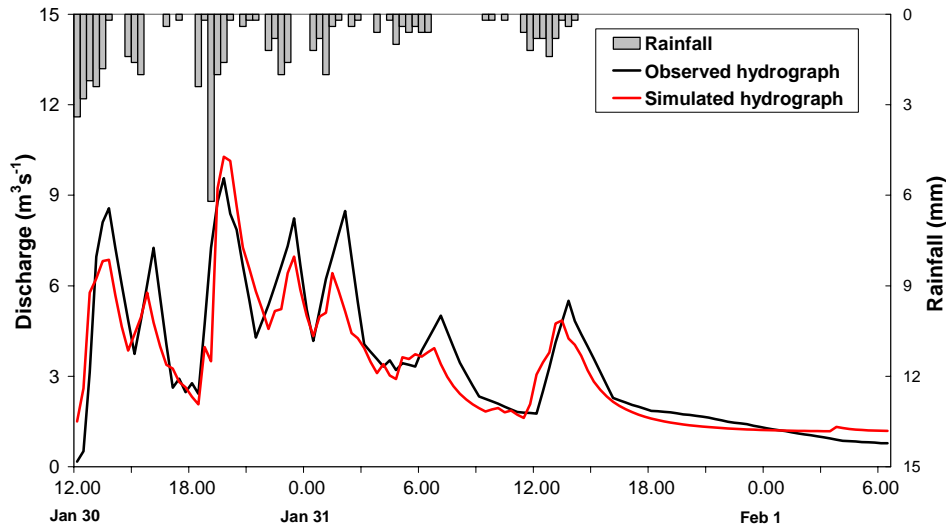
Figure 2. Comparison of simulated (red line) and observed hydrograph (black line) for the calibration event (storm I).

5.1. Validation against data

A traditional split-sample test was conducted against events not used for calibration. RISE was here applied like an event based model and only the parameter θ_0 was varied for each event to account for initial soil moisture conditions.

Summary results are shown in Table 3 in terms of R_{eff}, δV and δQ. On the whole the values of the adopted goodness-of-fit functions are of the same order of magnitude as during the calibration period.

Storm event	R_{eff}	δV (%)	δQ (%)
II	0.83	10.0	9.8
III	0.94	7.1	2.1
IV	0.77	15.3	14.1
V	0.08	23.6	3.1
VI	0.87	2.2	23.2
VII	0.85	12.9	11.5
VIII	0.87	15.7	2.2

Table 3. Model performance for the validation events.

Figures 3a and 3b provide a view of the comparison between the observed and simulated hydrographs for two events, storm III and V, which, according to Nash and Sutcliffe efficiency, represent the best and the worst results respectively. Event V is a long lasting, multi-peak storm event with a catchment response which was expected to be difficult to simulate. However, even in this case, the fit can be considered quite good, in view of the limited amount of data used for model calibration, and the small error affecting peak flow reproduction.
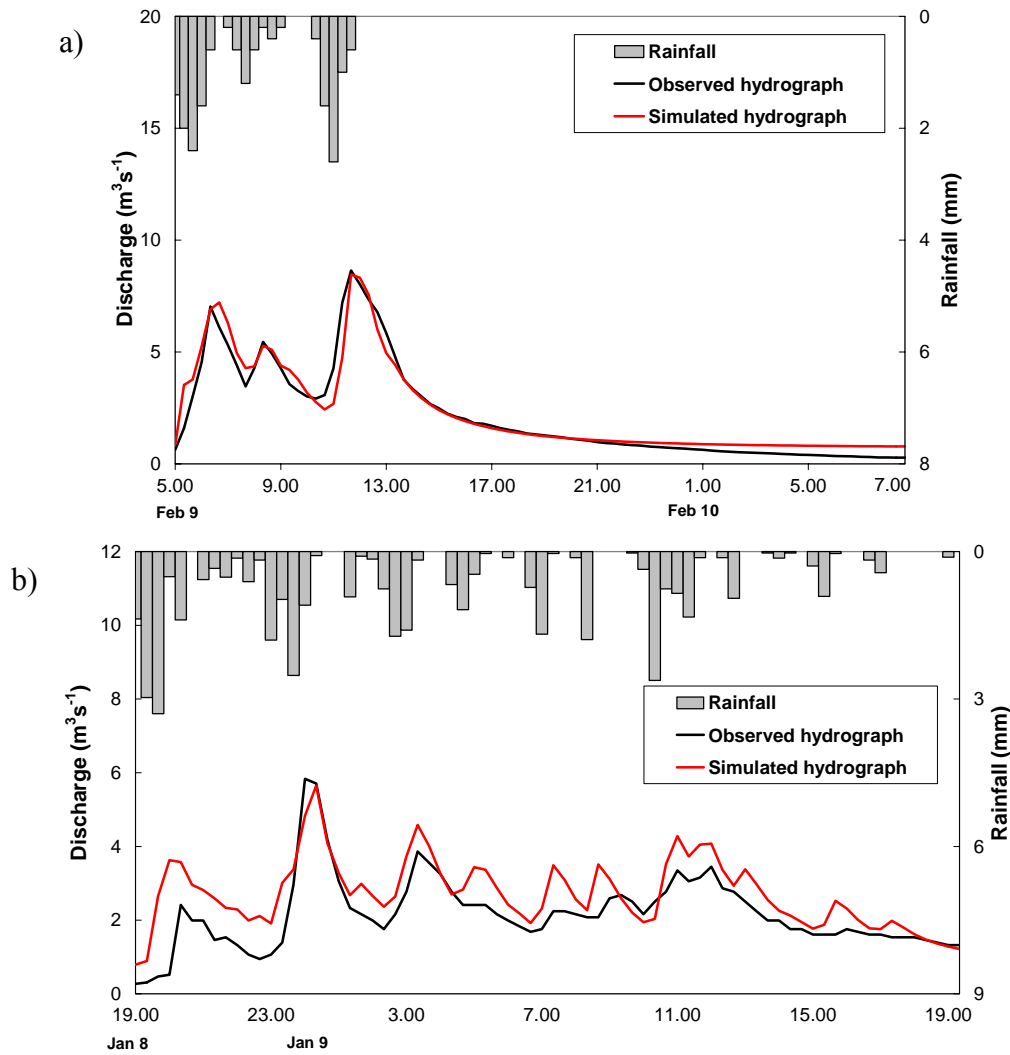
Figure 3. Comparison of simulated and observed hydrograph; a) validation event III; b) validation event V.

5.2. Validation against hydrological common sense

Several qualitative assessments were considered in the second phase of model validation: i) evaluation of model ability in reproducing different runoff generation mechanisms; ii) evaluation of estimated spatial delineation of runoff production source areas, and evaluation of simulated behaviour of internal variables; iii) evaluation of model response plausibility for 'virtual' applications representing different hydrological conditions.

The first check was performed simulating longer periods which alternate storm and interstorms sequences. For these applications potential evapotranspiration was calculated by means of the Penman-Monteith equation. Several variables (except for air temperature and wind speed) were taken from literature or estimated with simplified equations.

Figure 4 shows temporal variability of the different simulated contributions to total catchment runoff for the events occurred on January 2001 and December 2001. A reasonable agreement between simulated and observed discharge (not shown here) was reached: model efficiencies over the entire simulation period amounted respectively to 0.65 and 0.87.
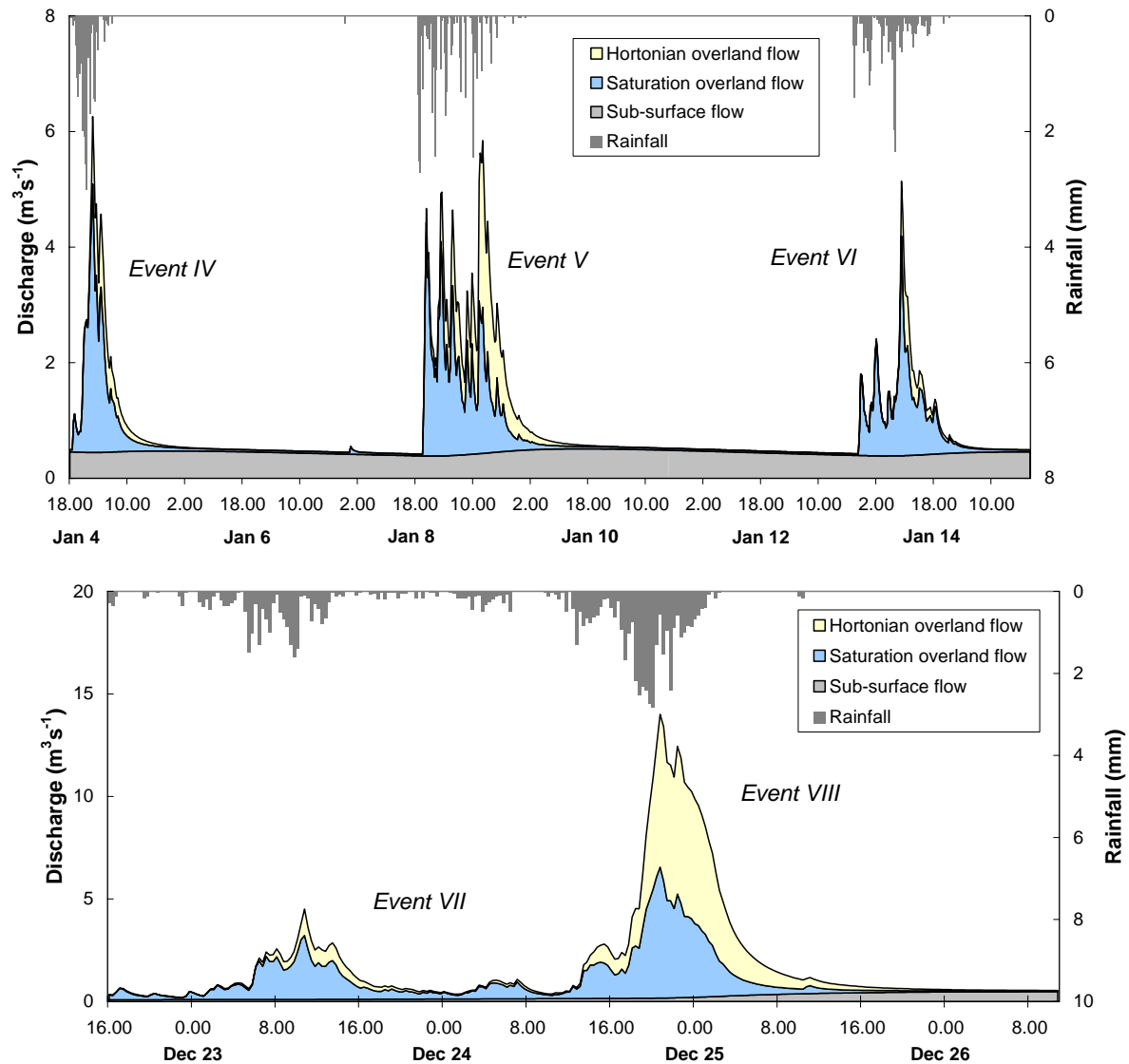
Figure 4. Partitioning of the simulated hydrographs according to runoff generation mechanisms.

Results suggest that catchment runoff is mainly produced by the saturation excess mechanism, while hortonian overland flow is associated with high intensity rainfall and/or with cells that approaching to saturation reduce their infiltration capacity. Return flow, which is included in saturation overland flow, also contributes to the total runoff after the storm event as saturation conditions still occurs in the riparian areas during recession period.

The potential and suitability of the RISE conceptualisation was also tested assessing, the spatial delineation of cells with the same dominant runoff generation processes during the event. Two snapshots illustrating the spatial distribution of contributing areas for different runoff production mechanisms, as resulted for time to peak of the events VII and VIII, are sketched respectively in Figures 5a and 5b.

Figure 5a shows that areas of surface saturation (including stream network) are mainly located at the bottom of hillslopes, in zones of convergent topography; hortonian overland flow is active as a runoff mechanism over a limited portion of the catchment.
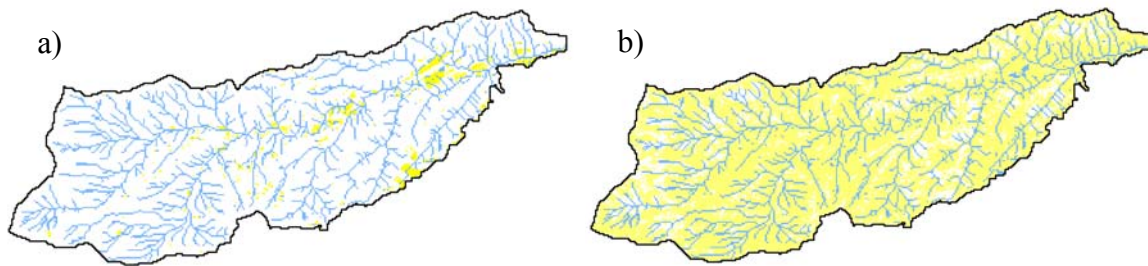
Figure 5. Simulated distributions of different runoff production areas (infiltration excess yellow
- and saturation excess – blue) for the peaks of the events VII and VIII.

In contrast, as indicated by the substantial number of yellow pixels in Figure 5b, infiltration excess is largely produced in the catchment, while saturation overland flow is restricted to near-channel saturated areas. Analyses of internal variables behaviour (not showed here, see *Biondi*, 2004) also showed model ability to realistically represent the role of different catchment landscape portions.

These results about the storm runoff generation processes can be considered quite appropriate for the examined catchment, even if the lack of spatial variability in soil properties may surely play a critical role in understanding the catchment behaviour and in identifying dominant processes taking place at a particular site. The widespread production of infiltration excess (Figure 5b), for example, is certainly due to the fact the soil properties in the simulation were uniformly assumed across the catchment.

Finally, a series of 'virtual experiments' were developed: the underlying philosophy of this approach is to use the model as a virtual landscape and to perform numerical experiments to explore and capture all major controls on simulated response.

One set of experiments were focused on the control exerted by rainfall intensity and initial soil moisture on flow and runoff generation mechanism.

Two types of rainfall event were designed: the first one was a long duration, low event with an intensity of 3 mm·h^{-1} which lasted 48 hours; the second was a high intensity rainfall with a total amount of 120 mm distributed over two hours. Two different values of θ_0, corresponding to 0.1 and 0.4, were assumed to represent a dry and a wet condition respectively. The outflow hydrograph of total runoff and its main contributions are shown in Figure 6.

The first row highlights for the high intensity event how the two initial soil moisture conditions yielded strongly different catchment responses. This is mainly due to the non linear conceptualisation of hortonian overland flow production, while, in both cases saturation overland flow do not vary significantly due the threshold nature of the process, which is evidently limited by catchment topography and take place only in riparian zones. The second row refers to the low event and shows quite the same behaviour. In the wet condition also a significant subsurface flow is activated because of the redistribution of near surface soil moisture. For both events, the peak discharge of the wet conditions almost increase fourfold that obtained in the dry case.
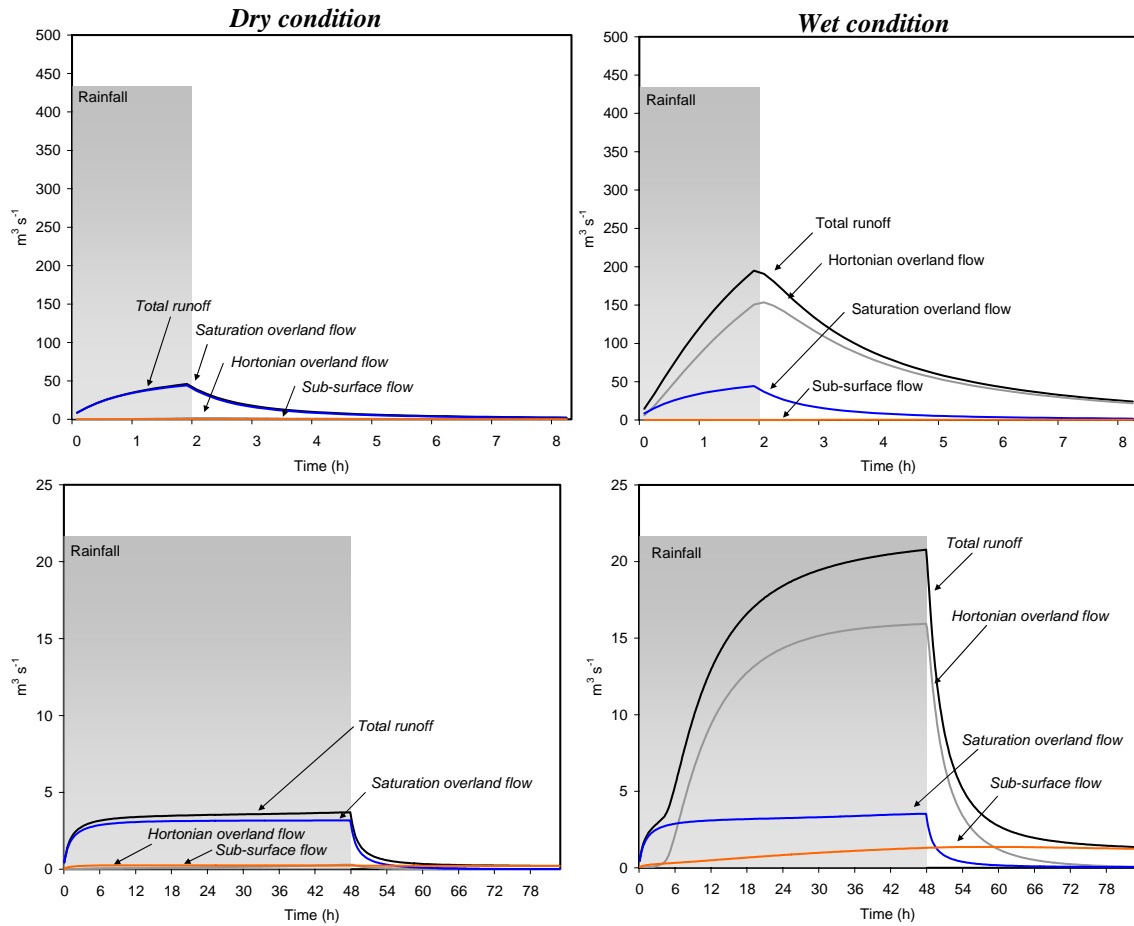
Figure 6. Effects of different initial soil moisture (dry and wet condition) and precipitation event on catchment runoff generation.

6. UNCERTAINTY ASSESSMENT

6.1 The GLUE approach

Model performance was assessed using the Generalised Likelihood Uncertainty Estimation (GLUE) procedure (*Beven and Binley*, 1992), which allows for the concept of equifinality of models and parameter sets in the evaluation of predictive uncertainty. Within the present application we will refer only to the propagation on simulated discharge of the uncertainty associated with parameters.

GLUE technique involves random generation of a large number of independent sets of parameter values. For each parameter set, a model simulation is performed, and the value of a goodness-of-fit function, or "likelihood measure", calculated. All parameter sets for which the likelihood measure falls below a specified threshold are rejected as "non-behavioural" according to the terminology introduced by *Spear and Hornberger* (1980).

The likelihood measure associated to behavioural simulations is then normalised and used to construct, at each time step, a cumulative distribution function of simulated discharge from which uncertainty bounds can be derived in a non linear modelling context. Likelihood weights, implicitly assuming stationary, can be used in prediction mode and updated through a Bayesian revision process, if new observations are available to improve the model evaluation.

257

6.2 GLUE application

As often remarked in literature, it is necessary to recognise that GLUE methodology introduces several degrees of subjectivity: the choice of the model, the period of data used in evaluation, the feasible ranges for each parameter value, the sampling strategy, the chosen likelihood measure and threshold value (*Beven*, 2001). Each choice made within this application is explicitly reported below.

Generation of parameter sets was based on Latin Hypercube Sampling (LHS), that has been showed (*Yu et al.*, 2001; *Sieber and Uhlenbrook*, 2005) to be a powerful tool for model uncertainty and sensitivity analyses because it requires a less computing power and significantly fewer simulations to represent adequately the parameter space than the conventional Monte Carlo random sampling.

In LHS the range of each parameter is subdivided into N equiprobable intervals, with N representing the number of required parameter combinations. A uniform distribution was assumed to represent the "prior information" about variation of the parameter values, therefore each interval was set to equal size. The generation was executed N times according to a stratified sampling, randomly pairing the parameters values. Parameters were sampled from the ranges listed in Table 4.

Parameter	Min	Max	Parameter	Min	Max
$A \ [m^2]$	8100	13500	$\theta_s \ [-]$	0.4	0.5
$Z \ [m]$	0.5	3	$\theta_r \ [-]$	0.01	0.12
$f_{max} \ [m \ s^{-1}]$	10^{-4}	10^{-2}	$\theta_0 \ [-]$	0.01	0.5
$f_{min} \ [m \ s^{-1}]$	10^{-9}	10^{-4}	$r \ [-]$	1	100
$K_h^{(s)} \ [m \ s^{-1}]$	10^{-9}	10^{-3}	$u_c \ [m \ s^{-1}]$	0.5	5
$n \ [-]$	1	20	$D_L \ [m^2 \ s^{-1}]$	10	100000
$c \ [-]$	5	20			

Table 4. Ranges of the parameters used within the GLUE framework.

In literature the assessment of the necessary number of model runs is usually performed by checking convergence of some model output statistics. Figures 7 show the value of mean and standard deviation of simulated peak discharge and runoff volume error obtained for storm event IV, which was chosen as the GLUE calibration event: all statistical measures quite yield convergence to constant values when N exceeds 400. Notwithstanding, the number of model runs was set to 1500, much more than ten times the number of investigated parameters, which is the value usually recommended.

Evaluation of acceptability of model realisations, to discriminate between behavioural and non-behavioural sets, was here performed according to what suggested by *Beven* (2006). A simulation was retained as suitable when its prediction falls within prior limits of acceptability which account for an appropriate level of error on observed data:

$$Q_{min}(t) < Q_{sim}(t) < Q_{max}(t) \tag{6}$$

for all time step t. Owing to our modelling task, emphasis was put on behavioural simulations associated with a good reproduction of higher rather than lower flows. In what follows the range of acceptability that brackets the observational data was:

$$Q_{min}(t) = 0.5 Q_{obs}(t) \ ; \ Q_{max}(t) = 1.5 Q_{obs}(t) \qquad \qquad if \ Q_{obs}(t) \geq 3 \ m^3 / s \tag{7}$$

Only the 7% of the simulations were classified as behavioural.
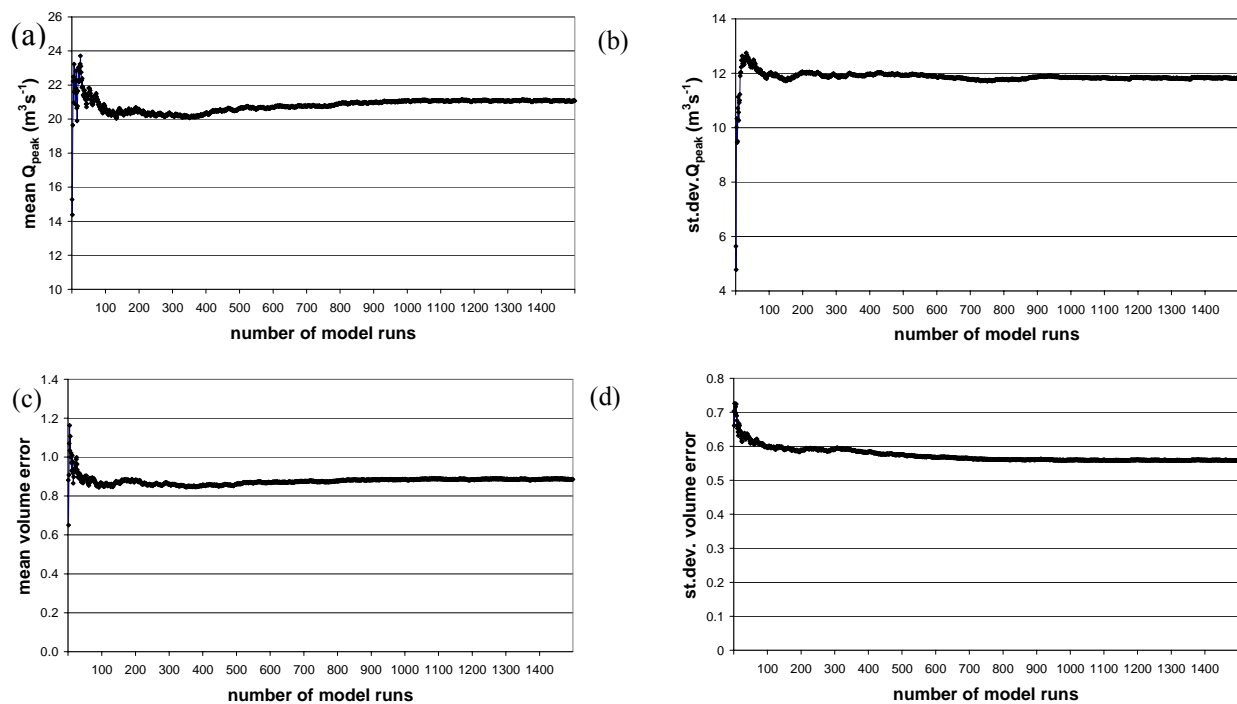
Figure 7. Mean and standard deviation of the simulated peak discharge Q_{peak} (a and b) and of volume error (c and d) for event IV versus the number of simulations.

For each time step a weight was assigned to the model prediction according to a simple triangular weighting scheme, with the peak at observation. It can be considered equivalent to a fuzzy membership function which reflects the level of goodness of fit and defines an acceptable error around an observed value. Then, to evaluate the prediction limits, these weights were summed and rescaled to provide a single weight associated with a particular set of parameter for the whole calibration period.

Uncertainty bounds were drawn at values of the simulated variable corresponding to selected quantiles of the distribution, the 5th and 95th percentiles.

As shown in Figures 8a and 8b for the calibration event and for one of the validation periods (including event VII and event VIII), the prediction bounds are broad and span the observed data. Despite the adopted criterion of acceptability, the proportion of observations bracketed by the prediction limits for the calibration and the validation period is equal to 87% and 80% respectively. In both cases the model performs more effectively around the higher flow and uncertainty limits include the observed peak.

GLUE has also been used as a valuable tool for testing model behaviour: indeed, deviations of prediction limits from the observations suggest that either can be structural or data errors. Actually the visual analysis of the results revealed that: i) the model often seems to anticipate the rising limb of the observed hydrographs; ii) the simulation of recession limbs or dry periods is apparently biased, with a systematic underestimation of flow. The first remark can possibly be a consequence of the value assumed for the limits of threshold area for channel initiation, which was not calibrated and that should produce an increase in the saturation excess response to precipitation. The latter notice obviously reflects the choice of the criterion (eq. 7) of acceptability; anyway it is an indication that drier periods seem to be the most difficult to model and that their dynamics may be more appropriately represented. This is a task for future studies.
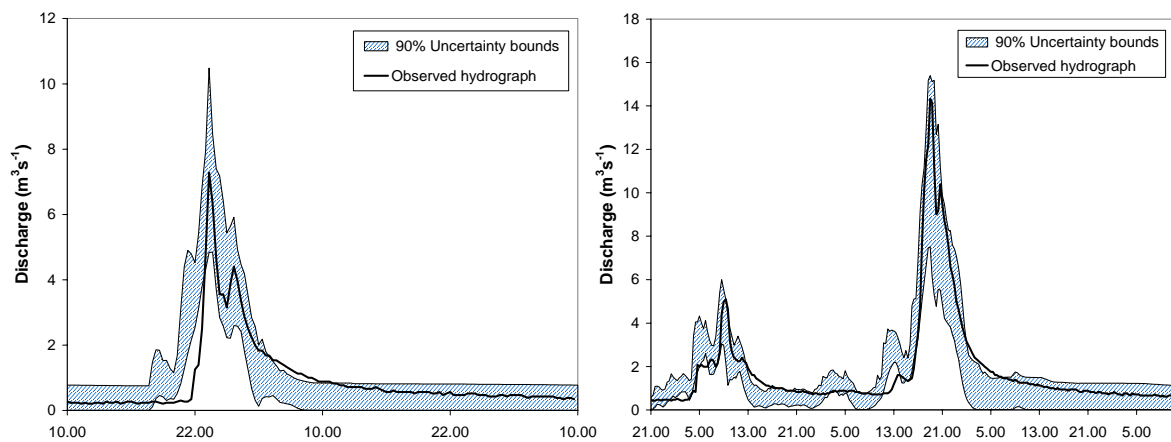
Figure 8. Observed hydrograph and 90% uncertainty bounds obtained with the GLUE approach. a) GLUE calibration event (storm IV); b) December 2001 validation period.

7. CONCLUSIONS

A modelling scheme for rainfall-runoff simulation, based on both infiltration and saturation excess mechanism, was tested on a Southern Italy basin. The model evaluation through a classic split-sample procedure, using several performance criteria, showed a quite good reproduction of the observed hydrographs both for calibration and validation events. A second set of simulations, performed against the hydrological common sense, gave further insight into model behaviour in reproducing different runoff generation mechanisms. Also virtual experiments showed model ability to realistically represent the role of different catchment landscape units on storm runoff production and internal variables behaviour. The GLUE assessment performed to evaluate propagation on simulated discharge of the uncertainty associated with parameters confirmed model ability to simulate high flow periods, with quite narrow uncertainty bounds including peak values. The last analysis also revealed some model shortcomings in reproducing low flow periods of the investigated events.

REFERENCES

Anderson, M.G., and P.D. Bates (eds.) (2001), *Model Validation: Perspectives in Hydrological Science*, Wiley, Chichester.

Beven, K.J., and A.M. Binley (1992), The Future of Distributed Models: Model Calibration and Predictive Uncertainty, *Hydrol. Proc., 6*, 279-298.

Beven, K.J. (2001), *Rainfall-Runoff Modelling: The Primer*, Wiley and Sons.

Beven, K.J. (2006), A manifesto for the equifinality thesis, *J. Hydrol., 320*, 18-36.

Biondi, D. (2004), Sviluppo, taratura e validazione dei modelli di trasformazione afflussi-deflussi, Ph.D. Dissertation, University of Calabria, Cosenza, Italy *(in Italian)*.

Christiaens, K., and J. Feyen (2002), Constraining soil hydraulic parameter and output uncertainty of the distributed hydrological MIKE-SHE model using the GLUE framework, *Hydrol. Proc., 16*, 373-391.

Duan, Q., S. Sorooshian, and V.K. Gupta (1992), Effective and efficient global minimization, *Water Resour. Res., 28*(4), 1015-1031.

Ewen, J., and G. Parkin (1996), Validation of catchment models for predicting lad-use and climate change impacts, *J. Hydrol.*, *175*, 583-594.

Grayson, R.B., I.D. Moore, and T.A. McMahon (1992), Physically Based Hydrologic Modeling 1. A Terrain-Based Model for Investigative Purposes, *Water Resour. Res.*, *28*(10), 2639-2658.

Grayson, R.B., and G. Blöschl (eds.) (2000), *Spatial Patterns in Catchment Hydrology: Observations and Modeling*, Cambridge University Press, Cambridge (UK).

Klemeš, V. (1986), Operational testing of hydrological simulation models, *Hydrol. Sciences J.*, *31*(1), 13-24.

Quinn P.F., K.J. Beven and R. Lamb (1995), The ln(a/tanβ) index: how to calculate it and how to use it in the TOPMODEL framework, *Hydrol. Proc., 9*, 161-182.

Refsgaard, J.C., and J. Knudsen (1996), Operational validation and intercomparison of different types of hydrological models, *Water Resour. Res.*, *32*(7), 2189-2202.

Rinaldo, A., G.K. Vogel, R. Rigon, and I. Rodriguez-Iturbe (1995), Can one gauge the shape of a basin?, *Water Resour. Res.*, *31*(4), 1119-1127.

Rosso, R. (1994), An introduction to spatially distributed modelling of basin response, in *Advances in Distributed Hydrology*, edited by R. Rosso, A. Peano, I. Becchi and G. Bemporad, pp. 3-30, *Water Resources Publications,* Highlands Ranch, Colorado.

Seibert, J., and J.J. McDonnell (2002), On the dialog between experimentalist and modeller in catchment hydrology: Use of soft data for multicriteria model calibration, *Water Resour. Res.*, *38*(11), 1241.

Sieber, A., and S. Uhlenbrook (2005), Sensitivity analyses of a distributed catchment model to verify model structure, *J. Hydrol.*, *310*, 216-235.

Taddei, A., and O. Terranova (1993), Areal Investigation of Surface Runoff Propensity in a Model Basin, in *Environmental Management, Geo-Water & Engineering Aspects*, edited by Chowdhury and Sivakumar, pp. 503-507, Balkema, Rotterdam.

Versace, P., D. Biondi, and B. Sirangelo (2004), La generazione dei deflussi nella simulazione delle piene fluviali, *Atti del XXIX Convegno di Idraulica e Costruzioni Idrauliche*, Vol. 2, pp. 855-862, Trento *(in Italian).*

Weiler, M., and J. McDonnell (2004), Virtual experiments: a new approach for improving process conceptualization in hillslope hydrology, *J. Hydrol.*, *285*, 3-18.

Wigmosta, M.S., L.W. Vail, and D.P. Lettenmaier (1994), A Distributed Hydrology-Vegetation Model for Complex Terrain, *Water Resour. Res.*, *30*(6), 1665-1679.

Yu, P.S., T.Ch. Yang, and S.J. Chen (2001), Comparison of uncertainty analysis methods for a distributed rainfall-runoff model, *J. Hydrol.*, *244*, 43-59.

Observing and modelling exceptional floods and rainfalls
Proceedings of the AMHY-FRIEND International Workshop on Hydrological Extremes,
held at University of Calabria, Cosenza (Italy), May 3-4, 2006

REGIONALIZATION OF EXTREME RAINFALL AND DISCHARGES IN SLOVENIA

M. Brilly, S. Rusjan, T. Srebrnič and M. Mikoš

Faculty of Civil and Geodetic Engineering, Chair of Hydrology and Hydraulic Engineering, University of Ljubljana, Slovenia

ABSTRACT

For planning of river engineering works (river regulation works, erection of hydro power plants and similar works) and other construction works along and in watercourses (bridges, retaining walls for roads and similar works) it is necessary to know the water regime of each single watercourse, where construction works are planned. Aiming at this, we analyzed the seasonality of discharges in Slovenia on the basis of standard hydrologic data, which are available through the Environmental Agency of the Republic of Slovenia, Ministry of the Environment and Physical Planning. For 305 river gauging stations on Slovenian watercourses we performed an analysis of seasonality of maximum annual discharges, maximum mean monthly discharges, and minimum mean monthly discharges. The results of the analysis are graphically shown in a map of Slovenia and they make it possible to plan the construction works outside the period of maximum discharges (high flows). As determined by the analysis of maximum annual discharges flood seasonality shows that floods in the alpine part of Slovenia should be expected in autumn. In the western part of Slovenia they typically happen in late autumn and in early winter, and in the eastern part of Slovenia they are observed in late summer. In the south-eastern part of Slovenia no pronounced flood seasonality can be observed, the reason may be the karstic lithological composition.

1. INTRODUCTION

Regional estimation of hydrological parameters has challenged hydrologists and different methodologies for regional estimation of parameters have been derived (*Bloschl and Sivapalan*, 1997). Regional analyzes help in understanding of hydrological processes and estimation of regimes on the rivers and streams without measurements. But there are some gaps in trying to delineate the regimes. The problem is how to incorporate the impact of upstream rainfall distribution on the downstream hydrological regime an how to recognize it.

Slovenia is situated close to the northern part of the Adriatic Sea, where the Alps and Dinaric Mountains clash and form a barrier between seaside and the Pannonian plain (Figure 1). The cyclones that contribute the largest amount of precipitation in Slovenia make their way from the Atlantic, south of the Alps, through the mountain slopes (Figure 2). The mean annual precipitation is highest in the Dinaric Alps. From the Alps towards the sea the annual amount of precipitation largely depends on the orographic factors and the gauging stations in dependence of altitude and position of surrounding mountains, show very different results at small distance. At the seaside, the precipitation is as low as 900 mm. From west and southwest towards east and north, the amount of precipitation

decreases, first rapidly, and then more gradually (Figure 3). Eastwards the precipitation further reduces to about 750 mm at the Pannonian Plain. The average annual precipitation in Slovenia is thus 1500 mm (*Brilly*, 1997).

Figure 1. Digital terrain model of Slovenia.
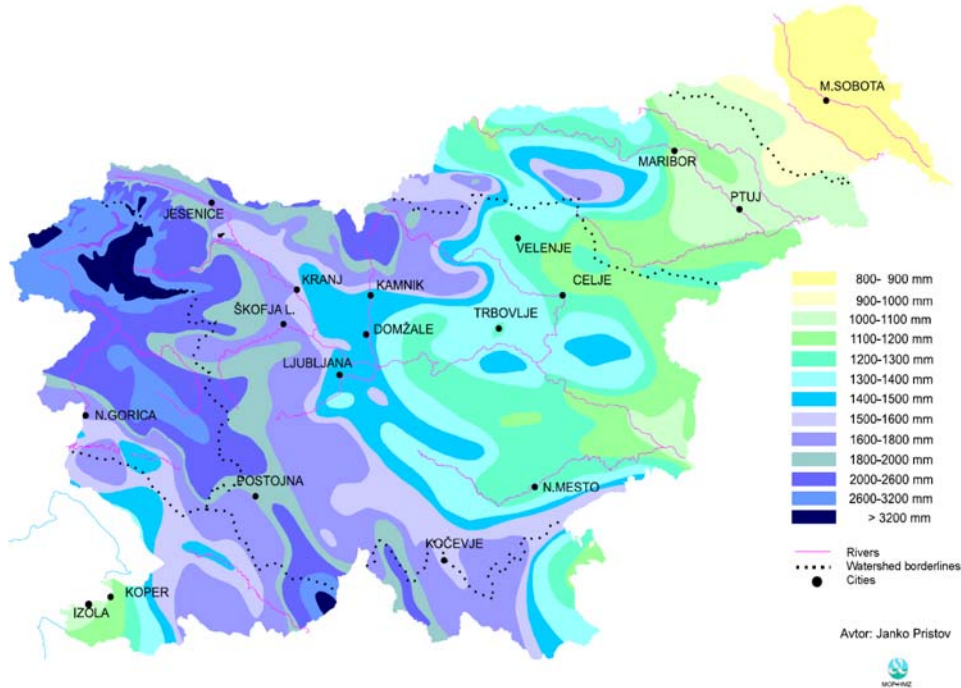
Figure 2. Map of precipitation of Slovenia for the period 1961–1990.
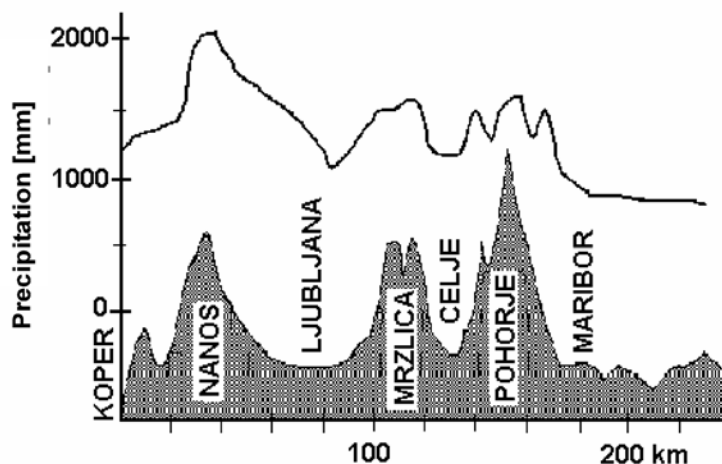
Figure 3. Change of annual precipitation with distance from the sea.

Rainfall distribution and runoff have a high variety. The quantity of annual precipitation changes with extremely short distance, therefore the regionalization of hydrological data and determination of (generally) valid simple empirical correlations of hydrological variables in the territory of Slovenia is not adequate. The phenomena are extremely versatile, and each area and each river are unique.

Due to soil composition and evapotranspiration, the distribution of surface runoff is somewhat more heterogeneous (Figure 4).
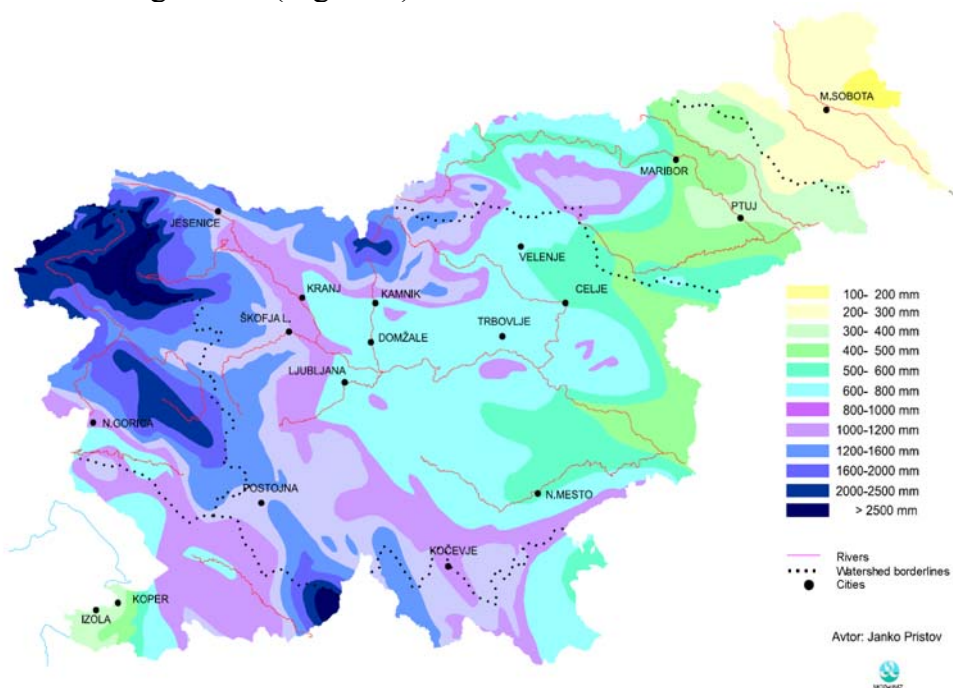
Figure 4. Runoff calculated for the period 1961–1990.

The most recent study of seasonality of single regions in Slovenia was performed in 1999 by M. Hrvatin from the Anton Melik Geographical Institute (Geografski instituta Antona Melika ZRC SAZU). All gauging stations with continuous measurements for the period 1961–1990 were considered. The regimes were determined by way of monthly runoff coefficients, and the hierarchical classification into groups was done by the Ward

method taking into consideration the Manhattan distances. 8 types of runoff types were identified that were named after the regional unit that they were characteristic of, and according to the origin of water source. Within the European project entitled "Flood estimation methods and associated impacts on design and management practices" the European countries have developed and proposed several methods for flood forecasting.

The expert group from the Technical University of Vienna developed an interesting approach, which included the spatial distribution of precipitation and runoff in Austria; based on the analysis of seasonality of these data they were able to establish the time of floods in different parts of Austria and the major reasons for their occurrence. In this paper, their method was applied to Slovenian territory using the data from Slovene meteorological and water stations.

2. METHODOLOGY

Floods are the result of meteorological and hydrological processes that intertwine and occasionally lead to extreme runoff. The emergence of floods is a complex process, lacking predictability, and hence the methods for prediction of probability of occurrence are based on analysis of probability of the event without any special analysis of the underlying physical reasons of the event. That is why the need has been identified to find an approach that would include a deeper understanding of physical processes in occurrence of floods (*Bloschl*, 2001).

All processes that bring about the occurrence of floods and relate to physical phenomena have specific characteristics, such as periodicity, seasonality, disproportionality and certain limits. We can infer from these characteristics, what are the most contributing processes. The advantage of such an approach is that it is based on standard hydrological and meteorological data obtained from a network of observation stations, and special data obtained with highly demanding and expensive research are not needed (*Bloschl*, 2001).

The method that was used in analysing the seasonality of occurrence of the highest annual discharges and the maximum annual daily precipitation, which was used also in the Austrian analysis (*Merz et al.*, 1999), was proposed by *Burn* (1997). First, the date (day, month) of occurrence of the annual maximum discharge and maximum annual daily precipitation for each station was transformed into the Julian Day (the consecutive day of the year), where 1st January is day 1 and 31st December is day 365 (Figure 5).

The Julian Day indicating the day of the year of maximum precipitation (peak) was transformed as:

$$\theta = \left(\text{julian day} \right) \times \left(\frac{2\pi}{365} \right) \tag{1}$$

The value of θ is angle in radians indicating the maximum in that particular year (θ=0 degrees means 1 January, θ=360 degrees means 31 December). The date of the occurrence of the maximum value can be interpreted as a vector, whose direction is determined by angle θ. If there are n-events available for a certain station (n is the number of years for which data are available), the procedure given above can be used for graphic representation of the date of the occurrence of the maximum.
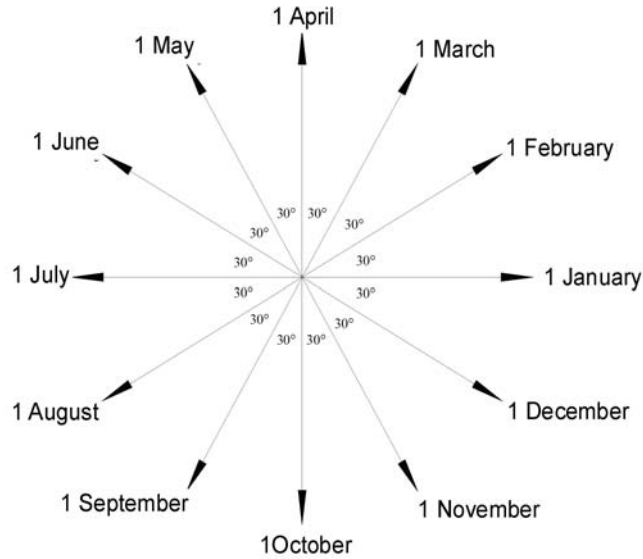
Figure 5. Definition of the vector direction, indicating the date of the maximum annual discharge and maximum annual daily precipitation.

From the set of n data (n is the number of years for which data are available) for each station the $\overline{x}$ and $\overline{y}$ coordinates of the average date of the occurrence of the maximum are calculated:

$$\overline{x} = \frac{1}{n} \sum_{i=1}^{n} \cos(\theta_i) \tag{2}$$

$$\overline{y} = \frac{1}{n} \sum_{i=1}^{n} \sin(\theta_i) \tag{3}$$

The values of $\overline{x}$ in $\overline{y}$ represent the x and y coordinates of the average date of the occurrence of the maximum. The average direction of the vector, showing the date of the maximum, is obtained in the following equation:

$$\overline{\theta} = \tan^{-1}\left(\frac{\overline{y}}{\overline{x}}\right) \tag{4}$$

In this way we obtained the average direction of the vector given in radians, however, it can be expressed as a Julian Day as:

$$MD = \overline{\theta}\frac{365}{2\pi} \tag{5}$$

The value of MD represents the mean day (Julian Day) of maximum annual discharge in each gauging station and mean day (Julian Day) of occurrence of annual daily precipitation in each meteorological station.

The length of the vector, representing the measure of variability of event in single stations, is defined as:

$$\overline{r} = \sqrt{\overline{x}^2 + \overline{y}^2} \tag{6}$$

The parameter $\overline{r}$, whose values spans between 0 and 1, is a dimensionless unit indicating the distribution of dates of flood water around the mean date of occurrence of high water in single stations. If the value $\overline{r}=1$ it means that in the data set the maximum occurs exactly on the same day in the year. If the value is $\overline{r}=0$, this means that there is a high variability in the data set and that high water happens on a different day in the year. Actually, the value of 1 is never reached, however one needs to know that with the value

267

of r̄ approaching 1, the seasonality of the event is more profound. For a further analysis and spatial representation by way of maps we used the AutoCAD software (Figure 6).

For the analysis we used the data that are regularly collected by the Environmental Agency of the Republic of Slovenia (ARSO) at the measuring network of meteorological and water stations in Slovenia. At the Agency, these data are kept in extensive databases and each year they are published in the Meteorological Annals, while the hydrological data are published in the Hydrological Yearbook.
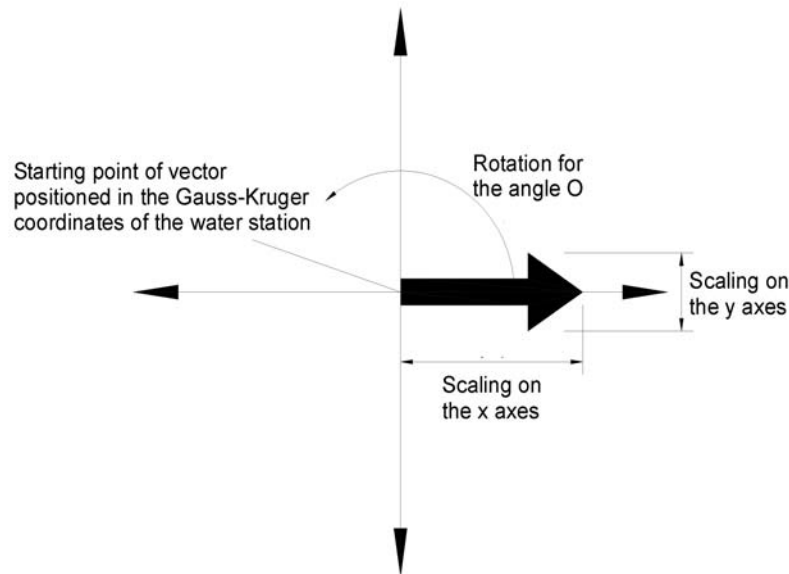
Figure 6. Principle of drawing vectors in AutoCAD Map.

3. ANALYSIS

3.1 Rainfall data

Since the mid-19th century, precipitation has been observed in Slovenia with the introduction of the hydro-meteorological service of the Austro-Hungarian Monarchy. Traditionally, in Slovenia the Hellmann-type rain gauges without shield are used. The number of rain gauges steadily increased until the 1980's when there were 342 rain gauges. Then the number started to decrease to 240 rain gauges of today. About 25 % are rain gauge recorders that also measure the intensity of rain (Figure 7).
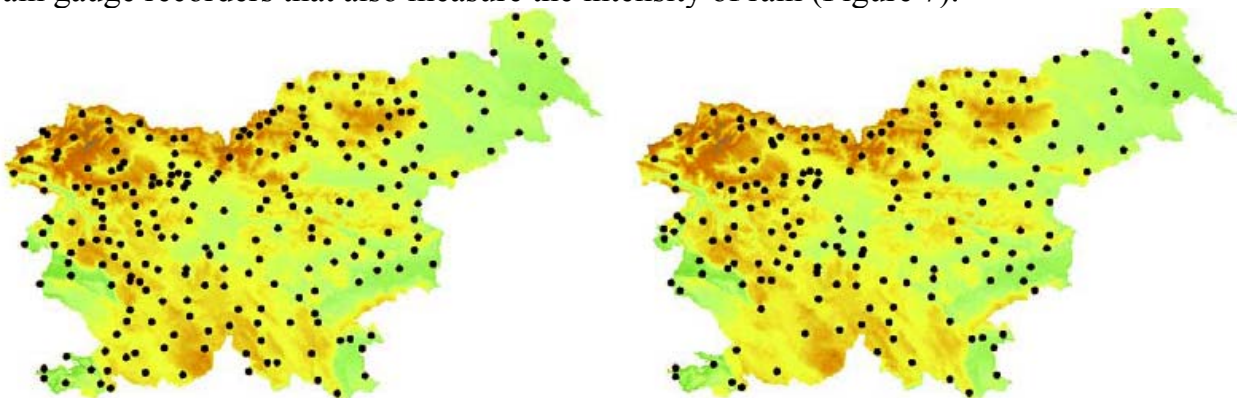
Figure 7. Spatial distribution of precipitation stations for 1975 (left) and 2001 (right)
(Source: Environmental Agency of the Republic of Slovenia (ARSO)).

For each meteorological station the data about the date of the highest annual precipitation, month of the highest mean monthly precipitation and quantity of precipitation were collected. The analysis included the data from all meteorological stations under the condition that they had been in operation for at least 5 years. Besides the date and month of the before mentioned values, we also recorded the type of precipitation. The database for analysis of seasonality of maximum annual daily precipitation thus contained the data on 370 stations. 2004 was the last year included into the database.

3.2 Runoff data

In Slovenia, there are about 160 water stations. On average, each station covers about 175 km of streams and an area of 125 km^2 (*Bat*, 2003). The water level and occasionally also discharge are measured in the water stations, which enable the making of discharge curves. The discharge is determined based on the water levels and discharge curves. Hence, in Slovenia the system of observations and measurements is based on the classic network of water stations.
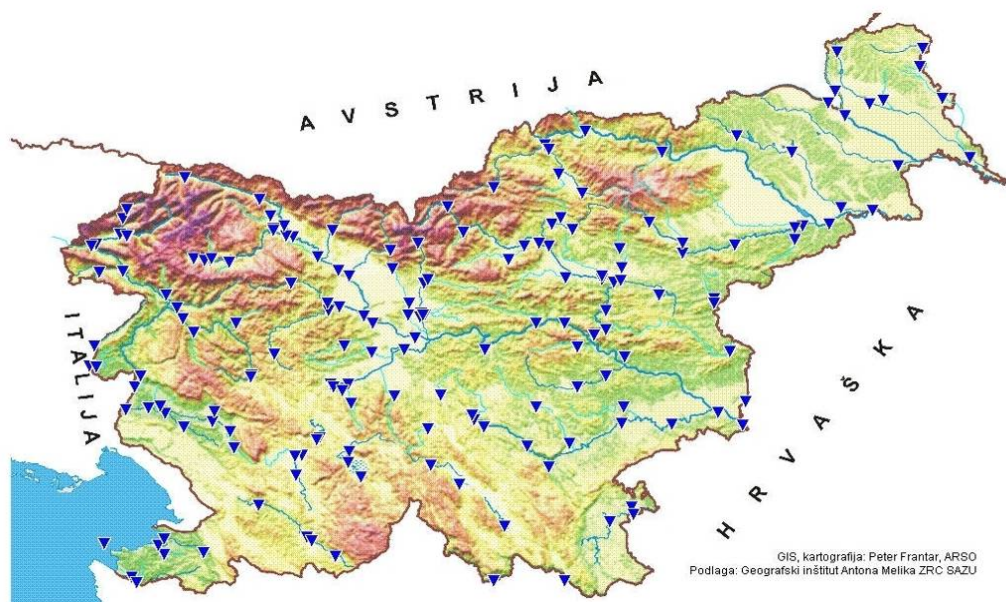
Figure 8. Distribution of water stations and terrain in Slovenia
(*Source: Environmental Agency of the Republic of Slovenia (ARSO)*)

The stations include 52 (27.4 %) water stations, 124 (65.3 %) water level recorders, and 14 or (7.4 %) automatic stations. With regard to density and importance of the river network, the setting up of the stations has been unevenly distributed. The network is less dense in south and east Slovenia and in the Karst region (*Kolbezen*, 1998). The number of water stations increased by the 1980's the same way as the number of rain gauge stations did, then it started to decrease.

3.3 Analysis of results

Based on the methodology and available data, seasonality maps of maximum annual precipitation, maximum monthly precipitation and maximum annual runoff were made (Figures 9, 10 and 11). The figures show the results from the stations with at least 20-

year data sets. Figures 9 and 10 show two completely separated areas, one under a strong influence of the Mediterranean Sea from the west, and the other one under a strong continental influence from the east.
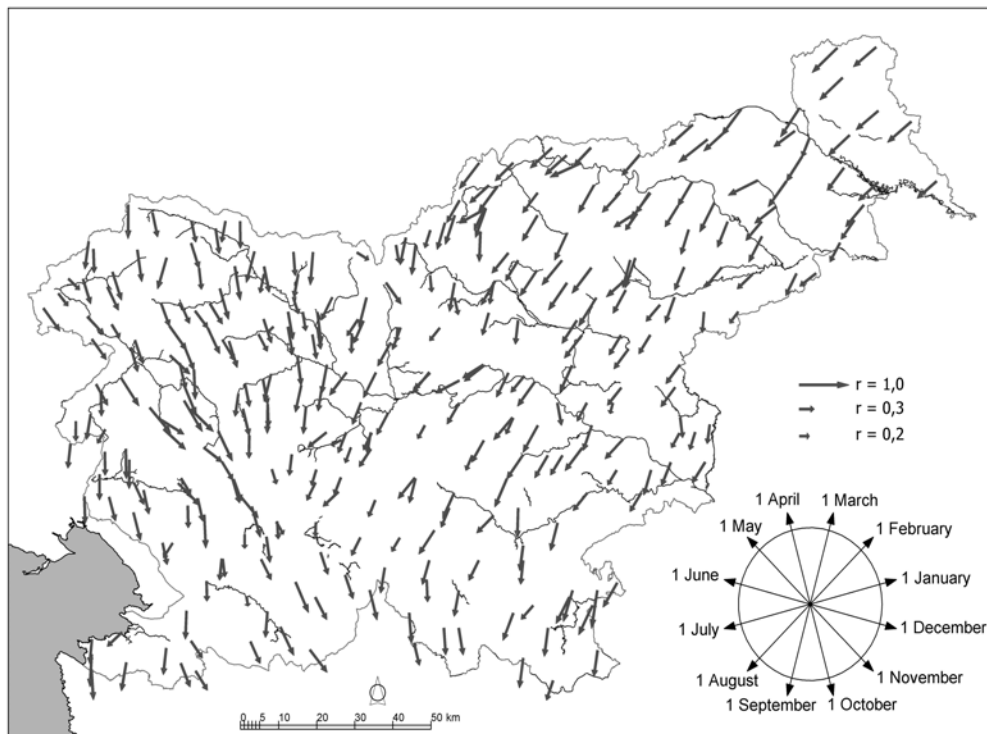
Figure 9. Graphic representation of the analysis of seasonality of occurrence of maximum daily precipitation in a year for 323 meteorological stations operating between 20 and 105 years.

In terms of maximum daily precipitation two areas are distinguished, having a rather narrow belt of 10÷20 km in-between. The areas are rather homogenous with a significant maximum of precipitation in October in the Mediterranean area and a maximum in the month of August in the continental area. The figure of monthly peak values is much more diversified, since the peaks in the Mediterranean part occur a little later, while in the continental areas they occur as daily peaks.

The peaks in the continental area may occur as early as in June or July. The belt bordering both areas is somewhat larger and deviates from the border belt of daily precipitation peaks. For such kind of representation the border belt with mixed effects is of interest, and it cannot be linked to any of the two areas, thus causing problems in regionalization, lacking a definite and unambiguous divide between the two areas.

In the area with continental influence, the difference in seasonality between maximum daily and maximum monthly precipitation is of interest. With small-sized streams, the seasonality of peak runoffs corresponds to the seasonality of precipitation, and with large streams the effects of upstream catchments are noticed, which can be attributed to the Mediterranean regime.

That is why the size of vectors in water stations in the lower Sava is relatively small, since the flood wave may occur in the upper part of the Sava River, being under the influence of the Mediterranean climate, as well as in the Savinja River, which is mostly under the influence of continental conditions.

270
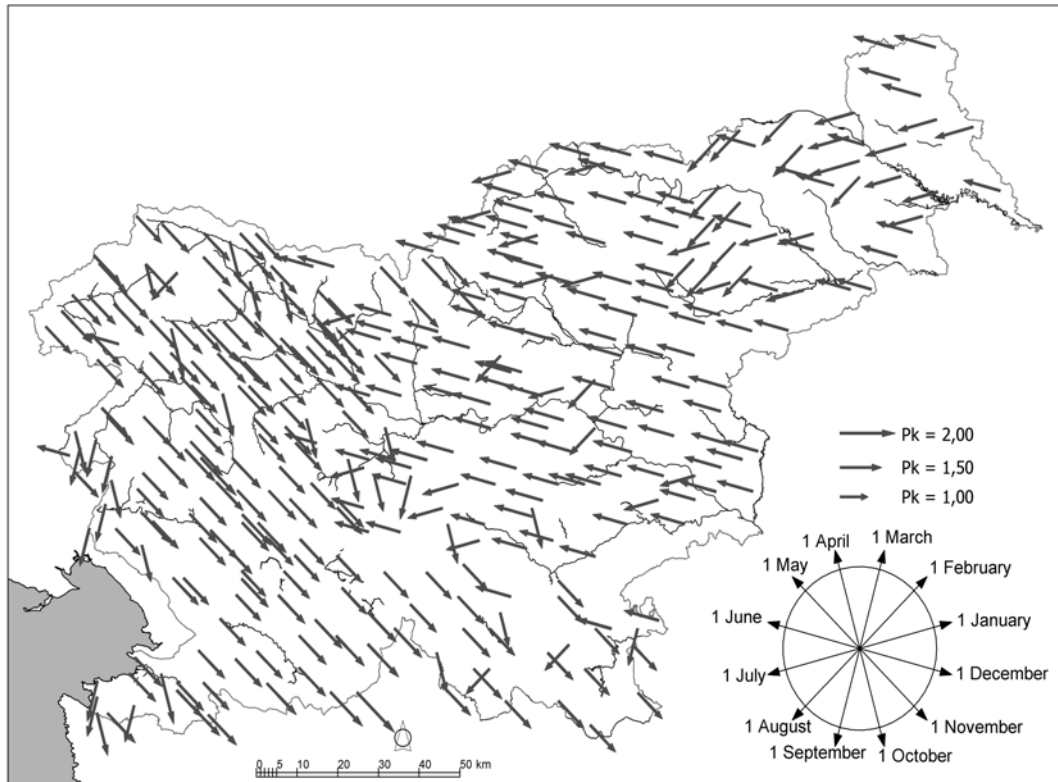
Figure 10. Analysis of seasonality of occurrence of maximum average monthly precipitation for 357 meteorological stations with sets of operation between 10 and 105 years.
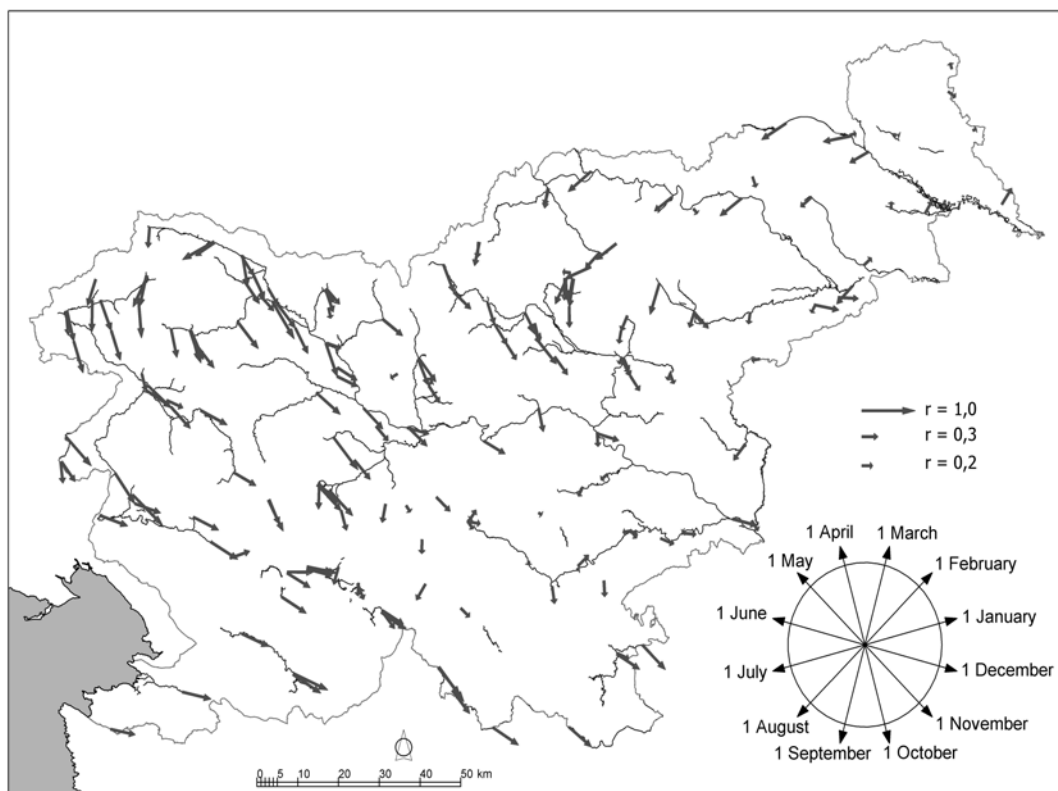
Figure 11. Analysis of seasonality of occurrence of peak annual runoff for 306 water stations, being in operation between 5 and 76 years.

4. CONCLUSIONS

The method represented here is highly applicable for diverse climatic conditions present in the territory of Slovenia, where in short distances the influences of different and powerful effects are mixed, such as the Mediterranean and continental climates. The method enables the analysis of seasonality under highly diverse conditions and clear representation of the scale and significance of bordering areas.

The analysis also clearly shows the need for a denser network of observation stations in the bordering areas, where despite the short distances, the simple correlation is not sufficient for analysis of the water regime.

REFERENCES

Bat, M., G. Beltram, T. Cegnar, et al. (2003), The water wealth in Slovenia, Ljubljana, Environmental Agency of the Republic of Slovenia, 131 str. (in Slovenian).

Bloschl, G. (2001), Flash-flood Risk Assessment under the impacts of land use changes and river Engineering works, Final Report, Wien, Technische Universitat Wien, 84 f.

Bloschl, G., and M. Sivapalan (1997), Process controls on regional flood frequency: Coefficient of variation and basin scale, *Water Resour. Res.*, *33*, 2967-2980.

Brilly, M., and M. Kobold (1997), Minimal discharges in Sloveniji, *Acta hydrotechnica*, *15*/17, 107-114.

Burn, D.H. (1997), Catchment similarity for regional flood frequency analysis using seasonality measures, *J. Hydrol.*, *202*, 212-230.

Merz, R., U. Piock-Ellena, G. Bloschl, and D. Gutknecht (1999), Seasonality of flood processes in Austria, *Hydrol. Extremes*, *255*, 273-278.

HYDROLOGICAL ANALYSIS OF A RAINFALL EVENT IN CALABRIA

T. Caloiero[1], F. Fusto[1], G. Iiritano[1] and G. Mendicino[2]

(1) Functional Centre of Calabria Region, Catanzaro, Italy.
(2) Soil Protection Department "V. Marone", University of Calabria, Cosenza, Italy.

ABSTRACT

Between 12th and 13th November 2004 a considerable rainfall event occurred in the Calabria region (southern Italy). This event started in the south part of Calabria and during its evolution it interested the entire region with remarkable damages.

The analysis of the cumulate precipitation recorded during the event, from 6:00 a.m. of the 12th November to 6:00 a.m. of the 13th November, and the evaluation of the return period for the maximum rainfall of 1 hour, 3 hours, 6 hours, 12 hours and 24 hours stored in some rain gauges were performed.

The hydrologic model WRROOM (Watershed Rainfall Runoff Object Oriented Model) was applied to study rainfall-runoff transformation in four of the principal basins of Calabria region: the Neto River at the closing section of Rocca di Neto and the Tacina River at the closing section of Serrarossa for the Ionian side, the Mesima River at the closing section of Sbarretta and the Petrace River at the closing section of Gonia for the Tyrrenian side.

Results of the hydrological analysis of the rainfall event occurred in Calabria in November 2004 are presented.

1. INTRODUCTION

Two of the main problems in hydrology are to estimate the magnitude of an event with a given return period and to determinate the rainfall-generated runoff. The first problem has been overcome by the use of some statistical distribution such as the Two Components Extreme Value (TCEV) distribution (*Rossi et al.*, 1984). In order to obtain a robust estimation of the parameters, statistical distributions need a large data set which is difficult to find, for this reason such kind of distributions are often used on regional basis. In Calabria a regionalized procedure has been developed in the VAPI project, based on the TCEV distribution (*Versace et al.*, 1989). The knowledge about the mechanism of transformation of rainfall in runoff is very important because it permits the integration of the runoff information, usually more limited than those on precipitation and often completely missing.

In literature there are several rainfall-runoff transformation models, and different classifications (*Maione,* 1977; *Moisello,* 1985). Among the various models, of remarkable interest are the "mathematical models of distributed type". A rainfall-runoff simulation improvement can be obtained by taking into consideration models of physically based distributed type which allow accounting for the heterogeneities of the topography, the vegetation and the soil, and the non uniform distribution of the precipitation inside a basin. The growing availability of cartography in digital form (DEM) and the coming of Geographic Information Systems (GIS) together with the

development of more and more progressive and powerful calculation means has directed the research toward this type of models in which the representation of the variables concerning the input and the basin features can be assumed as changing in time and space. In the mathematical modelling a simplification is made by identifying elementary cells in which these features are considered as uniform. However, the restrict description and simplification of the various hydrologic processes have put in evidence, in real cases, the limits of the applicability of these models both for the complexity of the calculations and for the information necessary to an acceptable knowledge of the morphological features of the basin and of the spatial and temporal distribution of the precipitation. For this reason, in the last few years, hydrologic studies of distributed type directed towards the analysis of special aspects of the hydrologic cycle (infiltration, propagation of flood in the network) have taken start.

2. METHODOLOGY

2.1 Two Components Extreme Value

The TCEV model (*Rossi et al.*, 1984; *Fiorentino et al.*, 1987; *Ferrari and Versace*, 1995; *Versace and Ferrari,* 1997; *Gabriele and Iiritano,* 1994; *Versiani and Carneiro* 2000), considers that there are two independent series of independent and identically distributed variables $Z_{1i,j}$ (j = 1,...,K_1) and $Z_{2i,j}$ (j = 1,...,K_2), generated by two Poisson processes, with respective parameters $\Lambda_1 = E\{K_1\}$ and $\Lambda_2 = E\{K_2\}$, with $\Lambda_1 > \Lambda_2$.

The cumulative distribution function (cdf) of the TCEV (Two Components Extreme Value) probability law is:

$$F_X(x) = \exp\left[-\Lambda_1 \exp\left(-x/\theta_1\right) - \Lambda_* \Lambda_1^{(1/\theta_*)} \exp\left(-x/\theta_* \theta_1\right)\right] \tag{1}$$

The parameters θ_* and Λ_* used in the regionalization procedure are defined by:

$$\theta_* = \frac{\theta_2}{\theta_1} \tag{2}$$

$$\Lambda_* = \frac{\Lambda_2}{\Lambda_1^{(1/\theta_*)}} \tag{3}$$

The parameters θ_1 and Λ_1 describe the most frequent events (the basic series), while θ_2 and Λ_2 describe the rarest events (the outlier series). The first level of the regionalization consists in searching for homogeneous regions characterised by similar coefficients of skewness, such that they can be considered as constant. In each region the parameters θ_* and Λ_* are assumed as not changing from site to site. The second and third levels of the regionalization method consist of the search of homogeneous sub-regions. In this level we assume that homogeneous sub-regions with respect to the coefficient of variation exist within the region where the coefficient of skewness is constant. In each sub-region the parameters θ_*, Λ_* and Λ_1 are assumed not to change from site to site.

2.2 Rainfall-Runoff model

The hydrologic model used for the rainfall-runoff simulations is a semi-distributed type. It has a limited number of lumped parameters with a clear physical meaning, and his structure considers the spatial and temporal variability of the fields of precipitation and of morphological features of the basin. It is a model of the type "object-oriented" and

so the basin is represented through the combination of "hydrologic objects" connected depending on the detail level of the simulation. The "objects" used in the schematization of a hydrographical basin are "sub-basin", "reservoir", "junction" and "channel".

Each of these "objects" is a linear element, with a hydrologic-hydraulic behaviour definable through opportune mathematical relations of link between points of outlet of sub-basin. In particular, every component can be characterized by one or more physical processes, in turn, can be simulated through one or more alternative mathematical procedures, defined methods. The topologic connection of the elements and the determination of their features take place automatically way using the information derived from the digital terrain models (DTM) due to techniques of integration between hydrologic modelling and geographic information system.

In relation to the number and to the geographic position of the hydrometric stations present in the basin, and in relation to the hydrologic features and to the level of detail of the rainfall-runoff simulation, it is possible to realize different topologic analysis schemes for the same network. Furthermore, the system is equipped with a calibration procedure totally automatic which is implemented on every hydrometric measurement station and at the outlet of the main basin. In this case the topologic scheme used to represent the basins has been limited to the use of an element "sub-basin" and a "junction", in the closing section, coinciding with the hydrometric station. That has been principally done to evaluate the hypothesis of using the model with pre-announcement purpose, to limit the calculation time necessary for the simulations.

2.3 Initial and constant rate loss model

The underlying concept of the initial and constant-rate loss model is that the maximum potential rate of precipitation loss, f_c, is constant throughout an event. An initial loss, I_a, is added to the model to represent interception and depression storage. Interception storage is a consequence of absorption of precipitation by surface cover, including plants in the watershed. Depression storage is a consequence of depressions in the watershed topography, water is stored in these and eventually infiltrates or evaporates. This loss occurs prior to the onset of runoff. Until the accumulated precipitation on the pervious area exceeds the initial loss volume, no runoff occurs.

2.4 SCS Curve Number loss model

The Soil Conservation Service (SCS) Curve Number (CN) model estimates precipitation excess as a function of cumulative precipitation, soil cover, land use, and antecedent moisture. This method is based on two parameters, the Initial Abstraction value and the Curve Number. The first one depends on the infiltration; the second one depends on the type and the use of the soil and on the antecedent moisture conditions. CN values range from 100 (for water bodies) to approximately 30 for permeable soils with high infiltration rates (*USACE*, 2000). Publications from the Soil Conservation Service (1971 and 1986) provide further background and details on use of the CN model.

2.5 Modified Clark model

The method schematizes the way between sub-zone k and the closing section through a combination of a channel and a reservoir, both linear, which describe the translation and the store phenomena. This method is based on two parameters, the mean velocity

value V_m, supposed constant, in each cell of the basin, and the value of the ratio between the delay time of the hypothetical linear reservoir at the closing section and the total resident time of the rainfall, β, inside the basin.

2.6 Diffusive model

For this scheme the function of answer $h_k(t)$, concerning the way which joins the generic cell of the DTM to the basin outlet, is obtained through a statistical distribution of the type "first-passage-time distribution". This method is based on two parameters, the mean velocity value V_m, in each cell of the basin, and the Peclet number of the cell. In this method so far considered it is assumed that the relationship $Pe=V_p l_p/d_p$ defined as number of Peclet of the single cell, remain constant in the entire basin (*Calabretta et al.*, 2000) and therefore it can be used as parameter of calibration which allows to determine, locally, the coefficient of dispersion d_p. Based on the formulated hypotheses the unitary hydrograph can be determined by estimating the two and parameters V_m e P_e.

2.7 Base-Flow model

For the simulation of the baseflow, low-pass method (*Chapman*, 1999) was applied. The baseflow value is computed weighing the value of the flow at time t and baseflow at the time t-1, using a parameter ρ.

3. APPLICATIONS

The Calabria region is in the furthest south of Italy, with an area of 15080 km^2 and a perimeter of about 818 km. Towards the north it borders Basilicata region for about 80 km, the south-eastern side is washed by the Ionian Sea and the western one by the Tyrrhenian Sea, for a total of 738 km of coasts. Calabria has an oblong shape with a length of 248 km and a width included between a maximum of 111 km (between Punta Alice and Capo Bonifati) and a minimum of 31 km (between Squillace's and S. Eufemia's Gulfs). Calabria is one of the most mountainous regions of Italy, since 42% of the land is mountainous, 49% hilly and only the 9% is flat. The maximum and average altitudes are 2267 m a.s.l. and 597 m a.s.l. respectively.

In Calabria there are 36 main hydrographical basins divided into 75 secondary and into 591 elementary. Even though they are hundreds, streams of Calabria are, however, all of short length, with basins of limited extension and high slopes. Due to the morphological features of the streams and to the presence of waterproof formation, rainfall swallowed quickly and the hydrometric regime depends on the meteoric inflows. Only some of the main streams, for most coming from the Sila Mountain, have a constant hydrometric regime (*Caloiero et al.*, 1990).

3.1 Spatial and temporal evolution

The evaluation of the return period for the maximum rainfalls of duration 1, 3, 6, 12 and 24 hours observed in some rain gauges during the event, from 6:00 a.m. of 12th November to 6:00 a.m. of 13th November, was performed.

In the first six hours, from 6:00 a.m. to 12:00 a.m. of 12th November, the event localized over Aspromonte Mountain and in the territories of Gioia Tauro. Maximum

precipitation values have been observed in the rain gauges of Santa Cristina d'Aspromonte (105.2 mm) and Gioia Tauro (42.6 mm) (Figure 1a).

From 12:00 a.m. to 18:00 p.m. of 12th November the event interested the other territories of the region and in particular the Amato River valley for province of Catanzaro and the middle-high Savuto River valley, the Crati River valley and the upper Ionian side for province of Cosenza. Maximum precipitation values have been observed in the rain gauges of Parenti (102.2 mm), Rogliano (74.4 mm), Tiriolo (59.2 mm), Gioia Tauro (54.4 mm) and Cropalati (47.2 mm) (Figure 1b).

From 18:00 p.m. to 24:00 p.m. of 12th November, the event interested all the territories of Catanzaro, Cosenza and Vibo Valentia with an increasing of intensity in Aspromonte Mountain and in the territories of Gioia Tauro. Maximum values precipitation have been observed in the rain gauges of Parenti (120.2 mm), Tiriolo (115.8 mm), Camigliatello (81 mm), Savelli and Cerenzia (68.4 mm), Feroleto della Chiesa (67.8 mm) and San Pietro di Caridà (67.4 mm) (Figure 1c).

In the last six hours of the event, from 00:00 a.m. to 6:00 a.m. of 13th November, precipitations decrease mainly in Crotone territory and, to a lesser extend, in the territories of Catanzaro and Cosenza. Maximum precipitation values are stored in the rain gauges of Cirò Marina Volvito (114.4 mm), Pagliarelle (97.2 mm), Cotronei (90.6 mm), Cerenzia (72.6 mm), Catanzaro (55.4 mm) and Albi (51.0 mm). During its evolution, from 6:00 a.m. of 12th November to 6:00 a.m. of 13th November the event interested the entire region. Maximum precipitation values are observed in the pluviometric stations of Parenti (223.6 mm), S. Cristina d'Aspromonte (206.4 mm), Tiriolo (181.6 mm), Cerenzia (158.2 mm), Cirò Marina Volvito (127.6 mm) and Savelli (125.2 mm).

3.2 Determination of the return period

For the rain gauges in which, during the evolution of the event, maximum values of precipitation were stored, a statistical analysis was performed to determine the values of the return period (T) at different levels of time aggregation (1 hour, 3 hours, 6 hours, 12 hours and 24 hours). The TCEV probabilistic model has been applied to hourly data recorded in the rain gauges listed in Table 1, that also show maximum rainfall values.

Code	Rain Gauge	Basin	Elevation (m)	h_{1hour} (mm)	h_{3hours} (mm)	h_{6hours} (mm)	$h_{12hours}$ (mm)	$h_{24hours}$ (mm)
1410	Cariati	Tra Trionto e Neto	10	39.8	64.4	87.6	88	133.8
1455	Cirò Marina Volv.	Tra Trionto e Neto	10	67.4	77.6	114.4	115.8	133.2
1570	Savelli	Neto	964	47.8	89.2	96.0	101.8	125.6
1580	Cerenzia	Neto	663	62.6	110.8	140.8	141.6	193.4
1724	Cotronei	Tacina	530	37.6	82.2	96	96.6	124
1830	Albi	Alli	710	51.4	90.4	90.8	92.4	105.4
2540	Santa Cristina	Petraie	510	78.8	139.0	145.0	205.8	206.6
2665	S.Pietro di Caridà	Mesima	750	50.4	66.8	67.4	73.4	105.8
2740	Rosarno	Mesima	61	34.6	43.6	44.2	84.2	100.8
2890	Tiriolo	Amato	690	81.4	120.2	120.2	174.6	181.2
2990	Parenti	Savuto	830	85.4	118.6	120.2	222.4	223.6
3000	Rogliano	Savuto	650	39.2	70.6	74.4	102.6	102.8

Table 1 – Maximum rainfall values observed with different levels of time aggregation.
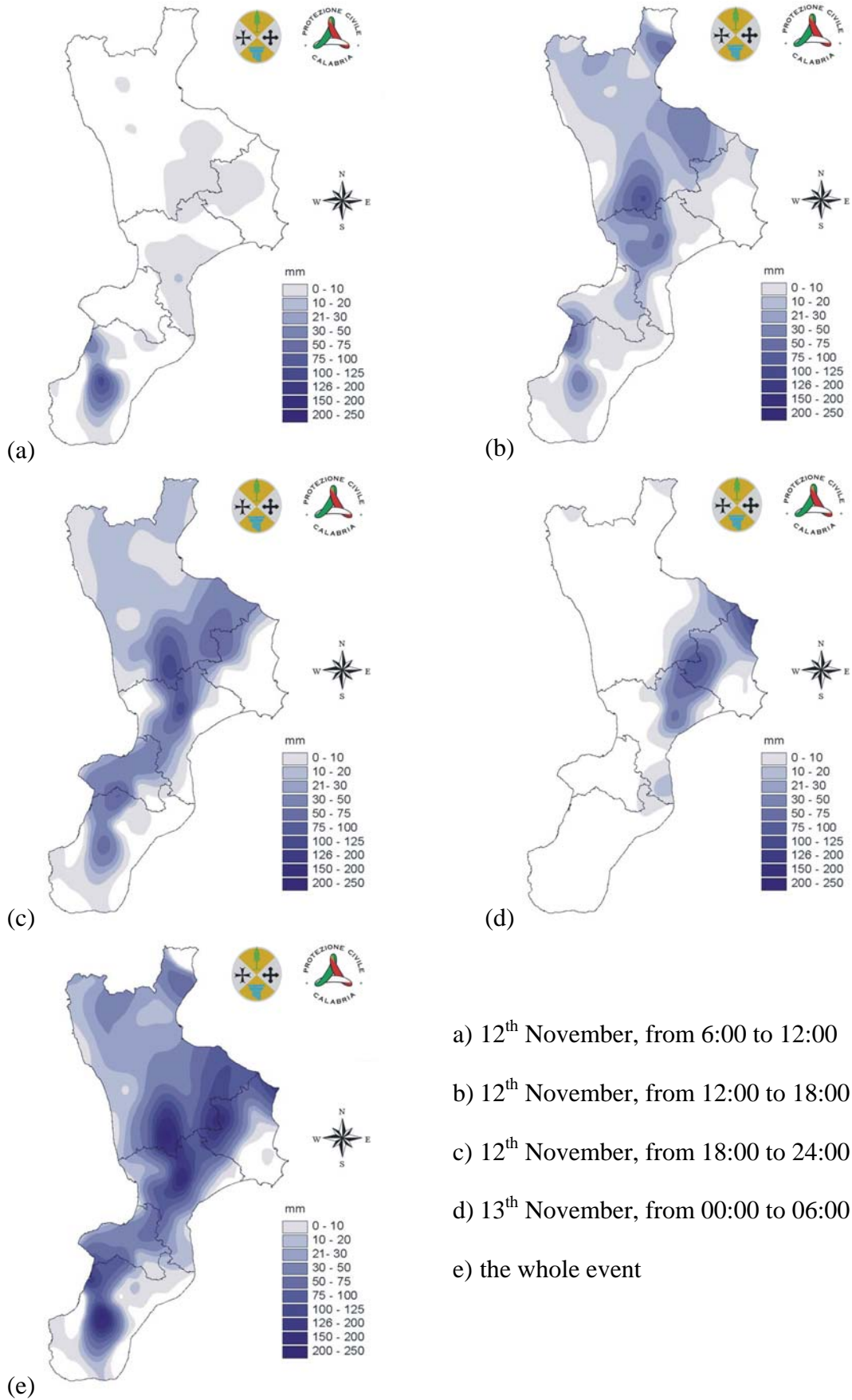
Figure 1. Maps of the cumulate precipitations stored during the event.

a) 12th November, from 6:00 to 12:00

b) 12th November, from 12:00 to 18:00

c) 12th November, from 18:00 to 24:00

d) 13th November, from 00:00 to 06:00

e) the whole event

The analysis with the TCEV model was performed at the first level of regionalization for the rain gauges with an historical dataset of minimum 30 years, at second level of regionalization for the rain gauges with an historical dataset of minimum 10 years. For all the stations the analysis was performed at the third level of regionalization (Figure 2).

From the analysis of the return period (Table 2), there are relevant results in Parenti rain gauge with return periods of 306 years, 220 years and 436 for aggregations of 1 hour, 3 hours and 12 hours respectively. There are other relevant results in Tiriolo rain gauge with return periods of 110 years and 87 years for aggregations of 1 hour and 3 hours respectively.

Other remarkable results point out from rain gauges of Rogliano with return periods of 84 years and 29 years for aggregations of 3 hours and 6 hours respectively and San Pietro di Caridà, Cirò Marina Volvito, Santa Cristina d'Aspromonte e Cerenzia with return periods of 65 years, 41 years, 34 years and 29 years respectively, for 1 hour aggregations.

Rain Gauge	Level	T (hours)				
		1	3	6	12	24
Albi	I	11	14	5	2	2
Cariati	III	5	6	8	3	4
Cerenzia	III	29	30	22	7	5
Cirò Marina Volvito	III	41	13	22	8	4
Cotronei	III	4	11	6	3	2
Parenti	III	306	220	52	436	75
Rogliano	I	18	84	29	22	8
Rosarno	I	4	11	2	22	4
San Pietro di Caridà	I	65	39	8	7	3
Santa Cristina	III	34	25	5	5	2
Savelli	II	11	14	5	2	2
Tiriolo	I	110	87	25	28	9

Table 2. Return period values.
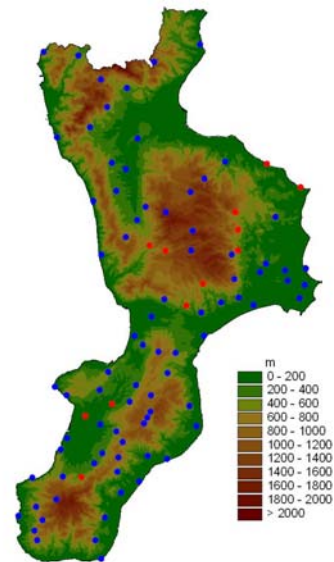
Figure 2. Maps of total rain gauges (in blue) and of rain gauges (in red) in which TCEV model was applied.

3.3 Rainfall-runoff simulation

A rainfall-runoff model was applied in four of the principal basins of the Calabria Region: the Neto River at the closing section of Rocca di Neto and the Tacina River at the closing section of Serrarossa for the Ionian side, the Mesima River at the closing section of Sbarretta and the Petrace River at the closing section of Gonia for the Tyrrhenian side. The initial and constant rate loss model, the SCS Curve Number loss model, the modified Clark model and the diffusive model were combined and applied for the simulations.

The combinations of different loss models and UH models applied with the same base-flow method are:
a. CN, Modified Clark, Low-pass;
b. Initial and Constant Rate, Modified Clark, Low-pass;
c. CN, Diffusive, Low-pass;
d. Initial and Constant Rate, Diffusive, Low-pass.

In Tables 3-6 the values of the parameters obtained by the simulations are shown:

Basin	Ia	CN	V_m	β	ρ	O.F.	EQ_{peak}	ET_{peak}	BIAS	E.C.
Neto	49.86	80.4	4.51	0.1	0.55	47.57	-3.246	-0.333	46.67	0.938
Tacina	37.01	60.52	4.61	0.61	0.99	12.25	-9.781	0.333	11.75	0.87
Mesima	0.01	39.23	4.81	0.84	0.98	11.36	-16.074	0.667	9.77	0.859
Petrace	0.01	34.43	4.72	0.1	0.5	96.03	-29.051	6.667	78.03	0.285

Table 3. Results using CN, Modified Clark, Low-pass.

Basin	Ia	CN	V_m	β	ρ	O.F.	EQ_{peak}	ET_{peak}	BIAS	E.C.
Neto	49.16	11.48	0.91	0.19	0.57	49.1	-6.419	-0.667	44.9	0.942
Tacina	28.37	19	1.53	0.66	0.99	11.17	-10.084	-0.333	10.75	0.891
Mesima	21.47	10.17	2.1	0.86	0.99	9.71	-14.307	0	8.41	0.895
Petrace	15.6	12.62	4.85	0.21	0.97	33.66	0.35	0	29.5	0.898

Table 4. Results using Initial and Constant Rate, Modified Clark, Low-pass.

Basin	Ia	CN	V_m	β	ρ	O.F.	EQ_{peak}	ET_{peak}	BIAS	E.C.
Neto	50	82.45	4.95	99.9	0.8	48.03	-4.797	-0.667	47.35	0.936
Tacina	50	77.71	0.51	94.3	0.98	12.85	-8.743	-0.333	12.86	0.844
Mesima	29.34	81.34	0.51	20.6	0.96	21.04	10.67	0	19.13	21.04
Petrace	0.012	34.67	2.99	99.5	0.5	97.06	-29.23	6.667	79.2	0.267

Table 5. Results using CN, Diffusive, Low-pass.

Basin	Ia	CN	V_m	β	ρ	O.F.	EQ_{peak}	ET_{peak}	BIAS	E.C.
Neto	50	9.2	0.54	100	0.77	95.74	-14.428	-1	91	0.764
Tacina	18.17	21.48	0.51	100	0.95	23.61	-4.463	-1	24.42	0.439
Mesima	35.71	2.18	0.51	22.4	0.97	23.14	19.051	-0.333	21.09	0.348
Petrace	21.77	10.38	2.28	30.9	0.95	24.96	-5.58	-0.333	24.48	0.93

Table 6. Results using Initial and Constant Rate, Diffusive, Low-pass.

where:

$$O.F. = \sqrt{\frac{\sum_{t=1}^{n}\left[Q_{obs}(t) - Q_{comp}(t)\right]^2 \cdot \frac{\left[Q_{obs}(t) + Q_m(t)\right]}{2Q_m}}{n}}$$

$Q_m = \dfrac{1}{n}\sum_{t=1}^{n} Q_{obs}(t)$ mean discharge observed

$Q_{obs}(t)$ discharge observed at time t (3)

$Q_{comp}(t)$ discharge computed at time t

$$EQ_{peak} = \frac{Q_{peakOBS} - Q_{peakCOMP}}{Q_{ppeakCOMP}} \tag{4}$$

$$ET_{peak} = \frac{T_{peakOBS} - T_{peakCOMP}}{T_{peakOBS}} \cdot \frac{\Delta t}{60} \tag{5}$$

$$BIAS = \sum_{t=1}^{n} \frac{Q_{obs}(t) - Q_{comp}(t)}{n} \tag{6}$$

280

$$EC = 1 - \frac{\sum\limits_{t=1}^{n}\left[Q_{obs}(t) - Q_{comp}(t)\right]^2}{\sum\limits_{t=1}^{n}\left[Q_{obs}(t) - Q_m(t)\right]^2} \qquad (7)$$

The Petrace River at the closing section of Gonia presents an area of 402.87 km^2 with a perimeter of 129.7 km and a slope of the main stream of 2.63 %. The application of the rainfall-runoff model gives good results (Figure 3) with the use of the initial and constant rate loss model. In particular the best simulation is made by using the initial and constant rate loss model and the diffusive model. The Mesima River at the closing section of Sbarretta presents an area of 461.94 km^2 with a perimeter of 141.92 km and a slope of the main stream of 0.82 %.

The application of the rainfall-runoff model gives acceptable results (Figure 4) with the use of the modified Clark model. In particular the best simulation is made by using the initial and constant rate loss model and the modified Clark model. The Neto River at the closing section of Rocca di Neto presents an area of 845.76 km^2 with a perimeter of 185.92 km and a slope of the main stream of 1.99 %. The application of the rainfall-runoff model gives good results (Figure 5) with the use of the modified Clark model. In particular the best simulation is made by using the SCS Curve Number loss model and the modified Clark model. The Tacina River at the closing section of Serrarossa presents an area of 241.17 km^2 with a perimeter of 114.88 km and a slope of the main stream of 3.74 %. The application of the rainfall-runoff model gives good results (Figure 6) with the use of the SCS Curve Number loss model. In particular the best simulation is made by using the SCS Curve Number loss model and the diffusive model.

CN + Clark

Initial and Constant + Clark

CN + diffusive

Initial and Constant + diffusive
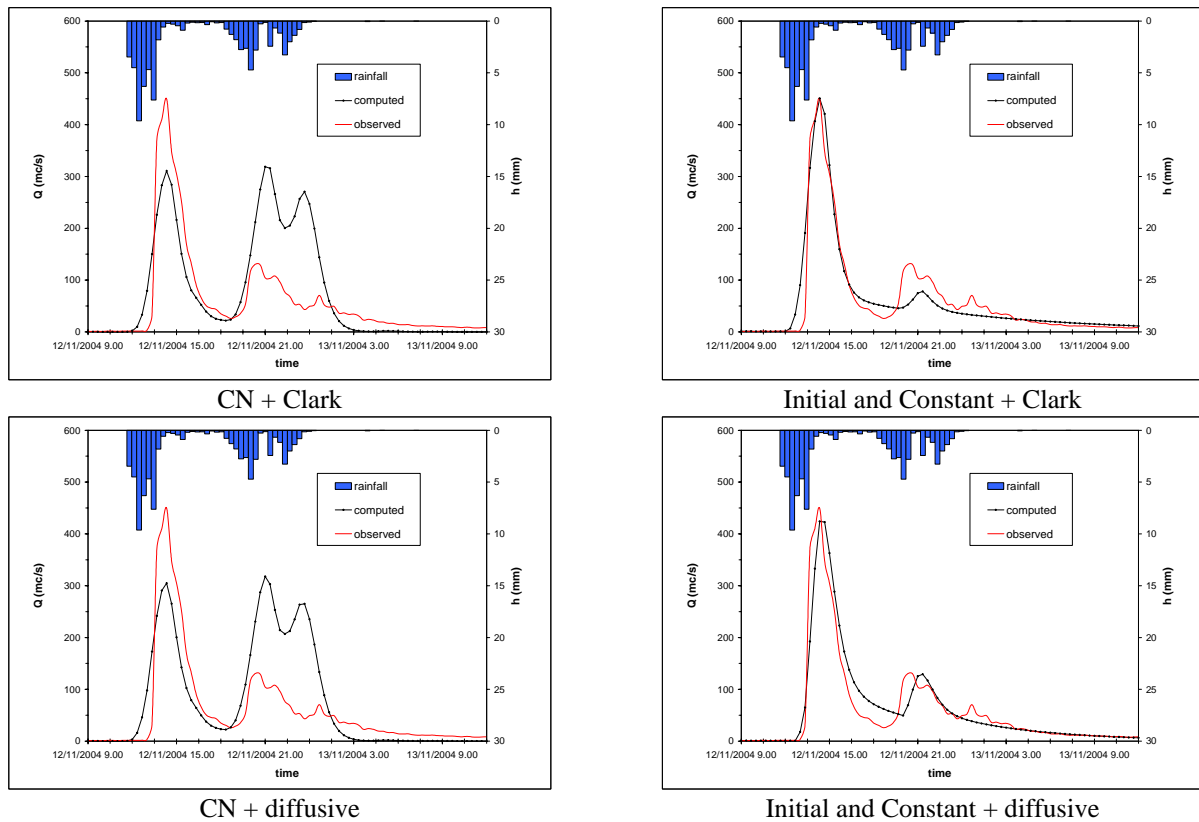
Figure 3. Rainfall-runoff simulation on the Petrace River.
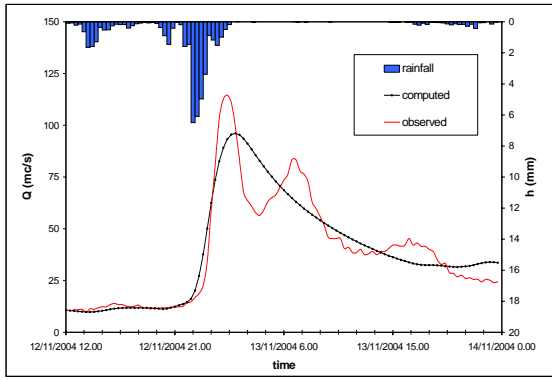
CN + Clark
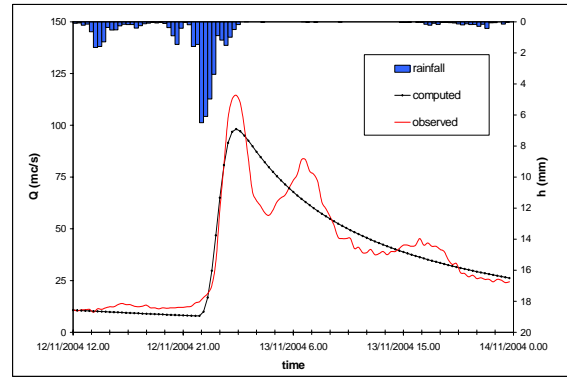
Initial and Constant + Clark
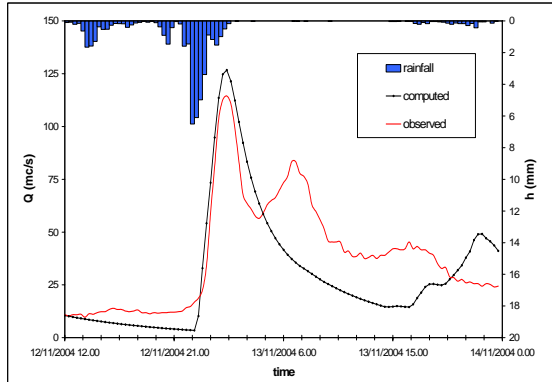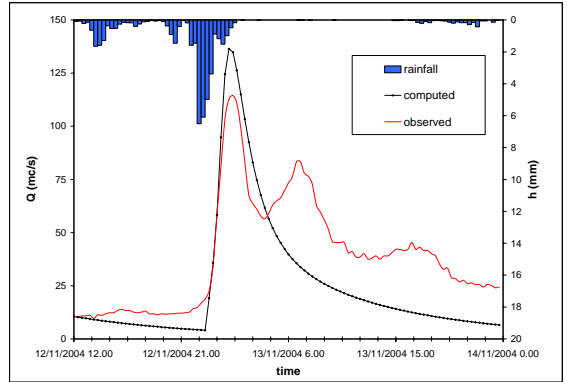
CN + diffusive

Initial and Constant + diffusive

Figure 4. Rainfall-runoff simulation on the Mesima River.
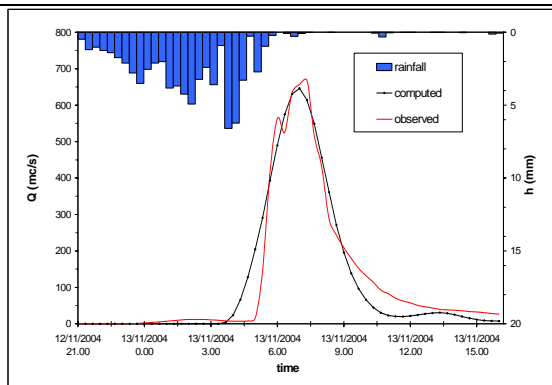
CN + Clark
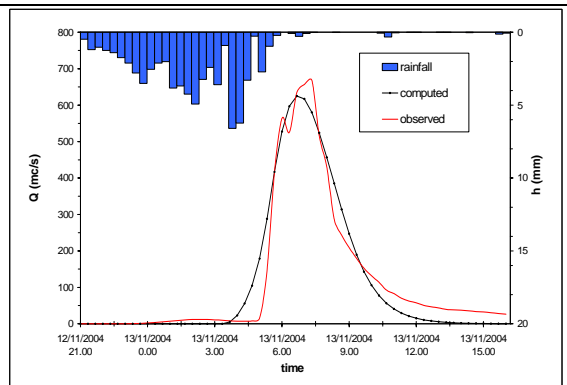
Initial and Constant + Clark
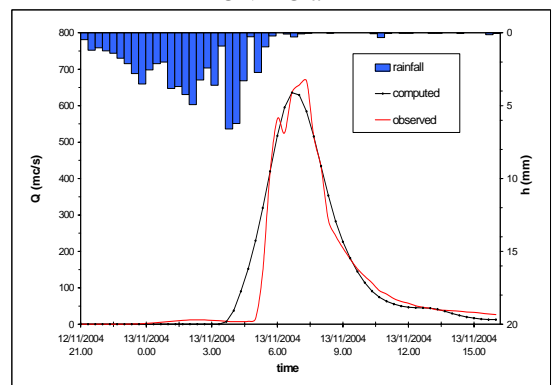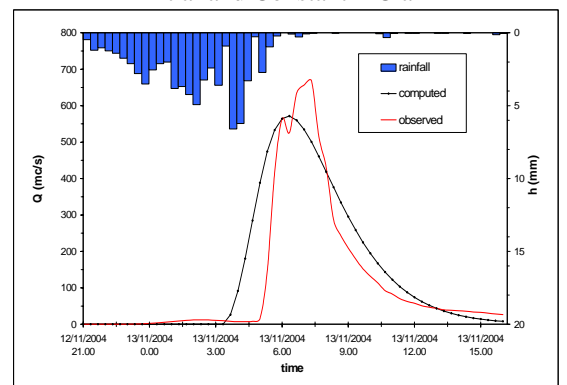
CN + diffusive

Initial and Constant + diffusive

Figure 5. Rainfall-runoff simulation on the Neto River.
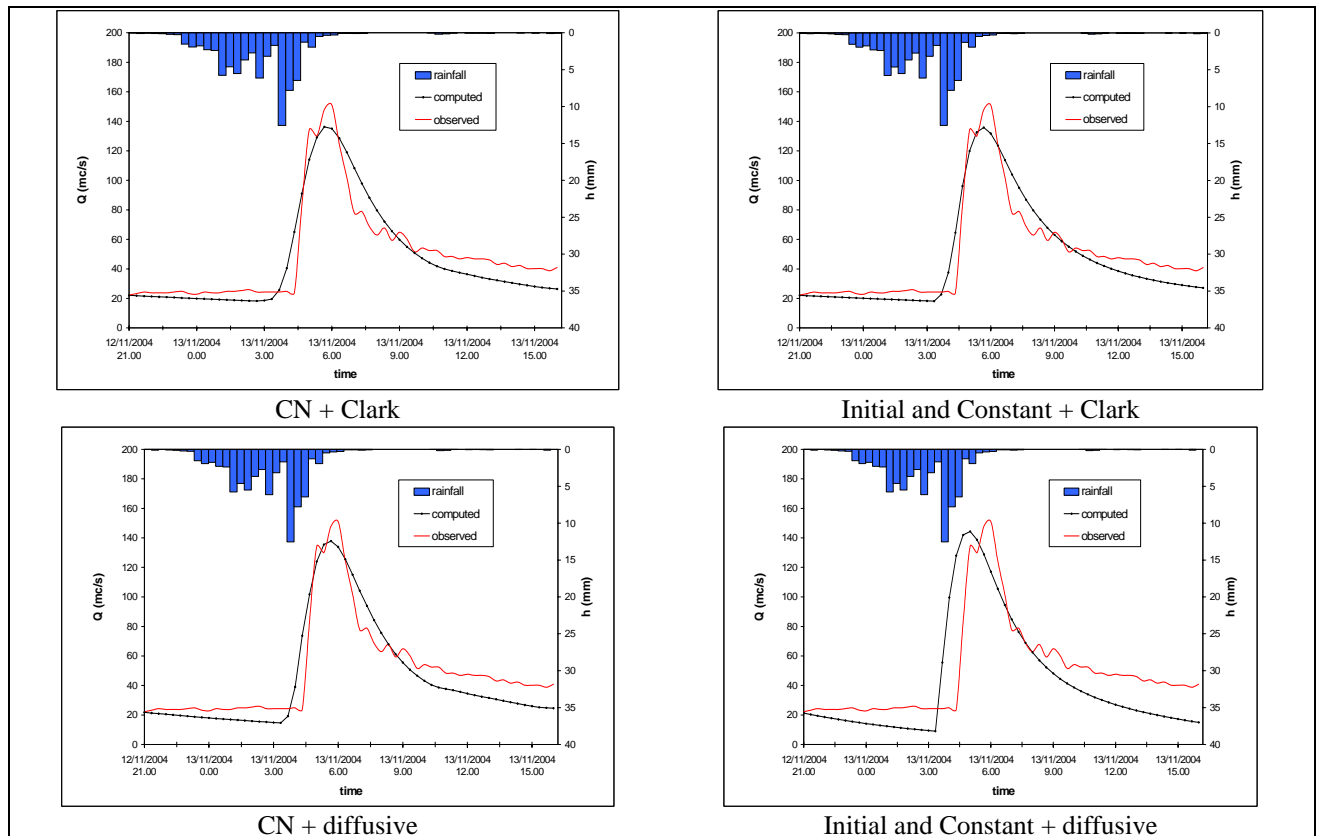
Figure 6. Rainfall-runoff simulation on the Tacina River.

4. CONCLUSIONS

The analysis of extreme rainfall events is very important, in particular in territories as the Calabria region in which many basins present areas less than 100 km^2. In fact, for those basins and in condition of high soil moisture, due to a extreme rainfall event flash flood can be generated.

The rainfall event occurred in Calabria between 12th and 13th November 2004 is one of the biggest of the last years. The analysis with the TCEV model has shown high return period of the rainfall in the entire region. The rainfall-runoff simulation has generally given good results. In particular, observed and computed hydrographs are very similar and there is a good correspondence in the time of the maximum curve peak. The results allow to set the WRROOM model for the basins interested by the event.

REFERENCES

Calabretta G., G. Mendicino, and P. Versace (2000), Un modello semidistribuito per la prevenzione delle piene fluviali in piccoli bacini idrografici, *Atti del XXVII Convegno di Idraulica e Costruzioni Idrauliche*, Genova, Italy *(in Italian)*.

Caloiero, D., R. Niccoli, and C. Reali (1990), Le precipitazioni in Calabria (1921-1980), CNR-IRPI, *Geodata N. 36*, Rende (CS), Italy *(in Italian)*.

Ferrari, E. and P. Versace (1995), Evaluation of index flood in Italy, IHP-UNESCO, FRIEND-AMHY Annual Conference, Thessaloniki, Greece.

Fiorentino, M., S. Gabriele, F. Rossi, and P. Versace (1987), Hierarchical approach for regional flood frequency analysis, in *Regional Flood Frequency Analysis*, edited by V.P. Singh, 35-49, D. Reidel Publishing Company, Dordrech, Holland.

Gabriele, S. and G. Iiritano (1994), Alcuni aspetti teorici ed applicativi nella regionalizzazione delle piogge con il modello TCEV, *Prediction and prevention of extreme hydrological events and their mitigation*, n. *1089*, GNDCI, CNR-IRPI (editor), Rende (CS), Italy *(in Italian)*.

Maidment, D.R., F. Olivera, A. Calver, A. Eatherall, and W. Fraczek (1996), Unit Hydrograph Derived from Spatially Distributed Velocity Field, *Hydrol. Proc.*, *10*, 831-844.

Maione, U. (1977), *Appunti di Idrologia*, *Le piene fluviali,* La Goliardica Pavese, Pavia *(in Italian)*.

Moisello, U. (1985), *Grandezze e fenomeni idrologici*, La Goliardica Pavese, Pavia (in Italian).

Rossi, F., M. Fiorentino, and P. Versace (1984), Two Component Extreme Value distribution for flood frequency analysis, *Water Resour. Res.*, *20*(7), 847-856.

Soil Conservation Service (1971), *National engineering handbook, Section 4: Hydrology*, USDA, Springfield, VA.

Soil Conservation Service (1986), *Urban hydrology for small watersheds*, Technical Release 55, USDA, Springfield, VA.

USACE (2000), HEC-HMS user's manual, Hydrologic Engineering Center, Davis, CA.

Versace, P., and E. Ferrari (1997), Regional hierarchical approach to flood frequency analysis. Floods, *'94-97 Report*, Chapter 4, FRIEND Project, IHP UNESCO.

Versace, P., E. Ferrari, S. Gabriele, and F. Rossi (1989), Valutazione delle piene in Calabria, GNDCI, CNR-IRPI (editor), Rende (CS), Italy *(in Italian)*.

Versiani, B.R., and R.M.F. Carneiro (2000), Regionalization analysis of maximum flood: study case of Minas Gerais, Brazil, *Proc. of 4th International Conference on Hydroscience and Engineering*, Seoul, Korea.

Weiler M., B.L. McGlynn, K. McGuire, and J.J. McDonnell (2003), How does rainfall become runoff ? A combined tracer and runoff transfer function approach, *Water Resour. Res.*, *39*(11), doi:10-1029/2003WR002331.

INVITED LECTURE

Observing and modelling exceptional floods and rainfalls
Proceedings of the AMHY-FRIEND International Workshop on Hydrological Extremes,
held at University of Calabria, Cosenza (Italy), May 3-4, 2006

REMOTE SENSING FOR PREVENTION ANALYSIS
OF TSUNAMI IN SRI LANKA

F. Ferrucci[1,2]

[1] Earth Sciences Dept., University of Calabria, Cosenza, Italy
[2] Decentralized Pole of Calabria University, Vibo Valentia, Italy

ABSTRACT

An inter-Government agreement established between Italy and Sri Lanka in the aftermath of the great 2004 Indian Ocean tsunami, led to design and carry out the operational project «HyperDEM» aimed to map in 3D the coastal areas of Sri Lanka. The products of HyperDEM, were transferred to the Government of Sri Lanka for enabling the carrying out of quantitative emergency planning in tsunami-prone areas. The work, based on integration of airborne Lidar and spaceborne Radar campaigns, started late in summer 2005, and was accomplished in spring 2006.

1. INTRODUCTION

Tsunamis are liquid gravitational waves that travel at speeds $V=\sqrt{h \cdot g}$, where h is the thickness of the water layer and g the gravity acceleration. V may easily exceed 700 km/h in blue waters whereas, in shallow waters, waves slow-down and wavefronts run-up to heights of metres.

Slowest velocities of tsunami waves are much larger than humans can run for escaping them. In terms of preparedness, this means that escape way solutions must be addressed well in advance, aimed to let people moving to the closest safe place at any moment. Indeed, unnoticeably elevated areas close to the shoreline can be good, and sometimes unexpected escape places to single out, map and include in emergency plans.

The main parameter that discriminates tsunamis from ordinary sea waves or swell, is wavelengths in the order of tens of kilometres in open seas, and increased spectrum complexity near the shore. As for wave heights, outstanding heights are obtained as a combination of a steep seafloor topographic gradient, and a short distance from the source. The worst such case is documented to have occurred in the near field of a M_W=8.0 earthquake in 1946 at Unimak Island, Alaska, where the Scotch Cap lighthouse was flushed away by a 35-metre high wave.

Reportedly, wave heights for the great Indian Ocean tsunami of 26th December 2004, may have exceed 15 m on the northern Sumatra coasts. In Sri Lanka, about 2000 km away from the epicentre of the M_W=9.0 earthquake, largest wave heights may have exceeded 10 m in the East, but at least 5000 lives were taken by waves not higher than 5 m, in the South and in the Southwest of the island.

All concepts as above, apply with some modifications also to storm-surges eventually associated to seasonal cyclogenesis in the Bay of Bengal, a threat provided with much higher probability of occurrence than tsunamis in Sri Lanka. Indeed, known tsunamis hitting the Central Indian Ocean before 2004, date back to 1945, 1881 and 1883 (the former, were earthquake-generated; the latter relates to the explosion of Krakatau

volcano, Indonesia) whereas the storm-surge disaster of 1970 in Bangladesh alone was responsible for about 500000 casualties at once.
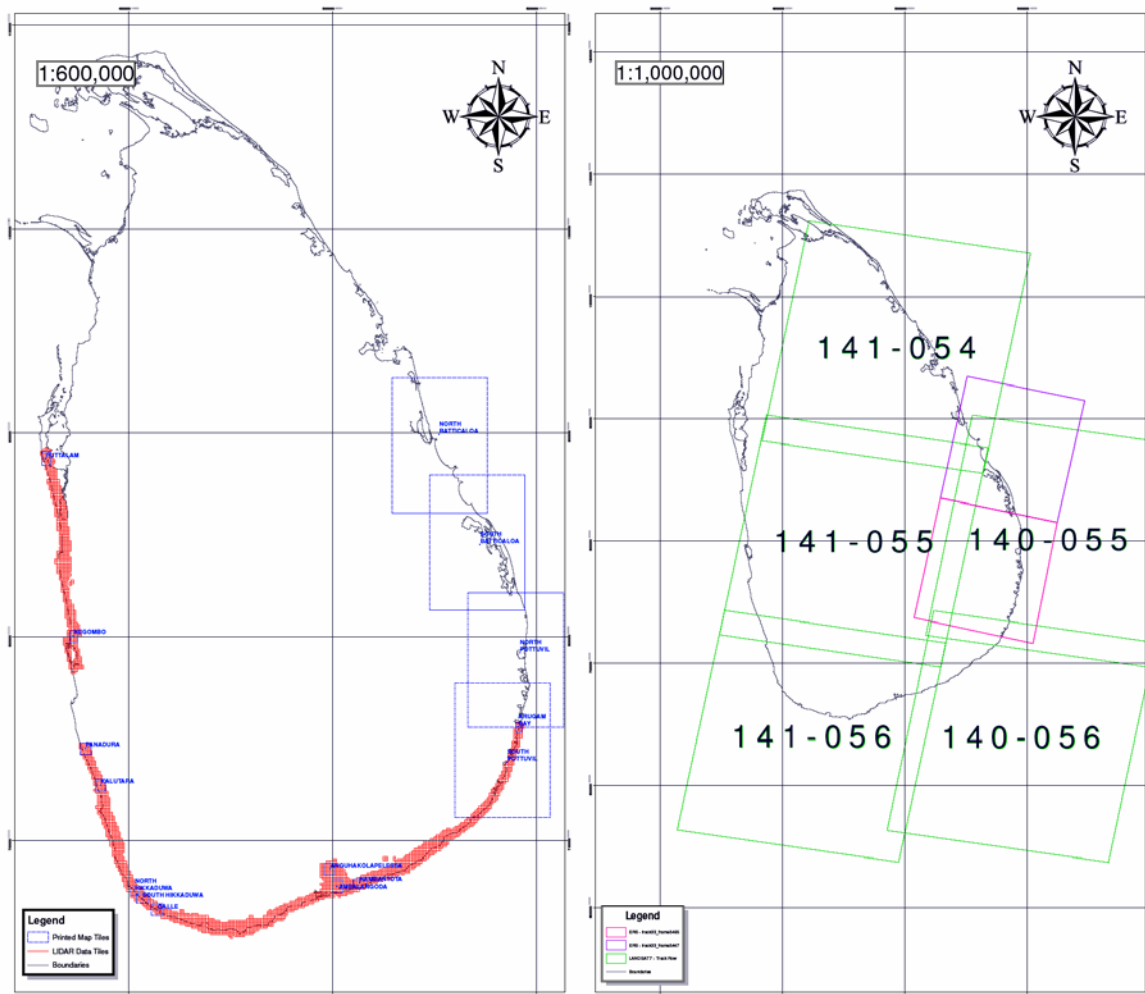
Figure 1. <u>Left:</u> location map of areas surveyed by airborne LiDAR (red squares) and spaceborne RaDAR (blue open squares). In the former, both Digital Elevation and Digital Surface Models were obtained at 1m resolution; in the latter, only DSM, at 30m resolution. <u>Right:</u> location of Landsat-7/ETM+ (green) and ERS-1/ERS-2/ENVISAT (violet) satellite frames used in HyperDEM. ASTER and QuickBird imagery was also used for satisfying interpretation needs eventually arisen during processing of the 2.7 TeraByte dataset.

2. THE "HYPERDEM" MODEL

Following an inter-Government agreement established between Italy and Sri Lanka five months after the 2004 tsunami, the operational project "'HyperDEM - The precise Digital Elevation Model of the coastal areas of Sri Lanka", was launched late early in September 2005, and accomplished in spring 2006.

The agreement focused on mapping in 3D and at very-high resolution, a portion of the coastal areas hosting at least two-thirds of damage and casualties observed in 2004. Overall, the island had suffered 34000 casualties and 2 millions near-permanently displaced persons. The percentage of affected coastal populations ranged from 35% in the northern coastal districts to 80% in the eastern districts, whereas southern districts displayed about 30% impact, albeit with scattered pockets of severe damage. In

consultation with the Sri Lankan Government, we decided to map the southern two-third of the island, including most of its eastern and western shores, as shown in Figure 1.

Since tsunami waves create maximum damage on land, the project was addressed to enable the drawing of scenarios, including the impact zone limits, the assessment of expected severity of impact, and the effect of buildings on absorption and/or dispersion of incoming energy. This target requires ground resolutions in the order of 1 m, and elevation precisions in the order of 0.2÷0.3 m to be achieved uniformly over large areas.

According to observed, inland penetration of tsunami waters, the size of coastal zones to map was fixed at an average 3 km. This pointed to an expected 1800 km² to map in 3D, in very short times (maximum one month), and with the resolutions/precisions as above: such target - clearly out of reach for standard topography missions - could be achieved only with use of State-of-the-Art active and passive remote sensing techniques.

We choose to combine airborne LiDAR and Hyperspectral – for top 3D resolution and simultaneous confidence qualification of elevation data – and spaceborne RaDAR (*Prati et al.*, 1994) with multispectral mapping (*Hirn and Ferrucci*, 2005), aimed to extend the DEM mapping to the whole of the areas indicated by the Sri Lankan Government.

3. THE AIR CAMPAIGN

Over 1780 km² of coastal areas were prospected during the airborne campaign of February 2006. The survey, planned for integrated operation and combined acquisition of active and passive instruments at once, was designed (Figure 2) on target ground resolutions of 1 m² for LiDAR, and 4 m² for hyperspectral.

We decided also to operate simultaneously a semi-metric digital camera with typical footprint in the order of 0.2 m (when operated at the same flight level giving rise to the nominal LiDAR resolution of 1 m) for assisting in the interpretation of ambiguous elevation features in the very-high resolution dataset.
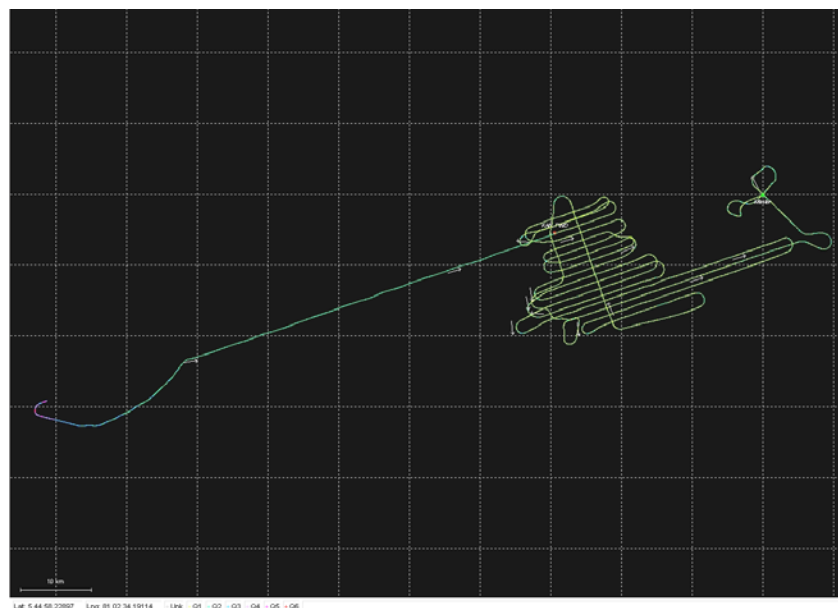
Figure 2. SBET (Best Estimated Trajectory) of the airborne platform near Hambantota, 16th February 2006. The SBET is constituted of fixes spaced about 0.15 m, and was characterized by residual r.m.s. errors < 0.3 m.

In cartography applications, indeed, LiDAR raw elevation data are systematically purged of false or misleading information as that due to lateral backscattering, multiple scattering, returns from strongly reflecting physical surfaces, and so forth (*Baltsavias*, 1999; *Kraus and Pfeifer*, 1998).

Such information-cleaning process is performed through a classification process that allows assigning physical meaning to scatterers provided with variable signal/noise ratios.

First pulses are typically associated to strongly reflecting objects, like trees, wires, roofs and bridges, whereas later (and weaker) pulses are either attributed to returns from "ground" (*Kraus and Pfeifer*, 1998). The average inland extension of prospected area is about 3 km, with a maximum of over 10 km in the area of the artificial basin and the dam of Angunakolapelessa (Figure 3) in the south. Airborne LiDAR, orthophotos and hyperspectral data were acquired between 11th and 21st February, with a five-day interval (17th to 20th February) devoted to processing and preliminary analysis of data acquired during the first leg (Figure 4).

Figure 3. Example of 3D rendering of combined LiDAR (1m planimetric resolution, 0.2 m precision in elevation on steady reflectors) and digital camera aerial scenery (planimetric resolution of 0.2 m). This picture was taken over the artificial lake of Angunakolapelessa, southern Sri Lanka.

The following payloads were installed on the airborne platform, a De Havilland DHC-3 "Beaver" operated by the Sri Lankan private operator Air Taxi :
• A LiDAR system Optech ALTM 3033. The instrument consists of a Near Infrared (λ=1064 nm) Laser beam with pulse repetition rate of 33KHz. A scanning mirror directs the Laser optical pulses across the flight path, providing coverage to either sides

of the flight direction. The forward motion of the aircraft provides coverage in the direction of flight.

- ALTM 3033 incorporates a GPS receiver and an Inertial Measurement Unit (IMU). Roll, pitch and yaw (attitude) of the aircraft are measured by the Inertial Navigation System unit at a frequency of 200 Hz.
- A Hyperspectral Radiometer AISA Eagle 1K by the Finnish firm SPECIM. It is a pushbroom scanner made up of a V-NIR hyperspectral sensor, a GPS/INS Applanix sensor, and a laptop implemented data acquisition unit.
- AISA Eagle 1K operates at wavelengths between 400-970 nm; it is able to record up to 244 bands (with spectral sampling of 2.3 nm/pixel) and 1024 spatial pixels. The system is flexible enough to allow acquiring data in almost every band combination, simultaneously acting on the number of bands and the bandwidth by use of a computer assisted procedure.
- A semi-metric digital camera ROLLEI 6008 db45, with digital back Phase-One, model H2O. The camera presents a pixel spacing is 9 micrometers, in a scene composed of 4080 x 5440 pixel with 48-bit dynamics. Acquisition is assisted by a camera compensation system to adjust the roll and pitch variations due to aircraft position and flight attitude.

Figure 4. Shaded relief, LiDAR derived DSM of the seafront (centre), the harbour (right) and the 17th Century Dutch fort (left) in the southern city of Galle. DSMs, obtained by mapping first returns from terrain - including buildings and vegetation - are better suited than DGMs to HyperDEM-like applications.

The flight zone (Figure 1, left) spanned between Puttalam, in the West, and Pottuvil, in the Southeast. For security reasons, authorized flight plans did not include the capital, Colombo, nor some specific damaged coastal zones in the East (Trincomalee, Batticaloa,

Ampara). Instead, eastern areas (Figure 1) were covered by spaceborne RaDAR, and qualified by high resolution spaceborne multispectral observation (Figure 1, right).

Flight heights ranged between 900-2700 metres, as a function of the desired ground resolution, the morphology and land-cover of surveyed areas, and the meteorological conditions.

Flight paths (Figure 2) were computed in real time by DGPS (differential kinematic GPS), using data simultaneously acquired by one GPS receiver onboard the aircraft and two, twin-frequency geodetic GPS receivers Ashtech (mod. Z-Extreme) at the fixed rate of one measurement per second. Twin-frequency GPS receivers were operated only on the benchmarks of an ad-hoc geodetic frame created by OGS, starting from a re-calculated benchmark of the Sri Lanka Survey Department, at the Katunayake International airport, north of Colombo.

All benchmarks of the new geodetic frame were calculated and located on ellipsoids WGS84 and Everest 1830 in the Transverse Mercator projection. Upon completion of the campaign, the Sri Lanka Survey Dept. was provided with the monographs of the new, OGS established benchmarks.
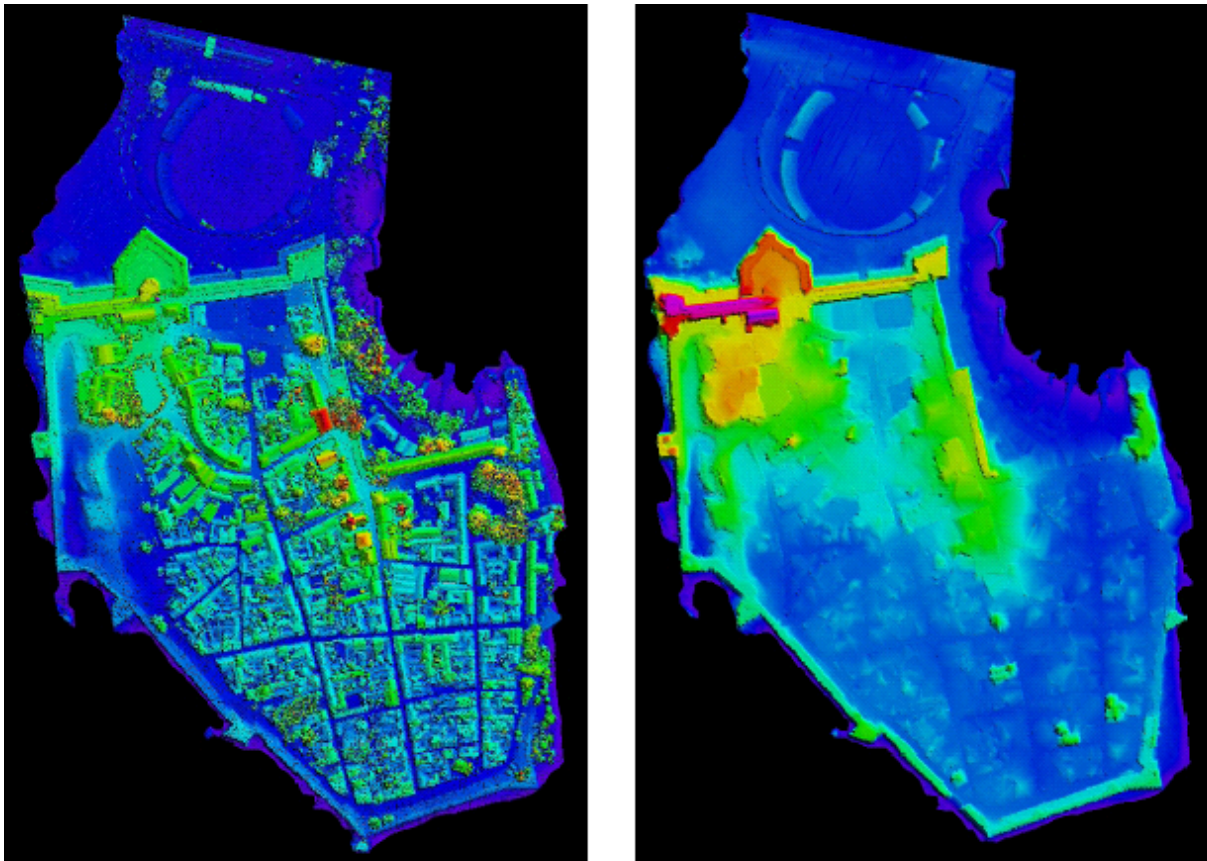
Figure 5. LiDAR-derived DSM (left) and DGM "ground" (right). The example relates to the 17th Century Dutch fort in Galle, whose thick defence walls are emphasized by removal of objects in DGM (right).

GPS data were integrated to Inertial Platform (IMU) data acquired at 200 Hz. The aircraft trajectory – called SBET (Best Estimated Trajectory; see Figure 2), and made up of fixes spaced ca. 15 cm from each other – is characterized by residual r.m.s. errors better than 0.3 metres, that are compatible with the required precision in elevation.

Range data were geo-referenced by use of spatial and orientation parameters; basic products are vectors of points, including the information on position, GPS time and backscattered LiDAR amplitude. All products were delivered in UTM (44 N) projection, on WGS84 ellipsoid.

LiDAR data were also corrected by use of a geodic model derived from the EGM96 model. In particular, Digital Elevation Models obtained by airborne LiDAR (Figures 4 and 5), were associated to co-registered airborne Hyperspectral data that underwent unsupervised, level-two classification for automatically discriminating bare soil from vegetation.

Finally, bare pixels (without vegetation) were weighted 1, vegetated pixels weighted 0, and vegetated pixels for which two LiDAR returns are available (an early reflection from the top of canopy, and a late reflection from the underlying ground) were marked 0.5.

This procedure has allowed creating automatically (i) a mask including all points whose elevation is fully reliable within the nominal error range, and (ii) a three-dimensional, level-two land-cover of subsets weighted 0.5 and 1.

The information was completed by carrying out same bare soil classification on multispectral, very high-resolution, pre-/post-tsunami QuickBird data. In spite of the comparable pixel footprint, however, the 4-band Visible/Near-Infrared spectral content of QuickBird provided much poorer information than the airborne 64-band Hyperspectral airborne radiometer.

4. The space campaign

The campaign relied upon same strategy as in the air campaign, with elevation data founded upon interferometric Synthetic Aperture RaDAR techniques (*Prati et al.*, 1994; *Ferretti et al.*, 1999, 2001), and pixel qualification carried out on Infra-Red multispectral satellite scenery (*Hirn and Ferrucci*, 2005).

Pixel qualification was based on the automated discrimination of bare soils, buildings and infrastructures from vegetation (*Ferrucci and Hirn*, 2005). These classes return highest confidence weight to RaDAR measured elevation values in the same pixel, whereas dense canopy returns lower or zero values. Overall, the space dataset is composed of 67 images, both RaDAR and multispectral, with resolutions ranging from metric (QuickBird) to decametric (ASTER, Landsat-7, ERS-1, ERS-2, Envisat).

To fit the requirements of HyperDEM, repeat-pass interferometry was carried out to provide for two different products: Permanent Scatterers (PS-InSAR™) data and DEM using ERS-1/ERS-2 'Tandem' pair combinations. PS-InSAR is a trademark of Politecnico di Milano.

The available SAR dataset was composed of 23 scenes along ERS/Envisat track 33 (Descending orbit), frames 3447 and 3465, acquired since 1992 at uneven rates. Accounting for the pixel dimensions (10m x 10m), and the lack of penetration of C-band RaDAR radiation across canopy, the elevation model mirrors the envelope of the Earth surface, including vegetation. In this article, consequently, "DEM" reads as Digital Surface Model.

The useable SAR dataset, composed of 42 scenes, was theoretically sufficient for carrying out thorough PS-InSAR analysis. Conversely, the characteristics of land cover - in combination with the characteristics specified above of Synthetic Aperture RaDARs

onboard the ESA spacecrafts - did not reveal suitable for thorough, Permanent Scatterer analysis (Figures 6, 7).
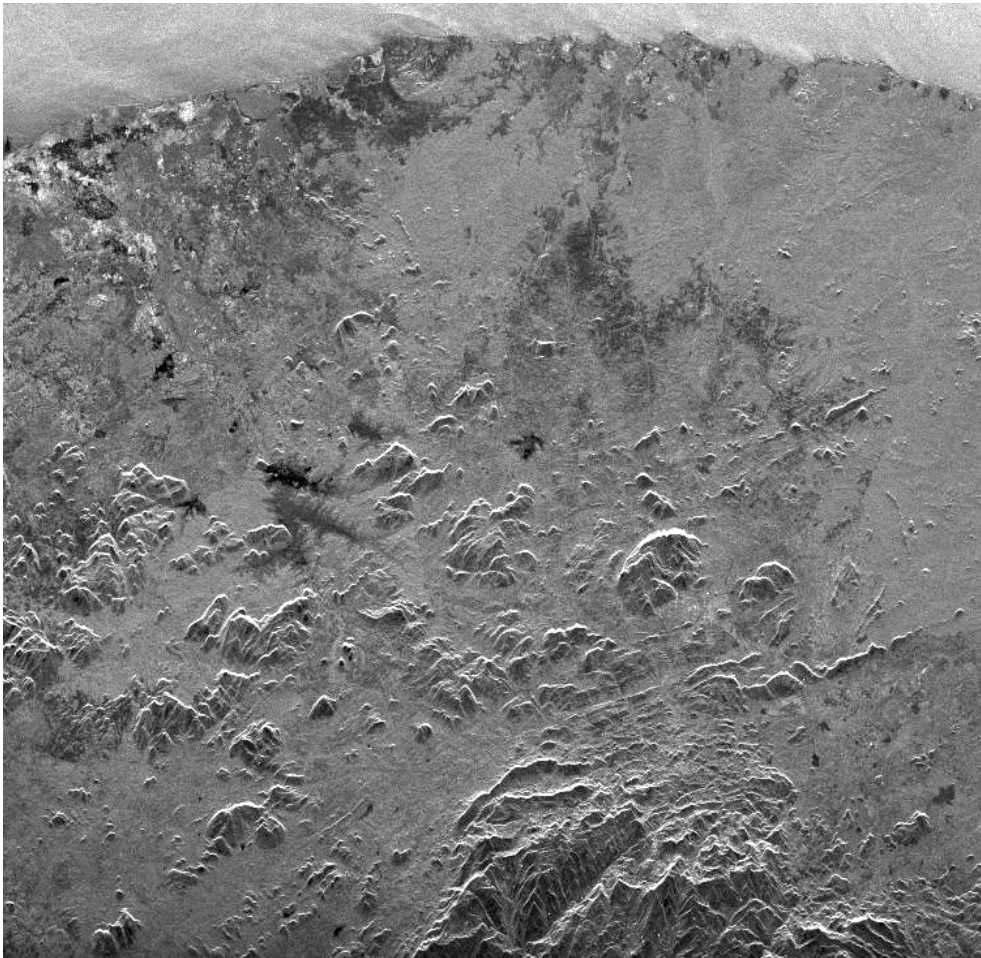
Figure 6. View of the eastern coast (North is to the left) from radar satellites ERS (Track 33 – Frame 3465) of the European Space Agency. Because of the overall limited dataset, and the characteristics of the eastern coast areas (alternating rain forest, extremely flat terrains and frequent water bodies), the technical choice switched from PS-InSAR to Multi-Baseline InSAR technique.

In particular, the characteristics of the land cover make this area very sensitive to temporal decorrelation, that is, the loss of coherence between two successive images due to a large time interval elapsed between acquisitions. For this reasons, basic RaDAR analysis was re-centred on past ERS-1/ERS-2 tandem pairs, with 1-day intervals between over passes and 35-day repeat times.

After elimination of tandem pairs with baseline larger than 1km, only 5 pairs for frame 3465, and only 3 for frame 3447 were left. This forced moving from the PS-InSAR™ technique to the Multi-Interferogram approach (*Prati et al.*, 1994; *Ferretti et al.*, 1999): which is less precise, but less sensitive to the quantity of data.

As for merge of the very-high resolution LiDAR, and moderate-to-high resolution other spatial data, it is worth recalling that raw data coming from the LiDAR airborne acquisition are in dual form, "first pulse" and "last pulse". First-pulses, allow mapping the reflecting envelope surface and give rise to DSM; whereas the last-pulses subset, the

DGM or "ground", is constituted of rays bouncing back from the ground after crossing void spaces in the canopy.
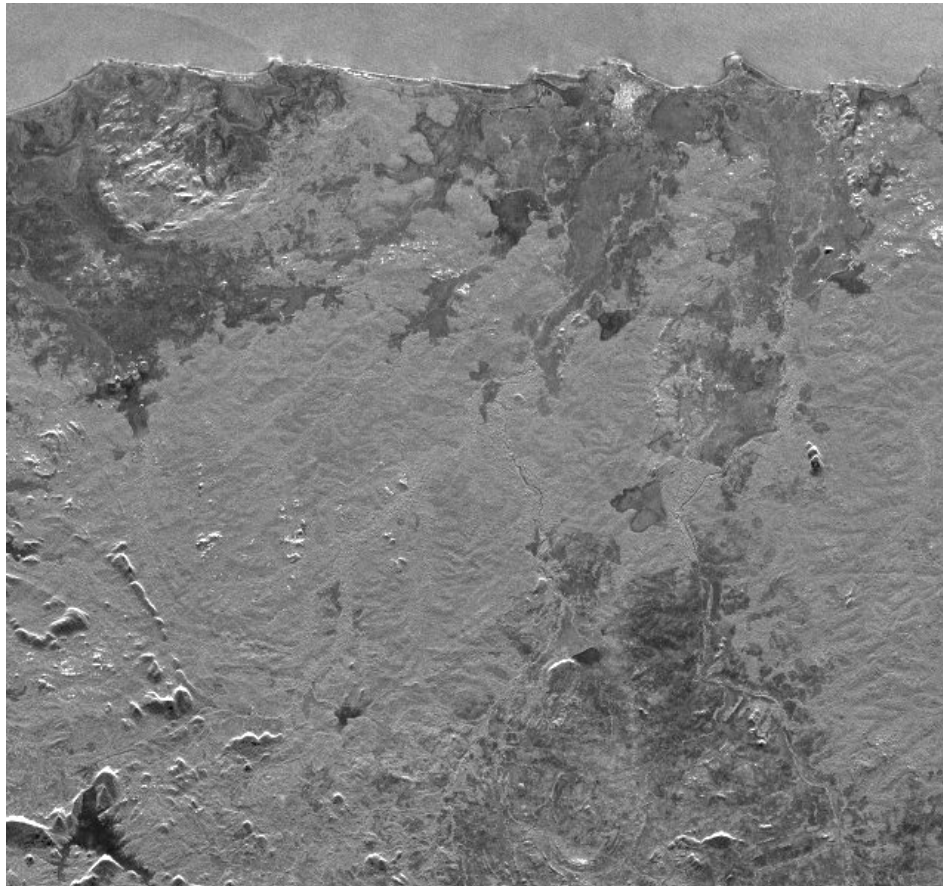
Figure 7. SAR Multi-Image Reflectivity map of a portion of the eastern coast (North is to the left). Dark shading indicates vegetation cover. In these areas, the Phase Stability Index is low since radar scattering de-organizes in the foliage, which points to an equally low probability of success of Permanent Scatterers interferometry. Indeed, much of the area within the image is covered by vegetation or water bodies, whose behaviour is incoherent within a multi-temporal sequence.

As for products obtained from processing and post-processing, we shall recall that the generic definition of "DEM" (Digital Elevation Model), applies to elevation of terrain referred to bare-Earth without vegetation and/or buildings. In order to deal with LiDAR and InSAR data at once, conversely, we split had to models into DGM ("ground") and DSM ("surface").

Definitely, DGM refers only to LiDAR, whereas DSM – that envelope the whole of reflectors on visible Earth – refers also to RaDAR. Consequently, a comparison between different results obtained in the East – by space and RaDAR – and in the West and South – by air and LiDAR – can be performed only on Digital Surface Models.

Comparison, done over the LiDAR-InSAR, DSM overlap area of Arugam Bay in the south-east (see Figures 10 and 11) leads to a satisfactory least standard deviation value of 2.56 metres. It is worth noting, however, that such comparison is carried out on products displaying a two-order of magnitude difference in ground resolution, that is, 1 square metre per pixel for LiDAR, vs. 100 square metres per pixel (10m x 10m) for InSAR.
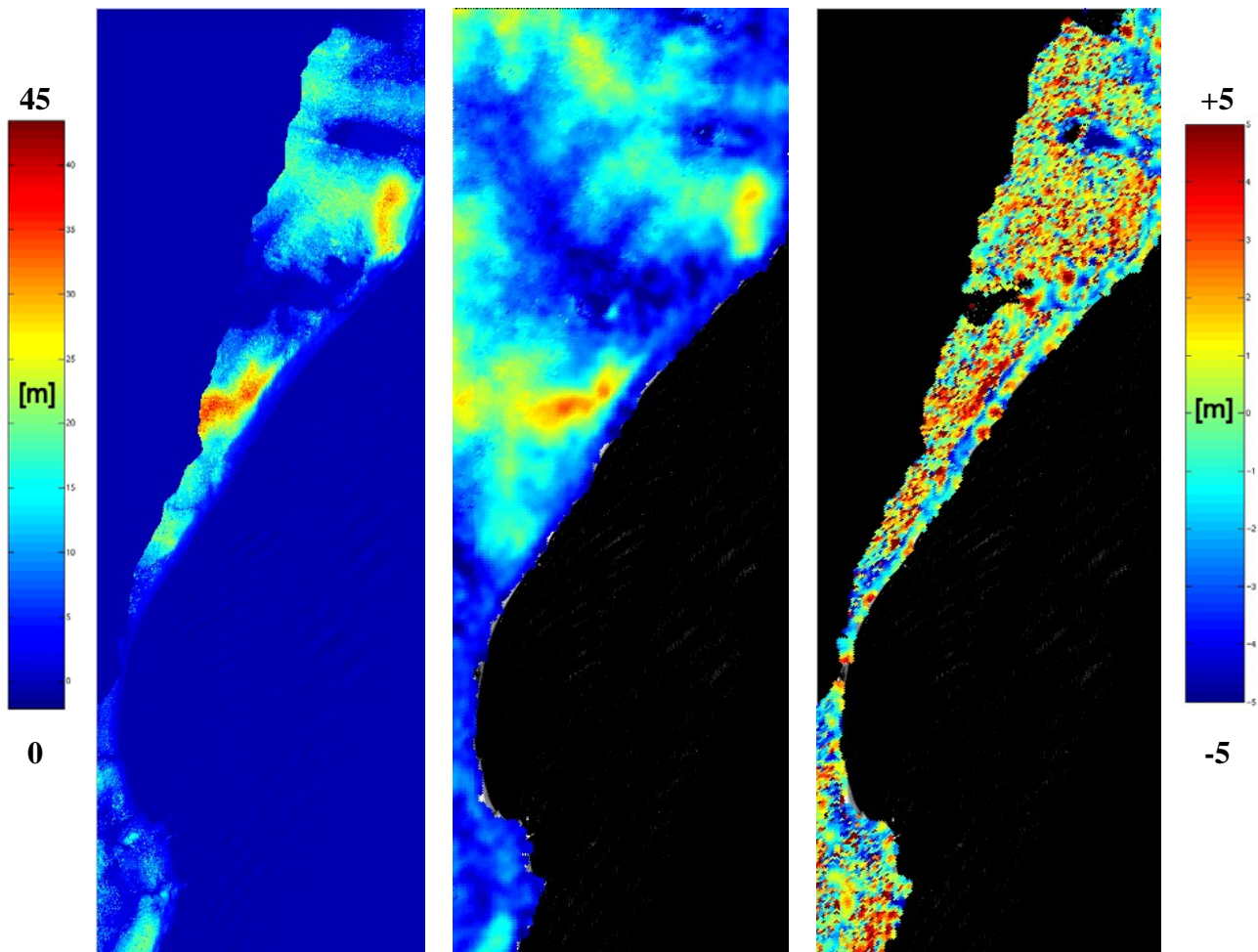
Figure 8. DSM obtained by LiDAR (left), by Multi-Interferogram InSAR (centre) and map of the LiDAR-InSAR elevation differences (right). Colorbars shown for elevation (left) and errors (right). Minimum standard deviation of 2.56 m is a good estimate of InSAR topography accuracy in the whole area.

5. DATA AND RESULTS

LiDAR models were arranged in tiles of 1000 x 1000 x 1 metre (excepting those along the shoreline), for as much as 4600 billion grid points measured in elevation (*Baltsavias*, 1999; *Kraus and Pfeifer*, 1998; *Axelsson*, 2000). Spaceborne RaDAR Digital Surface Models were arranged in two frames of 1811x3497 and 894x3202 (columns x rows) respectively, with 30-metre spacing of points, allowing for total 2.4 million grid points measured in elevation.

According to the inter-Government agreement, the Disaster Management Centre in Colombo (acting End User of HyperDEM), was provided also with a few inundation examples - as the one in Figure 9, centred on the urban area of Galle - aimed to demonstrate the procedures to be followed by the Sri Lankan Authorities for tsunami scenario building.

For the sake of simplicity, simulation was conducted not accounting for the - significant - dynamic component of the tsunami wavefront. It is worth noting, however, that this simplified "static" procedure – that does not allow calculating the energy budget, nor its distribution on obstacles on land – provided a good fit with observed inland

penetration of waters on 26th December 2004 (*Tinti et al.*, 2005; *Tinti et al.*, 2006). Products arisen from the work carried out (1780 km^2 of Digital Ground Model at 1-metre resolution, and about 2500 km^2 of Digital Surface Model at resolutions between 1 metre and 10 metres) were handed over by the Ambassador of Italy in Sri Lanka, and the Minister for Disaster Management and Humanitarian Affairs, on 7th December 2006, in Colombo.
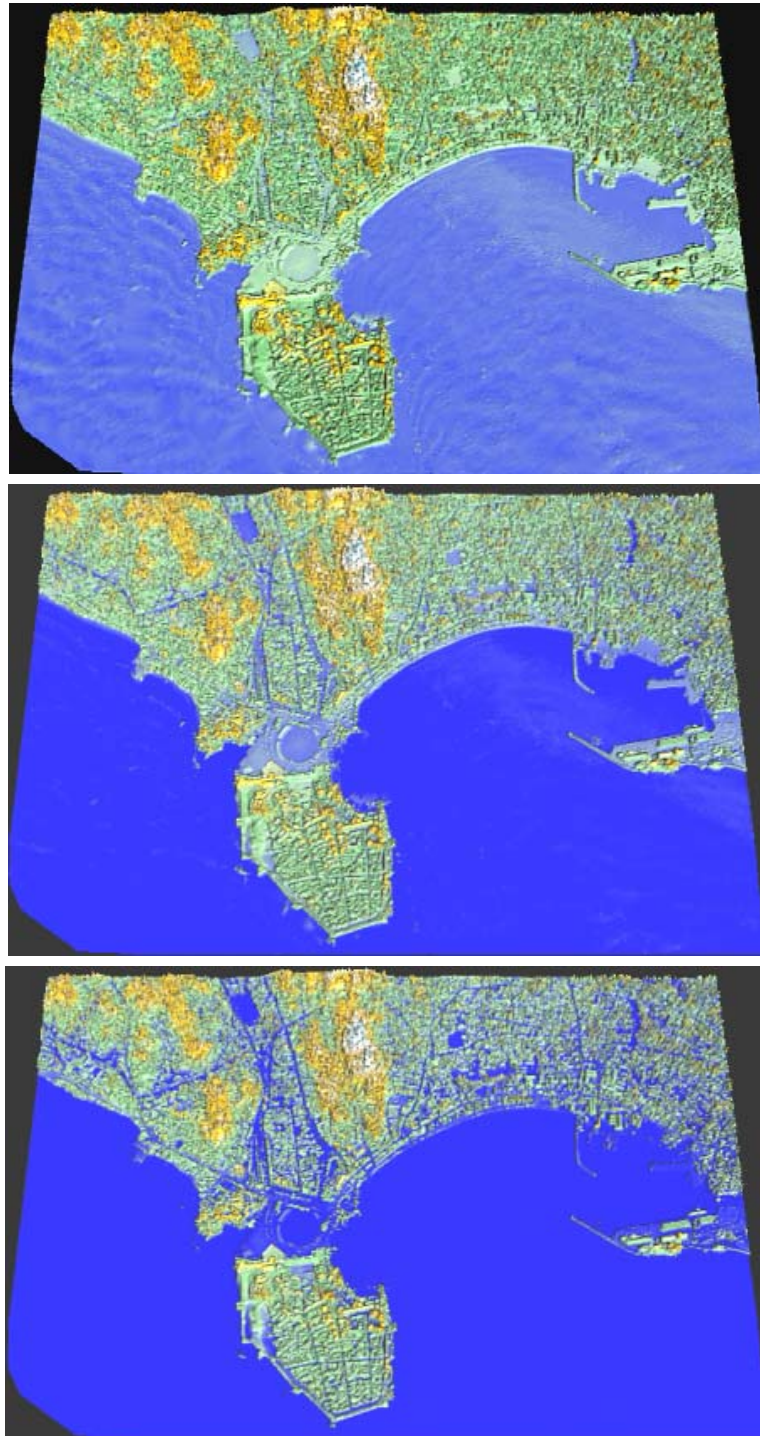
Figure 9. Digital Surface Model of the town of Galle (top), and inundation simulation by a 2-metre (centre) and a 4-metre (bottom) model *surge*. The synthetic scenario shown here, is satisfactorily consistent with the real case tsunami observed at Galle as of 26th December 2004.

REFERENCES

Axelsson, P. (2000), DEM Generation from Laser Scanner data Using Adaptive TIN Models, *International Archives of Photogrammetry and Remote Sensing, Vol. XXXIII*, B4. Amsterdam.

Baltsavias, E.P. (1999), Airborne laser scanning: basic relations and formulas, *ISPRS Journal of Photogrammetry & Remote Sensing, 54*, 199-214.

Ferretti, A., C. Prati, and F. Rocca (1999), Multibaseline InSAR DEM Reconstruction: the Wavelet Approach, *IEEE Trans. on Geoscience and Remote Sensing*, 37 (2), 705-715.

Ferretti, A., C. Prati, and F. Rocca (2001), Permanent scatterers in SAR interferometry, *IEEE Trans. on Geoscience and Remote Sensing*, 39(1).

Ferrucci, F., and B. Hirn (2005), An automated method for detecting and mapping, particularly for areas without vegetation, *International Patent*, PCT WO2005/005926A1, publ. 26th January 2005.

Hirn, B., and F. Ferrucci (2005), MYME2: a Multi-Payload Integrated Procedure for the Automated, High-Resolution Remote Sensing of Burn Scars, *IEEE-IGARSS*, paper n. 20238, pp.4, 25-29 July, Seoul, South Korea.

Kraus, K., and N. Pfeifer (1998), Determination of Terrain Models in Wooded Areas with Airborne laser Scanner data, *ISPRS Journal of Photogrammetry and Remote Sensing*, 53(4), 193-203.

Prati, C., F. Rocca, and A. Monti Guarnieri (1994), Topographic capabilities of SAR exemplified with ERS-1, *Geo Information System*, 7(1), 17-23.

Tinti, S., A. Armigliato, A. Manucci, G. Pagnoni, and F. Zaniboni (2005), Landslides and tsunamis of 30th December 2002 at Stromboli, Italy: numerical simulations, *Bollettino di Geofisica Teorica e Applicata, 46*, 153-168.

Tinti, S., A. Armigliato, A. Manucci, G. Pagnoni, F. Zaniboni, A.C. Yalçiner, and Y. Altinok (2006), The generating mechanism of the August 17, 1999 İzmit Bay (Turkey) tsunami: Regional (tectonic) and local (mass instabilities) causes, *Marine Geology, 225*, 311-330.

Index of Authors